BLOOD BIOMARKERS OF NEURODEGENERATIVE DISEASES

EDITED BY: Thomas K. Karikari, Nicholas James Ashton, Henrik Zetterberg and Kaj Blennow

PUBLISHED IN: Frontiers in Aging Neuroscience, Frontiers in Molecular Neuroscience and Frontiers in Neuroscience

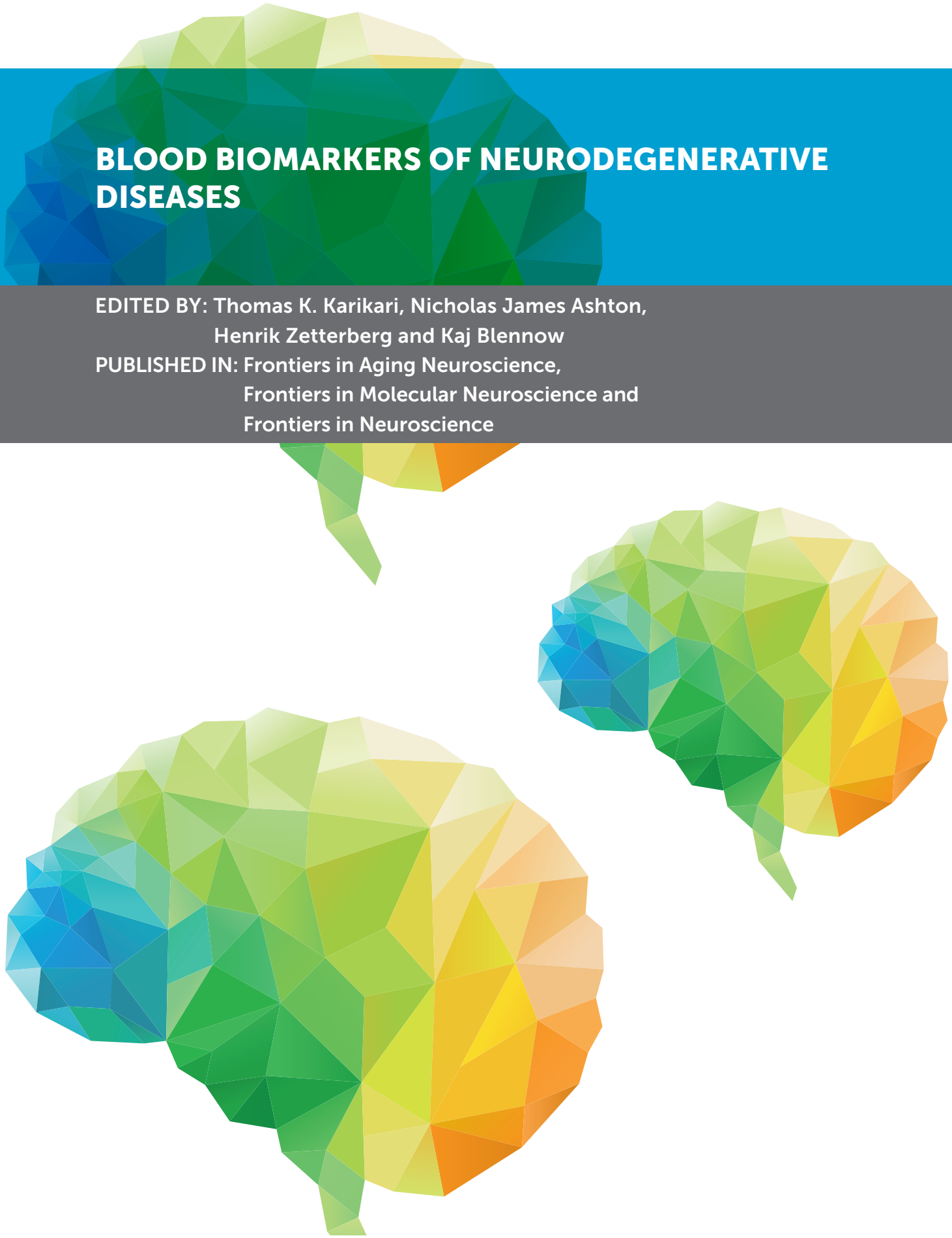

frontiers Research Topics

frontiers

ISSN 1664-8714
ISBN 978-2-88976-284-2
DOI 10.3389/978-2-88976-284-2

About Frontiers

Frontiers is more than just an open-access publisher of scholarly articles: it is a pioneering approach to the world of academia, radically improving the way scholarly research is managed. The grand vision of Frontiers is a world where all people have an equal opportunity to seek, share and generate knowledge. Frontiers provides immediate and permanent online open access to all its publications, but this alone is not enough to realize our grand goals.

Frontiers Journal Series

The Frontiers Journal Series is a multi-tier and interdisciplinary set of open-access, online journals, promising a paradigm shift from the current review, selection and dissemination processes in academic publishing. All Frontiers journals are driven by researchers for researchers; therefore, they constitute a service to the scholarly community. At the same time, the Frontiers Journal Series operates on a revolutionary invention, the tiered publishing system, initially addressing specific communities of scholars, and gradually climbing up to broader public understanding, thus serving the interests of the lay society, too.

Dedication to Quality

Each Frontiers article is a landmark of the highest quality, thanks to genuinely collaborative interactions between authors and review editors, who include some of the world's best academicians. Research must be certified by peers before entering a stream of knowledge that may eventually reach the public - and shape society; therefore, Frontiers only applies the most rigorous and unbiased reviews.
Frontiers revolutionizes research publishing by freely delivering the most outstanding research, evaluated with no bias from both the academic and social point of view. By applying the most advanced information technologies, Frontiers is catapulting scholarly publishing into a new generation.

What are Frontiers Research Topics?

Frontiers Research Topics are very popular trademarks of the Frontiers Journals Series: they are collections of at least ten articles, all centered on a particular subject. With their unique mix of varied contributions from Original Research to Review Articles, Frontiers Research Topics unify the most influential researchers, the latest key findings and historical advances in a hot research area! Find out more on how to host your own Frontiers Research Topic or contribute to one as an author by contacting the Frontiers Editorial Office: frontiersin.org/about/contact

BLOOD BIOMARKERS OF NEURODEGENERATIVE DISEASES

Topic Editors:
Thomas K. Karikari, University of Gothenburg, Sweden
Nicholas James Ashton, University of Gothenburg, Sweden
Henrik Zetterberg, University of Gothenburg, Sweden
Kaj Blennow, University of Gothenburg, Sweden

Citation: Karikari, T. K., Ashton, N. J., Zetterberg, H., Blennow, K., eds. (2022). Blood Biomarkers of Neurodegenerative Diseases. Lausanne: Frontiers Media SA. doi: 10.3389/978-2-88976-284-2

Table of Contents

frontiers | Frontiers in Molecular Neuroscience

EDITORIAL
published: 30 June 2022
doi: 10.3389/fnmol.2022.966139

Editorial: Blood Biomarkers of Neurodegenerative Diseases

Thomas K. Karikari[1,2]*, *Nicholas J. Ashton*[1,3,4,5], *Henrik Zetterberg*[1,6,7,8,9] *and Kaj Blennow*[1,6]

[1] Department of Psychiatry and Neurochemistry, Institute of Neuroscience and Physiology, The Sahlgrenska Academy, University of Gothenburg, Gothenburg, Sweden, [2] Department of Psychiatry, University of Pittsburgh, Pittsburgh, PA, United States, [3] Centre for Age-Related Medicine, Stavanger University Hospital, Stavanger, Norway, [4] King's College London, Institute of Psychiatry, Psychology & Neuroscience, Maurice Wohl Clinical Neuroscience Institute, London, United Kingdom, [5] National Institute for Health and Care Research (NIHR) Biomedical Research Centre for Mental Health & Biomedical Research Unit for Dementia at South London & Maudsley National Health Service (NHS) Foundation, London, United Kingdom, [6] Clinical Neurochemistry Laboratory, Sahlgrenska University Hospital, Mölndal, Sweden, [7] Department of Neurodegenerative Disease, University College London (UCL) Institute of Neurology, London, United Kingdom, [8] UK Dementia Research Institute at University College London (UCL), London, United Kingdom, [9] Hong Kong Center for Neurodegenerative Diseases, Hong Kong, China

Keywords: blood biomarker, Alzheimer's disease, tau, amyloid, neurofilament

Editorial on the Research Topic

Blood Biomarkers of Neurodegenerative Diseases

We are rapidly entering an era where the use of easily accessible blood tests give meaningful information about the pathophysiological basis of neurodegenerative diseases. Recent technical and methodological advances, aided by the rise of well-characterized research cohorts, have propelled the neurodegeneration field in a direction toward several important and sought-after applications of blood biomarkers; as screening or risk assessment tools, or as therapy monitoring in clinical trials. The key candidates include biomarkers fulfilling the AT(N) criteria for the definition and staging of Alzheimer's disease (AD) (Ashton et al., 2020; Teunissen et al., 2021; Karikari et al., 2022). However, the widespread applications of these biomarkers would require prior verification in diverse populations. Moreover, there is a need to characterize demographic, lifestyle and medical conditions that can affect the production and clearance of these blood biomarkers. Furthermore, blood biomarkers of other key molecular processes involved in AD (e.g., inflammation) and, importantly, other neurodegenerative diseases (e.g., TDP-43 and α-synuclein) are actively being explored to improve disease identification, characterization, and differential diagnosis.

We proposed a Research Topic focused on gathering further evidence on the aforementioned topics. Forty-five manuscripts were submitted for consideration and 25 of these were accepted for publication following the peer-review process. The accepted manuscripts are summarized below, divided into seven broad areas.

ALZHEIMER'S, PARKINSON'S AND OTHER NEURODEGENERATIVE DISEASES

In a study of 277 participants, Jiao et al. reported significant increases in plasma total-tau and NfL in AD vs. controls. A diagnostic model incorporating these blood biomarkers and age, sex, and *APOE* allele gave a diagnostic accuracy of 89%, sensitivity of 82% and specificity of 84%. In evaluating 463 AD patients and 1,389 controls matched according to age, sex and body mass index, Chen X. et al. found significantly higher levels of serum cystatin C in AD vs. control participants. Serum cystatin C levels did associate with cognitive function and the risk of cognitive impairment. In an investigation that combined experimental and bioinformatic approaches, Sabaie et al. showed that the *BCAS4/miR-185-5p/SHISA7* competing endogenous RNA axis in the blood and brains of people with AD.

OPEN ACCESS

Edited and reviewed by:
Jean-Marc Taymans, Institut National de la Santé et de la Recherche Médicale (INSERM), France

***Correspondence:**
Thomas K. Karikari
thomas.karikari@gu.se; karikari@pitt.edu

Specialty section:
This article was submitted to Molecular Signalling and Pathways, a section of the journal Frontiers in Molecular Neuroscience

Received: *10 June 2022*
Accepted: *16 June 2022*
Published: *30 June 2022*

Citation:
Karikari TK, Ashton NJ, Zetterberg H and Blennow K (2022) Editorial: Blood Biomarkers of Neurodegenerative Diseases. Front. Mol. Neurosci. 15:966139. doi: 10.3389/fnmol.2022.966139

Xu et al. sought to explore this association further by investigating relationships between heme oxygenase-1 levels, iron content and hemoglobin levels. The authors showed that in people with Parkinson's disease (PD) there were increased levels of heme oxygenase-1 and low levels of hemoglobin, which they concluded to be a putative mechanisms of iron deposition in PD. Hu et al. reported that concentrations of the anti-inflammatory neuropeptides pituitary adenylate-cyclase activating polypeptide (PACAP) and vasoactive intestinal peptide (VIP) were increased in people living with PD vs. unaffected controls. Measures of mood disorder and non-motor symptoms were associated with serum VIP and PACAP levels, respectively. Zhang W. et al. integrated experimental and computational methods to show that expression of the signal sequence receptor subunit 1 gene was significantly upregulated in the blood of animal models of PD.

Vacchiano et al. showed significant correlations between plasma and cerebrospinal fluid (CSF) levels of NfL in paired samples, and both showed high performances to difference ALS patients from ALS mimics despite CSF NfL being slightly superior (AUC = 92%) to plasma NfL (AUC = 87%). High concentrations of NfL in either CSF or plasma signified faster disease progression and poorer longitudinal survival.

In a publication on Huntingtin disease, Ingannato et al. showed that individuals with bulbar onset disease had higher plasma NfL levels and later age of onset compared with the spinal onset variant.

An original report by Ye et al. indicated that serum levels of cystatin C were associated with measures of disability in patients with multiple systems atrophy including those with predominant cerebellar ataxia (MSA-C) but not those with predominant Parkinsonism. MSA-C patients with low vs. high levels of serum cystatin C demonstrated a difference in the probability of survival over a 5-year duration. Guan et al. showed that serum uric acid levels were significantly decreased in people diagnosed with Meige's syndrome vs. controls and predicted severe clinical symptoms.

MILD COGNITIVE IMPAIRMENT

Liang et al. reported that interleukin-2, an immunoregulatory protein, is a potentially better blood biomarker for cognitive decline in amnestic mild cognitive decline than each of plasma Aβ42/Aβ40, total-tau and p-tau181. In a 9-year longitudinal study, Chen C. et al. reported that older adults with high uric acid levels in blood have reduced risk of developing mild cognitive impairment. Ngwa et al. described genome-wide DNA methylation patterns associated with aerobic exercise in people with mild cognitive impairment.

NORMAL AGING

Zecca et al. studied age effects on plasma Aβ42 levels, reporting a significant positive correlation in the whole cohort. When separated into age groups, they found a significant inverse association of plasma Aβ42 with age in individuals <35 years old, a significant positive correlation in those aged 35–65 years old, and no correlation in those over 65 years.

Orihashi et al. showed that soluble triggering receptor expressed on myeloid cells 2 (sTREM2) levels did not correlate with baseline or longitudinal changes in the volumes of specific brain regions closely linked with cognitive function in normal aging. In a report by Kapoor et al., the levels of endothelial progenitor cells and vascular endothelial growth factor D was each associated with small vessel disease after accounting for age and sex. In a study performed in an APP/PS1 mouse model, Zhang L. et al. explored dynamic changes in Aβ42 aggregates in peripheral vs. brain-derived sources. Using immunoassays that differentiate monomeric from oligomeric and total Aβ42 species, the authors showed that the levels of Aβ42 monomers and oligomers were significantly decreased and increased, respectively, in 9- vs. 3-month-old animals. Moreover, intestinal levels of Aβ42 were also higher at 9- vs. 3-months.

KIDNEY DISEASE AND RENAL FUNCTION

Hou et al. investigated the utility of plasma biomarkers in end-stage renal disease. They reported marginally higher levels of the plasma NfL in patients with vs. without cognitive impairment but the levels did not associate with cognitive function or biochemical parameters. However, the levels of plasma Aβ40, Aβ42 and total-tau were not different between end-stage renal disease participants with or without cognitive decline.

ANALYTICAL METHODS

Chatterton et al. reported a proof-of-concept study to detect cell-free DNA in blood plasma by combining bisulfite sequencing and computational processing approaches.

Chang et al. examined preanalytical handling protocols for the assessment of alpha-synuclein and NfL in plasma. The results showed that K_2-EDTA and K_3-EDTA tubes had equivalent performances for assessing both biomarkers. However, sample centrifugation at 4 °C led to lower and less reproducible levels of plasma α-synuclein measured.

GENOME-WIDE ASSOCIATION STUDIES

In a genome-wide association study, Chen H. et al. identified over 160 metabolites that did associate significantly with several neurodegenerative diseases. For instance, X-11529 and X-13429 was associated with frontotemporal dementia while 2-methoxyacetaminophen sulfate was associated with amyotrophic lateral sclerosis. Furthermore, Zhao et al. reported suggestive associations of interleukin-16 and macrophage inflammatory protein-1 beta with PD risk, but age of onset did not associate with inflammatory cytokine profiles.

REVIEW ARTICLES

Asadi et al. reviewed publications on the value of stress granules in the neurodegenerative diseases and the proteins that these

granules consist of. Guo et al. presented a narrative review of recent advances in peptide- and peptoid-based biomarker detection assays and technology platforms used in the AD field.

CONCLUSION

The articles published in this Research Topic cover a broad range of topics of direct relevance to the pathogenesis and etiology of neurodegenerative diseases. Other articles covered preanalytical handling and clinical performances of blood biomarkers, as well as lifestyle and age-related factors that can affect their performances.

AUTHOR CONTRIBUTIONS

TK prepared an initial draft of this editorial that was carefully revised by NA, HZ, and KB. All authors approved the final version for submission.

FUNDING

TK was funded by the Swedish Research Council (Vetenskapsrådet #2021-03244), the Alzheimer's Association Research Fellowship (#AARF-21-850325), the BrightFocus Foundation (#A2020812F), the Emil and Wera Cornells foundation, the International Society for Neurochemistry's Career Development Grant, the Swedish Alzheimer Foundation (Alzheimerfonden; #AF-930627), the Swedish Brain Foundation (Hjärnfonden; #FO2020-0240), the Swedish Dementia Foundation (Demensförbundet), the Swedish Parkinson Foundation (Parkinsonfonden), Gamla Tjänarinnor Foundation, the Aina (Ann) Wallströms and Mary-Ann Sjöbloms Foundation, the Agneta Prytz-Folkes & Gösta Folkes Foundation (#2020-00124), the Gun and Bertil Stohnes Foundation, and the Anna Lisa and Brother Björnsson's Foundation. NA was supported by the Swedish Alzheimer Foundation (Alzheimerfonden; #AF-931009), Hjärnfonden and the Swedish Dementia Foundation (Demensförbundet). HZ is a Wallenberg Scholar supported by grants from the Swedish Research Council (#2018-02532), the European Research Council (#681712), Swedish State Support for Clinical Research (#ALFGBG-720931), the Alzheimer Drug Discovery Foundation (ADDF), USA (#201809-2016862), the AD Strategic Fund and the Alzheimer's Association (#ADSF-21-831376-C, #ADSF-21-831381-C, and #ADSF-21-831377-C), the Olav Thon Foundation, the Erling-Persson Family Foundation, Stiftelsen för Gamla Tjänarinnor, Hjärnfonden, Sweden (#FO2019-0228), the European Union's Horizon 2020 research and innovation programme under the Marie Skłodowska-Curie grant agreement No 860197 (MIRIADE), European Union Joint Program for Neurodegenerative Disorders (JPND2021-00694), and the UK Dementia Research Institute at UCL.KB is supported by the Swedish Research Council (#2017-00915), the Alzheimer Drug Discovery Foundation (ADDF), USA (#RDAPB-201809-2016615), the Swedish Alzheimer Foundation (#AF-742881), Hjärnfonden, Sweden (#FO2017-0243), the Swedish state under the agreement between the Swedish government and the County Councils, the ALF-agreement (#ALFGBG-715986), and European Union Joint Program for Neurodegenerative Disorders (JPND2019-466-236). The funders had no role in data collection, analysis or decision to publish.

REFERENCES

Ashton, N. J., Hye, A., Rajkumar, A. P., Leuzy, A., Snowden, S., Suárez-Calvet, M., et al. (2020). An update on blood-based biomarkers for non-Alzheimer neurodegenerative disorders. *Nat. Rev. Neurol.* 16, 265–284. doi: 10.1038/s41582-020-0348-0

Karikari, T. K., Ashton, N. J., Brinkmalm, G., Brum, W. S., Andréa L. Benedet, Montoliu-Gaya, L., et al. (2022). Blood phospho-tau in Alzheimer's disease: analysis, interpretation, and clinical utility. *Nat. Rev. Neurol.* doi: 10.1038/s41582-022-00665-2. [Epub ahead of print].

Teunissen, C. E., Verberk, I. M. W., Thijssen, E. H., Vermunt, L., Hansson, O., Zetterberg, H., et al. (2021). Blood-based biomarkers for Alzheimer's disease: towards clinical implementation. *Lancet Neurol.* 21, 66–77. doi: 10.1016/S1474-4422(21)00361-6

Conflict of Interest: HZ has served at scientific advisory boards and/or as a consultant for Abbvie, Alector, ALZPath, Annexon, Apellis, Artery Therapeutics, AZTherapies, CogRx, Denali, Eisai, Nervgen, Novo Nordisk, Pinteon Therapeutics, Red Abbey Labs, reMYND, Passage Bio, Roche, Samumed, Siemens Healthineers, Triplet Therapeutics, and Wave, and has given lectures in symposia sponsored by Cellectricon, Fujirebio, Alzecure, Biogen, and Roche. KB has served as a consultant, at advisory boards, or at data monitoring committees for Abcam, Axon, BioArctic, Biogen, JOMDD/Shimadzu. Julius Clinical, Lilly, MagQu, Novartis, Ono Pharma, Pharmatrophix, Prothena, Roche Diagnostics, and Siemens Healthineers, HZ and KB are co-founders of Brain Biomarker Solutions in Gothenburg AB, a GU Ventures-based platform company at the University of Gothenburg.

The remaining authors declare that the research was conducted in the absence of any commercial or financial relationships that could be construed as a potential conflict of interest.

Publisher's Note: All claims expressed in this article are solely those of the authors and do not necessarily represent those of their affiliated organizations, or those of the publisher, the editors and the reviewers. Any product that may be evaluated in this article, or claim that may be made by its manufacturer, is not guaranteed or endorsed by the publisher.

frontiers in Aging Neuroscience

ORIGINAL RESEARCH
published: 18 March 2021
doi: 10.3389/fnagi.2021.656626

Elevated Heme Oxygenase-1 Correlates With Increased Brain Iron Deposition Measured by Quantitative Susceptibility Mapping and Decreased Hemoglobin in Patients With Parkinson's Disease

Jinghui Xu[1,2†], Chi Xiao[1†], Weizheng Song[3], Xiangqin Cui[1], Mengqiu Pan[4], Qun Wang[1], Yanqiu Feng[5‡] and Yunqi Xu[1*‡]*

[1]Department of Neurology, Nanfang Hospital, Southern Medical University, Guangzhou, China, [2]Department of Rehabilitation Medicine, The Third Affiliated Hospital, Sun Yat-sen University, Guangzhou, China, [3]Department of Neurosurgery, the Eighth People's Hospital of Chengdu, Chengdu, China, [4]Department of Neurology, Guangdong 999 Brain Hospital, Guangzhou, China, [5]Guangdong Provincial Key Laboratory of Medical Image Processing, Southern Medical University, Guangzhou, China

OPEN ACCESS

Edited by:
Thomas K. Karikari,
University of Gothenburg, Sweden

Reviewed by:
Maria Joao Gama,
University of Lisbon, Portugal
Agathe Vrillon,
Assistance Publique Hopitaux De Paris, France
Emmanuel Quansah,
Van Andel Institute, United States

***Correspondence:**
Yunqi Xu
xyqtf@smu.edu.cn
Yanqiu Feng
foree@163.com

†These authors have contributed equally to this work and share the first authorship

‡These authors have contributed equally to this work and share the last authorship

Received: 21 January 2021
Accepted: 26 February 2021
Published: 18 March 2021

Citation:
Xu J, Xiao C, Song W, Cui X, Pan M, Wang Q, Feng Y and Xu Y (2021) Elevated Heme Oxygenase-1 Correlates With Increased Brain Iron Deposition Measured by Quantitative Susceptibility Mapping and Decreased Hemoglobin in Patients With Parkinson's Disease. Front. Aging Neurosci. 13:656626. doi: 10.3389/fnagi.2021.656626

Background: Brain iron deposition, low hemoglobin (HGB), and increased heme oxygenase-1 (HO-1) have been implicated in Parkinson's disease (PD). However, the association among them in PD is poorly studied.

Objective: To explore the association of the level of HO-1 with brain iron deposition and low level of HGB in PD.

Methods: A total of 32 patients with PD and 26 controls were recruited for this study. C57BL/6 male mice were used in generating 1-methyl-4-phenyl-1,2,3,6-tetrahydropyridine (MPTP)-induced chronic PD model. The Levels of serum HO-1 and HGB of human subjects and mice were assayed by ELISA, blood routine test, respectively. Quantitative susceptibility mapping (QSM) was used to quantitatively analyze brain iron deposition in human subjects and mice. HO-1 inhibitor (Sn-protoporphyrin, SnPP) was used to suppress the function and expression of HO-1 in PD mice. Correlations between the concentration of serum HO-1 and iron deposition of the region of interests (ROIs), levels of HGB, between the three factors mentioned above, and scores of clinical scales were explored in PD patients.

Results: This study revealed significant elevation of the serum HO-1 concentration, iron deposition within bilateral substantial nigra (SN), red nucleus (RN), and putamen (PUT) and decrease of HGB level in PD patients. There was a significantly positive correlation between the serum HO-1 concentration and iron deposition within SN, an inverse correlation between the serum HO-1 concentration and HGB level in PD patients. A significant increase in HO-1 expression of serum and iron deposition in SN was also observed in the PD mouse model, and the SnPP could significantly reduce iron deposition in the SN.

Conclusions: The high level of HO-1 may be the common mechanism of iron deposition and low HGB in PD. Therefore, the findings presented in this study indicate that HO-1 correlates with brain iron deposition and anemia in PD.

Keywords: Parkinson's disease, heme oxygenase-1, brain iron deposition, low hemoglobin, quantitative susceptibility mapping

INTRODUCTION

Post-mortem and *in vivo* studies have demonstrated that high iron content is a prominent pathophysiological feature of PD (Dexter et al., 1987; Berg and Hochstrasser, 2006; Jin et al., 2011). Excessive iron induces cell death by altering the state between ferrous and ferric forms (Barnham et al., 2004). A series of studies have demonstrated the impact of iron deposition on the pathological aggregation of alpha synuclein (Ostrerova-Golts et al., 2000; Li et al., 2010; He et al., 2015). Although iron deposition is an important pathological hallmark of PD and promotes its pathological progress, the root cause of brain iron deposition is still unclear (He et al., 2015). Many theoretical hypotheses have been used to explain iron deposition in the nigrostriatal system, including an increase of iron intake, change of iron transporter, and increased permeability of the blood-brain barrier (Ward et al., 2014). Presently, no theory explains total iron deposition, thus the need for in-depth studies.

The change of HGB in patients with PD has been attracting the attention of researchers. Several studies revealed that patients with lower HGB were more susceptible to PD (Savica et al., 2009). Our previous study (Deng et al., 2017) showed that, compared with non PD patients, the HGB in PD patients decreased significantly, to the level of anemia, though a small sample-size study exhibited that the levels of HGB did not change in PD patients (Madenci et al., 2012). It is generally believed that HGB decreases significantly in PD patients during the whole period of the disease. However, the root cause of decreased HGB as well as the underlying relationship between PD and decreased HGB is not clear.

To date, most studies have revealed decreased HGB and iron deposition, but how they interact with each other in PD is still unknown. Considering that iron in the human body mainly exists in HGB, it is speculated that there is an internal correlation between iron deposition and reduction of HGB.

Heme oxygenase 1 (HO-1) is an enzyme that catalyzes the degradation of heme into biliverdin or bilirubin, ferrous iron, and carbon monoxide. The expression of HO-1 is maintained at a low level and is restricted to some scattered neurons and glia in the central nervous system (Barañano and Snyder, 2001). However, after exposure to oxidative challenge, the expression of HO-1 protein significantly increases. Recently, some studies revealed increased HO-1 in astrocytes, dopaminergic neurons in the substantia nigra and in the serum of PD patients (Schipper, 2004; Mateo et al., 2010). The increased levels of HO-1 in PD might reflect an activated antioxidant reaction induced by chronic oxidative stress state in PD patients.

Considering the close association between HO-1 and heme catabolism as well as iron metabolism, it was hereby hypothesized that over-expression of HO-1 may influence brain iron deposition and HGB levels in patients with PD. To the best of our knowledge, the association between the level of HO-1, brain iron deposition, and lower HGB level in patients with PD has not been reported. It is against this background that, this study was conducted.

The imaging method for investigating brain iron deposition has been applied extensively. Particularly, the application of QSM in the detection of iron deposition in PD patients has already been reported in recent studies (He et al., 2015; Wei et al., 2019) due to its capacity for distinguishing iron-rich structures from the surrounding background (Li et al., 2011; Xuan et al., 2017). Currently, QSM has become an increasingly useful diagnostic tool for diseases associated with iron deposition (Eskreis-Winkler et al., 2017).

This study utilized QSM to determine iron deposition in various brain regions of patients with PD as well as in age- and gender-matched control subjects, and in the MPTP-induced PD mice model. This study aims to explore whether increased HO-1 levels are correlated with iron deposits in selected brain regions and lower HGB levels in PD. Investigating this relationship would explain the pathogenesis of iron deposition and lower HGB in PD and provide potential therapeutic targets and diagnostic markers.

MATERIALS AND METHODS

Patients and Ethics Statement

This study was approved by the Ethics Committee of Nanfang Hospital. All subjects provided written informed consent before the start of the study. Thirty-two PD patients were enrolled from the Nanfang Hospital of Southern Medical University and Guangdong 999 Brain Hospital. PD diagnosis was conducted by at least two experienced neurologists according to the MDS clinical diagnostic criteria for PD (Postuma et al., 2015). Additionally, a total of 26 controls were recruited by at least two experienced neurologists who were blinded to the research objectives. Most of the patients in this group exhibited minor neurological deficits, such as mild headache, dizziness, etc. Both the PD patients and control groups (CG) were from Han ethnicity. All controls did not have extrapyramidal symptoms, brain trauma, hypothyroidism, psychiatric disease, anosmia, constipation, insomnia, and cognitive decline. Patients and controls who were malnourished, or had eating disorders, diagnosed with gastrointestinal disease or thalassemia, were not enrolled in this study.

Human Nervous System Assessment and Neuropsychological Testing

The severity of PD was assessed by the MDS-Unified PD Rating Scale and the Hoehn & Yahr Scale (Goetz et al., 2008) while cognitive level was assessed by CMMSE (Cui et al., 2011). Also, Hamilton Depression Scale (HAMD scale) and Hamilton Anxiety Scale (HAMA scale) were used to assess the mental state of the participants; PD Sleep Scale was used to assess sleep quantity and non-motor symptom scale (NMSS) was used to assess some non-symptoms, such as hyposmia and constipation. The scale was evaluated by a trained and experienced specialist who was also blinded to the research objectives. The onset of PD was recorded as the first time when a patient experienced typical motor symptoms such as bradykinesia, resting tremor, and rigidity.

Mouse Model

All experiments were approved by the Institutional Animal Care and Use Committee of Nanfang Hospital, Southern Medical University, and performed following the National Institutes of Health Guide for the Care and Use of Laboratory Animals. MPTP-HCl (Sigma, Italy) was dissolved in saline; 3-month-old male C57BL/6J mice (Laboratory Animal Center of Nanfang Hospital, China) were divided into four groups (n = 5 for each group). The control group received saline as a vehicle. MPTP (20 mg/kg i.p.) was injected twice a week for 5 weeks in the MPTP group (Jackson-Lewis and Przedborski, 2007), SnPP group received SnPP (40 μmol/kg/times) twice a week for 5 weeks and MPTP plus SnPP group received SnPP (40 μmol/kg/times) twice a week for 5 weeks an hour before MPTP injection. Twenty-four hours after the last MPTP injection, QSM examination and tissue sampling were performed.

Preparation and Preservation of Blood Samples

Whole blood and blood for serum preparation were collected from PD patients after 8 h of fasting via median cubital vein and mice by cardiac puncture. The samples were then put into EDTA-coated tubes and drying tubes, respectively. For serum preparation, blood was clotted in drying tubes for 2 h at room temperature and centrifuged at 1,500 g at 4°C for 10 min and the serum was carefully collected for analysis of HO-1.

HGB Testing

To observe the changes of HGB in PD patients and PD mice models, A KX21 automatic blood cell analyzer (Sysmex, Japan) and an Abaxis VetScan HM5 hematology analyzer (Abaxis, Union City, CA, USA) were used for routine blood tests from patients and mice, respectively.

Enzyme-Linked Immunosorbent Assay (ELISA)

HO-1 Sandwich ELISA kits (ab207621, Massachusetts, USA and LS-F4086, LSBio, USA) were used to measure the level of HO-1 in serum obtained from the PD patients and mice, respectively according to the manufacturer's instructions.

QSM Image Acquisition for PD Patients

A total of 24 patients and 20 age-and gender-matched controls were subjected to QSM test via clinical 3T MR imaging system (MK750, GE Healthcare, Milwaukee, WI), and data were acquired. Imaging parameters were as follows: TE/TR = 21 ms/15 ms; matrix size = 183 × 156; slice thickness = 2 mm; FOV = 182 × 220 mm^2; slice space = 0.6 mm; and Flip Angle = 10°. Before the reconstruction of QSM, two researchers independently graded the quality of the images and the unqualified images were excluded.

Image Acquisition for PD Model

For animal research, five mice in each group with qualified QSM images were included for analysis of iron deposition in the brain. The specimens were scanned on a 7 Tesla system with a Bruker console (Bruker Biospin, PharmaScan70/16, US). To obtain magnetic susceptibility maps, the specimens were scanned with a multi-echo 3D gradient-echo sequence (eight echo) under the following imaging parameters: TE1/△TE/TR = 5.37 ms/8.07 ms/250 ms, flip angle 35°.

QSM Image Reconstruction

QSM was processed using the STI Suite software (Duke University) after phase images in DICOM format were retrieved from the MRI scanner, as previously described (Kressler et al., 2010; Argyridis et al., 2014). Briefly, the phase images were unwrapped using a Laplacian-based phase unwrapping technique that relied on the sine and cosine functions of the phase angle (Li et al., 2011). The background phase was effectively removed using the harmonic artifact reduction for phase data with varying kernel sizes (VS.HARP; Li et al., 2011). The streaking artifact reduction for QSM (STAR-QSM; Kressler et al., 2010) was then used to improve the accuracy of magnetic susceptibility at the tissue edge. After the tissue field was inverted from field to source, the QSM images were finally obtained.

Statistical Analyses

All continuous variables (the HO-1, HGB concentrations, the age, and clinical scale) were expressed as the means ± standard deviations while categorical variables were expressed as frequencies and percentages. The data for serum HO-1, HGB, and the QSM values of the ROIs were symmetrically distributed, and group mean values were compared using the independent-samples T-test or one-way ANOVA if the data had no variance(see the "Results" section for further details). A partial correlation coefficient was determined using age as a covariate to evaluate the relationship between the concentration of serum HO-1, levels of HGB, and the QSM values of the ROIs. Spearman correlation coefficient was determined to evaluate the relationships between the three factors mentioned above and scores of clinical scales, as the scores of clinical scales were abnormal distribution. A p-value of less than 0.05 was considered to be statistically significant. All data were analyzed using the standard statistical package SPSS v. 22.0

(IBM, Chicago, IL, USA), and graphical representations were made using GraphPad Prism v. 7 (GraphPad Software, Inc. La Jolla, CA, USA).

RESULTS

Demographic and Clinical Characteristic

All recorded demographic and clinical characteristics of the subjects are presented in **Table 1** and there were no significant differences in patient's ages. All controls did not show typical non-motor symptoms for PD patients. Twenty-four PD cases and 20 controls with qualified QSM images were included for analysis of brain iron deposition (**Table 1**).

Comparison of Concentrations of Serum HO-1, ppm Value of QSM, and Level of HGB in PD Cases and Controls

The mean levels of serum HO-1 were higher in the PD group than in the control group ($p < 0.01$). The PD group exhibited significant elevation in the mean QSM value of bilateral substantia nigra ($p < 0.01$), red nucleus (RN; $p < 0.01$), and putamen ($p < 0.01$) as compared to the control group. There was no significant difference in the mean QSM value of a bilateral head of caudate nucleus (CN), globus pallidus (GP) between the PD and the control groups, although the value for the former was higher than the latter. The mean levels of HGB were significantly lower in the PD group than in the controls ($p = 0.027$), even after controlling the confusing effect of gender ($p = 0.044$; **Figure 1**, **Table 2**).

Correlation Between Serum HO-1 Levels and QSM Value, Level of HGB in Patients With PD

To explore the specific relationships between the elevation in serum HO-1 levels and increased QSM value as well as lower HGB of PD patients, a correlational analysis was conducted. The results revealed a statistically positive correlation between serum HO-1 levels and mean QSM values of bilateral substantial nigra ($r = 0.429$, $p = 0.041$), whereas there was no significant correlation between serum HO-1 levels and mean QSM values of other ROIs. The results also showed a significant, inverse correlation between serum HO-1 levels and mean levels of HGB in PD patients ($r = -0.607$, $p = 0.002$; **Figures 2A,B**). All *p*-values were adjusted for age.

TABLE 1 | Demographics of patients with Parkinson's disease (PD) and control group (CG).

	PD	CG	*p*
N	32	26	
M/F, *n*	11/21	12/14	0.362[a]
Age, years	60.97 ± 1.48	56.19 ± 2.34	0.092[b]
Duration, years	4.60 ± 1.10	/	/
Hoehn-Yahr stages	2.46 ± 0.26	/	/
UPDRS-III	28.91 ± 4.52	/	/

N, numbers; M, male; F, female; UPDRS-III, Unified Parkinson's Disease Rating Scale III and Data (mean ± SD). [a]Pearson chi-square test. [b]Independent-samples T test.

Correlation Between QSM Values of SN, Levels of HGB, Serum HO-1 Levels, and Scores of Clinical Scales in Patients With PD

To check whether the three factors (HO-1, HGB, and brain iron) correlate with worsening of PD or cognitive deficits, a correlational analysis was performed. The results revealed a statistically positive correlation between mean QSM values of bilateral substantial nigra and scores of UPDRS-III ($r = 0.409$, $p = 0.047$). The results also showed a significant, inverse correlation between levels of HGB and scores of UPDRS-III ($r = -0.361$, $p = 0.042$), H & Y stage ($r = -0.382$, $p = 0.031$). whereas there was no significant correlation between serum HO-1 levels and scores of clinical scales, between mean QSM values of bilateral SN, levels of HGB, and scores of MMSE (**Figures 2C-I**).

Comparison of HO-1, HGB, and Value of QSM in Mice

The results revealed changes in HO-1, HGB, and the value of QSM in MPTP-treated mice. To verify the role of HO-1 in iron deposition and HGB reduction, HO-1 inhibitor (SnPP) was used to alter the function of HO-1. It was found that the MPTP mice exhibited significant elevation in serum HO-1 and mean QSM value of bilateral substantia nigra compared with the control mice. Further, SnPP significantly reduced the mean QSM value of bilateral substantia nigra induced by MPTP, though it could not bring the mean QSM value of bilateral substantia nigra down to the level of control mice. However, there was no difference in HGB and mean QSM value of striatum between the MPTP group and the control group. The results indicate increased HO-1 in the serum and reveal the role of HO-1 in iron deposition in the substantia nigra (**Figure 3**, **Table 3**).

DISCUSSION

The current study suggests that the increase of iron deposition in the nervous system and the decrease of HGB may have common pathological factors. Further analysis showed that the abnormally high expression of HO-1 may be the foundation and bridge of the reported changes.

Studies have shown that iron deposition in the SN has a pivotal role in the necrosis of dopaminergic neurons (Dexter et al., 1987), the aggregation of α-synuclein (Ostrerova-Golts et al., 2000; Barnham et al., 2004), and promotes the progression of the disease. Iron deposition is not only an important pathological marker of Parkinson's disease (PD) but also an important driving factor for its progression. Currently, QSM is widely used in the examination and diagnosis of diseases characterized by iron deposition.

In addition to brain iron deposition, recent studies revealed that patients with anemia were more susceptible to PD. In other words, lower HGB may be a risk factor for PD (Savica et al., 2009). Our primary (Deng et al., 2017) and current results suggested that HGB levels were lower in PD patients

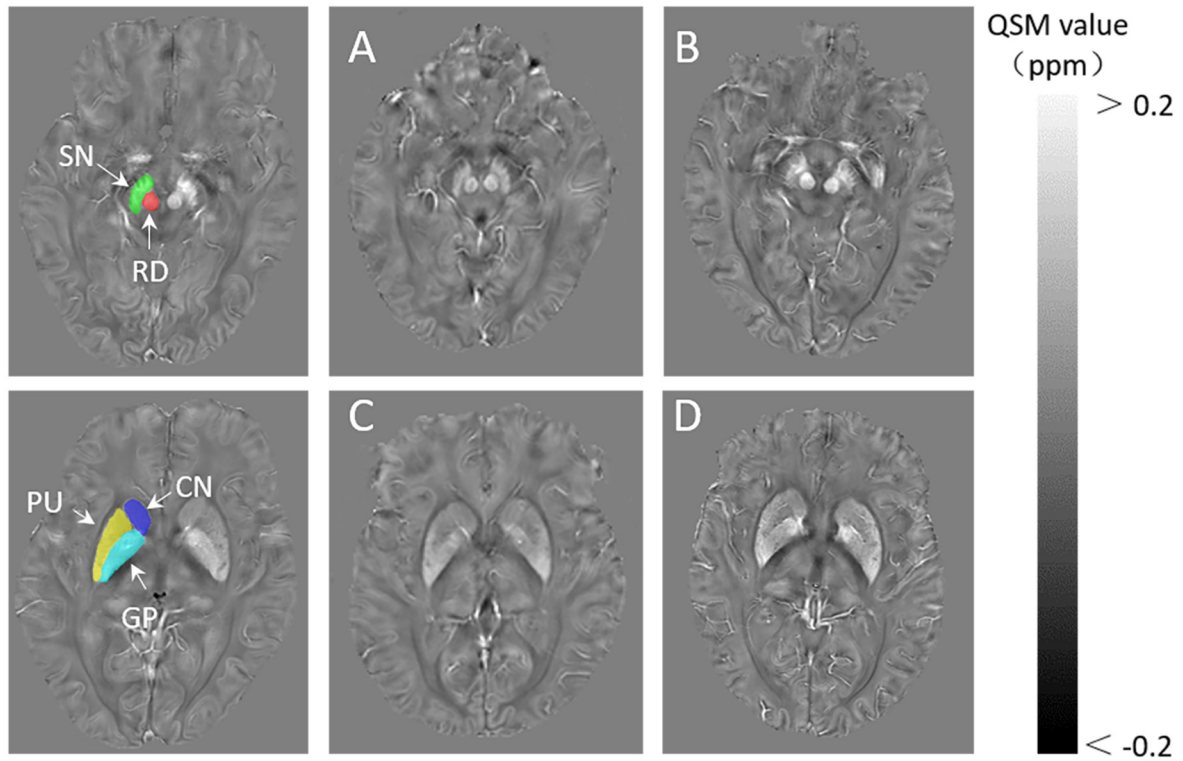

FIGURE 1 | The definition of regions of interest (ROIs).The bilateral substantia nigra (SN), globus pallidus (GP), red nucleus (RN), the head of the caudate nucleus (CN), and putamen (PUT) are included. Representative images of quantitative susceptibility mapping (QSM): a 60-year-old healthy man **(A,C)**, a 65-year-old woman with PD **(B,D)**.

TABLE 2 | Level of heme oxygenase-1 (HO-1), hemoglobin (HGB), and regional QSM values (*10^{-2}) in patients with PD and CG.

	PD	CG	*p*
N	32	26	/
HO-1(pg/ml)	85.685 ± 3.868	45.739 ± 3.686	0.000**
HGB (g/l)	127.500 ± 2.673	135.192 ± 1.827	0.044*
QSM value of ROIs			
SN	8.181 ± 1.548	6.623 ± 1.061	0.000**
RN	7.530 ± 2.003	5.657 ± 1.590	0.002**
CN	2.627 ± 0.848	2.410 ± 0.642	0.351
GP	7.700 ± 1.600	7.002 ± 1.071	0.104
PUT	3.568 ± 1.205	2.524 ± 0.811	0.002**

*QSM, quantitative susceptibility mapping; SN, substantia nigra; RN, red nucleus; CN, the head of caudate nucleus; GP, globus pallidus; PUT, putamen. *PD vs. CG $p < 0.05$; **PD vs. CG $p < 0.01$.*

compared to the controls. Some studies have shown that a decrease in HGB precedes the onset of motor symptoms. Therefore, this phenomenon could not be solely explained by nutritional disorders.

Nevertheless, the specific mechanisms of iron deposition and lower HGB level in PD are unclear. Iron deposition is certainly a complex and comprehensive process, but it must have a major fundamental process and cause. Increased iron uptake or failure of iron export might be contributing factors (He et al., 2015). The current study shows that PD is a disease involving multiple systems, anemia or lower HGB may indicate intrinsic pathological changes of PD. Also, since iron is an important metal ion bound to HGB, there is a need to consider the two pathological features together to establish the mutual underlying mechanism between them.

As an antioxidant, HO-1 has attracted more attention in the research of Parkinson's disease. In addition to the over-expression of HO-1 in the brain of PD patients (Schipper et al., 2019), some previous studies indicated possible overexpression of HO-1 in peripheral blood and saliva of PD patients, compared to the controls (Mateo et al., 2010; Song et al., 2018). Besides, Genetic studies also support the association of HMOX gene variations with the risk of PD, for instance, some HMOX1 gene variants increased the risk of some forms of PD (Ayuso et al., 2014). However, a previous study did not report a significant association between genetic markers in the HO-1 gene with increased susceptibility to PD (Funke et al., 2009). Based on the relevance of HO-1 in iron metabolism, investigations were carried out to determine the relationship between the level of HO-1 with brain iron deposition as well as the lower HGB level of PD patients. Consistent with previous findings (Mateo et al., 2010), the current study showed that serum HO-1 levels are increased in PD patients, compared with controls. More importantly, the elevation of HO-1 level positively correlated with the iron deposition of SN, and inversely with the HGB level in PD patients. The animal model study confirmed that HO-1 inhibitor could significantly reduce the iron deposition in

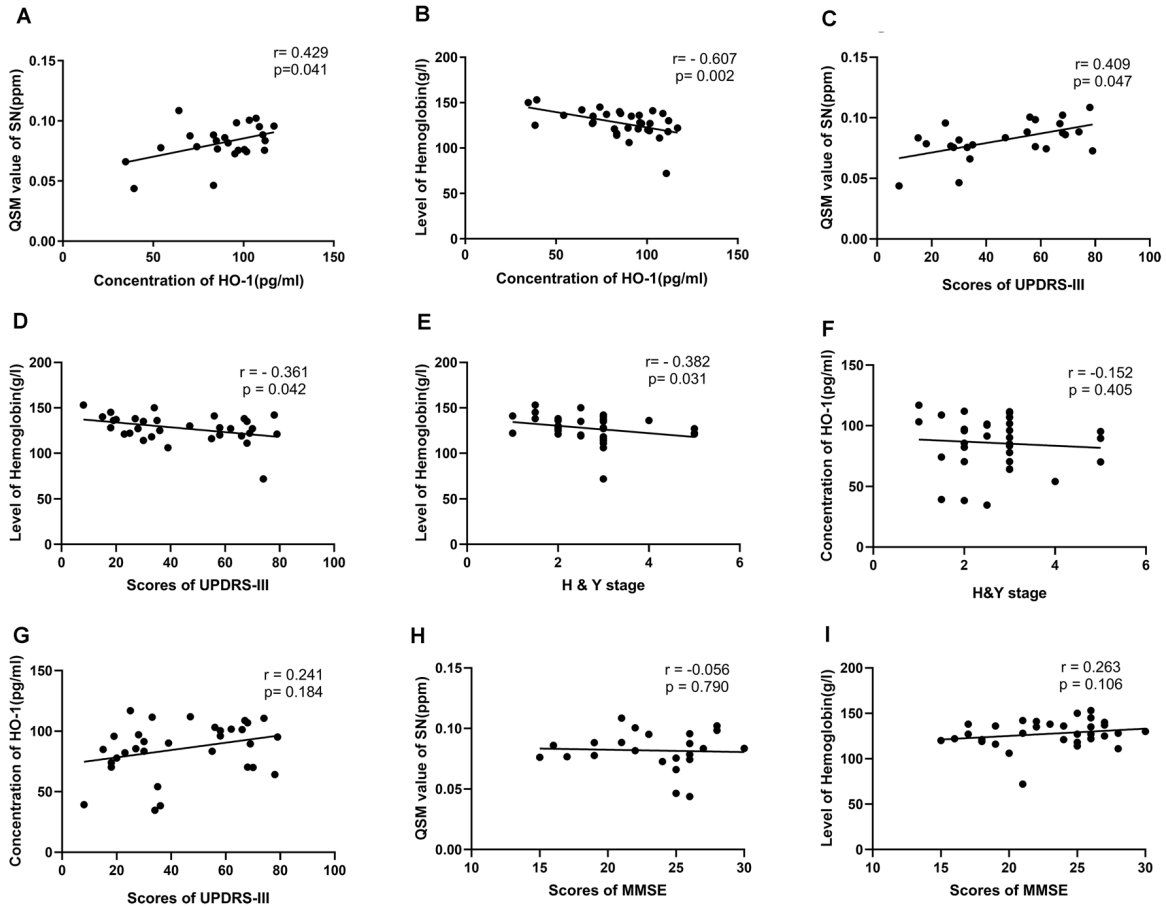

FIGURE 2 | Correlations between the level of heme oxygenase-1 (HO-1) and the QSM values or hemoglobin (HGB), between HO-1 levels, QSM value, level of HGB and scores of clinical scales in PD patients. Levels of HO-1 correlated positively with mean QSM values of bilateral SN, but correlated negatively with levels of HGB **(A,B)**. Mean QSM values of bilateral SN correlated positively with scores of UPDRS-III. Levels of HGB correlated negatively with scores of UPDRS-III and H & Y stage. There were no significant correlations between serum HO-1 levels and scores of clinical scales, between mean QSM values of bilateral SN, levels of HGB and scores of MMSE **(C–I)**.

SN. Therefore, it was suggested that the high expression of HO-1 in SN may be associated with iron deposition. Since the HO-1 is the key enzyme for heme catabolism, while heme is the main structure of HGB, the over-expression of HO-1 in peripheral blood and central nervous system in PD patients may increase the catabolism of heme, thus decrease the concentration of HGB. Though the current study did not test the heme decomposition products, a previous study (Macías-García et al., 2019) has concluded that overexpression of HO-1 could lead to higher peripheral bilirubin levels in PD, a major heme decomposition product. Also, with the catabolism of heme, the iron released from heme may aggravate the iron deposition in the brain. A previous study indicated that inhibition of heme oxygenase could ameliorate anemia and reduce iron overload in a β-thalassemia mouse model (Garcia-Santos et al., 2018).

Interestingly, the elevation of HO-1 positively correlates with the iron deposition of SN, but not in other regions. Some reasons could explain this interesting observation. First, although Parkinson's disease affects multiple nerve sites, dopaminergic neurons that are concentrated in the substantia nigra are still the main lesion. Both nigra neurons and astrocytes of PD brain specimens exhibited intense HO-1 immunostaining (Schipper et al., 1998), which suggested continuous oxidative stress. Over-expression of HO-1 could derange iron homeostasis and aggravate iron deposition in SN. Second, the over-expression of HO-1 and increased iron deposition of SN could be connected to chronic inflammation. Chronic neuroinflammation involves glial activation and peroxidation, and HO-1, as an important antioxidant factor, would play a role in this critical course. A previous study (Urrutia et al., 2014) indicated that a vicious cycle of exacerbated oxidative stress and increased iron accumulation could be promoted by inflammatory processes. On one hand, the gene expression of iron regulatory factors would change and iron deposition would exacerbate under inflammatory conditions (Recalcati et al., 2012). On the other hand, the increased iron deposition could generate secondary inflammatory response (Liu et al., 2017) and oxidative stress.

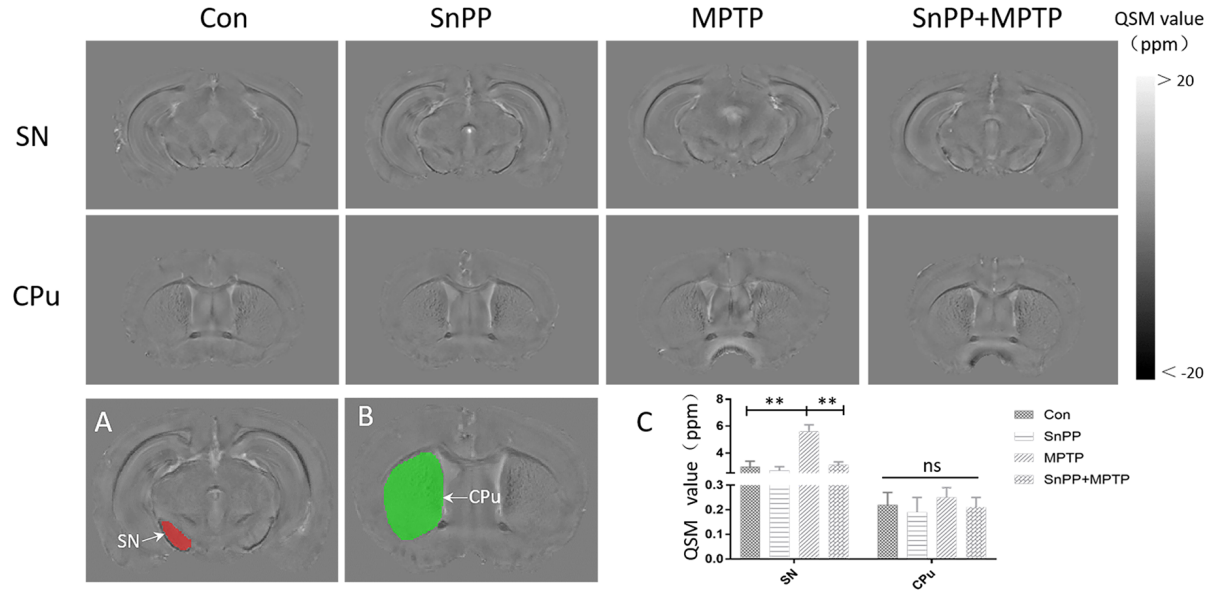

FIGURE 3 | Representative images of QSM in different mice groups and the definition of ROIs.The ROIs included the substantia nigra **(A)** and striatum **(B)**. MPTP increased iron deposition in the SN in mice, while the HO-1 inhibitor (SnPP) inhibited iron deposition in the SN. However, no significant elevation in the QSM values of bilateral striatum was observed in all mice **(C)**. $^{**}p < 0.01$; ns, not statistically significant.

TABLE 3 | The comparison of Level of HO-1, HGB and regional QSM values in different groups of mice.

	Con	SnPP	MPTP	SnPP+MPTP	P_1	P_2
N	5	5	5	5		
HO-1 (pg/ml)	41.15 ± 8.64	36.48 ± 3.25	94.15 ± 6.55	72.06 ± 3.99	<0.001	<0.001
HGB (g/l)	148 ± 7.7	143.8 ± 6.69	139 ± 8.65	141.80 ± 11.8	0.16	0.7
QSM value (ppm)						
SN	2.97 ± 0.14	2.73 ± 0.28	5.58 ± 0.52	3.1 ± 0.24	<0.001	<0.001
CPU	0.21 ± 0.04	0.19 ± 0.06	0.25 ± 0.04	0.23 ± 0.05	0.22	0.51

P-values are presented as follows: p_1: MPTP group vs. Con group; p_2: MPTP group vs. MPTP + SnPP group.

Also, the animal experiments revealed that although the serum HO-1 of PD model mice increased, the HGB did not decrease significantly. Two scenarios were considered as possible explanations for this observation. First, mice could have a great ability of compensation; second, the lesions involved in MPTP-induced PD model were different from PD patients, because PD patients' lesion is more extensive, including gastrointestinal tract/heart/spinal cord and other parts (Hawkes et al., 2007). Therefore, the source of HO-1 in PD patients may be more extensive and stable.

We found that iron deposition and levels of HGB were associated with motor symptoms, whereas there was no correlation between levels of HO-1 and disease severity. We speculate that one possible reason is the dynamic change of level of HO-1, higher in the early stage and lower in the late stage of the disease (Song et al., 2018). With the progression of the disease, the number of nigra neurons is greatly reduced, and the neuroinflammation may gradually weaken. Therefore, the expression of HO-1 would not sustain a high level.

It is noteworthy that this study had some limitations. First, the sample size was relatively small. Future research should be based on a larger sample size to verify the results. Second, a follow-up study was not conducted to evaluate dynamic changes of HO-1 and its association with brain iron deposition and HGB. Third, the gender ratio of this study might induce a bias, even after controlling the confusing effect. Last but not least, heme decomposition products were not analyzed in the current study. This calls for more comprehensive studies in the future. Despite these deficiencies, this study provides the first report on the association between peripheral HO-1 and HGB, brain iron deposition in PD patients.

CONCLUSION

In summary, the current study suggests that brain iron deposition is increased and HGB is significantly reduced in patients with PD, due to over-expression of HO-1.

DATA AVAILABILITY STATEMENT

The raw data supporting the conclusions of this article will be made available by the authors, without undue reservation.

ETHICS STATEMENT

The studies involving human participants were reviewed and approved by Ethics Committee of Nanfang Hospital. The patients/participants provided their written informed consent to participate in this study. The animal study was reviewed and approved by Ethics Committee of Nanfang Hospital.

AUTHOR CONTRIBUTIONS

JX: conceptualization, data curation, formal analysis, methodology, investigation, visualization, and writing—original draft. CX: data curation, formal analysis, methodology, investigation, visualization, and writing—original draft. WS: data curation, formal analysis, and investigation. XC: formal analysis, methodology, and supervision. MP: data curation, formal analysis, and methodology. QW: conceptualization, funding acquisition, and writing—review and editing. YF: methodology, supervision, validation, and writing—review and editing. YX: conceptualization, funding acquisition, methodology, resources, supervision, and writing—review and editing. All authors contributed to the article, read and approved the submitted version.

FUNDING

This work was supported by the Natural Science Foundation of Guangdong Province China (Grant No.: 2018A030313277) and the President Foundation of Nanfang Hospital, Southern Medical University (Grant Nos.: 2017B010 and 2014B008) awarded to YX and QW, respectively.

ACKNOWLEDGMENTS

We would like to thank all the participants in this study.

REFERENCES

Argyridis, I., Li, W., Johnson, G. A., and Liu, C. (2014). Quantitative magnetic susceptibility of the developing mouse brain reveals microstructural changes in the white matter. *NeuroImage* 88, 134–142. doi: 10.1016/j.neuroimage.2013.11.026

Ayuso, P., Martínez, C., Pastor, P., Lorenzo-Betancor, O., Luengo, A., Jiménez-Jiménez, F. J., et al. (2014). An association study between Heme oxygenase-1 genetic variants and Parkinson's disease. *Front. Cell. Neurosci.* 8:298. doi: 10.3389/fncel.2014.00298

Barañano, D. E., and Snyder, S. H. (2001). Neural roles for heme oxygenase: contrasts to nitric oxide synthase. *Proc. Natl. Acad. Sci. U S A* 98, 10996–11002. doi: 10.1073/pnas.191351298

Barnham, K. J., Masters, C. L., and Bush, A. I. (2004). Neurodegenerative diseases and oxidative stress. *Nat. Rev. Drug Discov.* 3, 205–214. doi: 10.1038/nrd1330

Berg, D., and Hochstrasser, H. (2006). Iron metabolism in Parkinsonian syndromes. *Mov. Disord.* 21, 1299–1310. doi: 10.1002/mds.21020

Cui, G.-H., Yao, Y.-H., Xu, R.-F., Tang, H.-D., Jiang, G.-X., Wang, Y., et al. (2011). Cognitive impairment using education-based cutoff points for CMMSE scores in elderly Chinese people of agricultural and rural Shanghai China. *Acta Neurol. Scand.* 124, 361–367. doi: 10.1111/j.1600-0404.2010.01484.x

Deng, Q., Zhou, X., Chen, J., Pan, M., Gao, H., Zhou, J., et al. (2017). Lower hemoglobin levels in patients with parkinson's disease are associated with disease severity and iron metabolism. *Brain Res.* 1655, 145–151. doi: 10.1016/j.brainres.2016.11.007

Dexter, D. T., Wells, F. R., Agid, F., Agid, Y., Lees, A. J., Jenner, P., et al. (1987). Increased nigral iron content in postmortem parkinsonian brain. *Lancet* 2, 1219–1220. doi: 10.1016/s0140-6736(87)91361-4

Eskreis-Winkler, S., Zhang, Y., Zhang, J., Liu, Z., Dimov, A., Gupta, A., et al. (2017). The clinical utility of QSM: disease diagnosis, medical management and surgical planning. *NMR Biomed.* 30:e3668. doi: 10.1002/nbm.3668

Funke, C., Tomiuk, J., Riess, O., Berg, D., and Soehn, A. S. (2009). Genetic analysis of heme oxygenase-1 (HO-1) in German Parkinson's disease patients. *J. Neural Transm.* 116, 853–859. doi: 10.1007/s00702-009-0237-6

Garcia-Santos, D., Hamdi, A., Saxova, Z., Fillebeen, C., Pantopoulos, K., Horvathova, M., et al. (2018). Inhibition of heme oxygenase ameliorates anemia and reduces iron overload in a beta-thalassemia mouse model. *Blood* 131, 236–246. doi: 10.1182/blood-2017-07-798728

Goetz, C. G., Tilley, B. C., Shaftman, S. R., Stebbins, G. T., Fahn, S., Martinez-Martin, P., et al. (2008). Movement disorder society, movement disorder society-sponsored revision of the unified Parkinson's Disease rating scale (MDS-UPDRS): scale presentation and clinimetric testing results. *Mov. Disord.* 23, 2129–2170. doi: 10.1002/mds.22340

Hawkes, C. H., Del Tredici, K., and Braak, H. (2007). Parkinson's disease: a dual-hit hypothesis. *Neuropathol. Appl. Neurobiol.* 33, 599–614. doi: 10.1111/j.1365-2990.2007.00874.x

He, N., Ling, H., Ding, B., Huang, J., Zhang, Y., Zhang, Z., et al. (2015). Region-specific disturbed iron distribution in early idiopathic Parkinson's disease measured by quantitative susceptibility mapping. *Hum. Brain Mapp.* 36, 4407–4420. doi: 10.1002/hbm.22928

Jackson-Lewis, V., and Przedborski, S. (2007). Protocol for the MPTP mouse model of Parkinson's disease. *Nat. Protoc.* 2, 141–151. doi: 10.1038/nprot.2006.342

Jin, L., Wang, J., Zhao, L., Jin, H., Fei, G., Zhang, Y., et al. (2011). Decreased serum ceruloplasmin levels characteristically aggravate nigral iron deposition in Parkinson's disease. *Brain* 134, 50–58. doi: 10.1093/brain/awq319

Kressler, B., de Rochefort, L., Liu, T., Spincemaille, P., Jiang, Q., and Wang, Y. (2010). Nonlinear regularization for per voxel estimation of magnetic susceptibility distributions from MRI field maps. *IEEE Trans. Med. Imaging* 29, 273–281. doi: 10.1109/TMI.2009.2023787

Li, W.-J., Jiang, H., Song, N., and Xie, J.-X. (2010). Dose- and time-dependent alpha-synuclein aggregation induced by ferric iron in SK-N-SH cells. *Neurosci. Bull.* 26, 205–210. doi: 10.1007/s12264-010-1117-7

Li, W., Wu, B., and Liu, C. (2011). Quantitative susceptibility mapping of human brain reflects spatial variation in tissue composition. *NeuroImage* 55, 1645–1656. doi: 10.1016/j.neuroimage.2010.11.088

Liu, Z., Shen, H.-C., Lian, T.-H., Mao, L., Tang, S.-X., Sun, L., et al. (2017). Iron deposition in substantia nigra: abnormal iron metabolism, neuroinflammatory mechanism and clinical relevance. *Sci. Rep.* 7:14973. doi: 10.1038/s41598-017-14721-1

Macías-García, D., Mendéz-Del Barrio, C., Jesús, S., Labrador, M. A., Adarmes-Gãmez, A., Vargas-González, L., et al. (2019). Increased bilirubin levels in Parkinson's disease. *Parkinsonism Relat. Disord.* 63, 213–216. doi: 10.1016/j.parkreldis.2019.01.012

Madenci, G., Bilen, S., Arli, B., Saka, M., and Ak, F. (2012). Serum iron, vitamin B12 and folic acid levels in Parkinson's disease. *Neurochem. Res.* 37, 1436–1441. doi: 10.1007/s11064-012-0729-x

Mateo, I., Infante, J., Sánchez-Juan, P., García-Gorostiaga, I., Rodríguez-Rodríguez, E., Vázquez-Higuera, J. L., et al. (2010). Serum heme oxygenase-1 levels are increased in Parkinson's disease but not in Alzheimer's disease. *Acta Neurol. Scand.* 121, 136–138. doi: 10.1111/j.1600-0404.2009.01261.x

Ostrerova-Golts, N., Petrucelli, L., Hardy, J., Lee, J. M., Farer, M., and Wolozin, B. (2000). The A53T alpha-synuclein mutation increases iron-dependent

aggregation and toxicity. *J. Neurosci.* 20, 6048–6054. doi: 10.1523/JNEUROSCI.20-16-06048.2000

Postuma, R. B., Berg, D., Stern, M., Poewe, W., Olanow, C. W., Oertel, W., et al. (2015). MDS clinical diagnostic criteria for Parkinson's disease. *Mov. Disord.* 30, 1591–1601. doi: 10.1002/mds.26424

Recalcati, S., Locati, M., Gammella, E., Invernizzi, P., and Cairo, G. (2012). Iron levels in polarized macrophages: regulation of immunity and autoimmunity. *Autoimmun. Rev.* 11, 883–889. doi: 10.1016/j.autrev.2012.03.003

Savica, R., Grossardt, B. R., Carlin, J. M., Icen, M., Bower, J. H., Ahlskog, J. E., et al. (2009). Anemia or low hemoglobin levels preceding Parkinson disease: a case-control study. *Neurology* 73, 1381–1387. doi: 10.1212/WNL.0b013e3181bd80c1

Schipper, H. M. (2004). Heme oxygenase expression in human central nervous system disorders. *Free Radic. Biol. Med.* 37, 1995–2011. doi: 10.1016/j.freeradbiomed.2004.09.015

Schipper, H. M., Liberman, A., and Stopa, E. G. (1998). Neural heme oxygenase-1 expression in idiopathic Parkinson's disease. *Exp. Neurol.* 150, 60–68. doi: 10.1006/exnr.1997.6752

Schipper, H. M., Song, W., Tavitian, A., and Cressatti, M. (2019). The sinister face of heme oxygenase-1 in brain aging and disease. *Prog. Neurobiol.* 172, 40–70. doi: 10.1016/j.pneurobio.2018.06.008

Song, W., Kothari, V., Velly, A. M., Cressatti, M., Liberman, A., Gornitsky, M., et al. (2018). Evaluation of salivary heme oxygenase-1 as a potential biomarker of early Parkinson's disease. *Mov. Disord.* 33, 583–591. doi: 10.1002/mds.27328

Urrutia, P. J., Mena, N. P., and Núñez, M. T. (2014). The interplay between iron accumulation, mitochondrial dysfunction and inflammation during the execution step of neurodegenerative disorders. *Front. Pharmacol.* 5:38. doi: 10.3389/fphar.2014.00038

Ward, R. J., Zucca, F. A., Duyn, J. H., Crichton, R. R., and Zecca, L. (2014). The role of iron in brain ageing and neurodegenerative disorders. *Lancet Neurol.* 13, 1045–1060. doi: 10.1016/S1474-4422(14)70117-6

Wei, H., Zhang, C., Wang, T., He, N., Li, D., Zhang, Y., et al. (2019). Precise targeting of the globus pallidus internus with quantitative susceptibility mapping for deep brain stimulation surgery. *J. Neurosurg.* 133, 1605–1611. doi: 10.3171/2019.7.JNS191254

Xuan, M., Guan, X., Gu, Q., Shen, Z., Yu, X., Qiu, T., et al. (2017). Different iron deposition patterns in early- and middle-late-onset Parkinson's disease. *Parkinsonism Relat. Disord.* 44, 23–27. doi: 10.1016/j.parkreldis.2017.08.013

Conflict of Interest: The authors declare that the research was conducted in the absence of any commercial or financial relationships that could be construed as a potential conflict of interest.

frontiers in Aging Neuroscience

ORIGINAL RESEARCH
published: 26 April 2021
doi: 10.3389/fnagi.2021.665612

Association Between sTREM2, an Immune Biomarker of Microglial Activation, and Aging-Related Brain Volume Changes in Community-Dwelling Older Adults: A 7-Year Follow-Up Study

Ryuzo Orihashi[1], Yoshito Mizoguchi[1], Yoshiomi Imamura[1], Shigeto Yamada[2] and Akira Monji[1]*

[1] Department of Psychiatry, Faculty of Medicine, Saga University, Saga, Japan, [2] St. Lucia's Hospital, Kurume, Japan

Background: This study aimed to investigate the association between serum levels of soluble triggering receptor expressed on myeloid cells 2 (sTREM2), a soluble form of an innate immune receptor expressed on the microglia, and brain volume in older adults.

Methods: The survey was conducted twice in Kurokawa-cho, Imari, Saga Prefecture, Japan, among people aged 65 years and older. We collected data from 596 residents. Serum sTREM2 level measurements, brain MRI, Mini-Mental State Examination (MMSE), and clinical dementia rating (CDR) were performed at Time 1 (2009–2011). Follow-up brain MRI, MMSE, and CDR were performed at Time 2 (2016–2017). The interval between Time 1 and Time 2 was approximately 7 years. Sixty-nine participants (16 men, mean age 72.69 ± 3.18 years; 53 women, mean age 72.68 ± 4.64 years) completed this study. We analyzed the correlation between serum sTREM2 levels (Time 1) and brain volume (Time 1, Time 2, and Time 1–Time 2 difference) using voxel-based morphometry implemented with Statistical Parametric Mapping.

Results: Participants in this study had lower MMSE and higher CDR scores 7 years after the baseline evaluation. However, analyses at the cluster level by applying multiple comparison corrections (family wise error; $P < 0.05$) showed no correlation between serum sTREM2 levels and volume of different brain regions, either cross-sectional or longitudinal.

Conclusion: Serum sTREM2 level could not serve as an immune biomarker of aging-related volume changes in brain regions closely related to cognitive function in older adults aged 65 years and above.

Keywords: sTREM2, brain volume, cognitive function, MRI, voxel-based morphometry

OPEN ACCESS

Edited by:
Thomas K. Karikari, University of Gothenburg, Sweden

Reviewed by:
Marc Suárez-Calvet, BarcelonaBeta Brain Research Center, Spain
Yuka Martens, Mayo Clinic Florida, United States
Shigeki Hirano, Chiba University, Japan

****Correspondence:***
Yoshito Mizoguchi
ymizo@cc.saga-u.ac.jp

Received: *08 February 2021*
Accepted: *30 March 2021*
Published: *26 April 2021*

Citation:
Orihashi R, Mizoguchi Y, Imamura Y, Yamada S and Monji A (2021) Association Between sTREM2, an Immune Biomarker of Microglial Activation, and Aging-Related Brain Volume Changes in Community-Dwelling Older Adults: A 7-Year Follow-Up Study. Front. Aging Neurosci. 13:665612. doi: 10.3389/fnagi.2021.665612

Abbreviations: AD, Alzheimer's disease; BMI, body mass index; CDR, clinical dementia rating; CSF, cerebrospinal fluid; DARTEL, diffeomorphic anatomical registration through exponentiated lie algebra; FWE, family wise error; FWHM, full width at half maximum; hs-CRP, high-sensitivity C-reactive protein; MMSE, Mini-Mental State Examination; MNI, Montreal Neurological Institute; SPM, Statistical Parametric Mapping; TREM2, triggering receptor expressed on myeloid cells 2; VBM, voxel-based morphometry.

INTRODUCTION

Dementia, including Alzheimer's disease (AD), is a major public health problem globally. Identifying biomarkers that could predict dementia at an early stage will be extremely beneficial. AD pathogenesis is associated with neuroinflammation mainly induced by the activation of microglia in the brain (Haraguchi et al., 2017; Podleśny-Drabiniok et al., 2020). Triggering receptor expressed on myeloid cells 2 (TREM2), a surface receptor of microglial cells, has important roles in microglial functions including phagocytosis and modulation of neuroinflammation (Ulrich and Holtzman, 2016). TREM2 has also been identified as one of the most potent genetic risk factors for AD (Ulrich et al., 2017). TREM2 is released into the extracellular space as a soluble form (sTREM2) and can be detected in the cerebrospinal fluid (CSF) and peripheral blood (Wunderlich et al., 2013; Kleinberger et al., 2014). Several studies reported an association between sTREM2 levels in the CSF or peripheral blood and AD (Hu et al., 2014; Henjum et al., 2016; Heslegrave et al., 2016; Piccio et al., 2016; Suárez-Calvet et al., 2016; Liu et al., 2018). However, to the best of our knowledge, not many studies have analyzed the association between sTREM2 level in peripheral blood and brain volume (Tan et al., 2017). If the association between sTREM2 level in peripheral blood and brain volume is clarified, it will strengthen the evidence that sTREM2 is a biomarker involved in the onset and progression of AD. This study aimed to evaluate serum sTREM2 levels in older adults living in a rural community and examine its relationship with brain volume using MRI. To address this, we designed a prospective cohort study in which healthy older adults without dementia were examined longitudinally for 7 years.

MATERIALS AND METHODS

Participant Characteristics

This was a longitudinal study conducted in Kurokawa-cho, Imari, Saga Prefecture, Japan, among people aged 65 years and above, as reported previously (Nabeta et al., 2014; Matsushima et al., 2015; Imamura et al., 2017; Orihashi et al., 2020). Kurokawa-cho is in northwestern Saga Prefecture and is a rural town somewhat cut-off from urban areas. The area of the town is 26.48 km^2. As of 2010, the population of Kurokawa-cho was 3253, with 932 people aged 65 years and older (28.7%). The town had 1134 households, and the average number of people per household was 2.87. The main industries are shipbuilding and primary industries.

In this study, we collected data from 596 older adults living in the community. These 596 participants comprised 63.9% of the population of Kurokawa-cho over 65 years of age. This survey was conducted twice. First, from October 2009 to March 2011, we conducted a baseline survey that we termed "Time 1." Second, we conducted from November 2016 to September 2017 (Time 2). Because most of the survey during Time 1 was conducted as a part of the national survey to obtain data to calculate the prevalence of dementia in Japan (Ikejima et al., 2012), not all participants underwent examinations during this period. Specifically, we and Ikejima et al. used the Diagnostic and Statistical Manual of Mental Disorders, third edition-revised, for the diagnosis of dementia with reference to MRI findings. MRI examinations were optional and executed in cases for which it was necessary for further assessment of dementia or the participants themselves requested it. Three hundred thirty-two participants underwent MRI examination and ten were diagnosed with dementia at Time 1. Seven years after conducting the first survey (Time 1), we had notified the investigation of Time 2 to all participants in Time 1 survey. However, only 71 participants (of Time 1) agreed to participate in the investigation of Time 2. Of the 71 participants, none were diagnosed with dementia at Time 1. Thus, 261 participants dropped out arbitrarily between Time 1 and Time 2 (**Figure 1**).

To select participants for analysis, we excluded two participants with no MRI samples or serum sTREM2 levels higher than three standard deviations from 71 participants. Consequently, we obtained sixty-nine participants (16 men, mean age 72.69 $\pm$ 3.18 years; 53 women, mean age 72.68 $\pm$ 4.64 years, at Time 1) for analysis.

This study was approved by the Ethics Committee of the Faculty of Medicine, Saga University, and all participants agreed to participate in the study according to the Declaration of Helsinki.

Cognitive Function Assessment

The Mini-Mental State Examination (MMSE) is a simple screening index that provides an estimate of cognitive function (Folstein et al., 1975). The clinical dementia rating (CDR) is used for dementia evaluation and severity staging (Hughes et al., 1982; Morris, 1993). All participants underwent MMSE and CDR for cognitive function assessment at Time 1 and Time 2.

Serum Samples

Blood samples for serum sTREM2 levels analysis were collected from participants either between 9:00 and 12:00 (AM) or between 12:00 and 15:00 (PM) during Time 1. On the same day, at Saga University, the samples were centrifuged and the serum was extracted and transferred to a container. The serum samples were immediately stored at −80°C.

Evaluation of Serum sTREM2 Levels and Other Risk Factors

Serum was thawed at room temperature. All samples were analyzed in duplicate. Serum sTREM2 levels were analyzed using a commercially available human TREM2 ELISA kit (RayBiotech, Norcross, GA, United States) according to the manufacturer's instructions (Tanaka et al., 2018, 2019; Ohara et al., 2019). The intra-assay coefficient of variation was 10% and the inter-assay coefficient of variation was 12%. The baseline survey also included metabolic status such as body mass index (BMI) and history of diabetes and dyslipidemia. Serum high-sensitivity C-reactive protein (hs-CRP) was analyzed using commercially available ELISA kits (R&D systems, Minneapolis, MN, United States) according to the manufacturer's instructions. The intra-assay coefficient of variation was 5.5% and the inter-assay coefficient of variation was 6.53%.

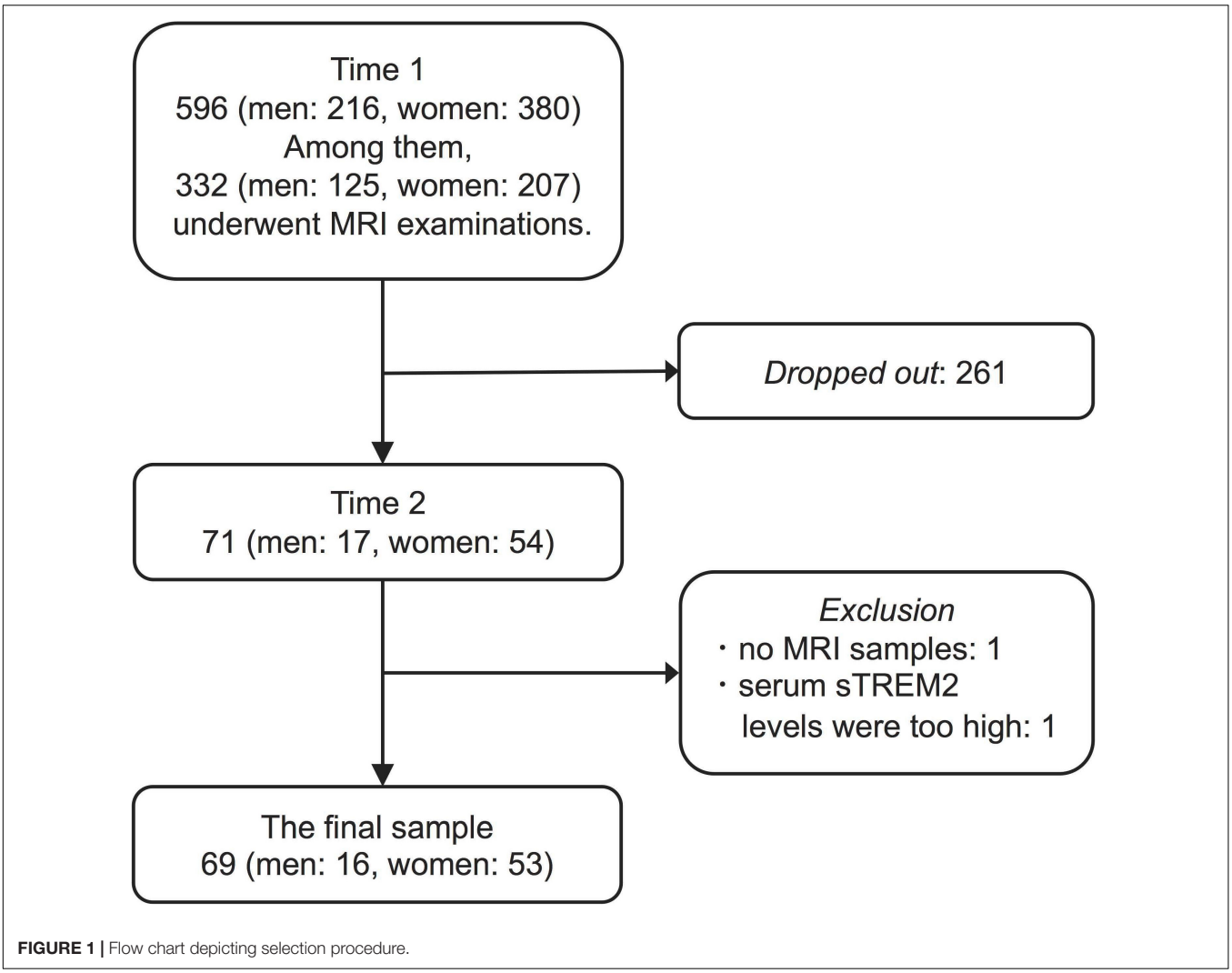

FIGURE 1 | Flow chart depicting selection procedure.

MRI Acquisition

MRI examinations were performed using a 1.5 Tesla device (Excelart Vantage AGV; Canon Medical Systems, Otawara, Japan). Three-dimensional T1-weighted structural images were acquired for each participant using a field echo three-dimensional (FE3D) method (TR, 21 ms; TE, 5.5 ms; flip angle, 20°; field of view, 240 × 240 mm; matrix, 256 × 256; slice thickness, 1.5 mm; number of slices, 124). The examination conditions were kept same for all participants and followed a standardized procedure.

Statistical Analysis

Participants' basic data were analyzed and compared using a commercially available statistical package (JMP 14.2.0; SAS Institute, Cary, NC, United States). The mean values were compared using Welch's *t*-test. Fisher's exact test was used to compare the prevalence of diabetes and dyslipidemia, and blood collection time. Multiple regression analysis was used to determine the effect of age, sex, hs-CRP, metabolic status, and blood collection time on serum sTREM2 levels. The Wilcoxon signed-rank test was used to compare MMSE and CDR scores at Time 1 and Time 2. Additionally, the serum sTREM2 levels were divided into quartile categories. We used linear mixed-effects models to estimate changes of averaged total brain volumes (gray matter volume and white matter volume) and averaged MMSE scores between Time 1 and Time 2 in each quartile category. Statistical significance was set at $P < 0.05$.

Preprocessing of the Brain MRI and Longitudinal Voxel-Based Morphometry Analysis

Brain MRI processing and analysis were conducted using voxel-based morphometry (VBM) (Ashburner and Friston, 2000) implemented with Statistical Parametric Mapping (SPM12; Wellcome Department of Cognitive Neurology, London, United Kingdom) in MATLAB R2016a (MathWorks, Natick, MA, United States). We used the same methodology described in a previous study (Orihashi et al., 2020).

T1-weighted MR images were first segmented for gray matter and white matter using the segmentation procedures implemented in SPM12. The diffeomorphic anatomical

registration through exponentiated lie algebra (DARTEL) tool described in SPM12 was used on the segmented gray matter and white matter images to construct a template for co-registration across participants (Ashburner and Friston, 2000; Ashburner, 2007). The segmented gray matter and white matter images were co-registered to the final DARTEL template and local volumes were preserved by modulating the image intensity of each voxel by the Jacobian determinants of the deformation fields computed by DARTEL. The registered images were smoothed with a Gaussian kernel with full width at half maximum (FWHM) of 8 mm and transformed into Montreal Neurological Institute (MNI) stereotactic space using affine and non-linear spatial normalization as implemented in SPM12. Preprocessing was conducted by Araya Brain Imaging (Tokyo, Japan).

Gray matter images were used for this analysis. After preparing the Time 1 and Time 2 images, the Time 1–Time 2 difference images were created by subtracting the Time 2 images from the Time 1 images (Ashburner and Ridgway, 2012). Correlation between serum sTREM2 levels at baseline (Time 1) and brain volume (Time 1, Time 2, and Time 1–Time 2 difference) was evaluated using gray matter images and multiple regression design. Men and women were analyzed together, with age, sex, handedness, and hs-CRP levels as covariates. Moreover, total brain volume at Time 1 and Time 2 was used as covariates during the respective time points. The masking toolbox was used to create mask images for analysis, and multiple comparison correction (family wise error) was performed. The initial voxel threshold was set to $P = 0.001$ uncorrected. Clusters were considered significant when they fell below the cluster-corrected P (family wise error) value (=0.05). Thus, analyses at the cluster level were performed to identify significant brain regions. After statistically significant brain regions were determined, the anatomical labels were identified using the automated anatomical labeling corresponding to the space of the MNI standard coordinate system (Tzourio-Mazoyer et al., 2002). Furthermore, using a similar method, analyses were performed on the association between MMSE or CDR scores (Time 1–Time 2 difference) and brain volume (Time 1, Time 2, and Time 1–Time 2 difference).

RESULTS

Participant Characteristics, Serum sTREM2 Levels, and MMSE and CDR Scores

There was no significant difference in serum sTREM2 levels between men (344.3 ± 305.4 pg/ml) and women (288.7 ± 277.0 pg/ml) at baseline. Further, the average interval between Time 1 and Time 2 brain MRI examinations was same in men and women. Moreover, no sex differences were observed in the prevalence of other risk factors and blood collection time (**Table 1**). Multiple regression analysis was performed to assess the association between serum sTREM2 levels and age, sex, hs-CRP, metabolic status, and blood collection time. Result showed that a history of diabetes may be one of the factors affecting serum sTREM2 levels ($P = 0.03$, standard partial regression coefficient = 0.279). Overall, participants' MMSE scores declined and CDR scores increased from Time 1 to Time 2 (**Table 2**). Moreover, serum sTREM2 levels did not correlate with changes (i.e., difference between Time 1 and Time 2) in either MMSE ($P = 0.38$) or CDR ($P = 0.47$) scores.

Voxel-Based Morphometry Findings

We analyzed the correlation between serum sTREM2 levels (Time 1) and brain volume (Time 1, Time 2, and Time 1–Time 2 difference). However, analyses at the cluster level by applying multiple comparison corrections (family wise error; significance level, $P < 0.05$) showed no correlation between serum sTREM2 levels and volume of different brain regions. Therefore, an uncorrected analysis at the peak level was performed (significance

TABLE 1 | Participant demographics.

	Overall	Men	Women	Statistical significance
N	69	16	53	
Age (years, Time 1), mean ± SD	72.68 ± 4.32	72.69 ± 3.18	72.68 ± 4.64	ns[a]
sTREM2 (pg/ml, Time 1), mean ± SD	301.6 ± 282.5	344.3 ± 305.4	288.7 ± 277.0	ns[a]
hs-CRP (ng/ml, Time 1), mean ± SD	1199.7 ± 1403.0	1014.3 ± 933.4	1255.7 ± 1519.5	ns[a]
Education (years), mean ± SD	9.90 ± 1.70	10.81 ± 2.10	9.62 ± 1.48	$P = 0.048$[a]
MRI interval (years, Time 1 to Time 2), mean ± SD	6.87 ± 0.63	6.86 ± 0.64	6.88 ± 0.63	ns[a]
BMI (kg/m^2), mean ± SD	23.90 ± 3.24	23.98 ± 2.73	23.87 ± 3.40	ns[a]
Diabetes, *n* (%)	14 (20.6)	3 (18.8)	11 (21.2)	ns[b]
Dyslipidemia, *n* (%)	26 (38.2)	3 (18.8)	23 (44.2)	ns[b]
Blood collection time, *n* (%)				
AM	35 (50.7)	6 (37.5)	29 (54.7)	ns[b]
PM	34 (49.3)	10 (62.5)	24 (45.3)	

Missing data: BMI (N = 2), Diabetes (N = 1), Dyslipidemia (N = 1). The blood collection time was defined as "AM" for 9:00 to 12:00 collection and "PM" for 12:00 to 15:00 collection.

[a] *Welch's t-test.*

[b] *Fisher's exact test.*

ns, not significant; sTREM2, soluble triggering receptor expressed on myeloid cells 2; hs-CRP, high-sensitivity C-reactive protein; BMI, body mass index.

TABLE 2 | MMSE and CDR scores at Time 1 and Time 2.

	Time 1	Time 2	Statistical significance
MMSE, mean ± SD	28.42 ± 1.45	26.43 ± 3.64	$P < 0.0001$
CDR, *n* (%)			
0	66 (95.7)	62 (89.9)	$P = 0.029$
0.5	3 (4.3)	6 (8.7)	
1		1 (1.4)	

Wilcoxon signed-rank test.
MMSE, Mini-Mental State Examination; CDR, clinical dementia rating.

level, $P < 0.001$). Results showed a positive correlation between serum sTREM2 level (Time 1) and volume of several brain regions (Time 2). These regions included the left putamen (coordinates −30, 5, 11), right lingual gyrus (coordinates 26, −53, 3), right olfactory cortex (coordinates 11, 21, −11), left middle frontal gyrus (coordinates −36, 50, −6), and right middle temporal gyrus (coordinates 57, −60, 14). The threshold for statistics were set to $T = 3.23$ for the height threshold and $k = 122$ voxels for the extent threshold. **Table 3** shows the VBM findings. These findings are also shown in **Figure 2** using standard brain MR images.

Analyses at the cluster level by applying multiple comparison correction (family wise error; significance level, $P < 0.05$) showed no association between MMSE score difference (Time 1–Time 2 difference) and brain volume. However, higher CDR scores were associated with decreased volumes (Time 2) of the brain regions containing the left and right hippocampus. The thresholds for statistics were set to $T = 3.22$ for the height threshold and $k = 2684$ voxels for the extent threshold (**Table 4**). The VBM findings on the significant clusters containing the left and right hippocampus are shown in **Figure 3** using standard brain MR images.

Additional Findings

We observed a decrease of both gray matter and total brain volume using paired *t*-test ($P < 0.0001$), by comparing Time 1 and Time 2. CDR (Time 1) scores were negatively associated with left hippocampus volume (Time 1) at the peak level ($P < 0.001$; the threshold for statistics were set to $T = 3.22$ for the height threshold and $k = 123$ voxels for the extent threshold). CDR (Time 2) scores were negatively associated with both hippocampus region's volume (Time 2) at the cluster level (family wise error; $P < 0.05$). CDR (Time 1) scores were positively associated with volumes (Time 2) of only two regions, left precentral gyrus and superior temporal gyrus, at the peak level ($P < 0.001$; the threshold for statistics were set to $T = 3.22$ for the height threshold and $k = 124$ voxels for the extent threshold). CDR (Time 1) scores were positively associated with change of right hippocampus region's volume (Time 1–Time 2 difference) at the cluster level (family wise error; $P < 0.05$). The change of CDR (Time 1–Time 2 difference) scores were negatively associated with change of whole brain regions' volume (Time 1–Time 2 difference) at the cluster level (family wise error; $P < 0.05$). Additionally, we had focused 7 participants whose CDR score was either 0.5 or 1.0 at Time 2. In our sample, there were 6 participants with CDR of 0.5 and one participant with CDR of 1.0. As a demographic, we did not find a significant age difference between 7 participants and remaining 62 participants (75.42 ± 3.45 vs. 72.37 ± 4.32, $P = 0.061$). In addition, we did not find a significant difference of serum sTREM2 levels between 7 participants and remaining 62 participants (219.1 ± 175.5 pg/ml vs. 310.9 ± 291.7 pg/ml, $P = 0.254$). Lastly, analyses at the cluster level (family wise error; $P < 0.05$) showed no correlation between serum sTREM2 levels and volume of different brain regions in these 7 participants. Moreover, there was no association between serum sTREM2 levels (Time 2) and brain volume (Time 2) in any regions at the cluster level (family wise error; $P < 0.05$). Serum sTREM2 levels significantly increased from 301.6 ± 282.5 pg/ml (at Time 1) to 977.8 ± 963.5 pg/ml (at Time 2). The Wilcoxon signed-rank test showed a significant difference ($P < 0.0001$). When we used age as a covariate, serum sTREM2 difference between Time 2 and Time 1 was associated with changes in CDR ($P = 0.016$) but not in MMSE ($P = 0.054$). Lastly, we divided all participants to three groups according to baseline serum sTREM2 levels: low, medium, and high, respectively. We compared changes in serum sTREM2 levels among the three groups. As a result, there was no significant difference ($P = 0.064$), suggesting that relatively higher baseline serum sTREM2 levels did not increase later further.

Lastly, we analyzed the association between changes in serum sTREM2 levels (Time 1–Time 2 difference) and brain volume at

TABLE 3 | Voxel-based morphometry (VBM) findings.

Cluster-level			Peak-level		MNI coordinates			
***P* FWE-corr**	***k*, Cluster size (voxels)**	***P* uncorr**	***T***	***P* uncorr**	***X* (mm)**	***Y* (mm)**	***Z* (mm)**	**Anatomical region**
0.709	148	0.253	4.52	<0.001	−30	5	11	Left putamen
0.601	198	0.188	4.35	<0.001	26	−53	3	Right lingual gyrus
0.767	122	0.298	4.23	<0.001	11	21	−11	Right olfactory cortex
0.543	227	0.160	4.17	<0.001	−36	50	−6	Left middle frontal gyrus
0.756	127	0.289	3.82	<0.001	57	−60	14	Right middle temporal gyrus

Positive correlation between serum sTREM2 level (Time 1) and brain volume (Time 2) by multiple regression analysis. Height threshold, T = 3.23; Extent threshold, k = 122 voxels; Expected voxels per cluster, k = 121.917; Degrees of freedom = (1.0, 62.0); FWHM = 16.1, 15.9, and 15.2 mm; 10.7, 10.6, and 10.2 voxels; Volume, 1263188 = 374278 voxels = 281.0 resels; Voxel size, 1.5 mm × 1.5 mm × 1.5 mm (resel = 1157.29 voxels). FWE, family wise error; corr, corrected; uncorr, uncorrected; MNI, Montreal Neurological Institute; FWHM, full width at half maximum. Labels are marked using automated anatomical labeling.

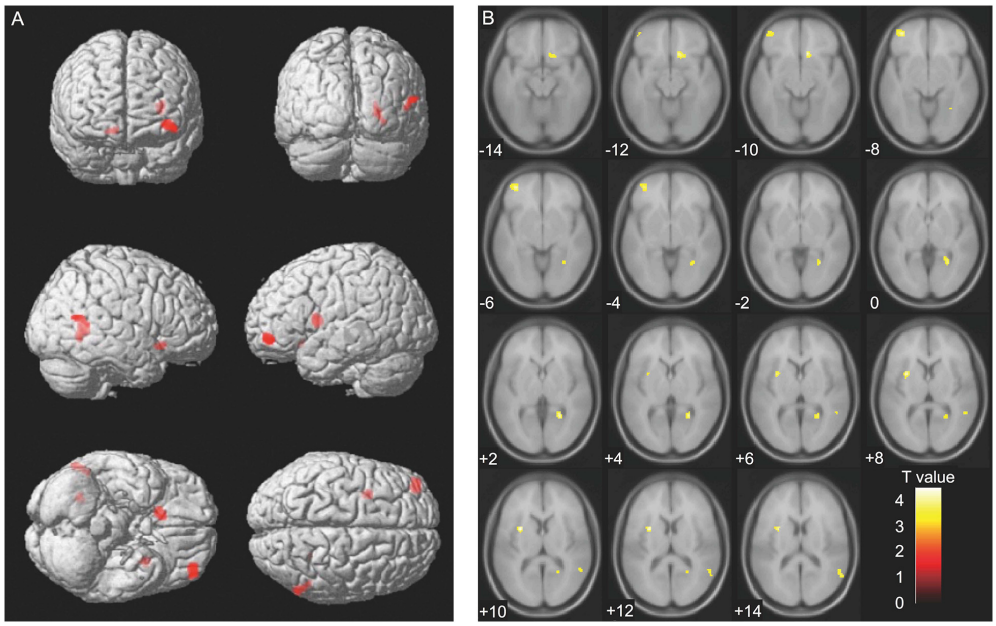

FIGURE 2 | Voxel-based morphometry findings: Association between serum sTREM2 levels (Time 1) and brain volume (Time 2). Positive correlation between serum sTREM2 levels (Time 1) and brain volume (Time 2), as shown by multiple regression analysis. The threshold for statistics were set to $T = 3.23$ for the height threshold and $k = 122$ voxels for the extent threshold. Volumes of the important regions are shown in **(A)** whole brain images and **(B)** axial images. The *T*-value applies to **(B)** axial images.

TABLE 4 | Voxel-based morphometry (VBM) findings.

Cluster-level			Peak-level		MNI coordinates			
***P* FWE-corr**	***k*, Cluster size (voxels)**	***P* uncorr**	***T***	***P* uncorr**	***X* (mm)**	***Y* (mm)**	***Z* (mm)**	**Anatomical region**
<0.001	4658	<0.001	6.30	<0.001	−21	−12	−26	Left hippocampus
<0.001	2684	<0.001	5.37	<0.001	24	−15	−27	Right hippocampus

Association between higher CDR scores and decreased brain volume (Time 2) by multiple regression analysis applying multiple comparison correction. These clusters contain the left and right hippocampus.
Height threshold, T = 3.22; Extent threshold, k = 2684 voxels; Expected voxels per cluster, k = 122.159;
Degrees of freedom = (1.0, 63.0); FWHM = 16.1, 15.9, and 15.2 mm; 10.7, 10.6, and 10.2 voxels;
Volume, 1263188 = 374278 voxels = 281.0 resels; Voxel size, 1.5 mm × 1.5 mm × 1.5 mm (resel = 1157.39 voxels).
FWE, family wise error; corr, corrected; uncorr, uncorrected; MNI, Montreal Neurological Institute; FWHM, full width at half maximum.
Labels are marked using automated anatomical labeling.

Time 1, at Time 2, and Time 1–Time 2 difference, respectively. As a result, analyses at the cluster level (family wise error; $P < 0.05$) showed no association between changes in serum sTREM2 levels (Time 1–Time 2 difference) and brain volume (both at Time 1 and at Time 2). However, changes in serum sTREM2 levels (Time 1–Time 2 difference) were positively associated with changes in brain volume (Time 1–Time 2 difference) of only two regions containing the left frontal lobe and the left hippocampus (family wise error; $P < 0.05$). Thus, these suggest that the change of sTREM2 could serve as an indicator of the volume changes of both left frontal lobe and left hippocampus.

DISCUSSION

In this study, we focused on the correlation between serum sTREM2 levels and brain volume in people aged over 65 years. Analyses at the cluster level by applying multiple comparison corrections (family wise error; $P < 0.05$) showed no correlation between serum sTREM2 levels and brain volume, either cross-sectional or longitudinal. However, when analyzed uncorrected, we observed that the baseline serum sTREM2 levels correlate positively with the volume of several brain regions 7 years later at the peak level. In our previous studies using similar methods, we observed that serum oxytocin levels in the older adults were positively correlated with the future hippocampus and amygdala volumes (Orihashi et al., 2020). The hippocampus and amygdala are closely related to cognitive function. Whereas hippocampus is involved in regulating memory functions, amygdala is associated with regulating emotional functions, and both of these structures coordinate and interact (Scoville and Milner, 1957; Fink et al., 1996; Klüver and Bucy, 1997). In this study, we observed that MMSE scores decreased and CDR scores increased in participants 7 years after the baseline evaluation

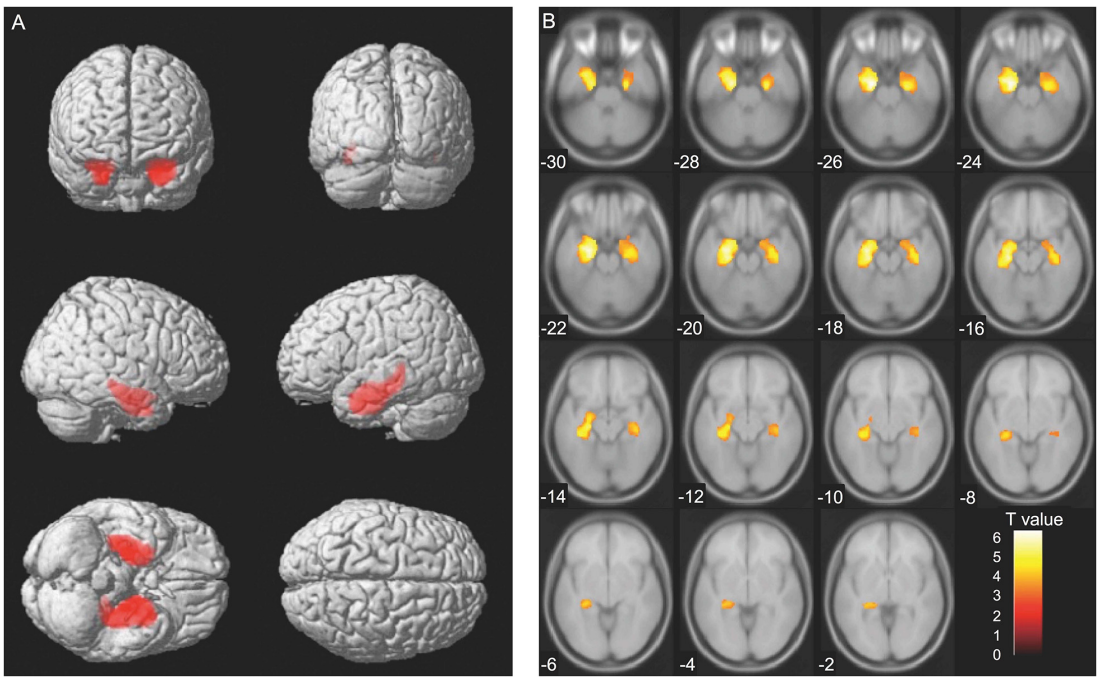

FIGURE 3 | Voxel-based morphometry findings: Association between changes in clinical dementia rating (CDR) scores and brain volume (Time 2). Association between higher CDR scores and decreased brain volume (Time 2) evaluated using multiple regression analysis. The thresholds for statistics were set to $T = 3.22$ for the height threshold and $k = 2684$ voxels for the extent threshold. Significant clusters containing the left and the right hippocampus are shown in **(A)** whole brain images and **(B)** axial images. The *T*-value applies to **(B)** axial images.

(**Table 2**). Moreover, higher CDR scores were also associated with decreased volume of the brain regions containing the left and right hippocampus (**Table 4**). Our results suggest that serum sTREM2 levels in older adults aged 65 years and above may not be significantly associated with later aging-related changes in the brain volume, especially in brain regions closely related to cognitive function.

Although previous studies have shown that CSF sTREM2 levels are higher in AD patients compared to healthy controls (Heslegrave et al., 2016; Piccio et al., 2016; Suárez-Calvet et al., 2016), others reported no difference between healthy controls and patients with AD or mild cognitive impairment (Henjum et al., 2016). Additionally, previous studies on sTREM2 levels in peripheral blood have also shown no difference between healthy controls and AD patients (Liu et al., 2018). Hu et al. reported an increased TREM2 expression at protein and mRNA levels on monocyte in AD, but plasma protein level was not significantly different in subjects with AD compared to controls (Hu et al., 2014). Moreover, there are also reports that high serum sTREM2 levels are associated with the development of dementia in the future (Ohara et al., 2019). These discrepancies in the results might be due to the characteristics of the participants. In the brain of AD patients, TREM2 expression may have a protective effect at an early stage (Ewers et al., 2019). However, in the later stages, there may be pathogenic effects through activation of the inflammatory response (Jay et al., 2017). A recent meta-analysis showed that sTREM2 level increases during the earlier course of AD development and is slightly attenuated at the dementia stage (Liu et al., 2018). There might be differences in sTREM2 expression and its clinical relevance between healthy individuals and patients at early and late stages of AD. Participants in our study were cognitively healthier at the baseline. This might be the reason that no association was observed between serum sTREM2 levels and future brain volume, especially in brain regions closely related to cognitive function. Additionally, the serum sTREM2 levels were divided into quartile categories (Q1 = 62.46–90.15 pg/ml, Q2 = 91.09–156.70 pg/ml, Q3 = 186.95–413.38 pg/ml, Q4 = 422.28–1415.8 pg/ml). We used linear mixed-effects models to estimate changes of averaged total brain volumes (A) and averaged MMSE scores (B) between Time 1 and Time 2 in each quartile category (**Supplementary Figure 1**). As a result, there were no interactions between serum sTRME2 levels and time, for total brain volume ($P = 0.78$) and MMSE ($P = 0.40$). Based on our results, serum sTREM2 levels in the older adults might not be considered as a biomarker for predicting a decline in future cognitive functions or brain volume. Recently, it has been suggested that higher CSF sTREM2 attenuates risk for cognitive decline and TREM2 may be protective against the development of AD (Franzmeier et al., 2020). Although measuring sTREM2 level in peripheral blood is less invasive and relatively easily, it might be necessary to analyze the relationship between the CSF sTREM2 levels and brain volume.

Our study has several major limitations. The evaluation of participants at Time 1 was conducted as part of a national survey for the prevalence of dementia in Japan. Importantly,

MRI examinations were optional and were executed when necessary for further assessment of dementia or upon request of participants. Thus, in our study, selection of participants may be biased and the cohort may not reflect the characteristics of a general rural older adults. Although our study was aimed to evaluate serum sTREM2 levels and examine its relationship with brain volume using MRI, we did not measure biomarkers other than sTREM2, such as amyloid-beta, t-tau, and p-tau. Additionally, we used only MMSE and CDR to assess cognitive function. Moreover, compared to previous studies on serum sTREM2 levels (Ohara et al., 2019), our sample size was smaller. Our study was limited by the high number of individuals who dropped out during Time 1 and Time 2.

CONCLUSION

Serum sTREM2 levels could not serve as an immune biomarker of aging-related volume changes in brain regions closely related to cognitive function in older adults aged 65 years and above.

DATA AVAILABILITY STATEMENT

The raw data supporting the conclusions of this article will be made available by the authors, without undue reservation.

ETHICS STATEMENT

The studies involving human participants were reviewed and approved by the Ethics Committee of the Faculty of Medicine, Saga University, and all participants agreed to participate in the study according to the Declaration of Helsinki. The patients/participants provided their written informed consent to participate in this study.

AUTHOR CONTRIBUTIONS

RO, YM, YI, SY, and AM designed the study. RO, YM, and YI acquired the data. RO analyzed the data and drafted the manuscript. YM edited the manuscript. All authors contributed to the article and approved the submitted version.

FUNDING

This study was supported by grants from the Japan Society for the Promotion of Science – Challenging Exploratory Research (to YM and YI).

ACKNOWLEDGMENTS

We would like to thank Takefumi Ueno and Hiroko Kunitake for their technical support.

SUPPLEMENTARY MATERIAL

The Supplementary Material for this article can be found online at: https://www.frontiersin.org/articles/10.3389/fnagi.2021.665612/full#supplementary-material

REFERENCES

Ashburner, J. (2007). A fast diffeomorphic image registration algorithm. *Neuroimage* 38, 95–113. doi: 10.1016/j.neuroimage.2007.07.007

Ashburner, J., and Friston, K. J. (2000). Voxel-based morphometry–the methods. *Neuroimage* 11, 805–821. doi: 10.1006/nimg.2000.0582

Ashburner, J., and Ridgway, G. R. (2012). Symmetric diffeomorphic modeling of longitudinal structural MRI. *Front. Neurosci.* 6:197. doi: 10.3389/fnins.2012.00197

Ewers, M., Franzmeier, N., Suárez-Calvet, M., Morenas-Rodriguez, E., Caballero, M. A. A., Kleinberger, G., et al. (2019). Increased soluble TREM2 in cerebrospinal fluid is associated with reduced cognitive and clinical decline in Alzheimer's disease. *Sci. Transl. Med.* 11:eaav6221. doi: 10.1126/scitranslmed.aav6221

Fink, G. R., Markowitsch, H. J., Reinkemeier, M., Bruckbauer, T., Kessler, J., and Heiss, W. D. (1996). Cerebral representation of one's own past: neural networks involved in autobiographical memory. *J. Neurosci.* 16, 4275–4282. doi: 10.1523/JNEUROSCI.16-13-04275.1996

Folstein, M. F., Folstein, S. E., and McHugh, P. R. (1975). Mini-mental state". A practical method for grading the cognitive state of patients for the clinician. *J. Psychiatr. Res.* 12, 189–198. doi: 10.1016/0022-3956(75)90026-6

Franzmeier, N., Suárez-Calvet, M., Frontzkowski, L., Moore, A., Hohman, T. J., Morenas-Rodriguez, E., et al. (2020). Higher CSF sTREM2 attenuates ApoE4-related risk for cognitive decline and neurodegeneration. *Mol. Neurodegener.* 15:57. doi: 10.1186/s13024-020-00407-2

Haraguchi, Y., Mizoguchi, Y., Ohgidani, M., Imamura, Y., Murakawa-Hirachi, T., Nabeta, H., et al. (2017). Donepezil suppresses intracellular Ca 2+ mobilization through the PI3K pathway in rodent microglia. *J. Neuroinflammation* 14:258. doi: 10.1186/s12974-017-1033-0

Henjum, K., Almdahl, I. S., Årskog, V., Minthon, L., Hansson, O., Fladby, T., et al. (2016). Cerebrospinal fluid soluble TREM2 in aging and Alzheimer's disease. *Alzheimers Res. Ther.* 8:17. doi: 10.1186/s13195-016-0182-1

Heslegrave, A., Heywood, W., Paterson, R., Magdalinou, N., Svensson, J., Johansson, P., et al. (2016). Increased cerebrospinal fluid soluble TREM2 concentration in Alzheimer's disease. *Mol. Neurodegener.* 11:3. doi: 10.1186/s13024-016-0071-x

Hu, N., Tan, M. S., Yu, J. T., Sun, L., Tan, L., Wang, Y. L., et al. (2014). Increased expression of TREM2 in peripheral blood of Alzheimer's disease patients. *J. Alzheimers Dis.* 38, 497–501. doi: 10.3233/JAD-130854

Hughes, C. P., Berg, L., Danziger, W. L., Coben, L. A., and Martin, R. L. (1982). A new clinical scale for the staging of dementia. *Braz. J. Psychiatry.* 140, 566–572. doi: 10.1192/bjp.140.6.566

Ikejima, C., Hisanaga, A., Meguro, K., Yamada, T., Ouma, S., Kawamuro, Y., et al. (2012). Multicentre population-based dementia prevalence survey in Japan: a preliminary report. *Psychogeriatrics* 12, 120–123. doi: 10.1111/j.1479-8301.2012.00415.x

Imamura, Y., Mizoguchi, Y., Nabeta, H., Haraguchi, Y., Matsushima, J., Kojima, N., et al. (2017). An association between belief in life after death and serum oxytocin in older people in rural Japan. *Int. J. Geriatr. Psychiatry* 32, 102–109. doi: 10.1002/gps.4453

Jay, T. R., von Saucken, V. E., and Landreth, G. E. (2017). TREM2 in Neurodegenerative Diseases. *Mol. Neurodegener.* 12:56. doi: 10.1186/s13024-017-0197-5

Kleinberger, G., Yamanishi, Y., Suárez-Calvet, M., Czirr, E., Lohmann, E., Cuyvers, E., et al. (2014). TREM2 mutations implicated in neurodegeneration impair cell surface transport and phagocytosis. *Sci. Transl. Med.* 6:243ra286. doi: 10.1126/scitranslmed.3009093

Klüver, H., and Bucy, P. C. (1997). Preliminary analysis of functions of the temporal lobes in monkeys. 1939. *J. Neuropsychiatry Clin. Neurosci.* 9, 606–620. doi: 10.1176/jnp.9.4.606

Liu, D., Cao, B., Zhao, Y., Huang, H., McIntyre, R. S., Rosenblat, J. D., et al. (2018). Soluble TREM2 changes during the clinical course of Alzheimer's disease: a meta-analysis. *Neurosci. Lett.* 686, 10–16. doi: 10.1016/j.neulet.2018.08.038

Matsushima, J., Kawashima, T., Nabeta, H., Imamura, Y., Watanabe, I., Mizoguchi, Y., et al. (2015). Association of inflammatory biomarkers with depressive symptoms and cognitive decline in a community-dwelling healthy older sample: a 3-year follow-up study. *J. Affect. Disord.* 173, 9–14. doi: 10.1016/j.jad.2014.10.030

Morris, J. C. (1993). The Clinical Dementia Rating (CDR): current version and scoring rules. *Neurology* 43, 2412–2414. doi: 10.1212/wnl.43.11.2412-a

Nabeta, H., Mizoguchi, Y., Matsushima, J., Imamura, Y., Watanabe, I., Tateishi, T., et al. (2014). Association of salivary cortisol levels and later depressive state in elderly people living in a rural community: a 3-year follow-up study. *J. Affect. Disord.* 158, 85–89. doi: 10.1016/j.jad.2014.02.003

Ohara, T., Hata, J., Tanaka, M., Honda, T., Yamakage, H., Yoshida, D., et al. (2019). Serum Soluble Triggering Receptor Expressed on Myeloid Cells 2 as a Biomarker for Incident Dementia: the Hisayama Study. *Ann. Neurol.* 85, 47–58. doi: 10.1002/ana.25385

Orihashi, R., Mizoguchi, Y., Imamura, Y., Yamada, S., Ueno, T., and Monji, A. (2020). Oxytocin and elderly MRI-based hippocampus and amygdala volume: a 7-year follow-up study. *Brain Commun.* 2:fcaa081. doi: 10.1093/braincomms/fcaa081

Piccio, L., Deming, Y., Del-Águila, J. L., Ghezzi, L., Holtzman, D. M., Fagan, A. M., et al. (2016). Cerebrospinal fluid soluble TREM2 is higher in Alzheimer disease and associated with mutation status. *Acta Neuropathol.* 131, 925–933. doi: 10.1007/s00401-016-1533-5

Podleśny-Drabiniok, A., Marcora, E., and Goate, A. M. (2020). Microglial Phagocytosis: a Disease-Associated Process Emerging from Alzheimer's Disease Genetics. *Trends Neurosci.* 43, 965–979. doi: 10.1016/j.tins.2020.10.002

Scoville, W. B., and Milner, B. (1957). Loss of recent memory after bilateral hippocampal lesions. *J. Neurol. Neurosurg. Psychiatry* 20, 11–21. doi: 10.1136/jnnp.20.1.11

Suárez-Calvet, M., Kleinberger, G., Araque Caballero, M., Brendel, M., Rominger, A., Alcolea, D., et al. (2016). sTREM2 cerebrospinal fluid levels are a potential biomarker for microglia activity in early-stage Alzheimer's disease and associate with neuronal injury markers. *EMBO Mol. Med.* 8, 466–476. doi: 10.15252/emmm.201506123

Tan, Y. J., Ng, A. S. L., Vipin, A., Lim, J. K. W., Chander, R. J., Ji, F., et al. (2017). Higher Peripheral TREM2 mRNA Levels Relate to Cognitive Deficits and Hippocampal Atrophy in Alzheimer's Disease and Amnestic Mild Cognitive Impairment. *J. Alzheimers Dis.* 58, 413–423. doi: 10.3233/JAD-161277

Tanaka, M., Honda, T., Yamakage, H., Hata, J., Yoshida, D., Hirakawa, Y., et al. (2018). A potential novel pathological implication of serum soluble triggering receptor expressed on myeloid cell 2 in insulin resistance in a general Japanese population: the Hisayama study. *Diabetes Res. Clin. Pract.* 146, 225–232. doi: 10.1016/j.diabres.2018.10.007

Tanaka, M., Yamakage, H., Masuda, S., Inoue, T., Ohue-Kitano, R., Araki, R., et al. (2019). Serum soluble TREM2 is a potential novel biomarker of cognitive impairment in Japanese non-obese patients with diabetes. *Diabetes Metab.* 45, 86–89. doi: 10.1016/j.diabet.2017.06.006

Tzourio-Mazoyer, N., Landeau, B., Papathanassiou, D., Crivello, F., Etard, O., Delcroix, N., et al. (2002). Automated anatomical labeling of activations in SPM using a macroscopic anatomical parcellation of the MNI MRI single-subject brain. *Neuroimage* 15, 273–289. doi: 10.1006/nimg.2001.0978

Ulrich, J. D., and Holtzman, D. M. (2016). TREM2 Function in Alzheimer's Disease and Neurodegeneration. *ACS Chem. Neurosci.* 7, 420–427. doi: 10.1021/acschemneuro.5b00313

Ulrich, J. D., Ulland, T. K., Colonna, M., and Holtzman, D. M. (2017). Elucidating the Role of TREM2 in Alzheimer's Disease. *Neuron* 94, 237–248. doi: 10.1016/j.neuron.2017.02.042

Wunderlich, P., Glebov, K., Kemmerling, N., Tien, N. T., Neumann, H., and Walter, J. (2013). Sequential proteolytic processing of the triggering receptor expressed on myeloid cells-2 (TREM2) protein by ectodomain shedding and γ-secretase-dependent intramembranous cleavage. *J. Biol. Chem.* 288, 33027–33036. doi: 10.1074/jbc.M113.517540

Conflict of Interest: The authors declare that the research was conducted in the absence of any commercial or financial relationships that could be construed as a potential conflict of interest.

frontiers in Aging Neuroscience

ORIGINAL RESEARCH
published: 28 May 2021
doi: 10.3389/fnagi.2021.670115

Better Identification of Cognitive Decline With Interleukin-2 Than With Amyloid and Tau Protein Biomarkers in Amnestic Mild Cognitive Impairment

*Chih-Sung Liang[1,2], Chia-Lin Tsai[3], Guan-Yu Lin[3], Jiunn-Tay Lee[3], Yu-Kai Lin[2,3], Che-Sheng Chu[4,5], Yueh-Feng Sung[3], Chia-Kuang Tsai[3], Ta-Chuan Yeh[6], Hsuan-Te Chu[1], Ming-Wei Su[7] and Fu-Chi Yang[2,3]**

[1] Department of Psychiatry, Beitou Branch, Tri-Service General Hospital, National Defense Medical Center, Taipei, Taiwan, [2] Graduate Institute of Medical Sciences, National Defense Medical Center, Taipei, Taiwan, [3] Department of Neurology, Tri-Service General Hospital, National Defense Medical Center, Taipei, Taiwan, [4] Department of Psychiatry, Kaohsiung Veterans General Hospital, Kaohsiung, Taiwan, [5] Center for Geriatric and Gerontology, Kaohsiung Veterans General Hospital, Kaohsiung, Taiwan, [6] Department of Psychiatry, Tri-Service General Hospital, National Defense Medical Center, Taipei, Taiwan, [7] Institute of Biomedical Sciences, Academia Sinica, Taipei, Taiwan

OPEN ACCESS

Edited by:
Thomas K. Karikari, University of Gothenburg, Sweden

Reviewed by:
Pedro Pesini, Araclon Biotech, Spain
Tobi Van Den Bossche, University of Antwerp, Belgium

***Correspondence:**
Fu-Chi Yang
fuji-yang@yahoo.com.tw

Received: *20 February 2021*
Accepted: *03 May 2021*
Published: *28 May 2021*

Citation:
Liang C-S, Tsai C-L, Lin G-Y, Lee J-T, Lin Y-K, Chu C-S, Sung Y-F, Tsai C-K, Yeh T-C, Chu H-T, Su M-W and Yang F-C (2021) Better Identification of Cognitive Decline With Interleukin-2 Than With Amyloid and Tau Protein Biomarkers in Amnestic Mild Cognitive Impairment. Front. Aging Neurosci. 13:670115. doi: 10.3389/fnagi.2021.670115

The rate of cognitive decline among patients with amnestic mild cognitive impairment (aMCI) varies, and it is thus crucial to accurately predict the probability of cognitive deterioration in patients with MCI. We compared the potential of cytokines with amyloid beta (Aβ) and tau biomarkers for predicting cognitive decline in patients with aMCI or Alzheimer's disease (AD). All participants (controls, aMCI, and AD patients) underwent plasma biomarker examinations for $A\beta_{1-40}$, $A\beta_{1-42}$, total tau (t-tau), tau phosphorylated at threonine 181 [*p*-Tau181]), and 29 cytokines and baseline cognitive tests, including Mini-Mental State Examination (MMSE). The correlation between biomarker levels and annual MMSE change during the follow-up was examined. Receiver operating characteristic (ROC) curve analysis was performed to determine whether the statistically significant plasma biomarkers could identify cognitive decline. Higher baseline levels of IL-2, sCD40L, IL-8, and VEGF were associated with a lower annual cognitive decline in the aMCI group, and higher baseline levels of $A\beta_{1-40}$, IFNγ, IL-5, IL-17A, IL-25, and FGF were associated with a rapid annual cognitive decline in the AD group. IL-2 had a high discriminatory capacity for identifying cognitive decline, with an area under curve (AUC) of 85.7% in the aMCI group, and the AUC was slightly increased when combining IL-2 with Aβ or tau biomarkers. However, none of the biomarkers had a satisfactory discriminatory capacity in the AD group. IL-2 may have a better discriminatory capacity for identifying cognitive decline than Aβ and tau biomarkers in patients with aMCI.

Keywords: predictive biomarkers, Alzheimer's disease, amnestic mild cognitive impairment, interleukin-2, beta amyloid, tau protein

INTRODUCTION

Amnestic mild cognitive impairment (aMCI) is a heterogenous, symptomatic pre-dementia condition that represents a transitional phase between normal ageing and dementia (and often Alzheimer's disease [AD]) (Petersen, 2011). The rate of cognitive decline among patients with aMCI varies, some patients progress to dementia, while others remain stable or even revert to normal cognition (Petersen, 2011). Depending on the population studied, the annual rate of conversion from aMCI to dementia ranges from less than 5–20% (Langa and Levine, 2014). However, many patients may not progress to dementia when followed up after 10 years (Mitchell and Shiri-Feshki, 2009), implying that patients diagnosed with aMCI may live with uncertainty for a long time (Langa and Levine, 2014). Therefore, it is crucial to accurately identify and predict the probability of cognitive deterioration in patients with aMCI.

In recent decades, significant effort has been devoted to diagnosing aMCI or dementia early using a variety of biomarkers. An accurate diagnosis and prognosis of aMCI is important for patients and their families to determine appropriate methods of care and future plans. The commonly suggested biomarkers are: an apolipoprotein E ε4 carrier status; atrophy on structural magnetic resonance imaging; hypometabolism on fludeoxyglucose F 18-positron emission tomography; and levels of several cerebrospinal fluid (CSF) biomarkers, such as amyloid β 1-42 peptide ($A\beta_{1-42}$), total tau, and tau phosphorylated at threonine 181 (*p*-Tau181) (Petersen et al., 2009). In recent years, plasma biomarkers have shown their potential for predicting the burden of Aβ in the brain and identifying rapid cognitive decline in patients with aMCI (Nakamura et al., 2018; Lue et al., 2019; Tsai et al., 2019, 2020). For example, a large cohort study reported that longitudinal changes of plasma *p*-Tau181 were associated with cognitive decline and neurodegeneration in the brain (Moscoso et al., 2021). Undoubtedly, biomarkers enable broader clinical access and efficient screening in individuals with risk factors of cognitive decline.

Although AD is characterized by a complex interplay between abnormal Aβ and tau proteins, evidence has suggested that the innate immune system-mediated inflammation drives the AD pathogenesis (Heneka et al., 2015; Heppner et al., 2015). Neuroinflammation may trigger a vicious cycle of microglial activation, release of pro-inflammatory factors, and neuronal damage in the preclinical stage of AD (Heneka et al., 2015; Heppner et al., 2015). Clinical studies have found that patients with aMCI or AD have significantly altered inflammatory biomarkers, such as interleukin (IL)-6 and IL-10 in both the peripheral and CSF (King et al., 2018; Shen et al., 2019). Furthermore, the peripheral levels of inflammatory biomarkers were found to be associated with future cognitive decline in patients with aMCI or AD (Bradburn et al., 2017; Morgan et al., 2019; Liang et al., 2020). For example, a cohort study reported that plasma levels of complement factor B and factor H were associated with aMCI progression to AD (Morgan et al., 2019). Another study reported plasma IL-33 expression was associated with cognitive preservation among patients with aMCI or AD (Liang et al., 2020). However, to date, no studies have compared the potential of cytokines versus Aβ- or tau-related biomarkers for predicting cognitive decline among patients with aMCI or AD.

The aim of this study was to compare the potential of 29 cytokines with Aβ and tau biomarkers for predicting cognitive decline among patients with aMCI or AD. We hypothesized that cytokines may have a better discriminatory ability than Aβ and tau biomarkers for predicting cognitive decline.

METHODS

Subjects and Study Design

The protocol was approved by the Institutional Review Board for the Protection of Human Subjects at the Tri-Service General Hospital (TSGHIRB 1-107-05-111). Written informed consent was obtained from all participants. Between January 2015 and December 2019, participants were recruited from the memory clinic of the Tri-Service General Hospital of the National Defense Medical Center, Taiwan. Individuals were eligible if they were aged 60 years or older and had negative findings on physical and neurological examinations, laboratory tests (assessment of creatinine, fasting blood sugar, free-thyroxine 4, high-sensitivity thyroid-stimulating hormone, vitamin B12, and folic acid; serologic test for syphilis; and routine blood tests) and neuroimaging examinations (brain computed tomography or magnetic resonance imaging).

Individuals were excluded if they had: (a) a history of major or uncontrolled medical conditions, such as heart failure, sepsis, liver cirrhosis, renal failure, chronic obstructive pulmonary disease, poorly controlled diabetes (Hemoglobin A1c $>$ 8.5), myocardial infarction, or malignancy; (b) substance abuse; (c) a history of major neurological disorders, such as stroke or Parkinson's disease; (d) a score >9 in the short-form Geriatric Depression Scale (GDS-S) or >3 for the modified Rankin Scale; and (e) a history of major psychiatric conditions that can impair cognition, such as major depressive disorder, bipolar disorder, or schizophrenia.

On recruitment, participants underwent the following examinations: Mini-Mental Status Examination (MMSE); Clinical Dementia Rating (CDR); short-form GDS-S; verbal fluency test; Hopkins Verbal Learning Test (HVLT); forward and backward digit span; Trail Making Test, Part A; Modified Boston Naming Test; and Hachinski Ischemia Scale (HIS). The second MMSE was conducted after the 1-year follow-up.

Participants were classified into the control, aMCI, and AD groups based on the results of HVLT, MMSE, and CDR examinations, as well as the recommendations from the National Institute on Aging and Alzheimer's Association (NIA-AA) workgroups on diagnostic guidelines for AD and aMCI due to AD (Albert et al., 2011; McKhann et al., 2011). A diagnosis of AD was made if patients satisfied the following criteria: (a) NIA-AA criteria (McKhann et al., 2011); (b) CDR $\geq$ 0.5; (c) MMSE $\leq$ 26 (middle school), MMSE score $\leq$ 22 (primary school), or MMSE score $\leq$ 19 (illiteracy); (d) HIS score $\leq$ 3; and (e) HVLT score $\leq$ 19 (Hogervorst et al., 2014). aMCI was diagnosed if patients satisfied the following criteria: (a)

NIA-AA criteria (Albert et al., 2011); (b) CDR = 0.5; (c) MMSE score > 26 (middle school), MMSE score > 22 (primary school), or MMSE score > 19 (illiteracy); (d) HIS score ≤ 3; and (e) HVLT score ≤ 22 (Hogervorst et al., 2014). Healthy controls were required to satisfy the following criteria: (a) no active neurological or psychiatric disorders; (b) no psychotropic drugs; (c) MMSE score > 26 (middle school), MMSE score > 22 (primary school), or MMSE score > 19 (illiteracy); and (d) CDR score = 0.

Plasma Preparation

Fasting blood was collected in 9-mL K3-EDTA tubes (455036, Greiner Bio-one GmbH, Kremsmünster, Austria), which were gently inverted three times immediately following blood collection. Blood samples were then centrifuged at 2,300 *g* for 10 min (4°C) using a swing-out (bucket) rotor (5202R, Eppendorf, Hamburg, Germany). Each 0.4-mL plasma sample was transferred to a fresh 2.0-mL tube (CryzoTraq, Ziath, Cambridge, United Kingdom). All plasma samples were stored in 0.5-ml aliquots within 8 h of blood collection at −80°C until further use.

Assessment of Plasma Aβ and Tau Levels

Immunomagnetic reduction (IMR), an ultra-sensitive analytical assay, can reliably assay ultra-low concentrations of Aβ and tau biomarkers, including $A\beta_{1-40}$, $A\beta_{1-42}$, total tau (t-Tau), and *p*-Tau181 (Tsai et al., 2019). The levels of plasma $A\beta_{1-40}$, $A\beta_{1-42}$, t-Tau, and *p*-Tau181 were assessed using IMR kits (MF-AB0-0060, MF-AB2-0060, MF-TAU-0060, and MF-PT1-0060, MagQu Co., New Taipei City, Taiwan). For each assay, 40 μL ($A\beta_{1-40}$, t-Tau, and *p*-Tau181) or 60 μL ($A\beta_{1-42}$) of plasma was mixed with 80 or 60 μL of reagent, respectively. Each reported biomarker concentration represented the average of 2 duplicated measurements. An IMR analyzer (XacPro-S, MagQu Co., New Taipei City, Taiwan) was used for all assays. The measured biomarker concentrations ranged from 0.17 to 1,000 pg/mL for $A\beta_{1-40}$, 0.77 to 30,000 pg/mL for $A\beta_{1-42}$, 0.026 to 3,000 pg/mL for t-Tau, and 0.0196 to 1,000 pg/mL for *p*-Tau181. Intra-assay or inter-assay coefficients of variations using IMR ranged from 7 to 10% and from 10 to 15% for high-concentration and low-concentration quality control samples of $A\beta_{1-40}$, $A\beta_{1-42}$, t-Tau, or *p*-Tau181, respectively. For each biomarker, two batches of reagents were used, and the quality of each batch of reagents was well-controlled by monitoring the particle size, particle concentration, and bioactivity. The variation in these reagent properties between batches was lower than 10%.

Measurement of Plasma Cytokines

A multiplex bead array assay was used to examine plasma cytokines levels. The detailed procedures for detection of soluble cytokines using the multiplex bead array assays have been previously reported (Ho et al., 2015, 2017). We examined 29 cytokines using a customized human cytokine magnetic bead panel (Bio-Rad; Yu-Shing Biotech., Ltd, Taipei, Taiwan) according to the manufacturer's instructions (Bio-Rad; Genmall Biotechnology Co., LTD., Taipei, Taiwan). The examined cytokines were IL-1β, IL-1 receptor antagonist (IL-1RA), IL-2, IL-4, IL-5, IL-6, IL-7, IL-8, IL-9, IL-10, IL-13, IL-17A, IL-23, IL-25, IL-31, interferon-gamma (IFNγ), tumor necrosis factor-alpha (TNFα), soluble CD40 ligand (sCD40L), IFNγ-induced protein 10 (IP10), monocyte chemoattractant protein 1 (MCP1), macrophage inflammatory protein 1-alpha (MIP1α), MIP1β, regulated upon activation, normal T cell expressed and secreted (RANTES), eotaxin, fibroblast growth factor (FGF), granulocyte colony-stimulating factor (GCSF), Granulocyte-macrophage colony-stimulating factor (GM-CSF), platelet-derived growth factor-BB (PDGF-BB), and vascular endothelial growth factor (VEGF). The median fluorescence intensities were assessed using a Bio-Plex 200 instrument (Bio-Rad) with Bio-Plex Manager software version 6.0 (Bio-Rad). Study samples were assessed in duplicates and the duplicate measurements were averaged for statistical analysis. Standard curves were created from duplicate values and all samples were analyzed as single determinants. All analyses were performed in one batch using kits from the same production lot.

Statistical Analyses

Group differences (aMCI vs controls and AD vs controls) in categorical variables were examined by using the Fisher's exact test. Group differences in continuous variables were examined by using the independent sample t-test or Mann–Whitney *U*-test. The temporal ordering (controls, aMCI, AD) of the cognitive tests, Aβ and tau biomarkers, and cytokines were examined by using the P trend analysis. The association between plasma biomarkers (including Aβ, tau, and cytokines biomarkers) and annual change in MMSE score in the aMCI and AD groups was assessed using partial correlation with adjustment for age, education level, body mass index, and apolipoprotein E (APOE) genotype (i.e., the proportion of individuals who carry the APOE ε4 allele). Receiver operating characteristic (ROC) curve analysis was performed for the statistically significant plasma biomarkers in the partial correlation analysis. Using cognitive decline (a change in the annual MMSE score ≥ 2) as the outcome, the utility of individual plasma biomarkers to identify the outcome was evaluated using the area under the ROC curve (AUC). The highest AUC value of the cytokine was combined with each Aβ and tau biomarker for a combined AUC analysis. The 95% confidence interval (CI) for the AUC was calculated using the DeLong's test. All tests were 2-tailed and $P < 0.05$ was considered statistically significant. No adjustment of multiple testing (multiplicity) was performed in this study. Data analyses were conducted using SPSS 25 (IBM SPSS Inc, Chicago, IL, United States).

RESULTS

Patient Demographics and Plasma Biomarkers

A total of 91 participants were included (aMCI = 51, AD = 28, controls = 12) (**Table 1**). Patients in the AD (78.3 ± 8.8 years) and aMCI groups (75.6 ± 8.6 years) were older than those in the control group (66.3 ± 5.9 years). All the cognitive tests

TABLE 1 | Baseline characteristics and IMR data of the enrolled participants.[a]

	Control	aMCI	AD[b]	*P* value		
Variable	**(*n* = 12)**	**(*n* = 51)**	**(*n* = 28)**	**P trend analysis**	**MCI vs. Control**	**AD vs. Control**
Demographics						
Male	3 (25.0)	11 (21.6)	7 (25.0)	na	0.532	0.663
Age, years	66.3 ± 5.9	75.6 ± 8.6	78.3 ± 8.8	na	**<0.001***	**<0.001***
Education, years	11.0 ± 3.9	8.2 ± 4.7	10.1 ± 5.1	na	**0.026***	0.489
BMI, kg/m^2	23.4 ± 2.1	24.7 ± 3.5	23.3 ± 3.4	na	0.064	0.708
Cognitive test						
Baseline MMSE	29.4 ± 0.5	24.7 ± 4.5	20.9 ± 5.4	**<0.001***	**<0.001***	**<0.001***
CDR	0 ± 0	0.25 ± 0.34	0.77 ± 0.50	**<0.001***	**<0.001***	**<0.001***
tCDR	0.46 ± 0.26	1.7 ± 1.7	3.4 ± 3.4	**<0.001***	**<0.001***	**<0.001***
HVLT	22.2 ± 4.9	17.0 ± 5.7	14.6 ± 6.0	**<0.001***	**0.003***	**<0.001***
Disease Index	11.3 ± 0.8	10.1 ± 2.1	8.2 ± 3.6	**0.001***	**0.01***	**<0.001***
fDS	11.6 ± 1.6	9.2 ± 2.7	9.0 ± 2.7	**0.006***	**<0.001***	**<0.001***
bDS	7.5 ± 3.0	4.3 ± 2.7	2.9 ± 2.0	**<0.001***	**<0.001***	**<0.001***
VFT	13.9 ± 2.2	11.2 ± 4.0	8.6 ± 3.6	**<0.001***	**<0.001***	**<0.001***
MBNT	14.5 ± 0.8	13.4 ± 1.6	13.2 ± 1.9	**0.023***	**0.002***	**0.004***
TMTA	48.6 ± 25.6	109.5 ± 85.9	132.0 ± 95.7	**0.005***	**<0.001***	**<0.001***
IMR data						
t-Tau, pg/ml	22.1 ± 3.1	25.5 ± 4.5	26.3 ± 4.5	**0.006***	**0.048***	**0.005***
p-Tau181, pg/ml	3.5 ± 0.5	3.9 ± 0.7	4.1 ± 1.0	**0.031***	0.168	**0.026***
$A\beta_{1-42}$, pg/ml	16.7 ± 0.7	17.1 ± 0.8	17.3 ± 1.0	**0.045***	0.131	**0.016***
$A\beta_{1-40}$, pg/ml	51.8 ± 5.3	51.8 ± 4.6	51.8 ± 3.9	0.961	0.908	0.876
α-synuclein, fg/ml	108 ± 78	138 ± 80	119 ± 64	0.584	0.254	0.505
$A\beta_{1-42}$ × t-Tau	370 ± 61	438 ± 92	458 ± 105	**0.007***	**0.047***	**0.008***
$A\beta_{1-42}$ × *p*-Tau181	58.1 ± 10.1	67.1 ± 13.7	71.0 ± 21.0	**0.022***	0.127	**0.021***
$A\beta_{1-42/}$ $A\beta_{1-40}$	0.32 ± 0.04	0.33 ± 0.03	0.34 ± 0.03	0.376	0.521	0.362
APOE ε4 (%)	3 (25.0)	12 (23.5)	9 (32.1)	0.521	0.797	0.651

Aβ, amyloid β; AD, Alzheimer's disease; aMCI, amnestic mild cognitive impairment; APOE, apolipoprotein E genotype; bDS, backward digit span; BMI, body mass index; CDR, Clinical Dementia Rating; fDS, forward digit span; HVLF, Hopkins Verbal Learning Test; IMR, ultra-sensitive immunomagnetic reduction; Modified Boston Naming Test (MBNT); MMSE, Mini-Mental Status Examination; na, not applicable; p-Tau181, tau phosphorylated at threonine 181; TMTA, Trail Making Test Part A; tCDR, total score of Clinical Dementia Rating; and t-Tau, total Tau.

[a] *Data are presented as frequency (percentage) or mean ± standard deviation.*

[b] *The diagnosis of AD was made according to clinical symptoms and cognitive tests not supported by postmortem examination or in vivo by biomarkers.*

Values in bold type indicates statistical significance.

showed a linear trend in the control, aMCI, and AD groups, and both the aMCI and AD groups had poorer cognitive test results than the control group. In terms of Aβ and tau biomarkers, five biomarkers showed a linear trend in the three groups, including t-Tau, *p*-Tua181, $A\beta_{1-42}$, $A\beta_{1-42}$ x t-Tau, and $A\beta_{1-42}$ x *p*-Tau181 levels. Compared with the control group, the AD group had higher levels of the above five biomarkers, and the aMCI group had higher levels of t-Tau and $A\beta_{1-42}$ x t-Tau. **Table 2** shows the plasma levels of the 29 cytokines. Among the control, aMCI, and AD groups, the MIP1β, RANTES, and PDFG-BB levels showed a linear trend. IL1RA was significantly higher in the aMCI group than the control group, and the levels of RANTES, IL-9, and PDGF-BB were significantly lower in the AD group than the control group.

Association Between Plasma Biomarkers and Cognitive Test Results

We examined whether the plasma biomarkers were associated with cognitive test results. As shown in the supplementary data (**Supplementary Tables 1–3**). Several plasma biomarkers were associated with cognitive test results in the three groups. In control group, the levels of t-Tau/$A\beta_{1-42}$ ratio, IL-4, IL-5, IL-7, IL-9, IL-13, IL-17A, eotaxin, FGF, MIP1β, PDFG-BB, RANTES, IL-23, IL-25, and sCD40L were associated with the cognitive test results. In the aMCI group, the levels of $A\beta_{1-40}$, $A\beta_{1-42}$/ $A\beta_{1-40}$ ratio, *p*-Tau/t-Tau ratio, IL-1β, IL-4, IL-8, IL-10, FGF, INFγ, IP-10, MIP1β, PDFG-BB, TNFα, IL-23, IL-31, and sCD40L were associated with the cognitive test results. In the AD group, the levels of t-Tau, $A\beta_{1-40}$, $A\beta_{1-42}$, α-Syn, t-Tau/ $A\beta_{1-42}$ ratio, $A\beta_{1-42}$/ $A\beta_{1-40}$ ratio, IL-1β, IL-2, IL-5, IL-10, FGF, GM-CSF, INFγ, MCP1, MIP1α, PDGF-BB, RANTES, IL-25, and IL-31 were associated with the cognitive test results.

Association Between Plasma Biomarkers and Annual Change in MMSE Score

We then examined the association between plasma biomarkers and annual changes in the MMSE score in the aMCI

TABLE 2 | Plasma levels of cytokines of the enrolled participants.[a]

		Control	aMCI	AD	*P* value		
	Cytokine, pg/ml	(*n* = 12)	(*n* = 51)	(*n* = 28)	P trend analysis	MCI vs. control	AD vs. control
Th1-related	IL-2	1.05 [0.91, 1.09]	1.14 [0.91, 1.56]	1.22 [0.64, 1.55]	0.447	0.165	0.258
	IFNγ	0.45 [0.42, 0.73]	0.54 [0.26, 0.70]	0.51 [0.40, 0.91]	0.943	0.861	0.627
	TNFα	5.6 [5.3, 7.0]	5.6 [4.8, 7.1]	6.1 [4.8, 8.2]		0.643	0.604
Th2-related	IL-4	0.94 [0.70, 1.14]	0.92 [0.79, 1.23]	1.05 [0.69, 1.38]	0.657	0.569	0.371
	IL-5	3.0 [1.3, 4.0]	3.2 [2.3, 4.0]	3.2 [2.3, 4.0]	0.153	0.306	0.280
	IL-6	0.30 [0.22, 0.42]	0.29 [0.20, 0.39]	0.32 [0.22, 0.49]	0.961	0.837	0.517
	IL-10	1.2 [1.0, 1.8]	0.9 [0.5, 1.5]	1.2 [0.4, 2.1]	0.979	0.438	0.925
	IL-13	0.92 [0.74, 1.31]	0.95 [0.74, 1.20]	1.00 [0.74, 1.29]	0.908	0.896	0.777
Th17-related	IL-1β	0.08 [0.07, 0.12]	0.09 [0.06, 0.13]	0.12 [0.08, 0.14]	0.536	0.699	0.168
	IL-17A	4.3 [3.1, 5.1]	4.4 [3.8, 5.1]	5.1 [3.4, 6.0]	0.195	0.540	0.149
	IL-23	5.4 [1.7, 8.9]	5.7 [3.1, 7.5]	5.2 [4.6, 8.5]	0.212	0.626	0.614
	IL-25	0.09 [0.07, 0.16]	0.06 [0.03, 0.14]	0.06 [0.04, 0.14]	0.498	0.301	0.653
	IL-31	36.1 [30.7, 43.7]	34.2 [24.1, 41.9]	34.1 [25.8, 43.5]	0.781	0.391	0.660
	sCD40L	25.5 [14.4, 34.7]	14.0 [9.3, 22.2]	12.5 [8.3, 19.7]	0.135	0.064	0.055
Chemokine	IL-8	0.90 [0.49, 1.08]	0.98 [0.66, 1.29]	1.15 [0.72, 1.33]	0.394	0.270	0.139
	IP10	569 [268, 758]	542.1 [303, 722]	379.3 [259, 568]	0.114	0.834	0.245
	MCP1	14.0 [9.0, 17.5]	11.7 [7.6, 17.1]	10.5 [6.4, 15.9]	0.190	0.558	0.362
	MIP1α	1.02 [0.82, 1.36]	1.14 [0.83, 1.33]	1.08 [0.86, 1.32]	0.698	0.739	0.615
	MIP1β	24.8 [18.1, 34.3]	18.7 [16.4, 24.3]	19.3 [16.7, 25.7]	**0.027***	0.096	0.177
	RANTES	1654 [1351, 1822]	1379 [861, 1710]	1079 [812, 1537]	**0.005***	0.146	**0.006***
	Eotaxin	43.7 [30.7, 55.4]	38.1 [29.6, 52.7]	36.4 [28.1, 53.2]	0.302	0.753	0.379
Others	IL-1RA	49.8 [39.0, 67.3]	78.8 [62.1, 103.0]	67.9 [50.5, 85.6]	0.161	**0.003***	0.118
	IL-7	7.6 [6.6, 9.3]	7.6 [6.7, 8.6]	8.2 [6.6, 10.7]	0.329	0.875	0.530
	IL-9	17.0 [16.6, 17.7]	16.4 [14.2, 18.1]	16.2 [14.6, 17.0]	0.658	0.263	**0.035***
	FGF	6.7 [6.4, 7.7]	7.3 [6.4, 9.3]	7.6 [6.9, 10.1]	0.318	0.293	0.106
	GCSF	86.2 [63.5, 106.5]	92.0 [75.4, 118.2]	91.5 [68.6, 112.7]	0.920	0.381	0.638
	GM-CSF	0.18 [0.14, 0.32]	0.28 [0.17, 0.49]	0.48 [0.14, 0.79]	0.209	0.383	0.342
	PDGF-BB	373 [192, 503]	216 [116, 355]	163 [55, 276]	**0.008***	0.052	**0.028***
	VEGF	25.4 [17.6, 36.8]	29.1 [21.8, 43.0]	33.3 [23.0, 44.4]	0.479	0.182	0.208

AD, Alzheimer's disease; aMCI, amnestic mild cognitive impairment; FGF, fibroblast growth factor; GCSF, granulocyte colony-stimulating factor; GM-CSF, granulocyte-macrophage colony-stimulating factor; IFNγ, interferon-gamma; IL, interleukin; IL-1RA, IL-1 receptor antagonist; IP10, IFNγ-induced protein 10; MCP1, monocyte chemoattractant protein 1; MIP1α, macrophage inflammatory protein 1-alpha; PDGF-BB, platelet-derived growth factor-BB; RANTES, regulated upon activation, normal T cell expressed and secreted; sCD40L, soluble CD40 ligand; Th, T helper; TNFα, tumor necrosis factor-alpha; VEGF, vascular endothelial growth factor.

[a]*Data are presented as median [25th, 75th percentile]; *P < 0.05.*

Values in bold type indicates statistical significance.

and AD groups. For both groups, there was no significant association of the Aβ and tau biomarkers with the annual change in MMSE score (**Table 3**), except for $A\beta_{1-40}$ in patients with AD ($r = -0.684$, $p = 0.042$). However, several cytokine levels were associated with annual MMSE changes. The aMCI group showed that higher baseline levels of IL-2 ($r = 0.420$, $p = 0.041$), sCD40L ($r = 0.419$, $p = 0.041$), IL-8 ($r = 0.410$, $p = 0.047$), and VEGF ($r = 0.491$, $p = 0.017$) were significantly correlated with a lower cognitive decline. In contrast, the AD group showed that the higher baseline levels of IFNγ ($r = -0.701$, $p = 0.036$), IL-5 ($r = -0.756$, $p = 0.019$), IL-17A ($r = -0.759$, $p = 0.021$), IL-25 ($r = -0.840$, $p = 0.036$), and FGF ($r = -0.780$, $p = 0.013$) were significantly correlated with more rapid cognitive decline. Interestingly, the MCI group had positive **associations** of cytokine levels with annual MMSE changes, while the AD group had negative associations of cytokine levels and annual MMSE changes.

Discriminatory Capacity of Plasma Biomarkers for Identifying Cognitive Decline

Several cytokines were correlated with annual MMSE score changes in the partial correlation analysis. We then compared these cytokines with the Aβ and tau biomarkers to assess their potential discriminatory capacity for identifying cognitive decline (a change in the annual MMSE score ≥ 2) in the aMCI (event number = 4) and the AD (event number = 4) groups. As shown in **Table 4**, none of the Aβ and tau biomarkers were able to predict cognitive decline in the aMCI and AD groups. In terms of cytokine levels, IL-2 had a satisfactory discriminatory capacity

TABLE 3 | Association of IMR data and cytokine levels with annual change in MMSE score.[a]

	Variable	aMCI		AD	
		Partial correlation	*P* value	Partial correlation	*P* value
IMR	t-Tau,	−0.067	0.757	−0.070	0.859
	$A\beta_{1-42}$	−0.039	0.858	0.024	0.952
	p-Tau181	−0.173	0.419	0.168	0.666
	$A\beta_{1-40}$	−0.173	0.409	**−0.684**	**0.042***
	α-synuclein	0.234	0.271	0.232	0.548
	$A\beta_{1-42}$ × t-Tau	−0.073	0.735	−0.109	0.781
	$A\beta_{1-42}$ × $A\beta_{1-40}$	0.127	0.554	0.419	0.261
	p-Tau × t-Tau	−0.167	0.435	0.364	0.336
Th1-related	IL-2	**0.420**	**0.041***	−0.025	0.949
	IFNγ	0.340	0.122	**−0.701**	**0.036***
	TNFα	0.185	0.387	0.194	0.617
Th2-related	IL-4	0.350	0.094	0.487	0.183
	IL-5	0.196	0.358	**−0.756**	**0.019***
	IL-6	0.205	0.349	0.112	0.811
	IL-10	−0.065	0.792	0.600	0.155
	IL-13	0.002	0.991	0.053	0.893
Th17-related	IL-1β	0.280	0.186	−0.266	0.524
	IL-17A	0.297	0.158	**−0.745**	**0.021***
	IL-23	−0.069	0.760	−0.492	0.178
	IL-25	−0.158	0.519	**−0.840**	**0.036***
	IL-31	0.264	0.213	−0.159	0.684
	sCD40L	**0.419**	**0.041***	−0.074	0.849
Chemokine	IL-8	**0.410**	**0.047***	0.460	0.213
	IP10	0.212	0.319	0.041	0.917
	MCP1	0.059	0.784	0.600	0.087
	MIP1α	0.292	0.167	−0.348	0.358
	MIP1β	−0.055	0.798	0.356	0.348
	RANTES	0.134	0.532	0.233	0.547
	Eotaxin	0.316	0.133	0.444	0.231
Others	IL-1RA	0.229	0.281	−0.201	0.603
	IL-7	0.172	0.423	0.008	0.984
	IL-9	0.111	0.606	0.098	0.801
	FGF	0.104	0.630	**−0.780**	**0.013***
	GCSF	0.321	0.126	0.261	0.497
	GM-CSF	0.386	0.139	−0.996	0.055
	PDGF-BB	0.147	0.494	0.011	0.977
	VEGF	**0.491**	**0.017***	−0.655	0.056

AD, Alzheimer's disease; aMCI; amnestic mild cognitive impairment; FGF, fibroblast growth factor; GCSF, granulocyte colony-stimulating factor; GM-CSF, granulocyte-macrophage colony-stimulating factor; IFNγ, interferon-gamma; IL, interleukin; IL-1RA, IL-1 receptor antagonist; IP10, IFNγ-induced protein 10; MCP1, monocyte chemoattractant protein 1; MIP1α, macrophage inflammatory protein 1-alpha; MMSE, Mini Mental Status Examination; PDGF-BB, platelet-derived growth factor-BB; RANTES, regulated upon activation, normal T cell expressed and secreted; sCD40L, soluble CD40 ligand; Th, T helper; TNFα, tumor necrosis factor-alpha; and VEGF, vascular endothelial growth factor.

[a]*Adjusted for age, education level, body mass index, and apolipoprotein E containing ε4.*

**P < 0.05.*

Values in bold type indicates statistical significance.

for detecting cognitive decline in the aMCI group (AUC = 85.7%, 95% CI = 69.7–100%). IL-25 had the best discriminatory capacity for identifying cognitive decline in the AD group; however, it did not reach statistical significance. The optimal cutoff was ≤ 1 pg/ml, with a sensitivity of 100% (95% CI = 39.8–100%) and specificity of 67.9% (95% CI = 47.6–84.1%). When assessing IL-2 with Aβ and tau biomarkers in the aMCI group, the combined AUC values increased to 88.4%. In contrast, when assessing IL-25 with each IMR biomarker in the AD group, all the combined AUC values were increased, but none of them were significant (**Table 4**).

Temporal Association of IL-2, Aβ, and Tau Between Controls, aMCI, and AD

Finally, we examined the temporal association in plasma IL-2, $A\beta_{1-42}$, and *p*-Tau181 levels between the three groups (**Figure 1**). We found that there was a linear trend for plasma $A\beta_{1-42}$ ($p = 0.045$) and *p*-Tau181 ($p = 0.031$) levels; however, the linear trend was not observed for plasma IL-2 levels. Indeed, the aMCI group had higher IL-2 levels (1.19 ± 0.53) than the control (0.95 ± 0.29) and AD (1.09 ± 0.62) groups, but there was no statistical significance (aMCI vs controls, $p = 0.165$; aMCI vs AD, $p = 0.460$).

DISCUSSION

This is the first clinical study to compare the discriminatory capacity of plasma cytokines versus plasma Aβ and tau biomarkers for identifying cognitive decline in patients with aMCI or AD. We found that plasma Aβ and tau biomarkers were not associated with annual changes in the MMSE score in both the aMCI and AD groups, while several plasma cytokines were associated with cognitive test results and annual changes in the MMSE score. In the aMCI group, higher baseline plasma levels of IL-2, sCD40L, and VEGF were associated with a lower cognitive decline, and in the AD group, higher baseline plasma levels of IFNγ, IL-5, IL-17A, IL-25, FGF, GM-CSF, and VEGF were associated with a more rapid cognitive decline. Among these plasma cytokines, plasma levels of IL-2 showed satisfactory discriminatory potential to identify cognitive decline in the aMCI group, and the AUC values were slightly increased when combining plasma levels of IL-2 with plasma levels of Aβ and tau biomarkers; however, in the AD group, all the investigated plasma cytokines did not reach significance for identifying cognitive decline. Briefly, our study suggests that initial plasma levels of several cytokines were associated with subsequent annual MMSE changes in patients with aMCI or AD, and that plasma levels of IL-2 may be a potential biomarker to detect rapid cognitive decline in the aMCI group.

In addition to Aβ plaques and neurofibrillary tangles, neuroinflammation in the central nervous system (CNS) has been suggested to play a key role in the pathology of AD (Heneka et al., 2015; Heppner et al., 2015). The CNS-intrinsic factors or systemic influences can induce neuroinflammatory responses in the brain, and activation of microglia and astroglia triggers an innate immune response characterized by the release of inflammatory mediators, including cytokines (Heneka et al., 2015; Heppner et al., 2015). This neuroinflammation contributes to disease progression and severity, and sufficiently drives the

TABLE 4 | Diagnostic utility of IMR data and cytokine levels for identifying cognitive decline (annual decline in MMSE score ≥ 2) in the aMCI and AD groups.

	Parameter	AUC, % (95% CI)	
		aMCI	AD
IMR data	t-Tau,	56.3 (22.4–90.1)	52.8 (16.8–88.7)
	$A\beta_{1-42}$	66.1 (28.4–100.0)	55.6 (12.9–98.2)
	p-Tau181	66.1 (42.3–89.9)	55.6 (14.8–96.3)
	$A\beta_{1-40}$	64.3 (26.3–100.0)	52.8 (10.0–84.4)
	α-synuclein	66.1 (42.9–89.2)	52.8 (5.7–88.7)
	$A\beta_{1-42}$ × t-Tau	46.4 (19.5–73.4)	52.8 (11.3–83.2)
	$A\beta_{1-42}$ × $A\beta_{1-40}$	69.6 (42.2–97.1)	50.0 (9.8–90.2)
	p-Tau × t-Tau	58.0 (33.1–83.0)	52.8 (11.1–94.5)
Cytokine	IL-2	**85.7 (69.7–100.0)*[a]**	50.0 (2.9–97.1)
	IFNγ	43.8 (23.0–64.5)	29.2 (0.0–76.4)
	IL-5	71.9 (38.5–100.0)	41.7 (0.0–91.3)
	IL-17A	67.9 (42.5–93.2)	44.4 (0.0–91.9)
	IL-25	53.6 (16.9–90.3)	73.6 (44.3–100.0)
	sCD40L	67.9 (34.9–100.0)	66.7 (33.7–99.6)
	FGF	62.5 (33.9–91.1)	66.7 (28.6–100.0)
	IL-8	69.1 (33.7–100.0)	73.6 (31.3–100.0)
	VEGF	67.4 (41.1–93.7)	43.1 (0.0–86.9)
Combined		IL-2 + IMR data	IL-25 + IMR data
	t-Tau	**88.4 (74.2–100.0)***	69.4 (37.5–100.0)
	$A\beta_{1-42}$	**85.7 (69.7–100.0)***	72.2 (33.9–100.0)
	p-Tau181	**84.8 (68.6–100.0)***	61.1 (18.4–100.0)
	$A\beta_{1-40}$	**86.6 (69.4–100.0)***	75.0 (46.5–100.0)
	α-synuclein	**88.4 (76.1–100.0)***	63.9 (19.3–100.0)
	$A\beta_{1-42}$ × t-Tau	**88.4 (75.3–100.0)***	72.2 (41.7–100.0)
	$A\beta_{1-42}$ × $A\beta_{1-40}$	**87.5 (71.8–100.0)***	72.2 (38.7–100.0)
	p-Tau × t-Tau	**87.5 (72.5–100.0)***	55.6 (4.1–100.0)

Aβ, amyloid β; AD, Alzheimer's disease; aMCI, amnestic mild cognitive impairment; AUC, area under the curve; FGF, fibroblast growth factor; CI, confidence interval; GM-CSF, granulocyte-macrophage colony-stimulating factor; IFNγ; interferon-gamma; IL, interleukin; IMR, ultra-sensitive immunomagnetic reduction; MMSE, Mini-Mental Status Examination; p-Tau181, tau phosphorylated at threonine 181; sCD40L, soluble CD40 ligand; Th helper; t-Tau, total Tau; and VEGF, vascular endothelial growth factor.

[a] The optimal cutoff was ≤ 1 pg/ml with a sensitivity of 100% (39.8–100%) and specificity of 67.9% (47.6–84.1%).

**P < 0.05.*

Values in bold type indicates statistical significance.

AD pathology. Our study found that higher baseline plasma levels of IL-2 were associated with a lower cognitive decline, and that plasma levels of IL-2 had a satisfactory discriminatory ability to detect cognitive decline in the aMCI group. Evidence suggests that IL-2 is involved in CNS development, normal brain physiology, and homeostatic repair mechanisms (Petitto et al., 2012). IL-2-knockout mice display impaired learning and memory reminiscent of AD as well as cytoarchitectural modifications and a reduced concentration of brain-derived neurotropic factor in the hippocampus (Petitto et al., 1999, 2012; Beck et al., 2005). An animal study found that peripheral low-dose IL-2 treatment could restore cognition in a mouse model of AD (Dansokho et al., 2016). Another animal study reported that low-dose IL-2 treatment improved the amyloid pathology, synaptic failure, and memory function in AD mice (Alves et al., 2017). The beneficial effects of IL-2 may be associated with amplification of regulatory T cells without a significant impact on conventional effector T cells and other immune effectors (Dansokho et al., 2016; Alves et al., 2017). In our study, patients with aMCI who had higher plasma levels of IL-2 may have more neuroprotective effects than those with lower plasma levels of IL-2, and these patients may thus have lesser cognitive decline.

In our study, the plasma levels of Aβ and tau biomarkers did not correlate with cognitive decline. Evidence suggests that the Aβ accumulation and tau-mediated neuronal injury and dysfunction precede clinical symptoms of aMCI and AD, and that substantial Aβ-plaque deposition alone may have no immediate effects on cognitive function (Petersen et al., 2009; Jack et al., 2013). The Aβ biomarkers plateau in the stage of aMCI and AD; therefore, cognitive decline does not significantly correlate with the rate of $A\beta_{1-42}$ accumulation in the CSF. Moreover, this demanding process is mediated by individual differences in brain resiliency, cognitive reserve, and comorbid pathological brain changes (Jack et al., 2013). The heterogeneous clinical presentation and pathological patterns of AD might also explain the non-linear relationship of tau biomarkers with cognitive impairment at the stage of aMCI and AD (Tatsuoka et al., 2013). For example, a recent neuroimaging study reported that patients with AD could be clustered into three subtypes with distinct topographical features of cortical atrophy and tau deposition (Jeon et al., 2019). Another study used multiple biomarkers (e.g., hippocampal volume, PET amyloid deposition, and CSF tau protein) and suggest that the neurobiological processes both act independently and interact in a nonlinear fashion during progression from aMCI to AD (Popescu et al., 2020).

For the control, aMC, and AD groups, we find a linear trend for plasma levels of $A\beta_{1-42}$ and *p*-Tau181; however, the linear trend was not observed for plasma levels of IL-2. The aMCI group had higher plasma levels of IL-2 than those of the control and AD groups, while they were not statistically significant. The mechanisms for the above study findings might be related to the beneficial role of IL-2 for AD pathology (Dansokho et al., 2016;

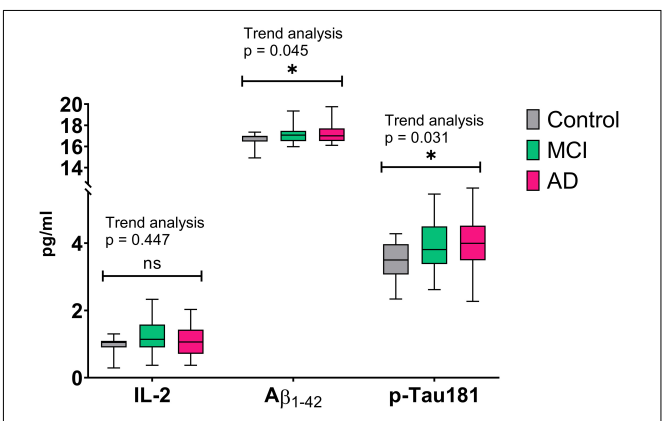

FIGURE 1 | Temporal association of plasma biomarkers between controls, aMCI, and AD groups. Aβ, amyloid β; AD, Alzheimer's disease; aMCI, amnestic mild cognitive impairment; IL, interleukin; ns, not statistically significant. *Indicates statistical significance.

Alves et al., 2017). In the aMCI group, higher plasma levels of IL-2 were associated with a lower cognitive decline. Therefore, the aMCI group with lower plasma levels of IL-2 might have higher risk of developing AD than those with higher plasma levels of IL-2. This might explain why the AD group might have lower plasma levels of IL-2 than the aMCI group. This finding warrants future large-scale studies into the association between IL-2 levels and AD conversion.

For Aβ measurement, our study used IMR assay which is quite different from the immunoprecipitation-mass spectrometry (IP-MS) and the single-molecule array (SIMOA) assays. The IMR assay quantifies the concentrations of analytes in a sample by measuring the percentage magnetic signal reduction after immunocomplex formation at the surface of magnetic nanobeads, and the magnetic signals are detected by a powerful magnetic sensor called a superconducting quantum interference device (Lue et al., 2019). The IP-MS assay quantifies Aβ-related peptides of different mass in mass spectrometry after they have been isolated and enriched from abundant plasma proteins by immunoprecipitation using the specific affinity of an antibody (Nakamura et al., 2018). The SIMOA assay is based on the use of capture antibodies coupled to paramagnetic beads and biotinylated detection antibodies, which in turn are detected by the action of a reporter enzyme: streptavidin β-galactosidase and resorufin β-D-galactopyranoside as the fluorescence substrate (Lue et al., 2019). For *p*-Tau181, the IMR assay differs from the SIMOA assay (Karikari et al., 2020, 2021) and the Meso Scale Discovery platform (Mielke et al., 2018). Importantly, the lower limit of quantification varies across different analytic methods. For example, in the current study using IMR assay, the lower limit of quantification of *p*-Tau181 was 0.0196 pg/ml; however, the lower limit of quantification of *p*-Tau181 was 0.5 pg/ml in SIMOA assay (Karikari et al., 2020). Therefore, our results may be affected by analytic differences and need to be validated for cross-method comparisons.

Our study has limitations that need to be considered when interpreting the results. First, the NIA-AA research framework defines AD as a biological construct rather than a clinical syndrome, and the diagnosis of AD focuses on Aβ deposition, pathologic tau, and neurodegeneration (Jack et al., 2018). Our study population was limited to patients who were clinically assessed and had positive findings on cognitive tests. We could not obtain CSF biomarkers and amyloid or tau positron emission tomography scans to define and stage the disease cross its entire spectrum as suggested by NIA-AA 2018 (Jack et al., 2018). Second, because of the absence of a transporter to the brain, IL-2 access into the brain is limited (Banks et al., 2004). Therefore, the correlation between peripheral levels of IL-2 and annual cognitive change may not be generalizable to the correlation between central levels of IL-2 and annual cognitive change. Third, cognitive decline is closely coupled with neurodegenerative biomarkers, such as hippocampal atrophy (Jack et al., 2013). The association between IL-2 and neurodegenerative biomarkers remains to be determined. Fourth, since the participants were recruited at a memory clinic, the findings of our study may not be generalizable to other study populations, such as community-dwelling elderly people. Fifth, our sample size was small. The low sample size in the control and ADD groups could bias the analysis because of overfitting due to low number of events per variable in the model therefore. Besides, the statistical power may also be decreased.

This is the first study to compare the discriminatory ability of identifying cognitive decline between cytokines, Aβ, and tau biomarkers in patients with aMCI and AD. We found that Aβ and tau biomarkers did not significantly predict annual cognitive change in both patients with aMCI and AD. Several cytokines were significantly associated with cognitive test results and annual cognitive change in patients with aMCI and AD. Plasma IL-2 levels had a satisfactory discriminating ability to detect cognitive decline in the aMCI group, and the discriminating potential was slightly increased when combined with Aβ and tau biomarkers. However, different inflammatory mechanisms might be responsible for different phases of neuroinflammation in aMCI and AD. Our study findings need to be replicated in future large longitudinal studies.

DATA AVAILABILITY STATEMENT

The raw data supporting the conclusions of this article will be made available by the authors, without undue reservation.

ETHICS STATEMENT

The studies involving human participants were reviewed and approved by the Institutional Review Board for the Protection of Human Subjects at the Tri-Service General Hospital (TSGHIRB 1-107-05-111). Written informed consent was obtained from all participants in the study.

AUTHOR CONTRIBUTIONS

C-SL managed the literature review, conducted the statistical analyses, interpreted the results, and wrote the first draft of the manuscript. C-LT played a major role in the acquisition of data and revised the manuscript for intellectual content. G-YL, C-SC, T-CY, H-TC, and M-WS interpreted the data and revised the manuscript for intellectual content. J-TL designed the study and provided conceptualization and theory used to integrate the findings, and edited the manuscript. Y-KL and C-KT interpreted the results and provided feedback and comments on the various versions of the manuscript. Y-FS provided the conceptualization and theory used to integrate the findings and edited the manuscript. F-CY designed the study, directed the data collection, provided the overall scientific supervision, interpreted the results, and edited the manuscript. All authors read and approved the final manuscript.

FUNDING

This study was supported by grants from the Ministry of Science and Technology of Taiwan (MOST 108-2314-B-016-023 and

MOST 108-2314-B-016-020), Tri-Service General Hospital (TSGH-C108-100, TSGH-C108-216, TSGH-D-109-101, TSGH-D-109-185, and TSGH-D-110048), and Beitou Branch, Tri-Service General Hospital (TSGH-BT-108-01).

ACKNOWLEDGMENTS

We thank Shieh-Yueh Yang at MagQu Co., Ltd. and MagQu LLC for assistance with the assays for plasma biomarkers and Ruei-Yi Chao for performing neuropsychological assessments during the study period. The study was conducted using resources from Taiwan Biobank and Biobank, Tri-Service General Hospital.one.

SUPPLEMENTARY MATERIAL

The Supplementary Material for this article can be found online at: https://www.frontiersin.org/articles/10.3389/fnagi.2021.670115/full#supplementary-material

REFERENCES

Albert, M. S., Dekosky, S. T., Dickson, D., Dubois, B., Feldman, H. H., Fox, N. C., et al. (2011). The diagnosis of mild cognitive impairment due to Alzheimer's disease: recommendations from the National Institute on Aging-Alzheimer's Association workgroups on diagnostic guidelines for Alzheimer's disease. *Alzheimers Dement* 7, 270–279.

Alves, S., Churlaud, G., Audrain, M., Michaelsen-Preusse, K., Fol, R., Souchet, B., et al. (2017). Interleukin-2 improves amyloid pathology, synaptic failure and memory in Alzheimer's disease mice. *Brain* 140, 826–842.

Banks, W. A., Niehoff, M. L., and Zalcman, S. S. (2004). Permeability of the mouse blood-brain barrier to murine interleukin-2: predominance of a saturable efflux system. *Brain Behav. Immun.* 18, 434–442. doi: 10.1016/j.bbi.2003.09.013

Beck, R. D. Jr., King, M. A., Ha, G. K., Cushman, J. D., Huang, Z., and Petitto, J. M. (2005). IL-2 deficiency results in altered septal and hippocampal cytoarchitecture: relation to development and neurotrophins. *J. Neuroimmunol.* 160, 146–153. doi: 10.1016/j.jneuroim.2004.11.006

Bradburn, S., Sarginson, J., and Murgatroyd, C. A. (2017). Association of peripheral interleukin-6 with global cognitive decline in non-demented adults: a meta-analysis of prospective studies. *Front. Aging Neurosci.* 9:438. doi: 10.3389/fnagi.2017.00438

Dansokho, C., Ait Ahmed, D., Aid, S., Toly-Ndour, C., Chaigneau, T., Calle, V., et al. (2016). Regulatory T cells delay disease progression in Alzheimer-like pathology. *Brain* 139, 1237–1251. doi: 10.1093/brain/awv408

Heneka, M. T., Carson, M. J., El Khoury, J., Landreth, G. E., Brosseron, F., Feinstein, D. L., et al. (2015). Neuroinflammation in Alzheimer's disease. *Lancet Neurol.* 14, 388–405.

Heppner, F. L., Ransohoff, R. M., and Becher, B. (2015). Immune attack: the role of inflammation in Alzheimer disease. *Nat. Rev. Neurosci.* 16, 358–372. doi: 10.1038/nrn3880

Ho, P. S., Yeh, Y. W., Huang, S. Y., and Liang, C. S. (2015). A shift toward T helper 2 responses and an increase in modulators of innate immunity in depressed patients treated with escitalopram. *Psychoneuroendocrinology* 53, 246–255. doi: 10.1016/j.psyneuen.2015.01.008

Ho, P. S., Yen, C. H., Chen, C. Y., Huang, S. Y., and Liang, C. S. (2017). Changes in cytokine and chemokine expression distinguish dysthymic disorder from major depression and healthy controls. *Psychiatry Res.* 248, 20–27. doi: 10.1016/j.psychres.2016.12.014

Hogervorst, E., Xin, X., Rahardjo, T., and Shifu, X. (2014). The Hopkins Verbal Learning Test and detection of MCI and mild dementia: a literature review. *J. Alzheimers Dis. Parkinsonism* 4:166. doi: 10.4172/2161-0460.1000166

Jack, C. R. Jr., Bennett, D. A., Blennow, K., Carrillo, M. C., Dunn, B., Haeberlein, S. B., et al. (2018). NIA-AA Research Framework: toward a biological definition of Alzheimer's disease. *Alzheimers Dement* 14, 535–562. doi: 10.1016/j.jalz.2018.02.018

Jack, C. R. Jr., Knopman, D. S., Jagust, W. J., Petersen, R. C., Weiner, M. W., Aisen, P. S., et al. (2013). Tracking pathophysiological processes in Alzheimer's disease: an updated hypothetical model of dynamic biomarkers. *Lancet Neurol.* 12, 207–216. doi: 10.1016/s1474-4422(12)70291-0

Jeon, S., Kang, J. M., Seo, S., Jeong, H. J., Funck, T., Lee, S. Y., et al. (2019). Topographical heterogeneity of Alzheimer's Disease based on MR Imaging, Tau PET, and Amyloid PET. *Front. Aging Neurosci.* 11:211. doi: 10.3389/fnagi.2019.00211

Karikari, T. K., Benedet, A. L., Ashton, N. J., Lantero Rodriguez, J., Snellman, A., Suárez-Calvet, M., et al. (2021). Diagnostic performance and prediction of clinical progression of plasma phospho-tau181 in the Alzheimer's Disease Neuroimaging Initiative. *Mol. Psychiatry* 2021, 429–442. doi: 10.1038/s41380-020-00923-z

Karikari, T. K., Pascoal, T. A., Ashton, N. J., Janelidze, S., Benedet, A. L., Rodriguez, J. L., et al. (2020). Blood phosphorylated tau 181 as a biomarker for Alzheimer's disease: a diagnostic performance and prediction modelling study using data from four prospective cohorts. *Lancet Neurol.* 19, 422–433. doi: 10.1016/s1474-4422(20)30071-5

King, E., O'brien, J. T., Donaghy, P., Morris, C., Barnett, N., Olsen, K., et al. (2018). Peripheral inflammation in prodromal Alzheimer's and Lewy body dementias. *J. Neurol. Neurosurg. Psychiatry* 89, 339–345. doi: 10.1136/jnnp-2017-317134

Langa, K. M., and Levine, D. A. (2014). The diagnosis and management of mild cognitive impairment: a clinical review. *JAMA* 312, 2551–2561. doi: 10.1001/jama.2014.13806

Liang, C. S., Su, K. P., Tsai, C. L., Lee, J. T., Chu, C. S., Yeh, T. C., et al. (2020). The role of interleukin-33 in patients with mild cognitive impairment and Alzheimer's disease. *Alzheimers Res. Ther.* 12:86.

Lue, L. F., Kuo, Y. M., and Sabbagh, M. (2019). Advance in plasma AD Core biomarker development: current findings from immunomagnetic reduction-based SQUID technology. *Neurol. Ther.* 8, 95–111. doi: 10.1007/s40120-019-00167-2

McKhann, G. M., Knopman, D. S., Chertkow, H., Hyman, B. T., Jack, C. R. Jr., Kawas, C. H., et al. (2011). The diagnosis of dementia due to Alzheimer's disease: recommendations from the National Institute on Aging-Alzheimer's Association workgroups on diagnostic guidelines for Alzheimer's disease. *Alzheimers Dement* 7, 263–269.

Mielke, M. M., Hagen, C. E., Xu, J., Chai, X., Vemuri, P., Lowe, V. J., et al. (2018). Plasma phospho-tau181 increases with Alzheimer's disease clinical severity and is associated with tau- and amyloid-positron emission tomography. *Alzheimers Dement* 14, 989–997. doi: 10.1016/j.jalz.2018.02.013

Mitchell, A. J., and Shiri-Feshki, M. (2009). Rate of progression of mild cognitive impairment to dementia–meta-analysis of 41 robust inception cohort studies. *Acta Psychiatr. Scand* 119, 252–265. doi: 10.1111/j.1600-0447.2008.01326.x

Morgan, A. R., Touchard, S., Leckey, C., O'hagan, C., Nevado-Holgado, A. J., Consortium, N., et al. (2019). Inflammatory biomarkers in Alzheimer's disease plasma. *Alzheimers Dement* 15, 776–787.

Moscoso, A., Grothe, M. J., Ashton, N. J., Karikari, T. K., Lantero Rodriguez, J., Snellman, A., et al. (2021). Longitudinal Associations of Blood Phosphorylated Tau181 and Neurofilament Light Chain With Neurodegeneration in Alzheimer Disease. *JAMA Neurol.* 78, 396–406.

Nakamura, A., Kaneko, N., Villemagne, V. L., Kato, T., Doecke, J., Dore, V., et al. (2018). High performance plasma amyloid-beta biomarkers for Alzheimer's disease. *Nature* 554, 249–254.

Petersen, R. C. (2011). Clinical practice. Mild cognitive impairment. *N. Engl. J. Med.* 364, 2227–2234.

Petersen, R. C., Roberts, R. O., Knopman, D. S., Boeve, B. F., Geda, Y. E., Ivnik, R. J., et al. (2009). Mild cognitive impairment: ten years later. *Arch. Neurol.* 66, 1447–1455.

Petitto, J. M., Mcnamara, R. K., Gendreau, P. L., Huang, Z., and Jackson, A. J. (1999). Impaired learning and memory and altered hippocampal neurodevelopment resulting from interleukin-2 gene deletion. *J. Neurosci. Res.*

56, 441–446. doi: 10.1002/(sici)1097-4547(19990515)56:4<441::aid-jnr11>3.0.co;2-g

Petitto, J. M., Meola, D., and Huang, Z. (2012). Interleukin-2 and the brain: dissecting central versus peripheral contributions using unique mouse models. *Methods Mol. Biol.* 934, 301–311. doi: 10.1007/978-1-62703-071-7_15

Popescu, S. G., Whittington, A., Gunn, R. N., Matthews, P. M., Glocker, B., Sharp, D. J., et al. (2020). Nonlinear biomarker interactions in conversion from mild cognitive impairment to Alzheimer's disease. *Hum. Brain Mapp.* 41, 4406–4418. doi: 10.1002/hbm.25133

Shen, X. N., Niu, L. D., Wang, Y. J., Cao, X. P., Liu, Q., Tan, L., et al. (2019). Inflammatory markers in Alzheimer's disease and mild cognitive impairment: a meta-analysis and systematic review of 170 studies. *J. Neurol. Neurosurg. Psychiatry* 90, 590–598. doi: 10.1136/jnnp-2018-319148

Tatsuoka, C., Tseng, H., Jaeger, J., Varadi, F., Smith, M. A., Yamada, T., et al. (2013). Modeling the heterogeneity in risk of progression to Alzheimer's disease across cognitive profiles in mild cognitive impairment. *Alzheimers Res. Ther.* 5:14. doi: 10.1186/alzrt168

Tsai, C. L., Liang, C. S., Lee, J. T., Su, M. W., Lin, C. C., Chu, H. T., et al. (2019). Associations between plasma biomarkers and cognition in patients with Alzheimer's Disease and amnestic mild cognitive impairment: a cross-sectional and longitudinal study. *J. Clin. Med.* 8:1893. doi: 10.3390/jcm8111893

Tsai, C. L., Liang, C. S., Yang, C. P., Lee, J. T., Ho, T. H., Su, M. W., et al. (2020). Indicators of rapid cognitive decline in amnestic mild cognitive impairment: the role of plasma biomarkers using magnetically labeled immunoassays. *J. Psychiatr. Res.* 129, 66–72. doi: 10.1016/j.jpsychires.2020.06.006

Conflict of Interest: The authors declare that the research was conducted in the absence of any commercial or financial relationships that could be construed as a potential conflict of interest.

frontiers in Aging Neuroscience

ORIGINAL RESEARCH
published: 28 May 2021
doi: 10.3389/fnagi.2021.657794

The Role of Plasma Neurofilament Light Protein for Assessing Cognitive Impairment in Patients With End-Stage Renal Disease

Yi-Chou Hou[1,2,3], Chuen-Lin Huang[4,5], Chien-Lin Lu[3,6], Cai-Mei Zheng[7,8,9], Yuh-Feng Lin[1,7,8,9,10], Kuo-Cheng Lu[11], Ya-Lin Chung[12] and Ruei-Ming Chen[13,14,15]**

[1] Graduate Institute of Clinical Medicine, College of Medicine, Taipei Medical University, Taipei, Taiwan, [2] Department of Internal Medicine, Cardinal Tien Hospital, New Taipei City, Taiwan, [3] School of Medicine, Fu Jen Catholic University, New Taipei City, Taiwan, [4] Department of Medical Research, Cardinal Tien Hospital, New Taipei City, Taiwan, [5] Department of Physiology and Biophysics, National Defense Medical Center, Graduate Institute of Physiology, Taipei, Taiwan, [6] Department of Nephrology, Fu Jen Catholic University Hospital, New Taipei City, Taiwan, [7] Division of Nephrology, Department of Internal Medicine, Taipei Medical University Shuang Ho Hospital, New Taipei City, Taiwan, [8] Division of Nephrology, Department of Internal Medicine, School of Medicine, College of Medicine, Taipei Medical University, Taipei, Taiwan, [9] Taipei Medical University-Research Center of Urology and Kidney, Taipei Medical University, Taipei, Taiwan, [10] National Defense Medical Center, Graduate Institute of Medical Sciences, Taipei, Taiwan, [11] Department of Nephrology, Taipei Tzu Chi Hospital, Buddhist Tzu Chi Medical Foundation, New Taipei City, Taiwan, [12] Department of Medical Laboratory, Cardinal-Tien Hospital, New Taipei City, Taiwan, [13] TMU Research Center of Cancer Translational Medicine, Graduate Institute of Medical Sciences, College of Medicine, Taipei Medical University, Taipei, Taiwan, [14] Cell Physiology and Molecular Image Research Center, Wan Fang Hospital, Taipei Medical University, Taipei, Taiwan, [15] Anesthesiology and Health Policy Research Center, Taipei Medical University Hospital, Taipei, Taiwan

OPEN ACCESS

Edited by:
Thomas K. Karikari,
University of Gothenburg, Sweden

Reviewed by:
Samir Abu-Rumeileh,
Ulm University Medical Center, Germany
Anniina Snellman,
University of Gothenburg, Sweden

***Correspondence:**
Kuo-Cheng Lu
kuochenglu@gmail.com
Ruei-Ming Chen
rmchen@tmu.edu.tw

Received: 24 January 2021
Accepted: 03 May 2021
Published: 28 May 2021

Citation:
Hou Y-C, Huang C-L, Lu C-L, Zheng C-M, Lin Y-F, Lu K-C, Chung Y-L and Chen R-M (2021) The Role of Plasma Neurofilament Light Protein for Assessing Cognitive Impairment in Patients With End-Stage Renal Disease. Front. Aging Neurosci. 13:657794. doi: 10.3389/fnagi.2021.657794

Introduction: End-stage renal disease (ESRD) is defined as the irreversible loss of renal function, necessitating renal replacement therapy. Patients with ESRD tend to have more risk factors for cognitive impairment than the general population, including hypertension, accumulative uremic toxin, anemia, and old age. The association between these risk factors and the pathologic protein was lacking. Blood-based assays for detecting pathologic protein, such as amyloid beta (Aβ), total tau protein, and neurofilament light chain (NfL), have the advantages of being less invasive and more cost-effective for diagnosing patients with cognitive impairment. The aim of the study is to validate if the common neurologic biomarkers were different in ESRD patients and to differentiate if the specific biomarkers could correlate with specific correctable risk factors.

Methods: In total, 67 participants aged >45 years were enrolled. The definition of ESRD was receiving maintenance hemodialysis for >3 months. Cognitive impairment was defined as a Mini-Mental State Examination score of <24. The participants were divided into groups for ESRD with and without cognitive impairment. The blood-based biomarkers (tau protein, Aβ1/40, Aβ1/42, and NfL) were analyzed through immunomagnetic reduction assay. Other biochemical and hematologic data were obtained simultaneously.

Summary of results: The study enrolled 43 patients with ESRD who did not have cognitive impairment and 24 patients with ESRD who had cognitive impairment

[Mini-Mental State Examination (MMSE): 27.60 ± 1.80 vs. 16.84 ± 6.40, $p < 0.05$]. Among the blood-based biomarkers, NfL was marginally higher in the ESRD with cognitive impairment group than in the ESRD without cognitive impairment group (10.41 ± 3.26 vs. 8.74 ± 2.81 pg/mL, $p = 0.037$). The concentrations of tau protein, amyloid β 1/42, and amyloid β 1/40 ($p = 0.504$, 0.393, and 0.952, respectively) were similar between the two groups. The area under the curve of NfL to distinguish cognitively impaired and unimpaired ESRD patients was 0.687 (95% confidence interval: 0.548–0.825, $p = 0.034$). There was no correlation between the concentration of NfL and MMSE among total population ($r = -0.153$, $p = 0.277$), patients with ($r = 0.137$, $p = 0.583$) or without cognitive impairment ($r = 0.155$, $p = 0.333$).

Conclusion: Patients with ESRD who had cognitive impairment had marginally higher plasma NfL concentrations. NfL concentration was not correlated with the biochemical parameters, total MMSE among total population or individual groups with or without cognitive impairment. The concentrations of Aβ1/40, Aβ1/42, and tau were similar between the groups.

Keywords: cognitive impairment, dementia, ESRD, neurofilament light chain, amyloid beta, tau

INTRODUCTION

Chronic kidney disease (CKD) is defined as the progressive loss of glomerular infiltration. CKD etiologies include diabetes mellitus, hypertension, dyslipidemia, hereditary kidney diseases such as polycystic kidney disease, and chronic exposure to nephrotoxic agents such as non-steroidal anti-inflammatory drugs. The progressive loss of glomerular filtration rate (GFR) induces multiple comorbidities, such as fluid retention, electrolyte imbalance, vitamin D deficiency, renal anemia mediated through insufficient erythropoietin (EPO) production by the kidney, and uremic toxin accumulation (Inker et al., 2014). The aforementioned comorbidities dysregulate the homeostasis of various organs and contribute to multiple disorders, such as vascular calcification, left ventricular hypertrophy, renal osteodystrophy, immune dysfunction, sarcopenia, and ischemic stroke (Li et al., 2015; Hou et al., 2017; Cherng et al., 2018). Renal replacement therapy, including hemodialysis, peritoneal dialysis, and kidney transplantation, was developed to remove excessive body fluid and uremic toxins to restore the homeostasis of the body in patients with end-stage renal disease (ESRD) (Mendu and Weiner, 2020). However, renal placement therapy also leads to several complications, such as immune dysregulation, malnutrition, arterial stiffness (Maraj et al., 2018), and insufficient toxin clearance because of the modality of renal replacement therapy and residual renal function preservation (van Gelder et al., 2020).

Clinically, cognitive impairment is recognized as progressive decline of cognitive, behavioral and sensorimotor function, which would therefore impair the memory and activity of daily life (Geda, 2012). Memory loss influences independent daily activities and further causes psychological stress and depressive mood. The screening for cognitive impairment is mostly based on psychiatric scales such as the Mini-Mental State Examination (MMSE), clinical dementia rating, and Montreal Cognitive Assessment (MoCA) (Malek-Ahmadi et al., 2014). The etiologies of cognitive impairment or dementia can be divided into vascular cognitive impairment, neurodegenerative disorders associated with the prion-like spreading, deposition of misfolded proteins (such as amyloid-beta, alfa-synuclein, hyperphosphorylated tau, transactive response DNA-binding protein 43 (TDP-43) or Lewy body) or frontotemporal dementia (Soto and Satani, 2011; Twohig and Nielsen, 2019; D'errico and Meyer-Luehmann, 2020; Hall et al., 2020; Jo et al., 2020). Cognitive impairment/dementia is commonly observed in patients with CKD. The incidence of cognitive impairment among patients with ESRD was reported to be 10–40%, which is higher than that among the general population (Drew et al., 2019). A study based on the National Health Insurance research database in Taiwan showed that the incidence of dementia was higher among patients with ESRD among in those without ESRD (Kuo et al., 2019). Patients with CKD tend to have more risk factors for dementia than members of the general population, including hypertension, diabetes mellitus, old age, and dyslipidemia (Chen et al., 2017b). In patients with CKD, the brain parenchyma may be injured, which induces vascular cognitive impairment because of insufficient blood flow due to ischemia, anemia associated with insufficient EPO (Hung et al., 2019), and intradialytic cerebral ischemia (MacEwen et al., 2017). Additionally, brain parenchymal cells might be damaged directly by uremic toxins, which could diffuse across the blood–brain barrier (e.g., indoxyl sulfate; Lin et al., 2019). Cohort studies have shown that plasma Aβ is associated with Alzheimer's disease (Lue et al., 2017). From the cohort studies for CKD patients, the plasma concentration of pathologic protein for cognitive impairment, such as Aβ,

Abbreviations: Aβ, amyloid beta; AUC, area under the curve; CKD, chronic kidney disease; CSF, cerebrospinal fluid; CI, confidence interval; EPO, erythropoietin; ESRD, end-stage renal disease; GFR, glomerular filtration rate; IMR, immunomagnetic reduction; MMSE, Mini-Mental State Exam; MoCA, Montreal Cognitive Assessment; NfL, neurofilament light chain; ROC curve, receiver operating characteristic curve.

was negatively correlated with the glomerular filtration rates (Gronewold et al., 2016), and the Aβ concentration was higher in the CKD patients with cognitive impairment than CKD patients without cognitive impairment (Vinothkumar et al., 2017). In patients with CKD, cognitive impairment is prevalent and cognitive impairment severity influences clinical outcomes; therefore, identifying a biomarker for the early detection of cognitive disorders and prediction of cognitive impairment severity is important.

For the early detection of cognitive impairment, biomarkers have been developed in different fields, including neuropsychological tests, neuroimaging, or biomarker detection in cerebrospinal fluid (CSF). Amyloid-beta peptides such as Aβ42 and Aβ40, and phosphorylated tau in CSF are well-validated biomarkers for the diagnosis of AD in clinical routine. In this regard several studies showed good correlations between the CSF biomarker levels and the correspondent neuropathological changes in AD brains (Tapiola et al., 2009; Lue et al., 2017; Baiardi et al., 2019). Neurofilament light chain (NfL), which is the main component of the cytoskeleton of myelinated neuron axons, is released from the damaged axons. NfL expression reflects subcortical neuronal damage and white matter damage (Gaetani et al., 2019). NfL in CSF increases in neurodegenerative diseases, such as Alzheimer disease, frontotemporal dementia, vascular dementia and even human-immunodeficiency virus associated cognitive impairment (Abu-Rumeileh et al., 2018; Anderson et al., 2018; Chatterjee et al., 2019; Martin et al., 2019). Akamine et al. (2020) demonstrated that the concentration of NfL increased along with the serum creatinine. The NfL is sensitive to detect the neuroaxonal damage, but it is not highly specific as overlapping levels exist among different neurodegenerative diseases except amyotrophic lateral sclerosis (Jeppsson et al., 2019; Verde et al., 2019; Gaetani et al., 2019). The report from Mattsson et al. (2017) demonstrated that the concentration of NfL in plasma was associated with severity of cognitive impairment. Plasma NfL was also associated also with other relevant variables such as neuroradiological markers of neurodegeneration, disease severity and survival in other neurodegenerative diseases such as frontotemporal dementia, Parkinson disease and prion disease (Lin et al., 2018; Abu-Rumeileh et al., 2020; Benussi et al., 2020; Spotorno et al., 2020). Moreover, plasma NfL was elevated in animal models of neurodegenerative disorders such as AD or Parkinson's disease (Loeffler et al., 2020). In the CSF of AD patients, the concentrations of pathologic proteins in CSF were sub-ng/mL or several ng/mL; their measured concentration in the blood might be as low as the pg/mL range (Yang et al., 2017). Therefore, ultrasensitive techniques should be applied, such as immunomagnetic reduction (IMR), for detecting them (Yang et al., 2017). In this cohort, we used IMR instead of enzyme-linked immunoassay (ELISA) or other methods. IMR involves the use of magnetic beads to pull down target molecules for increased sensitivity and specificity.

The aim of the study is to validate if the common neurologic biomarkers, such as Aβ, tau protein, and NfL, could differentiate the cognitive impairment in ESRD patients by immunomagnetic reduction. Besides, we would like to correlate the neurologic biomarkers with other clinical parameters in order to search for correctable risk factors for cognitive impairment in ESRD patients.

MATERIALS AND METHODS

Study Subjects

This study was conducted at a regional hospital in New Taipei City, Taiwan in accordance with the tenets outlined in the Declaration of Helsinki. The study protocol was approved by the Ethics Committee of Human Studies at Cardinal Tien Hospital (CTH-108-2-5-002). The study period was from August 2019 to December 2020. Patients receiving maintenance hemodialysis (three times per week) continuously for > 3 months were enrolled. All patients received conventional hemodialysis using a high-flux or high efficient dialyzer. The exclusion criteria were as follows: (1) age <45 years; (2) stroke within 6 months; and (3) aphasic, illiterate, or unable to write in or understand Chinese or Taiwanese. We obtained written informed consent from enrolled participants. Subsequently, patients were divided into two groups based on their MMSE score. Blood and urine samples were obtained. Demographic data were obtained from medical records in Cardinal Tien Hospital. Diagnoses of congestive heart failure, diabetes mellitus, and hypertension were confirmed using medical records. Stroke diagnosis 6 months before enrollment was confirmed. Body weight and height were measured after hemodialysis and body mass index was obtained. Pre-dialytic hematologic and biochemical parameters were obtained within the month after informed consent was obtained on the mid-day (Wednesday or Thursday) as follows: hemoglobin, platelet count, white blood cell count, glutamic oxaloacetic transaminase (GOT), glutamic pyruvic transaminase (GPT), albumin, blood sugar, uric acid, total cholesterol, triglyceride, sodium, potassium, calcium, phosphorus and intact parathyroid hormone. Estimated glomerular filtration rate (eGFR) was determined by the Modification of Diet in Renal Disease Study equation (Levey et al., 2006). Serum urea levels were recorded pre- and postdialysis to calculate single-pool fractional clearance of urea (Kt/V), which serves as the parameter of adequacy for dialysis (Daugirdas, 1995). The normalized protein catabolic rate (nPCR), as the parameter of dietary protein intake, was calculated by applying the 2-blood urea nitrogen (BUN) method for the predialysis BUN level from monthly kinetic modeling sessions, and the Daugirdas-Schniditz rate equation was used to estimate of the equilibrated postdialysis BUN level (Daugirdas, 1995).

Sample Collection

A non-fasting venous blood sample was drawn from each participant and then deposited in a dipotassium ethylenediaminetetraacetic acid (K2 EDTA) tube. The total volume of blood obtained was 10 mL. The sample was drawn before hemodialysis treatment midweek (Wednesday or Thursday). The blood samples were centrifuged at 2,500 × g for 15 min within 3 h of collection, and plasmas were aliquoted into cryotubes (1 mL per tube) and stored at –80°C (Liu et al., 2020). Each sample was given an identification number after collection. NfL, Aβ1/40, Aβ1/42, and tau concentrations were measured

using IMR technology for all the collected plasma samples. The reagent for magnetic nanoparticles was dispersed in a phosphoryl buffer solution at pH 7.2.

IMR Measurement

These immobilizing antibodies for reagent nanoparticles were produced for NfL (Santa Cruz/sc20011), Aβ1/40 (Sigma/A3981), Aβ1/42 (Abcam/ab34376), and tau protein (Sigma/T9450). The mean diameter of antibody functionalized magnetic nanoparticles was 50–60 nm. The magnetic concentration of each type of reagent was 12 mg-Fe/mL, except for NfL (10 mg/Fe/mL). The compositions of IMR reagents in the human plasma were as follows: 80 μL of Aβ1/40 reagent (MF-AB0–0060, MagQu) mixed with 40 μL of human plasma, 60 μL of Aβ1/42 reagent (MFAB2–0060, MagQu) with 60 μL of human plasma, 80 μL of tau reagent (MF-TAU-0060, MagQu) with 40 μL of human plasma, and 60 μL of NfL reagent with 60 μL of sample (Lue et al., 2017; Liu et al., 2020). The IMR reagent and human plasma were mixed at room temperature. A superconducting quantum interference device based on a magnetic susceptometer (XacPro-S MagQu) was used to detect the reduction in magnetic susceptibility. Biomarker concentrations were transformed from IMR signals. The detection range for total tau protein, Aβ42, Aβ40, and NfL was 0.1∼3,000 pg/mL, 1∼30,000 pg/mL, 1∼1,000 pg/mL, and 0.0033 ∼1,000 pg/mL respectively. The intra-assay or inter-assay coefficient of variation for assaying Aβ1-40, Aβ1-42, total-Tau, or NfL using IMR is within the range of 7–10%. The mean value for each sample was used for statistical analysis.

Cognitive Assessment

The Chinese version of the MMSE was employed by the same doctor for the entire study (Li et al., 2016). Cognitive impairment was defined as MMSE scores of 10–24. The normal cognitive function was defined as MMSE scores of 25–30 (Folstein et al., 1975). The MMSE was taken within the first hour of hemodialysis to avoid hemodynamic variation mediated by ultrafiltration.

Statistics

Continuous variables are presented as means ± standard deviations. Categorical values are expressed as the frequency of count and the percentage. Mann-Whitney Rank Sum Test was used for comparisons of continuous variables between the two groups, including biochemical and laboratory data, plasma neurologic biomarkers and the interaction of NfL with other neurologic biomarkers. The chi-square test was used to analyze the association between the category variables. Spearman's rank correlation coefficient was used to correlate NfL concentration with biochemical and hematologic results, the total and individual categories of the MMSE and the MMSE of participants with and without cognitive impairment. Receiver operating characteristic (ROC) curve analysis was conducted to differentiate the cognitive impairment in ESRD patients by NfL. Delong's non-parametric method was used to determine the confidence interval (CI) for the area under the curve (AUC), sensitivity, and specificity. All statistical analyses were performed using the statistical package SPSS for Windows (Version XVII; SPSS, Inc., Chicago, IL, United States). A two-sided *P*-value of < 0.05 was considered statistically significant.

RESULTS

Table 1 presented the demographic characteristics of the participants. In total, 67 participants were enrolled in the study. Of these, 24 participants had ESRD with cognitive impairment and 43 participants had ESRD without cognitive impairment (control group). Participants in the cognitive impairment group were older than those in the control group (74.80 ± 7.42 vs. 67.34 ± 8.45 years, $p < 0.05$). The proportion of women was higher in the cognitive impairment group than in the control group (60.3% vs. 21.9%, $p < 0.05$). In the patients with cognitive impairment, the percentage of educations year less than 6 years was higher than the patients without cognitive impairment (66.7% vs. 32.5%, $p < 0.05$). The educations years more than 10 years was higher in the patients without cognitive impairment than patients with cognitive impairment (58.1% vs. 12.5%, $p < 0.05$). **Table 2** presents the biochemical and hematological results of the participants. Predialysis creatinine (6.77 ± 1.93 mg/dL vs. 9.13 ± 2.28 mg/dL, $p < 0.05$), albumin (3.68 ± 0.26 g/dL vs. 3.90 ± 0.30 g/dL, $p < 0.05$), phosphorus (4.55 ± 1.10 mg/dL vs. 5.32 ± 1.56 mg/dL, $p < 0.05$) and hemoglobin (9.94 ± 1.34 g/dL vs. 10.16 ± 1.29 g/dL, $p < 0.05$) levels were lower in the cognitive impairment group than in the control group. The estimated GFR was higher in the cognitive impairment group (7.70 ± 3.03 mL/min/1.73 m^2 vs. 6.36 ± 2.89 mL/min/1.73 m^2, $p < 0.05$). Furthermore, the potassium concentration, white blood cell count, and platelet count were lower in the cognitive impairment group than in the control group, although the mean values were within the reference range. The Kt/V and normalized protein catabolic rate were similar between the groups.

Table 3 presents a comparison of neurological biomarkers between the groups. The NfL concentration was marginally

TABLE 1 | Demographic characteristics of the participants.

	ESRD without cognitive impairment	ESRD with cognitive impairment
Sample sizes	43	24
Age (year-old)	67.3 ± 8.5	74.8 ± 7.4*
Education level *		
0–6 years	14 (32.5%)	16 (66.7%)
7–9 years	4 (9.3%)	5 (20.8%)
≥10 years	25 (58.1%)	3 (12.5%)
Gender (female)	9 (22%)	14 (60%)*
Diabetes mellitus	24 (58%)	18 (78%)*
Hypertension	27 (66%)	13 (57%)*
Congestive heart failure	5 (12%)	7 (30%)
Stroke	4 (10%)	3 (13%)
BMI	25.1 ± 4.1	25.4 ± 5.4

ESRD, end-stage renal disease; BMI, body mass index.
**p < 0.05.*

higher in the cognitive impairment group than in the control group (10.65 ± 3.23 pg/mL vs. 8.66 ± 2.76 pg/mL, $p = 0.03$). Furthermore, the concentrations of total tau protein, Aβ1/42 and Aβ1/40 didn't differ between groups ($p = 0.45$, 0.35 and 0.91, respectively). **Figure 1** displays a comparison of neurological biomarkers between the groups. **Figure 2** displays the receiver operating characteristic curve of NfL to differentiate the cognitively impaired and unimpaired ESRD patients. The AUC for NfL was 0.687 ($p = 0.012$, 95% CI: 0.548–0.825).

Table 4 demonstrated the correlation between NfL and age and hematologic and biochemical data. As the concentration of NfL might correlate with the age (Vågberg et al., 2015), we performed the correlation between NfL and age ($r = -0.081$, $p = 0.530$). There was no correlation between the hematologic and biochemical parameters with NfL.

Table 5 presents a comparison of the two groups for different categories of the MMSE. The scores of orientation to time (2.29 ± 1.04 vs. 4.51 ± 0.66, $p < 0.05$) and place (3.41 ± 1.90 vs. 4.97 ± 0.15, $p < 0.05$), registration, attention and calculation, recall, and language were lower in patients who had ESRD with cognitive impairment than in those who had ESRD without cognitive impairment.

Table 6 demonstrated the correlation between NfL and MMSE (total and individual categories. The correlation coefficient between NfL and the category of orientation to place was –0.262 ($p = 0.036$). No correlation was observed with other subsets. **Figure 3** shows the correlation between the NfL and MMSE score and the different categories of the MMSE. There was no correlation between the concentration of NfL and MMSE among total population ($r = -0.153$, $p = 0.277$). **Figure 4** illustrated the correlation between the NfL and total MMSE in patients with ($r = 0.137$, $p = 0.583$) or without cognitive impairment ($r = 0.155$, $p = 0.333$).

TABLE 2 | Biochemical and laboratory data of the participants.

	ESRD without cognitive impairment	ESRD with cognitive impairment
Sample sizes	43	24
Blood urea nitrogen (mg/dL)	72 ± 18	61 ± 23
Creatinine (mg/dL)	9.13 ± 2.28	6.77 ± 1.93*
eGFR (mL/min/1.73 m^2)	6.36 ± 2.89	7.70 ± 3.03*
Sodium (mEq/L)	138 ± 3	137 ± 5
Potassium (mEq/L)	4.66 ± 0.70	4.20 ± 0.70*
Albumin (g/dL)	3.90 ± 0.30	3.68 ± 0.26*
Calcium (mg/dL)	8.95 ± 0.69	9.06 ± 0.81
Phosphorus (mg/dL)	5.32 ± 1.56	4.55 ± 1.10*
Blood sugar (mg/dL)	152 ± 65	169 ± 86
Triglyceride (mg/dL)	150 ± 107	144 ± 75
Total cholesterol (mg/dL)	149 ± 28	163 ± 86
Uric acid (mg/dL)	6.43 ± 1.84	6.45 ± 1.56
Intact parathyroid hormone (pg/mL)	357 ± 306	475 ± 400
White blood cell (/μL)	6,591 ± 1,932	5,367 ± 1,144*
Hemoglobin (g/dL)	10.16 ± 1.29	9.94 ± 1.34*
Platelet count (/μL)	182 ± 60	173 ± 44*
Kt/V	1.47 ± 0.80	1.48 ± 0.62
nPCR	1.07 ± 0.31	1.10 ± 0.43

ESRD, end-stage renal disease; eGFR, estimated glomerular filtration; Kt/V, single-pool fractional clearance of urea; nPCR, normalized protein catabolic rate.
**p < 0.05.*

DISCUSSION

Our cohort study revealed that the serum concentration of albumin is lower in patients with ESRD with cognitive impairment than in those with ESRD without cognitive impairment. The serum glucose concentration was higher in the patients with ESRD with cognitive impairment than in the controls. Among the serum biomarkers associating with cognitive impairment, the plasma concentrations of tau protein, Aβ1/40, and Aβ1/42 were similar between the groups. The NfL concentration was marginally higher in the patients who had ESRD with cognitive impairment than in the controls. There was no correlation between NfL, biochemical parameters and total MMSE.

Diagnostic Efficacy of the Scale for Cognitive Impairment in Patients With CKD

The scale for diagnosing cognitive impairment has been mostly discussed regarding its use for patients with CKD/ESRD. Commonly used scales include the MMSE, modified MMSE, MoCA, Mini-Cog, Digits Symbol Substitution, and Trial B. The aforementioned screening tests are used in different stages of CKD. Drew et al. showed that all the aforementioned screening tools have predictive value for cognitive impairment diagnosis in patients with ESRD receiving hemodialysis. MoCA had the best predictive value, with an AUC of 0.81 (95% CI: 0.730–0.890) (Drew et al., 2020). In contrast with other scales, MMSE serves as the screening assessment for patients with cognitive impairment (O'Bryant et al., 2008). In our study, MMSE score ≤ 24 was the definition of cognitive impairment adopted in this study. During the test, the MMSE was applied within the first hour of hemodialysis to avoid the influence of brain perfusion due to ultrafiltration during treatment. Moreover, categories involving memory, execution, and appraisal were lower in the cognitive impairment group than in the control group. Our results demonstrated that the education years less than 6 years were more common in the patients with cognitive impairment, which was coherent with studies on the MMSE and education level (Crum et al., 1993; Matallana et al., 2011). Therefore, other screening or diagnostic scales might be needed along with MMSE in the future studies.

The Role of NfL for Risk Assessment for Cognitive Impairment

Neurofilament is the cytoskeleton of neuron axons. On the basis of size and caliber, the neurofilament could be categorized as light (6 kDa), medium (145 kDa), or heavy (200 kDa). Studies have shown that myelinated neuron damage is common among

TABLE 3 | Plasma neurological biomarkers of the participants.

	ESRD without cognitive impairment	ESRD with cognitive impairment
Sample sizes	43	24
Tau protein, pg/mL	21.89 ± 2.77	22.03 ± 2.94
Amyloid beta 1/42, pg/mL	16.63 ± 0.65	16.69 ± 0.61
Amyloid beta 1/40, pg/mL	53.10 ± 5.30	52.50 ± 4.66
NfL, pg/mL	8.66 ± 2.76	10.65 ± 3.23*

ESRD, end-stage renal disease; NfL, neurofilament light chain.
**p < 0.05.*

patients with ESRD because of altered blood perfusion. Findlay et al. stated that the cerebral mean flow velocity decreases during dialysis in a time-dependent manner, and such a decline reflects the progression of white matter hyperintensity (Findlay et al., 2019). The decrease in cerebral blood flow velocity was correlated with MoCA score in patients on dialysis. Ultrafiltration during renal replacement might influence brain perfusion. Thus, the axons within white matter are vulnerable during ultrafiltration, and axon damage might explain the increase in plasma NfL. Additionally, sympathetic hyperactivity is a common phenomenon in patients with ESRD. In patients with ESRD, inflammation, hyperactivity of the renin–angiotensin–aldosterone system, or insulin resistance causes sympathetic hyperactivation (Kaur et al., 2017). Insufficient parasympathetic tone reduces acetylcholine release within the synaptic cleft. Sato et al. reported that cardiovascular mortality was low when treating patients with amnesia who were administered an acetylcholine esterase inhibitor (Sato et al., 2010). The transmitral flow in diastolic refilling was impaired in patients with dementia who were not treated with acetylcholine esterase inhibitors. Thus, sympathetic hyperactivity might contribute to cognitive impairment (Vistisen et al., 2014; Nicolini et al., 2020). The percentage of patients with diabetes mellitus was higher in

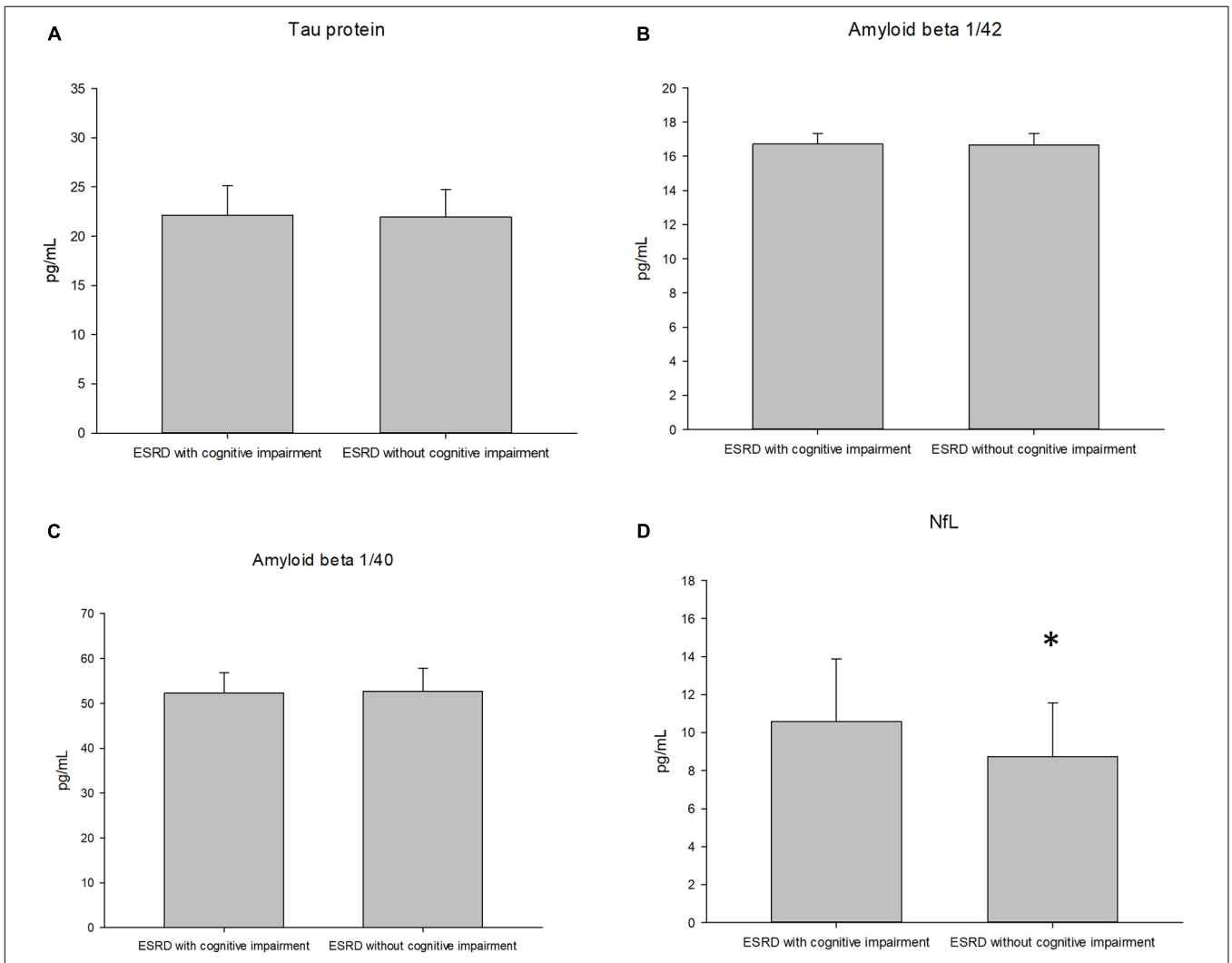

FIGURE 1 | The plasma concentration of the tau protein **(A)**, amyloid 1/42 **(B)**, amyloid 1/40 **(C)**, and neurofilament light chain [NfL, **(D)**] between groups of the subjects.

the cognitive impairment group than in the control group (78.2% vs. 58.5%). The NfL concentration was high in patients with diabetes mellitus during hypoglycemia and was negatively correlated with the gray matter volume of the frontal lobe (Sampedro et al., 2020). In our study, the NfL concentration was marginally higher in the cognitive impairment group and the AUC for diagnosis was 0.687. The correlation between NfL and other biochemical parameter was unable to be made. The possible explanation might be the multiple comorbidities in ESRD patients, such as unmeasured uremic toxin contributing to neuroinflammation within the glial cells (Adesso et al., 2017) or the hyperglycemic status disturbing morphology of neuronal structure (Flores-Gómez et al., 2019). The higher percentage of diabetes mellitus in cognitive impairment group might influence the performance of NfL.

In our cohort, NfL concentration was only negatively correlated with the category of orientation to place in the MMSE, but not total MMSE. In patients with Alzheimer disease or mild cognitive impairment, degenerative change occurs in the hippocampus and is a pathological hallmark, and its synaptic connection within a specific lobe, such as the prefrontal lobe, could directly influence the excitatory potential of neurons (Dégenètais et al., 2003). Moreover, recent reports have provided similar results. For instance, Dinomais et al. (2016) reported that MMSE score was correlated with gray matter damage within the limbic system. Several studies have investigated whether MMSE scores are correlated with damage within a specific area of the brain. Through the use of a 3D mapping technique, the MMSE was correlated with gray matter integrity in the frontal lobe, temporal lobe, and angular gyri (Apostolova et al., 2006). When different categories of the MMSE are being considered, deficit in a specific category could be correlated with specific cortical loss. Vasquez demonstrated that visual attention deficit was correlated with unilateral partial hypoperfusion (Vasquez et al., 2011). The superior and middle gyri of the frontal lobe are the functional areas during calculation (Wang and Wang, 2001). Moreover, Han et al. (2020) reported that patients with stroke with frontal cortex involvement had a lower MMSE score in the calculation category than healthy controls after adjustment for age. Since the correlation between NfL and the total MMSE was lacking, the

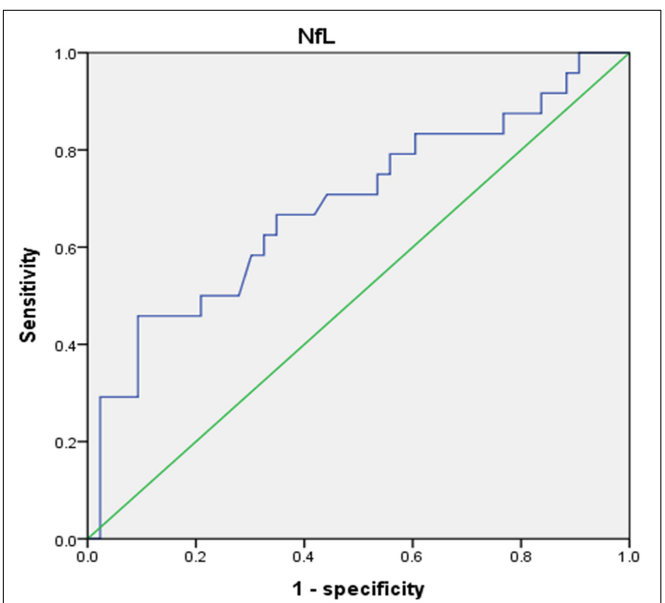

FIGURE 2 | The ROC curve of the NfL for cognitive impairment of in ESRD.

TABLE 4 | the correlation between and NfL and the biochemical/hematologic data in total population.

	Coefficient of correlation	*p*-value
Age	−0.081	0.530
Blood urea nitrogen (mg/dL)	0.131	0.373
Creatinine (mg/dL)	0.032	0.800
eGFR (mL/min/1.73 m^2)	0.057	0.790
Sodium (mEq/L)	−0.032	0.804
Potassium (mEq/L)	0.105	0.411
Albumin (g/dL)	0.088	0.492
Calcium (mg/dL)	0.146	0.279
Phosphorus (mg/dL)	−0.026	0.842
Blood sugar (mg/dL)	−0.084	0.525
Triglyceride (mg/dL)	−0.197	0.158
Total cholesterol (mg/dL)	0.095	0.498
Uric acid (mg/dL)	−0.131	0.338
Intact parathyroid hormone (pg/mL)	0.036	0.390
White blood cell (/μL)	−0.108	0.408
Hemoglobin (g/dL)	0.063	0.632
Platelet count (/μL)	0.00	0.998

TABLE 5 | Mini-mental state examination results of the participants.

	ESRD without cognitive impairment	ESRD with cognitive impairment
Sample sizes	43	24
MMSE (30 points maximum)	27.6 ± 1.8	18.0 ± 5.1*
Orientation to time (5 points maximum)	4.51 ± 0.66	2.29 ± 1.04*
Orientation to place (5 points maximum)	4.97 ± 0.15	3.41 ± 1.90*
Registration (3 points maximum)	2.97 ± 0.15	2.62 ± 0.57*
Attention and calculation (5 points maximum)	4.34 ± 1.08	1.45 ± 1.53*
Recall (3 points maximum)	2.44 ± 0.62	1.29 ± 1.04*
Language (9 points maximum)	8.27 ± 1.00	6.33 ± 1.80*

ESRD, end-stage renal disease; MMSE, Mini-Mental State Examination.
**p < 0.05.*

TABLE 6 | the correlation between and NfL and MMSE in total population.

	Coefficient of correlation	*p*-value
MMSE	−0.153	0.227
Orientation to time	−0.061	0.631
Orientation to place	−0.262	0.036*
Registration	−0.038	0.763
Attention and calculation	−0.195	0.123
Recall	−0.058	0.647
Language	−0.042	0.739

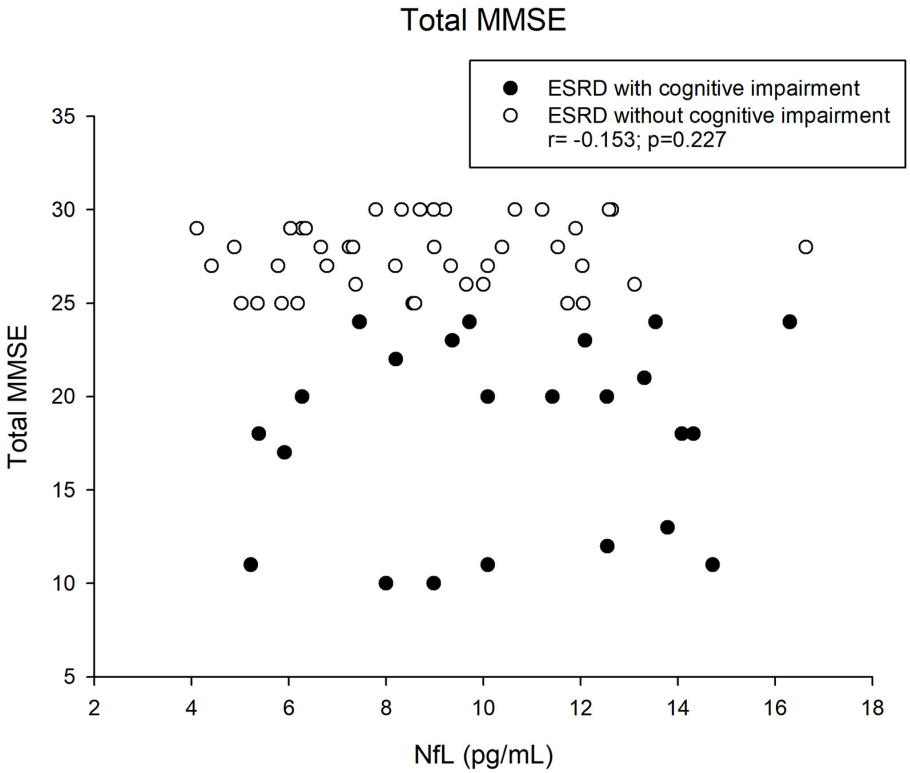

FIGURE 3 | Correlation between NfL and total MMSE in ESRD patients.

causes for the cognitive impairment in ESRD might be more than neurodegeneration.

Plasma Amyloid Beta or Tau Protein Were Not Associated With Cognitive Impairment in ESRD

Traditionally, Aβ aggregation and the hyperphosphorylation of tau protein are important pathogeneses of Alzheimer disease. In Alzheimer disease, the amyloid precursor protein within the cell membrane is cleaved by β- and γ-secretase, which forms insoluble amyloid monomers (Aβ1/42) as the plaque within the brain parenchyma. The soluble monomer Aβ1/40 reflected the less amyloid plaque formation within brain parenchyma (Chen et al., 2017a). As amyloid plaque deposition increases, the spread of phosphorylated tau within neurons is accelerated, forming a neurofibrillary tangle within the brain (Busche and Hyman, 2020). As tau or amyloid formation increases within the brain, the blood–brain barrier effluxes these pathological proteins into the plasma (Liu et al., 2012). *In vivo* research has suggested that the peripheral clearance of pathologic proteins could improve memory (Jin et al., 2017). The concentrations of tau protein and Aβ1/42 were similar in the cognitive impairment group than in the control group. One possible mechanism is that the efflux ability of the blood–brain barrier might be disturbed by protein-bounded uremic toxins (Bobot et al., 2020), thus interfering with biomarker detection. Second, other contributing factors might potentiate neuronal damage in patients with cognitive impairment, such as hypoalbuminemia and anemia.

Role of Hypoalbuminemia and Anemia in ESRD Patients With Cognitive Impairment

Hypoalbuminemia and anemia have been found to be contributing factors for Alzheimer disease (Llewellyn et al., 2010; Hong et al., 2013). Hypoalbuminemia is common in patients with ESRD. Malnutrition is common in patients with ESRD due to chronic inflammation, anorexia due to poor oral intake, hypercatabolism, and the gradual loss of amino acids during renal replacement therapy (Tonbul et al., 2006). In our study, the body mass index values were similar between the groups, confirming that the results were not confounded by obesity or underweight. Doorduijn et al. (2019) showed that patients with Alzheimer disease or mild cognitive impairment had a high incidence of malnutrition and less fat-free mass. Furthermore, CSF tau concentration was negatively correlated with fat-free mass and malnutrition severity (Doorduijn et al., 2019). In patients with Alzheimer's disease, malnutrition was closely associated with hyperhomocysteinemia (Sun et al., 2017). Homocysteine activates the phosphorylation of tau protein through protein phosphatase inactivation (Zhang et al., 2008). Renal anemia is caused by insufficient EPO production by tubulointerstitial cells and the resistance of erythropoietic precursor cells to EPO due to the accumulation of uremic toxins

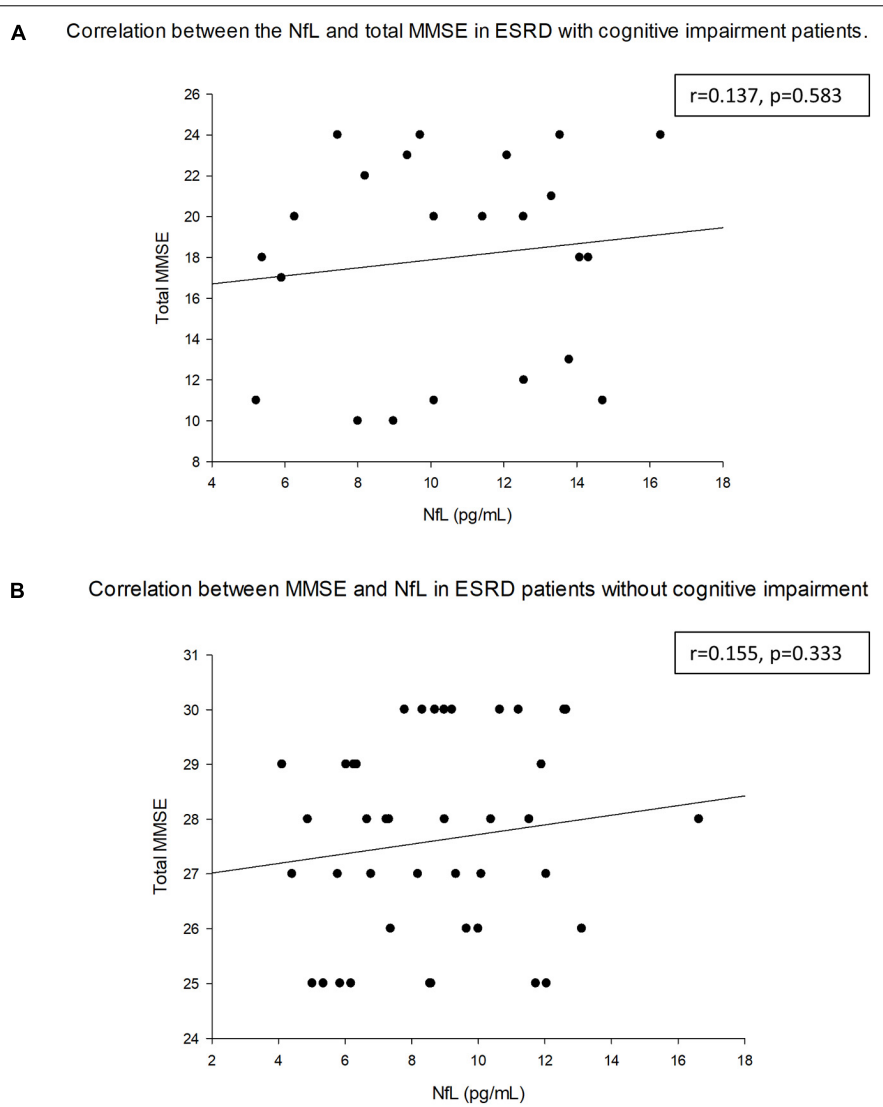

FIGURE 4 | Correlation between NfL and total MMSE with **(A)** and without **(B)** cognitive impairment.

and systemic inflammation (Batchelor et al., 2020). Vinothkumar et al. (2019) reported that the phosphorylated tau protein concentration was lower in patients with CKD treated with EPO than subjects without EPO treatment. Anemia was associated with neuron function in patients with CKD. Our previous study demonstrated that hemoglobin concentration was negatively correlated with striatum function in patients with ESRD (Hou et al., 2020). Mazumder et al. (2019) reported that mitochondrial dysfunction and oxidative stress accumulation within the brain were the main molecular mechanisms involved in cognitive impairment in an adenine-induced CKD animal model. Insufficient oxygen supply due to anemia might contribute to reactive oxygen species generation. EPO could increase tau phosphorylation during exposure to β-amyloid peptides (Sun et al., 2008). Our study showed that hypoalbuminemia and anemia might be associated with cognitive impairment, but further studies linking these risk factors with pathological characteristics, such as neurofibrillary tangle or amyloid plaque, may be required to determine the mechanism of cognitive impairment in patients with ESRD/CKD.

The Limitation of the Study

In our study, the average age of patients was higher in the ESRD with cognitive impairment group than in the other group. Furthermore, the cognitive impairment group had a higher proportion of women than the other group. Studies have shown that patients undergoing dialysis tend to belong to the elderly population (Yang et al., 2008; Stevens et al., 2010). We did not rank patients according to cognitive impairment severity or adjust for education level because of the low number of cases. Our cohort study used MMSE to group the subjects. However, MMSE alone might not be sufficient to distinguish the mild cognitive impairment or prodromal dementia (McKhann et al., 2011). Other sophisticated neurospsychological measurements

might be needed in addition to MMSE. Second, we chose to test for correlations between peripheral neurological biomarkers and traditional risk factors for cognitive impairment. Protein detection in plasma and CSF has been validated in previous studies. Although CSF and plasma measurements have been verified in other cohort studies, the association between the plasma and CSF neurological biomarkers has not been validated for patients with ESRD. Third, to correlate the peripheral biomarkers with radiologic studies was not performed. No image studies such as magnetic resonance image was performed during the study. The radiologic studies might provide further correlation between the pathologic change of the brain parenchyma and MMSE categories. Fourth, we didn't exclude the possible AD pathologic change by measuring Aβ and tau in the CSF or by positron emission tomography (Okamura et al., 2014). However, from the study by Gronewold et al. (2016), the CKD might contribute to elevated plasma Aβ concentration. It is still unknown if there is interaction between CKD and the pathologic change in AD. Further analysis of the correlations between plasma neurological biomarkers and the results of radiological studies may be warranted in the future. Finally, the depressive mood and hormonal dysregulation (such as hypothyroidism or growth hormone, which could influence cognitive function, were also the common comorbidities in CKD/ESRD patients (Drew et al., 2019; Rhee, 2019). In this cohort study these comorbidities were not excluded. In the future studies, these confounding disorders should be taken into consideration in the studies related for cognitive impairment in ESRD.

CONCLUSION

This case–control study compared the biomarkers for ESRD patients with and without cognitive impairment. Plasma NfL was marginally higher in the cognitive impairment group; the concentration of tau protein, Aβ 1/42, Aβ 1/40 were similar between groups. There was no correlation between NfL and biochemical parameters or total MMSE. Further studies, especially radiological studies, may be necessary to verify the role of these neurological biomarkers and the possible pathogenesis of cognitive impairment in patients with ESRD.

DATA AVAILABILITY STATEMENT

The raw data supporting the conclusions of this article will be made available by the authors, without undue reservation.

ETHICS STATEMENT

The studies involving human participants were reviewed and approved by the Cardinal Tien Hospital. The patients/participants provided their written informed consent to participate in this study.

AUTHOR CONTRIBUTIONS

Y-CH drafted the manuscript and obtained informed consent from the participants. C-LH and C-LL executed statistical analysis. C-MZ, Y-FL, and K-CL conducted the study. Y-LC was responsible for sample collection. R-MC designed the study. All authors contributed to the article and approved the submitted version.

FUNDING

The study was financially funded by the Ministry of Science and Technology (MOST 108-2314-B-303-029) and Cardinal Tien Hospital (CTH-109-AK2229). This study was supported by TMU Research Center of Cancer Translational Medicine from the Featured Areas Research Center Program within the framework of the Higher Education Sprout Project by the Ministry of Education (MOE), Taipei, Taiwan. The manuscript was edited by Wallace Academic Editing.

ACKNOWLEDGMENTS

We thank the MagQu company (New Taipei City, Taiwan) for providing the immunomagnetic reduction technique for detecting neurological biomarkers.

REFERENCES

Abu-Rumeileh, S., Baiardi, S., Ladogana, A., Zenesini, C., Bartoletti-Stella, A, Poleggi, A., et al. (2020). Comparison between plasma and cerebrospinal fluid biomarkers for the early diagnosis and association with survival in prion disease. *J. Neurol. Neurosurg. Psychiatry* 91, 1181–1188.

Abu-Rumeileh, S., Mometto, N., Bartoletti-Stella, A., Polischi, B., Oppi, F., Poda, R., et al. (2018). Cerebrospinal fluid biomarkers in patients with frontotemporal dementia spectrum: a single-center study. *J. Alzheimers Dis.* 66, 551–563. doi: 10.3233/jad-180409

Adesso, S., Magnus, T., Cuzzocrea, S., Campolo, M., Rissiek, B., Paciello, O., et al. (2017). Indoxyl sulfate affects glial function increasing oxidative stress and neuroinflammation in chronic kidney disease: interaction between astrocytes and microglia. *Front. Pharmacol.* 8:370. doi: 10.3389/fphar.2017.00370

Akamine, S., Marutani, N., Kanayama, D., Gotoh, S., Maruyama, R., Yanagida, K., et al. (2020). Renal function is associated with blood neurofilament light chain level in older adults. *Sci. Rep.* 10:20350.

Anderson, A. M., Easley, K. A., Kasher, N., Franklin, D., Heaton, R. K., Zetterberg, H., et al. (2018). Neurofilament light chain in blood is negatively associated with neuropsychological performance in HIV-infected adults and declines with initiation of antiretroviral therapy. *J. Neurovirol.* 24, 695–701. doi: 10.1007/s13365-018-0664-y

Apostolova, L. G., Lu, P. H., Rogers, S., Dutton, R. A., Hayashi, K. M., Toga, A. W., et al. (2006). 3D Mapping of mini-mental state examination performance in clinical and preclinical Alzheimer Disease. *Alzheimer Dis. Assoc. Disord.* 20, 224–231. doi: 10.1097/01.wad.0000213857.89613.10

Baiardi, S., Abu-Rumeileh, S., Rossi, M., Zenesini, C., Bartoletti-Stella, A., Polischi, B., et al. (2019). Antemortem CSF Aβ42/Aβ40 ratio predicts Alzheimer's disease pathology better than Aβ42 in rapidly progressive dementias. *Ann. Clin. Transl. Neurol.* 6, 263–273.

Batchelor, E. K., Kapitsinou, P., Pergola, P. E., Kovesdy, C. P., and Jalal, D. I. (2020). Iron deficiency in chronic kidney disease: updates on pathophysiology, diagnosis, and treatment. *J. Am. Soc. Nephrol.* 31, 456–468. doi: 10.1681/asn.2019020213

Benussi, A., Karikari, T. K., Ashton, N., Gazzina, S., Premi, E., Benussi, L., et al. (2020). Diagnostic and prognostic value of serum NfL and p-Tau181 in frontotemporal lobar degeneration. *J. Neurol. Neurosurg. Psychiatry* 91, 960–967. doi: 10.1136/jnnp-2020-323487

Bobot, M., Thomas, L., Moyon, A., Fernandez, S., Mckay, N., Balasse, L., et al. (2020). Uremic toxic blood-brain barrier disruption mediated by AhR Activation leads to cognitive impairment during experimental Renal Dysfunction. *J. Am. Soc. Nephrol.* 31, 1509–1521. doi: 10.1681/asn.2019070728

Busche, M. A., and Hyman, B. T. (2020). Synergy between amyloid-β and tau in Alzheimer's disease. *Nat. Neurosci.* 23, 1183–1193. doi: 10.1038/s41593-020-0687-6

Chatterjee, P., Zetterberg, H., Goozee, K., Lim, C. K., Jacobs, K. R., Ashton, N. J., et al. (2019). Plasma neurofilament light chain and amyloid-β are associated with the kynurenine pathway metabolites in preclinical Alzheimer's disease. *J. Neuroinflam.* 16:186.

Chen, G.-F., Xu, T.-H., Yan, Y., Zhou, Y.-R., Jiang, Y., Melcher, K., et al. (2017a). Amyloid beta: structure, biology and structure-based therapeutic development. *Acta Pharmacologica Sinica* 38, 1205–1235. doi: 10.1038/aps.2017.28

Chen, T.-B., Yiao, S.-Y., Sun, Y., Lee, H.-J., Yang, S.-C., Chiu, M.-J., et al. (2017b). Comorbidity and dementia: a nationwide survey in Taiwan. *PloS One* 12:e0175475. doi: 10.1371/journal.pone.0175475

Cherng, Y.-G., Lin, C.-S., Shih, C.-C., Hsu, Y.-H., Yeh, C.-C., Hu, C.-J., et al. (2018). Stroke risk and outcomes in patients with chronic kidney disease or end-stage renal disease: Two nationwide studies. *PLoS One* 13:e0191155. doi: 10.1371/journal.pone.0191155

Crum, R. M., Anthony, J. C., Bassett, S. S., and Folstein, M. F. (1993). Population-based norms for the mini-mental state examination by age and educational level. *JAMA* 269, 2386–2391. doi: 10.1001/jama.1993.03500180078038

Daugirdas, J. T. (1995). Simplified equations for monitoring Kt/V, PCRn, eKt/V, and ePCRn. *Adv.Renal Replacement Ther.* 2, 295–304. doi: 10.1016/s1073-4449(12)80028-8

Dégenètais, E., Thierry, A. M., Glowinski, J., and Gioanni, Y. (2003). Synaptic influence of hippocampus on pyramidal cells of the rat prefrontal cortex: an in vivo intracellular recording study. *Cereb Cortex* 13, 782–792. doi: 10.1093/cercor/13.7.782

D'errico, P., and Meyer-Luehmann, M. (2020). Mechanisms of pathogenic Tau and Aβ protein spreading in Alzheimer's Disease. *Front. Aging Neurosci.* 12:265. doi: 10.3389/fnagi.2020.00265

Dinomais, M., Celle, S., Duval, G. T., Roche, F., Henni, S., Bartha, R., et al. (2016). Anatomic correlation of the mini-mental state examination: a voxel-based morphometric study in older adults. *PloS One* 11:e0162889. doi: 10.1371/journal.pone.0162889

Doorduijn, A. S., Visser, M., van de Rest, O., Kester, M. I., de, Leeuw FA, Boesveldt, S., et al. (2019). Associations of AD biomarkers and cognitive performance with nutritional status: The NUDAD Project. *Nutrients* 11:1161. doi: 10.3390/nu11051161

Drew, D. A., Tighiouart, H., Rollins, J., Duncan, S., Babroudi, S., Scott, T., et al. (2020). Evaluation of screening tests for cognitive impairment in patients receiving maintenance hemodialysis. *J. Am. Soc. Nephrol.* 31, 855–864. doi: 10.1681/asn.2019100988

Drew, D. A., Weiner, D. E., and Sarnak, M. J. (2019). Cognitive impairment in CKD: pathophysiology, management, and prevention. *Am. J. Kidney Dis.* 74, 782–790. doi: 10.1053/j.ajkd.2019.05.017

Findlay, M. D., Dawson, J., Dickie, D. A., Forbes, K. P., Mcglynn, D., Quinn, T., et al. (2019). Investigating the relationship between cerebral blood flow and cognitive function in hemodialysis patients. *J. Am. Soc. Nephrol.* 30, 147–158. doi: 10.1681/asn.2018050462

Flores-Gómez, A. A., de Jesús Gomez-Villalobos, M., and Flores, G. (2019). Consequences of diabetes mellitus on neuronal connectivity in limbic regions. *Synapse* 73:e22082. doi: 10.1002/syn.22082

Folstein, M. F., Folstein, S. E., and Mchugh, P. R. (1975). "Mini-mental state". A practical method for grading the cognitive state of patients for the clinician. *J. Psychiatr. Res.* 12, 189–198.

Gaetani, L., Blennow, K., Calabresi, P., Di Filippo, M., Parnetti, L., and Zetterberg, H. (2019). Neurofilament light chain as a biomarker in neurological disorders. *J. Neurol. Neurosurg. Psychiatry* 90, 870–881. doi: 10.1136/jnnp-2018-320106

Geda, Y. E. (2012). Mild cognitive impairment in older adults. *Curr. Psychiatry Rep.* 14, 320–327.

Gronewold, J., Klafki, H.-W., Baldelli, E., Kaltwasser, B., Seidel, U. K., Todica, O., et al. (2016). Factors responsible for Plasma β-Amyloid accumulation in chronic kidney disease. *Mol. Neurobiol.* 53, 3136–3145. doi: 10.1007/s12035-015-9218-y

Hall, S., Janelidze, S., Londos, E., Leuzy, A., Stomrud, E., Dage, J. L., et al. (2020). Plasma Phospho-Tau Identifies Alzheimer's Co-Pathology in patients with lewy body disease. *Mov Disord.* 36, 767–771. doi: 10.1002/mds.28370

Han, M., Kim, D.-Y., Leigh, J.-H., and Kim, M.-W. (2020). Value of the frontal assessment battery tool for assessing the frontal lobe function in stroke patients. *Ann. Rehabil. Med.* 44, 261–272. doi: 10.5535/arm.19111

Hong, C. H., Falvey, C., Harris, T. B., Simonsick, E. M., Satterfield, S., Ferrucci, L., et al. (2013). Anemia and risk of dementia in older adults: findings from the Health ABC study. *Neurology* 81, 528–533. doi: 10.1212/wnl.0b013e31829e701d

Hou, Y. C., Fan, Y. M., Huang, Y. C., Chen, R. M., Wang, C. H., Lin, Y. T., et al. (2020). Tc-99m TRODAT-1 SPECT is a potential biomarker for restless leg syndrome in patients with end-stage renal disease. *J. Clin. Med.* 9:889. doi: 10.3390/jcm9030889

Hou, Y. C., Liu, W. C., Zheng, C. M., Zheng, J. Q., Yen, T. H., and Lu, K. C. (2017). Role of Vitamin D in Uremic Vascular calcification. *Biomed. Res. Int.* 2017:2803579. doi: 10.1155/2017/2803579

Hung, P.-H., Yeh, C.-C., Sung, F.-C., Hsiao, C.-Y., Muo, C.-H., Hung, K.-Y., et al. (2019). Erythropoietin prevents dementia in hemodialysis patients: a nationwide population-based study. *Aging* 11, 6941–6950. doi: 10.18632/aging.102227

Inker, L. A., Astor, B. C., Fox, C. H., Isakova, T., Lash, J. P., Peralta, C. A., et al. (2014). KDOQI US commentary on the 2012 KDIGO clinical practice guideline for the evaluation and management of CKD. *Am. J. Kidney Dis.* 63, 713–735. doi: 10.1053/j.ajkd.2014.01.416

Jeppsson, A., Wikkelsö, C., Blennow, K., Zetterberg, H., Constantinescu, R., Remes, A. M., et al. (2019). CSF biomarkers distinguish idiopathic normal pressure hydrocephalus from its mimics. *J. Neurol. Neurosurg. Psychiatry* 90, 1117–1123. doi: 10.1136/jnnp-2019-320826

Jin, W. S., Shen, L. L., Bu, X. L., Zhang, W. W., Chen, S. H., Huang, Z. L., et al. (2017). Peritoneal dialysis reduces amyloid-beta plasma levels in humans and attenuates Alzheimer-associated phenotypes in an APP/PS1 mouse model. *Acta Neuropathol.* 134, 207–220. doi: 10.1007/s00401-017-1721-y

Jo, M., Lee, S., Jeon, Y.-M., Kim, S., Kwon, Y., Kim, H.-J., et al. (2020). The role of TDP-43 propagation in neurodegenerative diseases: integrating insights from clinical and experimental studies. *Exper. Mol. Med.* 52, 1652–1662. doi: 10.1038/s12276-020-00513-7

Kaur, J., Young, B. E., and Fadel, P. J. (2017). Sympathetic overactivity in chronic kidney disease: consequences and mechanisms. *Int. J. Mol. Sci.* 18:1682. doi: 10.3390/ijms18081682

Kuo, Y.-T., Li, C.-Y., Sung, J.-M., Chang, C.-C., Wang, J.-D., Sun, C.-Y., et al. (2019). Risk of dementia in patients with end-stage renal disease under maintenance dialysis—a nationwide population-based study with consideration of competing risk of mortality. *Alzheimer's Res. Ther.* 11:31.

Levey, A. S., Coresh, J., Greene, T., Stevens, L. A., Zhang, Y. L., Hendriksen, S., et al. (2006). Using standardized serum creatinine values in the modification of diet in renal disease study equation for estimating glomerular filtration rate. *Ann. Intern. Med.* 145, 247–254. doi: 10.7326/0003-4819-145-4-200608150-00004

Li, C. I, Li, T. C., Lin, W. Y., Liu, C. S., Hsu, C. C., Hsiung, C. A., et al. (2015). Combined association of chronic disease and low skeletal muscle mass with physical performance in older adults in the Sarcopenia and Translational Aging Research in Taiwan (START) study. *BMC Geriatr.* 15:11. doi: 10.1186/s12877-015-0011-6

Li, H., Jia, J., and Yang, Z. (2016). Mini-mental state examination in elderly chinese: a population-based normative study. *J. Alzheimer's Dis.* 53, 487–496. doi: 10.3233/jad-160119

Lin, Y. S., Lee, W. J., Wang, S. J., and Fuh, J. L. (2018). Levels of plasma neurofilament light chain and cognitive function in patients with Alzheimer or Parkinson disease. *Sci. Rep.* 8:17368.

Lin, Y. T., Wu, P. H., Tsai, Y. C., Hsu, Y. L., Wang, H. Y., Kuo, M. C., et al. (2019). Indoxyl sulfate induces apoptosis through oxidative stress and mitogen-activated protein kinase signaling pathway inhibition in human astrocytes. *J. Clin. Med.* 8:191. doi: 10.3390/jcm8020191

Liu, H.-C., Lin, W.-C., Chiu, M.-J., Lu, C.-H., Lin, C.-Y., and Yang, S.-Y. (2020). Development of an assay of plasma neurofilament light chain utilizing immunomagnetic reduction technology. *PLoS One* 15:e0234519. doi: 10.1371/journal.pone.0234519

Liu, Y.-H., Giunta, B., Zhou, H.-D., Tan, J., and Wang, Y.-J. (2012). Immunotherapy for Alzheimer disease—the challenge of adverse effects. *Nat. Rev. Neurol.* 8, 465–469. doi: 10.1038/nrneurol.2012.118

Llewellyn, D. J., Langa, K. M., Friedland, R. P., and Lang, I. A. (2010). Serum albumin concentration and cognitive impairment. *Curr. Alzheimer Res.* 7, 91–96. doi: 10.2174/156720510790274392

Loeffler, T., Schilcher, I., Flunkert, S., and Hutter-Paier, B. (2020). Neurofilament-Light chain as biomarker of neurodegenerative and rare diseases with high translational value. *Front. Neurosci.* 14:579. doi: 10.3389/fnins.2020.00579

Lue, L.-F., Sabbagh, M. N., Chiu, M.-J., Jing, N., Snyder, N. L., Schmitz, C., et al. (2017). Plasma Levels of Aβ42 and Tau identified probable Alzheimer's Dementia: findings in two cohorts. *Front. Aging Neurosci.* 9:226. doi: 10.3389/fnagi.2017.00226

MacEwen, C., Sutherland, S., Daly, J., Pugh, C., and Tarassenko, L. (2017). Relationship between hypotension and cerebral ischemia during hemodialysis. *J. Am. Soc. Nephrol.* 28:2511. doi: 10.1681/asn.2016060704

Malek-Ahmadi, M., Davis, K., Belden, C. M., and Sabbagh, M. N. (2014). Comparative analysis of the Alzheimer questionnaire (AQ) with the CDR sum of boxes, MoCA, and MMSE. *Alzheimer Dis. Assoc. Disord.* 28, 296–298. doi: 10.1097/wad.0b013e3182769731

Maraj, M., Kuśnierz-Cabala, B., Dumnicka, P., and Gala-Błñdzińska, A. (2018). Malnutrition, Inflammation, Atherosclerosis syndrome (MIA) and diet recommendations among end-stage renal disease patients treated with maintenance hemodialysis. *Nutrients* 10:69. doi: 10.3390/nu10010069

Martin, S. J., Mcglasson, S., Hunt, D., and Overell, J. (2019). Cerebrospinal fluid neurofilament light chain in multiple sclerosis and its subtypes: a meta-analysis of case-control studies. *J. Neurol. Neurosurg. Psychiatry* 90, 1059–1067. doi: 10.1136/jnnp-2018-319190

Matallana, D., de Santacruz, C., Cano, C., Reyes, P., Samper-Ternent, R., Markides, K. S., et al. (2011). The relationship between education level and mini-mental state examination domains among older Mexican Americans. *J. Geriatr. Psychiatry Neurol.* 24, 9–18. doi: 10.1177/0891988710373597

Mattsson, N., Andreasson, U., Zetterberg, H., Blennow, K., and Alzheimer's Disease Neuroimaging Initiative. (2017). Association of plasma neurofilament light with neurodegeneration in patients with Alzheimer Disease. *JAMA Neurol.* 74, 557–566. doi: 10.1001/jamaneurol.2016.6117

Mazumder, M. K., Paul, R., Bhattacharya, P., and Borah, A. (2019). Neurological sequel of chronic kidney disease: from diminished Acetylcholinesterase activity to mitochondrial dysfunctions, oxidative stress and inflammation in mice brain. *Sci. Rep.* 9:3097.

McKhann, G. M., Knopman, D. S., Chertkow, H., Hyman, B. T., Jack, C. R. Jr., Kawas, C. H., et al. (2011). The diagnosis of dementia due to Alzheimer's disease: recommendations from the national institute on aging-Alzheimer's association workgroups on diagnostic guidelines for Alzheimer's disease. *Alzheimer's Dementia* 7, 263–269.

Mendu, M. L., and Weiner, D. E. (2020). Health policy and kidney care in the united states: core curriculum 2020. *Am. J. Kidney Dis.* 76, 720–730. doi: 10.1053/j.ajkd.2020.03.028

Nicolini, P., Mari, D., Abbate, C., Inglese, S., Bertagnoli, L., Tomasini, E., et al. (2020). Autonomic function in amnestic and non-amnestic mild cognitive impairment: spectral heart rate variability analysis provides evidence for a brain–heart axis. *Sci. Rep.* 10:11661.

O'Bryant, S. E., Humphreys, J. D., Smith, G. E., Ivnik, R. J., Graff-Radford, N. R., Petersen, R. C., et al. (2008). Detecting dementia with the mini-mental state examination in highly educated individuals. *Arch. Neurol.* 65, 963–967.

Okamura, N., Harada, R., Furumoto, S., Arai, H., Yanai, K., and Kudo, Y. (2014). Tau PET imaging in Alzheimer's disease. *Curr. Neurol. Neurosci. Rep.* 14:500.

Rhee, C. M. (2019). Thyroid disease in end-stage renal disease. *Curr. Opin. Nephrol. Hypertens* 28, 621–630.

Sampedro, F., Stantonyonge, N., Martínez-Horta, S., Alcolea, D., Lleó, A., Muñoz, L., et al. (2020). Increased plasma neurofilament light chain levels in patients with type-1 diabetes with impaired awareness of hypoglycemia. *BMJ Open Diabetes Res. Care* 8:e001516. doi: 10.1136/bmjdrc-2020-001516

Sato, K., Urbano, R., Yu, C., Yamasaki, F., Sato, T., Jordan, J., et al. (2010). The effect of donepezil treatment on cardiovascular mortality. *Clin. Pharmacol. Ther.* 88, 335–338. doi: 10.1038/clpt.2010.98

Soto, C., and Satani, N. (2011). The intricate mechanisms of neurodegeneration in prion diseases. *Trends Mol. Med.* 17, 14–24. doi: 10.1016/j.molmed.2010.09.001

Spotorno, N., Lindberg, O., Nilsson, C., Landqvist Waldö, M., van Westen, D., Nilsson, K., et al. (2020). Plasma neurofilament light protein correlates with diffusion tensor imaging metrics in frontotemporal dementia. *PLoS One* 15:e0236384. doi: 10.1371/journal.pone.0236384

Stevens, L. A., Viswanathan, G., and Weiner, D. E. (2010). Chronic kidney disease and end-stage renal disease in the elderly population: current prevalence, future projections, and clinical significance. *Adv. Chronic Kidney Dis.* 17, 293–301. doi: 10.1053/j.ackd.2010.03.010

Sun, J., Wen, S., Zhou, J., and Ding, S. (2017). Association between malnutrition and hyperhomocysteine in Alzheimer's disease patients and diet intervention of betaine. *J. Clin. Lab. Anal.* 31:e22090. doi: 10.1002/jcla.22090

Sun, Z. K., Yang, H. Q., Pan, J., Zhen, H., Wang, Z. Q., Chen, S. D., et al. (2008). Protective effects of erythropoietin on tau phosphorylation induced by beta-amyloid. *J. Neurosci. Res.* 86, 3018–3027. doi: 10.1002/jnr.21745

Tapiola, T., Alafuzoff, I., Herukka, S. K., Parkkinen, L., Hartikainen, P., Soininen, H., et al. (2009). Cerebrospinal fluid {beta}-amyloid 42 and tau proteins as biomarkers of Alzheimer-type pathologic changes in the brain. *Arch. Neurol.* 66, 382–389.

Tonbul, H. Z., Demir, M., Altintepe, L., Güney, I., Yeter, E., Türk, S., et al. (2006). Malnutrition-inflammation-atherosclerosis (MIA) syndrome components in hemodialysis and peritoneal dialysis patients. *Ren. Fail.* 28, 287–294. doi: 10.1080/08860220600583625

Twohig, D., and Nielsen, H. M. (2019). α-synuclein in the pathophysiology of Alzheimer's disease. *Mol. Neurodegen.* 14:23.

Vågberg, M., Norgren, N., Dring, A., Lindqvist, T., Birgander, R., Zetterberg, H., et al. (2015). Levels and age dependency of neurofilament light and glial fibrillary acidic protein in healthy individuals and their relation to the brain parenchymal fraction. *PloS One* 10:e0135886. doi: 10.1371/journal.pone.0135886

van Gelder, M. K., Middel, I. R., Vernooij, R. W. M., Bots, M. L., and Verhaar, M. C. (2020). Protein-Bound uremic toxins in hemodialysis patients relate to residual kidney function, are not influenced by convective transport, and do not relate to outcome. *Toxins (Basel)* 12:234. doi: 10.3390/toxins12040234

Vasquez, B. P., Buck, B. H., Black, S. E., Leibovitch, F. S., Lobaugh, N. J., Caldwell, C. B., et al. (2011). Visual attention deficits in Alzheimer's disease: relationship to HMPAO SPECT cortical hypoperfusion. *Neuropsychologia* 49, 1741–1750. doi: 10.1016/j.neuropsychologia.2011.02.052

Verde, F., Steinacker, P., Weishaupt, J. H., Kassubek, J., Oeckl, P., Halbgebauer, S., et al. (2019). Neurofilament light chain in serum for the diagnosis of amyotrophic lateral sclerosis. *J. Neurol. Neurosurg. Psychiatry* 90, 157–164.

Vinothkumar, G., Kedharnath, C., Krishnakumar, S., Sreedhar, S., Preethikrishnan, K., Dinesh, S., et al. (2017). Abnormal amyloid β(42) expression and increased oxidative stress in plasma of CKD patients with cognitive dysfunction: A small scale case control study comparison with Alzheimer's disease. *BBA Clin.* 8, 20–27. doi: 10.1016/j.bbacli.2017.06.001

Vinothkumar, G., Krishnakumar, S., Riya, and Venkataraman, P. (2019). Correlation between abnormal GSK3β, β Amyloid, total Tau, p-Tau 181 levels and neuropsychological assessment total scores in CKD patients with cognitive dysfunction: impact of rHuEPO therapy. *J. Clin. Neurosci.* 69, 38–42. doi: 10.1016/j.jocn.2019.08.073

Vistisen, S. T., Hansen, T. K., Jensen, J., Nielsen, J. F., and Fleischer, J. (2014). Heart rate variability in neurorehabilitation patients with severe acquired brain injury. *Brain Inj.* 28, 196–202. doi: 10.3109/02699052.2013.860477

Wang, M., and Wang, L. (2001). Localization of the brain calculation function area with MRI. *Chinese Sci. Bull.* 46:1889. doi: 10.1007/bf02901165

Yang, S.-Y., Chiu, M.-J., Chen, T.-F., and Horng, H.-E. (2017). Detection of plasma biomarkers using immunomagnetic reduction: a promising method for the early diagnosis of Alzheimer's Disease. *Neurol. Ther.* 6, 37–56.

Yang, W.-C., Hwang, S.-J., and Nephrology, T. S. O. (2008). Incidence, prevalence and mortality trends of dialysis end-stage renal disease in Taiwan from 1990 to 2001: the impact of national health insurance. *Nephrol. Dialysis Transpl.* 23, 3977–3982. doi: 10.1093/ndt/gfn406

Zhang, C.-E., Tian, Q., Wei, W., Peng, J.-H., Liu, G.-P., Zhou, X.-W., et al. (2008). Homocysteine induces tau phosphorylation by inactivating protein phosphatase 2A in rat hippocampus. *Neurobiol. Aging* 29, 1654–1665. doi: 10.1016/j.neurobiolaging.2007.04.015

Conflict of Interest: The authors declare that the research was conducted in the absence of any commercial or financial relationships that could be construed as a potential conflict of interest.

frontiers in Aging Neuroscience

REVIEW
published: 23 June 2021
doi: 10.3389/fnagi.2021.650740

Stress Granules and Neurodegenerative Disorders: A Scoping Review

Mohammad Reza Asadi[1,2], Marziyeh Sadat Moslehian[2], Hani Sabaie[2], Abbas Jalaiei[2], Soudeh Ghafouri-Fard[3], Mohammad Taheri[4] and Maryam Rezazadeh[1,2]**

[1] Molecular Medicine Research Center, Tabriz University of Medical Sciences, Tabriz, Iran, [2] Department of Medical Genetics, Faculty of Medicine, Tabriz University of Medical Sciences, Tabriz, Iran, [3] Department of Medical Genetics, School of Medicine, Shahid Beheshti University of Medical Sciences, Tehran, Iran, [4] Skull Base Research Center, Loghman Hakim Hospital, Shahid Beheshti University of Medical Sciences, Tehran, Iran

Cytoplasmic ribonucleoproteins called stress granules (SGs) are considered as one of the main cellular solutions against stress. Their temporary presence ends with stress relief. Any factor such as chronic stress or mutations in the structure of the components of SGs that lead to their permanent presence can affect their interactions with pathological aggregations and increase the degenerative effects. SGs involved in RNA mechanisms are important factors in the pathophysiology of neurodegenerative disorders such as amyotrophic lateral sclerosis (ALS), frontotemporal degeneration (FTD), and Alzheimer's diseases (AD). Although many studies have been performed in the field of SGs and neurodegenerative disorders, so far, no systematic studies have been executed in this field. The purpose of this study is to provide a comprehensive perspective of all studies about the role of SGs in the pathogenesis of neurodegenerative disorders with a focus on the protein ingredients of these granules. This scoping review is based on a six-stage methodology structure and the PRISMA guideline. A systematic search of seven databases for qualified articles was conducted until December 2020. Publications were screened independently by two reviewers and quantitative and qualitative analysis was performed on the extracted data. Bioinformatics analysis was used to plot the network and predict interprotein interactions. In addition, GO analysis was performed. A total of 48 articles were identified that comply the inclusion criteria. Most studies on neurodegenerative diseases have been conducted on ALS, AD, and FTD using human post mortem tissues. Human derived cell line studies have been used only in ALS. A total 29 genes of protein components of SGs have been studied, the most important of which are TDP-43, TIA-1, PABP-1. Bioinformatics studies have predicted 15 proteins to interact with the protein components of SGs, which may be the constituents of SGs. Understanding the interactions between SGs and pathological aggregations in neurodegenerative diseases can provide new targets for treatment of these disorders.

Keywords: stress granules, pathological aggregations, neurodegenerative disorders, amyotrophic lateral sclerosis, Alzheimer's, TDP-43, TIA-1, PABP-1

OPEN ACCESS

Edited by:
Thomas K. Karikari, University of Gothenburg, Sweden

Reviewed by:
Manuela Basso, University of Trento, Italy
Basant K. Patel, Indian Institute of Technology Hyderabad, India
Nicole Liachko, University of Washington, United States

***Correspondence:**
Mohammad Taheri
mohammad_823@yahoo.com
Maryam Rezazadeh
rezazadehm@tbzmed.ac.ir

Received: *07 January 2021*
Accepted: *17 May 2021*
Published: *23 June 2021*

Citation:
Asadi MR, Sadat Moslehian M, Sabaie H, Jalaiei A, Ghafouri-Fard S, Taheri M and Rezazadeh M (2021) Stress Granules and Neurodegenerative Disorders: A Scoping Review. Front. Aging Neurosci. 13:650740. doi: 10.3389/fnagi.2021.650740

INTRODUCTION

Cell function is divided between the organelles sited inside the cell. Based on the presence of lipid membrane, organelles can be divided into main two groups. Nucleus, mitochondria, endoplasmic reticulum, and Golgi apparatus are the major membranous organelles. Membraneless organelles are ribosomes (Turi et al., 2019), stress granules (Arrigo et al., 1988), p-body (Sheth and Parker, 2003), and nucleolus (Shaw and Jordan, 1995) that are formed during a process called the liquid-liquid phase separation phase (Marnik and Updike, 2019). The existence of stress at the cellular level can lead to a variety of responses, including global translational inhibition, leading to the formation of stress granules (SG) (Aulas et al., 2018). SGs, membraneless ribonucleoproteins containing mRNA, are cytoplasmic accumulations being stopped at the initiation of translation and disappear after the end of stress induction (Boncella et al., 2020). These stresses in mammalian cells include viral infections (biotic stress), induction of redox stress with sodium arsenite, heat and UV radiation which are environmental stress conditions (Kedersha et al., 2013). Three groups can form the protein component of stress granules: RNA-binding proteins, translation initiation factors, and non-RNA-binding proteins (Cao et al., 2020; Samadian et al., 2021). Stoppage at the critical stage of translation initiation due to biotic or environmental stress leads to the isolation of the translating polysomes resulting in the creation of a huge reservoir of RNA and related proteins that build and increase the number of SGs. On the other hand, relieving stress and increasing translated mRNAs is associated with disassembly and reduction in the number of these granules (Panas et al., 2016; Marnik and Updike, 2019).

There are two mechanisms for stopping translation initiation at the cellular level. Phosphorylation of the α subunit of eIF2 transcription initiation factor and prevention of the eIF-4F complex assembly. eIF2 is present in the ternary complex and is responsible for transferring the initiator tRNA to the pre-initiation complex at the 5'-ends of mRNAs. The result of eIF2 phosphorylation is reduction in its binding to GTP and loss of its ability to transfer the initiator tRNA to ribosomes for start codon recognition. Four stress associated kinases (HRI, PERK, PKR, GCN2) have the ability to phosphorylate the α subunit in the eIF2 factor (Aulas et al., 2017; Wolozin and Ivanov, 2019). eIF-4F complex is responsible for detecting the structure of the cap at the 5' mRNA end, and assembly of this complex is controlled by the PI3K-mTOR kinase cascade. eIF4E is inactivated in phosphorylated form and this phosphorylation is performed by mTOR, a member of the phosphatidylinositol 3-kinase-related kinase family of protein kinases (Mitra et al., 2015). eIF4E in active mode prevents the eIF-4F complex assembly and the translation process halts at the initiation point (Gingras et al., 1999; Aulas et al., 2017; Wolozin and Ivanov, 2019).

No specific function can be considered for SGs, but they can be considered as a "decision point" (Wolozin and Ivanov, 2019) for the fate of mRNA trapped in its structure. SG can define the fate of an mRNA that could be subjected to storage, degeneration, or re-initiation of translation. The probability of mRNA being in the SGs structure is sequence-independent but is directly related to the low translatability and the increase in the length of encoded region as well as the UTR region in the mRNA (Khong et al., 2017). Since proteins and RNAs with important roles can be included in SGs, this would affect biological interactions (Arimoto-Matsuzaki et al., 2008).

Traces of SGs have been found in many diseases, such as cancer (Gao et al., 2019), neurodegenerative disorders (Wolozin, 2012) and autoimmune conditions (McCormick and Khaperskyy, 2017). Neurodegenerative diseases include as amyotrophic lateral sclerosis (ALS) (Baron et al., 2013), Alzheimer's disease (AD) (Ash et al., 2014), and multiple sclerosis (MS) (Salapa et al., 2018). The neurodegeneration process involves atrophy and loss of neuronal activity (Wolozin and Ivanov, 2019). In neurodegenerative diseases, many mutations and misfolding events have been identified in this protein components of SGs, which can lead to the accumulation of abnormal proteins and the formation of SGs. Pathological symptoms appear when the presence of SGs becomes permanent due to an increase in their formation resulting from chronic stress (Brown et al., 2020) and a decrease in their deletion due to mutations in genes involved in the process of autophagy (Chitiprolu et al., 2018; Brown et al., 2020).

So far, many studies have been done on the nature of SGs, their components, structures and their pathological characteristics in various neurodegenerative diseases, and useful results have been obtained. In this study, we tried to establish a strong correlation between clinical evidence and genetic characteristics in neurodegenerative diseases in the form of a scoping review study by summarizing all human clinical studies and human-derived cell lines in the field of SGs.

METHODS

General Framework for Review

The writing strategy of this article is based on the methodology proposed by Arksey and O'Malley (2005). This strategy was later improved by Levac et al. (2010) and Colquhoun et al. (2014). In this review, 5 steps of the 6-step framework have been followed which includes (1) Development of research questions, (2) Search strategy, (3) Study eligibility criteria, (4) Data extraction, (5) Collating, summarizing and reporting the results. The sixth step, consultation, is optional and is not included in this article. Also, in order to observe the principles of clarity and transparency in writing the article, the Preferred Reporting Items for Systematic Reviews and Meta-Analyses Extension for Scoping Reviews (PRISMA-ScR) Checklist has been used well (Tricco et al., 2018).

Abbreviations: SGs, Stress granules; ALS, amyotrophic lateral sclerosis; FTD, frontotemporal degeneration; AD, Alzheimer's diseases; MS, multiple sclerosis; PRISMA-ScR, Preferred Reporting Items for Systematic Reviews and Meta-Analyses Extension for Scoping Reviews; MeSH, medical subject heading; GO, Gene ontology; FTLD, frontotemporal lobar degeneration; NIFID, neuronal intermediate filament inclusion disease; BIBD, basophilic inclusion body disease; MND, motor neuron disease; IHC, immunohistochemistry; IP, immunoprecipitation; MNs, motor neurons; LMN, lower MNs; TDP-43, TAR DNA-binding protein 43; HRE, Hexanucleotide repeat expansion; GEF, guanine nucleotide exchange factor; hnRNPA1, Heterogeneous nuclear ribonucleoprotein A1.

Development of Research Questions

To survey, summarize and discuss the studies on SGs in human and human-derived cell lines in neurodegenerative diseases, our review was guided by the following questions:

1. What exactly have been done on SGs in humans with neurodegenerative disease?
2. Exactly what studies have been done on SGs in human-derived cell lines in neurodegenerative disease?

Search Strategy

The publications were searched using seven databases: PubMed, Scopus, Cochrane, Google Scholar, Embase, Web of Science, and ProQuest, based on the search method of each database and was not limited to the date, language, subject or type of publication. Also, review articles published in this field were reviewed to reduce the possibility of losing related articles. "Neurodegeneration" keyword was the medical subject heading (MeSH) used in search strategy if available. PubMed and Embase related search strategies are shown in **Appendix I**. The last search was conducted on December 8, 2020. The references were managed using EndNote X8.1.

Study Eligibility Criteria

Studies in neurodegenerative diseases in relation to SGs in humans or in human-derived cell lines were screened from publications obtained during the search process. All types of publications were reviewed, including journal articles, conference presentations, conference abstracts and reports. Non-English articles with English abstracts were also included. Screening was done in two stages. At first, both researchers (MRA, MSM) screened articles separately based on title and abstract, according to the inclusion criteria mentioned above. In the next step, full texts of the selected articles were investigated to measure its relevance to the research question. Finally, appropriate articles were selected based on the eligibility criteria. Any contradiction was resolved in agreement with the opinion of the third person.

Data Extraction

Two separate charts were designed for human samples and human-derived cell lines in Microsoft Excel to help extracting the data. Chart related to human sample articles included author's name, year of publication, diagnosed neurodegenerative disease (number of patients), age and country, sample and method of analysis, protein component of SGs and major findings. The chart related to human-derived cell lines articles included the author's name, year of publication, origin of cell lines, age at biopsy, country, sample, method of analysis, mutation, and major findings. Two researchers (MRA, MSM) separately extracted data from articles based on charts.

Collating, Summarizing, and Reporting the Results

Quantitative and qualitative analysis was performed on the data obtained from the publications. In the quantitative analysis section, a descriptive numerical summary of the extent, nature and distribution of the studies were reviewed. In the qualitative analysis section, based on the research question mentioned earlier, a narrative review was performed on the available information with affirmation on the broader context suggested by Levac et al. (2010).

Bioinformatics Analysis

Two disease-protein interaction networks were designed using Cytoscape v3.8.0 software (Shannon et al., 2003) based on data extracted from articles. One was the network of neurodegenerative diseases with protein components of SGs and their interactions according to the results of human studies and the other was the protein components of SGs studied in human-derived cell lines from ALS. Therefore, the gene/proteins found from the literature search were used as input. The output was the interaction network between these proteins. Gene ontology (GO) analysis was performed using Enrichr's web-based tools and services (Kuleshov et al., 2016) on the genes of SGs protein components in neurodegenerative diseases and ALS. Protein-protein interaction was predicted using the string-db cytoscape plugin (Doncheva et al., 2019) on the data extracted from the articles. The analyzed graph of GO was ranked based on $p < 0.05$.

RESULT

Keyword-based searches in various databases yielded 1,087 related records. Also, 7 records from other sources were added to the results. Of these, 758 duplicates were identified. After excluding the duplicates, the number of articles with potential to be related to the research question reached 329. A total of 262 articles were excluded from the study by screening titles and abstracts and 61 articles remained. By reviewing the full text of the remaining articles, 49 articles were included in the study, of which 5 articles were conference abstracts. The process of selecting eligible studies is detailed in the flowchart in **Figure 1**. **Table 1** provides an overview of the included articles.

Summary of Methods of Studies Performed in Human Subjects

The studies were published from 2008 to 2020. The total number of neurodegenerative cases in this study is 258. These studies were conducted ALS (Fujita et al., 2008; Colombrita et al., 2009; Volkening et al., 2009; Dormann et al., 2010; Liu-Yesucevitz et al., 2010; Bentmann et al., 2012; Farg et al., 2013, 2014; McGurk et al., 2014; Cohen et al., 2015; Lim et al., 2016; Manghera et al., 2016; Dreser et al., 2017; Hirsch-Reinshagen et al., 2017; Mackenzie et al., 2017; Bennett et al., 2018; Chen and Cohen, 2019; Mann et al., 2019; Montalbano et al., 2020; Vassileff et al., 2020), ALS/FTD (Hirsch-Reinshagen et al., 2017; Mackenzie et al., 2017), ALS/frontotemporal lobar degeneration (FTLD) (Mann et al., 2019), AD (Castellani et al., 2011; Vanderweyde et al., 2012; Ivanov et al., 2016; Maziuk et al., 2018; Silva et al., 2019; Montalbano et al., 2020; Younas et al., 2020), MS (Salapa et al., 2018, 2020; Levin et al., 2020), FTD (McGurk et al., 2014; Montalbano et al., 2020), FTDP-17 (Vanderweyde et al., 2012), FTLD-u (Fujita et al., 2008; Dormann et al., 2010; Liu-Yesucevitz et al., 2010), FTLD

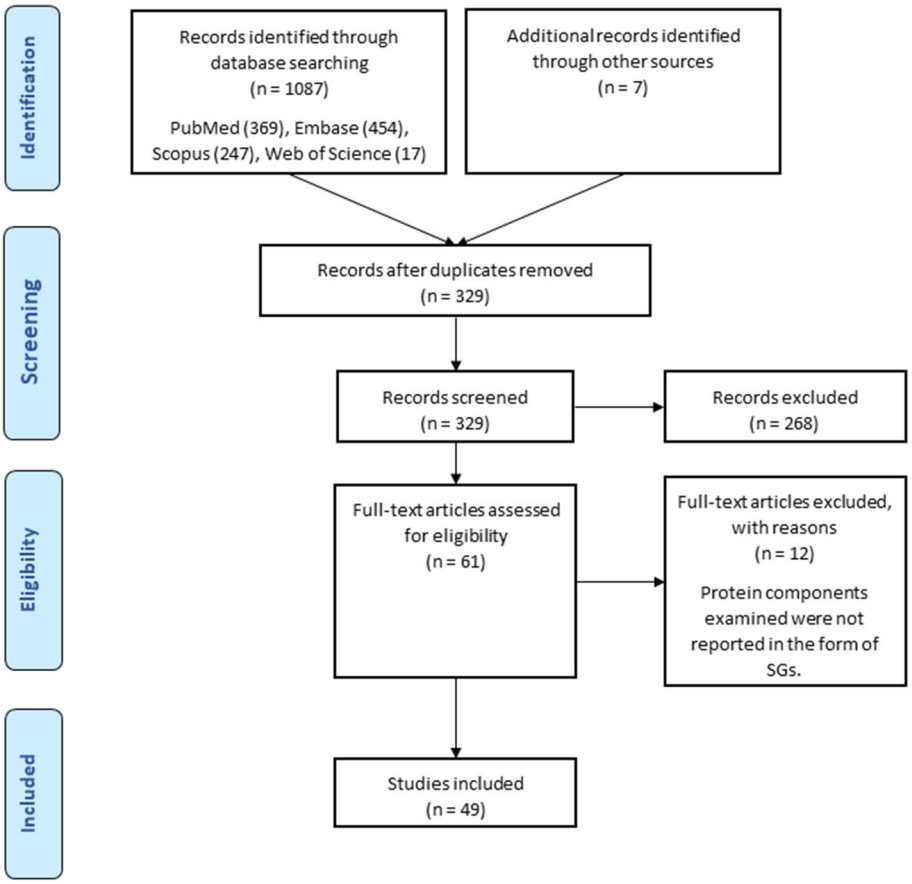

FIGURE 1 | Search strategy flow chart based on the PRISMA flow diagram.

TABLE 1 | Detailed characteristics of included publications.

Characteristic	Number ($n = 49$)	Percentage (%)
Type		
Journal article	44	89.7
Conference abstract	5	10.20
Year		
<2010	3	6.12
2010–2015	8	16.32
2015–2020	38	77.55

with TDP-43 inclusions (FTLD-TDP) (Dormann et al., 2010; Bentmann et al., 2012; Cohen et al., 2015), FTLD-FUS (Hock et al., 2018), neuronal intermediate filament inclusion disease (NIFID) (Dormann et al., 2010), basophilic inclusion body disease (BIBD) (Dormann et al., 2010; McGurk et al., 2014) and motor neuron disease (MND) (Fujita et al., 2008), which are summarized in **Table 2**. Cases in this study include both sexes, but because the gender of the cases was not mentioned in many studies, it was not indexed in **Table 2**. The samples used in the studies were brain, spinal cord and blood, of which twelve studies used only brain (Castellani et al., 2011; Vanderweyde et al., 2012; Manghera et al., 2016; Hock et al., 2018; Maziuk et al., 2018; Salapa et al., 2018, 2020; Silva et al., 2019; Levin et al., 2020; Montalbano et al., 2020; Vassileff et al., 2020; Younas et al., 2020), seven studies used only spinal cord (Colombrita et al., 2009; Farg et al., 2013, 2014; McGurk et al., 2014; Dreser et al., 2017; Mackenzie et al., 2017; Chen and Cohen, 2019), ten studies used both tissues (Fujita et al., 2008; Volkening et al., 2009; Dormann et al., 2010; Liu-Yesucevitz et al., 2010; Bentmann et al., 2012; Cohen et al., 2015; Lim et al., 2016; Hirsch-Reinshagen et al., 2017; Bennett et al., 2018; Mann et al., 2019) and one study used blood samples (Ivanov et al., 2016). The analysis methods of most studies were immunohistochemistry (IHC), but immunoprecipitation (IP) (Volkening et al., 2009; Farg et al., 2013; Montalbano et al., 2020), immunofluorescent microscope imager (Ivanov et al., 2016), RNA-FISH (Mann et al., 2019), mass spectrometry (Vassileff et al., 2020) and confocal microscopy (Volkening et al., 2009; Montalbano et al., 2020) were also used. The protein component of the SGs examined in the studies is also summarized in **Figure 2**. The included studies have been conducted in the United States, Canada, Australia, Germany, the Netherlands, Japan, Italy, Russia, South Korea, China and the United Kingdom. Based

TABLE 2 | Stress Granules and neurodegenerative disorders in human samples.

Author(s)	Year of publication	Country	Diagnosed neurodegenerative disease (number of patients)	Age	Sample	Analysis method(s)	Protein component of stress granules	Major findings	References
Fujita et al.	2008	Japan	• MND (2) • ALS (3) • FTLD-u (2)	MND Patients (45 and 58 years old) ALS patients (63.7 and 81 years old) FTLD-u with MND patients (62 and 63 years old)	Spinal cord Brain (hippocampus)	IHC	PABP-1 TIA-1 TDP-43 rpS6	• The presence of RNA in the Basophilic inclusions in the diagnosed disorders. • The Basophilic inclusions were labeled for PABP-1, TIA-1 and ribosomal protein S6; In contrast the BIs were not immune-positive for TDP-43.	Fujita et al., 2008
Volkening et al.	2009	Canada	• ALS (7(3 SOD associated)	NR	Spinal cord Brain	IP and western blot Biotin-labeled NFL 3′UTR RNA, IHC and confocal microscopy, RNA-IP-PCR	TDP-43 TIA-1 STAUFEN SOD1	• TDP-43 showed colocalization in ALS motor neurons with mutants or WT-SOD1. • TDP-43 showed colocalization in ALS's MNs and controls with STAUFEN. • The frequency of SGs and P-bodies in ALS's MNs were higher than controls and showed colocalization with TDP-43. • NFL mRNA processing in ALS's MNs is severely altered by TDP-43.	Volkening et al., 2009
Colombrita et al.	2009	Italy	• ALS (3)	NR	Spinal cord	IHC	TDP-43 TIAR HuR	• Mis-localization of TDP-43 was evident in the cytoplasm as a granular distribution. • No co-localization was observed between TIAR and HuR with TDP-43 inclusions.	Colombrita et al., 2009
Liu-Yesucevitz et al.	2010	United States	• ALS (4) • FTLD-u (5)	ALS Patients ranging from 63 to 79, mean 69 years FTLD-U Patients ranging from 72 to 83, mean 75.6 years	Spinal cord Brain (Frontal Cortex)	IHC	TDP-43 eIF3 TIA-1	• Colocalization were found between pTDP-43 inclusions and TIA-1 and eIF3 proteins. • Inclusions containing TDP-43 in ALS's spinal cord and FTD's brain can contain stress granule proteins.	Liu-Yesucevitz et al., 2010
Dormann et al.	2010	Canada	• ALS (1) • FTLD-u (3) • NIFID (3) • BIBD (1) • FTLD-TDP (2)	NR	Spinal cord Brain (hippocampus)	IHC	PABP-1 eIF4G	• PABP-1 and eIF4G are present in NCIs in patients with FUS pathology. • PABP-1 IHC shows highly immunoreactivity in NCIs in ALS's spinal cord MNs, BIBD, FTLD-u's hippocampus and NIFID but not detected in FTLD-TDP's hippocampus. • PABP-1 colocalized with p62 in same brain regions in ALS, FTLD-u, NIFID and BIBD but not in FTLD-TDP. • eIF4G was not detected in FTLD-TDP.	Dormann et al., 2010
Castellani et al.	2011	United States	AD (13)	Patients ranging from 67 to 89, mean 77.7 years	Brain (hippocampus)	IHC	rpS6	• IHC analysis showed that neurons in the AD's hippocampus containing 20 times more rPS6-positive granules compared to age-matched groups. • rPS6-positive granules were more common in neurons lacking NFT. • GVD granules colocalized with rPS6 in pyramidal neurons.	Castellani et al., 2011
Bentmann et al.	2012	Germany	• FTLD-TDP (5) • ALS (4)	NR	Brain (hippocampus) Spinal cord	IHC	TDP-43 PABP-1	• In ALS's spinal cord TDP-43 (N-terminal and C-terminal) labeled in NCIs but in FTLD-TDP's hippocampus only C-terminal of TDP-43 were labeled. • Double-labeling of PABP-1 and pTDP-43 of the same cases showed positive inclusions in spinal cord but not in cortical inclusions.	Bentmann et al., 2012

(Continued)

TABLE 2 | Continued

Author(s)	Year of publication	Country	Diagnosed neurodegenerative disease (number of patients)	Age	Sample	Analysis method(s)	Protein component of stress granules	Major findings	References
								• Inclusions in the FTLD's cortex, which have C-terminal fragments, were not labeled with PABP-1, whereas components in the spinal cord, which include full-length TDP-43, were positive for this protein marker.	
Vanderweyde et al.	2012	United States	• AD (6) • FTDP-17 (5)	AD's Patients ranging from 65 to 96, mean 82.5 years FTDP-17 Patients ranging from 44 to 53, mean 50.6 years	Brain (hippocampus) Brain (Frontal Cortex)	IHC	TIA-1 TDP-43 TTP G3BP1	• In ADs, TIA-1 colocalization was observed with Tau aggregations (pathological-phosphorylated-total) in all cases. • Larger Tau aggregations tended to be more colocalized with TIA-1 than smaller one. • Examination of controls showed small sparse aggregations of Tau. Also, by examining older controls, the presence of SGs in them was confirmed but they were not related to Tau pathology and its aggregations. • FUS inclusions moderately colocalized with TIA-1 inclusions, TDP-43 colocalized with TIA-1 inclusions infrequently. • Presence of TTP and G3BP1 in AD's brain was confirmed. G3BP1 not aggregated with TIA-1. TTP strongly colocalized with Tau inclusions. • Similar results observed in 5 cases of FTDP-17. • TIA-1-positive SGs were observed in both microglia, and astrocytes cell types.	Vanderweyde et al., 2012
Farg et al.	2012	Australia	ALS (3)	ALS Patients ranging from 42 to 55, mean 50 years	Spinal cord	IHC IP	ATXN2 FUS	• Ataxin-2 is present in the structure of SGs, which rapidly respond to stress and insults that affect the cell, and preventing translation of incorporate mRNA. • In controls, ataxin-2 was rarely observed in FUS inclusions Whereas in the ALS's, ataxin-2 was often seen with FUS cytoplasmic inclusions. • IP revealed that FUS was co-precipitated with ataxin-2 and not in controls. • Interaction between ataxin-2 and FUS is also RNA-independent, which was completed with RNase treatment.	Farg et al., 2013
McGurk et al.	2014	United States	• ALS [14 (2 with C9orf72 mutation and 3 with ATXN2 mutation)] • ALS-D [8 (6 with C9orf72 mutation and 1 with ATXN2 mutation)] • FTD (1) • BIBD (2)	ALS Patients ranging from 52 to 79, mean 65.7 years ALS-D Patients ranging from 46 to 67, mean 55.8 years FTD Patient with 47 years old BIBD patients with 65 and 75 years old	Spinal cord	IHC	PABP-1 TDP-43 FUS	• PABP-1 is colocalized with mature TDP-43 inclusions, not with TDP-43 pre-inclusions. • PABP-1, colocalized with TDP-43 inclusions, in the ALS's with ATXN2 and C9orf72 mutations. • The frequency of PABP-1 colocalization with TDP-43 inclusions in ALS's without mutation is 36%, in ALS's with ATXN2 mutation is 47% and in ALS's with C9orf72 mutation is 67%. • In patients with FUS pathology, PABP-1 observed with pathologic FUS in the motor neurons.	McGurk et al., 2014
Farg et al.	2014	Australia	ALS (1)	74 years old patient	Spinal cord	IHC	hnRNPA1 hnRNPA2B1	• Increased colocalization between C9orf72 and rab7 and rab11 in ALS's compared to controls • Poor regulation of cell trafficking in patients with C9orf72 mutation	Farg et al., 2014

(Continued)

TABLE 2 | Continued

Author(s)	Year of publication	Country	Diagnosed neurodegenerative disease (number of patients)	Age	Sample	Analysis method(s)	Protein component of stress granules	Major findings	References
Cohen et al.	2015	United States	• ALS (6) • FTLD-TDP (3)	ALS Patients ranging from 39 to 81, mean 56.8 years FTLD Patients ranging from 54 to 75, mean 64 years	Spinal cord Brain	IHC	TDP-43	• FTLD brain was highly immunoreactive for TDP-43 inclusions. • TDP-43 is full length (N-/C-terminal) and highly acetylated in ALS's TDP-43 inclusions. • Changes in acetylation plays an important role in loss of function and accumulation of TDP-43 in stress granules.	Cohen et al., 2015
Manghera et al.	2016	United States	ALS (5)	ALS Patients ranging from 50 to 76, mean 61.4 years	Brain (frontal cortex)	IHC	TDP-43 G3BP1	• Simultaneous expression of ERVK and TDP-43 is one of the hallmarks of ALS. • An increase in expression of G3BP1 was seen in ALSs vs. controls. This may be due to the increased expression of TDP-43 seen in ERVK+ cortical neurons. • No colocalization was observed between G3BP1 and ERVK. • SGs and viroplasms segregation can be a trigger to increased expression of ERVK viral proteins in ALS.	Manghera et al., 2016
Ivanov et al.	2016	Russia	AD(26)	AD's Patients ranging from 72 to 82, mean 76 years	Blood	MI	eIF3	• Significant heterogeneity in the distribution of eIF3 in neutrophils of patients' blood samples compared to controls. • Heterogeneity of eIF3 in patients' neutrophils is associated with the formation of SGs.	Ivanov et al., 2016
Lim et al.	2016	• South Korea	ALS (2)	ALS Patients with 34 and 57 years old, mean 45.5 years	Brain Spinal cord	IHC	FUS	• Distribution of FUS in controls and ALS samples is limited to the nucleus. • Oxidative stress induces the amassment of cytoplasmic FUS in stress granules, thus mimicking pathological characteristics recognized in mutant FUS in ALS patient. • Cytoplasmic aggregation of FUS was observed in G504Wfs mutant carrier sample in contrast to the control and ALS samples. • In G504Wfs mutant ALSs, FUS proteins emerges from the nucleus and undergoes cytoplasmic localization.	Lim et al., 2016
Dreser et al.	2017	Netherland	ALS (28(9 with c9orf72 mutation and 4 with FUS pathology)	NR	Spinal cord	IHC	MATRIN-3	• Cytoplasmic accumulations of matrin-3 were detected in C9orf72 and FUS cases. • Increased nuclear matrin-3 staining in all cases.	Dreser et al., 2017
Hirsch-Reinshagen et al.	2017	Canada	• ALS (1) • ALS/FTD (4)	ALS Patients with FTD ranging from 30 to 79, mean 58 years ALS Patient with 59 years old	Spinal cord Brain	IHC	TDP-43 TIA-1 PABP-1	• IHC showed a large number of granular TDP-43 in prefrontal cortex and primary motor cortex. • In all cases, Hippocampal dentate granule cells and dopaminergic neurons in the substantia nigra was affected. • NCIs were seen in granular, filamentous, round and compact form in LMN. • IHC failed to show abnormality using a number of TIA-1 antibodies. • The staining patterns were similar in ALSs with and without TIA-1 mutation and with normal control group, and no aggregations were	Hirsch-Reinshagen et al., 2017

(Continued)

TABLE 2 | Continued

Author(s)	Year of publication	Country	Diagnosed neurodegenerative disease (number of patients)	Age	Sample	Analysis method(s)	Protein component of stress granules	Major findings	References
								detected in cases with TIA-1 mutation. • Colocalization between TIA-1 and pTDP-43 was not detected.	
Mackenzie et al.	2017	United States	ALS/FTD (5)	ALS Patients with FTD ranging from 30 to 79, mean 58.2 years	Spinal cord	IHC	TDP-43 TIA-1	• Numerous rounds and hyaline TDP-43 inclusions were observed in all five autopsy cases. • TIA-1 mutations increase the tendency of TIA-1 protein to phase transition.	Mackenzie et al., 2017
Bennett et al.	2018	• United States	ALS (2)	NR	Brain Spinal cord	IHC	TDP-43	• TDP-43 was accumulated in stress granules seen in the cytoplasm of ALS lumbar cord MNs. • These cytosolic accumulations were associated with nuclear clearance. • TDP-43 ectopic position is a feature of ALS in humans.	Bennett et al., 2018
Silva et al.	2018	• United States	AD (NR)	NR	Brain (Temporal cortex)	IHC	DDX6 PABP-1	• IHC revealed DDX6 and PABP-1 were localized around p-TAUs. • The proximity and increased presence of DDX6 and PABP-1 can be attributed to the pathology caused by Tau aggregations.	Silva et al., 2019
Hock et al.	2018	• United kingdom	FTLD-FUS (4)	NR	Brain	IHC	FUS TNPO1	• Hypertonic stress leads to cytoplasmic transmission and loss of neuronal FUS function in SGs-independent manner. • Hypertonic Stress-mediated FUS transmission is caused by disruption of nuclear imports mediated by transport (TNPO1). • FTLD's frontal cortex was positive for TNPO1 neuronal cytoplasmic inclusion. • Astrocytes are resistant to FUS transmission and damage caused by hypertonic stress.	Hock et al., 2018
Maziuk et al.	2018	• United States	AD (7)	AD's Patients ranging from 57 to 97, mean 81.4 years	Brain	IHC	DDX6 hnRNPA0	• DDX6 and hnRNPA0 IHC indicated the presence of RBP inclusions in the cortex. • Location of RBPs indicated an inverse association compared to mature NFTs. It was observed that RBPs are found as pathological inclusions around mature tangles, thus RBP aggregates form near pathological TAUs but are strongly separated from them.	Maziuk et al., 2018
Salapa et al.	2018	• Canada	MS (1)	51 years old patient	Brain	IHC	TIA-1 hnRNPA1	• TIA-1 and hnRNPA1 normally have nuclear and cytoplasmic distribution in contrast, In MS's hnRNPA1 nuclear depletion was observed in brain neurons. • Accumulations of TIA-1 in large SGs formed in the cytoplasm of MS's brain neurons, but not in the nucleus. • In MS's brain neurons unlike control, hnRNPA1 and TIA-1 colocalized in cytoplasmic granules in double-label staining.	Salapa et al., 2018
Chen et al.	2019	• United States	ALS (6)	ALS Patients ranging from 39 to 81, mean 56.8 years.	Spinal cord	IHC	FMRP TDP-43 TIA-1 TIAR	• The observed immunohistochemical patterns of FMRP and p-FMRP are cytoplasmic and not related to the pathology of TDP-43.	Chen and Cohen, 2019

(Continued)

TABLE 2 | Continued

Author(s)	Year of publication	Country	Diagnosed neurodegenerative disease (number of patients)	Age	Sample	Analysis method(s)	Protein component of stress granules	Major findings	References
								• Different forms of TDP-43 with FMRP and p-FMRP co-localized in Double-Labeling. • TIA-1 and TIAR Double-labeling presented limited colocalization with TDP-43 inclusions. • TIA-1 was placed next to the TDP-43 inclusions and TIAR showed a stippled pattern in the cytoplasm of MNs and were not directly colocalized with TDP-43 inclusions.	
Mann et al.	2019	United States	ALS/FTLD (NR)	NR	Brain (hippocampus) Spinal cord	IHC RNA-FISH	TDP-43 G3BP1 ATKN2	• optoTDP-43 accumulations are similar to TDP-43 accumulations in TDP-43 proteinopathy. • RNA-FISH performed on ALSs' spinal cord and FTLDs' brain with a poly-T probe and failed to found TDP-43/mRNA colocalization. TDP-43 inclusions lacked mRNA. • No colocalization between TDP-43 and G3BP1/ATKN2 inclusions was detected.	Mann et al., 2019
Salapa et al.	2020	• Canada	MS (12)	MS Patients ranging from 44 to 65, mean 52.1 years.	Brain	IHC	TDP-43 hnRNPA1	Localization of TDP-43 and hnRNPA1 in MS's showed severe nuclear depletion and robust cytoplasmic localization compared with controls.	Salapa et al., 2020
Younas et al.	2020	• Germany	AD (16)	AD's Patients ranging from 56 to 93, mean 77.7 years	Brain	IHC	SFPQ TIA-1	• Examination of SFPQ in AD's brain tissue showed down-regulation. • SFPQ in AD's brain showed nuclear depletion and cytoplasmic colocalization with TIA-1. • SFPQ showed extra-nuclear colocalization with p-Tau in AD's brain legions. • There is probably a link between SFPQ and Tau oligomers in oligomerization and misfolding.	Younas et al., 2020
Vassileff et al.	2020	• Australia	ALS (10)	NR	Brain	Mass Spectrometry	STAU1 DHX30 TDP-43	• MECV examination in ALS compared to controls identified 16 protein packages that were statistically significant. • Up-regulation of two basic proteins from RNA-binding proteins in the dynamic pathway of SGs in ALS compared to controls.	Vassileff et al., 2020
Levin et al.	2020	• Canada	MS (14)	NR	Brain	IHC	TDP-43 hnRNPA1	• Nuclear depletion and cytoplasmic localization of TDP 43 in MS's neurons compared with controls. • Both TDP-43 and hnRNPA1 were colocalized in structure of SGs in the cytoplasm.	Levin et al., 2020
Montalbano et al.	2020	• United States	• AD (3) • ALS (3) • FTD (2)	AD's Patients ranging from 81 to 86, mean 83.3 years. ALS Patients ranging from 64 to 84, mean 72 years. FTD Patients with 56 and 60 years old, mean 58 years.	Brain (frontal cortex)	IHC IP confocal microscopy	TDP-43	• The interaction between the Tau and TDP-43 may be involved in the pathogenesis of AD, ALS and FTD. • TDP-43 is detected in stress granules in FTD and ALS.	Montalbano et al., 2020

SG, Stress Granule; MND, motor neuron disease; ALS, Amyotrophic lateral sclerosis; FTLD-u, Frontotemporal lobar degeneration; IHC, Immunohistochemistry; BI, Basophilic inclusion; IP, immunoprecipitation; PCR, polymerase chain reaction; WT, Wild Type; MN, Motor Neurons; FTD, Frontotemporal Degeneration; NIFID, Neuronal intermediate filament inclusion disease; BIBD, Basophilic Inclusion Body Disease; NCI, neuronal cytoplasmic inclusion; AD, Alzheimer's disease; NFT, Neurofibrillary tangle; GVD, granule vascular degeneration; ALS-D, Amyotrophic lateral sclerosis with dementia; ERVK, Endogenous retrovirus-K; LMN, Lower Motor Neurons; RBP, RNA Binding Protein; MS, Multiple Sclerosis; MECV, Motor cortex extracellular vesicles.

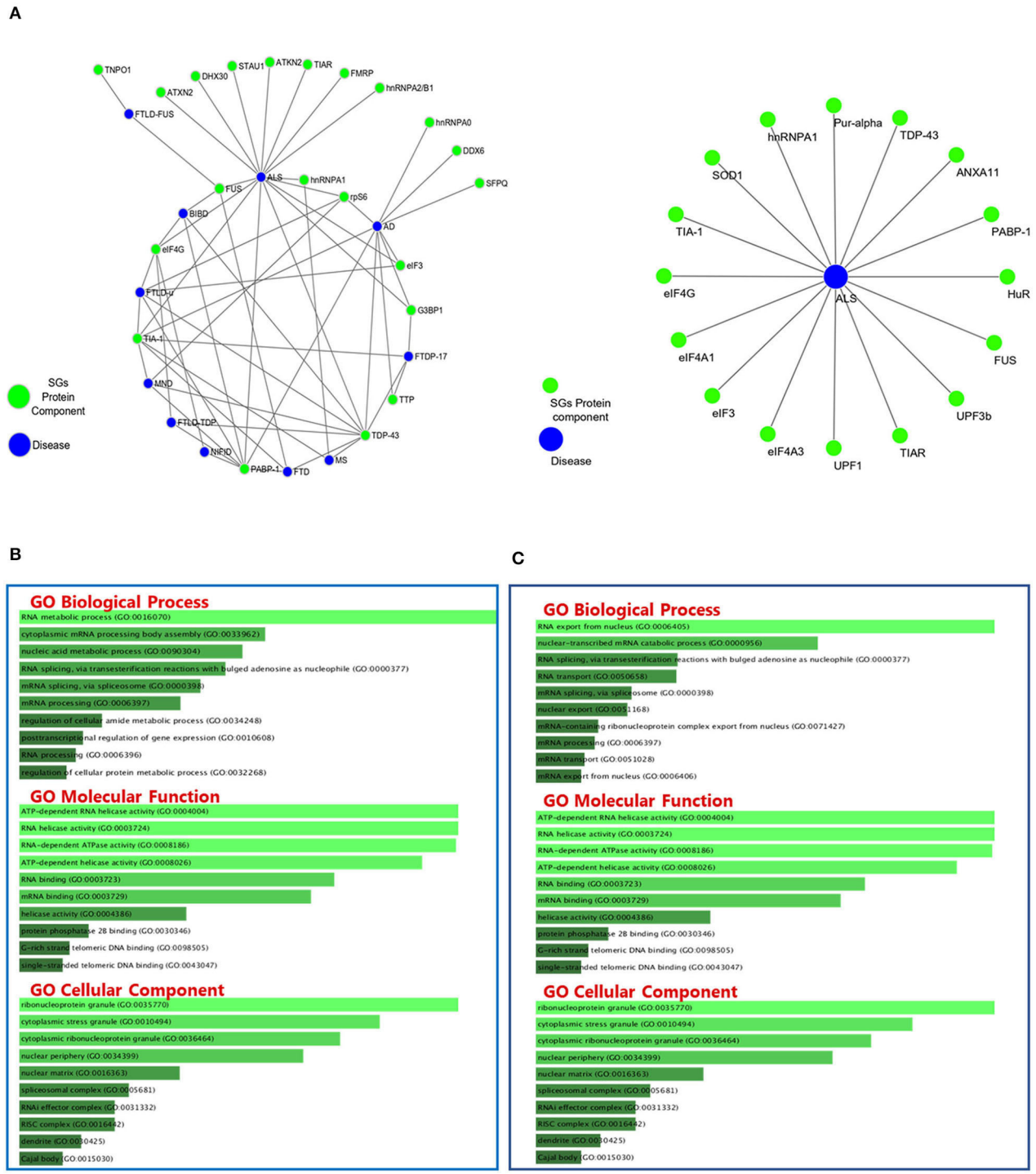

FIGURE 2 | Protein-Protein Interactions and Top 10 GO analysis of target genes in SGs protein components in neurodegenerative disease. The network of neurodegenerative diseases with protein components of SGs and their interactions. **(A)** Gene ontology analysis of the genes in **Table 2 (B)** and **Table 3 (C)** has been performed. The length of each bar represents the degree of significance in that particular category sorted by *p*-value. Note that the lower the color intensity of the bars, the greater the relationship with that category.

on the bioinformatics studies using the string-db Cytoscape plugin, 15 new genes were predicted to interact with the genes extracted from these studies, including HNRNPC, HNRNPDL, KHDRBS1, HNRNPH1, EDC4, DCP1A, ELAVL1, MATR3, TAF15, HNRNPF, PTBP1, CAPRIN1, PABPC1, KHSRP, AND ILF3.

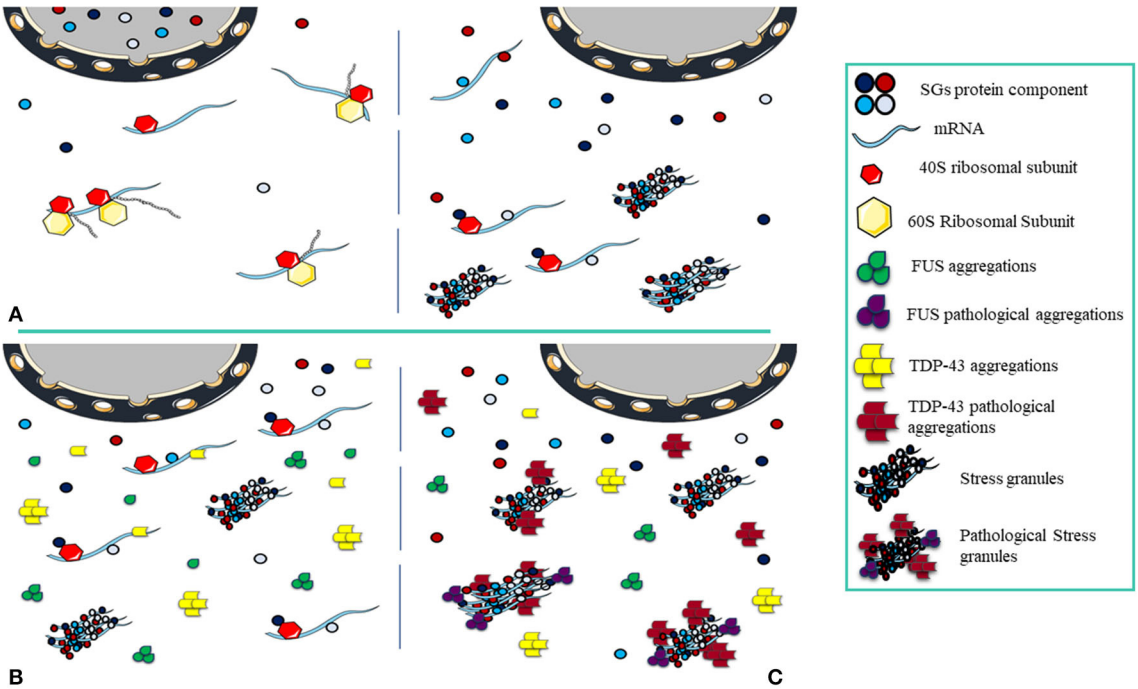

FIGURE 3 | Pathological Stress Granules Formation. **(A)** The cell is in equilibrium, and as stress arrives, nuclear depletion of SGs components occurs, the translation process halts and the structure of transient SGs is formed. Once the stress is relieved, the cell returns to normal and SGs disassemble. **(B)** The cell is exposed to acute stress, the components of SGs and protein aggregations (FUS and TDP-43) localize to the cytoplasm. In this condition, FUS and TDP-43 aggregations have not become pathological and do not interact with SGs, the number of SGs decreases as stress is relieved. **(C)** Under chronic stress, FUS and TDP-43 aggregations become pathological and in interaction with SGs, under the constant presence, pathological effects appear.

Summary of Methods of Studies Performed in Human-Derived Cell Lines

The studies were published from 2016 to 2020. In this ward, only ALS patients were sampled, whose numbers were around 50 as their number has not been reported in 5 studies. The average age of the people reported in this section is 47.6 years. Samples used in the studies included human skin fibroblasts in 18 studies, hair follicle cells (Japtok et al., 2015) and human B-lymphoblastoid cells (Daigle et al., 2016) each in one study. The protein component of SGs examined in these studies includes G3BP1, TIA-1, hnRNPA1, TDP-43, PABP-1, FUS, TIAR, eIF4A3, eIF4A1, eIF3, eIF4G, UPF1, UPF3b, HuR, ANXA11, Pur-alpha, which are also summarized in **Figure 3**. The cell lines used in this study carry missense mutations in SOD1 (Gal et al., 2016; Rajpurohit et al., 2020), TARDBP (Orrù et al., 2016; Loginov et al., 2018; Ratti et al., 2020), FUS (Japtok et al., 2015; Lenzi et al., 2015; Daigle et al., 2016; Ichiyanagi et al., 2016; Lim et al., 2016; Lo Bello et al., 2017; Kamelgarn et al., 2018; Arenas et al., 2020), TDP-43 (Kreiter et al., 2018; Loginov et al., 2018; Feneberg et al., 2020) and ANXA11 (Gieseler et al., 2019) genes and frameshift mutations in FUS (Japtok et al., 2015; Lim et al., 2016) gene and hexanucleotide repeat expansion mutations in C9ORF72 gene (Dafinca et al., 2016; Loginov et al., 2018; Ratti et al., 2020). Studies were conducted in the United States, Italy, Germany, France, Japan, South Korea, India and the United Kingdom.

SGs: From Assembly to Disequilibrium and Pathogenesis

Inhibition of translation due to stress is the main factor for SGs assembly. The size of the SGs can vary from 100 to 1,000 nm (Kedersha et al., 1999). SG assembly needs inhibition of the assembly of polysomes so that only the 40S ribosome subunit remains attached. Non-translated mRNAs are attached to other RNA binding proteins at the nucleation phase in the SGs formation. These proteins at the nucleation phase, also known as SG nucleators, are generally multi-domain proteins in which the IDR "intrinsically disordered region" and RBD domains are prominent (Kedersha et al., 2005) and facilitate the assembly of SGs (Gilks et al., 2004). The nucleation phase continues with the formation of a repository of mRNPs *in situ*, where it is accompanied by interactions between RNA-RNA and RNA-protein to create a stable form of SG cores. Increasing the interactions with the growth of these cores brings the concentration to the critical level, initiates the phase changes (Kedersha et al., 2005; Molliex et al., 2015; Patel et al., 2015) and creates the primary biphasic core/shell structures. The composition of biphasic SGs creates a larger mature assembly during the microtubule-dependent process (Wheeler et al., 2016). The opposite point of assembling SGs is disassembly. In general, disassembly involves the return of non-translated mRNAs trapped in the SG structures to the translation process and is caused by a variety of factors including chaperones in the stress

relief phase (Mazroui et al., 2007), microtubules (Loschi et al., 2009), autophagy mechanisms (Dormann et al., 2010), and post-translational modifications (Stoecklin et al., 2004). Assembling and disassembling of SGs are in equilibrium with polysomes (Kedersha et al., 2000). Since biotic or environmental stress stops translation and increases the number of SGs, relieving stress and increasing the number of translated mRNAs is associated with return to equilibrium and disassembly of SGs (Panas et al., 2016; Marnik and Updike, 2019). When the condition progresses toward disequilibrium, by increasing the assembly of SGs and decreasing the clearance, pathogenic processes would be evolved (Wolozin, 2012; Chen and Liu, 2017) (**Figure 3**).

This pathogenesis links SGs to a wide range of neurodegenerative diseases including ALS (Colombrita et al., 2009; Volkening et al., 2009; Farg et al., 2013; Manghera et al., 2016; Dreser et al., 2017; Chen and Cohen, 2019), AD (Castellani et al., 2011; Vanderweyde et al., 2012; Ivanov et al., 2016; Maziuk et al., 2018; Silva et al., 2019; Younas et al., 2020), FTD (Hirsch-Reinshagen et al., 2017; Mackenzie et al., 2017; Hock et al., 2018; Montalbano et al., 2020), and FTDP (Vanderweyde et al., 2012). Many of the protein components of SGs such as TIA-1 (Fujita et al., 2008; Volkening et al., 2009; Liu-Yesucevitz et al., 2010; Vanderweyde et al., 2012; Dafinca et al., 2016; Gal et al., 2016; Hirsch-Reinshagen et al., 2017; Mackenzie et al., 2017; Salapa et al., 2018; Chen and Cohen, 2019; Younas et al., 2020), PABP-1 (Fujita et al., 2008; Dormann et al., 2010; Bentmann et al., 2012; McGurk et al., 2014; Dafinca et al., 2016; Gal et al., 2016; Hirsch-Reinshagen et al., 2017; Kamelgarn et al., 2018; Silva et al., 2019), G3BP1 (Vanderweyde et al., 2012; Daigle et al., 2016; Gal et al., 2016; Ichiyanagi et al., 2016; Lim et al., 2016; Manghera et al., 2016; Orrù et al., 2016; Loginov et al., 2018; Mann et al., 2019), eIF4G (Dormann et al., 2010; Lim et al., 2016; Kamelgarn et al., 2018), TTP (Vanderweyde et al., 2012) and TIAR (Colombrita et al., 2009; Lenzi et al., 2015; Lo Bello et al., 2017; Codron et al., 2018; Loginov et al., 2018; Chen and Cohen, 2019; Ratti et al., 2020) have been studied in neurodegenerative diseases. IHC has revealed the colocalization of pathological accumulations of proteins such as TDP-43 (Fujita et al., 2008; Colombrita et al., 2009; Volkening et al., 2009; Liu-Yesucevitz et al., 2010; Bentmann et al., 2012; Vanderweyde et al., 2012; McGurk et al., 2014; Gal et al., 2016; Manghera et al., 2016; Orrù et al., 2016; Chen and Liu, 2017; Hirsch-Reinshagen et al., 2017; Mackenzie et al., 2017; Bennett et al., 2018; Kreiter et al., 2018; Loginov et al., 2018; Chen and Cohen, 2019; Mann et al., 2019; Feneberg et al., 2020; Levin et al., 2020; Montalbano et al., 2020; Ratti et al., 2020; Salapa et al., 2020; Vassileff et al., 2020) or FUS (Farg et al., 2013; McGurk et al., 2014; Japtok et al., 2015; Lenzi et al., 2015; Daigle et al., 2016; Lim et al., 2016; Lo Bello et al., 2017; Hock et al., 2018; Kamelgarn et al., 2018; Arenas et al., 2020) with SGs in neurodegeneration, indicating a strong association of SGs with the pathogenic mechanisms. In this study, by reviewing all studies on SGs and neurodegenerative diseases in humans, we tried to answer the question that SGs can act as nests or sources for these pathological aggregations, or disruption and mutations in the main components of these accumulations can disrupt the balance of SGs.

ALS and FTD Disorders and SGs

ALS is a neurodegenerative disease specific to motor neurons (MNs), and with progressive loss of upper MNs (UMN) in the motor cortex of the brain and lower MNs (LMN) in the brain stem and the spinal cord (Robberecht and Philips, 2013), muscle weakness and atrophy appear (Hardiman et al., 2017). The main pathological signature of ALS is the presence of inclusion bodies in the cytoplasmic region of MNs. The key component of these inclusions in 95% of cases is TDP-43 in the form of hyperphosphorylated, Ubiquitinated, and truncated (Neumann et al., 2006; Nonaka et al., 2016). FUS and SOD1 are other proteins that can be involved in the formation of these inclusions (Volkening et al., 2009; Farg et al., 2013). TDP-43 and FUS are RNA-binding proteins that are often nuclear localized but can commute between the nucleus and the cytoplasm (Kapeli et al., 2017). The nuclear activity of these proteins is summarized in transcription, pre-mRNA splicing and processing non-coding RNAs (Ederle and Dormann, 2017). In the cytoplasm, these proteins can contribute in the regulation of mRNA stability, mRNA transport, translation, autophagy, and stress response and LLPS (Birsa et al., 2020). SOD1 is a superoxide dismutase enzyme. Mutations in this gene can result in these accumulation (Volkening et al., 2009). Based on bioinformatics studies and overlap in the function of these proteins in pathological aggregations and impairment of mRNA mechanisms, these proteins can be considered as pathological factors in these disorders (Liu-Yesucevitz et al., 2010; Wolozin, 2012; Ramaswami et al., 2013). One of the symptoms of impaired mRNA mechanisms is the disequilibrium of SGs. Numerous studies have been performed on the presence of SGs and their association with pathological aggregations in humans using post mortem tissue (brain, spinal cord) and blood, which are summarized in **Table 2**. To investigate the presence of SGs in the target tissue, SG markers were used, which include TIA-1, G3BP1, PABP-1, TIAR, HuR, and TTP. Studies of human-derived cell lines have been mostly performed using autopsy skin fibroblasts and differentiation into motor (Dimos et al., 2008). These studies have allowed the study of mutations in the TDP-43, FUS, SOD1, and C9orf72 genes and their effects on cell and other components of pathological aggregations and SGs, which are summarized in **Table 3**.

TAR DNA-binding protein 43 (TDP-43), product of the TARDBP gene, plays the largest role in the formation of pathological aggregations. Most of the changes observed in this protein in aggregations include phosphorylation (Liu-Yesucevitz et al., 2010; Bentmann et al., 2012; Cohen et al., 2015; Hirsch-Reinshagen et al., 2017; Ratti et al., 2020), acetylation (Cohen et al., 2015), and cleavage at N/C terminals (Bentmann et al., 2012; Cohen et al., 2015). General observations suggest that hyperphosphorylation and acetylation may predispose TDP-43 to accumulation. TDP-43 has been studied in both full-length and cleaved (Cohen et al., 2015) forms in aggregations in spinal cord (McGurk et al., 2014; Chen and Cohen, 2019) and brain (Liu-Yesucevitz et al., 2010; Manghera et al., 2016; Hirsch-Reinshagen et al., 2017; Vassileff et al., 2020). In studies of colocalization of

TABLE 3 | Stress Granules and ALS in human derived cell lines.

	Year of publication	Country	Cell line origin	Diagnosed neurodegenerative disease (number of patients)	Age at biopsy	Mutation	Mutation type	Analysis method(s)	Protein component of stress granules	Major findings	References
Daigle et al.	2015	United States	Human B-lymphoblastoid cells	ALS	NR	FUS-R521C FUS-R518G	Missense	Culturing human lymphoblastoid cells, Immunofluorescence, Generation of deletion constructs, Western blotting, Quantitative PCR, Assessment of neuronal viability, Propidium iodide staining, TUNEL assay, Stress granule induction, and quantification	Pur-alpha G3BP1 FUS	• Pur-alpha was identified as a new component of stress granules in mutant-carrying cells. • Pur-alpha colocalized along with FUS in structural SGs. • Pur-alpha is essential for the formation of SGs. • FUS mislocalization and toxicity caused by its mutations are suppressed by improper expression of Pur-alpha.	Daigle et al., 2016
Japtok et al.	2015	Germany	Human skin fibroblast hair follicle cells (keratinocyte)	ALS (2 case and 3 control)	ALS Patients with 58 and 29 years old	FUS- R521C FUS-R495QfsX527	Missense frameshift	Generation and expansion of iPSCs, *In vitro* differentiation of embryoid bodies, AP staining and immunofluorescence on iPSC colonies, Immunofluorescence on cortical neurons, Karyotyping, Genotyping, Differentiation of human iPSCs into cortical neurons, Sodium arsenite treatment, Quantification, and statistics	FUS	• Type of FUS mutation determines the quantity of FUS accumulation in stress granules and cellular susceptibility to exogenous stress.	Japtok et al., 2015
Lenzi et al.	2015	Italy	Human skin fibroblast	ALS (3 case and 1 control)	NR	FUS-R514S FUS-R521C FUS-P525L	Missense	Generation and maintenance of human iPSCs, Differentiation of iPSCs into ventral spinal cord neural cells, RT-PCR, RT-qPCR and western blot analyses, Immunostaining and confocal imaging, Quantification of nuclear/cytoplasmic and SG FUS distribution and line scan analysis, TALEN-directed mutagenesis	FUS TIAR	• FUS mislocalization and its application in the structure of stress granules is specific to different types of mutant FUSs and occurs only under stress. • The amount of FUS used in the structure of SGs depends on the type of mutation and the amount of FUS proteins in the cytoplasm.	Lenzi et al., 2015
Gal et al.	2016	United States	Human skin fibroblast	ALS (1 case and 1 control)	ALS Patient with 63 years old Healthy control with 64 years old	SOD1- L144F	Missense	Skin Biopsy and Fibroblast Culture, Fluorescence microscopy, Coimmunoprecipitation assays, Western blotting, *In silico* docking, Stress granule induction and analysis	SOD1 G3BP1 TIA-1 hnRNPA1 TDP-43 PABP-1	• Co-localization was observed between mutant SOD1 (L144F) with G3BP1unlike WT-SOD1 protein in fibroblast cells. • The slight association of mutant SOD1 protein with several other RNA-binding proteins in ALS indicated that these interactions were more specific to the G3BP1 protein. • The RRM domain of G3BP1 and two phenylalanine residues (F380 and F382) are important for desired interactions. • SOD1 mutations and their effects on SG dynamics can be strongly associated with the characteristics and pathogenesis of ALS.	Gal et al., 2016
Dafinca et al.	2016	United kingdom	Human skin fibroblast	ALS(NR)	NR	C9orf72 mutation	HRE	Generation and Culture of iPSC Lines, Assessment of Genome Integrity and Tracking, Sendai Clearance Assay, Pluri Test, Flow Cytometry, Differentiation of iPSCs to MNs, Differentiation of iPSCs to CNs, IHC, Immunoblotting, Propidium Iodide Staining,	TIA-1 PABP-1	• Abnormal accumulation of proteins and stress granules was observed in c9orf72 IPSC-derived MNs. • Decreased survival of these cells may be due to disruption of mitochondrial membrane potential and calcium homeostasis, increased ER stress and decreased BCL2 protein levels.	Dafinca et al., 2016

(Continued)

TABLE 3 | Continued

	Year of publication	Country	Cell line origin	Diagnosed neurodegenerative disease (number of patients)	Age at biopsy	Mutation	Mutation type	Analysis method(s)	Protein component of stress granules	Major findings	References
								Mitochondrial Staining, ER Calcium Imaging, RNA-FISH, Electrophysiology, Southern Blotting, qRT-PCR, Repeat-Primed PCR, Electron Microscopy		• By examining the effects of C9orf72 mutations on calcium signaling pathways, the importance of this pathway as a therapeutic target in neurodegenerative disease was determined.	
Lim et al.	2016	South Korea	Human skin fibroblast	ALS (Shaw and Jordan, 1995) Healthy control (Shaw and Jordan, 1995)	ALS Patients ranging from 31 to 57, mean 39 years	FUS-Q519E FUS-G504Wfs FUS-R495	Missense frameshift	Conversion of human skin fibroblasts to iNeurons, Immunocytochemistry and confocal microscopy, Nuclear-cytoplasmic fractionation and immunoblot analysis	FUS eIF4G G3BP1	• Mislocalization of FUS proteins and nuclear clearance were seen in patient-derived cells. • Oxidative stress causes cytoplasmic FUS protein accumulations. • The pathological features of P.Q519E mutation were detected only in patient derived-ineuron cells as opposed to fibroblasts and transfected cells.	Lim et al., 2016
Ichiyanagi et al.	2016	Japan	Human skin fibroblast	ALS (2 case and 1 control)	ALS Patients with 39 and 43 years old	FUS-H517D	Missense	Isolation of Human Skin Fibroblasts and Generation of iPSCs, Motor Neuron Differentiation, Immunocytochemistry, High-Content Analysis, Quantitative RT-PCR, Sequence Analysis, Exon Array for MPCs	FUS G3BP1	• The produced cell line showed several characteristics of neurodegenerative diseases such as FUS mislocalization and SG production against stress. • Aberrant gene expression or incorrect splicing, was detected in MPCs using exon array analysis and CLIP-seq dataset. • The IPSC produced in this study can be well used to assess the characteristics of motor neuron diseases.	Ichiyanagi et al., 2016
Orru et al.	2016	Italy	Human skin fibroblast	ALS (2 case without mutations and 2 mutant carrier and 3 healthy control)	NR	TARDBP-A382T	Missense	Cell culture and treatments, IHC, Transfection, qPCR, Western blot Quantification of cells, forming SGs and SG size, Cell viability assays	TDP-43 HuR G3BP1	• TDP-43 did not participate directly in the structure of SGs, it helps to form SG by regulating the G3BP1 core protein. • A382T mutation meaningfully reduced the number of SGs per cell. • Stress stimulation for cells with the A382T mutation reduced survival due to the loss of TDP-43 function in SGs nucleation. • TDP-43 protein mislocalization was not detected as a pathological factor in cell death.	Orrù et al., 2016
Lo Bello et al.	2017	Italy	Human skin fibroblast	ALS (2 case without mutations and 2 mutant carrier and 2 healthy control)	NR	FUS-P525L	Missense	Skin Biopsy and Fibroblast Culture, Stress Treatment, Subcellular Fractionation, SDS-PAGE and Western Blotting, Immunofluorescence, Subcellular FUS Expression, Time Course of the Number of Fibroblasts Containing Stress Granules, Evaluation of the Number of Stress Granules per Cell	FUS TIAR	• High nuclear FUS expression was observed in fibroblasts in both controls and patients. Protein placement in mutant carriers was seen in both nucleus and cytoplasm (mostly cytoplasm). • Stress treatment caused the mis-localization of large amounts of FUS proteins in the cytoplasm and placement in the structure of SGs, instead time-dependent reduction was seen in all cases. • Fibroblasts mutant carriers had more SGs than ALS and control samples and persevere in the cell longer.	Lo Bello et al., 2017

(Continued)

TABLE 3 | Continued

	Year of publication	Country	Cell line origin	Diagnosed neurodegenerative disease (number of patients)	Age at biopsy	Mutation	Mutation type	Analysis method(s)	Protein component of stress granules	Major findings	References
Codron et al.	2018	France	Human skin fibroblast	ALS (6 case and 4 control)	ALS Patients ranging from 54 to 76, mean 63.8 years Healthy controls with a mean age of 59.7	NR	NR	Cell culture, Cell growth assay, Immunofixation, 3D fluorescence microscopy, Super resolution microscopy (dStorm), Reactive oxygen species detection Reactive oxygen species detection	TDP-43 TIAR	• There was no difference between fibroblast cell growth, shape and spreading in patients and controls cells. • Mislocalization and accumulation of TDP-43 were not detected in patients and controls cells. • The cytoskeleton appeared completely normal in cells and no difference was observed in the distribution of mitochondria. • The rate of ROS production and its stress response in patient-derived cells and controls showed similarity. • Patient-derived fibroblasts are not suitable for pathological and prognostic studies of ALS.	Codron et al., 2018
Kamelgarn et al.	2018	United States	Human skin fibroblast	ALS (6 case and 5 control)	ALS Patients ranging from 26 to 58, mean 42.1 years	FUS-R521G FUS-P525R	Missense	Skin Biopsy and Fibroblast Culture, Protein Translation Assays, NMD Activity Assays	FUS eIF4A3 eIF4A1 eIF3 eIF4G UPF1 UPF3b PABP-1	• Development of a new protocol for the separation of positive cytoplasmic granules. • The mutant FUS in fibroblast cell line derived from ALS's and can interfere with the translation process. • The mutant FUS interfered with the automatic regulation of NMD and increased its activity by increasing its promoting factors (UPF1, UPF3b) and decreasing its negative regulatory factors (UPF3a).	Kamelgarn et al., 2018
Kreiter et al.	2018	Germany	Human skin fibroblast	ALS (2 case and 4 control)	NR	TDP-43-S393L TDP-43-G294V	Missense	Generation of iPSC lines, Trilineage differentiation potential, Karyotyping, Genotyping Differentiation of human NPCs to spinal motor neurons, Immunofluorescence of spinal motor neurons, Microfluidic chambers, Live cell imaging, Tracking analysis, Static analysis of cell organelles, Electrophysiology	TDP-43	• In the early stages of neuronal differentiation, no difference was seen between TDP-43 mutant cell lines and WTs. • Neuronal loss and pathological neurofilament abnormalities were seen in the aging stage in mutant TDP-43 cell lines. • Abnormal phenotypes in terms of shape, size, and motility were observed in mitochondria and lysosomes that were not due to mis-localization or accumulation of TDP-43 in the motor neurons carrying the TDP-43 mutations in the aging phase. • Axon trafficking in motor neurons was improved by D-sorbitol, but no TDP-43 accumulations or mis-localizations were observed. • S393L and G294V Mutations can cause motor neuron degeneration but are independent of the cytoplasmic accumulation of TDP-43.	Kreiter et al., 2018

(Continued)

TABLE 3 | Continued

	Year of publication	Country	Cell line origin	Diagnosed neurodegenerative disease (number of patients)	Age at biopsy	Mutation	Mutation type	Analysis method(s)	Protein component of stress granules	Major findings	References
Colombrita et al.	2018	Italy	Human skin fibroblast	ALS (6 case and 3 control)	NR	TARDBP -A382T C9orf72 mutation	Missense HRE	Cell culture and treatments, Quantification of cells forming SGs and SG size	TDP-43 TIAR	• Stress granules formed by arsenite treatment are larger than SGs formed by acute stress. • SGs examined in C9orf72 and TARDBP mutant cells were different in size and number. • Arsenic-induced SGs used TDP-43 in mutant cells, while TDP-43 was not found in acute stress SGs. • Filamentous and round pTDP-43 inclusions were found in mutant-carrying cells after chronic arsenite stress.	Theme 4 Human cell biology and pathology, 2018
Dafinca et al.	2018	United kingdom	Human skin fibroblast	ALS (2 case and 2 control)	NR	TDP-43M337V TDP-43 I383T	Missense	Skin Biopsy and Fibroblast Culture, Generation of iPSC lines, HI-FI CRISPR/Cas9, Stress granule analysis, Nucleo-cytoplasmic Transport investigation	TDP-43 G3BP1	• TDP-43 mutations devastate protein degradation in IPSC derived MNs. • TDP-43 mutations have a devastating effect on the mechanism of protein transport between the nucleus and the cytoplasm.	Theme 4 Human cell biology and pathology, 2018
Hedges	2019	United Kingdom	Human skin fibroblast	ALS(NR)	NR	ANXA11- D40G ANXA11- G38R ANXA11- R235Q	Missense	Opera Phenix imaging platform, super resolution microscopy, live imaging	TDP-43 ANXA11	• TDP-43 protein mislocalization was detected in ANXA11 mutant motor neurons. • Altering the location of ANXA11 protein with stress granules (reduction in co-localization).	Gieseler et al., 2019
Rajpurohit et al.	2020	India	Human skin fibroblast	ALS(NR)	NR	SOD1-L39R	Missense	Reprogramming of iPSCs and Culture, Differentiation of iPSCs into Astrocytes and Motor Neurons, Stress Granule Dynamics, Endoplasmic Reticulum Stress, Autophagy Studies, Non-Cell Autonomous Neurotoxicity Studies, IHC Analysis,	SOD1 G3BP1	High expression of G3BP1 and co-localization with SOD1-L39R in ALS's MNs and astrocytes is associated with increased AIF1-mediated autophagy activity and caspase 7/3 upregulation.	Rajpurohit et al., 2020
Arenas et al.	2020	United States	Human skin fibroblast	ALS (5 case and 5 control)	ALS Patients ranging from 26 to 58, mean 39.4 years.	FUS-R521G FUS-P525R	Missense	Patient skin fibroblast isolation and culture, Generation of the anti-acetylated-K510 FUS antibody	FUS	• FUS acetylations in lysine 510, located in the NLS sequence, disrupts the interaction between FUS and Transportin-1 and results in FUS mis-localization in the cytoplasm resembling SG aggregations. • ALS fibroblasts showed greater acetylations in lysine compared to controls.	Arenas et al., 2020
Feneberg et al.	2020	United Kingdom	Human skin fibroblast	ALS (1)	NR	TDP-43M337V	Missense	Human cellular models, Mass spectrometry and bioinformatics, IHC and microscopy, Stress granule analysis, Immunoprecipitation and immunoblotting, Ultrafiltration liquid chromatography and extracellular vesicle Characterization, Transmission electron microscopy	TDP-43 eIF4A1	TDP-43M337V can increase the formation of stress granules by degrading interprotein interactions to increase binding to eIF4A1 and endoplasmic reticulum chaperone Grp78.	Feneberg et al., 2020

(Continued)

TABLE 3 | Continued

	Year of publication	Country	Cell line origin	Diagnosed neurodegenerative disease (number of patients)	Age at biopsy	Mutation	Mutation type	Analysis method(s)	Protein component of stress granules	Major findings	References
Ratti et al.	2020	Italy	Human skin fibroblast	ALS (2 case and 1 control)	ALS Patients with 56 and 48 years old. Healthy control with 45 years old.	TARDBP -A382T C9orf72 mutation	Missense HRE	iPSC-derived motoneurons, Arsenite treatment, Cell viability assay, Immunofluorescence, Quantitative analyses of SG, Colocalization image analysis, TEM, Quantitative analysis of TEM data	TDP-43 TIAR	• Recruitment of TDP-43 as pTDP-43 in SGs structure due to chronic stress and increase in P62. • Genetics play a key role in responding to cellular stress and the size and number of SGs. • Disruption of autophagy mechanisms may be involved in TDP-43 aggregations. • Arsenite stress relief was associated with a decrease in number of SGs and TDP-43 aggregations in 72 h, but P62 remained, so Disruption of autophagy mechanisms may be involved in TDP-43 aggregations.	Ratti et al., 2020

SG, Stress Granule; ALS, Amyotrophic lateral sclerosis; PCR, polymerase chain reaction; iPSC, Induced pluripotent stem cells; RT-PCR, Reverse Transcriptase PCR; Q-PCR, Quantitative PCR; TALEN, Transcription activator-like effector nucleases; HRE, hexanucleotide repeat expansion; CN, cortical neurons; MN, Motor Neurons; IHC, Immunohistochemistry; ER, Endoplasmic Reticulum; qRT-PCR, Quantitative Reverse Transcription PCR; MPC, motor neuron precursor cell; NMD, Non-sense Mediated mRNA Decay; NPC, neural precursor cell; HI-FI, high-fidelity; NLS, nuclear localizing sequence; TEM, Transmission Electron Microscopy.

TDP-43 with SGs, it is most often colocalized with TIA-1, PABP-1, G3BP1, TIAR, and HuR, which are markers for the presence of SGs in cell and are the core proteins in nucleation phase in the assembly of SGs (Kedersha et al., 2005). In addition, in MNs differentiated from fibroblasts, the effect of TDP43 on nucleation phase and interaction with G3BP1 in CORE formation has been determined (Orrù et al., 2016). TDP-43 is colocalized with STAUFEN and FMRP, which play important roles in mRNA mechanisms. STAUFEN (Volkening et al., 2009; Vassileff et al., 2020), encoded by the STAU1 gene, is involved in the transport of mRNA to different subcellular compartments and organelles (Thomas et al., 2005). FMRP is involved in the nucleocytoplasmic shuttling and dendritic localization of mRNA (Antar et al., 2005). So far, the effects of TDP-43 mutants including S393L (Kreiter et al., 2018), G294V (Kreiter et al., 2018), M337V (Loginov et al., 2018; Feneberg et al., 2020), I383T (Loginov et al., 2018) and TARDBP-A382T (Orrù et al., 2016; Loginov et al., 2018; Ratti et al., 2020) mutations in human-derived cell line studies have been considered. S393L, G294V missense mutations can cause neurodegeneration in MNs in a TDP-43 accumulation independent manner (Kreiter et al., 2018). The TDP-43 M337V mutant can increase the assembly of SGs by interfering with the function of eIF4A1 and endoplasmic reticulum chaperone Grp78 (Feneberg et al., 2020). In contrast, TARDBP-A382T mutation due to loss of TDP-43 function significantly has reduced the number of SGs in cells (Orrù et al., 2016).

FUS (fused in sarcoma) is present in pathological aggregations with a lower percentage than TDP-43 and its association and effects on SGs have been studied. The mechanism of FUS toxicity is not fully understood, but due to its cytoplasmic localization, loss of nuclear activity and acquisition of cytoplasmic function might be involved (Kino et al., 2015). Studies in post-mortem tissue have shown the association of FUS aggregations with SGs through colocalization with ATAXIN2 (Farg et al., 2013) and PABP-1 (McGurk et al., 2014). FUS aggregations are directly affected by the type of mutation, benign and malignant (Japtok et al., 2015). The amount of mislocalization and recruitment in the structure of SGs is related to the type of mutation (Lenzi et al., 2015). FUS in the cell carrying the P525L mutation has more cytoplasmic localization than in control, and when exposed to stress, this localization increases leading to nuclear depletion (Lim et al., 2016). After stress relief, the mutant carrier cell needs more time to return to normal than control. SGs are more numerous in this cell and have a longer persistence, which indicates the direct effect of FUS mutations on SGs (Lo Bello et al., 2017). Post-transcription modifications, such as acetylation in lysine 510, which is located in the NLS sequence, disrupts the interaction between FUS and transportin1, causing its cytoplasmic mislocalization, which is more common in the pathogenesis of ALS than in controls (Arenas et al., 2020). The localization of SOD1 has been confirmed in both mutant and WT form with TDP-43 accumulations in spinal cord motor neurons (Volkening et al., 2009). Mutations that occur in SOD1 can also affect the dynamics of SGs. The mutant types SOD1-L144F (Gal et al., 2016) and SOD1-L39R (Rajpurohit et al., 2020) colocalize with G3BP1 in fibroblast-derived motor neurons, whereas SOD1-WT does

not colocalize with SGs (Gal et al., 2016; Rajpurohit et al., 2020).

Hexanucleotide repeat expansion (HRE) is another common mutation in ALS that is associated with an increase in the number of G4C2 repeats in the C9orf72 gene. The number of repeats in normal people are between 20 and 30, but in people with mutations, the number of repeats increases to hundreds (Khan et al., 2012). Three mechanisms explain the effect of C9orf72 mutations on SGs.

1. C9orf72-related RNA transcripts accumulate in the nucleus and cytoplasm causing sequestration of RNA-binding proteins, including proteins involved in SG dynamics (Rossi et al., 2015; Dafinca et al., 2016). Colocalization of PABP-1 with TDP-43 inclusions was higher in ALS patients with C9orf72 mutation (67%) than in patients with ATXN2 mutation (47%) and patients without any mutation (36%) (McGurk et al., 2014).
2. The effect of mutations on C9orf72 protein function and the destruction of interactions with other proteins is another proposed mechanism. DENNL72 is another name for C9orf72, which stands for differentially expressed in normal and neoplastic cells and One of the molecular roles envisaged for it is acting as a guanine nucleotide exchange factor (GEF) (Levine et al., 2013). The interaction of C9orf72 as GEF with Rab proteins (Tang, 2016) is involved in autophagy and cellular trafficking mechanisms such as Rab7 and Rab11 (Farg et al., 2014) and disruption of these pathways can lead to cytoplasmic accumulations of TDP-43 (Ratti et al., 2020) and decreased clearance of SGs (Monahan et al., 2016).
3. The transcript of the mutant C9orf72 gene containing GGGGCC repeats can be translated during the non-ATG translation mechanism and produce 5 different types of dipeptide repeats (DPRs) (Mori et al., 2013). Among these, arginine-containing dipeptide repeats can interact with a number of SG protein components that have the IDR domain. DPRs containing glycine and proline also play a role in the assembly of SGs by inhibiting the translation and phosphorylation of eIF2a and G3BP1 (Lee et al., 2016).

FTD is one of the most common types of dementia that affects people under the age of 65 (Bird et al., 1999) and represents a diverse range of subtypes with neurodegenerative disorders such as FTLD (Faber, 1999). Due to common characteristics in clinical observations, ALS and FTD now form a broad continuum of neurodegeneration that can occur in an individual or a family. Like ALS, studies on post-mortem tissue, specifically the brain of FTD patients, have revealed the association and development of the disease with SGs (Dormann et al., 2010; Liu-Yesucevitz et al., 2010; Hirsch-Reinshagen et al., 2017; Mackenzie et al., 2017). Most pathological mechanisms and aggregations such as TDP43, FUS, and C9orf72 mutations overlap with ALS. But FTD has some distinctive features. No colocalization was observed between PABP-1 and eIF4G with cytoplasmic neuronal inclusions in FTLD-TDP brain (Dormann et al., 2010), and acetylated and full-length pTDP-43 have no effects in the pathogenesis of FTLD-TDP (Cohen et al., 2015).

AD and SGs

AD is a chronic neurodegenerative disease that is accompanied by death of neurons and loss of synapses in the cerebral cortex and certain subcortical regions of the brain (Tiraboschi et al., 2004; Burns and Iliffe, 2009). The most common form of dementia is AD, which occurs with abnormal structures (Wang et al., 2018), extracellular senile plaques, composed mainly of small proteins called Aβ42 (Bate et al., 2006), and intraneuronal neurofibrillary tangles, which are the result of accumulations of hyperphosphorylated Tau proteins (Bancher et al., 1989). Tau proteins are a group of six protein isoforms produced by alternative splicing of the MAPT (microtubule-associated protein Tau) gene (Goedert et al., 1989). The main function of Tau proteins is to maintain the stability of microtubules in axons due to their high expression in CNS neurons (Haritani et al., 1994), which are highly soluble in the cytoplasm and contribute to the dynamic and functions of microtubules (Arendt et al., 2016). Tau undergoes many post-translational modifications, including hyperphosphorylation (Grundke-Iqbal et al., 1986), acetylation (Min et al., 2010), C-terminal truncation (Zhao et al., 2016), and n-glycosylation (Wang et al., 1996), which can play a role in regulating its localization and functions. Usually, Tau is non-phosphorylated in interaction with microtubules in the axons. When stress is applied, it is phosphorylated near the microtubule binding domain and loses its ability to bind to microtubules (Trinczek et al., 1995). The hyperphosphorylated form of Tau is seen in all six isoforms in neurofibrillary tangles (Hernández and Avila, 2007). Hyperphosphorylation increases the affinity of Tau proteins for each other and binds together to form oligomers and misfolded Taus. Oligomers bind to other units to form Tau deposits, which are the Elements of NFTs that bind together to form NFTs (Shafiei et al., 2017).

Tau can act as a negative regulator of protein translation by binding to ribosomes and reducing protein synthesis (Meier et al., 2016). Stopping translation and providing RNA-binding proteins to mRNA are key elements in the formation of SGs. TIA-1 and TTP are among the core nucleation proteins. The size of Tau aggregations is directly related to TIA-1 colocalization. The larger the Tau aggregations, the greater the rate of TIA-1 colocalization (Vanderweyde et al., 2012). PABP-1 and DDX6 are also proteins found near Tau aggregations in the temporal cortex neurons of AD (Silva et al., 2019). The association of aggregations between RNA-binding proteins and the formation of SGs with Tau aggregates has not been well-studied. Tau aggregations might promote the dynamic equilibrium of SGs toward further assembly or to SGs disequilibrium pave the way for the accumulation of Tau proteins. The formation of RBPs pathological aggregations close to the Tau pathological aggregates supports this hypothesis (Maziuk et al., 2018). Tau proteins have interaction with rps6, which is a component of the 40s ribosome complex, and affects translation inhibition (Koren et al., 2019). Notably, hippocampal neurons in AD patients have more positive rps6 granules than controls (Castellani et al., 2011). Moreover, the colocalization of rps6 with TIA-1 and PABP-1 in basophilic inclusions may indicate one of the main shared mechanisms between Tau aggregations and stress granules (Fujita et al., 2008).

The association of TDP-43 oligomers with Tau aggregations has also been suggested as one of the interactions involved in the pathogenesis of Tau (Montalbano et al., 2020).

MS and SGs

MS is a demyelinating disease in which the cover of nerve cells in the brain and spinal cord is damaged (Noyes and Weinstock-Guttman, 2013). The causative mechanism of the disease is summarized in the destruction of myelin sheath by the immune system and defects in myelin-producing cells (Nakahara et al., 2011). The disease has three main features, including the formation of lesions in the CNS, inflammation and destruction of the myelin sheath (Compston and Coles, 2008). Neurodegeneration is also an important feature in the pathology of MS (Frohman et al., 2006; Lassmann and van Horssen, 2011), but so far, no specific mechanism has been proposed for it. The impact of SGs on neurodegeneration and neurodegenerative diseases has been fully discussed so far. Heterogeneous nuclear ribonucleoprotein A1 (hnRNPA1) is a major component in the formation of SGs (Guil et al., 2006) and is discussed as a factor in the pathogenesis of autoimmune mediated CNS neurological diseases and as a link between SGs and autoimmune neurological diseases (Douglas et al., 2016). The interaction between TIA-1 and hnRNPA1 in cytoplasmic granules and its nuclear depletion in MS patients is significant. The aggregations of TIA-1 in the structure of large SGs in the cytoplasm can be a link between degeneration in neurons and MS (Salapa et al., 2018). Nuclear depletion of TDP-43 and interaction with hnRNPA1 and colocalization of both in the structure of SGs also emphasizes the importance of SGs in MS (Levin et al., 2020; Salapa et al., 2020).

Bioinformatics Perspective

GO classifies relationships between genes by annotating and categorizing them into three levels: biological process, molecular function, and cellular component. Biological process describes the cellular or physiological role performed on a larger scale by a gene in relation to other genes. The molecular function describes the molecular activity of the desired gene, and the cellular component determines where the gene product executes its function (The Gene Ontology Consortium., 2019). GO analysis was performed on the list of genes associated with SGs in neurodegenerative diseases (**Figure 3A**) and the list of genes associated with SGs in ALS disease was extracted from human derived cell lines studies (**Figure 3C**) using Enrichr's web-based tools and services (Kuleshov et al., 2016). Most of the proteins in the structure of SGs are RBPs (Kedersha et al., 2005), and GO analysis confirms this. According to the GO biological process, the connections that can be made in one biological pathway with other proteins are more involved in the RNA metabolic pathways and, as expected, all of these proteins act in conjunction with RNAs, including cytoplasmic mRNA, body assembly, and RNA splicing. Further use of these proteins in

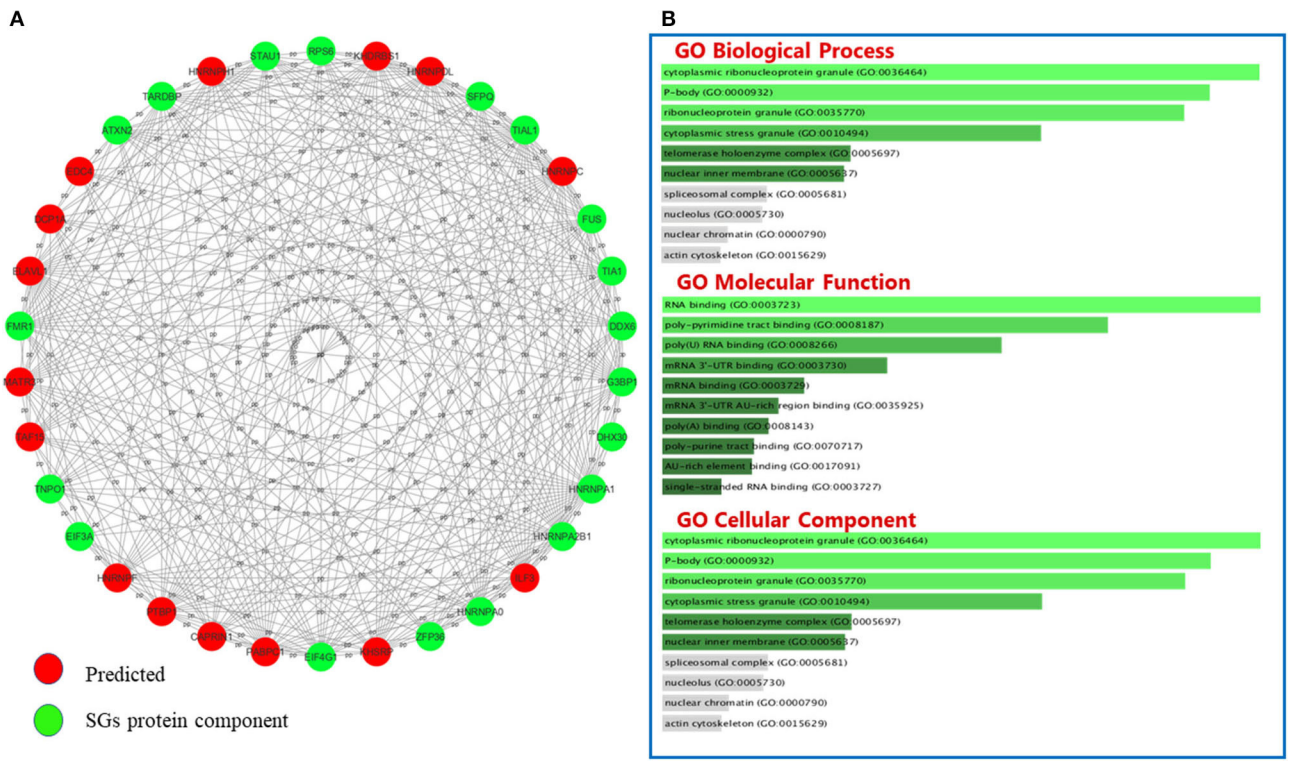

FIGURE 4 | The interactions between SGs protein components and predicted proteins and GO analysis on predicted ones in neurodegenerative disease. **(A)** Fifteen new proteins were predicted by interaction with SGs protein components using the Cytoscape string-db plugin on data extracted from articles. **(B)** Fifteen new proteins were predicted by interaction with SGs protein components using the Cytoscape string-db plugin on data extracted from articles. GO analysis was performed on the predicted proteins in three biological processes: molecular function and cellular component. The length of each bar indicates the importance in that particular category sorted by *p*-value. Note that the lower the color intensity of the bars, the greater the relationship with that category.

the structure of ribonucleoprotein granules, cytoplasmic SGs and cytoplasmic ribonucleoprotein granules was confirmed by GO cellular component analysis. In ALS, the biological association of these proteins with other proteins, based on the GO biological process, significantly confirmed their role in RNA export from nucleus. This was expected, given that these proteins are mostly shuttling between nucleus and cytoplasm. Gene prediction was performed on the gene list extracted in neurodegenerative disease in **Table 3** by string-db cytoscape plugin (Doncheva et al., 2019). GO biological process showed these proteins interact with other proteins in p-bodies, cytoplasmic ribonucleoprotein granules and cytoplasmic SGs. Overall, bioinformatics analysis determined the association of these proteins and genes with RNA-related mechanisms that are specifically involved in the formation and assembly of ribonucleoprotein granules. Their functional position is also shared between nucleus and cytoplasm and is an evidence to trafficking and shuttling of SGs protein components between them (**Figure 4**).

Conclusions

Equilibrium is the most important point in SGs. SGs are in the nature of the cell and are considered as cell solutions to stress. They are temporary constructions and when the stress is relieved, they are disassembled and reduced in number, and the cell condition returns to normal. If under any circumstances the presence of SGs becomes permanent and leads to disequilibrium, in interaction with pathological aggregations such as TDP and FUS aggregations, they can lead to pathological conditions such as neuron degeneration. SGs have been studied in many neurodegenerative diseases in humans, including ALS, FTD, AD, and MS. These studies have indicated common features in SG biology among neurodegenerative diseases. At least 15 proteins have been predicted to interact with the protein components of SGs in mentioned neurodegenerative disorders. Therefore, it seems that SG biology is common between these disorders. Yet, some components of SGs might be specific to these disorders. Based on the rarity of comparative analysis between these disorders, it is not possible to male conclusive interpretations in this regard. We have tried to provide a comprehensive summary of these studies and an overview of SGs in neurodegenerative diseases. To conclude, more studies can be done in diseases such as AD and MS and the association of the Tau protein with other protein components of SGs or the association of inflammatory pathways with the formation of SGs could also be assessed.

AUTHOR CONTRIBUTIONS

MT, SG-F, and MR wrote the manuscript and contributed in study design. MA, MS, HS, and AJ contributed in the data collection, designed the tables and figures. All authors approved the manuscript.

SUPPLEMENTARY MATERIAL

The Supplementary Material for this article can be found online at: https://www.frontiersin.org/articles/10.3389/fnagi.2021.650740/full#supplementary-material

REFERENCES

Antar, L. N., Dictenberg, J. B., Plociniak, M., Afroz, R., and Bassell, G. J. (2005). Localization of FMRP-associated mRNA granules and requirement of microtubules for activity-dependent trafficking in hippocampal neurons. *Genes Brain Behav.* 4, 350–359. doi: 10.1111/j.1601-183X.2005.00128.x

Arenas, A., Chen, J., Kuang, L., Barnett, K., Kasarskis, E., Gal, J., et al. (2020). Lysine acetylation regulates the RNA binding, subcellular localization and inclusion formation of FUS. *Hum. Mol. Genet.* 29, 2684–2697. doi: 10.1093/hmg/ddaa159

Arendt, T., Stieler, J. T., and Holzer, M. (2016). Tau and tauopathies. *Brain Res. Bull.* 126(Pt 3), 238–292. doi: 10.1016/j.brainresbull.2016.08.018

Arimoto-Matsuzaki, K., Fukuda, H., Imajoh-Ohmi, S., Saito, H., and Takekawa, M. (2008). Formation of stress granules inhibits apoptosis by suppressing stress-responsive MAPK pathways. *Nat. Cell Biol.* 10, 1324–1332. doi: 10.1038/ncb1791

Arksey, H., and O'Malley, L. (2005). Scoping studies: towards a methodological framework. *Int. J. Soc. Res. Methodol.* 8, 19–32. doi: 10.1080/1364557032000119616

Arrigo, A. P., Suhan, J. P., and Welch, W. J. (1988). Dynamic changes in the structure and intracellular locale of the mammalian low-molecular-weight heat shock protein. *Mol. Cell. Biol.* 8, 5059–5071. doi: 10.1128/MCB.8.12.5059

Ash, P. E. A., Vanderweyde, T. E., Youmans, K. L., Apicco, D. J., and Wolozin, B. (2014). Pathological stress granules in Alzheimer's disease. *Brain Res.* 1584, 52–58. doi: 10.1016/j.brainres.2014.05.052

Aulas, A., Fay, M. M., Lyons, S. M., Achorn, C. A., Kedersha, N., Anderson, P., et al. (2017). Stress-specific differences in assembly and composition of stress granules and related foci. *J. Cell Sci.* 130:927. doi: 10.1242/jcs.199240

Aulas, A., Lyons, S. M., Fay, M. M., Anderson, P., and Ivanov, P. (2018). Nitric oxide triggers the assembly of "type II" stress granules linked to decreased cell viability. *Cell Death Dis.* 9:1129. doi: 10.1038/s41419-018-1173-x

Bancher, C., Brunner, C., Lassmann, H., Budka, H., Jellinger, K., Wiche, G., et al. (1989). Accumulation of abnormally phosphorylated τ precedes the formation of neurofibrillary tangles in Alzheimer's disease. *Brain Res.* 477, 90–99. doi: 10.1016/0006-8993(89)91396-6

Baron, D. M., Kaushansky, L. J., Ward, C. L., Sama, R. R. K., Chian, R. J., Boggio, K. J., et al. (2013). Amyotrophic lateral sclerosis-linked FUS/TLS alters stress granule assembly and dynamics. *Mol. Neurodegen.* 8:30. doi: 10.1186/1750-1326-8-30

Bate, C., Kempster, S., Last, V., and Williams, A. (2006). Interferon-gamma increases neuronal death in response to amyloid-beta1-42. *J. Neuroinflamm.* 3:7. doi: 10.1186/1742-2094-3-7

Bennett, C. L., Dastidar, S. G., Ling, S. C., Malik, B., Ashe, T., Wadhwa, M., et al. (2018). Senataxin mutations elicit motor neuron degeneration phenotypes and yield TDP-43 mislocalization in ALS4 mice and human patients. *Acta Neuropathol.* 136, 425–443. doi: 10.1007/s00401-018-1852-9

Bentmann, E., Neumann, M., Tahirovic, S., Rodde, R., Dormann, D., and Haass, C. (2012). Requirements for stress granule recruitment of fused in sarcoma (FUS) and TAR DNA-binding protein of 43 kDa (TDP-43). *J. Biol. Chem.* 287, 23079–23094. doi: 10.1074/jbc.M111.328757

Bird, T. D., Nochlin, D., Poorkaj, P., Cherrier, M., Kaye, J., Payami, H., et al. (1999). A clinical pathological comparison of three families with frontotemporal dementia and identical mutations in the tau gene (P301L). *Brain* 122, 741–756. doi: 10.1093/brain/122.4.741

Birsa, N., Bentham, M. P., and Fratta, P. (2020). Cytoplasmic functions of TDP-43 and FUS and their role in ALS. *Semin. Cell Dev. Biol.* 99, 193–201. doi: 10.1016/j.semcdb.2019.05.023

Boncella, A. E., Shattuck, J. E., Cascarina, S. M., Paul, K. R., Baer, M. H., Fomicheva, A., et al. (2020). Composition-based prediction and rational manipulation of prion-like domain recruitment to stress granules. *Proc. Natl. Acad. Sci. U.S.A.* 117, 5826–5835. doi: 10.1073/pnas.1912723117

Brown, D. G., Shorter, J., and Wobst, H. J. (2020). Emerging small-molecule therapeutic approaches for amyotrophic lateral sclerosis and frontotemporal dementia. *Bioorgan. Med. Chem. Lett.* 30:126942. doi: 10.1016/j.bmcl.2019.126942

Burns, A., and Iliffe, S. (2009). Alzheimer's disease. *BMJ* 338:b158. doi: 10.1136/bmj.b158

Cao, X., Jin, X., and Liu, B. (2020). The involvement of stress granules in aging and aging-associated diseases. *Aging Cell* 19:e13136. doi: 10.1111/acel.13136

Castellani, R. J., Gupta, Y., Sheng, B., Siedlak, S. L., Harris, P. L., Coller, J. M., et al. (2011). A novel origin for granulovacuolar degeneration in aging and Alzheimer's disease: parallels to stress granules. *Lab. Invest.* 91, 1777–1786. doi: 10.1038/labinvest.2011.149

Chen, L., and Liu, B. (2017). Relationships between stress granules, oxidative stress, and neurodegenerative diseases. *Oxidat. Med. Cell. Long.* 2017:1809592. doi: 10.1155/2017/1809592

Chen, Y., and Cohen, T. J. (2019). Aggregation of the nucleic acid-binding protein TDP-43 occurs via distinct routes that are coordinated with stress granule formation. *J. Biol. Chem.* 294, 3696–3706. doi: 10.1074/jbc.RA118.006351

Chitiprolu, M., Jagow, C., Tremblay, V., Bondy-Chorney, E., Paris, G., Savard, A., et al. (2018). A complex of C9ORF72 and p62 uses arginine methylation to eliminate stress granules by autophagy. *Nat. Commun.* 9:2794. doi: 10.1038/s41467-018-05273-7

Codron, P., Cassereau, J., Vourc'h, P., Veyrat-Durebex, C., Blasco, H., Kane, S., et al. (2018). Primary fibroblasts derived from sporadic amyotrophic lateral sclerosis patients do not show ALS cytological lesions. *Amyotroph. Lat. Scl. Frontotemp. Degener.* 19, 446–456. doi: 10.1080/21678421.2018.1431787

Cohen, T. J., Hwang, A. W., Restrepo, C. R., Yuan, C. X., Trojanowski, J. Q., and Lee, V. M. Y. (2015). An acetylation switch controls TDP-43 function and aggregation propensity. *Nat. Commun.* 6:5845. doi: 10.1038/ncomms6845

Colombrita, C., Zennaro, E., Fallini, C., Weber, M., Sommacal, A., Buratti, E., et al. (2009). TDP-43 is recruited to stress granules in conditions of oxidative insult. *J. Neurochem.* 111, 1051–1061. doi: 10.1111/j.1471-4159.2009.06383.x

Colquhoun, H. L., Levac, D., O'Brien, K. K., Straus, S., Tricco, A. C., Perrier, L., et al. (2014). Scoping reviews: time for clarity in definition, methods, and reporting. *J. Clin. Epidemiol.* 67, 1291–1294. doi: 10.1016/j.jclinepi.2014.03.013

Compston, A., and Coles, A. (2008). Multiple sclerosis. *Lancet* 372, 1502–1517. doi: 10.1016/S0140-6736(08)61620-7

Dafinca, R., Scaber, J., Ababneh, N., Lalic, T., Weir, G., Christian, H., et al. (2016). C9orf72 hexanucleotide expansions are associated with altered endoplasmic reticulum calcium homeostasis and stress granule formation in induced pluripotent stem cell-derived neurons from patients with amyotrophic lateral sclerosis and frontotemporal dementia. *Stem Cells.* 34, 2063–2078. doi: 10.1002/stem.2388

Daigle, J. G., Krishnamurthy, K., Ramesh, N., Casci, I., Monaghan, J., McAvoy, K., et al. (2016). Pur-alpha regulates cytoplasmic stress granule dynamics and ameliorates FUS toxicity. *Acta Neuropathol.* 131, 605–620. doi: 10.1007/s00401-015-1530-0

Dimos, J. T., Rodolfa, K. T., Niakan, K. K., Weisenthal, L. M., Mitsumoto, H., Chung, W., et al. (2008). Induced pluripotent stem cells generated from patients with ALS can be differentiated into motor neurons. *Science*. (2008) 321, 1218–1221. doi: 10.1126/science.1158799

Doncheva, N. T., Morris, J. H., Gorodkin, J., and Jensen, L. J. (2019). Cytoscape stringapp: network analysis and visualization of proteomics data. *J. Proteome Res.* 18, 623–632. doi: 10.1021/acs.jproteome.8b00702

Dormann, D., Rodde, R., Edbauer, D., Bentmann, E., Fischer, I., Hruscha, A., et al. (2010). ALS-associated fused in sarcoma (FUS) mutations disrupt transportin-mediated nuclear import. *EMBO J.* 29, 2841–2857. doi: 10.1038/emboj.2010.143

Douglas, J. N., Gardner, L. A., Salapa, H. E., Lalor, S. J., Lee, S., Segal, B. M., et al. (2016). Antibodies to the RNA-binding protein hnRNP A1 contribute to neurodegeneration in a model of central nervous system autoimmune inflammatory disease. *J. Neuroinflamm.* 13:178. doi: 10.1186/s12974-016-0647-y

Dreser, A., Vollrath, J. T., Sechi, A., Johann, S., Roos, A., Yamoah, A., et al. (2017). The ALS-linked E102Q mutation in Sigma receptor-1 leads to ER stress-mediated defects in protein homeostasis and dysregulation of RNA-binding proteins. *Cell Death Diff.* 24, 1655–1671. doi: 10.1038/cdd.2017.88

Ederle, H., and Dormann, D. (2017). TDP-43 and FUS en route from the nucleus to the cytoplasm. *FEBS Lett.* 591, 1489–1507. doi: 10.1002/1873-3468.12646

Faber, R. (1999). Frontotemporal lobar degeneration: a consensus on clinical diagnostic criteria. *Neurology* 53:1159. doi: 10.1212/WNL.53.5.1158-b

Farg, M. A., Soo, K. Y., Warraich, S. T., Sundaramoorthy, V., Blair, I. P., and Atkin, J. D. (2013). Ataxin-2 interacts with FUS and intermediate-length polyglutamine expansions enhance FUS-related pathology in amyotrophic lateral sclerosis. *Hum. Mol. Genet.* 22, 717–728. doi: 10.1093/hmg/dds479

Farg, M. A., Sundaramoorthy, V., Sultana, J. M., Yang, S., Atkinson, R. A., Levina, V., et al. (2014). C9ORF72, implicated in amytrophic lateral sclerosis and frontotemporal dementia, regulates endosomal trafficking. *Hum. Mol. Genet.* 23, 3579–3595. doi: 10.1093/hmg/ddu068

Feneberg, E., Gordon, D., Thompson, A., Finelli, M., Dafinca, R., Candalija Iserte, A., et al. (2020). An ALS-linked mutation in TDP-43 disrupts normal protein interactions in the motor neuron response to oxidative stress. *Neurobiol. Dis.* 144:105050. doi: 10.1016/j.nbd.2020.105050

Frohman, E. M., Racke, M. K., and Raine, C. S. (2006). Multiple sclerosis–the plaque and its pathogenesis. *N. Engl. J. Med.* 354, 942–955. doi: 10.1056/NEJMra052130

Fujita, K., Ito, H., Nakano, S., Kinoshita, Y., Wate, R., and Kusaka, H. (2008). Immunohistochemical identification of messenger RNA-related proteins in basophilic inclusions of adult-onset atypical motor neuron disease. *Acta Neuropathol.* 116, 439–445. doi: 10.1007/s00401-008-0415-x

Gal, J., Kuang, L., Barnett, K. R., Zhu, B. Z., Shissler, S. C., Korotkov, K. V., et al. (2016). ALS mutant SOD1 interacts with G3BP1 and affects stress granule dynamics. *Acta Neuropathol.* 132, 563–576. doi: 10.1007/s00401-016-1601-x

Gao, X., Jiang, L., Gong, Y., Chen, X., Ying, M., Zhu, H., et al. (2019). Stress granule: a promising target for cancer treatment. *Br. J. Pharmacol.* 176, 4421–4433. doi: 10.1111/bph.14790

Gieseler, A., Hillert, R., Krusche, A., and Zacher, K. H. (2019). Theme 5 human cell biology and pathology. *Amyotroph. Lat. Scl. Frontotemp. Degen.* 20, 188–205. doi: 10.1080/21678421.2019.1646993

Gilks, N., Kedersha, N., Ayodele, M., Shen, L., Stoecklin, G., Dember, L. M., et al. (2004). Stress granule assembly is mediated by prion-like aggregation of TIA-1. *Mol. Biol. Cell.* 15, 5383–5398. doi: 10.1091/mbc.e04-08-0715

Gingras, A. C., Raught, B., and Sonenberg, N. (1999). eIF4 initiation factors: effectors of mRNA recruitment to ribosomes and regulators of translation. *Annu. Rev. Biochem.* 68, 913–963. doi: 10.1146/annurev.biochem.68.1.913

Goedert, M., Spillantini, M. G., Jakes, R., Rutherford, D., and Crowther, R. A. (1989). Multiple isoforms of human microtubule-associated protein tau: sequences and localization in neurofibrillary tangles of Alzheimer's disease. *Neuron* 3, 519–526. doi: 10.1016/0896-6273(89)90210-9

Grundke-Iqbal, I., Iqbal, K., Tung, Y. C., Quinlan, M., Wisniewski, H. M., and Binder, L. I. (1986). Abnormal phosphorylation of the microtubule-associated protein tau (tau) in Alzheimer cytoskeletal pathology. *Proc. Natl Acad. Sci. U.S.A.* 83, 4913–4917. doi: 10.1073/pnas.83.13.4913

Guil, S., Long, J. C., and Cáceres, J. F. (2006). hnRNP A1 relocalization to the stress granules reflects a role in the stress response. *Mol. Cell. Biol.* 26, 5744–5758. doi: 10.1128/MCB.00224-06

Hardiman, O., Al-Chalabi, A., Chio, A., Corr, E. M., Logroscino, G., Robberecht, W., et al. (2017). Amyotrophic lateral sclerosis. *Nat. Rev. Dis. Prim.* 3:17085. doi: 10.1038/nrdp.2017.85

Haritani, M., Spencer, Y. I., and Wells, G. A. H. (1994). Hydrated autoclave pretreatment enhancement of prion protein immunoreactivity in formalin-fixed bovine spongiform encephalopathy-affected brain. *Acta Neuropathol.* 87, 86–90. doi: 10.1007/BF00386258

Hernández, F., and Avila, J. (2007). Tauopathies. *Cell. Mol. Life Sci.* 64, 2219–2233. doi: 10.1007/s00018-007-7220-x

Hirsch-Reinshagen, V., Pottier, C., Nicholson, A. M., Baker, M., Hsiung, G. R., Krieger, C., et al. (2017). Clinical and neuropathological features of ALS/FTD with TIA1 mutations. *Acta Neuropathol. Commun.* 5:96. doi: 10.1186/s40478-017-0493-x

Hock, E. M., Maniecka, Z., Hruska-Plochan, M., Reber, S., Laferrière, F., Sahadevan, M. K. S., et al. (2018). Hypertonic stress causes cytoplasmic translocation of neuronal, but not astrocytic, FUS due to impaired transportin function. *Cell Rep.* 24, 987–1000.e7. doi: 10.1016/j.celrep.2018.06.094

Ichiyanagi, N., Fujimori, K., Yano, M., Ishihara-Fujisaki, C., Sone, T., Akiyama, T., et al. (2016). Establishment of *in vitro* FUS-associated familial amyotrophic lateral sclerosis model using human induced pluripotent stem cells. *Stem Cell Rep.* 6, 496–510. doi: 10.1016/j.stemcr.2016.02.011

Ivanov, P. A., Mikhaylova, N. M., and Klyushnik, T. P. (2016). Distribution of translation initiation factor eIF3 in neutrophils in Alzheimer disease. *Biochem. Suppl. A Memb. Cell Biol.* 10, 328–332. doi: 10.1134/S1990747816030053

Japtok, J., Lojewski, X., Naumann, M., Klingenstein, M., Reinhardt, P., Sterneckert, J., et al. (2015). Stepwise acquirement of hallmark neuropathology in FUS-ALS

iPSC models depends on mutation type and neuronal aging. *Neurobiol. Dis.* 82, 420–429. doi: 10.1016/j.nbd.2015.07.017

Kamelgarn, M., Chen, J., Kuang, L., Jin, H., Kasarskis, E. J., and Zhu, H. (2018). ALS mutations of FUS suppress protein translation and disrupt the regulation of nonsense-mediated decay. *Proc. Natl. Acad. Sci. U.S.A.* 115, E11904–E11913. doi: 10.1073/pnas.1810413115

Kapeli, K., Martinez, F. J., and Yeo, G. W. (2017). Genetic mutations in RNA-binding proteins and their roles in ALS. *Hum. Genet.* 136, 1193–1214. doi: 10.1007/s00439-017-1830-7

Kedersha, N., Cho, M. R., Li, W., Yacono, P. W., Chen, S., Gilks, N., et al. (2000). Dynamic shuttling of TIA-1 accompanies the recruitment of mRNA to mammalian stress granules. *J. Cell. Biol.* 151, 1257–1268. doi: 10.1083/jcb.151.6.1257

Kedersha, N., Ivanov, P., and Anderson, P. (2013). Stress granules and cell signaling: more than just a passing phase? *Trends Biochem. Sci.* 38, 494–506. doi: 10.1016/j.tibs.2013.07.004

Kedersha, N., Stoecklin, G., Ayodele, M., Yacono, P., Lykke-Andersen, J., Fritzler, M. J., et al. (2005). Stress granules and processing bodies are dynamically linked sites of mRNP remodeling. *J. Cell. Biol.* 169, 871–884. doi: 10.1083/jcb.200502088

Kedersha, N. L., Gupta, M., Li, W., Miller, I., and Anderson, P. (1999). RNA-binding proteins TIA-1 and TIAR link the phosphorylation of eIF-2 alpha to the assembly of mammalian stress granules. *J. Cell. Biol.* 147, 1431–1442. doi: 10.1083/jcb.147.7.1431

Khan, B. K., Yokoyama, J. S., Takada, L. T., Sha, S. J., Rutherford, N. J., Fong, J. C., et al. (2012). Atypical, slowly progressive behavioural variant frontotemporal dementia associated with C9ORF72 hexanucleotide expansion. *J. Neurol. Neurosurg. Psychiatry* 83, 358–364. doi: 10.1136/jnnp-2011-301883

Khong, A., Matheny, T., Jain, S., Mitchell, S. F., Wheeler, J. R., and Parker, R. (2017). The stress granule transcriptome reveals principles of mRNA accumulation in stress granules. *Mol. Cell.* 68, 808–20.e5. doi: 10.1016/j.molcel.2017.10.015

Kino, Y., Washizu, C., Kurosawa, M., Yamada, M., Miyazaki, H., Akagi, T., et al. (2015). FUS/TLS deficiency causes behavioral and pathological abnormalities distinct from amyotrophic lateral sclerosis. *Acta Neuropathol. Commun.* 3:24. doi: 10.1186/s40478-015-0202-6

Koren, S. A., Hamm, M. J., Meier, S. E., Weiss, B. E., Nation, G. K., Chishti, E. A., et al. (2019). Tau drives translational selectivity by interacting with ribosomal proteins. *Acta Neuropathol.* 137, 571–583. doi: 10.1007/s00401-019-01970-9

Kreiter, N., Pal, A., Lojewski, X., Corcia, P., Naujock, M., Reinhardt, P., et al. (2018). Age-dependent neurodegeneration and organelle transport deficiencies in mutant TDP43 patient-derived neurons are independent of TDP43 aggregation. *Neurobiol. Dis.* 115, 167–181. doi: 10.1016/j.nbd.2018.03.010

Kuleshov, M. V., Jones, M. R., Rouillard, A. D., Fernandez, N. F., Duan, Q., Wang, Z., et al. (2016). Enrichr: a comprehensive gene set enrichment analysis web server 2016 update. *Nucleic Acids Res.* 44, W90–W97. doi: 10.1093/nar/gkw377

Lassmann, H., and van Horssen, J. (2011). The molecular basis of neurodegeneration in multiple sclerosis. *FEBS Lett.* 585, 3715–3723. doi: 10.1016/j.febslet.2011.08.004

Lee, K. H., Zhang, P., Kim, H. J., Mitrea, D. M., Sarkar, M., Freibaum, B. D., et al. (2016). C9orf72 dipeptide repeats impair the assembly, dynamics, and function of membrane-less organelles. *Cell* 167, 774–788.e17. doi: 10.1016/j.cell.2016.10.002

Lenzi, J., De Santis, R., de Turris, V., Morlando, M., Laneve, P., Calvo, A., et al. (2015). ALS mutant FUS proteins are recruited into stress granules in induced pluripotent stem cell-derived motoneurons. *Dis. Models Mech.* 8, 755–766. doi: 10.1242/dmm.020099

Levac, D., Colquhoun, H., and O'Brien, K. K. (2010). Scoping studies: advancing the methodology. *Implement. Sci.* 5:69. doi: 10.1186/1748-5908-5-69

Levin, M., Salapa, H., Libner, C., Hutchinson, C., and Popescu, B. (2020). A role for dysfunctional RNA binding proteins in the pathogenesis of neurodegeneration in MS (2669). *Neurology* 94(Suppl. 15):2669.

Levine, T. P., Daniels, R. D., Gatta, A. T., Wong, L. H., and Hayes, M. J. (2013). The product of C9orf72, a gene strongly implicated in neurodegeneration, is structurally related to DENN Rab-GEFs. *Bioinformatics* 29, 499–503. doi: 10.1093/bioinformatics/bts725

Lim, S. M., Choi, W. J., Oh, K. W., Xue, Y., Choi, J. Y., Kim, S. H., et al. (2016). Directly converted patient-specific induced neurons mirror the neuropathology of FUS with disrupted nuclear localization in amyotrophic lateral sclerosis. *Mol Neurodegener.* 11:8. doi: 10.1186/s13024-016-0075-6

Liu-Yesucevitz, L., Bilgutay, A., Zhang, Y. J., Vanderweyde, T., Citro, A., Mehta, T., et al. (2010). Tar DNA binding protein-43 (TDP-43) associates with stress granules: analysis of cultured cells and pathological brain tissue. *PLoS ONE.* 5:e13250. doi: 10.1371/journal.pone.0013250

Lo Bello, M., Di Fini, F., Notaro, A., Spataro, R., Conforti, F. L., and La Bella, V. (2017). ALS-related mutant FUS protein is mislocalized to cytoplasm and is recruited into stress granules of fibroblasts from asymptomatic FUS P525L mutation carriers. *Neuro Degen. Dis.* 17, 292–303. doi: 10.1159/000480085

Loginov, V. I., Burdennyy, A. M., Filippova, E. A., Pronina, I. V., Kazubskaya, T. P., Kushlinsky, D. N., et al. (2018). [Hypermethylation of miR-107, miR-130b, miR-203a, miR-1258 genes associated with ovarian cancer development and metastasis]. *Molekul. Biol.* 52, 801–809. doi: 10.1134/S0026893318050102

Loschi, M., Leishman, C. C., Berardone, N., and Boccaccio, G. L. (2009). Dynein and kinesin regulate stress-granule and P-body dynamics. *J. Cell. Sci.* 122(Pt 21), 3973–3982. doi: 10.1242/jcs.051383

Mackenzie, I. R., Nicholson, A. M., Sarkar, M., Messing, J., Purice, M. D., Pottier, C., et al. (2017). TIA1 mutations in amyotrophic lateral sclerosis and frontotemporal dementia promote phase separation and alter stress granule dynamics. *Neuron* 95, 808–816.e9. doi: 10.1016/j.neuron.2017.07.025

Manghera, M., Ferguson-Parry, J., and Douville, R. N. (2016). TDP-43 regulates endogenous retrovirus-K viral protein accumulation. *Neurobiol. Dis.* 94, 226–236. doi: 10.1016/j.nbd.2016.06.017

Mann, J. R., Gleixner, A. M., Mauna, J. C., Gomes, E., DeChellis-Marks, M. R., Needham, P. G., et al. (2019). RNA binding antagonizes neurotoxic phase transitions of TDP-43. *Neuron* 102, 321–338.e8. doi: 10.1016/j.neuron.2019.01.048

Marnik, E. A., and Updike, D. L. (2019). Membraneless organelles: P granules in Caenorhabditis elegans. *Traffic* 20, 373–379. doi: 10.1111/tra.12644

Maziuk, B. F., Apicco, D. J., Cruz, A. L., Jiang, L., Ash, P. E. A., da Rocha, E. L., et al. (2018). RNA binding proteins co-localize with small tau inclusions in tauopathy. *Acta Neuropathol. Commun.* 6:71. doi: 10.1186/s40478-018-0574-5

Mazroui, R., Marco, S., Kaufman, R., and Gallouzi, I. E. (2007). Inhibition of the ubiquitin-proteasome system induces stress granule formation. *Mol. Biol. Cell.* 18, 2603–2618. doi: 10.1091/mbc.e06-12-1079

McCormick, C., and Khaperskyy, D. A. (2017). Translation inhibition and stress granules in the antiviral immune response. *Nat. Rev. Immunol.* 17:647. doi: 10.1038/nri.2017.63

McGurk, L., Lee, V. M., Trojanowksi, J. Q., Van Deerlin, V. M., Lee, E. B., and Bonini, N. M. (2014). Poly-A binding protein-1 localization to a subset of TDP-43 inclusions in amyotrophic lateral sclerosis occurs more frequently in patients harboring an expansion in C9orf72. *J. Neuropathol. Exp. Neurol.* 73, 837–845. doi: 10.1097/NEN.0000000000000102

Meier, S., Bell, M., Lyons, D. N., Rodriguez-Rivera, J., Ingram, A., Fontaine, S. N., et al. (2016). Pathological tau promotes neuronal damage by impairing ribosomal function and decreasing protein synthesis. *J. Neurosci.* 36, 1001–1007. doi: 10.1523/JNEUROSCI.3029-15.2016

Min, S. W., Cho, S.-H., Zhou, Y., Schroeder, S., Haroutunian, V., Seeley, W. W., et al. (2010). Acetylation of tau inhibits its degradation and contributes to tauopathy. *Neuron* 67, 953–966. doi: 10.1016/j.neuron.2010.08.044

Mitra, A., Luna, J. I., Marusina, A. I., Merleev, A., Kundu-Raychaudhuri, S., Fiorentino, D., et al. (2015). Dual mTOR inhibition is required to prevent TGF-β-mediated fibrosis: implications for scleroderma. *J. Invest. Dermatol.* 135, 2873–2876. doi: 10.1038/jid.2015.252

Molliex, A., Temirov, J., Lee, J., Coughlin, M., Kanagaraj, A. P., Kim, H. J., et al. (2015). Phase separation by low complexity domains promotes stress granule assembly and drives pathological fibrillization. *Cell* 163, 123–133. doi: 10.1016/j.cell.2015.09.015

Monahan, Z., Shewmaker, F., and Pandey, U. B. (2016). Stress granules at the intersection of autophagy and ALS. *Brain. Res.* 1649(Pt B), 189–200. doi: 10.1016/j.brainres.2016.05.022

Montalbano, M., McAllen, S., Cascio, F. L., Sengupta, U., Garcia, S., Bhatt, N., et al. (2020). TDP-43 and tau oligomers in alzheimer's disease, amyotrophic lateral sclerosis, and frontotemporal dementia. *Neurobiol. Dis.* 146:105130. doi: 10.1016/j.nbd.2020.105130

Mori, K., Weng, S. M., Arzberger, T., May, S., Rentzsch, K., Kremmer, E., et al. (2013). The C9orf72 GGGGCC repeat is translated into aggregating dipeptide-repeat proteins in FTLD/ALS. *Science* 339, 1335–1338. doi: 10.1126/science.1232927

Nakahara, J., Maeda, M., Aiso, S., and Suzuki, N. (2011). Current concepts in multiple sclerosis: autoimmunity versus oligodendrogliopathy. *Clin. Rev. Allergy Immunol.* 42, 26–34. doi: 10.1007/s12016-011-8287-6

Neumann, M., Sampathu, D. M., Kwong, L. K., Truax, A. C., Micsenyi, M. C., Chou, T. T., et al. (2006). Ubiquitinated TDP-43 in frontotemporal lobar degeneration and amyotrophic lateral sclerosis. *Science* 314, 130–133. doi: 10.1126/science.1134108

Nonaka, T., Suzuki, G., Tanaka, Y., Kametani, F., Hirai, S., Okado, H., et al. (2016). Phosphorylation of TAR DNA-binding protein of 43 kDa (TDP-43) by truncated casein kinase 1δ triggers mislocalization and accumulation of TDP-43. *J. Biol. Chem.* 291, 5473–5483. doi: 10.1074/jbc.M115.695379

Noyes, K., and Weinstock-Guttman, B. (2013). Impact of diagnosis and early treatment on the course of multiple sclerosis. *Am. J. Manag. care.* 19(Suppl. 17), s321–s331. doi: 10.1155/2013/713627

Orrù, S., Coni, P., Floris, A., Littera, R., Carcassi, C., Sogos, V., et al. (2016). Reduced stress granule formation and cell death in fibroblasts with the A382T mutation of TARDBP gene: evidence for loss of TDP-43 nuclear function. *Hum. Mol. Genet.* 25, 4473–4483. doi: 10.1093/hmg/ddw276

Panas, M. D., Ivanov, P., and Anderson, P. (2016). Mechanistic insights into mammalian stress granule dynamics. *J. Cell. Biol.* 215, 313–323. doi: 10.1083/jcb.201609081

Patel, A., Lee, H. O., Jawerth, L., Maharana, S., Jahnel, M., Hein, M. Y., et al. (2015). A liquid-to-solid phase transition of the ALS protein FUS Accelerated By Disease Mutation. *Cell* 162, 1066–1077. doi: 10.1016/j.cell.2015.07.047

Rajpurohit, C. S., Kumar, V., Cheffer, A., Oliveira, D., Ulrich, H., Okamoto, O. K., et al. (2020). Mechanistic insights of astrocyte-mediated hyperactive autophagy and loss of motor neuron function in SOD1(L39R) linked amyotrophic lateral sclerosis. *Mol. Neurobiol.* 57, 4117–4133. doi: 10.1007/s12035-020-02006-0

Ramaswami, M., Taylor, J. P., and Parker, R. (2013). Altered ribostasis: RNA-protein granules in degenerative disorders. *Cell* 154, 727–736. doi: 10.1016/j.cell.2013.07.038

Ratti, A., Gumina, V., Lenzi, P., Bossolasco, P., Fulceri, F., Volpe, C., et al. (2020). Chronic stress induces formation of stress granules and pathological TDP-43 aggregates in human ALS fibroblasts and iPSC-motoneurons. *Neurobiol. Dis.* 145:105051. doi: 10.1016/j.nbd.2020.105051

Robberecht, W., and Philips, T. (2013). The changing scene of amyotrophic lateral sclerosis. *Nat. Rev. Neurosci.* 14, 248–264. doi: 10.1038/nrn3430

Rossi, S., Serrano, A., Gerbino, V., Giorgi, A., Di Francesco, L., Nencini, M., et al. (2015). Nuclear accumulation of mRNAs underlies G4C2-repeat-induced translational repression in a cellular model of C9orf72 ALS. *J. Cell. Sci.* 128, 1787–1799. doi: 10.1242/jcs.165332

Salapa, H. E., Hutchinson, C., Popescu, B. F., and Levin, M. C. (2020). Neuronal RNA-binding protein dysfunction in multiple sclerosis cortex. *Anna. Clin. Transl. Neurol.* 7, 1214–1224. doi: 10.1002/acn3.51103

Salapa, H. E., Johnson, C., Hutchinson, C., Popescu, B. F., and Levin, M. C. (2018). Dysfunctional RNA binding proteins and stress granules in multiple sclerosis. *J. Neuroimmunol.* 324, 149–156. doi: 10.1016/j.jneuroim.2018.08.015

Samadian, M., Gholipour, M., Hajiesmaeili, M., Taheri, M., and Ghafouri-Fard, S. (2021). The eminent role of microRNAs in the pathogenesis of Alzheimer's disease. *Front Aging Neurosci.* 13:107. doi: 10.3389/fnagi.2021.641080

Shafiei, S. S., Guerrero-Muñoz, M. J., and Castillo-Carranza, D. L. (2017). Tau oligomers: cytotoxicity, propagation, and mitochondrial damage. *Front Aging Neurosci.* 9:83. doi: 10.3389/fnagi.2017.00083

Shannon, P., Markiel, A., Ozier, O., Baliga, N. S., Wang, J. T., Ramage, D., et al. (2003). Cytoscape: a software environment for integrated models of biomolecular interaction networks. *Genome Res.* 13, 2498–2504. doi: 10.1101/gr.1239303

Shaw, P. J., and Jordan, E. G. (1995). The nucleolus. *Annu. Rev. Cell Dev. Biol.* 11, 93–121. doi: 10.1146/annurev.cb.11.110195.000521

Sheth, U., and Parker, R. (2003). Decapping and decay of messenger RNA occur in cytoplasmic processing bodies. *Science* 300, 805–808. doi: 10.1126/science.1082320

Silva, J. M., Rodrigues, S., Sampaio-Marques, B., Gomes, P., Neves-Carvalho, A., Dioli, C., et al. (2019). Dysregulation of autophagy and stress granule-related proteins in stress-driven Tau pathology. *Cell Death Diff.* 26, 1411–1427. doi: 10.1038/s41418-018-0217-1

Stoecklin, G., Stubbs, T., Kedersha, N., Wax, S., Rigby, W. F. C., Blackwell, T. K., et al. (2004). MK2-induced tristetraprolin:14-3-3 complexes prevent stress granule association and ARE-mRNA decay. *EMBO J.* 23, 1313–1324. doi: 10.1038/sj.emboj.7600163

Tang, B. L. (2016). C9orf72's interaction with rab GTPases-modulation of membrane traffic and autophagy. *Front. Cell. Neurosci.* 10:228. doi: 10.3389/fncel.2016.00228

The Gene Ontology Consortium. (2019). The Gene Ontology Resource: 20 Years and still GOing strong. *Nucleic Acids Res.* 47, D330–D338. doi: 10.1093/nar/gky1055

Theme 4 Human cell biology and pathology. (2018). *Amyotroph. Lat. Scl. Frontotemp. Degen.* 19, 154–177. doi: 10.1080/21678421.2018.1510571

Thomas, M. G., Martinez Tosar, L. J., Loschi, M., Pasquini, J. M., Correale, J., Kindler, S., et al. (2005). Staufen recruitment into stress granules does not affect early mRNA transport in oligodendrocytes. *Mol. Biol. Cell.* 16, 405–420. doi: 10.1091/mbc.e04-06-0516

Tiraboschi, P., Hansen, L., Thal, L. J., and Corey-Bloom, J. (2004). The importance of neuritic plaques and tangles to the development and evolution of AD. *Neurology* 62, 1984–1989. doi: 10.1212/01.WNL.0000129697.01779.0A

Tricco, A. C., Lillie, E., Zarin, W., O'Brien, K. K., Colquhoun, H., Levac, D., et al. (2018). PRISMA extension for scoping reviews (PRISMA-ScR): checklist and explanation. *Ann. Intern. Med.* 169, 467–473. doi: 10.7326/M18-0850

Trinczek, B., Biernat, J., Baumann, K., Mandelkow, E. M., and Mandelkow, E. (1995). Domains of tau protein, differential phosphorylation, and dynamic instability of microtubules. *Mol. Biol. Cell.* 6, 1887–1902. doi: 10.1091/mbc.6.12.1887

Turi, Z., Lacey, M., Mistrik, M., and Moudry, P. (2019). Impaired ribosome biogenesis: mechanisms and relevance to cancer and aging. *Aging* 11, 2512–2540. doi: 10.18632/aging.101922

Vanderweyde, T., Yu, H., Varnum, M., Liu-Yesucevitz, L., Citro, A., Ikezu, T., et al. (2012). Contrasting pathology of the stress granule proteins TIA-1 and G3BP in tauopathies. *J. Neurosci.* 32, 8270–8283. doi: 10.1523/JNEUROSCI.1592-12.2012

Vassileff, N., Vella, L. J., Rajapaksha, H., Shambrook, M., Kenari, A. N., McLean, C., et al. (2020). Revealing the proteome of motor cortex derived extracellular vesicles isolated from amyotrophic lateral sclerosis human postmortem tissues. *Cells* 9:1709. doi: 10.3390/cells9071709

Volkening, K., Leystra-Lantz, C., Yang, W., Jaffee, H., and Strong, M. J. (2009). Tar DNA binding protein of 43 kDa (TDP-43), 14-3-3 proteins and copper/zinc superoxide dismutase (SOD1) interact to modulate NFL mRNA stability. Implications for altered RNA processing in amyotrophic lateral sclerosis (ALS). *Brain Res.* 1305, 168–182. doi: 10.1016/j.brainres.2009.09.105

Wang, J. Z., Grundke-Iqbal, I., and Iqbal, K. (1996). Glycosylation of microtubule-associated protein tau: an abnormal posttranslational modification in Alzheimer's disease. *Nat. Med.* 2, 871–875. doi: 10.1038/nm0896-871

Wang, Z.-H., Liu, P., Liu, X., Yu, S. P., Wang, J.-Z., and Ye, K. (2018). Delta-secretase (AEP) mediates tau-splicing imbalance and accelerates cognitive decline in tauopathies. *J. Exp. Med.* 215, 3038–3056. doi: 10.1084/jem.20180539

Wheeler, J. R., Matheny, T., Jain, S., Abrisch, R., and Parker, R. (2016). Distinct stages in stress granule assembly and disassembly. *Elife.* 5:e18413. doi: 10.7554/eLife.18413

Wolozin, B. (2012). Regulated protein aggregation: stress granules and neurodegeneration. *Mol. Neurodegen.* 7:56. doi: 10.1186/1750-1326-7-56

Wolozin, B., and Ivanov, P. (2019). Stress granules and neurodegeneration. *Nat. Rev. Neurosci.* 20, 649–666. doi: 10.1038/s41583-019-0222-5

Younas, N., Zafar, S., Shafiq, M., Noor, A., Siegert, A., Arora, A. S., et al. (2020). SFPQ and Tau: critical factors contributing to rapid progression of Alzheimer's disease. *Acta Neuropathol.* 140, 317–339. doi: 10.1007/s00401-020-02178-y

Zhao, X., Kotilinek, L. A., Smith, B., Hlynialuk, C., Zahs, K., Ramsden, M., et al. (2016). Caspase-2 cleavage of tau reversibly impairs memory. *Nat. Med.* 22, 1268–1276. doi: 10.1038/nm.4199

Conflict of Interest: The authors declare that the research was conducted in the absence of any commercial or financial relationships that could be construed as a potential conflict of interest.

frontiers in Molecular Neuroscience

ORIGINAL RESEARCH
published: 02 July 2021
doi: 10.3389/fnmol.2021.672614

Bisulfite Amplicon Sequencing Can Detect Glia and Neuron Cell-Free DNA in Blood Plasma

Zac Chatterton[1,2,3,4,5], Natalia Mendelev[1,2,3,4], Sean Chen[1,2,3,4], Walter Carr[6,7], Gary H. Kamimori[6], Yongchao Ge[3], Andrew J. Dwork[8,9,10] and Fatemeh Haghighi[1,2,3,4]*

[1] Friedman Brain Institute, Icahn School of Medicine at Mount Sinai, New York, NY, United States, [2] Department of Neuroscience, Icahn School of Medicine at Mount Sinai, New York, NY, United States, [3] Department of Neurology, Icahn School of Medicine at Mount Sinai, New York, NY, United States, [4] Medical Epigenetics, James J. Peters VA Medical Center, New York, NY, United States, [5] Brain and Mind Centre, School of Medical Science, Faculty of Medicine and Health, The University of Sydney, Sydney, NSW, Australia, [6] Walter Reed Army Institute of Research, Silver Spring, MD, United States, [7] Oak Ridge Institute for Science and Education, Oak Ridge, TN, United States, [8] Department of Pathology and Cell Biology, Columbia University, New York, NY, United States, [9] Department of Psychiatry, Columbia University, New York, NY, United States, [10] Molecular Imaging and Neuropathology Division, New York State Psychiatric Institute, New York, NY, United States

OPEN ACCESS

Edited by:
Robert J. Harvey,
University of the Sunshine Coast, Australia

Reviewed by:
Katja Kobow,
University Hospital Erlangen, Germany
Matthew B. Veldman,
Medical College of Wisconsin, United States

***Correspondence:**
Zac Chatterton
zac.chatterton@sydney.edu.au

Specialty section:
This article was submitted to Molecular Signalling and Pathways, a section of the journal Frontiers in Molecular Neuroscience

Received: 26 February 2021
Accepted: 14 June 2021
Published: 02 July 2021

Citation:
Chatterton Z, Mendelev N, Chen S, Carr W, Kamimori GH, Ge Y, Dwork AJ and Haghighi F (2021) Bisulfite Amplicon Sequencing Can Detect Glia and Neuron Cell-Free DNA in Blood Plasma. Front. Mol. Neurosci. 14:672614. doi: 10.3389/fnmol.2021.672614

Sampling the live brain is difficult and dangerous, and withdrawing cerebrospinal fluid is uncomfortable and frightening to the subject, so new sources of real-time analysis are constantly sought. Cell-free DNA (cfDNA) derived from glia and neurons offers the potential for wide-ranging neurological disease diagnosis and monitoring. However, new laboratory and bioinformatic strategies are needed. DNA methylation patterns on individual cfDNA fragments can be used to ascribe their cell-of-origin. Here we describe bisulfite sequencing assays and bioinformatic processing methods to identify cfDNA derived from glia and neurons. In proof-of-concept experiments, we describe the presence of both glia- and neuron-cfDNA in the blood plasma of human subjects following mild trauma. This detection of glia- and neuron-cfDNA represents a significant step forward in the translation of liquid biopsies for neurological diseases.

Keywords: cfDNA, diagnostic, epigenetic, neuron, glia, neurotrauma

INTRODUCTION

It has been two decades since the first descriptions of fetal-derived cell-free DNA (cfDNA) within maternal plasma (Lo et al., 1997) and the identification of tumor-derived cfDNA within patient blood (Nawroz et al., 1996; Anker et al., 1997). Next-generation sequencing (NGS) of these rare DNA fragments has established a minimally invasive technique for the diagnosis and disease tracking of cancer and graft rejection, and prenatal genetic testing. The technological advancements in NGS have increased the limits of detection of these techniques (Newman et al., 2014) to ∼0.02%, which hold promise of early detection of smaller cancers and more sensitive clinical patient tracking.

In the absence of genetic markers, DNA methylation has been used to delineate fetal from maternal DNA (Nygren et al., 2010). Fetal-derived cfDNA is detectable in mothers' blood from 7 weeks of gestation when the fetus weighs < 1 g (Lo et al., 1998). Considering the average

adult human brain weighs ∼1.3 kg and can undergo extensive tissue loss as a result of both neurotrauma and degeneration, it is likely that apoptotic or necrotic DNA is shed from the brain into the peripheral blood following neurological damage. The use of cfDNA to identify fetal genetic abnormalities and to diagnose cancers largely removes the risk of serious fetal injury and patient (Crowley et al., 2013). This aspect is also particularly attractive for the diagnosis of neurological disease. Indeed, genotyping neurological tumors is possible using cfDNA, e.g., neuroblastoma by MYCN (Combaret et al., 2002), and glioblastoma by EGFR mutations (Salkeni et al., 2013). A seminal study also identified the presence of brain-derived cfDNA in blood from subjects who had suffered a traumatic brain injury (TBI), ischemic brain damage following cardiac arrest, and multiple sclerosis (Lehmann-Werman et al., 2016), providing the first evidence of brain-derived cfDNA associated with varying modes of neurological damage.

DNA methylation is an epigenetic modification in which methyl groups are covalently bound to cytosines within a CpG context. Uniquely to neurons, global DNA methylation is gained postnatally within the CpH context (H = any base other than guanine) (Lister et al., 2013), providing unique DNA methylation markers of neuronal cell identity. Within this study, we first identify genomic regions harboring CpG DNA methylation specific to glia and neurons, and CpH DNA methylation specific to neurons. We then validate bisulfite amplicon sequencing assays targeting CpG and CpH loci. We recently describe an analytical framework that identifies the glia and neuron origin of cfDNA within cerebrospinal fluid following Whole-Genome Bisulfite Sequencing (WGBS) using DNA methylation k-mers (Ye et al., 2021). We extend this method to the analysis of bisulfite amplicon sequencing data for precise annotation of glia- and neuron-cfDNA. Finally, in proof-of-concept experiments, we apply our bisulfite amplicon sequencing assays to cfDNA from 47 blood plasma samples taken from subjects pre- and post-acute pressure exposure, representing a mild trauma, and identify the presence of both glia- and neuron-cfDNA in blood plasma.

MATERIALS AND METHODS

Informed consent for the collection of the postmortem brain specimens for research and psychological autopsy interview of the relatives was obtained, as approved by the Institutional Review Board of the New York State Psychiatric Institute (NYSPI)/Department of Psychiatry of Columbia University (Protocol #6477R). Collection of samples from male participants at U.S. Army explosive entry training sites (special operations and combat engineer courses) was approved by the Institutional Review Boards of the Naval Medical Research Center and the Walter Reed Army Institute of Research (NMRC#2011.0002; WRAIR#1796).

Brain Tissue Samples and Processing

All brains were from the Macedonian/NYSPI Brain Collection (Rosoklija et al., 2013). Autopsies were performed at the Institute for Forensic Medicine in Skopje, Macedonia on individuals who died suddenly. Family members gave informed consent for use of the autopsy tissue for research, review of medical records, and a "Psychological Autopsy" interview (Kelly and Mann, 1996) with a Macedonian psychiatrist or psychologist trained in the procedure at NYSPI. For this study, individuals with schizophrenia, major depressive disorder and individuals with no history of neuropsychiatric disorder were matched by age and sex. Samples from individuals with a history of substance or alcohol use disorders were excluded. The samples included a broad age range (22–72 years) with a mean of 50 years (full subject details in **Supplementary Table 1**). All dissections were performed by a trained neuropathologist (AJD).

Neuronal and non-neuronal nuclei (consisting mainly of glia) were separated following protocols described in Matevossian and Akbarian (2008). Briefly, frozen sections of the dorsolateral prefrontal cortex (DLPFC) (∼100 mg) from each patient (n = 72) were homogenized on ice, cells were lyzed, and nuclei were isolated by high-speed centrifugation through a sucrose buffer. Nuclei were immunostained using the Alexa-Fluor conjugated Anti-NeuN antibody (Abcam, ab190195) and isolated by fluorescent activated nuclei sorting (FANS) (BD FACS-Aria).

DNA Methylation Microarray Profiling and Data Processing

DNA was isolated from 216 brain specimens [DLPFC NeuN + (Neuron), DLPFC NeuN- (Glia), and ventral white matter (VWM)], bisulfite converted (Zymo) and CpG methylation was determined by Illumina Infinium HumanMethylationBeadChip microarray (HM450) analysis, described previously (Bibikova et al., 2006). Raw data files (.idat) were processed by minfi package (Aryee et al., 2014). All samples displayed a mean probe-wise detection call p-value for the 485512 array probes < 0.0005. Samples were removed that did not match phenotypic sex and methylation-based sex calling using the getSex function of minfi. Samples with non-matching genotypes (HM450 SNP interrogating probes) between tissues of the same individual were removed resulting in 192 samples for downstream analysis (69 Neuron, 66 Glia, and 67 VWM). Probes mapping to the X and Y chromosomes, affected by SNPs and cross hybridizing probes were removed (as outlined in Naeem et al., 2014), leaving 301,397 probes for analysis.

Statistical Analysis of DNA Methylation Microarray Data

To identify genomic regions with DNA methylation specific to glia and neurons, we combined our in-house generated HM450 data (above) with public HM450 data of neurons from the occipital frontal cortex (OFC) (n = 12, GSE50798) to define our neuron group (n = 71). To define our glia group (n = 78), we combined our in-house glia HM450 data (above) with public HM450 data of OFC glia (n = 12, GSE50798). Differentially methylated positions (DMPs) were identified by independent linear modeling of glia or neurons and publicly available HM450 data from blood cells (n = 47 from GSE41169 and GSE32148) using limma (blood contrast) (Smyth, 2005). Additionally, DMPs were identified by independent

linear modeling between glia or neurons and publicly available HM450 data from several "other" cell-types (n = 36, detailed in **Supplementary Table 2**) using limma (other contrast) (Smyth, 2005). Differentially methylated regions (DMRs) were identified between the same contrasts as described for DMP's through use of the bumphunter software (Jaffe et al., 2012). The most significant hypermethylated neuron or glia DMPs [false discovery rate (fdr) corrected p-value] that resided within both "blood contrast" and "other contrast" DMRs were selected (**Figure 1A**). Genomic regions ± 150 bp of these DMPs were prioritized for bisulfite amplicon design (below). Neuron DMPs (±150 bp) were intersected with Blood and Brain DNase hypersensitivity narrow peaks (ENCODE, **Supplementary Table 3**) using GenomicRanges software (Lawrence et al., 2013) to identify neuron DMP's that reside within blood euchromatin and brain heterochromatin.

Statistical Analysis of WGBS Data

To identify CpH DNA methylation specific to neurons, we used WGBS data from FANS sorted NeuN+ (neuron) and NeuN- (glia) nuclei derived from the prefrontal cortex of two male and two female adults (GSE47966). We applied a coverage threshold of 5X, removed X and Y chromosomes, and selected CpH sites that displayed 100% DNA methylation difference between neuron and glia. The density of hypermethylated CpH sites ± 50bp of each other was calculated within neurons, and genomic regions with ≥5 hypermethylated CpH within ± 50bp were prioritized for bisulfite amplicon design.

Bisulfite Amplicon Assay Design

Genomic DNA (gDNA) sequences ± 5000 bp from the desired target cytosine (CpG/CpH) were acquired from Ensembl. Assays were designed to interrogate the target cytosine using Pyromark ADSW v1.0 software (Qiagen, Pyrosequencing), in combination with manual assessment. PCR primers were designed to avoid extremely low complexity regions, CpG sites, and high-frequency polymorphisms.

Bisulfite Amplicon Assay Testing

DNA Methylation Standards

CpG methylation standards were purchased (Zymo) and CpH DNA methylation standards were constructed from pooled ratios of neuron gDNA and peripheral blood mononuclear cell (PBMC) gDNA. Bisulfite conversion of 100 ng of DNA was performed using the EZ DNA Methylation Kit (Zymo) and a modified protocol optimized for low input DNA. Briefly, 500 μg of resuspended VX Carrier RNA (Qiagen, 950280) was added to the M-binding buffer to improve binding efficacy and total yield after bisulfite treatment. Bisulfite-modified DNA was purified as per the manufacturer's protocol and eluted in 46 μL of M-Elution buffer.

Multiplex Assay Design

In silico designed assays were divided into two groups based on the amplicon size, primer Tm, and GC content, while also avoiding overlapping primer pairs. PCRs were performed on the DNA methylation controls using the PCR multiplex protocols and thermal cycling conditions reported in **Supplementary Material I**. Capillary electrophoresis (CE) of the PCR products was performed using the Agilent 2100 Bioanalyzer system and DNA 1000 chips (Agilent). Based on the QC results, nested PCRs were performed to recover amplicons that did not sufficiently amplify in the initial reaction.

Bisulfite Amplicon Sequencing (Ion Torrent) of DNA Methylation Standards

Prior to library construction, PCR products were pooled and purified using QIAquick PCR Purification Kit columns (Qiagen). Libraries were prepared using the KAPA Library Preparation Kit for Ion Torrent Platforms (KK8310) and IonXpress™ Barcode Adapters (Thermo Fisher). Next, library molecules were purified using Agencourt AMPure XP beads (Beckman Coulter) and quantified by real-time PCR using the KAPA Library Quantification Kit (KK4827). Barcoded samples were then pooled in an equimolar fashion before template preparation was performed on 340 million library molecules using the Ion PGM Templating OT2 200 kit (Thermo Fisher). Following this, enriched, template-positive library molecules were then sequenced on the Ion Torrent PGM sequencer using the Ion PBM™ Sequencing 200 Kit v2 kit with Ion 314™ v2 Chips (Thermo Fisher). FASTQ files from the Ion Torrent PGM server were aligned to the local reference database using Bismark software (Krueger and Andrews, 2011). Methylation levels were calculated for cytosines covered by a minimum of 30 total reads. For CpG methylation assays, an R^2 value of >0.9 was required for validation. Each CpH assay had >1 CpH loci with an R^2 value of >0.75. The final protocol includes 33 assays targeting genomic regions with brain-specific DNA methylation in addition to two assays targeting spiked in Lambda phage gDNA to control for bisulfite conversion efficiency (detailed in **Supplementary Table 4**). To limit repeated re-design of the multiplex cycling conditions, all assays were applied to the validation (cellular DNA) and proof-of-concept (cfDNA) samples; however, only assays that past signal-to-noise thresholding (below) are reported.

Protocol for Bisulfite Amplicon Sequencing of cfDNA

The full protocol is supplied as **Supplementary Material I** that includes all necessary information for cfDNA extraction, cfDNA quantification, Lambda gDNA spike-in, bisulfite conversion, PCR, amplicon pooling, and methods for Illumina library construction and pooling.

Blood Plasma Processing

In collaboration with the Walter Reed Army Institute of Research, to investigate the effects of repeated blast wave exposure in explosive entry personnel (Breachers), plasma samples were taken from 12 breachers following training days 1, 7, 8, and 9. Blood samples were taken 1.5–2.5 h post-blast exposure. All samples were from male subjects with an average age of 29.67 years (SD 3.87 years) (detailed in **Supplementary Table 5**). Briefly, plasma was separated by centrifugation at 3000 g for 15 min at room temp and was clarified by additional centrifugation at 10,000 g for 10 min; 4°C and stored at −80°C.

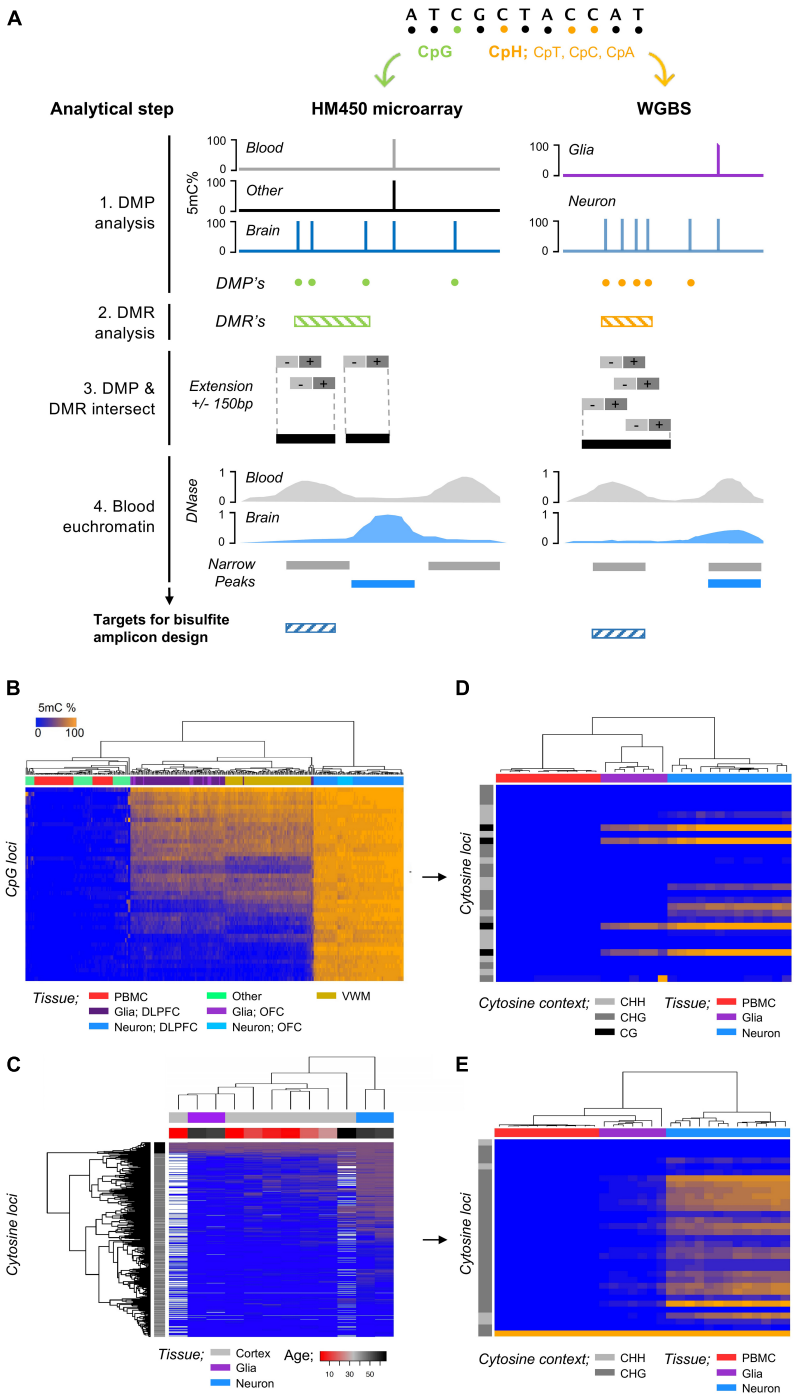

FIGURE 1 | Discovery and validation of regions of the genome that harbor glia and neuron DNA methylation (5mC). **(A)** Strategy for characterization of genomic region/cytosine loci selection for glia and neuron cfDNA methylation analysis. (1) DMPs were identified by linear regression between glia/neurons (brain cells) and blood cells and other tissues of the human body, (2) DMRs were identified by bumphunter analysis between brain cells, blood cells, and other tissues, and (3) brain-cell DMP and DMRs were intersected (GenomicRanges) to refine DMPs within genomic regions with DNA methylation specific to a brain cells. The DMPs were extended ± 150 bp for assay design, and (4) target genomic regions for bisulfite amplicon design were refined to euchromatic regions of blood cells and heterochromatic regions of brain cells. **(B)** Heatmap shows unsupervised hierarchical clustering of samples by cell-type using the DNA methylation (CpG microarray) of 45 CpG found hypermethylated within neurons compared to blood (>90%) and "other" cells/tissue types (>80%). DLPFC, dorsolateral prefrontal cortex; OFC, occipital frontal cortex; VWM, ventral white matter. **(C)** Heatmap shows unsupervised hierarchical clustering of samples by cell-type (neuron/glia) and developmental age (cortex; gray matter) using the DNA methylation (WGBS; Lister et al., 2013) of 741 cytosine loci within 28 regions found within "high-density" regions of hypermethylated CpH within neurons. **(D)** Heatmap shows unsupervised hierarchical clustering of samples by cell-type using the DNA methylation of CpG and CpH loci following bisulfite amplicon sequencing. **(E)** Heatmap shows unsupervised hierarchical clustering of samples by cell-type using the DNA methylation of CpH loci following bisulfite amplicon sequencing.

Bisulfite Amplicon Sequencing and Alignment

Bisulfite amplicon sequencing libraries were created from neuron (n = 13) and glia gDNA (n = 7) from samples used for HM450 analysis (above) and PBMC (n = 11) from Breachers training day 1, and cfDNA (n = 47) from Breachers training days 1, 7, 8, and 9 following the protocols in **Supplementary Material I**. Libraries were denatured following Illumina protocols and sequenced on either the Illumina MiSeq using 2 × 26bp sequencing or the Illumina HiSeq2500 using 2 × 50bp sequencing. Paired-end (PE) 50 bp reads were trimmed to 26 bp using fastqutils truncate function for combined analysis with 26 bp PE reads. Read trimming was performed with cutadapt (<Q30). A targeted bisulfite reference genome was generated using bismark command bismark_genome_preparation and a fasta file that included all 33 assay targets and Lambda genome. Trimmed PE reads from neuron, glia, and PBMC samples were mapped to the targeted bisulfite reference genome using bismark (–bowtie2 –non_directional) (Krueger and Andrews, 2011) and stacked DNA methylation calls and coverage were obtained using bismark_methylation_extractor (-p –comprehensive –merge_non_CpG –cytosine_report –CX). The bisulfite conversion efficiency of each sample was calculated using the mean DNA methylation% of all cytosines within the two Lambda assays.

DNA Methylation k-mer Analysis

We extended our analytical framework that identifies the glia and neuron origin of cfDNA using DNA methylation k-mers (Ye et al., 2021) to bisulfite amplicon sequencing. Briefly, we apply a threshold value to the DNA methylation of each cytosine within each cell-type, annotating "C" for DNA methylation ≥ 50%, while DNA methylation < 50% are annotated "T." The values are stored in .vcf format and converted to fasta format using gatk -T FastaAlternateReferenceMaker, resulting in unique reference sequence for each cell-type. These scripts are available at https://github.com/zchatt/methylK. We use the Kallisto index function to index k-mers (31-mer) from the fasta files (Bray et al., 2016). Assignment (pseudoalignment) of raw bisulfite sequencing reads was then performed using Kallisto (Bray et al., 2016). F1-statistics were calculated for the correct assignment of reads to either glia or neuron and PBMC for all possible co-methylation events, i.e., 1, 2. . .26 (read length) methylated cytosines. The point of inflection between a signal-to-noise ratio, e.g., correct assignment/incorrect assignment, and the F1-statistic was used to define the signal-to-noise thresholds for reads to be assigned as neuron (>2920:1) and glia (>2870:1).

Statistical Analysis of Glia and Neuron-cfDNA

Assignment of raw bisulfite sequencing reads from cfDNA libraries to glia or neuron origin was performed by Kallisto software (Bray et al., 2016) using the k-mer index with signal-to-noise thresholds applied. Glia- and neuron-cfDNA were normalized to each samples sequencing depth. These values contained an excess of zeros (zero inflation score test, p-val < 2.2×10^{-16}) (van den Broek, 1995) and followed a negative binomial distribution; therefore zero-inflated negative binomial regression (ZINBR) was used to model glia- and neuron-cfDNA measurements against Peak Impulse (psi/ms) with the covariate bisulfite conversion efficiency.

RESULTS

Discovery of Genomic Regions Harboring DNA Methylation Specific to Glia and Neurons

Cell-free DNA is predominantly derived from blood cells (∼85%) and other cell-types of the body (Moss et al., 2018); we therefore implemented a discovery pipeline (**Figure 1A**) that identified genomic regions harboring CpG methylation specific to glia or neurons by contrasting HM450 DNA methylation microarray profiles from glia or neurons to those from blood cells (n = 47) and several other human tissues/cell-types (n = 36) that could potentially contribute to the cfDNA fraction, e.g., liver (methods). We identified 45 CpG specifically hypermethylated within neurons (fdr p < 0.05 and >0.8 delta-beta) (**Figure 1B**) and 13 CpG specifically hypermethylated within glia (fdr p < 0.05 and >0.5 delta-beta) that were prioritized for bisulfite amplicon design. To identify regions of the genome harboring CpH methylation specific to neurons, we analyzed publicly available WGBS data (Lister et al., 2013) and contrast neurons and glia isolated from the prefrontal cortex of two adults (methods). We identified 309,452 CpH that displayed 100% DNA methylation difference between neuron and glia (hypermethylated in neurons) of which 29,336 were within genomic regions (±50 bp) of additional CpH hypermethylated in neurons. CpH methylation is obtained postnatally (Lister et al., 2013) and contributes largely to cell specification of neuronal subtypes (Luo et al., 2017), and thus we show the developmentally acquiescence of the CpH in **Figure 1C** using additional WGBS data from Lister et al. taken across neurodevelopment. We identified 28 genomic regions with ≥ 5 CpH sites hypermethylated in neurons that were prioritized for bisulfite amplicon design.

Validation of Bisulfite Sequencing Assays and Optimization of Assay Sensitivity and Specificity for Quantifying Glia and Neuron DNA

We designed PCR assays to amplify genomic regions with hypermethylated CpG/CpH specific to neurons or glia (methods). Each assay was validated by sequencing of DNA methylation standards; all CpG methylation assays had an $R^2 > 0.9$ and CpH assays had > 1 CpH with $R^2 > 0.75$. The final bisulfite amplicon pool includes 33 assays targeting genomic regions harboring glia and neuron DNA methylation in addition to two assays targeting spiked in Lambda phage gDNA to control for bisulfite conversion efficiency (detailed in **Supplementary Table 4** and **Supplementary Material I**). Using this protocol, we performed bisulfite amplicon sequencing of gDNA from neuron

(n = 13), glia (n = 7), and PBMC (n = 11) and observed that samples clustered distinctly by cell-type using the CpG and CpH methylation (**Figures 1D,E**).

CfDNA derived from a glia or neuron is likely rare, necessitating the annotation of cfDNA to its cell-of-origin at the single-read level. For this purpose, we leverage an approach we recently established to assign WGBS reads to their cell-of-origin (Ye et al., 2021) by first indexing DNA methylation sequence substrings (k-mers) of cell-types and then, second, performing k-mer lookup of bisulfite sequencing reads from cfDNA to assign their cell-of-origin (**Figure 2A**). Using this approach, we found that the k-mer lookup method assigned 13% more reads than read alignment by bismark (Student's t-test $p = 1.2 \times 10^{-14}$, **Figure 2B**). DNA methylation k-mers could be shared between cell-types, but we found that 24% of reads could be assigned to a single "unique" cell-type (**Figure 2A**). Importantly, sequencing reads derived from a cell-type were "correctly" assigned to the same cell-type at a high efficiency, e.g., bisulfite sequencing of neuron DNA assigned to neurons ($p < 2 \times 10^{-16}$, **Figures 2C,D**).

We observed that true-positive assigned reads had a significantly greater number of methylated cytosines within the read (co-methylation) than false-positives for neuron ($p < 2 \times 10^{-16}$) and glia ($p = 4.7 \times 10^{-8}$), and the amount of co-methylation was correlated to the signal-to-noise ratio for both neuron ($r = 0.22$, $p = 1.57 \times 10^{-10}$, **Figure 2F**) and glia ($r = 0.17$, $p = 0.001$). To define a signal-to-noise threshold of co-methylation to assign a read as neuron or glia, we used the point of inflection of the F1-statistic calculated from the accuracy in assigning neuron (**Figure 2F**) or glia reads (not shown) with increasing of signal-to-noise ratio thresholds. Intriguingly, the signal-to-noise thresholds were almost identical for neuron and glial cell-types (2920:1 and 2870:1, F1 = 0.9997). Signal-to-noise thresholding reduced the assignment of PBMC reads to neurons (false-positives) by 878-fold (0.2% to 2×10^{-4}%, $p = 2.8 \times 10^{-10}$) and correctly assigned 0.9% of reads from neurons, 3836-fold higher than false-positives ($p = 7.27 \times 10^{-7}$).

Proof-of-Concept Detection of Glia- and Neuron-cfDNA Within Blood Plasma Following Explosive Pressure Exposure

We investigated the effects of human blast wave exposure on glia- and neuron-cfDNA levels in blood plasma samples taken from explosive entry personnel (Breachers) during a 2-week training exercise using explosives. CfDNA was isolated from Breachers (n = 12) on training day 1 (prior to exposure) and days 7, 8, and 9. We performed bisulfite amplicon sequencing of cfDNA extracted from 47 blood plasma samples using protocols described in **Supplementary Material I**. Deep sequencing was performed, generating a mean of 656,935 sequencing reads per sample (±501,045 sd) from which glia- and neuron-cfDNA were quantified (methods). We observed evidence of glia- and neuron-cfDNA within 79% (37/47) and 49% (23/47) of subject samples, respectively. Our assay has increased sensitivity to detect neuron-cfDNA. Within our optimization studies, 0.9% of neuron gDNA was correctly assigned compared to 0.14% of glia gDNA. Adjusting for these assay biases, we observed higher amounts of glia-cfDNA (Student paired t-test, $p = 0.05$, **Figure 3A**). The highest levels of glia- and neuron-cfDNA detected were 7.2×10^{-4} and 1.9×10^{-4} (adjusted fraction of reads), respectively. We observed that 17 subject samples had detectable levels of both glia- and neuron-cfDNA from which we estimate that glia-cfDNA is 10.8-fold more abundant than neuron-cfDNA; however, the levels were only weakly correlated ($r = 0.17$).

On day 7 of training, the Breachers were exposed to significantly higher pressure than other training days (Student's t-test, $p = 3.1 \times 10^{-13}$, **Figure 3C**). The Peak Impulse (psi/ms) represents a measure of energy from a blast wave that is imparted on the subject. We observed a significant increase in neuron-cfDNA post-blast on day 7 compared to pre-blast levels on day 1 (ZINBR $p = 0.03$, **Figure 3C**). No significant increase was observed between pre-blast and post-blast glia-cfDNA levels. Notably, neuron-cfDNA levels detected within a subject's blood plasma were significantly associated with the Peak Impulse (psi/ms) exposure received by the subject prior to blood draw (ZINBR $p = 0.004$). We observed high levels ($>1 \times 10^{-4}$ adj. fraction of reads) of neuron-cfDNA within four subject samples that were twofold higher than any other observations (**Figure 3C**). Notably, three of the four samples were taken following the highest blast wave pressure exposure on day 7 of training and were accompanied by increases in glia-cfDNA (**Figures 3D–F**). Notably, within three of these four subjects, the levels of neuron-cfDNA were reduced >60-fold 1 day following their peak levels (**Figure 3C**; subject 3A02, 3A05, and 3D05), while the other subject (3D04) had a reduction of 3.2-fold 1 day following their peak with undetectable levels 2 days following peak neuron-cfDNA levels (**Figure 3C**). No association was observed between glia-cfDNA and Peak Impulse (psi/ms) exposure (ZINBR $p = 0.49$). Unexpectedly, we detected a high level of glia-cfDNA on day 1 of training in one subject (**Figure 3D**; subject 3 × 01), who did not have a day 7 sample to compare. Five subjects exhibited increases in glia-cfDNA on day 7, and four subjects exhibited increases in glia-cfDNA on day 9 of training that were > 25-fold higher than pre-exposure levels (**Figure 3D**). The results show evidence of glia- and neuron-cfDNA within patient blood plasma following mild trauma.

DISCUSSION

Here we report bisulfite amplicon sequencing assays and bioinformatic strategies using DNA methylation k-mer lookup that, combined, can detect glia- and neuron-cfDNA within blood plasma. The "correct" assignment of cfDNA fragments to a cell-of-origin is essential for clinical utility of cfDNA. Cell-type specific DNA methylation patterns are analogous to gene sequence substrings (k-mers) that can delineate between the DNA of organisms (Breitwieser et al., 2018) and transcripts (Bray et al., 2016). Similarly, DNA methylation embedded within the genomic context can be used as a medium for k-mer indexing and subsequent k-mer lookup strategies (Ye et al., 2021). This represents a strategy for on-the-fly single-read cell-of-origin assignment that is scalable to the whole genome (Ye et al., 2021).

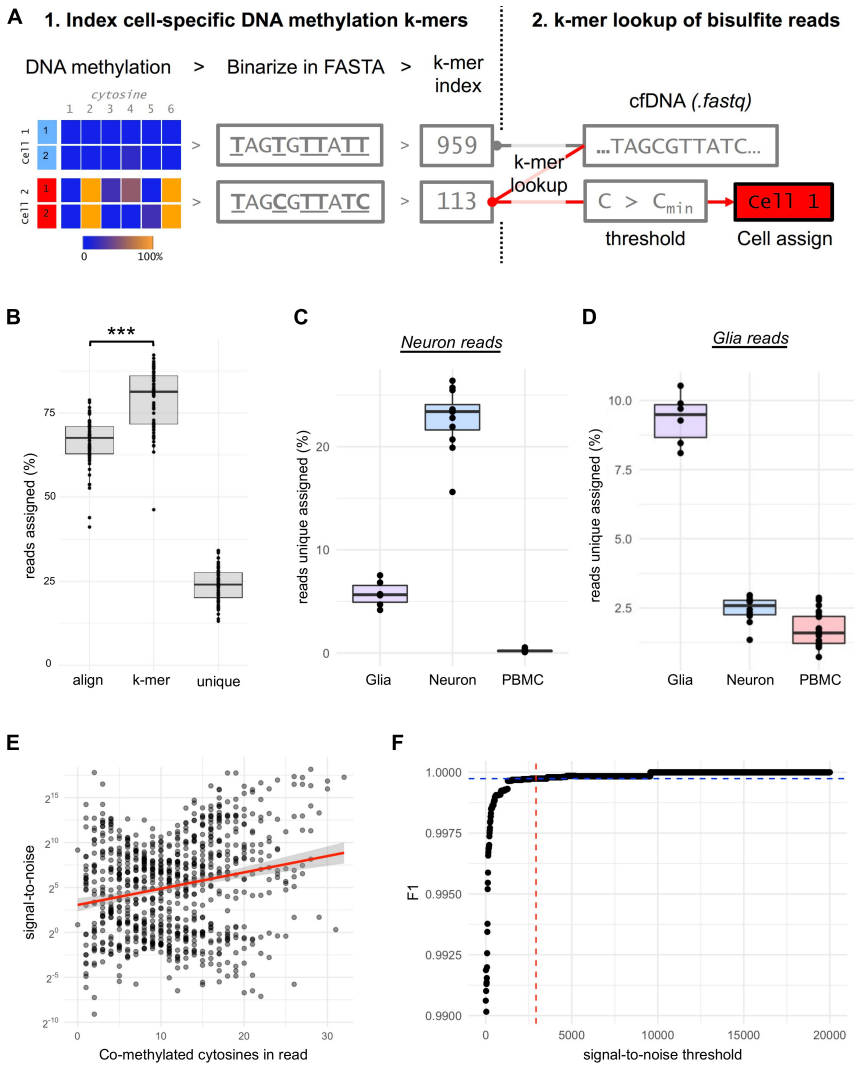

FIGURE 2 | Optimizing the sensitivity and specificity for neuron and glia DNA detection. **(A)** Procedures for creating cell-specific DNA methylation k-mers. DNA methylation signals (%) of each cytosine are summarized across all samples of a cell-type and binarized (>/<50%). The binarized DNA methylation is then inserted into genomic context in FASTA format from which k-mers are indexed. Then raw bisulfite sequencing reads (.fastq eg. from cfDNA) are assigned to cell-types by hash table lookup of indexed k-mers. Co-methylation thresholds, based on signal-to-noise ratios, are then applied to each uniquely assigned read before the read is assigned to its cell-of-origin. **(B)** Boxplot shows the % of reads from glia (n = 7), neuron (n = 13) and PBMC's (n = 11) assigned by alignment (bismark) and k-mer assignment to any cell-type (Kallisto) or uniquely assigned to a cell-type. *** *p*-value = 1.2 x 10–14 **(C)** Boxplot shows the % of uniquely assigned reads from neuron cells to glia, neuron or PBMC's. **(D)** Boxplot shows the % of uniquely assigned reads from glia cells to glia, neuron or PBMC's. **(E)** Correlation plot between the signal-to-noise ratio and co-methylation events for each assay for the neuron cell-type. **(F)** Plot showing the selection of optimal signal-to-noise threshold to accurately assign neuron DNA fragments using the point of inflection (red-blue) of the F1-statistic.

Considering the diversity of cell-types within the human body, we anticipate that cfDNA methylation analysis will be expanded to incorporate many genomic sites of interest to define various cell-types. As our k-mer approach is deterministic, the approach will improve with the addition of single-cell DNA methylation profiles that are currently being established.

The bisulfite sequencing assays used within the current study target regions of the genome that harbor CpG and, uniquely to neurons, CpH DNA methylation. We note that the glia and neuron DNA methylation profiles were discovered from the DLPFC and OFC brain-regions. Considering DNA methylation can exhibit brain-region specificity (Lunnon et al., 2016) and cell sub-type specificity (Luo et al., 2017), future studies will be needed to establish whether the assays are specific for all glia/neurons of the human brain. We show a proof-of-concept study using a unique population of explosive entry personnel with pre- and post-exposure biospecimens that neuron-cfDNA is significantly elevated in response to pressure exposure. Career breachers have reported a range of physical, emotional, and cognitive symptoms, including headache, sleep issues, anxiety, and lower cognitive performance, akin to some symptoms of mild TBI and notably, increased brain activity

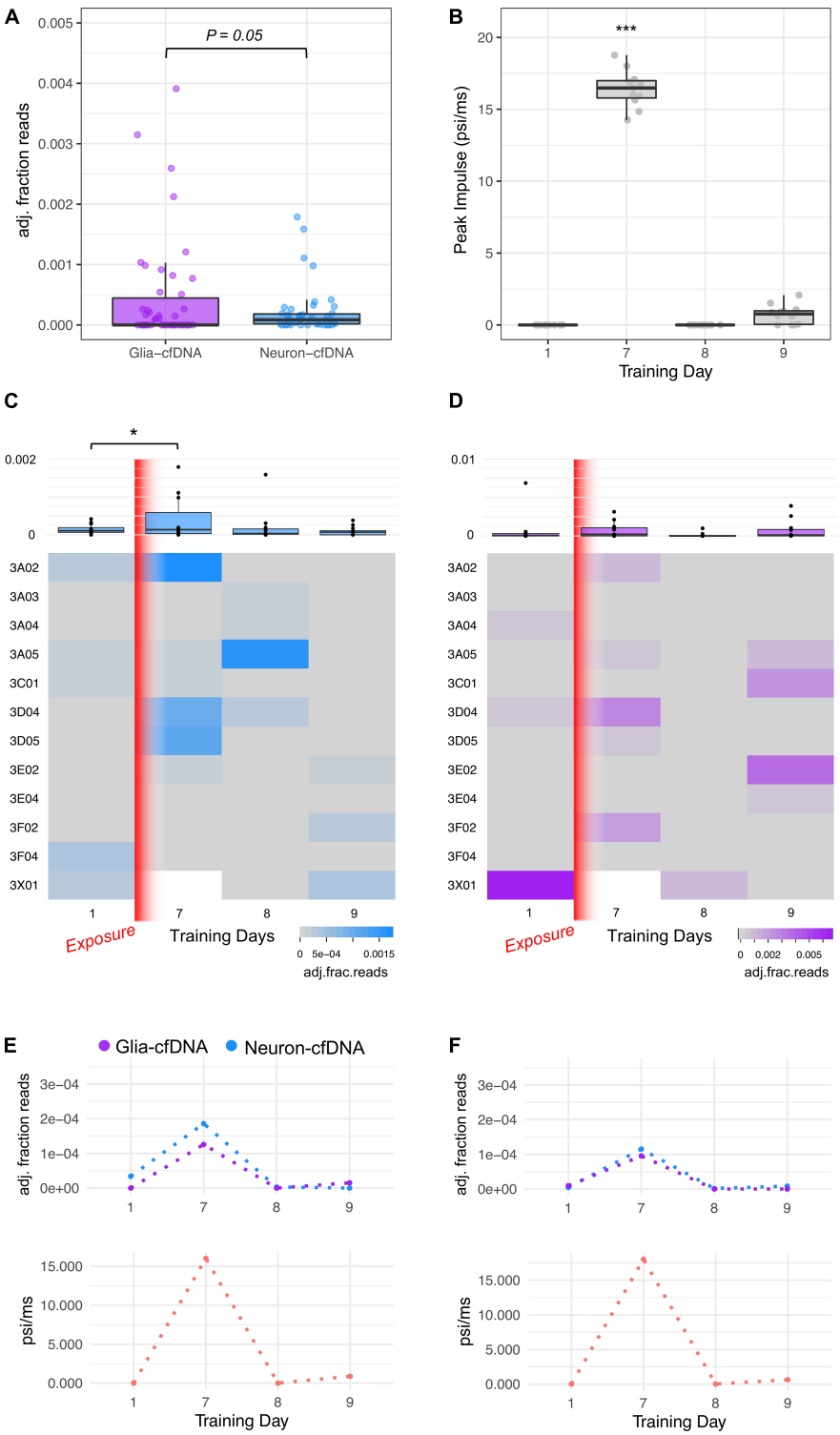

FIGURE 3 | Glia- and neuron-cfDNA measurements within 47 breacher blood plasma samples. **(A)** Boxplot of glia-cfDNA and neuron-cfDNA measurements within breacher samples, measured as adjusted fraction of sequencing reads (adj. fraction reads). **(B)** Boxplot of peak impulse exposure (psi/ms) measurements of breachers on training days 1, 7, 8, and 9 recorded by pressure monitoring devices mounted on each subject. **(C)** Heatmap and boxplots of the neuron-cfDNA measurements across days 1, 7, 8, and 9 of training. **(D)** Heatmap and boxplots of the glia-cfDNA measurements across days 1, 7, 8, and 9 of training. **(E,F)** Longitudinal glia and neuron-cfDNA measurements (top) and peak impulse exposure (psi/ms) of two breacher subjects with highest neuron-cfDNA levels. $^{*}p = 0.03$ and $^{***}p = 3.1 \times 10^{-13}$.

post-exposure (Carr et al., 2016). Reports have shown elevation of neurological proteins (e.g., NfL) within breachers serum post pressure exposure (Boutte et al., 2019). It should be noted that the breacher personnel did not report clinical symptoms associated with mild-TBI following exposure. We note the small sample size of the population as a limitation to the current study. To our knowledge, this is the first investigation of glia- and neuron-cfDNA following low-level blast exposure within a longitudinal operational breaching training.

Looking ahead, glia- and neuron-cfDNA represent a new class of peripheral biomarkers that can characterize the cell-type affected by neurological damage. While this is a proof-of-concept study, the methods we establish have great potential to be extended to various neuronal cell-types and brain regions. Following acute neurotrauma, such as TBI, serum levels of glia and neuron derived proteins (e.g., GFAP and NfL) are increased, and can improve the standard of care within affected patients by indicating injury extent and the need for a CT-scan (Bazarian et al., 2018; Czeiter et al., 2020; Shahim et al., 2020). Importantly, the half-life of cfDNA is much lower than proteins (∼1 h vs 3–4 days GFAP or ∼3 weeks NfL) (Gauthier et al., 1996; Barry et al., 2007; Diehl et al., 2008; Moody et al., 2017); however, the dynamics in which brain-derived cfDNA is deposited and cleared are not currently understood. Future studies of brain-derived cfDNA within animal models of brain injury will be important to understand these dynamics. We hypothesize that glia- and neuron-cfDNA may have application in assessing the extent of neurological injury in the acute phase following injury and represent new important biomarkers to evaluate within acute trauma. Similarly, NfL levels are increased in chronic neurodegenerative diseases such as dementia (Steinacker et al., 2018) highlighting a possible application for glia- and neuron-cfDNA in the diagnosis, subtyping, and disease tracking in chronic neurodegenerative disease.

DATA AVAILABILITY STATEMENT

The datasets analyzed for this study can be found at Gene Expression Omnibus (https://www.ncbi.nlm.nih.gov/geo/) under the accession numbers GSE50798, GSE41169, GSE32148, and GSE47966. The datasets presented in this study can be found at Gene Expression Omnibus under accession number GSE126663.

ETHICS STATEMENT

The studies involving human participants were reviewed and approved by the Institutional Review Board at the Icahn School of Medicine at Mount Sinai. The patients/participants provided their written informed consent to participate in this study.

AUTHOR CONTRIBUTIONS

ZC and FH conceived the study, coordinated experiments, and wrote the manuscript, with contributions from all authors. AD performed post-mortem brain tissue dissections. ZC, NM, and SC performed nuclei isolation and fluorescent activated nuclei sorting. ZC and YG performed bioinformatic and statistical analysis. ZC performed the bisulfite amplicon sequencing analysis and conceived and programmed the methylK pipeline. WC and GK recruited and collected breacher subjects for this study. All authors read and approved the final manuscript.

FUNDING

This study was supported by a postdoctoral fellowship to ZC from the NIDA T32 postdoctoral training program in Interdisciplinary Training in Drug Abuse Research, and VA Merit grants CX001728, CX001395, BX003794, and RX001705 to FH at the James J. Peters VA Medical Center. Also, FH is a recipient of the VA CSR&D Research Career Scientist Award (CX002074). Sample collections (GK) were supported by Broad Agency Announcement Award No. W81XWH-16-2-0001. This research was supported in part by an appointment to the Research Participation Program at the Walter Reed Army Institute of Research administered by the Oak Ridge Institute for Science and Education through an interagency agreement between the U.S. Department of Energy and USAMRMC. Acquisition and sampling of postmortem brain was supported by grants R01 MH64168 and R01 MH098786ORK from the National Institute of Mental Health and the Fogarty International Center at the National Institutes of Health. This work was also supported in part through the computational resources and staff expertise provided by Scientific Computing at the Icahn School of Medicine at Mount Sinai.

ACKNOWLEDGMENTS

We thank Liying Yan (EpigenDX) and her team for their help in assay design and synthesis.

SUPPLEMENTARY MATERIAL

The Supplementary Material for this article can be found online at: https://www.frontiersin.org/articles/10.3389/fnmol.2021.672614/full#supplementary-material

REFERENCES

Anker, P., Lefort, F., Vasioukhin, V., Lyautey, J., Lederrey, C., Chen, X. Q., et al. (1997). K-ras mutations are found in DNA extracted from the plasma of patients with colorectal cancer. *Gastroenterology* 112, 1114–1120. doi: 10.1016/s0016-5085(97)70121-5

Aryee, M. J., Jaffe, A. E., Corrada-Bravo, H., Ladd-Acosta, C., Feinberg, A. P., Hansen, K. D., et al. (2014). Minfi: a flexible and comprehensive Bioconductor package for the analysis of Infinium DNA methylation microarrays. *Bioinformatics* 30, 1363–1369. doi: 10.1093/bioinformatics/btu049

Barry, D. M., Millecamps, S., Julien, J. P., and Garcia, M. L. (2007). New movements in neurofilament transport, turnover and disease. *Exp. Cell. Res.* 313, 2110–2120. doi: 10.1016/j.yexcr.2007.03.011

Bazarian, J. J., Biberthaler, P., Welch, R. D., Lewis, L. M., Barzo, P., Bogner-Flatz, V., et al. (2018). Serum GFAP and UCH-L1 for prediction of absence of intracranial

injuries on head CT (ALERT-TBI): a multicentre observational study. *Lancet Neurol.* 17, 782–789. doi: 10.1016/s1474-4422(18)30231-x

Bibikova, M., Lin, Z., Zhou, L., Chudin, E., Garcia, E. W., Wu, B., et al. (2006). High-throughput DNA methylation profiling using universal bead arrays. *Genome Res.* 16, 383–393. doi: 10.1101/gr.4410706

Boutte, A. M., Thangavelu, B., LaValle, C. R., Nemes, J., Gilsdorf, J., Shear, D. A., et al. (2019). Brain-related proteins as serum biomarkers of acute, subconcussive blast overpressure exposure: a cohort study of military personnel. *PLoS One* 14:e0221036. doi: 10.1371/journal.pone.0221036

Bray, N. L., Pimentel, H., Melsted, P., and Pachter, L. (2016). Near-optimal probabilistic RNA-seq quantification. *Nat. Biotechnol.* 34, 525–527. doi: 10.1038/nbt.3519

Breitwieser, F. P., Baker, D. N., and Salzberg, S. L. (2018). KrakenUniq: confident and fast metagenomics classification using unique k-mer counts. *Genome Biol.* 19:198.

Carr, W., Stone, J. R., Walilko, T., Young, L. A., Snook, T. L., Paggi, M. E., et al. (2016). Repeated Low-Level Blast Exposure: a Descriptive Human Subjects Study. *Mil. Med.* 181, 28–39. doi: 10.7205/milmed-d-15-00137

Combaret, V., Audoynaud, C., Iacono, I., Favrot, M. C., Schell, M., Bergeron, C., et al. (2002). Circulating MYCN DNA as a tumor-specific marker in neuroblastoma patients. *Cancer Res.* 62, 3646–3648.

Crowley, E., Di Nicolantonio, F., Loupakis, F., and Bardelli, A. (2013). Liquid biopsy: monitoring cancer-genetics in the blood. *Nat. Rev. Clin. Oncol.* 10, 472–484. doi: 10.1038/nrclinonc.2013.110

Czeiter, E., Amrein, K., Gravesteijn, B. Y., Lecky, F., Menon, D. K., Mondello, S., et al. (2020). Blood biomarkers on admission in acute traumatic brain injury: relations to severity. CT findings and care path in the CENTER-TBI study. *EBioMed.* 56:102785. doi: 10.1016/j.ebiom.2020.102785

Diehl, F., Schmidt, K., Choti, M. A., Romans, K., Goodman, S., Li, M., et al. (2008). Circulating mutant DNA to assess tumor dynamics. *Nat. Med.* 14, 985–990. doi: 10.1038/nm.1789

Gauthier, V. J., Tyler, L. N., and Mannik, M. (1996). Blood clearance kinetics and liver uptake of mononucleosomes in mice. *J. Immunol.* 156, 1151–1156.

Jaffe, A. E., Murakami, P., Lee, H., Leek, J. T., Fallin, M. D., Feinberg, A. P., et al. (2012). Bump hunting to identify differentially methylated regions in epigenetic epidemiology studies. *Int. J. Epidemiol.* 41, 200–209. doi: 10.1093/ije/dyr238

Kelly, T. M., and Mann, J. J. (1996). Validity of DSM-III-R diagnosis by psychological autopsy: a comparison with clinician ante-mortem diagnosis. *Acta Psychiatr. Scand.* 94, 337–343. doi: 10.1111/j.1600-0447.1996.tb09869.x

Krueger, F., and Andrews, S. R. (2011). Bismark: a flexible aligner and methylation caller for Bisulfite-Seq applications. *Bioinformatics* 27, 1571–1572. doi: 10.1093/bioinformatics/btr167

Lawrence, M., Huber, W., Pages, H., Aboyoun, P., Carlson, M., Gentleman, R., et al. (2013). Software for computing and annotating genomic ranges. *PLoS Comput. Biol.* 9:e1003118. doi: 10.1371/journal.pcbi.1003118

Lehmann-Werman, R., Neiman, D., Zemmour, H., Moss, J., Magenheim, J., Vaknin-Dembinsky, A., et al. (2016). Identification of tissue-specific cell death using methylation patterns of circulating DNA. *Proc. Natl. Acad. Sci. U. S. A.* 113, E1826–E1834.

Lister, R., Mukamel, E. A., Nery, J. R., Urich, M., Puddifoot, C. A., Johnson, N. D., et al. (2013). Global epigenomic reconfiguration during mammalian brain development. *Science* 341:1237905. doi: 10.1126/science.1237905

Lo, Y. M., Corbetta, N., Chamberlain, P. F., Rai, V., Sargent, I. L., Redman, C. W., et al. (1997). Presence of fetal DNA in maternal plasma and serum. *Lancet* 350, 485–487.

Lo, Y. M., Tein, M. S., Lau, T. K., Haines, C. J., Leung, T. N., Poon, P. M., et al. (1998). Quantitative analysis of fetal DNA in maternal plasma and serum: implications for noninvasive prenatal diagnosis. *Am. J. Hum. Genet.* 62, 768–775.

Luo, C., Keown, C. L., Kurihara, L., Zhou, J., He, Y., Li, J., et al. (2017). Single-cell methylomes identify neuronal subtypes and regulatory elements in mammalian cortex. *Science* 357, 600–604. doi: 10.1126/science.aan3351

Lunnon, K., Hannon, E., Smith, R. G., Dempster, E., Wong, C., Burrage, J., et al. (2016). Variation in 5-hydroxymethylcytosine across human cortex and cerebellum. *Genome Biol.* 17:27.

Matevossian, A., and Akbarian, S. (2008). Neuronal nuclei isolation from human postmortem brain tissue. *J. Vis. Exp.* 20:914. doi: 10.3791/914

Moody, L. R., Barrett-Wilt, G. A., Sussman, M. R., and Messing, A. (2017). Glial fibrillary acidic protein exhibits altered turnover kinetics in a mouse model of Alexander disease. *J. Biol. Chem.* 292, 5814–5824. doi: 10.1074/jbc.m116.772020

Moss, J., Magenheim, J., Neiman, D., Zemmour, H., Loyfer, N., Korach, A., et al. (2018). Comprehensive human cell-type methylation atlas reveals origins of circulating cell-free DNA in health and disease. *Nat. Commun.* 9:5068.

Naeem, H., Wong, N. C., Chatterton, Z., Hong, M. K., Pedersen, J. S., Corcoran, N. M., et al. (2014). Reducing the risk of false discovery enabling identification of biologically significant genome-wide methylation status using the HumanMethylation450 array. *BMC Genom.* 15:51. doi: 10.1186/1471-2164-15-51

Nawroz, H., Koch, W., Anker, P., Stroun, M., and Sidransky, D. (1996). Microsatellite alterations in serum DNA of head and neck cancer patients. *Nat. Med.* 2, 1035–1037. doi: 10.1038/nm0996-1035

Newman, A. M., Bratman, S. V., To, J., Wynne, J. F., Eclov, N. C., Modlin, L. A., et al. (2014). An ultrasensitive method for quantitating circulating tumor DNA with broad patient coverage. *Nat. Med.* 20, 548–554. doi: 10.1038/nm.3519

Nygren, A. O., Dean, J., Jensen, T. J., Kruse, S., Kwong, W., van den Boom, D., et al. (2010). Quantification of fetal DNA by use of methylation-based DNA discrimination. *Clin. Chem.* 56, 1627–1635. doi: 10.1373/clinchem.2010.146290

Rosoklija, G., Duma, A., and Dwork, A. J. (2013). Psychiatric brain collection in Macedonia: general lessons for scientific collaboration among countries of differing wealth. *Pril* 34, 95–98.

Salkeni, M. A., Zarzour, A., Ansay, T. Y., McPherson, C. M., Warnick, R. E., Rixe, O., et al. (2013). Detection of EGFRvIII mutant DNA in the peripheral blood of brain tumor patients. *J. Neurooncol.* 115, 27–35. doi: 10.1007/s11060-013-1209-0

Shahim, P., Politis, A., van der Merwe, A., Moore, B., Ekanayake, V., Lippa, S. M., et al. (2020). Time course and diagnostic utility of NfL, tau. GFAP, and UCH-L1 in subacute and chronic TBI. *Neurology* 95, e623–e636.

Smyth, G. K. (2005). *Limma: linear Models for Microarray Data*. New York: Springer.

Steinacker, P., Anderl-Straub, S., Diehl-Schmid, J., Semler, E., Uttner, I., von Arnim, C. A. F., et al. (2018). Serum neurofilament light chain in behavioral variant frontotemporal dementia. *Neurology* 91, e1390–e1401. doi: 10.1212/WNL.0000000000006318

van den Broek, J. (1995). A score test for zero inflation in a Poisson distribution. *Biometrics* 51, 738–743. doi: 10.2307/2532959

Ye, Z., Chatterton, Z., Pflueger, J., Damiano, J. A., McQuillan, L., Harvey, A. S., et al. (2021). Cerebrospinal fluid liquid biopsy for detecting somatic mosaicism in brain. *Brain Commun.* 3:fcaa235.

Disclaimer: Material has been reviewed by the Walter Reed Army Institute of Research. There is no objection to its presentation and/or publication. The opinions or assertions contained herein are the private views of the authors and are not to be construed as official, or as reflecting true views of the Department of the Army or the Department of Defense. The investigators have adhered to the policies for protection of human subjects as prescribed in AR 70-25.

Conflict of Interest: The authors declare that the research was conducted in the absence of any commercial or financial relationships that could be construed as a potential conflict of interest.

frontiers in Molecular Neuroscience

ORIGINAL RESEARCH
published: 27 August 2021
doi: 10.3389/fnmol.2021.723317

Dynamic Changes in the Levels of Amyloid-β_{42} Species in the Brain and Periphery of APP/PS1 Mice and Their Significance for Alzheimer's Disease

*Liding Zhang[1,2], Changwen Yang[1,2], Yanqing Li[1,2], Shiqi Niu[1,2], Xiaohan Liang[1,2], Zhihong Zhang[1,2,3], Qingming Luo[1,2,3] and Haiming Luo[1,2]**

[1] Britton Chance Center for Biomedical Photonics, Wuhan National Laboratory for Optoelectronics, Huazhong University of Science and Technology, Wuhan, China, [2] MoE Key Laboratory for Biomedical Photonics, School of Engineering Sciences, Huazhong University of Science and Technology, Wuhan, China, [3] School of Biomedical Engineering, Hainan University, Haikou, China

OPEN ACCESS

Edited by:
Thomas K. Karikari,
University of Gothenburg, Sweden

Reviewed by:
Kristin Michaelsen-Preusse,
Technische Universitat Braunschweig, Germany
Zheng Chen,
University of Texas Health Science Center at Houston, United States

***Correspondence:**
Haiming Luo
hemluo@hust.edu.cn

Specialty section:
This article was submitted to Methods and Model Organisms, a section of the journal Frontiers in Molecular Neuroscience

Received: 10 June 2021
Accepted: 09 August 2021
Published: 27 August 2021

Citation:
Zhang L, Yang C, Li Y, Niu S, Liang X, Zhang Z, Luo Q and Luo H (2021) Dynamic Changes in the Levels of Amyloid-β_{42} Species in the Brain and Periphery of APP/PS1 Mice and Their Significance for Alzheimer's Disease. Front. Mol. Neurosci. 14:723317. doi: 10.3389/fnmol.2021.723317

Although amyloid-β_{42} ($A\beta_{42}$) has been used as one of the core biomarkers for Alzheimer's disease (AD) diagnosis, the dynamic changes of its different forms in the brain, blood, and even intestines and its correlation with the progression of AD disease remain obscure. Herein, we screened $A\beta_{42}$-specific preferred antibody pairs 1F12/1F12 and 1F12/2C6 to accurately detect $A\beta_{42}$ types using sandwich ELISA, including total $A\beta_{42}$, $A\beta_{42}$ oligomers ($A\beta_{42}$Os), and $A\beta_{42}$ monomers ($A\beta_{42}$Ms). The levels of $A\beta_{42}$ species in the brain, blood, and intestines of different aged APP/PS1 mice were quantified to study their correlation with AD progression. Total $A\beta_{42}$ levels in the blood were not correlated with AD progression, but $A\beta_{42}$Ms level in the blood of 9-month-old APP/PS1 mice was significantly reduced, and $A\beta_{42}$Os level in the brain was significantly elevated compared to 3-month-old APP/PS1, demonstrating that the levels of $A\beta_{42}$Ms and $A\beta_{42}$Os in the blood and brain were correlated with AD progression. Interestingly, in 9-month-old APP/PS1 mice, the level of $A\beta_{42}$ in the intestine was higher than that in 3-month-old APP/PS1 mice, indicating that the increased level of $A\beta_{42}$ in the gastrointestinal organs may also be related to the progression of AD. Meanwhile, changes in the gut microbiota composition of APP/PS1 mice with age were also observed. Therefore, the increase in Aβ derived from intestinal tissues and changes in microbiome composition can be used as a potential early diagnosis tool for AD, and further used as an indicator of drug intervention to reduce brain amyloid.

Keywords: Alzheimer's disease, blood $A\beta_{42}$, intestinal Aβ, dynamic distribution, ELISA – enzyme-linked immunosorbent assay

INTRODUCTION

Alzheimer's disease (AD) is an age-related, irreversible form of dementia that affects nearly 50 million people worldwide (Collaborators, 2019). A defining pathological feature of AD is the presence of extracellular deposits of aggregated amyloid-β (Aβ) in the form of senile plaques in specific brain tissues and vascular walls (Murphy and LeVine, 2010), the main components of

which are the peptide isoforms $A\beta_{40}$ and $A\beta_{42}$, of which $A\beta_{42}$ predominates in neuritic plaques of AD (Gu and Guo, 2013; Hong and Yaqub, 2019). Autopsy and Aβ positron emission tomography (PET) have indicated that Aβ deposition precedes cognitive decline by a decade or more (Driscoll et al., 2006; Sperling et al., 2011; Oxtoby et al., 2018). Aβ, a 4–4.5 kDa peptide containing 39–42 residues, is produced by sequential proteolytic cleavage of amyloid precursor protein (APP), which is expressed in brain cells and peripheral tissues (such as adrenal gland, kidney, heart, liver, spleen, muscles, and blood vessels) (Roher et al., 2009). Considering that skeletal muscle, accounting for 40% of total body weight (Kim et al., 2016), is only one of many peripheral sources of Aβ, peripheral Aβ may account for a large portion of total Aβ. As observed in human and animal models, brain-derived Aβ peptides can be transported from the brain to peripheral blood (Roberts et al., 2014; Xiang et al., 2015). The communication between the periphery organs and the brain allows for active and dynamic Aβ exchange in distinct reservoirs. The brain accumulation of Aβ aggregates is affected by the levels of $A\beta_{42}$ in the brain and peripheral tissues, but the contribution of peripheral Aβ toward the progression of AD is poorly understood.

$A\beta_{42}$ monomers ($A\beta_{42}$Ms), mainly α-helical and random coil structures, easily aggregate to form various soluble oligomers. The transition of monomers to oligomers triggers the aggregation and pathogenic transformation of Aβ peptides (Nag et al., 2011). A high concentration of $A\beta_{42}$ peptide promotes the formation of its aggregates from soluble monomers into toxic $A\beta_{42}$ oligomers ($A\beta_{42}$Os), and eventually forms extracellular neurotoxic plaques. It has been shown that the brain level of $A\beta_{42}$ increases in the early stage of AD, but decreases with the decline of cognitive ability in the late-stage AD (Naslund et al., 2000). The balance between Aβ production and clearance determines the concentration of Aβ in various reservoirs (Wang et al., 2006). Increasing evidence has implicated that diffusible and soluble Aβ oligomers (Bernstein et al., 2009), rather than insoluble fibrils and small monomers, are the main form of neurotoxicity. These oligomers induce neurotoxic intracellular signaling pathways such as neuronal injury (Wang W. et al., 2019), inflammatory (Salminen et al., 2008), mitochondrial dysfunction, and oxidative stress (Mucke and Selkoe, 2012). The fluctuation of amyloid subtypes in cerebrospinal fluid and blood mainly depends on $A\beta_{42}$Ms and $A\beta_{42}$Os, which are used as core biomarkers to reflect the progression of AD (Benilova et al., 2012). Therefore, dynamic measurement of the levels and profile of $A\beta_{42}$Ms and $A\beta_{42}$Os in the brain and periphery is crucial for studying their physiological metabolism and their substantial correlation with AD progression.

The reliable detection of $A\beta_{42}$Ms and $A\beta_{42}$Os is technically challenging because $A\beta_{42}$Os are transient, heterogeneous, and in dynamic equilibrium with $A\beta_{42}$Ms. In this study, we screened two sequence- and conformation-specific antibodies 1F12 and 2C6, that recognize different epitopes of $A\beta_{42}$. The preferred antibody pairs 1F12/2C6 and 1F12/1F12 were chosen to evaluate the potential significance of various sources and pools of $A\beta_{42}$ on the overall pathology of AD. The correlation between blood $A\beta_{42}$ levels and brain $A\beta_{42}$ levels in APP/PS1 and age-matched C57BL/6J mice at 3 and 9 months was dynamically assessed. Another comprehensive longitudinal study determined the potential effects of intestinal tissue-derived $A\beta_{42}$ on blood and brain $A\beta_{42}$ levels in APP/PS1 mice. We expect that our research will promote the understanding of the role of $A\beta_{42}$Ms and $A\beta_{42}$Os in the progression of AD.

MATERIALS AND METHODS

Chemicals and Materials

The $A\beta_{3-9}$, $A\beta_{13-19}$, $A\beta_{18-25}$, $A\beta_{29-36}$, $A\beta_{36-42}$, $A\beta_{40}$, and $A\beta_{42}$ were custom-synthesized as lyophilized powders by Royo Biotech Co., Ltd (Shanghai, China) with a purity of >95%. Anti-Aβ (6E10) antibody was obtained from Invitrogen. The goat anti-mouse IgG (H + L), protein A resin, and protein L resin were ordered from GenScript (Nanjing, China). The mouse monoclonal antibody isotyping kit was purchased from Southern Biotech (Birmingham, AL, United States). The Pierce streptavidin-coupled poly-HRP and protein marker were ordered from Thermo Scientific (Massachusetts, United States). Thioflavin S, BSA, Freund's complete adjuvant, and Freund's incomplete adjuvant were obtained from Sigma-Aldrich. Cy3-NHS ester and Biotin-PEG4-NHS ester were provided by Lumiprobe (Hannover, Germany). All other chemicals were purchased from commercial suppliers and used as received.

Oligomeric and Monomeric Aβ Preparations

The $A\beta_{40}$ monomers ($A\beta_{40}$Ms) and $A\beta_{42}$Ms were obtained by dissolving lyophilized $A\beta_{40}$, $A\beta_{42}$ peptides in 1,1,1,3,3,3-hexafluoroisopropanol (HFIP), followed by incubation overnight at room temperature. HFIP was evaporated with nitrogen gas to form a film, and the Aβ was redissolved in dimethyl sulfoxide. The prepared $A\beta_{40}$, $A\beta_{42}$ monomers solution (50 μM) was stored at −20°C as stock solution. The $A\beta_{40}$ oligomers ($A\beta_{40}$Os) and $A\beta_{42}$ oligomers ($A\beta_{42}$Os) were obtained from 24 h incubation of 50 μM $A\beta_{40}$ and $A\beta_{42}$ monomer solutions at 37°C in the dark, respectively.

Cryo-Transmission Electron Microscopy

The patterns of the prepared $A\beta_{42}$Ms and $A\beta_{42}$Os were confirmed by cryo-transmission electron microscopy (Cryo-TEM). In brief, 5 μL of each sample was deposited on a copper grid, and the excess liquid was removed using a filter paper, leaving a thin film of the solution on the grid. The Tecnai G20 transmission electron microscope (FEI Ltd., United States) was used to characterize the morphology of the above-mentioned samples.

Generation and Purification of 1F12 and 2C6

The antigen was prepared using lyophilized synthetic $A\beta_{42}$ peptide dissolved in 10 mM NaOH and diluted with PBS to a final concentration of 1 mg/mL. In the first immunization, BALB/c mice were immunized with 50 μg $A\beta_{42}$ peptide

mixed with Freund's complete adjuvant. In the second and third immunizations, $A\beta_{42}$ peptides and Freund's incomplete adjuvant mixtures were used (Zhang et al., 2018). After the third immunizations, 50 μg $A\beta_{42}$ peptide was used for booster immunization. Three days later, spleen cells were collected from the immunized mice and fused with SP2/0 cells via PEG at 37°C (Wang X. et al., 2019). The fused cells were maintained in HAT medium for 7 days and then cultured in HT medium. The positive hybridomas in each plate were screened by the limited dilution method (Kohler and Milstein, 1975). Three positive hybridoma cell lines were screened from the initial positive wells and cultured to prepare ascites. The immunoglobulins of 1F12, 2C6, and 2E2 were purified using protein A resin, according to the manufacturer's instructions.

Dot Blot Assay

One microgram of each $A\beta_{42}$ truncated peptide including $A\beta_{3-9}$, $A\beta_{13-19}$, $A\beta_{18-25}$, $A\beta_{29-36}$, and $A\beta_{36-42}$ was pipetted onto a PVDF membrane activated by methanol. After the peptide samples were deposited, the PVDF membrane was air-dried and blocked in 5% skimmed milk in phosphate-buffered saline (PBS) with Tween-20 detergent (PBS-T) at 37°C for 1 h. The membranes were then incubated with mAb 1F12 (1:1000) or 2C6 (1:1000) at 37°C for 2 h. After washing three times in PBS-T, the membrane was incubated with the secondary antibody HRP-conjugated goat anti-mouse IgG (H + L) at 37°C for 2 h, and the immunological signals were detected with ECL-substrate (Vazyme, China) using Tanon 5200 Muiti (Shanghai, China).

Biotinylated 1F12 or 2C6 Antibody Preparation

The biotinylated antibodies were generated based on the reaction of amino groups of 1F12 or 2C6 antibody with biotin *N*-hydroxysuccinimide (NHS) ester. Briefly, 10 nmol of 1F12 or 2C6 antibody was dissolved in PBS, and the solution pH was adjusted to 8.5 with Na_2CO_3 (0.1 M), followed by a reaction with 20 nmol biotin-PEG4-NHS esters in DMSO at room temperature for 2 h. The biotin-modified 1F12 or 2C6 antibody was purified using size exclusion PD-10 columns with PBS as the mobile phase. Indirect ELISA determined the activities and titers of biotinylated 1F12 or 2C6. The indirect ELISA assay was performed using serially diluted biotin-labeled antibodies (from 1:100 to 1:409,600) instead of the primary antibody. After incubation with the Pierce streptavidin-coupled poly-HRP, the immunoreaction was visualized with a soluble TMB substrate solution.

Measurement of the Titer and Binding Affinity of 1F12 or 2C6 Antibody

The 96-well plates were coated with 0.5 μg/well of $A\beta_{42}$ and blocked with 5% skimmed milk dissolved in a PBS-T buffer for 2 h at room temperature. Subsequently, series of diluted 1F12 or 2C6 ranging from 1:100 to 1:409,600 were added into each well for 2-h incubation at 22°C. The subsequent steps were performed as described in the ELISA section above. The binding affinities of 1F12 or 2C6 with $A\beta_{42}$ species were determined using serially diluted preparations of 1F12 or 2C6 with serials of concentrations (from 10 μg/mL to 10 ng/mL) instead of different dilutions (from 1:100 to 1:409,600). After incubation with the HRP-conjugated goat anti-mouse IgG (H + L), the immunoreaction was visualized with a soluble TMB substrate solution.

Screening of Preferred Antibody Pairs for Total $A\beta_{42}$ and $A\beta_{42}$Os Sandwich ELISA

Preferred antibody pairs of total $A\beta_{42}$ and $A\beta_{42}$Os sandwich ELISA were screened from the combination of different antibody pairs. The screening process of antibody pairs for total $A\beta_{42}$ was as follows: 96-well plate was coated with 1 μg/well of 1F12 or 2C6 as the capture antibody for 2 h at room temperature, and then blocked with 5% skimmed milk. Five ng total $A\beta_{42}$ containing $A\beta_{42}$Ms and $A\beta_{42}$Os or $A\beta_{42}$Os was loaded into each well and incubated 2 h at room temperature, followed by the addition of biotinylated 2C6 or 1F12 as the detection antibody. Finally, streptavidin-coupled poly-HRP was used to visualize the immunoreaction of each well.

Sandwich ELISA for the Detection of Total $A\beta_{42}$ and $A\beta_{42}$Os

The 96-well plates were coated with 1 μg/well of 1F12 in the citrate-buffered saline buffer for 2 h, and then blocked with 5% skimmed milk dissolved in PBS-T for 2 h at room temperature. A standard series of synthetic Aβ peptides ($A\beta_{40}$Ms, $A\beta_{42}$Ms, $A\beta_{40}$Os, and $A\beta_{42}$Os) and the biological samples (mouse blood and organ homogenization) to be analyzed were added to the plates in triplicates and incubated for 40 min at room temperature. The plate was washed three times with PBS-T and incubated with biotinylated mAb 2C6 for total $A\beta_{42}$ detection or biotinylated mAb 1F12 for $A\beta_{42}$Os detection, followed by incubation with streptavidin-coupled poly-HRP for 1 h at room temperature. The immunoreaction in each well was detected using TMB substrate solution.

Quantification of Aβ Peptides in Blood, Brain, and Intestinal Tissue

All procedures involving animal studies were reviewed and approved by the Institutional Animal Care and Use Committee of Huazhong University of Science and Technology. Herein, 3-month-old APP/PS1 mice (six mice for blood collection including three female and three male mice, and four mice for tissue collection, including two female and two male mice), 9-month-old APP/PS1 mice (six mice for blood collection including three female and three male mice, n = 4 for tissue collection, including two female and two male mice), and age-matched non-transgenic C57BL/6J mice (six mice for blood collection, including three female and three male mice, and four mice for tissues collection, including two female and two male mice) were anesthetized with 0.4 mL Avertin (25 mg/mL) and intracardially perfused with 0.9% saline solution. The mouse blood was collected, and tissues were organically extracted with antigen extraction tris-buffered saline (TBS, 20 mM Tris and 137 mM NaCl, pH 7.6) at a ratio of 1:50 (w/v) using a tissue grinder. The TBS included a complete protease inhibitor cocktail

(Roche). The supernatant of homogenates was centrifuged at 10,000 *g* for 30 min in Type 60 Ti fixed angle rotor at 4°C to obtain TBS-soluble proteins. The collected mouse blood, prepared brain, and intestinal tissue samples were used for $A\beta_{42}$ quantification by the above-prepared sandwich ELISA.

Immunoprecipitation and Western Blotting

The homogenates of organ tissues (brain, stomach, duodenum, jejunum, ileum, cecum, colon, and intestinal lysates) or blood were incubated for 30 min at room temperature with 40 μg/mL of 1F12 antibody conjugated on the protein A/G magnetic bead, according to the manufacturer's instructions. The immunoprecipitated proteins were eluted with 0.1 M glycine (pH 3.0) and immediately neutralized to pH 7.4 using a neutralization buffer (1 M Tris-HCl, pH 8.5). The samples were then denatured in loading buffer (Boster Biotech, United States) and boiled for 10 min. Following this, the proteins were run on a 12% reduced tris-tricine SDS-polyacrylamide gel via SDS-PAGE. Proteins were transferred onto a polyvinylidene fluoride membrane at 160 mA for 1 h, at 4°C. Membranes were blocked with 5% skimmed milk dissolved in 1 × PBS-T and incubated with 1F12 or 2C6 for 2 h at 37°C. Subsequently, the membranes were washed in PBS-T followed by 1 h incubation with secondary antibody HRP-conjugated goat anti-mouse IgG (H + L), and the immunological signals were detected using the ECL-substrate (Vazyme, China) on Tanon 5200 Muiti (Shanghai, China).

Immunofluorescence Assays of Tissues

The mice were anesthetized with 0.4 mL Avertin (25 mg/mL), and cardiac perfusion was performed with 4% paraformaldehyde (PFA) for 30 min. The tissues (brain, duodenum, jejunum, ileum, cecum, and colon) from mice were collected, fixed in 4% PFA, and dehydrated in sucrose solution. After embedding in OCT compound (Tissue-Tek; Sakura Finetek, Netherlands, United States), 15 μm coronal frozen sections of tissue samples were serially cut on a Leica CM3050 S cryostat. Each slice was mounted on glass slides and permeabilized with 0.2% Triton X-100 overnight at 4°C. The slice was blocked with 3% BSA for 2 h at room temperature and incubated with thioflavin S or commercially available anti-Aβ antibody 6E10, Cy3-conjugated 1F12 or 2C6 overnight at 4°C. All slides were washed five times with PBS and stained with thioflavin S. The Zeiss LSM710 microscope was used to image slides with red, green, and blue fluorescence filters.

Sequencing Data and Statistical Analyses

Sequencing data from an independent study of the APP/PS1 mice gut microbiota was obtained. Raw 16S sequences were downloaded from SRA accession PRJNA543965 and preprocessed using the 'dada2' R package. Reads were truncated at 150 bp, then a maximum expected error rate threshold of 1 was imposed. Taxonomy was assigned using the Silva v138 rRNA database using the default classify algorithm of dada2 (v1.16.0).

Downstream analysis was performed by several R packages including 'phyloseq,' 'MicrobiotaProcess,' 'DESeq2,' and 'ggplot2.' Beta diversity was measured by principal coordinate analysis (PCoA) based on weighted UniFrac phylogenetic distance. The significantly differed genus between groups was determined using 'DESeq2,' and their significance of difference was assessed by Wilcoxon rank-sum test. The significance cut-off was set at $^{*}p < 0.05$.

The data, except for sequencing data, are presented as means ± SEM. One-way or two-way analysis of variance (ANOVA) was used for multiple group comparisons. Statistical significance is represented in the figure by $^{*}p < 0.05$, $^{**}p < 0.01$, $^{***}p < 0.001$, $^{****}p < 0.0001$, and n.s. (indicating no significance). All statistical analyses were performed with GraphPad Prism7.0 software.

RESULTS

Screening and Identification of $A\beta_{42}$ Sequence- and Conformation-Specific Antibodies

BALB/c mice were immunized with human $A\beta_{42}$ peptide preparations, and a pool of approximately 1,500 clones was generated via hybridoma technology. In addition, 75 of these clones reacted with Aβ monomers and oligomers in ELISA (**Supplementary Figure 1A**). Then three positive hybridoma clones 1F12, 2C6, and 2E2 were selected, and their immunoglobulin isotypes were determined. The results showed that the isotype of 1F12 and 2C6 was IgG2a, and the isotype of 2E2 was IgA, and the light chains of these three monoclonal antibodies (mAbs) all belonged to the kappa chain (**Figure 1A**). Reduced SDS-PAGE identified the purity and molecular weight of these three mAbs (**Supplementary Figure 1B**). Therefore, 1F12 and 2C6 were chosen to characterize their reactivity by Western blotting brain natural $A\beta_{42}$ and immunostaining brain slices of APP/PS1 mice. The results displayed strong bands of $A\beta_{42}$ peptides recognized by 1F12 and 2C6, comparable to those obtained with 6E10 (**Supplementary Figure 1C**). Immunofluorescence imaging (using thioflavin S or commercially available anti-Aβ antibody 6E10) showed that Aβ plaques were colocalized with Cy3-labeled 1F12 (**Figure 1B** and **Supplementary Figure 2A**) or 2C6 (**Supplementary Figures 1D, 2B**). The titer of mAbs was determined by indirect ELISA and calculated as 1:204800 for 1F12, 1:102400 for 2C6, 1:51200 for 2E2 (**Supplementary Figure 1E**).

To identify the linear fragments (epitopes) of $A\beta_{42}$ recognized by 1F12 and 2C6, we performed epitope mapping experiments using a series of peptides starting from +3 to +42 in the $A\beta_{42}$ sequence. Based on a series of dot-blot analyses, we observed that 1F12 displayed a linear epitope, amino acids 3–9 located in the N-terminal region of the $A\beta_{42}$ peptide (**Figure 1C**, left). In contrast, 2C6 exhibited discrete epitopes, including four distinct $A\beta_{42}$ fragments (**Figure 1C**, right). To confirm the binding efficacy of 1F12 and 2C6 to $A\beta_{42}$ and $A\beta_{40}$ peptides, indirect ELISAs were performed on separate $A\beta_{42}$ and $A\beta_{40}$ coated plates.

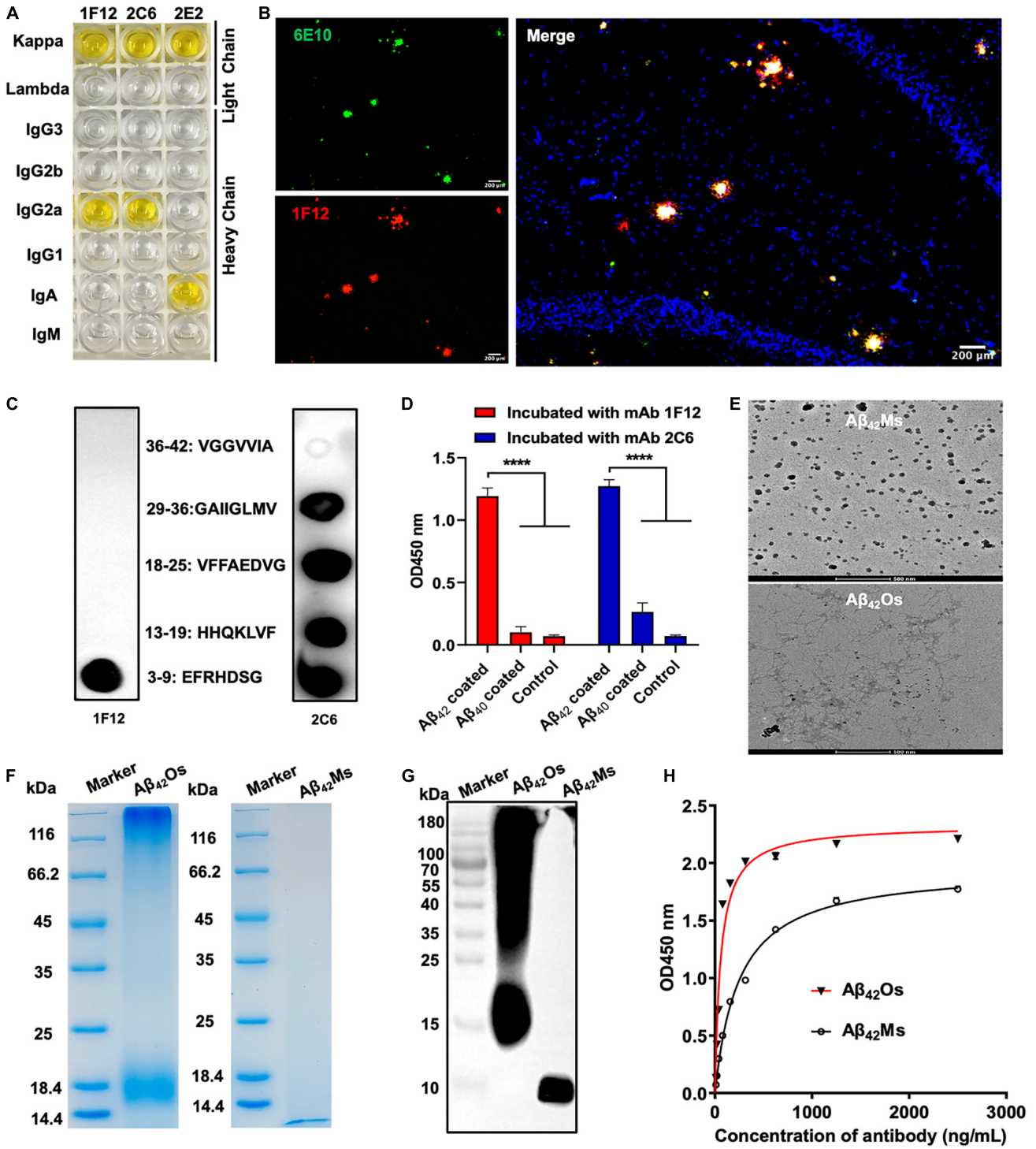

FIGURE 1 | Characterization of sequence and conformation-specific antibodies for $A\beta_{42}$Ms and $A\beta_{42}$Os. **(A)** The isotypes of the prepared monoclonal antibodies. **(B)** Confocal fluorescence images of murine APP/PS1 brain sections using Cy3-labeled anti-$A\beta_{42}$ monoclonal antibody 1F12 and commercially available anti-Aβ antibody 6E10. (Scale bar: 200 μm). **(C)** Linear epitopes of $A\beta_{42}$ recognized by 1F12 and 2C6. **(D)** The binding affinities of 1F12 and 2C6 to $A\beta_{42}$ and $A\beta_{40}$ were determined by indirect ELISA. **(E)** The morphologies of $A\beta_{42}$Ms and $A\beta_{42}$Os were analyzed by cryo-transmission electron microscopy in parallel. (Scale bar: 500 nm). The purity and molecular weight of freshly prepared $A\beta_{42}$Ms and $A\beta_{42}$Os were determined by 12% reduced SDS-PAGE using Coomassie blue staining **(F)** and Western blotting with 1F12 **(G)**. **(H)** The K_d value of 1F12-binding $A\beta_{42}$Ms and $A\beta_{42}$Os was detected with indirect ELISA. Data are presented as means ± SEM. One-way analysis of variance (ANOVA) was used for multigroup comparisons. Statistical significance is indicated in the figures by $^{****}p < 0.0001$.

The 1F12 and 2C6 detection signals of $A\beta_{42}$ were significantly higher than those of $A\beta_{40}$ (**Figure 1D**). Taken together, 1F12 and 2C6 were $A\beta_{42}$ sequence-specific antibodies, and both showed a preference for the conformational epitope presented by $A\beta_{42}$ rather than $A\beta_{40}$.

Binding Affinities and Selectivity of 1F12 and 2C6 for Different $A\beta_{42}$ Species

We further evaluated the binding affinity of 1F12 and 2C6 to $A\beta_{42}$Ms and $A\beta_{42}$Os with different conformations. Cyo-TEM confirmed the morphology of the prepared Aβ42Ms and Aβ42Os. The results showed that the morphology of $A\beta_{42}$Ms was α-helical and random coil structures (**Figure 1E**, up), while $A\beta_{42}$Os formed a β-sheet and typical fibril three-dimensional structures (**Figure 1E**, down). 12% reduced SDS-PAGE gel confirmed the purity and molecular weight of the prepared $A\beta_{42}$Ms and $A\beta_{42}$Os (**Figure 1F**), and their components were verified by Western blotting (**Figure 1G** and **Supplementary Figure 1F**). Indirect ELISA results showed that the K_d values of 1F12 bound to $A\beta_{42}$ species were 1.66 ± 0.09 nM for $A\beta_{42}$Ms and 0.38 ± 0.04 nM for $A\beta_{42}$Os (**Figure 1H**), while the K_d values of 2C6 were 3.59 ± 0.27 nM for $A\beta_{42}$Ms and 0.61 ± 0.03 nM for $A\beta_{42}$Os (**Supplementary Figure 1G**). Taken together, 1F12 and 2C6 were $A\beta_{42}$ sequence- and conformation-specific antibodies and could bind $A\beta_{42}$ species with different conformations.

Preferred Antibody Pairs for Specific Detection of Total $A\beta_{42}$ and $A\beta_{42}$Os

The screening of capture and detecting antibodies for sandwich ELISA is a prerequisite for developing techniques to detect and quantify $A\beta_{42}$Ms and $A\beta_{42}$Os. Both 1F12 and 2C6 were biotinylated, and indirect ELISA showed that their bioactivities and titers were high (**Supplementary Figures 1H,I**). To achieve the specific detection of total $A\beta_{42}$ and $A\beta_{42}$Os, a combination of different antibody pairs (1F12/2C6, 1F12/2E2, 2C6/1F12, 2C6/2E2, 2E2/1F12, 2E2/2C6) was screened for preferred antibody pairs by comparing their susceptibility to total $A\beta_{42}$ and $A\beta_{42}$Os in sandwich ELISA (**Figure 2A**). The capture/detection antibody pair 1F12/2C6 had the highest detection signal and specificity for total $A\beta_{42}$ among the six antibody pairs in ELISA (**Figures 2B,C**), while the 1F12/1F12 antibody pair was significantly more effective and specificity in detecting $A\beta_{42}$Os (**Figures 2D,E**).

Dynamic Monitoring of Changes in Total $A\beta_{42}$, $A\beta_{42}$Os, and $A\beta_{42}$Ms in Blood and Brain

To dynamically monitor the changes of total $A\beta_{42}$, $A\beta_{42}$Os, and $A\beta_{42}$Ms in the brain and periphery blood, 1F12/2C6 and 1F12/12 ELISAs were performed to quantify $A\beta_{42}$ in peripheral blood and brain extracts of 3 and 9-month-old APP/PS1 mice. The results showed that regardless of age (at 3- or 9-month-old), the total $A\beta_{42}$ in blood and brain extracts of APP/PS1 mice was significantly higher than that in the tissue extracts of C57BL/6J (**Figure 3A**). 1F12/2C6 ELISA showed that compared with the 3-month-old APP/PS1, the total $A\beta_{42}$ levels in the blood of the 9-month-old APP/PS1 did not change significantly ($p = 0.1787$), but the $A\beta_{42}$ content in the brain tissue was significantly increased ($p = 0.0062$, **Figure 3A**). In comparison, 1F12/1F12 ELISA showed that the $A\beta_{42}$Os level in the blood ($p = 0.005$) and brain ($p < 0.0001$) of APP/PS1 at 9 months old were significantly higher than that of APP/PS1 mice at 3 months old (**Figure 3B**). The amount of $A\beta_{42}$Ms was calculated by subtracting the total $A\beta_{42}$ from $A\beta_{42}$Os. The level of $A\beta_{42}$Ms in the blood of APP/PS1 mice at 9 months old was significantly lower than that of APP/PS1 mice at 3 months old ($p = 0.0004$, **Figure 3C**). The levels of total $A\beta_{42}$, $A\beta_{42}$Os, and $A\beta_{42}$Ms in C57BL/6J mice between 3 and 9 months old did not change significantly (**Figures 3A–C**). To further validate the 1F12/2C6 and 1F12/1F12 ELISA results, an immunoprecipitation (IP) assay was performed using blood and brain extracts of 3- and 9-month-old APP/PS1 mice. As shown in **Figure 3D**, a clear single band was observed in the blood and brain extracts of 3-month-old APP/PS1, and its molecular weight was similar to $A\beta_{42}$Ms. The results were consistent with the ELISA results as above-mentioned, confirming that the level of $A\beta_{42}$Ms at the early stage of AD (3-month-old APP/PS1) was high and the level of $A\beta_{42}$Os in the late stage of AD (9-month-old APP/PS1) were elevated. Western blotting analysis of immunoprecipitated proteins in blood and brain extracts of 9-month-old APP/PS1 mice revealed a prominent $A\beta_{42}$Os band with a molecular weight of more than 5 kDa and several clear bands of monomers to tetramers (**Figure 3E**). Taken together, $A\beta_{42}$ mainly existed as a monomer in the blood at the early stage of AD (e.g., 3-month-old APP/PS1 mice with less Aβ plaque load and Iba 1-positive cells staining, **Figures 3F–H**), whereas it appears as oligomers in blood and brain extracts at the late state (e.g., 9-month-old APP/PS1 mice with more Aβ plaque load and Iba 1-positive cells staining, **Figures 3F–H**).

Correlation of Total $A\beta_{42}$, $A\beta_{42}$Os, and $A\beta_{42}$Ms Level in the Gastrointestinal System With AD Progression

Apart from blood and brain, we also paid attention to the distribution of $A\beta_{42}$ in the intestinal system of APP/PS1 mice, such as duodenum, jejunum, ileum, colon, cecum, and their lysates. Several research groups have reported that AD may begin in the intestine and is closely related to the imbalance of intestinal flora (Hu et al., 2016; Harach et al., 2017; Jiang et al., 2017; Mancuso and Santangelo, 2018). To detect the distribution of total $A\beta_{42}$, $A\beta_{42}$Ms, and $A\beta_{42}$Os in the intestinal systems and explore its potential correlation with the pathogenesis of AD, organs extracted from different parts of intestines (duodenum, jejunum, ileum, colon, and cecum) and their lysates from 3- and 9-month-old APP/PS1 mice were collected for 1F12/2C6 and 1F12/1F12 ELISA. No $A\beta_{42}$ was detected in the different parts of intestines in 3-month-old APP/PS1 mice, but a certain amount of $A\beta_{42}$ was observed in jejunum lysate and colonic lysate (**Figure 4A**). Further analysis revealed $A\beta_{42}$ subtype in the jejunum and colon lysates. It was found that $A\beta_{42}$Os were observed in both jejunum and colonic lysate, with higher levels of $A\beta_{42}$Os in colon lysates (**Figure 4B**). But for $A\beta_{42}$Ms, a weak signal was only observed in the colonic lysate (**Figure 4C**). However, for 9-month-old

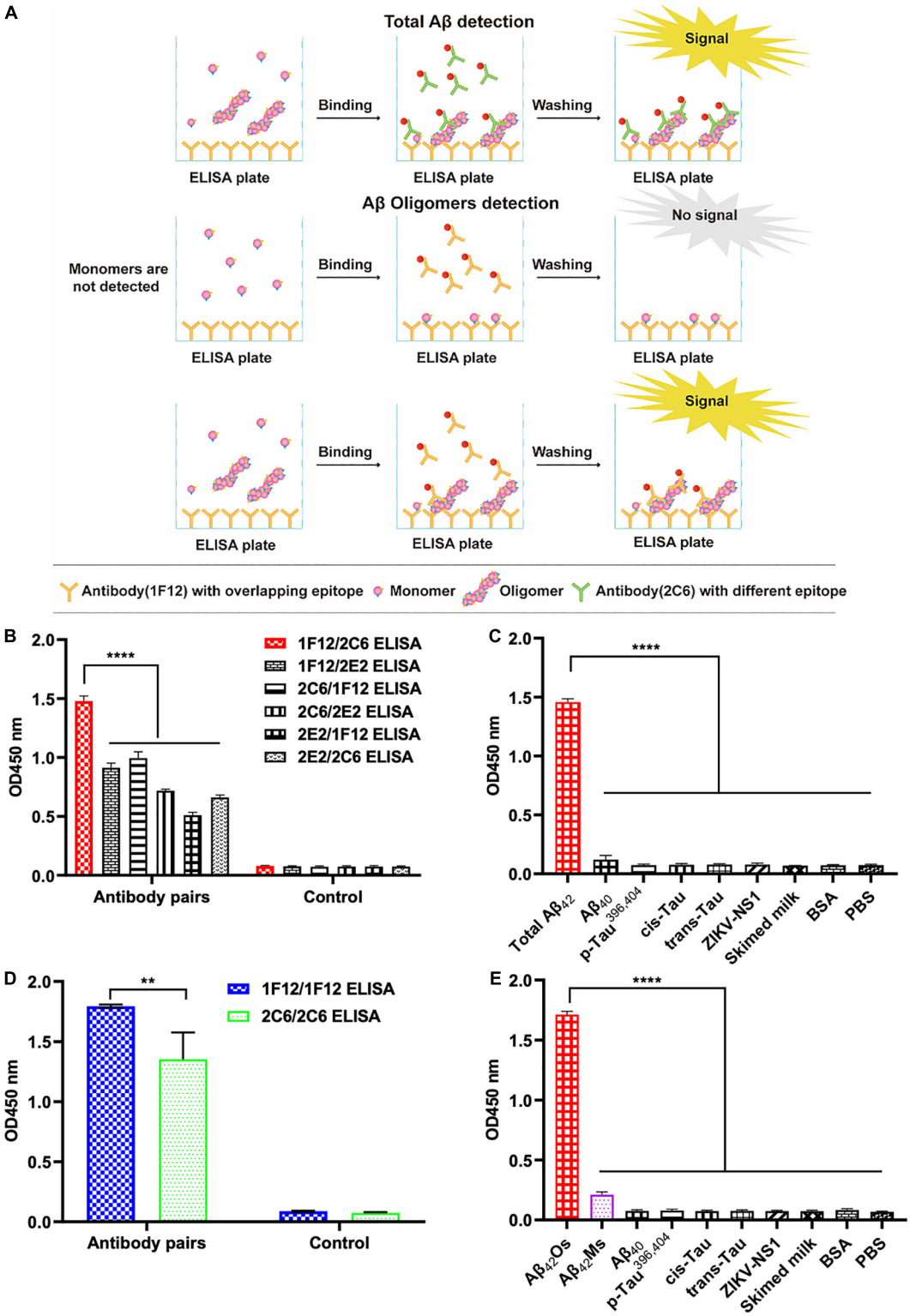

FIGURE 2 | Screening of preferred antibody pairs 1F12/2C6 and 1F12/1F12 against $A\beta_{42}$Ms and $A\beta_{42}$Os. **(A)** Schematic representation of 1F12/2C6, 1F12/1F12 ELISA to detect total $A\beta_{42}$, $A\beta_{42}$Os, respectively. **(B)** Preferred antibody pairs were screened for the detection of total $A\beta_{42}$. **(C)** The specificity assay of 1F12/2C6 ELISA for total $A\beta_{42}$ detection. **(D)** Preferred antibody pairs were screened for the detection of $A\beta_{42}$Os. **(E)** The specificity assay of 1F12/1F12 ELISA for $A\beta_{42}$Os detection. Data are presented as means ± SEM. Two-way analysis of variance (ANOVA) was used for **(B,D)** and One-way analysis of variance (ANOVA) was used for **(C,E)**. Statistical significance is indicated in the figures by $^{**}p < 0.01$ and $^{****}p < 0.0001$.

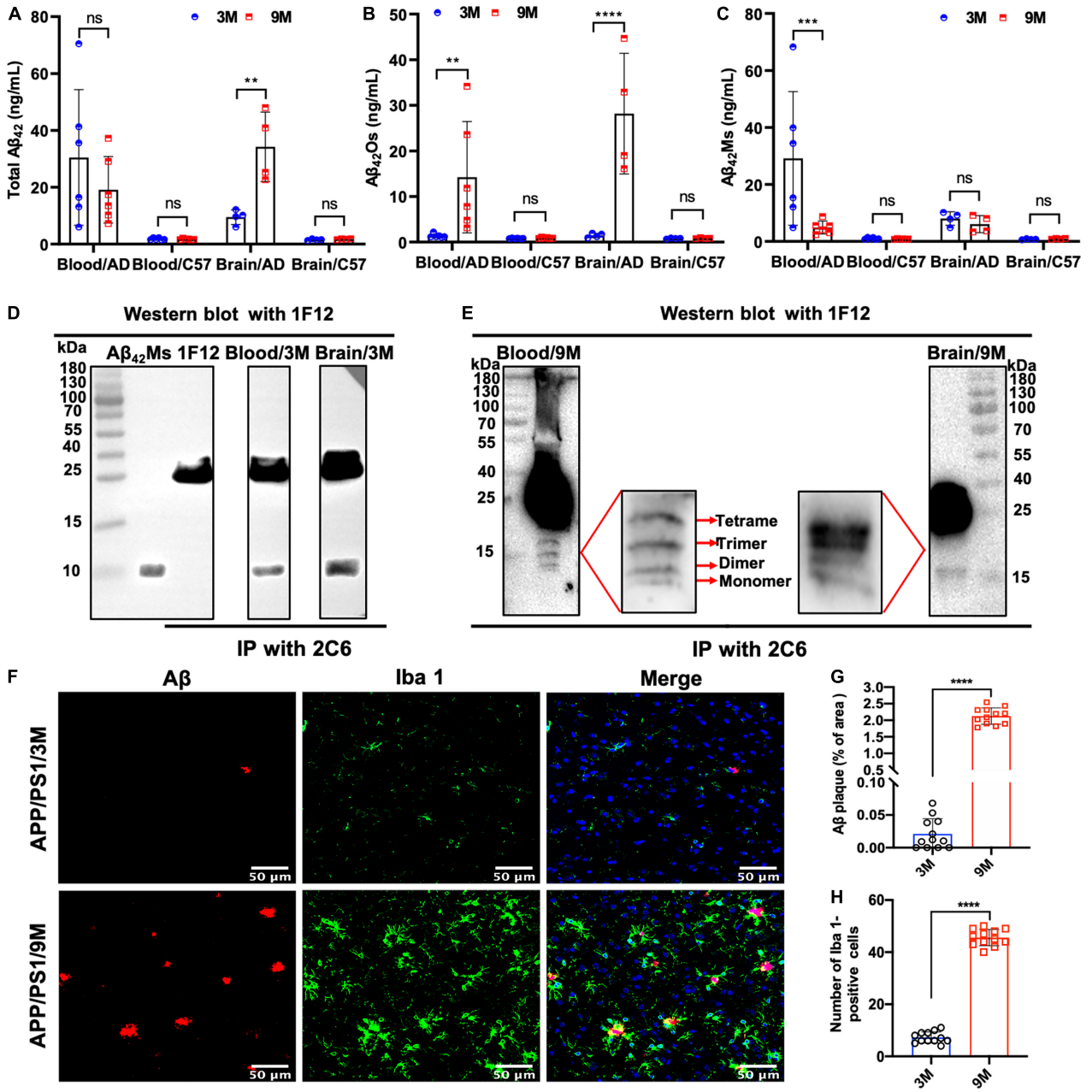

FIGURE 3 | Dynamic detection of the changes of $A\beta_{42}$Ms and $A\beta_{42}$Os in blood and brain of APP/PS1 mice by 1F12/2C6 and 1F12/1F12 ELISA. The level of total $A\beta_{42}$ **(A)**, $A\beta_{42}$Os **(B)**, and $A\beta_{42}$Ms **(C)** in the blood (n = 6) and brain (n = 4) of 3- and 9-month-old APP/PS1 and C57BL/6J mice. Total $A\beta_{42}$ in the blood and brain of 3 **(D)** or 9-month-old **(E)** APP/PS1 mice were enriched with immunoprecipitation (2C6) and visualized via Western blotting (1F12). **(F)** Confocal fluorescence images of Aβ plaque and Iba 1-positive cells staining in 3 or 9-month-old APP/PS1 mice. Aβ plaque **(G)** and Iba 1-positive **(H)** areas in the brains of 3- or 9-month-old APP/PS1 mice. Data are presented as means ± SEM. Two-way analysis of variance (ANOVA) was used in **(A–C)** for multigroup comparisons. Unpaired t-test was used in **(G,H)** for two-group comparisons. Statistical significance is indicated in the figures by $^{**}p < 0.01$, $^{***}p < 0.001$, $^{****}p < 0.0001$, and n.s. (indicating no significance).

APP/PS1 mice, total $A\beta_{42}$ signals were clearly observed in all gastrointestinal organs and their lysates, except for duodenum, duodenum lysates, and colonic lysates (**Figure 4A**). In a detailed analysis, we found that $A\beta_{42}$ mainly existed in the form of oligomers and was detected in all gastrointestinal organs except for the duodenum (**Figure 4B**). For the lysates, the result was opposite to the $A\beta_{42}$Ms level, and only two oligomers were detected with weak signals in the jejunum and ileum lysates (**Figure 4C**). For 3 or 9-month-old C57BL/6J mice, no significant differences were observed in the gastrointestinal organs and their lysates (**Supplementary Figures 3A,D**). Interestingly, the monomeric (**Supplementary Figures 3C,F**) or oligomeric

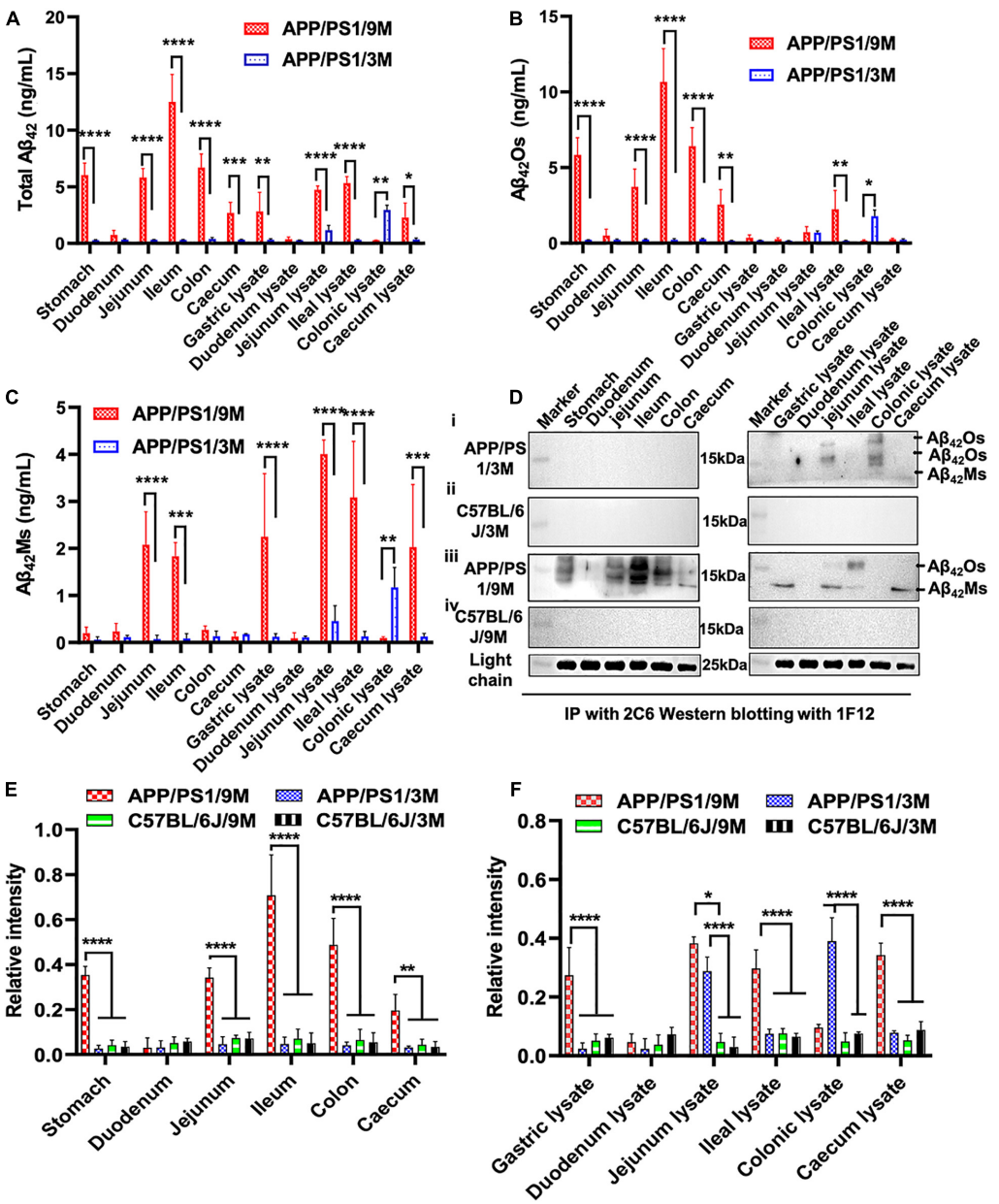

FIGURE 4 | Dynamic changes in the levels of $A\beta_{42}$Ms and $A\beta_{42}$Os in the intestines were detected and quantified via 1F12/2C6 and 1F12/1F12 ELISA. The level of total $A\beta_{42}$, $A\beta_{42}$Os, and $A\beta_{42}$Ms in the stomach, duodenum, jejunum, ileum, colon, and cecum and their lysates from 3-month-old APP/PS1 ($n = 4$; **A–C**), 9-month-old APP/PS1 ($n = 4$; **A–C**). **(D)** Representative IP-Western blotting data to analyze the distribution of $A\beta_{42}$ in the stomach, duodenum, jejunum, ileum, colon, and cecum and their lysates from 3-month-old APP/PS1 (i), 9-month-old APP/PS1 (iii), and C57BL/6J mice (ii,iv) at the same ages. **(E,F)** The Western blotting results for $A\beta_{42}$ in APP/PS1 or C57BL/6J mice were quantified. Data are presented as means ± SEM. Two-way analysis of variance (ANOVA) was used for multigroup comparisons. Statistical significance is indicated in the figures by $^{*}p < 0.05$, $^{**}p < 0.01$, $^{***}p < 0.001$, and $^{****}p < 0.0001$.

(**Supplementary Figures 3B,E**) forms of $A\beta_{42}$ levels in APP/PS1 mice were significantly higher than those in the C57BL/6J at 3 or 9 months old. Altogether, the ELISA results confirmed that both $A\beta_{42}$Ms and $A\beta_{42}$Os exist in the gastrointestinal system, and their distributions are different in APP/PS1 mice, but their levels increase with age.

Meanwhile, IP-Western blotting further confirmed the presence of $A\beta_{42}$ in the intestine through 1F12/2C6 and 1F12/1F12 ELISA. The $A\beta_{42}$Os signal was only observed in jejunal lysates and colon lysates of 3-month-old APP/PS1 mice (**Figure 4D, i**). In comparison, no $A\beta_{42}$ species were detected in 3-month-old C57BL/6J mice (**Figure 4D, ii**). Compared with 3-month-old APP/PS1 mice, the distribution of $A\beta_{42}$Os and $A\beta_{42}$Ms in 9-month-old APP/PS1 mice was quite different. In 9-month-old APP/PS1 mice, obvious $A\beta_{42}$Os bands were observed in the stomach, jejunum, ileum, colon, cecum, jejunum lysate,

and ileum lysate, while $A\beta_{42}$Ms levels were detected in low in the jejunum, ileum, and in high in the lysates of stomach, jejunum, and cecum (**Figure 4D, iii**). However, in age-matched C57BL/6J mice, no bands of $A\beta_{42}$Ms or/and $A\beta_{42}$Os were observed (**Figure 4D, iv**). The light chain of 1F12 was used as an internal reference to ensure that the same amount of immunomagnetic beads was added to each sample. The quantitative data of Western blotting (**Figures 4E,F**) were consistent with the 1F12/2C6 and 1F12/1F12 ELISA results (**Figures 4A–C** and **Supplementary Figures 3A–F**), indicating that both the levels of $A\beta_{42}$Ms and $A\beta_{42}$Os and their distributions in the gastrointestinal system are correlated with AD progression.

Based on the results of IP-Western blotting and sandwich ELISA, we further investigated the accumulation of insoluble Aβ plaques in the intestine because $A\beta_{42}$Ms and $A\beta_{42}$Os were the core components of amyloid plaques. The immunofluorescence assay (IFA) showed that the weak fluorescent signals of thioflavin S and Cy3-1F12 were colocalized in the duodenum of 3-month-old mice (**Figure 5**, left). However, in 9-month-old APP/PS1 mice, obvious fluorescent colocalization signals of thioflavin S and Cy3-1F12 were observed in the duodenum, ileum, and cecum, which of their fluorescence signals were significantly stronger than that of 3-month-old APP/PS1 mice (**Figure 5**, right). In comparison, in 3- or 9-month-old C57BL/6J mice, no fluorescent signals of thioflavin S and Cy3-1F12 were observed (**Supplementary Figure 3** and **Figure 4**). Overall, the results of sandwich ELISA (**Figures 4A–C**), IP-Western blotting (**Figure 4D**), and IFA (**Figure 5**) convincingly demonstrated that Aβ exists in the intestine of APP/PS1 mice, and their levels correlate to AD progression.

Dynamic Changes in Microbiome Composition of APP/PS1 Mice With Age

To investigate the changes in microbiome composition of APP/PS1 mice with age, we compared relative microbial abundance at genus levels among 3-month-old APP/PS1 mice, 9-month-old APP/PS1 mice, and age-matched C57BL/6J mice. Among all three groups, the abundance of Lachnospiraceae fluctuated with age (**Figure 6A**). To further characterize the microbiome composition, a beta diversity analysis was performed based on PCoA and weighted UniFrac distance in 3 and 9-month-old APP/PS1 mice (**Figure 6B**). The PERMANOVA results revealed that the microbiome structure was reshaped during the development of AD (**Figure 6C**). Then, representative bacterial taxa that differed significantly across two APP/PS1 groups were determined by 'DESeq2' R package based on the negative binomial distribution. Taxa were sorted by fold change between the two groups at the genus level (**Figure 6D**). In addition, the content of Turicibacter, Atopostipes, and

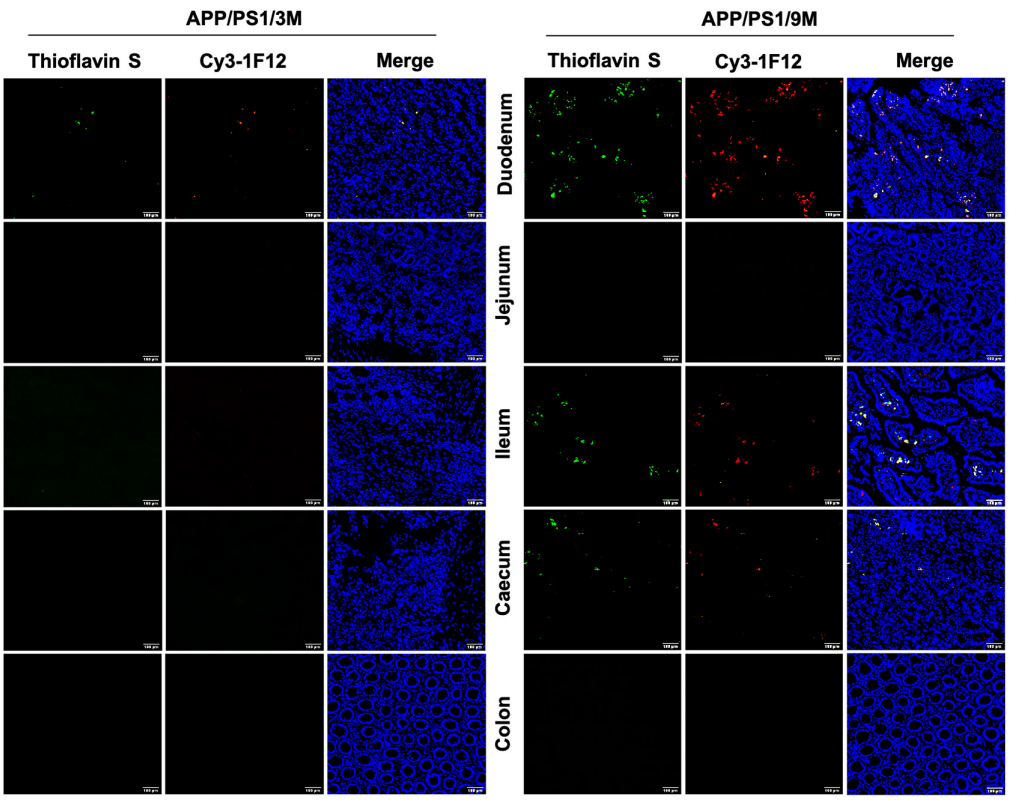

FIGURE 5 | Immunofluorescence assay for insoluble Aβ plaques in different parts of the intestines of APP/PS1 mice. The levels of insoluble Aβ plaques in the duodenum, jejunum, ileum, cecum, and colon of 3-month-old **(left)** and 9-month-old **(right)** APP/PS1 mice were evaluated by double-staining with thioflavin S and Cy3-IF12 (Scale bar: 100 μm).

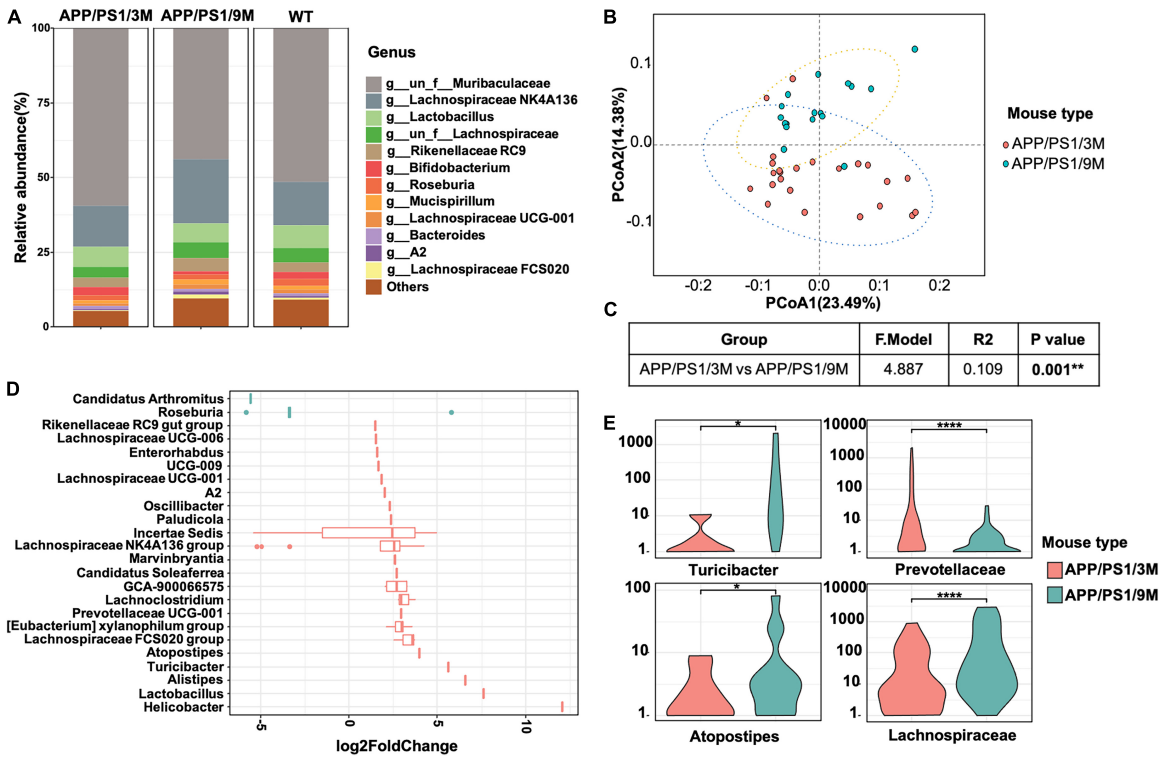

FIGURE 6 | Comparison of microbiome composition of APP/PS1 mice at 3 and 9 months old. **(A)** The relative abundance of top microorganisms in the feces of 3 and 9-month-old APP/PS1 mice and age-matched C57/BL/6 mice. **(B)** Principal coordinate analysis (PCoA) based on weighted UniFrac phylogenetic distance to compare 3 and 9-month-old APP/PS1 mice. **(C)** Comparison of beta diversity between 3 and 9-month-old APP/PS1 mice based on weighted UniFrac phylogenetic distance. The data was calculated using permutational multivariate analysis of variance (PERMANOVA) by R package 'vegan.' $^{**}p < 0.01$. **(D)** Significant difference in the bacterial genus with relative abundance ≥ 0.01% between 3 and 9-month-old APP/PS1 mice. **(E)** The main genus of APP/PS1 mice with significant differences at 3 and 9 months. Comparisons of the relative abundance of gut microbiota between groups at the genus level were performed using two-tailed Wilcoxon rank-sum tests. Statistical significance is indicated in the figures by $^{*}p < 0.05$, $^{**}p < 0.01$, and $^{****}p < 0.0001$.

Lachnospiraceae in 9-month-old APP/PS1 mice was significantly higher than that in 3-month-old mice (**Figure 6E**). Meanwhile, the Prevotellaceae was less abundant in aged APP/PS1 mice (**Figure 6E**). Collectively, these results illustrated that in the early stages of AD, the composition of the gut microbiota shows a significant difference.

DISCUSSION

In this study, we screened $A\beta_{42}$ sequence- and conformation-specific antibodies 1F12 and 2C6 and selected preferred antibody pairs 1F12/2C6 and 1F12/1F12 for sandwich ELISA to accurately detect $A\beta_{42}$Ms and $A\beta_{42}$Os in blood and organs. Of note, in the results of identifying the epitopes of 1F12 and 2C6, we find that the 2C6 exhibited discrete epitopes. Presently, there are about five epitopes on the surface of $A\beta_{42}$ peptides, mainly including $A\beta_{3-9}$, $A\beta_{13-19}$, $A\beta_{18-25}$, $A\beta_{29-36}$, and $A\beta_{36-42}$ and several antibodies have been designed for the corresponding epitopes (De et al., 2019). Interestingly, our prepared 2C6 can recognize the $A\beta_{3-9}$, $A\beta_{13-19}$, $A\beta_{18-25}$, $A\beta_{29-36}$, but not for $A\beta_{36-42}$. In the detailed analysis of the immune response of $A\beta_{36-42}$, we used the keyhole limpet hemocyanin-coupled $A\beta_{36-42}$ peptides to immunize BALB/c mice, but only one of three mice showed a weak immune response with a low titer. The inadequate immune response may be due to the $A\beta_{36-42}$ peptides (VGGVVIA) containing many hydrophobic amino acids, such as V, I, and A, making it difficult for animals to absorb and followed to produce antibodies. Therefore, the explanation of why 2C6 exhibits discrete epitopes is that there are more hydrophilic or neutral amino acids instead of hydrophobic amino acids in the region of $A\beta_{1-36}$, making it easier to be exposed and recognized by antibodies. Besides, the successful preparation of mAb A8978 (against the intermediate epitope $A\beta_{13-28}$) and mAb 78 (against $A\beta_{7-11}$, $A\beta_{18-24}$, and $A\beta_{26-32}$) indicate that it is possible to generate multiple epitope antibodies in the $A\beta_{1-36}$ region (Hatami et al., 2014; Nabers et al., 2018), and all these results also further confirm our explanation. Studies describing the different roles of $A\beta_{42}$ sequence region in the toxicity mechanisms have been reported by several groups. In general, the C-terminal area of $A\beta_{42}$ plays a significant role in inducing bilayer permeability (De et al., 2019), while the middle and N-terminal parts of $A\beta_{42}$ are effective in causing microglial inflammation and TLR signaling (Colvin et al., 2017; De et al., 2019). Therefore, antibodies targeting the C-terminal region of $A\beta_{42}$ are more effective in reducing membrane

permeability induced by Aβ_{42} aggregates, whereas antibodies targeting the middle and N-terminal areas of Aβ_{42} are more potent in reducing the inflammatory response induced by Aβ_{42} aggregates. These differences may be due to the accessibility of solvent-exposed N-terminal fragments in larger aggregates formed in the later stages of Aβ_{42} aggregation. Altogether, the functional effect of antibodies with more epitopes may be far greater than that of single-epitope antibodies, especially in terms of immunotherapy.

The 1F12/2C6 and 1F12/1F12 ELISAs provided sufficient sensitivity to detect the levels of Aβ_{42}Ms and Aβ_{42}Os in blood and tissue extracts of APP/PS1 mice, and the results were not affected by the peripheral expression of APP or Aβ_{40} because the prepared 1F12 and 2C6 showed more preference for Aβ_{42} species. The results of ELISA and immunoprecipitation (IP) performed in blood and brain extracts of 3- and 9-month-old APP/PS1 mice well confirmed that no APP protein brand was observed or detected, except for Aβ_{42}Ms and several small Aβ_{42}Os (**Figures 1D**, **2C,E**, **3D,E**). Longitudinal studies of blood Aβ_{42}Ms and Aβ_{42}Os levels showed extensive temporal variation within and among APP/PS1 mice that participated in our research. Based on the 1F12/2C6 and 1F12/1F12 ELISA tests, it was found that the decrease in the levels of total Aβ_{42} in blood was accompanied by its increase in the brain, but total Aβ_{42} levels in blood were not correlated with AD progression ($p = 0.2146$, **Figure 3A**). The results are unexpectedly consistent with the literature on Aβ_{42} detection because the Aβ_{42} level in previous reports did not show a significant change (Hoglund et al., 2005) using a pair of antibodies that recognize different Aβ_{42} epitopes, which is similar to 1F12/2C6 ELISA. In contrast, soluble Aβ_{42}Os, whose levels are elevated in AD patients, are easily mis-detected in the measurement of Aβ_{42}, resulting in underestimation of Aβ_{42}Ms level and poor performance in assessing the progression of AD (Yang et al., 2013; Liu et al., 2017). However, based on our method, we found obvious decrease in the level of Aβ_{42}Ms and significantly increased level of Aβ_{42}Os in blood, and prominently elevated level of Aβ_{42}Os in the brains of 3 and 9-month-old APP/PS1 mice (**Figures 3B,C**). Therefore, the levels of Aβ_{42}Ms and Aβ_{42}Os in blood and brain are closely associated with AD progression, which is helpful for us to further understanding of the pathogenesis of AD.

Increasing evidence indicates that the intestine or intestinal flora is associated with the progression of AD. However, to date, almost no literature directly reports the presence of Aβ_{42} in the intestinal tissues and further elaborates the relationship between Aβ_{42} in the intestine and AD progression. Our study showed that significantly increased levels of Aβ_{42} were observed in the gastrointestinal organs (including stomach, jejunum, ileum, colon, cecum, jejunum lysate, ileal lysate, and cecum lysate) of 9-month-old APP/PS1 mice but not in 3-month-old APP/PS1 mice or age-matched C57BL/6J mice (**Figures 4**, **5**). The level of Aβ_{42}Ms in the blood and brain of 3-month-old APP/PS1 mice was significantly higher than that in the intestine, indicating that the human Aβ produced by APP/PS1 mice is mainly distributed in the blood and brain. While the increasing Aβ_{42} levels in the gastrointestinal organs still needed more evidence to confirm whether it originates from the brain or/and blood. Presently, several potential mechanisms of how brain Aβ is released into peripheral tissues have been mentioned. Some convincing evidence suggests that brain-derived soluble Aβ_{42}Ms and Aβ_{42}Os can be absorbed by neurons and enter the intestine along the vagus nerve (Foley et al., 2020). In contrast, the administration of Aβ_{42} into the gastrointestinal tract may induce amyloidosis in the central nervous system (CNS) and AD-related pathologies, such as dementia (Sun et al., 2020). Besides, a study provided by Cintron et al. (2015) demonstrated the ability of peripheral monocytes to transport Aβ_{42} aggregates from the abdominal cavity to the brain, spleen, and liver. Several other groups claimed that Aβ seeds could be transported via axons (Clavaguera et al., 2014; Guo and Lee, 2014; Boluda et al., 2015; Ye et al., 2015). In addition, the levels of Aβ_{42} in the peripheral blood neuronal-derived exosomes in AD patients were higher than those in aMCI and healthy people, indicating that exosomes could also act as transport vehicles for Aβ_{42} (Jia et al., 2019; Lakshmi et al., 2020). Altogether, neurons, axons, neuronal-derived exosomes, and peripheral monocytes can be used as potential carriers of Aβ_{42} delivery, and there is currently evidence supporting axonal transport as a critical mode of disease propagation within the nervous system. In addition to the brain, other non-neural tissues, including the pancreas, kidney, spleen, heart, liver, testis, aorta, lung, skin, adrenal glands, and thyroid, also express amyloid-β protein precursor (APP). It is worth noting that the peripheral expression of APP will have the opportunity to be hydrolyzed to produce Aβ_{42} when APP is transferred to its resident site tans-Golgi network (TGN), where β- and γ-secretase are distributed (Roher et al., 2009; Querfurth and LaFerla, 2010; Sakono and Zako, 2010; Hodson, 2018). The produced Aβ_{42} is recycled to the cell membrane surface, which may increase the level of Aβ_{42} in peripheral tissues. However, to date, it is difficult to evaluate the impact of APP produced by peripheral tissues on Aβ levels in the brain and blood. The current evidence supports the brain as the primary source of Aβ pools because Aβ levels are the highest. Whether the source of APP or/and Aβ in peripheral tissues contributes to the Aβ pool of brain, blood or gastrointestinal organs and its influence on the detection of Aβ_{42} levels in the brain and blood need to be further confirmed to clarify.

In a detailed analysis of the intestinal origin of Aβ_{42}, we found that Aβ_{42}Ms and Aβ_{42}Os were first detected in colonic lysates of 3-month-old APP/PS1 (**Figures 4B–D, i**). Interestingly, this phenomenon is partly consistent with the study reported by Hui et al. (2012) that the colon is considered the first segment of the gastrointestinal tract where Aβ deposits occur. This phenomenon may be explained that in the early stage of AD, the Aβ_{42}, especially Aβ_{42} monomers or small oligomers from the brain and blood pools, can be easily transmitted through the enteric nervous system (ENS) to the digestive tract of the stomach and intestines. According to reports, the colon contains the most neurons (Gershon, 1998; Rao and Gershon, 2016; Brierley et al., 2018; Borgmann et al., 2021), and the monomers that gradually accumulate in the colon can be aggregated into small molecular weight oligomers. It is worth noting that the colon undergoes vital processes to ensure our health. These processes are coordinated by transmitting sensory signals from the periphery to the central

nervous system, allowing communication from the intestine to the brain via the "gut-brain axis" (Brierley et al., 2018). Foley et al. (2020) have confirmed that soluble $A\beta_{42}$Ms and $A\beta_{42}$Os could be absorbed by neurons and enter the intestine along the vagus nerve. Therefore, there is a strong correlation between the colon and degenerative neurological disease. In general, our results and previous evidence may well explain the observation of $A\beta_{42}$ in colon lysates, but the precise correlation of $A\beta_{42}$ and the intestine still needs to be studied. Besides, the intestine and enteric nervous systems play an important role in neurological disorders and deserve our attention.

Compared to 3-month-old APP/PS1, we did not observe an increase in $A\beta_{42}$ peptides in colonic lysates, although the levels of $A\beta_{42}$Ms and $A\beta_{42}$Os increased sharply in 9-month-old APP/PS1 (**Figures 4B–D, iii**). The significant difference in $A\beta_{42}$ levels in colonic lysates of 3- and 9-month-old APP/PS1 mice may be due to the migration of $A\beta_{42}$ in the colon from the colon to other gastrointestinal organs. This migration process has been confirmed by multiple groups (Cintron et al., 2015; Sun et al., 2020). In addition, high $A\beta_{42}$ levels were detected in the cecum, ileum, jejunum, and even stomach of 9-month-old APP/PS1 mice. Among them, the $A\beta_{42}$ level in the ileum was more significant and higher than that in the colon or colon lysate. These results further confirmed the ability of $A\beta_{42}$ peptides to spread in the colon as seeds. Thus, the disappeared $A\beta_{42}$ peptide in the colonic lysate of 9-month-old APP/PS1 may have migrated to other gastrointestinal organs such as the cecum, ileum, jejunum, and stomach because their $A\beta_{42}$ levels were significantly higher than colon lysates. In summary, our study, together with previous studies, confirms the ability of $A\beta_{42}$ peptides to spread as seeds, which leads to extensive changes in $A\beta_{42}$ levels within and between different APP/PS1 mice.

In this study, we monitored the dynamic changes of $A\beta_{42}$Ms and $A\beta_{42}$Os levels in the intestines and studied their significance for AD. Indeed, our results convincingly demonstrated that Aβ exists in the intestines of APP/PS1 mice, and their levels are correlated with AD progression. However, a current controversy is whether the gastrointestinal organs can directly produce $A\beta_{42}$. Several studies have reported that microorganisms including *Bacillus subtilis*, *Shigella*, *Escherichia coli*, *Salmonella enterica*, *Staphylococcus aureus*, and *Mycobacterium tuberculosis* can produce functional extracellular amyloid proteins but not for $A\beta_{42}$ peptides (Hufnagel et al., 2013; Schwartz and Boles, 2013; Friedland, 2015; Pistollato et al., 2016). In fact, it seems that there is insufficient evidence to show that $A\beta_{42}$ peptides could be directly produced in the organs of the gastrointestinal tract. In addition, the practical and accurate distinction between locally produced and transported $A\beta_{42}$ peptides is crucial for helping to understand the pathology of AD. Distinguishing the local production and transportation of $A\beta_{42}$ peptides is our next research plan.

In addition to finding elevated levels of soluble $A\beta_{42}$, several insoluble $A\beta_{42}$ plaques were observed in the intestines of 3-month-old APP/PS1 mice. However, it is in the early stages of AD, and there were only a few plaques in the brain (**Figure 5**, left). With the progression of AD, more plaques were observed in the intestines of 9-month-old APP/PS1 mice (**Figure 5**, right). Interestingly, changes in microbiome composition were observed in 9-month-old APP/PS1 mice. The effect of increased levels of $A\beta_{42}$ in the intestine on the changes in its microbial composition remains obscure. There is no doubt that the observed toxicity of $A\beta_{42}$, especially small oligomers, is the most effective in inducing inflammation of microglia or macrophages, and it causes more damage in inducing bilayer permeability (Flagmeier et al., 2017; Fusco et al., 2017; De et al., 2019). It is certain that in the current investigation, the abundance of Lachnospiraceae fluctuated with age (**Figures 6C,D**). The content of Turicibacter, Atopostipes, and Lachnospiraceae in aged APP/PS1 mice was significantly higher than in young APP/PS1 mice, but the abundance of Prevotellaceae in old APP/PS1 mice was lower (**Figure 6**). Overall, these results indicated that the significant difference in gut microbiota composition is accompanied by the sharply increased soluble $A\beta_{42}$ and insoluble Aβ plaques during AD progression, but whether this change affects or is affected by the change in gut-derived $A\beta_{42}$ needs to be further explored.

In summary, based on our screened antibody pairs 1F12/2C6 and 1F12/1F12 in sandwich ELISA for specific detection of $A\beta_{42}$Ms and $A\beta_{42}$Os, we observed apparent fluctuation in the levels of $A\beta_{42}$Ms and $A\beta_{42}$Os in blood and intestines of APP/PS1 mice during the progression of AD. The identification of $A\beta_{42}$ abnormalities in the gastrointestinal tract could provide new ideas for AD therapeutic interventions that are only used to evaluate $A\beta_{42}$ levels in peripheral blood and the brain. Furthermore, studying the relationship between the levels of $A\beta_{42}$Ms and $A\beta_{42}$Os in peripheral tissues and the progression of AD may help to understand the causes of AD, and may provide new treatment strategies for improving AD or other Aβ-related dementias.

DATA AVAILABILITY STATEMENT

The datasets presented in this study can be found in online repositories. The names of the repository/repositories and accession number(s) can be found in the article.

ETHICS STATEMENT

The animal study was reviewed and approved by the Institutional Animal Care and Use Committee of Huazhong University of Science and Technology.

AUTHOR CONTRIBUTIONS

HL, QL, and ZZ coordinated the writing of the manuscript and provided writing guidance and manuscript revision. LZ completed all experiments and contributed to writing the first draft. YL and SN participated in most experiments. XL was involved in APP/PS1 mice breeding and schematic figure preparations. CY performed the bioinformatics data analysis. All authors reviewed and approved the final manuscript.

FUNDING

This study was financially supported by grants from the Major Research Plan of the National Natural Science Foundation of China (Grant No. 91749209), the National Natural Science Foundation of China (Grant No. 81971025), and the Startup Fund of Huazhong University of Science and Technology.

ACKNOWLEDGMENTS

We thank the Optical Bioimaging Core Facility and the Center for Nanoscale Characterization & Devices (CNCD) of WNLO-HUST for support with data acquisition, the Analytical and Testing Center of HUST for performing spectral measurements, and the Research Core Facilities for Life Science (HUST) for using cryo-transmission electron microscopy.

SUPPLEMENTARY MATERIAL

The Supplementary Material for this article can be found online at: https://www.frontiersin.org/articles/10.3389/fnmol.2021.723317/full#supplementary-material

Supplementary Figure 1 | Characterization of sequence- and conformation-specific antibodies 1F12 and 2C6 against $A\beta_{42}$Ms and $A\beta_{42}$Os. **(A)** The preferred hybridoma colonies were screened via indirect ELISA. **(B)** The purity and molecular weight of purified 1F12, 2C6, and 2E2 were confirmed via 12% reduced SDS-PAGE with Coomassie blue staining. **(C)** The bioactivities of 1F12, 2C6, and commercial antibody 6E10 toward natural $A\beta_{42}$ peptides extracted from murine APP/PS1 brain were evaluated via Western blotting. **(D)** Confocal fluorescence images of murine APP/PS1 brain sections using Cy3-labeled anti-$A\beta_{42}$ monoclonal antibody 2C6 and commercially available anti-Aβ antibody 6E10 **(E)**. (Scale bar: 200 μm). **(E)** Titers of 1F12, 2C6, and 2E2. **(F)** The purity and molecular weight of freshly prepared $A\beta_{42}$Ms and $A\beta_{42}$Os were determined by Western blotting with 2C6. **(G)** Binding affinities of 2C6 toward $A\beta_{42}$Ms and $A\beta_{42}$Os were evaluated via indirect ELISA. The activities **(H)** and titers **(I)** of the biotinylated 1F12 or 2C6 antibody.

Supplementary Figure 2 | Confocal fluorescence images of whole murine APP/PS1 brain sections using Cy3-labeled anti-$A\beta_{42}$ monoclonal antibody 1F12 **(A)** or 2C6 **(B)** and thioflavin S.

Supplementary Figure 3 | Comparison of the dynamic distribution of $A\beta_{42}$ in APP/PS1 and C57BL/6J. The levels of total $A\beta_{42}$ **(A,D)**, $A\beta_{42}$Os **(B,E)**, and $A\beta_{42}$Ms **(C,F)** in the stomach, duodenum, jejunum, ileum, colon, and cecum and their lysates from APP/PS1 and C57BL/6J at 3-month-old (n = 4) or 9-month-old APP/PS1 (n = 4). Data are presented as means ± SEM. Two-way analysis of variance (ANOVA) was used for multigroup comparisons. Statistical significance is indicated in the figures by $^{**}p < 0.01$, $^{***}p < 0.001$ and $^{****}p < 0.0001$.

Supplementary Figure 4 | Representative confocal fluorescence images of the duodenum, jejunum, ileum, cecum, and colon of 3-month-old C57BL/6J mice double-stained with thioflavin S and Cy3-1F12 (Scale bar: 100 μm).

Supplementary Figure 5 | Representative confocal fluorescence images of the duodenum, jejunum, ileum, cecum, and colon of 9-month-old C57BL/6J mice double-stained with thioflavin S and Cy3-1F12 (Scale bar: 100 μm).

REFERENCES

Benilova, I., Karran, E., and De Strooper, B. (2012). The toxic Aβ oligomer and Alzheimer's disease: an emperor in need of clothes. *Nat. Neurosci.* 15, 349–357. doi: 10.1038/nn.3028

Bernstein, S. L., Dupuis, N. F., Lazo, N. D., Wyttenbach, T., Condron, M. M., Bitan, G., et al. (2009). Amyloid-beta protein oligomerization and the importance of tetramers and dodecamers in the aetiology of Alzheimer's disease. *Nat. Chem.* 1, 326–331. doi: 10.1038/nchem.247

Boluda, S., Iba, M., Zhang, B., Raible, K. M., Lee, V. M., and Trojanowski, J. Q. (2015). Differential induction and spread of tau pathology in young PS19 tau transgenic mice following intracerebral injections of pathological tau from Alzheimer's disease or corticobasal degeneration brains. *Acta Neuropathol.* 129, 221–237. doi: 10.1007/s00401-014-1373-0

Borgmann, D., Ciglieri, E., Biglari, N., Brandt, C., Cremer, A. L., Backes, H., et al. (2021). Gut-brain communication by distinct sensory neurons differently controls feeding and glucose metabolism. *Cell Metab.* 33, 1466–1482.e1467. doi: 10.1016/j.cmet.2021.05.002

Brierley, S. M., Hibberd, T. J., and Spencer, N. J. (2018). Spinal afferent innervation of the colon and rectum. *Front. Cell. Neurosci.* 12:467. doi: 10.3389/fncel.2018.00467

Cintron, A. F., Dalal, N. V., Dooyema, J., Betarbet, R., and Walker, L. C. (2015). Transport of cargo from periphery to brain by circulating monocytes. *Brain Res.* 1622, 328–338. doi: 10.1016/j.brainres.2015.06.047

Clavaguera, F., Grueninger, F., and Tolnay, M. (2014). Intercellular transfer of tau aggregates and spreading of tau pathology: implications for therapeutic strategies. *Neuropharmacology* 76 (Pt A), 9–15. doi: 10.1016/j.neuropharm.2013.08.037

Collaborators, G. B. D. D. (2019). Global, regional, and national burden of Alzheimer's disease and other dementias, 1990-2016: a systematic analysis for the Global Burden of Disease Study 2016. *Lancet Neurol.* 18, 88–106. doi: 10.1016/S1474-4422(18)30403-4

Colvin, B. A., Rogers, V. A., Kulas, J. A., Ridgway, E. A., Amtashar, F. S., Combs, C. K., et al. (2017). The conformational epitope for a new Aβ42 protofibril-selective antibody partially overlaps with the peptide N-terminal region. *J. Neurochem.* 143, 736–749. doi: 10.1111/jnc.14211

De, S., Wirthensohn, D. C., Flagmeier, P., Hughes, C., Aprile, F. A., Ruggeri, F. S., et al. (2019). Different soluble aggregates of Aβ42 can give rise to cellular toxicity through different mechanisms. *Nat. Commun.* 10:1541. doi: 10.1038/s41467-019-09477-3

Driscoll, I., Resnick, S. M., Troncoso, J. C., An, Y., O'brien, R., and Zonderman, A. B. (2006). Impact of Alzheimer's pathology on cognitive trajectories in nondemented elderly. *Ann. Neurol.* 60, 688–695. doi: 10.1002/ana.21031

Flagmeier, P., De, S., Wirthensohn, D. C., Lee, S. F., Vincke, C., Muyldermans, S., et al. (2017). Ultrasensitive measurement of Ca(2+) influx into lipid vesicles induced by protein aggregates. *Angew. Chem. Int. Ed Engl.* 56, 7750–7754. doi: 10.1002/anie.201700966

Foley, A. R., Roseman, G. P., Chan, K., Smart, A., Finn, T. S., Yang, K., et al. (2020). Evidence for aggregation-independent, PrP(C)-mediated Aβ cellular internalization. *Proc. Natl. Acad. Sci. U.S.A.* 117, 28625–28631. doi: 10.1073/pnas.2009238117

Friedland, R. P. (2015). Mechanisms of molecular mimicry involving the microbiota in neurodegeneration. *J. Alzheimers Dis.* 45, 349–362. doi: 10.3233/jad-142841

Fusco, G., Chen, S. W., Williamson, P. T. F., Cascella, R., Perni, M., Jarvis, J. A., et al. (2017). Structural basis of membrane disruption and cellular toxicity by α-synuclein oligomers. *Science* 358, 1440–1443. doi: 10.1126/science.aan6160

Gershon, M. D. (1998). *The Second Brain: The Scientific Basis of Gut Instinct*. New York, NY: Harper Collins.

Gu, L., and Guo, Z. (2013). Alzheimer's Abeta42 and Abeta40 peptides form interlaced amyloid fibrils. *J. Neurochem.* 126, 305–311. doi: 10.1111/jnc.12202

Guo, J. L., and Lee, V. M. (2014). Cell-to-cell transmission of pathogenic proteins in neurodegenerative diseases. *Nat. Med.* 20, 130–138. doi: 10.1038/nm.3457

Harach, T., Marungruang, N., Duthilleul, N., Cheatham, V., Mc Coy, K. D., Frisoni, G., et al. (2017). Reduction of Abeta amyloid pathology in APPPS1 transgenic mice in the absence of gut microbiota. *Sci. Rep.* 7:41802. doi: 10.1038/srep41802

Hatami, A., Albay, R. III, Monjazeb, S., Milton, S., and Glabe, C. (2014). Monoclonal antibodies against Aβ42 fibrils distinguish multiple aggregation

state polymorphisms in vitro and in Alzheimer disease brain. *J. Biol. Chem.* 289, 32131–32143. doi: 10.1074/jbc.M114.594846

Hodson, R. (2018). Alzheimer's disease. *Nature* 559:S1. doi: 10.1038/d41586-018-05717-6

Hoglund, K., Thelen, K. M., Syversen, S., Sjogren, M., Von Bergmann, K., Wallin, A., et al. (2005). The effect of simvastatin treatment on the amyloid precursor protein and brain cholesterol metabolism in patients with Alzheimer's disease. *Dement. Geriatr. Cogn. Disord.* 19, 256–265. doi: 10.1159/000084550

Hong, K. S., and Yaqub, M. A. (2019). Application of functional near-infrared spectroscopy in the healthcare industry. *J. Inn. Opt. Health Sci.* 12. doi: 10.1142/S179354581930012X

Hu, X., Wang, T., and Jin, F. (2016). Alzheimer's disease and gut microbiota. *Sci. China Life Sci.* 59, 1006–1023. doi: 10.1007/s11427-016-5083-9

Hufnagel, D. A., Tükel, C., and Chapman, M. R. (2013). Disease to dirt: the biology of microbial amyloids. *PLoS Pathog* 9:e1003740. doi: 10.1371/journal.ppat.1003740

Hui, L., Chen, X., and Geiger, J. D. (2012). Endolysosome involvement in LDL cholesterol-induced Alzheimer's disease-like pathology in primary cultured neurons. *Life Sci.* 91, 1159–1168. doi: 10.1016/j.lfs.2012.04.039

Jia, L., Qiu, Q., Zhang, H., Chu, L., Du, Y., Zhang, J., et al. (2019). Concordance between the assessment of Aβ42, T-tau, and P-T181-tau in peripheral blood neuronal-derived exosomes and cerebrospinal fluid. *Alzheimers Dement.* 15, 1071–1080. doi: 10.1016/j.jalz.2019.05.002

Jiang, C., Li, G., Huang, P., Liu, Z., and Zhao, B. (2017). The gut microbiota and Alzheimer's disease. *J. Alzheimers Dis.* 58, 1–15. doi: 10.3233/jad-161141

Kim, K. M., Jang, H. C., and Lim, S. (2016). Differences among skeletal muscle mass indices derived from height-, weight-, and body mass index-adjusted models in assessing sarcopenia. *Korean J. Intern. Med.* 31, 643–650. doi: 10.3904/kjim.2016.015

Kohler, G., and Milstein, C. (1975). Continuous cultures of fused cells secreting antibody of predefined specificity. *Nature* 256, 495–497. doi: 10.1038/256495a0

Lakshmi, S., Essa, M. M., Hartman, R. E., Guillemin, G. J., Sivan, S., and Elumalai, P. (2020). Exosomes in Alzheimer's disease: potential role as pathological mediators, biomarkers and therapeutic targets. *Neurochem. Res.* 45, 2553–2559. doi: 10.1007/s11064-020-03111-1

Liu, L., Chang, Y., Yu, J., Jiang, M., and Xia, N. (2017). Two-in-one polydopamine nanospheres for fluorescent determination of beta-amyloid oligomers and inhibition of beta-amyloid aggregation. *Sens. Actuators B Chem.* 251, 359–365.

Mancuso, C., and Santangelo, R. (2018). Alzheimer's disease and gut microbiota modifications: the long way between preclinical studies and clinical evidence. *Pharmacol. Res.* 129, 329–336. doi: 10.1016/j.phrs.2017.12.009

Mucke, L., and Selkoe, D. J. (2012). Neurotoxicity of amyloid beta-protein: synaptic and network dysfunction. *Cold Spring Harb. Perspect. Med.* 2:a006338. doi: 10.1101/cshperspect.a006338

Murphy, M. P., and LeVine, H. III (2010). Alzheimer's disease and the amyloid-beta peptide. *J. Alzheimers Dis.* 19, 311–323. doi: 10.3233/JAD-2010-1221

Nabers, A., Perna, L., Lange, J., Mons, U., Schartner, J., Güldenhaupt, J., et al. (2018). Amyloid blood biomarker detects Alzheimer's disease. *EMBO Mol. Med.* 10:e8763. doi: 10.15252/emmm.201708763

Nag, S., Sarkar, B., Bandyopadhyay, A., Sahoo, B., Sreenivasan, V. K., Kombrabail, M., et al. (2011). Nature of the amyloid-beta monomer and the monomer-oligomer equilibrium. *J. Biol. Chem.* 286, 13827–13833. doi: 10.1074/jbc.M110.199885

Naslund, J., Haroutunian, V., Mohs, R., Davis, K. L., Davies, P., Greengard, P., et al. (2000). Correlation between elevated levels of amyloid beta-peptide in the brain and cognitive decline. *JAMA* 283, 1571–1577. doi: 10.1001/jama.283.12.1571

Oxtoby, N. P., Young, A. L., Cash, D. M., Benzinger, T. L. S., Fagan, A. M., Morris, J. C., et al. (2018). Data-driven models of dominantly-inherited Alzheimer's disease progression. *Brain* 141, 1529–1544. doi: 10.1093/brain/awy050

Pistollato, F., Sumalla Cano, S., Elio, I., Masias Vergara, M., Giampieri, F., and Battino, M. (2016). Role of gut microbiota and nutrients in amyloid formation and pathogenesis of Alzheimer disease. *Nutr. Rev.* 74, 624–634. doi: 10.1093/nutrit/nuw023

Querfurth, H. W., and LaFerla, F. M. (2010). Alzheimer's disease. *N. Engl. J. Med.* 362, 329–344. doi: 10.1056/NEJMra0909142

Rao, M., and Gershon, M. D. (2016). The bowel and beyond: the enteric nervous system in neurological disorders. *Nat. Rev. Gastroenterol. Hepatol.* 13, 517–528. doi: 10.1038/nrgastro.2016.107

Roberts, K. F., Elbert, D. L., Kasten, T. P., Patterson, B. W., Sigurdson, W. C., Connors, R. E., et al. (2014). Amyloid-beta efflux from the central nervous system into the plasma. *Ann. Neurol.* 76, 837–844. doi: 10.1002/ana.24270

Roher, A. E., Esh, C. L., Kokjohn, T. A., Castano, E. M., Van Vickle, G. D., Kalback, W. M., et al. (2009). Amyloid beta peptides in human plasma and tissues and their significance for Alzheimer's disease. *Alzheimers Dement.* 5, 18–29. doi: 10.1016/j.jalz.2008.10.004

Sakono, M., and Zako, T. (2010). Amyloid oligomers: formation and toxicity of Abeta oligomers. *FEBS J.* 277, 1348–1358. doi: 10.1111/j.1742-4658.2010.07568.x

Salminen, A., Ojala, J., Suuronen, T., Kaarniranta, K., and Kauppinen, A. (2008). Amyloid-beta oligomers set fire to inflammasomes and induce Alzheimer's pathology. *J. Cell. Mol. Med.* 12, 2255–2262. doi: 10.1111/j.1582-4934.2008.00496.x

Schwartz, K., and Boles, B. R. (2013). Microbial amyloids–functions and interactions within the host. *Curr. Opin. Microbiol.* 16, 93–99. doi: 10.1016/j.mib.2012.12.001

Sperling, R. A., Aisen, P. S., Beckett, L. A., Bennett, D. A., Craft, S., Fagan, A. M., et al. (2011). Toward defining the preclinical stages of Alzheimer's disease: recommendations from the National Institute on Aging-Alzheimer's Association workgroups on diagnostic guidelines for Alzheimer's disease. *Alzheimers Dement.* 7, 280–292. doi: 10.1016/j.jalz.2011.03.003

Sun, Y., Sommerville, N. R., Liu, J. Y. H., Ngan, M. P., Poon, D., Ponomarev, E. D., et al. (2020). Intra-gastrointestinal amyloid-β1-42 oligomers perturb enteric function and induce Alzheimer's disease pathology. *J. Physiol.* 598, 4209–4223. doi: 10.1113/jp279919

Wang, W., Hou, T. T., Jia, L. F., Wu, Q. Q., Quan, M. N., and Jia, J. P. (2019). Toxic amyloid-beta oligomers induced self-replication in astrocytes triggering neuronal injury. *EBioMedicine* 42, 174–187. doi: 10.1016/j.ebiom.2019.03.049

Wang, X., Sun, G., Feng, T., Zhang, J., Huang, X., Wang, T., et al. (2019). Sodium oligomannate therapeutically remodels gut microbiota and suppresses gut bacterial amino acids-shaped neuroinflammation to inhibit Alzheimer's disease progression. *Cell Res.* 29, 787–803. doi: 10.1038/s41422-019-0216-x

Wang, Y. J., Zhou, H. D., and Zhou, X. F. (2006). Clearance of amyloid-beta in Alzheimer's disease: progress, problems and perspectives. *Drug Discov. Today* 11, 931–938. doi: 10.1016/j.drudis.2006.08.004

Xiang, Y., Bu, X. L., Liu, Y. H., Zhu, C., Shen, L. L., Jiao, S. S., et al. (2015). Physiological amyloid-beta clearance in the periphery and its therapeutic potential for Alzheimer's disease. *Acta Neuropathol.* 130, 487–499. doi: 10.1007/s00401-015-1477-1

Yang, T., Hong, S., O'malley, T., Sperling, R. A., Walsh, D. M., and Selkoe, D. J. (2013). New ELISAs with high specificity for soluble oligomers of amyloid β-protein detect natural Aβ oligomers in human brain but not CSF. *Alzheimers Dement.* 9, 99–112.

Ye, L., Hamaguchi, T., Fritschi, S. K., Eisele, Y. S., Obermüller, U., Jucker, M., et al. (2015). Progression of seed-induced Aβ deposition within the limbic connectome. *Brain Pathol.* 25, 743–752. doi: 10.1111/bpa.12252

Zhang, L., Wei, Q., Han, Q., Chen, Q., Tai, W., Zhang, J., et al. (2018). Detection of *Shigella* in milk and clinical samples by magnetic immunocaptured-loop-mediated isothermal amplification assay. *Front. Microbiol.* 9:94. doi: 10.3389/fmicb.2018.00094

Conflict of Interest: The authors declare that the research was conducted in the absence of any commercial or financial relationships that could be construed as a potential conflict of interest.

Publisher's Note: All claims expressed in this article are solely those of the authors and do not necessarily represent those of their affiliated organizations, or those of the publisher, the editors and the reviewers. Any product that may be evaluated in this article, or claim that may be made by its manufacturer, is not guaranteed or endorsed by the publisher.

frontiers in Aging Neuroscience

ORIGINAL RESEARCH
published: 31 August 2021
doi: 10.3389/fnagi.2021.698571

The Role of Age on Beta-Amyloid$_{1–42}$ Plasma Levels in Healthy Subjects

Chiara Zecca[1], Giuseppe Pasculli[2], Rosanna Tortelli[1], Maria Teresa Dell'Abate[1], Rosa Capozzo[1], Maria Rosaria Barulli[1], Roberta Barone[1], Miriam Accogli[1], Serena Arima[3], Alessio Pollice[4], Vincenzo Brescia[5] and Giancarlo Logroscino[1,6]**

[1]Center for Neurodegenerative Diseases and the Aging Brain, Department of Clinical Research in Neurology of the University of Bari "Aldo Moro" at "Pia Fondazione Card G. Panico" Hospital Tricase, Lecce, Italy, [2]Department of Computer, Control, and Management Engineering Antonio Ruberti (DIAG), La Sapienza University, Rome, Italy, [3]Department of History, Society and Human Studies, University of Salento, Lecce, Italy, [4]Department of Economics and Finance, University of Bari "Aldo Moro", Bari, Italy, [5]Unit of Laboratory Medicine, "Pia Fondazione Card. G. Panico" Hospital Tricase, Lecce, Italy, [6]Department of Basic Medicine Sciences, Neuroscience, and Sense Organs, University of Bari "Aldo Moro", Bari, Italy

OPEN ACCESS

Edited by:
Nicholas James Ashton,
University of Gothenburg, Sweden

Reviewed by:
Amy Renee Nelson,
University of South Alabama, United States
Wagner Scheeren Brum,
Federal University of Rio Grande do Sul, Brazil

***Correspondence:**
Giancarlo Logroscino
giancarlo.logroscino@uniba.it
Chiara Zecca
chiarazecca.cz@gmail.com

Received: 21 April 2021
Accepted: 09 August 2021
Published: 31 August 2021

Citation:
Zecca C, Pasculli G, Tortelli R, Dell'Abate MT, Capozzo R, Barulli MR, Barone R, Accogli M, Arima S, Pollice A, Brescia V and Logroscino G (2021) The Role of Age on Beta-Amyloid$_{1–42}$ Plasma Levels in Healthy Subjects. Front. Aging Neurosci. 13:698571. doi: 10.3389/fnagi.2021.698571

Beta-amyloid (Aβ) plaques have been observed in the brain of healthy elderlies with frequencies strongly influenced by age. The aim of the study is to evaluate the role of age and other biochemical and hematological parameters on Aβ$_{1–42}$ plasma levels in cognitively and neurologically normal individuals. Two-hundred and seventy-five normal subjects stratified by age groups (<35 years, 35–65 years, and >65 years) were included in the study. Aβ$_{1–42}$ plasma levels significantly correlated with age (r_s = 0.27; $p < 0.0001$) in the whole sample, inversely correlated with age in the first age group (r_s = −0.25, p = 0.01), positively correlated in the second group (r_s = 0.22, p = 0.03), while there was no significant correlation in the older group (r_s = 0.02, p = 0.86). Both age (β-estimate = 0.08; $p < 0.001$) and cholesterol (β-estimate = 0.03; p = 0.009) were significantly associated with Aβ$_{1–42}$ plasma level in multivariable analysis. However, only the association with age survived *post hoc* adjustment for multiple comparisons. The different effects of age on the Aβ level across age groups should be explored in further studies to better understand the age-dependent variability. This could better define the value of plasma Aβ as a biomarker of the Alzheimer neuropathology.

Keywords: beta amyloid, Alzheimer's disease, biomarker, age, plasma

INTRODUCTION

Alzheimer's disease (AD) is a progressive neurodegenerative disorder developed as a result of multiple factors rather than a single cause (Alzheimer's Association, 2019). Age is one of the main risk factors, with the vast majority of people with Alzheimer's dementia being age 65 or older. The percentage of people with AD increases dramatically with age: 3% of people age 65–74, 17% of people age 75 to 84, and 32% of people age 85 or older (Hebert et al., 2013; Alzheimer's Association, 2019).

Beta-amyloid (Aβ) deposition is part of the histopathological definition of AD and *in vivo* biomarkers of this process have been included in 2011 by the National Institute on Aging and Alzheimer's Association (NIA-AA) in the new diagnostic criteria for all the preclinical and clinical stages of the disease (Sperling et al., 2011; Jack et al., 2012). In addition to NIA-AA, the International Work Group (IWG) in 2014 has established diagnostic guidelines for AD that incorporate imaging and cerebrospinal fluid (CSF) biomarkers (Dubois et al., 2014). Based on the IWG criteria, the diagnosis of AD requires the presence of cognitive symptoms plus biomarker evidence of AD pathophysiologic processes. The central role of these biomarkers has been confirmed in the 2018 NIA-AA research framework that biologically defined AD throughout the entire course of the disease (Jack et al., 2018).

Aβ is supposed to trigger a series of biochemical processes that determine tau-deposition, neuronal disruption, neuronal death, and finally clinically manifest AD ("amyloid cascade" hypothesis; Hardy and Allsop, 1991).

Sequential cleavage of Aβ precursor protein (AβPP) by β— and γ—secretases results in the production of multiple Aβ species, the main forms containing 40 ($A\beta_{1-40}$) or 42 amino acids ($A\beta_{1-42}$; Selkoe, 2001). Studies have shown that Aβ exists in a dynamic equilibrium of soluble monomeric, oligomeric, protofibrillar, and fibrillar forms (Dahlgren et al., 2002), reflecting a balance between their production and removal from the brain. $A\beta_{1-40}$ is more soluble, less prone to parenchymal deposition, but more likely to accumulate in the walls of cerebrocortical and leptomeningeal blood vessels, whereas $A\beta_{1-42}$ is relatively insoluble in the interstitial fluid and prone to parenchymal deposition (Iwatsubo et al., 1994; Gravina et al., 1995).

Excessive accumulation of $A\beta_{1-42}$ increases the aggregation of Aβ to form oligomers and fibrils (Pauwels et al., 2012).

Although Aβ plaques are supposed to trigger the AD pathophysiologic process, they are also commonly observed in the brains of clinically normal (CN) older individuals, but the age at which Aβ plaque deposition begins is unknown (Mormino, 2014). This feature has consistently been observed in postmortem studies and has been replicated in amyloid imaging studies (Jack et al., 2014). These studies reveal a low proportion of Aβ deposition in CN individuals younger than 60 years, followed by a linear increase in the proportion of Aβ in CN subjects after the age of 60 (∼30% of CN are Aβ positive at age 75; Mormino, 2014).

Many investigators have examined the association between Aβ and brain changes in CN to determine whether Aβ accumulation in normal subjects could signal AD preclinical state, but often with inconsistent results (Hardy and Selkoe, 2002; Jack et al., 2013; Villemagne et al., 2013; Fandos et al., 2017). However, little is known about the general demographic, clinical, biochemical, and hematological factors impacting plasma Aβ levels. Studies have investigated different biochemical blood parameters such as creatinine (Arvanitakis et al., 2002; Irizarry et al., 2005; Luchsinger et al., 2007; Metti et al., 2013; Rajagopalan et al., 2013), total cholesterol, High-density Lipoprotein (HDL) cholesterol, bilirubin, platelets (Toledo et al., 2011), and Thyroid Stimulating Hormone (TSH; Tan et al., 2008; Choi et al., 2017) with uncertain and variable results.

The goal of this study is to evaluate plasma levels of $A\beta_{1-42}$ in a sample of cognitively and neurologically normal individuals with a wide age-range 19–89 years, in order to study the variability and trends in $A\beta_{1-42}$ plasma levels by age, and whether plasma levels are influenced by biochemical and hematological blood parameters.

MATERIALS AND METHODS

Study Population

The sampling strategy included the enrollment of a broad age-range population. Three age-groups (<35 years; 35–65 years; >65 years) were then considered for statistical purposes and the number of enrolled subjects was equally distributed among groups.

Younger (<35) and middle-aged subjects (35–65 years) were enrolled from the blood-donor service of the donation site located in the "Azienda Ospedaliera Card. G. Panico," Tricase Lecce (Panico cohort); all donors were informed of the possibility to join the study within the normal donation process. Past medical history (presence of any identified neurological or medical condition) was investigated through a structured questionnaire administered before the blood draw.

The older participants (>65 years) were enrolled from the GreatAGE Study, a population-based study on neurological and psychiatric age-related diseases with a focus on nutrition and age-related hearing loss as predictors of late-life cognitive decline and depression, conducted in the area of Castellana Grotte, Southern Italy (GreatAGE cohort; Lozupone et al., 2018).

A detailed description of the methods used for the clinical assessment of the study population has been published elsewhere (Zecca et al., 2018).

Exclusion criteria considered for this study were: (1) the presence of signs/symptoms of any neurological or psychiatric diseases (or previous diagnosis) documented at the time of enrollment; (2) pharmacological therapy at the time of enrollment; (3) any illness in the previous 3 months that required medical intervention; (4) history of chronic liver, kidney or thyroid diseases; and (5) current drug or alcohol addiction.

The present study was approved by the Ethics Committee of ASL Lecce and by the Institutional Review Board of the "National Institute of Gastroenterology "S. De Bellis". All participants gave written informed consent.

Blood Sampling, Biochemical Determinations, and $A\beta_{1-42}$ Measurements

Venous blood was drawn by venipuncture in the morning after an overnight fast. Plasma samples were collected in EDTA vacutainers, which were immediately centrifuged for 5 min at 3,000 *g* at room temperature. Blood samples were routinely processed for hematologic and biochemical measurements, according to routine clinical standards. Plasma samples were aliquoted into polypropylene tubes and stored at −80°C until biochemical analyses (without being thawed and re-frozen) for blood amyloid testing. Samples were thawed at

room temperature before analysis. Only plasma samples free from hemoglobin, bilirubin, and triglycerides, which could interfere with the analytical methods, were considered eligible for analysis.

Quantification of Aβ_{1-42} in plasma was performed using a specific ELISA kit (Innotest β-amyloid$_{1-42}$, Innogenetics, Belgium), according to the manufacturer's instructions. The assay involved the use of a high sensitivity conjugate for the detection of the protein in plasma samples. Briefly, immunocoated plates were incubated with 100 μl of sample or calibrator for 3 h at room temperature on an orbital shaker. After several wash steps, a biotinylated antibody was added to the plates and incubated for 1 h at room temperature. This antibody was then detected by a peroxidase-labeled streptavidin. After the addition of substrate solution, positive samples developed a blue color. The reaction was stopped by the addition of sulfuric acid and the absorbance was then measured at 450 nm. All samples were analyzed in duplicate for each test run. Plasma Aβ_{1-42} levels were presented as pg/ml. A reference interval of 8.12–29.00 pg/ml for Aβ_{1-42} plasma levels was considered (Zecca et al., 2018).

The following biochemical parameters were examined: glucose, urea, creatinine, aspartate aminotransferase (AST), alanine aminotransferase (ALT), gamma glutamyl transpeptidase (gamma-GT), total bilirubin, total cholesterol, triglycerides, high-density lipoprotein (HDL) cholesterol, phosphorus, calcium, thyroid-stimulating hormone (TSH), full blood cell count (white cells with differentials, red cells, and platelets), hemoglobin (Hb) and erythrocyte sedimentation rate (ESR).

Statistical Analysis

Summary results are presented as mean ± standard deviation (SD) for normal continuous variables, the median-interquartile range for the non-normally distributed ones, and as absolute frequencies (with percentage frequencies in brackets) for categorical variables. The Shapiro-Wilk test was used to assess the normal distribution of the continuous variable residuals in a linear model against age categories. Continuous and categorical variables were compared across age subgroups using the Kruskal-Wallis, ANOVA, and the Pearson Chi-Square tests, respectively for continuous (non-normally and normally distributed) and categorical covariates. Spearman correlation corrected for multiple tests (Benjamini-Hochberg procedure) was used to test for the proportion of variance in the ranks shared between continuous covariates and Aβ_{1-42} levels.

Unpaired *t*-test was used to evaluate differences of Aβ_{1-42} levels between males and females stratifying by the three age groups. One-way analysis of means not assuming equal variances (Welch's F Test) was used to test differences in Aβ_{1-42} levels between males and females in the overall (not age-stratified) dataset. The latter test was also used to compare Aβ_{1-42} levels between different age groups (as a result of significative Levene's test for homogeneity Aβ levels variance across age groups, $p < 0.01$). All *p*-values obtained by age groups pairwise comparison were adjusted for family-wise error with the Bonferroni method. Non-parametric (Kruskal-Wallis) or parametric (Linear ANOVA) methods were used according to linear regression residual distributions to compare levels of other covariates between the three age groups. Piecewise cubic polynomial 97.5% confidence intervals (**Figure 2**) were obtained after $n = 1{,}000$ bootstraps data points replicates.

Finally, stepwise (both direction selection) multivariable linear regression models were run with Aβ_{1-42} as a dependent variable to determine which factors predicted Aβ_{1-42} protein levels. We used a stepwise selection process with significance levels $\alpha = 0.05$ for covariate deletions and $\alpha = 0.20$ for covariate additions, in order to determine the final multivariable models. All analyses were performed using R version 3.6.2 running under Windows 10 x64 (build 18362).

RESULTS

Two hundred and seventy-five cognitively and neurologically normal subjects were enrolled (120 women and 155 men; age range, 19–89 years; mean age ± SD, 51.61 ± 21.08 years). According to the sampling strategy, the number of subjects was equally distributed among age groups, with 93 subjects in the younger age group (<35 years), 89 subjects in the middle-age group (35–65 years), and 93 subjects in the older age-group (>65 years).

Descriptive statistics of the demographic characteristics, and of the biochemical and hematological indices of the whole sample as long as of the three subgroups are shown in **Table 1**.

Aβ_{1-42} plasma levels fitted a normal distribution in the whole study population ($p = 0.06$) as well as in the age subgroups ($p = 0.59$ for <35 age subgroup; $p = 0.73$ for 35–65 age subgroup; $p = 0.38$ for >65 age subgroup). The mean value (± SD) of the biomarker was 17.76 (±5.97) pg/ml in the whole group, 14.76 (±4.16) in the first age group, 19.96 (±5.96) in the second age group, and 18.67 (±6.36) in the third age group.

The Aβ_{1-42} plasma levels significantly differed between the three age groups ($p < 0.001$). Such significant overall difference between age groups was also confirmed for two of the subgroups with pairwise comparisons using *t*-tests with non-pooled SD as a *post hoc* analysis (<35 vs. 35–65 $p < 0.0001$; <35 vs. >65 $p < 0.0001$; 35–65 vs. >65 $p = 0.36$; **Figure 1**).

Furthermore, statistically significant differences were found also for most of the biochemical and hematological parameters between age subgroups (**Table 1**). No differences were found for erythrocytes (Kruskal-Wallis test, $p = 0.90$), Hb (Linear Model Anova, $p = 0.65$) among the three age groups.

The correlations between Aβ_{1-42} plasma levels and demographic and clinical parameters in the whole sample and in the three age strata are described in **Table 2**.

There were no differences in the mean plasma levels of Aβ_{1-42} between women (mean = 17.59, SD = 5.31) and men (mean = 17.89, SD = 6.45; $p = 0.67$) in the whole age group nor in any of the three age-related strata ($p = 0.71$ for <35 age group, $p = 0.20$ for 35–65 age group, $p = 0.94$ for >65 age group).

Aβ_{1-42} plasma levels correlated significantly with age ($r_s = 0.27$; $p < 0.0001$), in the whole group.

These evidences suggest that Aβ_{1-42} levels in cognitively normal individuals overall increased with age although this trend was not linear as demonstrated by fitting a cubic smoothing spline to our data (**Figure 2**).

TABLE 1 | Demographic characteristics and baseline biochemical and hematological indices.

	<35	35–65	>65	Total	*p* value
N	93	89	93	275	
Age (years)	27.17 (4.53)	52.30 (9.19)	75.40 (6.78)	51.61 (21.08)	<0.001[1]
Sex					<0.001[2]
F	57 (61.29%)	38 (42.70%)	25 (26.88%)	120 (43.64%)	
M	36 (38.71%)	51 (57.30%)	68 (73.12%)	155 (56.36%)	
Aβ$_{1-42}$ (pg/ml)	14.76 (4.16)	19.96 (5.96)	18.67 (6.36)	17.76 (5.97)	<0.001[3]
AST (U/L)	23.41 (9.46)	25.82 (8.73)	23.46 (12.56)	24.21 (10.43)	0.002[1]
ALT (U/L)	24.89 (6.09)	26.03 (9.09)	22.44 (13.61)	24.43 (10.17)	<0.001[1]
GGT (U/L)	25.49 (8.20)	26.17 (11.88)	22.30 (23.65)	24.63 (16.08)	<0.001[1]
Bilirubin (μmol/L)	0.76 (0.43)	0.75 (0.34)	0.64 (0.31)	0.72 (0.37)	0.047[1]
Cholesterol (mmol/L)	179.06 (26.53)	180.56 (29.59)	179.20 (35.86)	179.60 (30.82)	0.937[4]
HDL (mmol/L)	49.51 (10.49)	42.88 (10.16)	48.41 (13.11)	46.99 (11.67)	<0.0011
Triglycerides (mmol/L)	110.97 (45.86)	108.46 (33.32)	97.96 (50.95)	105.78 (44.32)	0.005[1]
Creatinine (μmol/L)	0.69 (0.26)	0.70 (0.24)	0.96 (0.32)	0.79 (0.30)	<0.001[1]
Glucose (mmol/L)	81.62 (10.94)	85.34 (15.62)	101.38 (20.89)	89.51 (18.43)	<0.001[1]
Total Protein (g/L)	7.29 (0.52)	7.31 (0.58)	6.88 (0.48)	7.16 (0.56)	<0.001[1]
TSH (mIU/L)	1.58 (0.73)	1.38 (0.66)	1.72 (0.95)	1.56 (0.80)	
Urea (mmol/L)	27.80 (6.41)	28.00 (9.67)	42.18 (10.66)	32.73 (11.31)	<0.001[1]
WBC (10E9/L)	6.45 (1.66)	6.21 (1.54)	5.82 (1.54)	6.16 (1.60)	
Erythrocytes (10E12/L)	4.89 (0.55)	4.85 (0.56)	4.85 (0.56)	4.86 (0.56)	0.898[1]
Platelets (10E9/L)	242.14 (54.80)	244.35 (58.75)	205.81 (49.05)	230.57 (56.92)	<0.001[1]
Hb (g/L)	13.58 (1.53)	13.69 (1.55)	13.78 (1.61)	13.68 (1.56)	0.674[4]

AST, aspartate aminotransferase; ALT, alanine aminotransferase; GGT, gamma glutamyl transpeptidase; HDL-cholesterol, high-density lipoprotein cholesterol; TSH, thyroid-stimulating hormone; WBC, white blood cells; Hb, hemoglobin. The results are reported as mean ± standard deviation (SD) Comparisons by age groups. [1]Kruskal-Wallis rank sum test. [2]Pearson's Chi-squared test. [3]One-way analysis of means (not assuming equal variances). [4]Linear Model ANOVA.

In fact, Aβ$_{1-42}$ plasma levels decreased in the first age group and then steadily increased in the second age group, to end up with another slight decrease up to a steady level in the third age group. In order to detect these age-dependent fluctuations of the protein levels and to study the effect of possible confounders, a subgroup correlation analysis was conducted. Spearman correlations in the three age groups, confirmed that Aβ$_{1-42}$ plasma levels negatively correlated with age in the first age group ($r_s = -0.25$; $p = 0.01$), positively correlated in the middle-age group ($r_s = 0.22$; $p = 0.03$), while no significant correlation was detected in the third age group ($r_s = 0.02$; $p = 0.86$,). After correcting for multiple tests, the correlation with age was confirmed in the whole group (p.adj = < 0.0001) and not confirmed in the first and middle-age group (p.adj = 0.56 and p.adj = 0.52, respectively) although such values were found significant in the crude analysis (**Table 2**).

Finally, for the whole sample and for each subgroup, a bidirectional stepwise multivariable linear regression model was fitted. Results are shown in **Table 3**.

In the model for the whole sample, a significant regression equation was found ($p < 0.01$), with an R^2 of 0.1. Both age (β-estimate = 0.08; $p < 0.001$) and cholesterol (β-estimate = 0.03; $p = 0.009$) were significantly associated with biomarker levels although the latter, differently from the more solid age findings, might be an artifact product of the stepwise regression analysis. Age was confirmed to be significantly associated with biomarker levels also in the first (β-estimate = −0.24; $p = 0.011$) and second (β-estimate = 0.14; $p = 0.038$) age groups. No significant associations were found between age and Aβ$_{1-42}$ levels in the stepwise multivariable linear regression model for the third age group (age covariate was omitted after the stepwise selection process for this age group). In addition, Aβ$_{1-42}$ levels were significantly associated with TSH (β-estimate = 2.30; $p = 0.016$) in the 35–65 age group and with total cholesterol and total proteins (β-estimate = 0.04, $p = 0.042$; β-estimate = −3.40, $p = 0.012$) in the last age group (>65 age). Assumption tests for statistical modeling were undertaken on the overall final model and were reported in **Supplementary Material**.

DISCUSSION

In the present study, we evaluated the Aβ$_{1-42}$ plasma levels in cognitively normal individuals with a wide range of age (19–89 years) in order to study if and how they are influenced by age.

We found an overall positive correlation between Aβ$_{1-42}$ plasma levels and age. Our results suggested that Aβ$_{1-42}$ levels, in cognitively normal individuals, increase with age although this trend is not linear: we observed a reduction of Aβ$_{1-42}$ plasma levels in the younger cases, followed by an increase in the adult age class and subsequent stabilization over 65 years.

This is in line with previous studies (Fukumoto et al., 2003; Toledo et al., 2013; Miners et al., 2014) that have highlighted the association of age with differential changes in protein levels, although, a study, dividing 391 subjects by 10-years intervals starting from age 20–29 years, reported a negative correlation between age and Aβ$_{1-42}$ plasma concentration, and no age-group differences (Lue et al., 2019). Probably the differences with this study may be due to the different analytical methods.

Our findings on protein levels in subjects over 65 years were comparable with those found by de Wolf et al. (2020) in a population-based cohort study including subjects of the same age

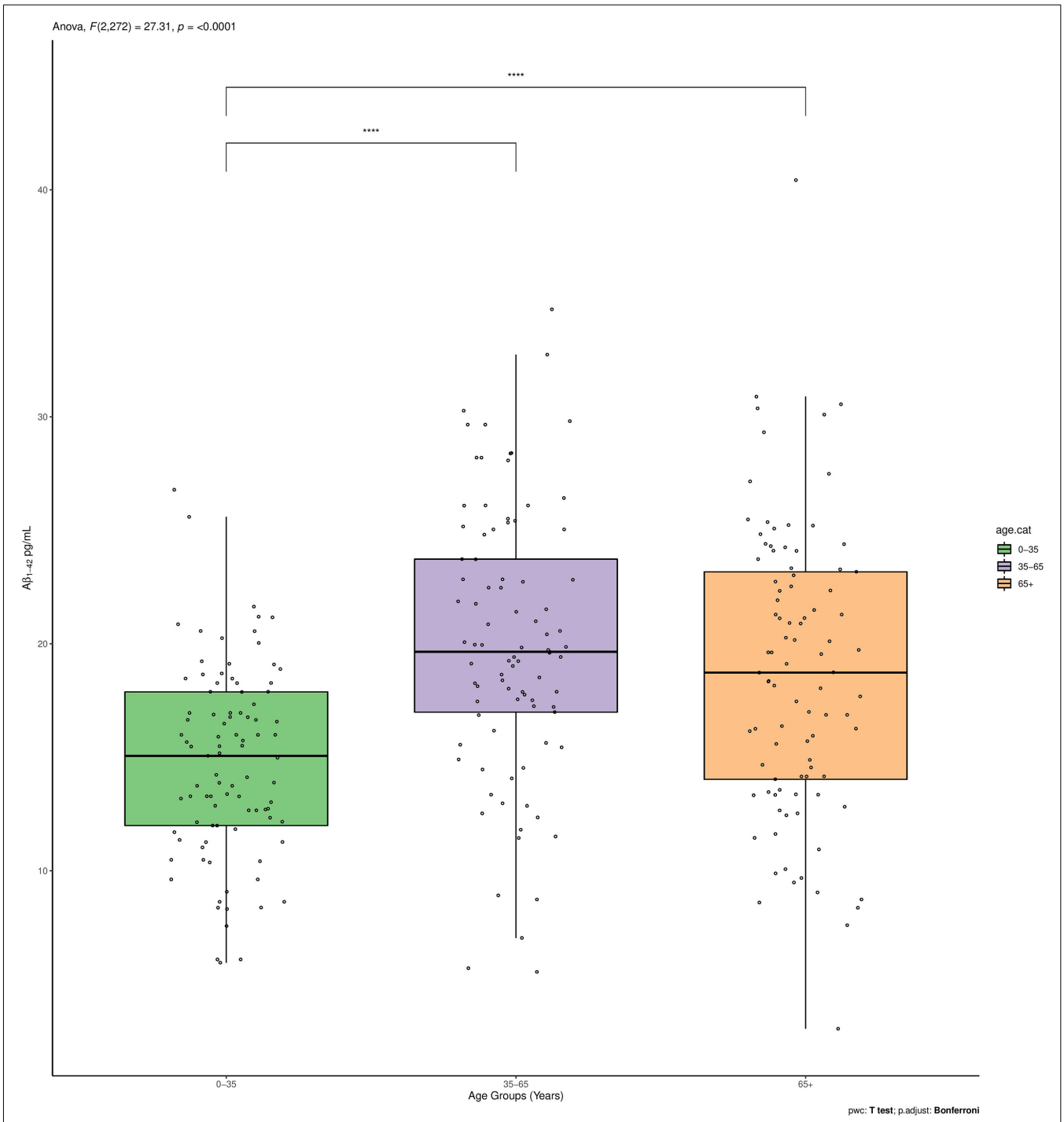

FIGURE 1 | Aβ$_{1-42}$ plasma levels between the three age groups (<35, 35–65, >65). ****$p < 0.001$.

group. The authors investigated whether levels of Aβ$_{1-42}$ plasma of non-demented subjects >60 years of age were associated with AD dementia, arguing that lower Aβ$_{1-42}$ plasma levels are significantly associated with incident AD dementia. In line with our results, there was no correlation between Aβ$_{1-42}$ and age in the 65-year-old subjects.

Age represents an important factor to consider when evaluating the accuracy of a diagnostic test and is an additive information to the biochemical data. A recent study (West et al., 2021) based on plasma Aβ42/40 ratio has in fact highlighted how plasma Aβ42/40 concentration ratio determined using the Mass Spectrometry assay can accurately identify brain amyloid

TABLE 2 | Correlations between A$\beta_{1–42}$ measurements and clinical parameters observed in this study.

		Overall			1st Group			2nd Group			3rd Group		
Variable		**Aβ_{1-42}/r$_s$**	***p*-value**	**adj.p**	**Aβ_{1-42}/r$_s$**	***p*-value**	**adj.p**	**Aβ_{1-42}/r$_s$**	***p*-value**	**adj.p**	**Aβ_{1-42}/r$_s$**	***p*-value**	**adj.p**
Sex	M	17.89 ± 6.45	0.67		14.55 ± 5.00	0.71		21.09 ± 6.06	0.20		18.85 ± 6.88	0.94	
	F	17.59 ± 5.31			14.89 ± 3.57			18.95 ± 5.76			18.31 ± 4.77		
Age		0.27	**<0.0001**	**<0.0001**	−0.25	**0.01**	0.56	0.22	**0.03**	0.52	0.02	0.86	0.95
ALT		−0.06	0.31	0.66	0.03	0.76	0.78	0.08	0.47	0.98	−0.17	0.09	0.58
AST		−0.04	0.48	0.50	−0.16	0.12	0.97	−0.01	0.93	0.87	−0.12	0.25	0.37
GGT		−0.01	0.86	0.91	−0.01	0.94	0.99	0.2	0.06	0.56	0.02	0.85	0.95
Bilirubin		−0.01	0.84	0.90	0.07	0.51	0.96	−0.05	0.65	0.95	−0.06	0.55	0.82
Cholesterol		0.12	**0.04**	0.13	−0.06	0.56	0.97	0.2	0.06	0.56	0.18	0.08	0.34
HDL		−0.06	0.31	0.41	0.12	0.25	0.97	−0.05	0.62	0.95	0.06	0.56	0.26
Triglycerides		0.07	0.22	0.50	−0.04	0.67	0.93	0.03	0.80	0.95	0.21	**0.04**	0.82
Creatinine		0.08	0.17	0.35	0.02	0.82	0.97	−0.07	0.49	0.87	0.13	0.22	0.55
Glucose		0.09	0.14	0.37	−0.11	0.27	0.93	−0.02	0.88	0.98	0.08	0.46	0.78
Total proteins		−0.11	**0.05**	0.16	0.1	0.36	0.93	−0.15	0.15	0.78	−0.2	**0.05**	0.29
TSH		0.06	0.37	0.50	−0.09	0.38	0.93	0.1	0.37	0.87	0.22	0.04	0.24
Urea		0.09	0.13	0.31	−0.01	0.93	0.99	0.04	0.74	0.95	0.03	0.8	0.95
RBC		−0.06	0.28	0.34	−0.13	0.22	0.97	0.09	0.42	0.99	−0.14	0.18	0.51
WBC		−0.09	0.15	0.48	0.05	0.67	0.93	0	0.99	0.87	−0.15	0.16	0.53
Platelets		−0.04	0.56	0.71	−0.1	0.34	0.93	0.08	0.44	0.87	−0.01	0.93	0.99
Hb		0.02	0.70	0.83	−0.03	0.78	0.97	0.04	0.74	0.95	0.01	0.93	0.99

P-values refer to the Spearman correlation test (adj.p for Benjamini-Hochberg procedure for multiple testing) for continuous variables and to the t-test (Welch test for unequal variances for the overall groups) for categorical variable. Bold values denote statistical significance at the p ≤ 0.05 level.

status, and that including additional risk factors for amyloid pathology in the model, as age or ApoE4 status, improved the model accuracy. Given the central role for Aβ in AD and the need for biomarkers that can be used as reliable diagnostic tools, many studies have examined the temporal dynamics of Aβ in biological samples (Huang et al., 2012a,b; Moghekar et al., 2012) and it has also been largely investigated whether Aβ concentration can be influenced by age (Mayeux et al., 2003; Song et al., 2011; Toledo et al., 2011), by testing the longitudinal changes in plasma Aβ levels in cognitively stable individuals vs. those who develop AD dementia and the concentration across time at different stages of the disease. In cognitively stable individuals, plasma Aβ levels increase slightly with age. It has been hypothesized that the age-related increase of Aβ species in plasma may reflect in the periphery the increased Aβ production or decreased Aβ clearance in the brain leading to increased Aβ deposition and AD with aging (Fukumoto et al., 2003).

In subjects who eventually develop clinical AD, protein levels are elevated in the pre-dementia stage, reach a peak and then diminish prior to the development of clinical AD symptoms (Song et al., 2011).

The decrease of plasma amyloid level during the Alzheimer's process could be explained by the decrease of Aβ clearance from the brain to the peripheral fluid (blood) because of alteration of blood-brain barrier permeability, glymphatic system, or vascular or microglial activation troubles (Ramanathan et al., 2015).

What emerged in our study found agreement with imaging (Rodrigue et al., 2012; Jack et al., 2014) and postmortem (Price et al., 2009) studies, that showed a steady increase in plaque deposition across the age span of 26–95 years, with a slowing of the age-related increase in plaques at the older end of the lifespan. Savva and colleagues (Savva et al., 2009) conducted neuropathological examinations on the brains of about 500 older individuals (aged 69–103 years) for whom the dementia status was known from assessments conducted, on average, 1.5 years before death. The density of Alzheimer-type pathology (neurofibrillary tangles and neuritic plaques) and the severity of other pathologies (atrophy, cerebrovascular disease, and Lewy bodies) were evaluated in the cerebral cortex and hippocampus of these brains, and five age groups for analysis (≤80, 80–84, 85–89, 90–94 and ≥95 years of age) were considered. The study highlighted that the prevalence of Alzheimer-type pathology progressively increased with age in both brain regions of individuals without dementia. In contrast, in the brains of people with dementia, the prevalence of such pathology remained constant or decreased with increasing age. The findings from the study indicated that in the younger old (<80 years of age) the presence of moderate or severe Alzheimer-type pathology was strongly associated with dementia, but the strength of the associations progressively declined with age and was at its weakest in the oldest old (≥95 years of age).

Aβ peptides are generated outside of the central nervous system in appreciable quantities by the skeletal muscle, platelets, and vascular walls (Roher et al., 2009). As well as, amyloid precursor protein (APP), the only member of

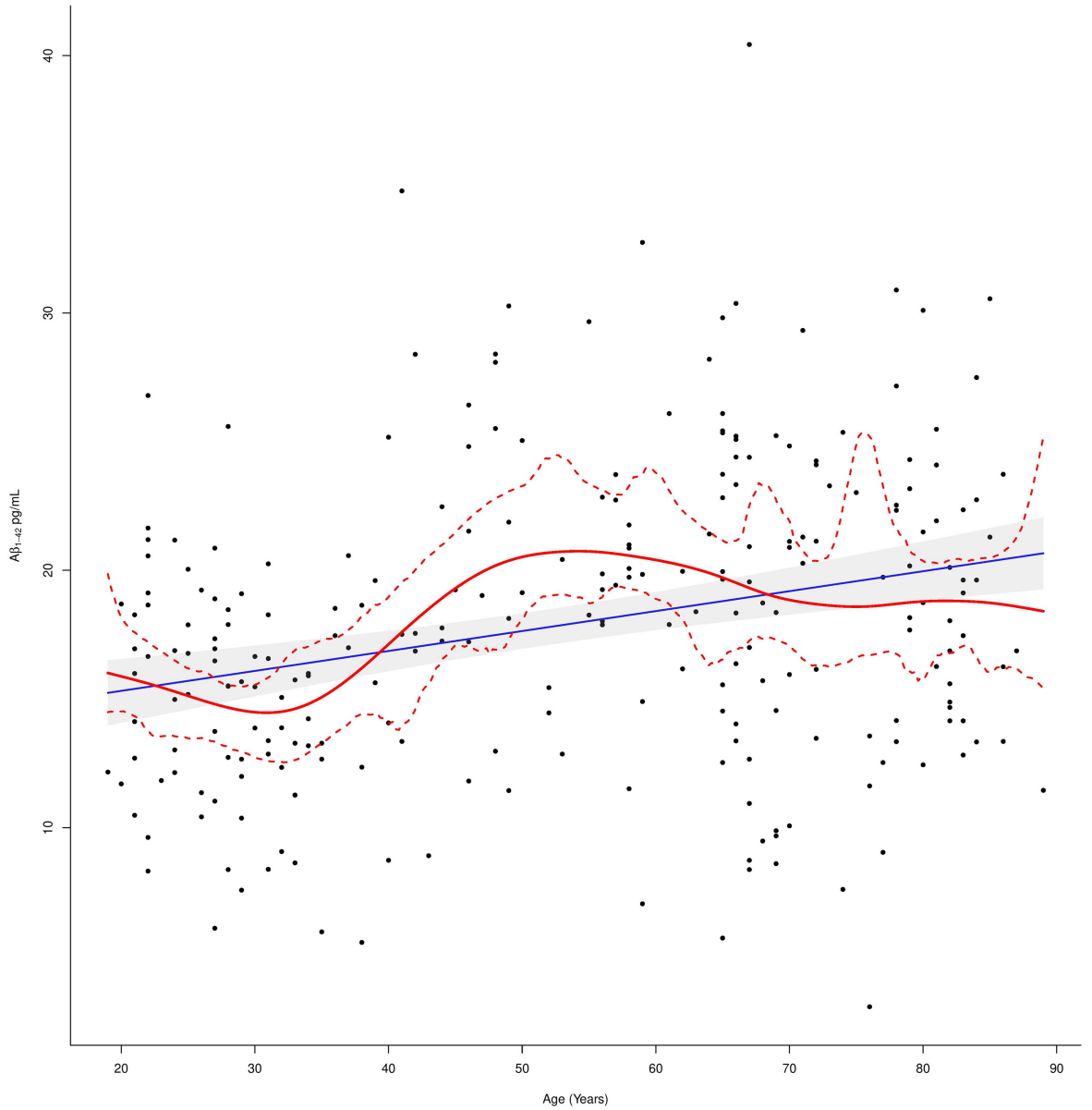

FIGURE 2 | Plasma Aβ$_{1-42}$ levels in relation to age. The linear regression fit line (blue line) and the cubic smoothing spline (red line) were added. The 97.5% confidence limits around the main spline estimate are based on 1,000 bootstrap re-samplings of the data points in the scatterplot.

the family encoding Aβ peptides, is expressed in endothelial cells of cerebral and peripheral arteries, with physiological and pathological implications, from atherosclerosis to cerebral amyloid angiopathy (d'Uscio et al., 2017). It has been demonstrated that APP and Aβ are increased in plasma of patients with coronary heart disease (Stamatelopoulos et al., 2015).

Moreover, recent studies have identified Aβ as an antimicrobial peptide (AMP), and suggest Aβ deposition may be a protective innate immune response to infection (Soscia et al., 2010; Kumar et al., 2016; Eimer et al., 2018). Such peptides act both by directly inactivating pathogens, and also by modulating responses of innate immune cells, including phagocytes. These antimicrobial properties have been attributed to Aβ oligomers that form fibrils in the presence of bacterial surface epitopes (Voth et al., 2020). Amyloids, particularly Aβ42, polymerizes into fibrils upon contact with bacterial surface epitopes and actively agglutinate bacteria prior to bactericidal activity. It has been shown that pathogens responsible for nosocomial pneumonia, including *Pseudomonas aeruginosa*, *Klebsiella pneumonia*, and *Staphylococcus aureus*, elicit lung endothelial production and release of amyloids (Voth et al., 2020). So, all these potential sources of Aβ should be taken into consideration when evaluating peripheral levels of the protein.

TABLE 3 | Stepwise multivariable (both directions selection) linear regression analysis exploring factors correlated with $A\beta_{1-42}$.

	Overall			Group1 (<35)			Group2 (35–65)			Group3 (>65)		
Predictors	**β-Estimate**	**96% CI**	***p*-value**	**β-Estimate**	**96% CI**	***p*-value**	**β-Estimate**	**96% CI**	***p*-value**	**β-Estimate**	**96% CI**	***p*-value**
(Intercept)	8.50	4.15–12.84	**<0.001**	25.35	17.56–33.15	**<0.001**	9.37	1.43–17.30	**0.021**	35.40	16.03–54.76	**<0.001**
Age	0.08	0.04–0.11	**<0.001**	−0.24	−0.42 to −0.05	**0.011**	0.14	0.01–0.28	**0.038**			
Total Cholesterol	0.03	0.01–0.05	**0.009**							0.04	0.00–0.07	**0.042**
Creatinine				2.75	−0.43–5.93	0.089						
Glucose				−0.07	−0.15–0.00	0.055						
TSH							2.30	0.43–4.17	**0.016**			
Total Proteins										−3.40	−6.03 to −0.76	**0.012**
Observations	274			93			89			92		
R^2 / R^2 adjusted	0.096/0.089			0.123/0.093			0.095/0.074			0.111/0.091		

Bold values denote statistical significance at the $p \leq 0.05$ level.

In order to assess whether other factors may affect Aβ protein, the relationships between $A\beta_{1-42}$ plasma levels and biochemical/hematological blood parameters have also been explored in the present study.

In line with previous studies (Toledo et al., 2011; Metti et al., 2013; Ruiz et al., 2013), we found an association between $A\beta_{1-42}$ and cholesterol, total protein, creatinine, HDL, and platelets.

According to these studies, the age and the above mentioned parameters were independent predictors for $A\beta_{1-40}$ and $A\beta_{1-42}$ and explained 12.1% and 12.9% of the variability of their respective concentrations, underscoring the importance of using multivariable models that adjust for possible confounders (Toledo et al., 2011).

In our study, both directions stepwise multivariable linear regression models were examined for $A\beta_{1-42}$ in the whole sample and in each subgroup to determine which factors independently predict biomarker levels. In the model for the whole sample, biomarker levels were significantly predicted by age and total cholesterol. Our results agree with a population-based study of subjects over 75 that found higher total cholesterol and higher LDL cholesterol predicted plasma $A\beta_{1-42}$ levels (Blasko et al., 2011). The proposed mechanism by which cholesterol might accelerate the production of Aβ is by shifting Aβ precursor protein (AβPP) metabolism from forming alpha to beta cleavage products (Blasko et al., 2011). Also in the study of Toledo and coworkers, $A\beta_{1-40}$ and $A\beta_{1-42}$ plasma levels were mainly predicted by creatinine, total protein, and total cholesterol (Toledo et al., 2011); however, another study did not support these findings, showing different significant predictors of plasma $A\beta_{1-40}$ and $A\beta_{1-42}$ (history of diabetes, HDL cholesterol; Metti et al., 2013).

The stepwise linear regression analysis stratified by age subgroups detected various relations inside the three groups; age was significantly associated with plasma protein concentrations in the first group (<35 years), age and TSH in the second group (35-65 years), and total cholesterol and total proteins in the third group (>65 years). A study has shown a positive correlation between TSH and triglycerides and $A\beta_{1-42}$ plasma levels in cognitively intact subjects over 65 (Tan et al., 2008). Several *in vitro* and *in vivo* studies have shown that thyroid hormone regulates the gene expression of amyloid precursor protein (APP), increasing APP expression and consequently, Aβ peptide and Aβ levels (O'Barr et al., 2006).

The presence of conflicting results between studies assessing plasma Aβ peptides can be explained, in part, by the high variability in the methods for $A\beta_{1-42}$ measurements, not yet standardized; different technologies have been used to measure plasma Aβ (ELISA, Luminex, or Simoa technology), with different diagnostic performance. But also, the study designs or the different ages of subjects enrolled can affect the comparison of results.

Some limitations need to be considered in this study. Firstly, we did not have any CSF and positron emission tomography (PET) measurements of $A\beta_{1-42}$ and thus it was not possible to correlate plasma $A\beta_{1-42}$ to measurements or burden of $A\beta_{1-42}$ in CSF to corroborate our results. Secondly, the value

of plasma Aβ42/40 ratio as surrogate biomarkers of cortical Aβ deposition was not available. The ratio appears to be a better predictor of the presence of brain amyloid than just the plasma Aβ_{1-42} concentration. Moreover, the ratio, instead of single peptide measurements, could also attenuate possible bias in single Aβ peptide levels due to pre-analytical and analytical variables. Thirdly, the use of a classic ELISA method for plasma quantification of protein levels. From a molecular biology point of view, a more sensitive methodology would have been optimal for better detection and accuracy in measuring blood amyloid protein. The recent introduction of new ultrasensitive assays, such as a single-molecule array, allows detection at a single molecule level, significantly improving analytical sensitivity, and their use in research is strongly recommended. Sensitive measurement of plasma Aβ levels in a large patient group is required to clarify the clinical, demographic, and genetic factors that influence plasma Aβ levels, and as a prerequisite for proposing plasma Aβ as a biomarker for diagnosis, progression, and treatment effects.

We point out that the data we analyzed came from a retrospective study that, as we know from literature (Cowie et al., 2017), are important tools in medical research. Nonetheless, we are conscious that such kinds of studies have several limitations owing to their design such as selection or recall biases (Talari and Goyal, 2020). However, the main strengths of this study are the large sample size and the wide age range of healthy individuals, but also the assessment of normality, especially for the older participants (>65 years), with an extensive geriatric and neurological examination and standardized cognitive tests. Moreover, all the Aβ measurements were undertaken in a single-center laboratory, eliminating inter-center variability.

To conclude, after age 65 Aβ_{1-42} does not increase in normal subjects, and in the whole cohort age and Aβ_{1-42} are strongly associated.

Our findings open new insights to better understand the effect of age on plasma Aβ peptides.The possible relationship of Aβ with age should be further explored in larger longitudinal studies, especially exploring the oldest age, and comparing data from wet biomarkers with imaging and neuropsychological data. Furthermore, our results may be important to better define the diagnostic value of plasma Aβ in studies of age-related diseases.

DATA AVAILABILITY STATEMENT

The raw data supporting the conclusions of this article will be made available by the authors, without undue reservation.

ETHICS STATEMENT

The studies involving human participants were reviewed and approved by Ethic Committee of ASL Lecce. The patients/participants provided their written informed consent to participate in this study.

AUTHOR CONTRIBUTIONS

Manuscript design and writing: CZ, RT, MTD, and GL. Data analysis: GP, AP, and SA. Data collection: CZ, RT, MTD, RC, MB, RB, and MA. Supervision: GL, VB, AP, and SA. Critical discussion and final revision: RT and GL. All authors contributed to the article and approved the submitted version.

FUNDING

This work was supported by "Establishment of the TECNOPOLO for Precision Medicine" funded by the Puglia Region CUP B84I18000540002.

SUPPLEMENTARY MATERIAL

The Supplementary Material for this article can be found online at: https://www.frontiersin.org/articles/10.3389/fnagi.2021.698571/full#supplementary-material.

REFERENCES

Alzheimer's Association. (2019). Alzheimer's disease facts and figures. *Alzheimers Dement.* 15, 321–387. doi: 10.1016/j.jalz.2019.01.010

Arvanitakis, Z., Lucas, J. A., Younkin, L. H., Younkin, S. G., and Graff-Radford, N. R. (2002). Serum creatinine levels correlate with plasma amyloid β protein. *Alzheimer Dis. Assoc. Disord.* 16, 187–190. doi: 10.1097/00002093-200207000-00009

Blasko, I., Kemmler, G., Jungwirth, S., Wichart, I., Weissgram, S., Jellinger, K., et al. (2011). Prospective study on association between plasma amyloid β-42 and atherosclerotic risk factors. *J. Neural Transm. (Vienna)* 118, 663–672. doi: 10.1007/s00702-011-0599-4

Choi, H. J., Byun, M. S., Yi, D., Sohn, B. K., Lee, J. H., Lee, J.-Y., et al. (2017). Associations of thyroid hormone serum levels with *in vivo* Alzheimer's disease pathologies. *Alzheimers Res. Ther.* 9:64. doi: 10.1186/s13195-017-0291-5

Cowie, M. R., Blomster, J. I., Curtis, L. H., Duclaux, S., Ford, I., Fritz, F., et al. (2017). Electronic health records to facilitate clinical research. *Clin. Res. Cardiol.* 106, 1–9. doi: 10.1007/s00392-016-1025-6

d'Uscio, L. V., He, T., and Katusic, Z. S. (2017). Expression and processing of amyloid precursor protein in vascular endothelium. *Physiology (Bethesda)* 32, 20–32. doi: 10.1111/bcp.15029

Dahlgren, K. N., Manelli, A. M., Stine, W. B., Baker, L. K., Krafft, G. A., LaDu, M. J., et al. (2002). Oligomeric and fibrillar species of amyloid-β peptides differentially affect neuronal viability. *J. Biol. Chem.* 277, 32046–32053. doi: 10.1074/jbc.M201750200

de Wolf, F., Ghanbari, M., Licher, S., McRae-McKee, K., Gras, L., Weverling, G. J., et al. (2020). Plasma tau, neurofilament light chain and amyloid-β levels and risk of dementia; a population-based cohort study. *Brain* 143, 1220–1232. doi: 10.1093/brain/awaa054

Dubois, B., Feldman, H. H., Jacova, C., Hampel, H., Molinuevo, J. L., Blennow, K., et al. (2014). Advancing research diagnostic criteria for Alzheimer's disease: the IWG-2 criteria. *Lancet Neurol.* 13, 614–629. doi: 10.1016/S1474-4422(14)70090-0

Eimer, W. A., Vijaya Kumar, D. K., Navalpur Shanmugam, N. K., Rodriguez, A. S., Mitchell, T., Washicosky, K. J., et al. (2018). Alzheimer's disease-associated β-amyloid is rapidly seeded by herpesviridae to protect against brain infection. *Neuron* 99, 56–63. e3. doi: 10.1016/j.neuron.2018.06.030

Fandos, N., Pérez-Grijalba, V., Pesini, P., Olmos, S., Bossa, M., Villemagne, V. L., et al. (2017). Plasma amyloid β 42/40 ratios as biomarkers for amyloid β cerebral deposition in cognitively normal individuals. *Alzheimers Dement. (Amst)* 8, 179–187. doi: 10.1016/j.dadm.2017.07.004

Fukumoto, H., Tennis, M., Locascio, J. J., Hyman, B. T., Growdon, J. H., Irizarry, M. C., et al. (2003). Age but not diagnosis is the main predictor of plasma amyloid β-protein levels. *Arch. Neurol.* 60, 958–964. doi: 10.1001/archneur.60.7.958

Gravina, S. A., Ho, L., Eckman, C. B., Long, K. E., Otvos, L., Younkin, L. H., et al. (1995). Amyloid β protein (Aβ) in Alzheimer's disease brain. Biochemical and immunocytochemical analysis with antibodies specific for forms ending at Aβ 40 or Aβ 42(43). *J. Biol. Chem.* 270, 7013–7016. doi: 10.1074/jbc.270.13.7013

Hardy, J., and Allsop, D. (1991). Amyloid deposition as the central event in the aetiology of Alzheimer's disease. *Trends Pharmacol. Sci.* 12, 383–388. doi: 10.1016/0165-6147(91)90609-v

Hardy, J., and Selkoe, D. J. (2002). The amyloid hypothesis of Alzheimer's disease: progress and problems on the road to therapeutics. *Science* 297, 353–356. doi: 10.1126/science.1072994

Hebert, L. E., Weuve, J., Scherr, P. A., and Evans, D. A. (2013). Alzheimer disease in the United States (2010–2050) estimated using the 2010 census. *Neurology* 80, 1778–1783. doi: 10.1212/WNL.0b013e31828726f5

Huang, Y., Potter, R., Sigurdson, W., Kasten, T., Connors, R., Morris, J. C., et al. (2012a). β-amyloid dynamics in human plasma. *Arch. Neurol.* 69, 1591–1597. doi: 10.1001/archneurol.2012.18107

Huang, Y., Potter, R., Sigurdson, W., Santacruz, A., Shih, S., Ju, Y.-E., et al. (2012b). Effects of age and amyloid deposition on Aβ dynamics in the human central nervous system. *Arch. Neurol.* 69, 51–58. doi: 10.1001/archneurol.2011.235

Irizarry, M. C., Gurol, M. E., Raju, S., Diaz-Arrastia, R., Locascio, J. J., Tennis, M., et al. (2005). Association of homocysteine with plasma amyloid β protein in aging and neurodegenerative disease. *Neurology* 65, 1402–1408. doi: 10.1212/01.wnl.0000183063.99107.5c

Iwatsubo, T., Odaka, A., Suzuki, N., Mizusawa, H., Nukina, N., Ihara, Y., et al. (1994). Visualization of A β 42(43) and A β 40 in senile plaques with end-specific A β monoclonals: evidence that an initially deposited species is A β 42(43). *Neuron* 13, 45–53. doi: 10.1016/0896-6273(94)90458-8

Jack, C. R., Bennett, D. A., Blennow, K., Carrillo, M. C., Dunn, B., Haeberlein, S. B., et al. (2018). NIA-AA research framework: toward a biological definition of Alzheimer's disease. *Alzheimers Dement.* 14, 535–562. doi: 10.1016/j.jalz.2018.02.018

Jack, C. R., Knopman, D. S., Jagust, W. J., Petersen, R. C., Weiner, M. W., Aisen, P. S., et al. (2013). Tracking pathophysiological processes in Alzheimer's disease: an updated hypothetical model of dynamic biomarkers. *Lancet Neurol.* 12, 207–216. doi: 10.1016/S1474-4422(12)70291-0

Jack, C. R., Knopman, D. S., Weigand, S. D., Wiste, H. J., Vemuri, P., Lowe, V., et al. (2012). An operational approach to national institute on aging-Alzheimer's association criteria for preclinical Alzheimer disease. *Ann. Neurol.* 71, 765–775. doi: 10.1002/ana.22628

Jack, C. R., Wiste, H. J., Weigand, S. D., Rocca, W. A., Knopman, D. S., Mielke, M. M., et al. (2014). Age-specific population frequencies of cerebral β-amyloidosis and neurodegeneration among people with normal cognitive function aged 50–89 years: a cross-sectional study. *Lancet Neurol.* 13, 997–1005. doi: 10.1016/S1474-4422(14)70194-2

Kumar, D. K. V., Choi, S. H., Washicosky, K. J., Eimer, W. A., Tucker, S., Ghofrani, J., et al. (2016). Amyloid-β peptide protects against microbial infection in mouse and worm models of Alzheimer's disease. *Sci. Transl. Med.* 8:340ra72. doi: 10.1126/scitranslmed.aaf1059

Lozupone, M., Panza, F., Piccininni, M., Copetti, M., Sardone, R., Imbimbo, B. P., et al. (2018). Social dysfunction in older age and relationships with cognition, depression and apathy: the greatage study. *J. Alzheimers Dis.* 65, 989–1000. doi: 10.3233/JAD-180466

Luchsinger, J. A., Tang, M.-X., Miller, J., Green, R., Mehta, P. D., Mayeux, R., et al. (2007). Relation of plasma homocysteine to plasma amyloid β levels. *Neurochem. Res.* 32, 775–781. doi: 10.1007/s11064-006-9207-7

Lue, L.-F., Pai, M.-C., Chen, T.-F., Hu, C.-J., Huang, L.-K., Lin, W.-C., et al. (2019). Age-dependent relationship between plasma Aβ40 and Aβ42 and total tau levels in cognitively normal subjects. *Front. Aging Neurosci.* 11:222. doi: 10.3389/fnagi.2019.00222

Mayeux, R., Honig, L. S., Tang, M.-X., Manly, J., Stern, Y., Schupf, N., et al. (2003). Plasma A[β]40 and A[β]42 and Alzheimer's disease: relation to age, mortality and risk. *Neurology* 61, 1185–1190. doi: 10.1212/01.wnl.0000091890.32140.8f

Metti, A. L., Cauley, J. A., Ayonayon, H. N., Harris, T. B., Rosano, C., Williamson, J. D., et al. (2013). The demographic and medical correlates of plasma aβ40 and aβ42. *Alzheimer Dis. Assoc. Disord.* 27, 244–249. doi: 10.1097/WAD.0b013e318260a8cb

Miners, J. S., Jones, R., and Love, S. (2014). Differential changes in Aβ42 and Aβ40 with age. *J. Alzheimers Dis.* 40, 727–735. doi: 10.3233/JAD-132339

Moghekar, A., Goh, J., Li, M., Albert, M., and O'Brien, R. J. (2012). Cerebrospinal fluid Aβ and tau level fluctuation in an older clinical cohort. *Arch. Neurol.* 69, 246–250. doi: 10.1001/archneurol.2011.732

Mormino, E. C. (2014). The relevance of β-amyloid on markers of Alzheimer's disease in clinically normal individuals and factors that influence these associations. *Neuropsychol. Rev.* 24, 300–312. doi: 10.1007/s11065-014-9267-4

O'Barr, S. A., Oh, J. S., Ma, C., Brent, G. A., and Schultz, J. J. (2006). Thyroid hormone regulates endogenous amyloid-β precursor protein gene expression and processing in both *in vitro* and *in vivo* models. *Thyroid* 16, 1207–1213. doi: 10.1089/thy.2006.16.1207

Pauwels, K., Williams, T. L., Morris, K. L., Jonckheere, W., Vandersteen, A., Kelly, G., et al. (2012). Structural basis for increased toxicity of pathological aβ42:aβ40 ratios in Alzheimer disease. *J. Biol. Chem.* 287, 5650–5660. doi: 10.1074/jbc.M111.264473

Price, J. L., McKeel, D. W., Buckles, V. D., Roe, C. M., Xiong, C., Grundman, M., et al. (2009). Neuropathology of nondemented aging: presumptive evidence for preclinical Alzheimer disease. *Neurobiol. Aging* 30, 1026–1036. doi: 10.1016/j.neurobiolaging.2009.04.002

Rajagopalan, P., Refsum, H., Hua, X., Toga, A. W., Jack, C. R., Weiner, M. W., et al. (2013). Mapping creatinine- and cystatin C-related white matter brain deficits in the elderly. *Neurobiol. Aging* 34, 1221–1230. doi: 10.1016/j.neurobiolaging.2012.10.022

Ramanathan, A., Nelson, A. R., Sagare, A. P., and Zlokovic, B. V. (2015). Impaired vascular-mediated clearance of brain amyloid β in Alzheimer's disease: the role, regulation and restoration of LRP1. *Front. Aging Neurosci.* 7:136. doi: 10.3389/fnagi.2015.00136

Rodrigue, K. M., Kennedy, K. M., Devous, M. D., Rieck, J. R., Hebrank, A. C., Diaz-Arrastia, R., et al. (2012). β-amyloid burden in healthy aging: regional distribution and cognitive consequences. *Neurology* 78, 387–395. doi: 10.1212/WNL.0b013e318245d295

Roher, A. E., Esh, C. L., Kokjohn, T. A., Castaño, E. M., Van Vickle, G. D., Kalback, W. M., et al. (2009). Amyloid β peptides in human plasma and tissues and their significance for Alzheimer's disease. *Alzheimers Dement.* 5, 18–29. doi: 10.1016/j.jalz.2008.10.004

Ruiz, A., Pesini, P., Espinosa, A., Pérez-Grijalba, V., Valero, S., Sotolongo-Grau, O., et al. (2013). Blood amyloid β levels in healthy, mild cognitive impairment and Alzheimer's disease individuals: replication of diastolic blood pressure correlations and analysis of critical covariates. *PLoS One* 8:e81334. doi: 10.1371/journal.pone.0081334

Savva, G. M., Wharton, S. B., Ince, P. G., Forster, G., Matthews, F. E., Brayne, C., et al. (2009). Age, neuropathology and dementia. *N. Engl. J. Med.* 360, 2302–2309. doi: 10.1056/NEJMoa0806142

Selkoe, D. J. (2001). Alzheimer's disease: genes, proteins and therapy. *Physiol. Rev.* 81, 741–766. doi: 10.1152/physrev.2001.81.2.741

Song, F., Poljak, A., Valenzuela, M., Mayeux, R., Smythe, G. A., and Sachdev, P. S. (2011). Meta-analysis of plasma amyloid-β levels in Alzheimer's disease. *J. Alzheimers Dis.* 26, 365–375. doi: 10.3233/JAD-2011-101977

Soscia, S. J., Kirby, J. E., Washicosky, K. J., Tucker, S. M., Ingelsson, M., Hyman, B., et al. (2010). The Alzheimer's disease-associated amyloid β-protein is an antimicrobial peptide. *PLoS One* 5:e9505. doi: 10.1371/journal.pone.0009505

Sperling, R. A., Aisen, P. S., Beckett, L. A., Bennett, D. A., Craft, S., Fagan, A. M., et al. (2011). Toward defining the preclinical stages of Alzheimer's disease: recommendations from the national institute on aging-Alzheimer's association workgroups on diagnostic guidelines for Alzheimer's disease. *Alzheimers Dement.* 7, 280–292. doi: 10.1016/j.jalz.2011.03.003

Stamatelopoulos, K., Sibbing, D., Rallidis, L. S., Georgiopoulos, G., Stakos, D., Braun, S., et al. (2015). Amyloid-β (1–40) and the risk of death from cardiovascular causes in patients with coronary heart disease. *J. Am. Coll. Cardiol.* 65, 904–916. doi: 10.1016/j.jacc.2014.12.035

Talari, K., and Goyal, M. (2020). Retrospective studies - utility and caveats. *J. R. Coll. Physicians Edinb.* 50, 398–402. doi: 10.4997/JRCPE.2020.409

Tan, Z. S., Beiser, A., Vasan, R. S., Au, R., Auerbach, S., Kiel, D. P., et al. (2008). Thyroid function and the risk of Alzheimer disease: the Framingham Study. *Arch. Intern. Med.* 168, 1514–1520. doi: 10.1001/archinte.168.14.1514

Toledo, J. B., Shaw, L. M., and Trojanowski, J. Q. (2013). Plasma amyloid β measurements—a desired but elusive Alzheimer's disease biomarker. *Alzheimers Res. Ther.* 5:8. doi: 10.1186/alzrt162

Toledo, J. B., Vanderstichele, H., Figurski, M., Aisen, P. S., Petersen, R. C., Weiner, M. W., et al. (2011). Factors affecting Aβ plasma levels and their utility as biomarkers in ADNI. *Acta Neuropathol.* 122, 401–413. doi: 10.1007/s00401-011-0861-8

Villemagne, V. L., Burnham, S., Bourgeat, P., Brown, B., Ellis, K. A., Salvado, O., et al. (2013). Amyloid β deposition, neurodegeneration and cognitive decline in sporadic Alzheimer's disease: a prospective cohort study. *Lancet Neurol.* 12, 357–367. doi: 10.1016/S1474-4422(13)70044-9

Voth, S., Gwin, M., Francis, C. M., Balczon, R., Frank, D. W., Pittet, J.-F., et al. (2020). Virulent *Pseudomonas aeruginosa* infection converts antimicrobial amyloids into cytotoxic prions. *FASEB J.* 34, 9156–9179. doi: 10.1096/fj.202000051RRR

West, T., Kirmess, K. M., Meyer, M. R., Holubasch, M. S., Knapik, S. S., Hu, Y., et al. (2021). A blood-based diagnostic test incorporating plasma Aβ42/40 ratio, ApoE proteotype and age accurately identifies brain amyloid status: findings from a multi cohort validity analysis. *Mol. Neurodegener.* 16:30. doi: 10.1186/s13024-021-00451-6

Zecca, C., Tortelli, R., Panza, F., Arcuti, S., Piccininni, M., Capozzo, R., et al. (2018). Plasma β-amyloid 1–42 reference values in cognitively normal subjects. *J. Neurol. Sci.* 391, 120–126. doi: 10.1016/j.jns.2018.06.006

Conflict of Interest: The authors declare that the research was conducted in the absence of any commercial or financial relationships that could be construed as a potential conflict of interest.

Publisher's Note: All claims expressed in this article are solely those of the authors and do not necessarily represent those of their affiliated organizations, or those of the publisher, the editors and the reviewers. Any product that may be evaluated in this article, or claim that may be made by its manufacturer, is not guaranteed or endorsed by the publisher.

frontiers in Neuroscience

ORIGINAL RESEARCH
published: 03 September 2021
doi: 10.3389/fnins.2021.695049

Neurofilament Light Chain and Intermediate HTT Alleles as Combined Biomarkers in Italian ALS Patients

*Assunta Ingannato[1], Silvia Bagnoli[1], Salvatore Mazzeo[1], Valentina Bessi[1], Sabrina Matà[2], Monica Del Mastio[2], Gemma Lombardi[3], Camilla Ferrari[1], Sandro Sorbi[1,3] and Benedetta Nacmias[1,3]**

[1] NEUROFARBA Department, University of Florence, Florence, Italy, [2] SOD Neurologia 1, Dipartimento Neuromuscolo-Scheletrico e Degli Organi di Senso, Azienda Ospedaliero Universitaria Careggi, Florence, Italy, [3] IRCCS Fondazione Don Carlo Gnocchi, Florence, Italy

Objective: To study the possible implication of the two biomarkers, intermediate alleles (IAs) of the Huntingtin (HTT) gene and neurofilament light chain (NfL) levels in plasma, in amyotrophic lateral sclerosis (ALS) patients.

Methods: We analyzed IAs in a cohort of 106 Italian ALS patients and measured the plasma NfL levels in 20% of the patients of the cohort. We correlated the two biomarkers with clinical phenotypes.

Results: Intermediate alleles were present in 7.5% of the patients of our cohort, a frequency higher than that reported in general population. Plasma NfL levels increased with age at onset ($p < 0.05$). Patients with bulbar onset (BO) had higher plasma NfL concentration (CI −0.61 to −0.06, $p = 0.02$) and a later age at onset of the disease (CI −24.78 to −4.93, $p = 0.006$) with respect to the spinal onset (SO) form. Additionally, two of the patients, with IAs and plasma NfL concentration lower with respect to normal alleles' carriers, presented an age at onset higher than the mean of the entire cohort.

Conclusion: According to our findings, plasma NfL and IAs of HTT gene may represent potential biomarkers in ALS, providing evidence of a possible implication in clinical phenotype.

Keywords: amyotrophic lateral sclerosis, neurofilament light chain, CAG repeat expansion, HTT gene, biomarkers

OPEN ACCESS

Edited by:
Thomas K. Karikari, University of Gothenburg, Sweden

Reviewed by:
Rodolfo Gabriel Gatto, University of Illinois at Chicago, United States
Ilaria Puxeddu, University of Pisa, Italy

****Correspondence:***
Benedetta Nacmias
benedetta.nacmias@unifi.it

Specialty section:
This article was submitted to Neurodegeneration, a section of the journal Frontiers in Neuroscience

Received: *14 April 2021*
Accepted: *06 August 2021*
Published: *03 September 2021*

Citation:
Ingannato A, Bagnoli S, Mazzeo S, Bessi V, Matà S, Del Mastio M, Lombardi G, Ferrari C, Sorbi S and Nacmias B (2021) Neurofilament Light Chain and Intermediate HTT Alleles as Combined Biomarkers in Italian ALS Patients. Front. Neurosci. 15:695049. doi: 10.3389/fnins.2021.695049

INTRODUCTION

Amyotrophic lateral sclerosis (ALS) is a neurodegenerative disorder characterized by degeneration of upper and lower motoneurons, leading to progressive weakness, paralysis, and, in the end, death typically within 3–5 years from symptom onset (Hardiman et al., 2011; van Es et al., 2017). To date, the causes of ALS remain unknown; most cases are sporadic, whereas only 5–10% of the patients have a familiar form caused by a mutation in a known gene (Taylor et al., 2016). The most common pathogenic mutations are in the causative genes superoxide dismutase 1 (SOD1), TAR DNA binding protein (TARDBP or *TDP-43*), and chromosome 9 open reading frame 72

(C9orf72) (Yousefian-Jazi et al., 2020). The diagnosis of ALS is based on clinical findings and arrives only many months after symptom onset (Paganoni et al., 2014), so there is an urgency to find biological markers that could be helpful in diagnosis and prognosis and that could be included in common medical practice. Neurofilament light chain (NfLs) is the most promising biomarker in neurodegenerative diseases, and in the last years, it has been studied extensively in different neurological diseases (Bacioglu et al., 2016; Khalil et al., 2018; Gaetani et al., 2019). NfLs are subunits of neurofilaments, neuron-specific proteins belonging to the intermediate filament family, highly expressed in large caliber myelinated axons (Herrmann and Aebi, 2016). NfL levels increase in biological fluids, such as cerebrospinal fluids (CSF) and blood, proportionally to the degree of the axonal damage (Reiber, 1994). An elevated concentration of NfLs in CSF or blood indicates neuronal degeneration (Gaiottino et al., 2013). An innovative ultrasensitive single-molecule technology, called Simoa, can detect proteins at femtomolar concentration in blood, allowing precise quantification of NfLs (Rissin et al., 2010). Recently, several studies have focused on the potential diagnostic performance of NfLs as a biomarker in ALS (Lu et al., 2015; Li et al., 2018; Poesen and Van Damme, 2018; Verde et al., 2019). Their levels in CSF and blood are higher in ALS patients compared with healthy controls and also correlate with the disease progression rate and survival (Tortelli et al., 2012; Boylan et al., 2013; Lu et al., 2015; De Schaepdryver et al., 2018; Gille et al., 2019). Furthermore, recent studies are also trying to highlight the role of CAG repeat expansion in different neurological disorders (Dewan et al., 2021; Leotti et al., 2021). Expansions of the CAG repeat in the ATXN2 gene, which cause spinocerebellar ataxia type 2, have been associated with increased risk of ALS (Sproviero et al., 2017), while patients carrying CAG triplet expansion in the Huntingtin (HTT) gene in a range between 27 and 35, referred to as an intermediate allele (IA), showed motor and cognitive changes (Cubo et al., 2016; Jot, 2019; Savitt and Jankovic, 2019). A correlation between susceptibility to neurodegenerative diseases and HTT CAG repeat expansion was reported in 2019, suggesting that IAs might have a role also in the pathogenesis of Alzheimer's disease, increasing disease risk (Menéndez-González et al., 2019). The reported frequency of IAs in the general population is around 6% (Savitt and Jankovic, 2019), not so different from that observed in neurodegenerative disorders (Menéndez-González et al., 2019). For these reasons, further studies are still needed. The aim of our study was to test, for the first time, in an Italian cohort of ALS patients, the implication in the disease of the two biomarkers, plasma NfLs and IAs of the HTT gene focusing on disease susceptibility, age at onset, and site of onset (bulbar versus spinal). Finally, we examined whether there was a correlation between the two biomarkers.

MATERIALS AND METHODS

ALS Patients and Clinical Characteristics

The study does include ALS patients, with a defined diagnosis according to El Escorial diagnostic criteria for ALS (Brooks, 1994), recruited at the Neurological Clinic I of Careggi Hospital in Florence and consecutively enrolled from March 2009 to November 2020. Patients carrying a pathogenic mutation in a causative gene (SOD1, TDP43, and C9orf72) were excluded from the study. In fact, pathogenic mutation in causative genes could potentially act as a confounding factor in the overall analysis. Moreover, the presence of all other disease processes was an exclusion criterion. The study finally included a cohort of 106 Italian ALS patients where, at the first visit, all patients underwent a neurologic and functional assessment and venipuncture for blood collection. A minority of the patients (seven patients, with concomitant dementia at the onset) were evaluated with an extensive neuropsychological battery as described in more detail elsewhere (Bracco et al., 1990) and with SAND for language evaluation (Screening for Aphasia in NeuroDegeneration) (Catricalà et al., 2017), and received a clinical diagnosis of FTD according to the current criteria, including the behavioral variant (bv-FTD) and the non-fluent variant of primary progressive aphasia (nfv-PPA) (Neary et al., 1998; Gorno-Tempini et al., 2011). The study protocol was approved by the local ethics committee and conducted in accordance with the provisions of the Declaration of Helsinki.

Genetic Testing

High-molecular-weight DNA was isolated from whole blood using a QIAamp DNA blood mini QIAcube Kit (Qiagen, Germany), as described by the manufacturer. The amount of DNA for each sample has been determined using a NanoDrop ND-3300® Fluorospectrometer. DNA samples were aliquoted and stored at −20°C until use. HTT CAG repeat expansion was determined by a polymerase chain reaction (PCR) amplification assay using the following primers: 5′-[6-FAM] GACCCTGGAAAAGCTGATGA-3′ and 5′-GGCTGAGGAAGCTGAGGAG-3′. The forwarded primer was modified with 6-carboxyfluorescein (6-FAM), a fluorescent dye for labeling oligonucleotides (Jama et al., 2013). The size of the PCR product was determined by capillary electrophoresis using an ABI 3130X automated DNA sequencer and the GeneMapper version 4.0 software (Applied Biosystems). A set of HTT CAG alleles, whose lengths were confirmed by DNA sequencing, was used to provide standard size. CAG repeat expansions were considered as follows: normal alleles with CAG expansion under 27 repeats, IAs with 27–35 repetitions, and pathologic allele with expansions size > 35 repeats.

Plasma Sample Collection and NfL Analysis

Plasma was isolated from peripheral blood sample within 2 h of collection. Blood sample was centrifuged at 1300 rcf at 4° for 10 min, and the supernatant was immediately frozen and stored at −80°C until tested. Plasma NfL concentration was detected with the ultrasensitive single-molecule array (Simoa) technology provided by Quanterix Corporation (Lexington, MA, United States) (Rissin et al., 2010), on the automatized Simoa SR-X platform (GBIO, Hangzhou, China), following the instructions of the manufacturer. A Simoa NF-Light SR-X kit (Cat. No 103400) for human samples was used according to the protocol

provided by Quanterix. All plasma samples were analyzed in a single run basis. Plasma samples and controls were diluted at a 1:4 ratio and measured in duplicate with calibrators. A calibration curve was calculated from measurements of serially diluted calibrators. The lower limit of quantification (LLOQ) and the limit of detection (LOD) provided by the kit were 0.316 and 0.0552 pg/ml, respectively. The quality control with low NfL concentration had a mean concentration of 5.08 pg/ml; the quality control with high NfL concentration had a mean of 169 pg/ml.

Statistical Analysis

Statistical analysis was performed using R software v4.0.3 (The R Foundation) and SPSS software version 27 (IBM SPSS Statistics). We tested the correlations between continuous variables using Pearson's correlation analysis; $p < 0.05$ was set as significant. Multiple linear regression was performed between the log function of NfL measurement and clinical parameters. Shapiro–Wilk's test was executed to test the data normal distribution. To evaluate variable differences between groups, we used independent-samples *t*-test and Mann–Whitney *U*-test. Welch *t*-test was run when the assumption of homogeneity of variances was violated. To test whether the difference between two proportions is statistically significant, we used Fisher's exact test.

RESULTS

Italian ALS Cohort: Clinical Phenotype

The Italian cohort included 106 ALS patients (**Table 1**); 51 were female (48.1%) and 55 were male (51.9%). Disease clinical presentation at onset was ALS for 99 patients (93.4%) and ALS and bv-FTD for six patients (5.7%), and one patient (0.9%) showed ALS and nfv-PPA. The age at onset was available for 94 patients of the entire cohort, with a mean age of 67.04 ± 11.54 years. About 66% (70 out of 106) of ALS patients had a spinal onset (SO); 34% (36 patients) had ALS with a bulbar onset (BO). The mean age at onset of SO was 63.66 ± 11.91 years (64 out of 70 patients); the mean age at onset of BO was 74.30 ± 6.232 years (30 out of 36 patients).

TABLE 1 | Clinical information of the Italian cohort of ALS patients.

	ALS patients n = 106
Gender	
Female, n (%)	51 (48.1)
Male, n (%)	55 (51.9)
Site of onset	
SO, n (%)	70 (66)
BO, n (%)	36 (34)
Age at onset *(n = 94), mean*	67.04 ± 11.54
Clinical presentation at onset	
ALS, n (%)	99 (93.4)
ALS and bv-FTD, n (%)	6 (5.7)
ALS and nfv-PPA, n (%)	1 (0.9)

Abbreviations: ALS, amyotrophic lateral sclerosis; SO, spinal onset; BO, bulbar onset; bv-FTD, behavioral variant of frontotemporal dementia; nfv-PPA, non-fluent variant of primary progressive aphasia.

IAs in ALS Patients

Out of 106 ALS, eight patients (7.5%) were carrying IAs of the HTT gene, and 98 patients (92.5%) presented normal alleles. No one showed a pathological allele expansion. Seven patients had IAs and SO, and one patient had IA and BO. Of the 98 ALS patients with normal alleles, 63 had SO and 35 had BO. There was no statistically significant association between IAs' presence and site at onset, as assessed by Fisher's exact test ($p = 0.174$), and neither with gender ($p = 0.316$). Moreover, IAs' presence was not linearly related with age at onset [$F(1,92) = 0.41$, $p = 0.840$, and adjusted $R^2 = -0.010$]. A Mann–Whitney *U*-test was run, and the mean ranks of age at onset for patients with IAs (41.94) and normal alleles (48.02) were not statistically significantly different, $U = 299.5$, $z = -0.604$, $p = 0.546$, using an exact sampling distribution for *U* (Dineen and Blakesley, 1973). The mean age at onset of IA carriers (eight out of 94) was 66.25 ± 7.78 years, and in normal allele carriers (86 out of 94), it was 67.12 ± 11.86 years.

Plasma NfL Levels in ALS Patients

The plasma sample was available for a subgroup of 21 patients out of 106 ALS patients. To gain normally distributed data for all independent variables, we used the log function of NfL concentration (LogNfL) for analysis. The mean of plasma LogNfL detected in the entire cohort was 1.98 ± 0.32 pg/ml. There was a statistically significant, moderate positive correlation between LogNfL and age at onset (β 0.039; $p < 0.05$). In our subgroup, the mean age at onset was 67.20 ± 14.617 years. A linear regression model established that there were significant linear relationships between LogNfL and clinical data, age at onset [$F(1,18) = 4.96$, $p < 0.05$, and adjusted $R^2 = 0.17$], and site of onset [$F(1,19) = 6.47$, $p < 0.05$, and adjusted $R^2 = 0.21$]. Moreover, a statistically significant linear relationship emerged between age at onset and site at onset [$F(1,18) = 5.92$, $p < 0.05$, and adjusted $R^2 = 0.21$]. There was univariate normality, as assessed by Shapiro–Wilk's test ($p > 0.05$). No significant relationship was found with gender [$F(1,19) = 0.4$, $p = 0.535$, and adjusted $R^2 = -0.031$].

Out of 21 ALS patients, 14 (66.7%) had an SO and seven (33.3%) had a BO. Independent-samples *t*-test determined that LogNfL was higher in BO (2.21 ± 0.32 pg/mL) than SO (1.87 ± 0.27 pg/mL), a statistically significant difference of −0.34 (95% CI, −0.61 to −0.06), $t(19) = -2.54$, $p = 0.020$, and there was homogeneity of variances, as assessed by Levene's test for equality of variances ($p = 0.906$) (**Figure 1**). We ran a receiver operating characteristic (ROC) analysis, and a cutoff level of 2.1028 pg/ml discriminated between BO and SO with 78.6% sensitivity and 71.4% specificity (95% CI 54.5–98.6%). The mean age at onset of SO was 62 ± 4.33 years, and BO had a mean age at onset of 76.86 ± 1.74 years, a statistically significant difference of −14.86 (95% CI, −24.78 to −4.93), $t(15.377) = -3.18$, $p = 0.006$ (**Figure 2**). No statistically significant differences in LogNfL emerged in gender.

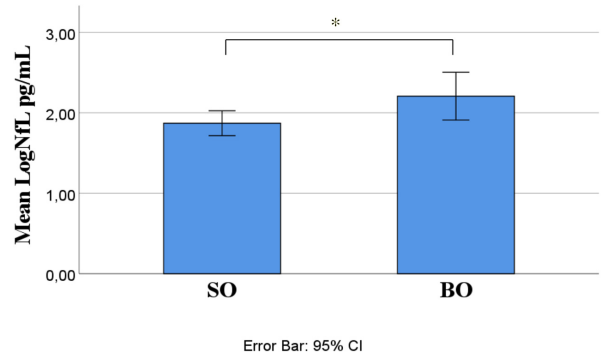

FIGURE 1 | ALS site of onset compared for mean LogNfL levels. Mean LogNfL was higher in BO than SO (2.21 + 0.32 versus 1.87 + 0.27 pg/mL; $p = 0.020$). Abbreviations: LogNfL, log of NfL concentration; SO, spinal onset; BO, bulbar onset.

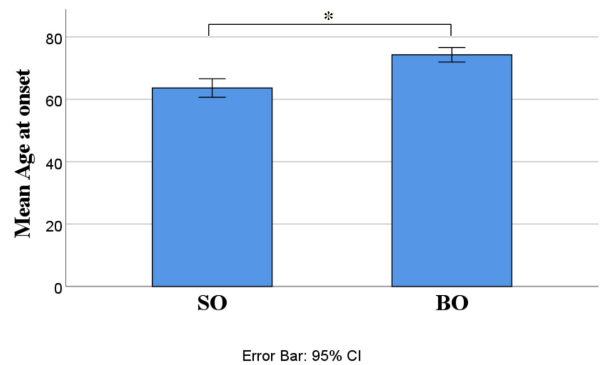

FIGURE 2 | ALS site of onset compared for mean age at onset. Mean age at onset was higher in BO than SO (62 + 4.33 versus 76.86 + 1.74. $p = 0.006$). Abbreviations: LogNfL, log of NfL concentration; SO, spinal onset; BO, bulbar onset.

Out of 21 patients, seven had a BO and normal alleles. Of 14 patients with SO, 12 had normal alleles and two were carrying IAs. The ALS age at onset of these two patients with IAs was, respectively, 73 and 77 years old.

IAs and NfL in ALS Patients

No significant relationship was found between IA presence and LogNfL [$F(1,19) = 1.07$, $p = 0.314$ and adjusted $R^2 = 0.004$]. Of 21 patients, two (9.52%) were carrying IAs with a mean LogNfL of 1.76 ± 0.2 pg/ml. The remaining 19 patients (90.47%) had normal alleles and a mean LogNfL of 2.0 ± 0.8 pg/ml.

DISCUSSION AND CONCLUSION

The first aim of this study was to investigate for the first time in an Italian cohort of ALS patients the distribution of two potential biomarkers, IAs of the HTT gene and plasma NfL levels, and to examine their possible implication with clinical-demographic data, as gender, age at onset, and site of symptoms onset (SO or BO). Another aim of our work was to detect the possible interaction between the two biomarkers. IAs were present in 7.5% of our cohort, a frequency higher than that reported in the general population (Savitt and Jankovic, 2019), but with no one statistically significant association with clinical-demographic variables. Analysis of plasma NfL concentration in a subgroup (20%) of the cohort provided evidence for a statistically significant correlation with disease age at onset and site of onset. Plasma NfL levels increased with progressing age at onset. BO had higher plasma NfL concentration, suggesting a neurodegeneration degree more elevated than in spinal form. A significant correlation also resulted between the ALS site of onset and age at onset. Patients with BO had a later age at onset of disease. BO and higher age at symptom onset have been identified as negative prognostic factors for the disease (Arora and Khan, 2021; Ferraro et al., 2021), so we could hypothesize that elevated NfL concentration is a negative factor for the progression of the disease.

NfLs are highly expressed in axons (Lee and Cleveland, 1996). Damage to the axon scaffold, with a consequent impaired trafficking, has been supposed at the base of the ALS pathogenesis (Falzone et al., 2021). Several studies explored the potential value of NfL as a biomarker in ALS and demonstrated that ALS patients presented higher levels of NfL compared with healthy controls and with pathological controls affected by other forms of motor neuron disease (MND) (Steinacker et al., 2016; Xu et al., 2016; Rossi et al., 2018; Gagliardi et al., 2019). In our study, NfL concentration was analyzed with the Simoa platform in plasma samples, and we detected elevated NfL levels in Italian ALS patients. The mean concentration detected in our Italian cohort was comparable with the plasma data of ALS worldwide populations (Li et al., 2018; Gille et al., 2019; Verde et al., 2019). So, our study could contribute to extend the results of previous studies on NfL levels in ALS worldwide population and, also, prove the diagnostic value of plasma NfL in Italian ALS population as a non-invasive biomarker. Several studies investigated the NfL biomarker in Italian ALS patients but always in CSF (Gagliardi et al., 2019, 2021; Abu-Rumeileh et al., 2020). NfL levels are more elevated and, consequentially, easily detectable in CSF compared to peripheral blood, but a lumbar puncture is required. The innovative Simoa technology remarkably improved the analytical sensitivity, allowing measurement of the lowest NfL concentrations in blood samples (Rissin et al., 2010), and NfL levels in CFS and blood values are comparable (Kuhle et al., 2016; Steinacker et al., 2016). Blood-based biomarkers are preferable because they require minimally invasive collection compared to CSF sampling and also present the other important advantages to be simple, inexpensive, and readily available. In fact, clinical application of plasma NfLs, because they are an easily accessible biomarker, has been recently investigated in several neurodegenerative disorders, such as in multiple sclerosis, Alzheimer's disease, frontotemporal dementia, Huntington's disease, Parkinson and atypical Parkinsonian disorders, and traumatic brain injury (Shahim et al., 2016; Hansson et al., 2017; Ljungqvist et al., 2017; Barro et al., 2018; Lewczuk et al., 2018; Sánchez-Valle et al., 2018; Rojas et al., 2021; Sampedro et al., 2021). The potential of NfLs

has also been indagated in oncology, microbiology, and infection diseases (Duffy, 2012; Schubert et al., 2015; Song et al., 2015).

We also observed that patients with incremented NfL levels were carrying normal alleles of the HTT gene. Two patients showed IAs and lower plasma NfL concentration. In addition, they had SO and an age at onset higher than the mean of the entire cohort. These preliminary data could indicate for IAs of the HTT gene a possible neuronal protective effect from neurodegeneration.

With regard to the second biomarker, the misfolded HTT protein, generated by the expansion of the CAG repeats in exon I of the HTT gene, is cleaved in mutated protein fragments that generate nuclear aggregates (Vonsattel and DiFiglia, 1998). Contrasting results were reported about their toxicity. A neuroprotective effect was seen in a HD transgenic mouse model with a strong reduction in susceptibility to excitotoxicity. It was suggested that at the basis of the imbalance toward the toxic or neuroprotective effect, there is the length of the fragments generated after the cleavage of the poly-Q stretch that could interact with proteins mediating resistance. Also, a full-length HTT protein folded differently than a shorter structure and could expose the exon I in a different manner leading to altered interactions (Slow et al., 2005; Zuchner and Brundin, 2008). Lee et al. (2018) described an "inverted U relationship" between the number of the CAG repeats of the HTT gene and a beneficial effect on cognitive functions. They demonstrated that the number of CAG repeats under 35 gives advantageous changes in brain structure and cognitive functions that becomes a disadvantage with an increasing length above 39 repetitions (Lee et al., 2017, 2018). Above the 39 CAG repeats, poly-Q tract would be non-functional in protein interactions, but below this threshold, HTT protein could show an increasingly greater flexibility, with an advantage in protein conformation and function and mediating changes in brain structure (Cattaneo et al., 2005; Schaefer et al., 2012; Caron et al., 2013). All these data support a possible neuronal protective effect of IAs in ALS patients.

Moreover, misfolded HTT protein and damaged axonal neurofilaments result in impaired trafficking and, consequently, in the loss of the neuronal connectivity. The impaired trafficking is a potential common mechanism at the base of ALS and HD pathogenesis (Morfini et al., 2013; Gatto et al., 2015).

In interpreting our findings, a few limitations should be considered. The sample size was relatively small, especially the subgroup (20% of patients) with data on plasma NfL. Moreover, not all patients were evaluated with a neuropsychological battery, so we did not control for the presence of associated cognitive symptoms that could act as confounding factors. Another limitation was the lack of a control group. IA frequency and plasma NfL levels were compared to literature data. This is a monocentric study, and a multicentric study would be useful to confirm these results. On the other hand, all samples were collected prospectively, processed, and stored using the same standardized method, and measurements of plasma NfL were done in a single batch, ensuring good reproducibility. As blood was collected at the first visit, when patients underwent a neurologic and functional assessment and venipuncture for blood collection, the correlation with disease progression was not considered. Our findings seem to reinforce the hypothesis that IAs could confer an advantage in degenerative brain disease, delaying the development of pathology and protecting from neuronal death. These preliminary findings indicate that both plasma NfL and IAs of the HTT gene may represent potential biomarkers for age at onset and site of onset (bulbar versus spinal), thus suggesting possible implication in clinical phenotype.

DATA AVAILABILITY STATEMENT

The raw data supporting the conclusions of this article will be made available by the authors, without undue reservation.

ETHICS STATEMENT

The studies involving human participants were reviewed and approved by the AOU-Careggi Ethical Committee. The patients/participants provided their written informed consent to participate in this study.

AUTHOR CONTRIBUTIONS

BN and SS: project design. SMaz, VB, SMat, MD, GL, CF, and SS: recruitment of patients. AI and SB: genetics analysis. AI, SB, SMaz, and BN: acquisition and analysis of data. AI, SB, and BN: writing of the manuscript. AI, SB, VB, SMaz, and BN: revision of the manuscript. All authors contributed to the article and approved the submitted version.

FUNDING

This work was supported by Fondi Ricerca UNIFI 2021 (BN) and RF-2018-12366665 (SS).

REFERENCES

Abu-Rumeileh, S., Vacchiano, V., Zenesini, C., Polischi, B., de Pasqua, S., Fileccia, E., et al. (2020). Diagnostic-prognostic value and electrophysiological correlates of CSF biomarkers of neurodegeneration and neuroinflammation in amyotrophic lateral sclerosis. *J. Neurol.* 267, 1699–1708. doi: 10.1007/s00415-020-09761-z

Arora, R. D., and Khan, Y. S. (2021). "Motor neuron disease," in *StatPearls [Internet]*. Treasure Island, FL: StatPearls.

Bacioglu, M., Maia, L. F., Preische, O., Schelle, J., Apel, A., Kaeser, S. A., et al. (2016). Neurofilament light chain in blood and CSF as marker of disease progression in mouse models and in neurodegenerative diseases. *Neuron* 91, 56–66. doi: 10.1016/j.neuron.2016.05.018

Barro, C., Benkert, P., Disanto, G., Tsagkas, C., Amann, M., Naegelin, Y., et al. (2018). Serum neurofilament as a predictor of disease worsening and brain and spinal cord atrophy in multiple sclerosis. *Brain* 141, 2382–2391. doi: 10.1093/brain/awy154

Boylan, K. B., Glass, J. D., Crook, J. E., Yang, C., Thomas, C. S., Desaro, P., et al. (2013). Phosphorylated neurofilament heavy subunit (pNF-H) in peripheral blood and CSF as a potential prognostic biomarker in amyotrophic lateral sclerosis. *J. Neurol. Neurosurg. Psychiatry* 84, 467–472. doi: 10.1136/jnnp-2012-303768

Bracco, L., Amaducci, L., Pedone, D., Bino, G., Lazzaro, M. P., Carella, F., et al. (1990). Italian multicentre study on dementia (SMID): a neuropsychological test battery for assessing Alzheimer's disease. *J. Psychiatr. Res.* 24, 213–226.

Brooks, B. R. (1994). El Escorial World federation of neurology criteria for the diagnosis of amyotrophic lateral sclerosis. Subcommittee on motor neuron diseases/amyotrophic lateral sclerosis of the World federation of neurology research group on neuromuscular diseases and the El Escorial "clinical limits of amyotrophic lateral sclerosis" workshop contributors. *J. Neurol. Sci.* 124, 96–107. doi: 10.1016/0022-510X(94)90191-0

Caron, N. S., Desmond, C. R., Xia, J., and Truant, R. (2013). Polyglutamine domain flexibility mediates the proximity between flanking sequences in huntingtin. *Proc. Natl. Acad. Sci. U. S. A.* 110, 14610–14615.

Catricalà, E., Gobbi, E., Battista, P., Miozzo, A., Polito, C., Boschi, V., et al. (2017). SAND: a screening for aphasia in neurodegeneration. development and normative data. *Neurol. Sci.* 38, 1469–1483. doi: 10.1007/s10072-017-3001-y

Cattaneo, E., Zuccato, C., and Tartari, M. (2005). Normal huntingtin function: an alternative approach to Huntington's disease. *Nat. Rev. Neurosci.* 6, 919–930.

Cubo, E., Ramos-Arroyo, M. A., Martinez-Horta, S., Martínez-Descalls, A., Calvo, S., Gil-Polo, C., et al. (2016). Clinical manifestations of intermediate allele carriers in Huntington disease. *Neurology* 87, 571–578. doi: 10.1212/WNL.0000000000002944

De Schaepdryver, M., Jeromin, A., Gille, B., Claeys, K. G., Herbst, V., Brix, B., et al. (2018). Comparison of elevated phosphorylated neurofilament heavy chains in serum and cerebrospinal fluid of patients with amyotrophic lateral sclerosis. *J. Neurol. Neurosurg. Psychiatry* 89, 367–373. doi: 10.1136/jnnp-2017-316605

Dewan, R., Chia, R., Ding, J., Hickman, R. A., Stein, T. D., Abramzon, Y., et al. (2021). Pathogenic Huntingtin repeat expansions in patients with frontotemporal dementia and amyotrophic lateral sclerosis. *Neuron* 109, 448–460.e4. doi: 10.1016/j.neuron.2020.11.005

Dineen, L. C., and Blakesley, B. C. (1973). Algorithm AS 62: generator for the sampling distribution of the Mann–Whitney U statistic. *Appl. Stat.* 22, 269–273. doi: 10.2307/2346934

Duffy, D. C. (2012). Ultra-sensitive protein detection using single molecule arrays (Simoa): the potential for detecting single molecules of botulinum toxin. *Botulinum J.* 2, 164–167.

Falzone, Y. M., Russo, T., Domi, T., Pozzi, L., Quattrini, A., Filippi, M., et al. (2021). Current application of neurofilaments in amyotrophic lateral sclerosis and future perspectives. *Neural Regen. Res.* 16, 1985–1991. doi: 10.4103/1673-5374.308072

Ferraro, P. M., Cabona, C., Meo, G., Rolla-Bigliani, C., Castellan, L., Pardini, M., et al. (2021). Age at symptom onset influences cortical thinning distribution and survival in amyotrophic lateral sclerosis. *Neuroradiology* 63, 1481–1487. doi: 10.1007/s00234-021-02681-3

Gaetani, L., Blennow, K., Calabresi, P., Di Filippo, M., Parnetti, L., and Zetterberg, H. (2019). Neurofilament light chain as a biomarker in neurological disorders. *J. Neurol. Neurosurg. Psychiatry* 90, 870–881. doi: 10.1136/jnnp-2018-320106

Gagliardi, D., Faravelli, I., Meneri, M., Saccomanno, D., Govoni, A., Magri, F., et al. (2021). Diagnostic and prognostic value of CSF neurofilaments in a cohort of patients with motor neuron disease: a cross-sectional study. *J. Cell. Mol. Med.* 25, 3765–3771. doi: 10.1111/jcmm.16240

Gagliardi, D., Meneri, M., Saccomanno, D., Bresolin, N., Comi, G. P., and Corti, S. (2019). Diagnostic and prognostic role of blood and cerebrospinal fluid and blood neurofilaments in amyotrophic lateral sclerosis: a review of the literature. *Int. J. Mol. Sci.* 20:4152. doi: 10.3390/ijms20174152

Gaiottino, J., Norgren, N., Dobson, R., Topping, J., Nissim, A., Malaspina, A., et al. (2013). Increased neurofilament light chain blood levels in neurodegenerative neurological diseases. *PLoS One* 8:e75091. doi: 10.1371/journal.pone.0075091

Gatto, R. G., Chu, Y., Ye, A. Q., Price, S. D., Tavassoli, E., Buenaventura, A., et al. (2015). Analysis of YFP(J16)-R6/2 reporter mice and postmortem brains reveals early pathology and increased vulnerability of callosal axons in Huntington's disease. *Hum. Mol. Genet.* 24, 5285–5298.

Gille, B., De Schaepdryver, M., Goossens, J., Dedeene, L., De Vocht, J., Oldoni, E., et al. (2019). Serum neurofilament light chain levels as a marker of upper motor neuron degeneration in patients with amyotrophic lateral sclerosis. *Neuropathol. Appl. Neurobiol.* 45, 291–304.

Gorno-Tempini, M. L., Hillis, A. E., Weintraub, S., Kertesz, A., Mendez, M., Cappa, S. F., et al. (2011). Classification of primary progressive aphasia and its variants. *Neurology* 76, 1006–1014.

Hansson, O., Janelidze, S., Hall, S., Magdalinou, N., Lees, A. J., Andreasson, U., et al. (2017). Blood-based NfL: a biomarker for differential diagnosis of parkinsonian disorder. *Neurology* 88, 930–937. doi: 10.1212/WNL.0000000000003680

Hardiman, O., van den Berg, L. H., and Kiernan, M. C. (2011). Clinical diagnosis and management of amyotrophic lateral sclerosis. *Nat. Rev. Neurol.* 7, 639–649.

Herrmann, H., and Aebi, U. (2016). Intermediate filaments: structure and assembly. *Cold Spring Harb. Perspect. Biol.* 8:a018242.

Jama, M., Millson, A., Miller, C. E., and Lyon, E. (2013). Triplet repeat primed PCR simplifies testing for Huntington disease. *J. Mol. Diagn.* 15, 255–262.

Jot, S. (2019). Parkinsonism with a hint of Huntington's from 29 CAG Repeats in HTT. *Brain Sci.* 9:245. doi: 10.3390/brainsci9100245

Khalil, M., Teunissen, C. E., Otto, M., Piehl, F., Sormani, M. P., Gattringer, T., et al. (2018). Neurofilaments as biomarkers in neurological disorders. *Nat. Rev. Neurol.* 14, 577–589.

Kuhle, J., Barro, C., Andreasson, U., Derfuss, T., Lindberg, R., Sandelius, A., et al. (2016). Comparison of three analytical platforms for quantification of the neurofilament light chain in blood samples: ELISA, electrochemiluminescence immunoassay and Simoa. *Clin. Chem. Lab. Med.* 54, 1655–1661. doi: 10.1515/cclm-2015-1195

Lee, J. K., Conrad, A., Epping, E., Mathews, K., Magnotta, V., Dawson, J. D., et al. (2018). Effect of trinucleotide repeats in the Huntington's gene on intelligence. *EBioMedicine* 31, 47–53. doi: 10.1016/j.ebiom.2018.03.031

Lee, J. K., Ding, Y., Conrad, A. L., Cattaneo, E., Epping, E., Mathews, K., et al. (2017). Sex-specific effects of the Huntington gene on normal neurodevelopment. *J. Neurosci. Res.* 95, 398–408.

Lee, M. K., and Cleveland, D. W. (1996). Neuronal intermediate filaments. *Annu. Rev. Neurosci.* 19, 187–217.

Leotti, V. B., de Vries, J. J., Oliveira, C. M., de Mattos, E. P., Te Meerman, G. J., Brunt, E. R., et al. (2021). CAG repeat size influences the progression rate of spinocerebellar ataxia type 3. *Ann. Neurol.* 89, 66–73. doi: 10.1002/ana.25919

Lewczuk, P., Ermann, N., Andreasson, U., Schultheis, C., Podhorna, J., Spitzer, P., et al. (2018). Plasma neurofilament light as a potential biomarker of neurodegeneration in Alzheimer's disease. *Alzheimers Res. Ther.* 10:71.

Li, D. W., Ren, H., Jeromin, A., Liu, M., Shen, D., Tai, H., et al. (2018). Diagnostic performance of neurofilaments in chinese patients with amyotrophic lateral sclerosis: a prospective study. *Front. Neurol.* 9:726. doi: 10.3389/fneur.2018.00726

Ljungqvist, J., Zetterberg, H., Mitsis, M., Blennow, K., and Skoglund, T. (2017). Serum neurofilament light protein as a marker for diffuse axonal injury: results from a case series study. *J. Neurotrauma* 34, 1124–1127. doi: 10.1089/neu.2016.4496

Lu, C. H., Macdonald-Wallis, C., Gray, E., Pearce, N., Petzold, A., Norgren, N., et al. (2015). Neurofilament light chain: a prognostic biomarker in amyotrophic lateral sclerosis. *Neurology* 84, 2247–2257. doi: 10.1212/WNL.0000000000001642

Menéndez-González, M., Clarimón, J., Rosas-Allende, I., Blázquez, M., San Martín, E. S., García-Fernández, C., et al. (2019). HTT gene intermediate alleles in neurodegeneration: evidence for association with Alzheimer's disease. *Neurobiol. Aging* 76, 215.e9–215.e14. doi: 10.1016/j.neurobiolaging.2018.11.014

Morfini, G. A., Bosco, D. A., Brown, H., Gatto, R., Kaminska, A., Song, Y., et al. (2013). Inhibition of fast axonal transport by pathogenic SOD1 involves activation of p38 MAP kinase. *PLoS One* 8:e65235. doi: 10.1371/journal.pone.0065235

Neary, D., Snowden, J. S., Gustafson, L., Passant, U., Stuss, D., Black, S., et al. (1998). Frontotemporal lobar degeneration: a consensus on clinical diagnostic criteria. *Neurology* 51, 1546–1554.

Paganoni, S., Macklin, E. A., Lee, A., Murphy, A., Chang, J., Zipf, A., et al. (2014). Diagnostic timelines and delays in diagnosing amyotrophic lateral sclerosis

(ALS). *Amyotroph. Lateral Scler. Frontotemporal. Degener.* 15, 453–456. doi: 10.3109/21678421.2014.903974

Poesen, K., and Van Damme, P. (2018). Diagnostic and prognostic performance of neurofilaments in ALS. *Front. Neurol.* 9:1167. doi: 10.3389/fneur.2018.01167

Reiber, H. (1994). Flow rate of cerebrospinal fluid (CSF)—a concept common to normal blood-CSF barrier function and to dysfunction in neurological diseases. *J. Neurol. Sci.* 122, 189–203.

Rissin, D. M., Kan, C. W., Campbell, T. G., Howes, S. C., Fournier, D. R., Song, L., et al. (2010). Single-molecule enzyme-linked immunosorbent assay detects serum proteins at subfemtomolar concentrations. *Nat. Biotechnol.* 28, 595–599. doi: 10.1038/nbt

Rojas, J. C., Wang, P., Staffaroni, A. M., Heller, C., Cobigo, Y., Wolf, A., et al. (2021). Plasma neurofilament light for prediction of disease progression in familial frontotemporal lobar degeneration. *Neurology* 96, e2296–e2312. doi: 10.1212/WNL.0000000000011848

Rossi, D., Volanti, P., Brambilla, L., Colletti, T., Spataro, R., and La Bella, V. (2018). CSF neurofilament proteins as diagnostic and prognostic biomarkers for amyotrophic lateral sclerosis. *J. Neurol.* 265, 510–521. doi: 10.1007/s00415-017-8730-6

Sampedro, F., Pérez-Pérez, J., Martínez-Horta, S., Pérez-González, R., Horta-Barba, A., Campolongo, A., et al. (2021). Cortical microstructural correlates of plasma neurofilament light chain in Huntington's disease. *Parkinsonism Relat. Disord.* 85, 91–94. doi: 10.1016/j.parkreldis.2021.03.008

Sánchez-Valle, R., Heslegrave, A., Foiani, M. S., Bosch, B., Antonell, A., Balasa, M., et al. (2018). Serum neurofilament light levels correlate with severity measures and neurodegeneration markers in autosomal dominant Alzheimer's disease. *Alzheimers Res. Ther.* 10:113. doi: 10.1186/s13195-018-0439-y

Savitt, D., and Jankovic, J. (2019). Clinical phenotype in carriers of intermediate alleles in the huntingtin gene. *J. Neurol. Sci.* 15, 57–61. doi: 10.1016/j.jns.2019.05.010

Schaefer, M. H., Wanker, E. E., and Andrade-Navarro, M. A. (2012). Evolution and function of CAG/polyglutamine repeats in protein-protein interaction networks. *Nucleic Acids Res.* 40, 4273–4287.

Schubert, S. M., Arendt, L. M., Zhou, W., Baig, S., Walter, S. R., Buchsbaum, R. J., et al. (2015). Ultra-sensitive protein detection via single molecule arrays towards early stage cancer monitoring. *Sci. Rep.* 5:11034. doi: 10.1038/srep11034

Shahim, P., Gren, M., Liman, V., Andreasson, U., Norgren, N., Tegner, Y., et al. (2016). Serum neurofilament light protein predicts clinical outcome in traumatic brain injury. *Sci. Rep.* 6:36791. doi: 10.1038/srep36791

Slow, E. J., Graham, R. K., Osmand, A. P., Devon, R. S., Lu, G., Deng, Y., et al. (2005). Absence of behavioral abnormalities and neurodegeneration in vivo despite widespread neuronal huntingtin inclusions. *Proc. Natl. Acad. Sci. U. S. A.* 102, 11402–11407. doi: 10.1073/pnas.0503634102

Song, L., Zhao, M., Duffy, D. C., Hansen, J., Shields, K., Wungjiranirun, M., et al. (2015). Development and validation of digital enzyme-linked immunosorbent assays for ultrasensitive detection and quantification of clostridium difficile toxins in stool. *J. Clin. Microbiol.* 53, 3204–3212. doi: 10.1128/JCM.01334-15

Sproviero, W., Shatunov, A., Stahl, D., Shoai, M., van Rheenen, W., Jones, A. R., et al. (2017). ATXN2 trinucleotide repeat length correlates with risk of ALS. *Neurobiol. Aging* 51, 178.e1–178.e9.

Steinacker, P., Feneberg, E., Weishaupt, J., Brettschneider, J., Tumani, H., Andersen, P. M., et al. (2016). Neurofilaments in the diagnosis of motoneuron diseases: a prospective study on 455 patients. *J. Neurol. Neurosurg. Psychiatry* 87, 12–20. doi: 10.1136/jnnp-2015-311387

Taylor, J. P., Brown, R. H., and Cleveland, D. W. (2016). Decoding ALS: from genes to mechanism. *Nature* 539, 197–206.

Tortelli, R., Ruggieri, M., Cortese, R., D'Errico, E., Capozzo, R., Leo, A., et al. (2012). Elevated cerebrospinal fluid neurofilament light levels in patients with amyotrophic lateral sclerosis: a possible marker of disease severity and progression. *Eur. J. Neurol.* 19, 1561–1567. doi: 10.1111/j.1468-1331.2012.03777.x

van Es, M. A., Hardiman, O., Chio, A., Al-Chalabi, A., Pasterkamp, R. J., Veldink, J. H., et al. (2017). Amyotrophic lateral sclerosis. *Lancet* 390, 2084–2098. doi: 10.1016/S0140-6736(17)31287-4

Verde, F., Steinacker, P., Weishaupt, J. H., Kassubek, J., Oeckl, P., Halbgebauer, S., et al. (2019). Neurofilament light chain in serum for the diagnosis of amyotrophic lateral sclerosis. *J. Neurol. Neurosurg. Psychiatry* 90, 157–164. doi: 10.1136/jnnp-2018-318704

Vonsattel, J. P., and DiFiglia, M. (1998). Huntington disease. *J. Neuropathol. Exp. Neurol.* 57, 369–384.

Xu, Z., Henderson, R. D., David, M., and McCombe, P. A. (2016). Neurofilaments as biomarkers for amyotrophic lateral sclerosis: a systematic review and meta-analysis. *PLoS One* 11:e0164625. doi: 10.1371/journal.pone.0164625

Yousefian-Jazi, A., Seol, Y., Kim, J., Ryu, H. L., Lee, J., and Ryu, H. (2020). Pathogenic genome signatures that damage motor neurons in amyotrophic lateral sclerosis. *Cells* 9:2687. doi: 10.3390/cells9122687

Zuchner, T., and Brundin, P. (2008). Mutant huntingtin can paradoxically protect neurons from death. *Cell Death Differ.* 15, 435–442. doi: 10.1038/sj.cdd.4402261

Conflict of Interest: The authors declare that the research was conducted in the absence of any commercial or financial relationships that could be construed as a potential conflict of interest.

Publisher's Note: All claims expressed in this article are solely those of the authors and do not necessarily represent those of their affiliated organizations, or those of the publisher, the editors and the reviewers. Any product that may be evaluated in this article, or claim that may be made by its manufacturer, is not guaranteed or endorsed by the publisher.

frontiers in Aging Neuroscience

ORIGINAL RESEARCH
published: 08 September 2021
doi: 10.3389/fnagi.2021.689939

Correlation of Decreased Serum Pituitary Adenylate Cyclase-Activating Polypeptide and Vasoactive Intestinal Peptide Levels With Non-motor Symptoms in Patients With Parkinson's Disease

Shiyu Hu[1,2], Shen Huang[1,3], Jianjun Ma[1,2,3], Dongsheng Li[1,2,3], Zhenxiang Zhao[1,2,3], Jinhua Zheng[1,2,3], Mingjian Li[1,2], Zhidong Wang[1,3], Wenhua Sun[1,3] and Xiaoxue Shi[1,3]*

[1] Department of Neurology, Henan Provincial People's Hospital, Zhengzhou, China, [2] Department of Neurology, People's Hospital of Henan University, Zhengzhou, China, [3] Department of Neurology, People's Hospital of Zhengzhou University, Zhengzhou, China

Objective: Pituitary adenylate-cyclase activating polypeptide (PACAP) and vasoactive intestinal peptide (VIP) are two neuropeptides that exhibit anti-inflammatory and neuroprotective properties, modulating the production of cytokines and chemokines, and the behavior of immune cells. However, the relationship between PACAP and VIP levels and Parkinson's disease (PD) are not clear. The aim of the current study was to evaluate serum PACAP and VIP levels in PD patients and to analysis the correlation between neuropeptide levels and non-motor symptoms.

Methods: In this cross-sectional study, we enrolled 72 patients with idiopathic PD and 71 healthy volunteers. Serum PACAP and VIP levels were measured using an enzyme-linked immunosorbent assay (ELISA) kit. Non-motor symptoms were assessed with the Non-Motor Symptoms Scale (NMSS) for PD, including total and single-item scores.

Results: The serum PACAP levels of PD patients were significantly lower than those of healthy controls [(76.02 ± 43.78) pg/ml vs. (154.96 ± 76.54) pg/ml, $P < 0.001$]; and the serum VIP levels of PD patients were also significantly lower than those of healthy controls [(109.56 ± 15.39) pg/ml vs. (136.46 ± 24.16) pg/ml, $P < 0.001$]. PACAP levels were inversely correlated only with the score on NMSS item five, assessing Attention/memory ($r = -0.276$, $P < 0.05$) and lower serum PACAP levels were detected in the cognitive dysfunction subgroup than in the cognitively intact subgroup [(61.87 ± 32.66) pg/ml vs. (84.51 ± 47.59) pg/ml, $P < 0.05$]; meanwhile, VIP levels were inversely correlated with the NMSS total score ($r = -0.285$, $P < 0.05$) and the single-item scores for item one, assessing Cardiovascular ($r = -0.257$, $P < 0.05$) and item three, assessing Mood/cognition ($r = -0.373$, $P < 0.05$), and lower serum VIP levels were detected in the anxiety subgroup and depression subgroup than in the non-anxiety subgroup and non-depression subgroup, respectively [(107.45 ± 15.40) pg/ml vs. (116.41 ± 13.67) pg/ml, $P < 0.05$]; [(104.45 ± 15.26) pg/ml vs. (113.43 ± 14.52) pg/ml, $P < 0.05$].

OPEN ACCESS

Edited by:
Thomas K. Karikari, University of Gothenburg, Sweden

Reviewed by:
Jifeng Guo, Central South University, China
Jairo Ramos Temerozo, Oswaldo Cruz Foundation (Fiocruz), Brazil
Corey Smith, Case Western Reserve University, United States

***Correspondence:**
Jianjun Ma
majj1124@163.com

Received: *01 April 2021*
Accepted: *16 August 2021*
Published: *08 September 2021*

Citation:
Hu S, Huang S, Ma J, Li D, Zhao Z, Zheng J, Li M, Wang Z, Sun W and Shi X (2021) Correlation of Decreased Serum Pituitary Adenylate Cyclase-Activating Polypeptide and Vasoactive Intestinal Peptide Levels With Non-motor Symptoms in Patients With Parkinson's Disease. Front. Aging Neurosci. 13:689939. doi: 10.3389/fnagi.2021.689939

Conclusion: The serum PACAP and VIP levels of PD patients were significantly lower than those of healthy controls. The non-motor symptoms significantly negatively correlated with serum PACAP level was cognitive dysfunction, while mood disorder was significantly correlated with serum VIP level.

Keywords: Parkinson's disease, pituitary adenylate cyclase-activating polypeptide, vasoactive Intestinal peptide, non-motor symptoms, cross-sectional study

INTRODUCTION

Parkinson's disease (PD) is a chronic neurodegenerative disorder involving the loss of dopaminergic neurons and the formation of Lewy pathology [mainly a-synuclein (a-syn)] in the substantia nigra (Qian et al., 2020). Its typical characteristics include motor symptoms such as bradykinesia, tremor at rest, and rigidity, which commonly present along with gait impairment. At the same time, non-motor symptoms such as hyposmia, constipation, pain, cognitive dysfunction, sleep, and mood disturbances often occur as well (Garcia-Ruiz et al., 2014; Lotankar et al., 2017). Although the pathogenesis of PD is not clear, neuroinflammation, in particular glia activation, has been identified as key factors in the progression of the disease (Gelders et al., 2018; Hall et al., 2018). In neuropathological studies, activated microglia has been found close to dopaminergic neurons in PD patients and cytokines have been found in higher levels in the striatum and substantia nigra of PD brains (Garcia-Esparcia et al., 2014). Anti-inflammatory and neuroprotective effects of neuropeptides, such as pituitary adenylate cyclase-activating polypeptide (PACAP) and vasoactive intestinal peptide (VIP), have been widely demonstrated in PD models *in vivo* and *in vitro* (Joers et al., 2017; Campos-Acuna et al., 2019; Panicker et al., 2019). PACAP and VIP are two neuropeptides that are structurally related, which have three known receptors, VPAC1, VPAC2, and PAC1, that belong to the G-protein-coupled receptor (GPCR) family. The VPAC1/2 receptors recognize VIP with high affinity, while PAC1 receptor binds to PACAP with higher affinity than VIP (Moody et al., 2011). Data from experimental studies have revealed that VIP and PACAP receptors are widely distributed in the nervous, endocrine, and immune systems among others (Moody et al., 2011; Hirabayashi et al., 2018). They exhibit anti-inflammatory and neuroprotective properties, modulating the production of cytokines and chemokines, and the behavior of immune cells (de Souza et al., 2020). Furthermore, studies in cellular models revealed that PACAP and VIP Protect against Aβ-mediated toxicity in PC12 cells (Onoue et al., 2002). In animal models of PD, VIP Prevents oxidative stress and apoptosis in 6-hydroxydopamine (6-OHDA)-lesioned rats (Tuncel et al., 2012) and PACAP improves learning and memory in three different paradigms of the water-maze task in MPTP-injected mice (Onoue et al., 2002). More importantly, PACAP and VIP have been detected in plasma (Baranowska-Bik et al., 2013; Han et al., 2015; Ma et al., 2015; Jiang et al., 2016), serum (Cernuda-Morollon et al., 2016), and cerebrospinal fluid (CSF) (Gjerris et al., 1984; Baranowska-Bik et al., 2013; Han et al., 2014) of some diseases in humans, such as multiple sclerosis, Alzheimer disease, cerebral hemorrhage, migraineur, atypical depression, and et al. However, there is a dearth of data on the levels of these neuropeptides in PD patients, and there are no previous studies exploring the potential relationship between serum PACAP and VIP levels and non-motor symptoms of PD. Therefore, the purposes of this study were (1) to evaluate the levels of PACAP and VIP in the serum in PD patients and healthy controls, and (2) to investigate whether there is any correlation between neuropeptide levels and non-motor symptoms in patients with PD.

MATERIALS AND METHODS

Participants

Patients with PD from December 2018 to October 2020 at the clinic of the Henan Provincial People's Hospital, Henan Province, China. PD patients were all clinically diagnosed according to the International Parkinson and Movement Disorder Society (MDS) Clinical Diagnostic Criteria for the diagnosis of PD (Postuma et al., 2015). The exclusion criteria were as follows: (1) patients diagnosed with neurological disease except PD (Alzheimer disease, epilepsy, cerebrovascular disease, severe head trauma, etc.); (2) patients who might have been pregnant or breastfeeding; (3) patients who might have a history of headache; and (4) patients who had severe complications. Healthy, age- and gender-matched volunteer controls were recruited at the same time from the health examination center. A total of 71 healthy volunteers participated in this study. The exclusion criteria were applied to both patients and controls. All subjects were made aware of the contents of the study, and a written informed consent document was obtained. The research protocol was approved by the Ethics Committee of Henan Provincial People's Hospital of Medical Science.

Clinical Assessment

For all included participants, demographic data and medical history were recorded. Motor symptom severity was evaluated in terms of Unified Parkinson's Disease Rating Scale (UPDRS) part III motor scores and Hoehn–Yahr (H-Y) stages. Non-motor symptoms were assessed with the Non-Motor Symptoms Scale (NMSS) (Chaudhuri et al., 2007) for PD, including total and single-item scores. Cognition was examined with the Mini-Mental State Examination (MMSE), adjusted for age and educational level. Mood symptoms were measured with the 14-item Hamilton Anxiety Rating Scale (HAMA-14) and the 17-item Hamilton Depression Rating Scale (HAMD-17). We have partitioned our data into two categories: no anxiety symptomatology ($0 \leq$ HAMA-14 ≤ 6) and had anxiety

symptomatology (HAMA-14 $\geq$ 7). A higher HAMA-14 score indicates a higher level of anxiety. The optimal threshold to utilize for maximum discrimination between depressed and non-depressed PD patients was reached at a cut-off score of 13/14 for the HAMD-17 (Huang et al., 2020). Therefore, we have divided our data into two categories:little to no depression symptomatology (0 $\leq$ HAMD-17 $\leq$ 13) and mild to marked depression symptomatology (HAMD-17 $\geq$ 14). A higher HAMD-17 score indicates a higher level of depression. The personal levodopa equivalent daily dose (LEDD) was finally calculated for each PD patient. All scale assessments were completed once in the patient's off period.

Blood Sample Collection

We collected peripheral blood (5 mL) from each participant into tubes without anticoagulant between 8:00 and 9:00 AM prior to clinical assessment (12 h of fasting). Samples were allowed to clot at room temperature for 30 min before centrifugation for 15 min at 1000 $\times$ *g*. Serum samples were then divided into several aliquots and immediately stored at −80°C until assay.

Measurement of Serum PACAP and VIP

Serum PACAP levels were measured using an enzyme-linked immunosorbent assay (ELISA) kit (HUFI01234; ELISA Genie, Dublin, Ireland). The detection range of this kit is 7.8–500 pg/ml, with a sensitivity of 4.688 pg/ml, and the intra- and inter-assay variability were <8 and <10%, respectively. Serum VIP levels were measured using an ELISA kit (EK-064-16; Phoenix Pharmaceuticals, Burlingame, CA, United States). The detection range of this kit is 0–25 ng/ml, with a sensitivity of 0.08 pg/ml, and the intra- and interassay variability were <10 and <15%, respectively. Samples were analyzed in duplicate on the same plate in accordance with the manufactures' instructions. PACAP and VIP levels were in all cases above the limit of detection.

Statistical Analysis

The Kolmogorov–Smirnov test and the Levene test were used to check the data for normality and homogeneity of variances. Numerical variables are expressed as the mean ± SD. Data that did not have a normal distribution are expressed as medians (interquartile ranges). Nominal variables are expressed as percentages. Two groups of normally distributed data were compared by an independent-sample Student's *t*-test. Multiple groups of data consistent a with normal distribution and homogeneity of variance were compared by one-way analysis of variance, and a *post hoc* least significant difference (LSD) test was used to further compare differences. For variables that violated the assumptions of normality or homoscedasticity, the groups were compared with the non-parametric Mann–Whitney U test (for 2 groups) or Kruskal–Wallis test (for >2 groups). Pearson's (or Spearman's) correlation analysis was conducted according to whether the variables were normally distributed. Receiver operating curve (ROC) analysis and cut-off points calculation were performed to estimate diagnostic sensitivity (Se) and specificity (Sp) values of biomarkers. Statistical analysis was performed using SPSS version 22.0 (IBM Corporation, Armonk, NY, United States) and GraphPad Prism 7 (GraphPad Software, Inc., San Diego, CA, United States). *P*-value <0.05 was considered statistically significant.

RESULTS

Clinical Characteristics

In this study, 72 PD patients (mean age 64.75 ± 11.75 years, 52.8% male, and 47.2% female) and 71 controls (mean age 62.08 ± 8.69 years, 52.1% male, and 47.9% female) were enrolled from the Henan Provincial People's Hospital between December 2018 and October 2020. In the PD group, the median number of years of education was 8, and the median duration of disease was 5 years. According to the levodopa equivalent conversion formula, the median LEDD was 337.5 mg, and the average score of the third part of the UPDRS was 45.88 scores (**Table 1**). There were no significant differences in gender or age between PD patients and healthy controls ($P > 0.05$).

Serum PACAP and VIP Levels in PD Patients and in Healthy Controls

Serum PACAP levels were significantly lower in PD patients than in healthy controls [(76.02 ± 43.78) pg/ml vs. (154.96 ± 76.54)

TABLE 1 | Clinical characteristics and serum PACAP and VIP levels of participants in individual groups in the current study.

Characteristics	PD (*n* = 72)	Controls (*n* = 71)	t/χ^2	*P*-Value
Age, y	64.75 ± 11.75	62.08 ± 8.69	1.540	0.126
Male, %	38 (52.8%)	37 (52.1%)	0.006	0.937
PACAP levels, pg/ml	76.02 ± 43.78	154.96 ± 76.54	7.583	< 0.001
VIP levels, pg/ml	109.56 ± 15.39	136.46 ± 24.16	7.950	< 0.001
Disease duration, y	5 (2,7)	NA	NA	NA
Education, y	8 (5,10.25)	NA	NA	NA
UPDRS III score	45.88 ± 18.96	NA	NA	NA
H-Y stage	2 (2,3)	NA	NA	NA
LEDD, mg/day	337.5 (200,500)	NA	NA	NA
MMSE score	25 (20.75,27)	NA	NA	NA

Mean ± standard deviation or median (interquartile range). PACAP, Pituitary Adenylate Cyclase-activating Polypeptide; VIP, Vasoactive Intestinal Peptide; UPDRS, Unified Parkinson's Disease Rating Scale; H-Y stage, Hoehn–Yahr stage; LEDD, levodopa equivalent daily dose; MMSE, Mini-Mental State Examination; NA, not applicable.

pg/ml, $P < 0.001$] and serum VIP levels were significantly lower in PD patients than in the healthy controls [(109.56 ± 15.39) pg/ml vs. (136.46 ± 24.16) pg/ml, $P < 0.001$]. The differences were significant (**Figure 1**).

Correlation Between Serum PACAP and VIP Levels

We found a positive correlation between serum levels of PACAP and VIP ($r = 0.478$, $P < 0.001$). When analyzed, respectively, there was a positive correlation between serum levels of PACAP and VIP in the healthy controls ($r = 0.288$, $P < 0.05$), and there was a positive correlation in the PD Patients ($r = 0.261$, $P < 0.05$) (**Figure 2**).

PACAP and VIP Levels in PD Patients at Different H-Y Stages

According to the H-Y stage, PD patients were divided into stages I and II as early-stage ($n = 39$), stage III as medium-stage ($n = 17$), and stages IV and V as advanced-stage ($n = 16$). Compared to PD patients with early-stage disease, PACAP and VIP levels in the medium-stage and advanced-stage PD patients were lower, while there were no significant differences in PACAP ($\chi 2 = 4.828$; df = 2; and $P > 0.05$) and VIP ($\chi^2 = 4.158$; df = 2; and $P > 0.05$) levels across the three groups (**Figure 3**).

Correlation of Serum PACAP and VIP Levels With Disease Duration and Disease Severity in PD Patients

We found a negative correlation between serum PACAP levels and disease duration ($r = -0.257$, $P < 0.05$), and a negative correlation between serum VIP levels and UPDRS part III score ($r = -0.256$, $P < 0.05$) (**Figure 4**). In addition, there was no significant correlation between serum PACAP or VIP levels and LEDD.

Receiver Operating Curve Analysis of PACAP and VIP Diagnosis of PD

Diagnostic accuracy was determined in PD patients and healthy controls by the ROC curve analysis. PACAP (AUC = 0.843; $P < 0.001$, 95% CI 0.781-0.906), at the cut-off value of 106.54 pg/ml showed 74.6% Se and 80.6% Sp. VIP (AUC = 0.838; $p < 0.001$, 95% CI 0.775-0.901), at the cut-off value of 114.90 pg/ml showed 84.5% Se and 70.8% Sp (**Figure 5**).

Correlation Analysis of Non-motor Symptoms and Serum PACAP and VIP Levels in PD Patients

Correlation analysis revealed that PACAP levels were inversely correlated only with the score for NMSS item five, assessing Attention/memory ($r = -0.276$, $P < 0.05$). Additionally, VIP levels were inversely correlated with the NMSS total score ($r = -0.285$, $P < 0.05$) as well as the single-item scores for items one, assessing Cardiovascular ($r = -0.257$, $P < 0.05$) and three, assessing Mood/cognition ($r = -0.373$, $P < 0.05$). The remaining non-motor symptoms were not associated with serum PACAP or VIP levels ($P \geq 0.05$) (**Table 2**).

Next, we used the significantly correlated non-motor symptoms as a grouping criterion to evaluate differences in PACAP and VIP levels between the two subgroups. This study included 72 patients with PD, including 27 with cognitive dysfunction (37.5%) (12 with 1–6 years of education, MMSE score <20, 10 with 7–9 years of education, MMSE score <24, and 5 with ≥10 years of education, MMSE score <26). Moreover, 55 with HAMA-14 score ≥7 who had anxiety (76.4%) and 30 with HAMA-17 score ≥14 who had depression (43.1%), 44 with NMSS item one score > 0 who had cardiovascular symptom (61.1%).

This further analysis found that lower serum PACAP levels were detected in the cognitive dysfunction subgroup than in the cognitively intact subgroup [(61.87 ± 32.66) pg/ml vs. (84.51 ± 47.59) pg/ml, $P < 0.05$], while serum VIP levels in the cognitive dysfunction subgroup were lower than in the cognitively intact subgroup [(108.04 ± 14.79) pg/ml vs. (110.48 ± 15.85) pg/ml], there was no statistically significant difference ($P > 0.05$). Additionally, we found that lower serum VIP levels were detected in the anxiety subgroup and depression subgroup than in the non-anxiety subgroup and non-depression subgroup [(107.45 ± 15.40) pg/ml vs. (116.41 ± 13.67) pg/ml, $P < 0.05$]; [(104.45 ± 15.26) pg/ml vs. (113.43 ± 14.52) pg/ml, $P < 0.05$]. However, we found no statistically significant difference in VIP levels between the cardiovascular symptom subgroup and the negative cardiovascular symptom subgroup in PD patients. The values are presented as the mean and standard deviation (**Figure 6**).

DISCUSSION

In recent years, some progress has been made in studies on the neuroprotective effects of some newly-discovered brain-gut peptides, such as pituitary adenylate cyclase activating polypeptide, vasoactive intestinal polypeptide and et al. PACAP is a neuropeptide isolated from sheep hypothalamus, which has potential to increase adenylate cyclase activity in the pituitary gland (Miyata et al., 1989) and VIP, which has potent and diverse biological action, was isolated from the small intestine of the hog. It is now completely clear that PACAP is packaged and released throughout the peripheral autonomic nervous system. In the sympathetic nervous system, it acts as a primary neurotransmitter and in the parasympathetic it appears to play a neuromodulatory role. PACAP is released at significant levels throughout the periphery upon stressor activation. Likewise, VIP is also released throughout the peripheral nervous system, including in the gut and other organs. The role of PACAP and VIP and in neurodegenerative murine models has been widely explored, particularly in PD models, which exhibits anti-inflammatory and neuroprotective effects. Therefore, we measured the serum levels of PACAP and VIP in PD patients and analyze the relationship with non-motor symptoms for the first time.

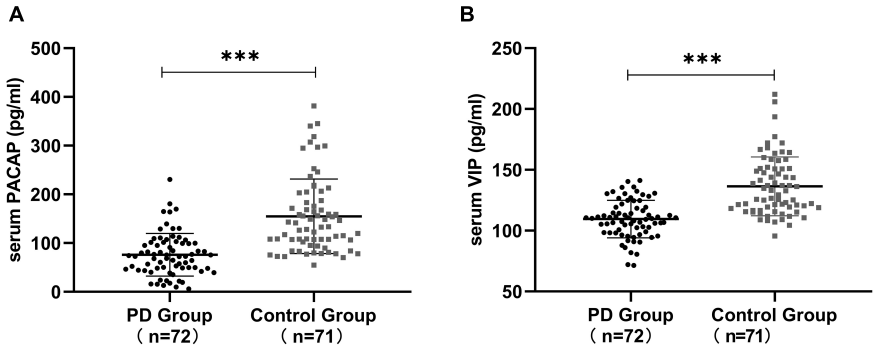

FIGURE 1 | Serum PACAP and VIP levels in Parkinson's disease (PD) patients and in healthy controls. **(A)** Lower serum PACAP levels were detected in PD patients than in healthy controls. **(B)** Lower serum VIP levels were detected in PD patients than in healthy controls. Values are presented as the mean ± standard deviation. ***$P < 0.001$. PACAP, pituitary adenylate cyclase-activating polypeptide; VIP, vasoactive intestinal peptide.

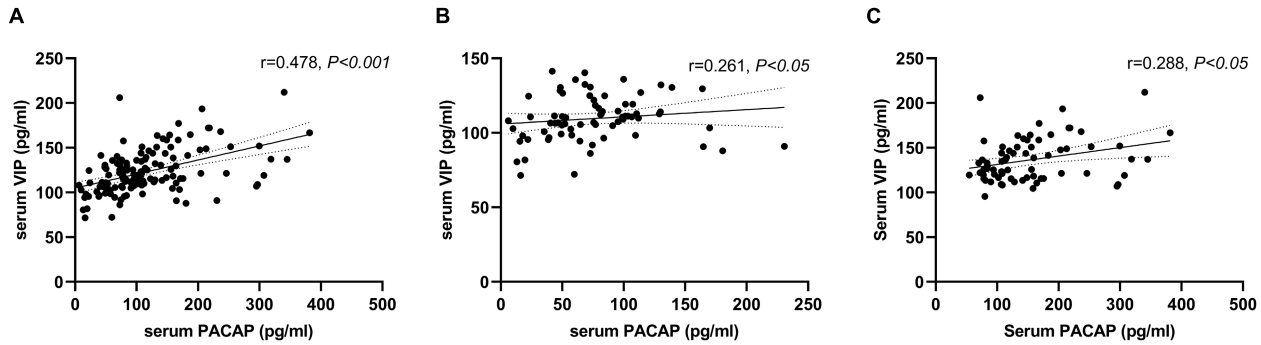

FIGURE 2 | Correlation between serum pituitary adenylate-cyclase activating polypeptide (PACAP) and vasoactive intestinal peptide (VIP) levels. **(A)** A positive correlation between serum levels of PACAP and VIP in the total groups (Pearson's correlation coefficient $r = 0.478$, $P < 0.001$, and $n = 143$). **(B)** A positive correlation between serum levels of PACAP and VIP in the PD group (Pearson's correlation coefficient $r = 0.261$, $P < 0.05$, and $n = 72$). **(C)** A positive correlation between serum levels of PACAP and VIP in the healthy control group (Pearson's correlation coefficient $r = 0.288$, $P < 0.05$, and $n = 71$).

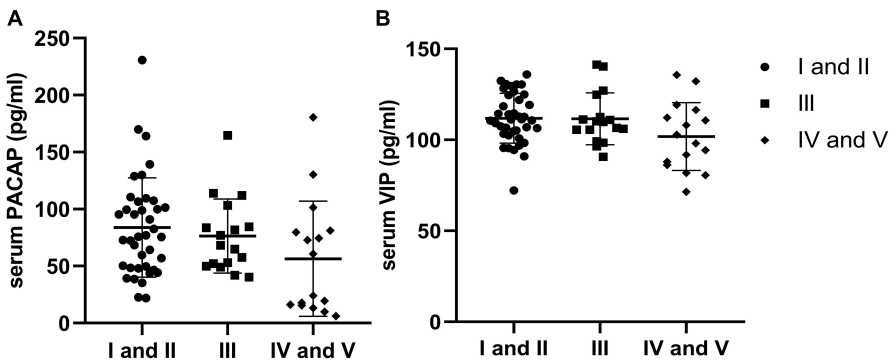

FIGURE 3 | Distribution of serum levels of pituitary adenylate-cyclase activating polypeptide (PACAP) and vasoactive intestinal peptide (VIP) by Hoehn–Yahr (H-Y) stage. **(A)** There were no significant differences in the distribution of serum PACAP levels by H-Y stage in Parkinson's disease (PD) patients ($P > 0.05$). **(B)** There were no significant differences in the distribution of serum VIP levels by H-Y stage in PD patients ($P > 0.05$).

To our knowledge, there is only a single report describing PACAP levels in the CSF of PD patients. Han and colleagues included only eight PD patients and found that PACAP levels were not significantly different in the CSF between the PD group and the healthy control group (Han et al., 2014), while no study has been found to measure VIP levels in PD patients. Of interest, our study first found a reduction in peripheral PACAP and VIP levels in PD patients. In addition, after H-Y classification, PACAP and VIP levels were significantly lower in PD patients with early, medium, and advanced stages than in healthy controls, and were

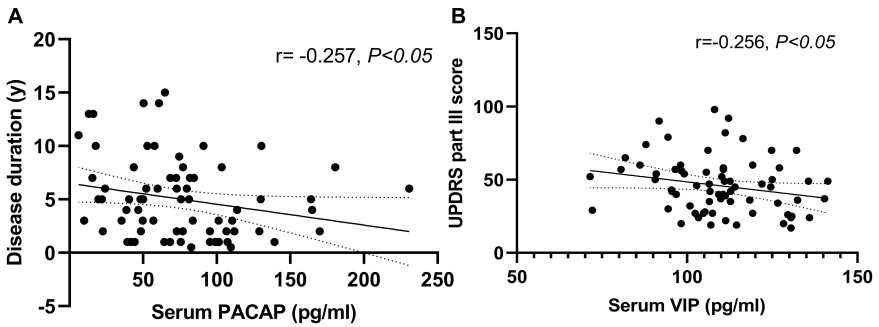

FIGURE 4 | Correlation of serum pituitary adenylate-cyclase activating polypeptide (PACAP) and vasoactive intestinal peptide (VIP) levels with disease duration and disease severity in PD patients. **(A)** Serum PACAP levels were negatively correlated with disease duration (Spearman's correlation coefficient $r = –0.257$, $P < 0.05$, and $n = 72$). **(B)** Serum VIP levels were negatively correlated with UPDRS part III scores (Pearson's correlation coefficient $r = –0.256$, $P < 0.05$, and $n = 72$).

gradually reduced with progression of the disease. We consider the following reasons for the observed decrease in serum PACAP and VIP levels in PD patients. First, PACAP is discovered as a hypothalamic peptide (Miyata et al., 1989). Moreover, a recent study found that the precursor of PACAP mRNA in the rat brain is present in different brain areas, especially the highest concentrations of PACAP in the hypothalamic area. As PD progresses, the hypothalamus shows varying degrees of damage (Jellinger, 2002). Collectively, endogenous PACAP levels may be reduced in the serum of PD patients. Second, PACAP and VIP act as anti-inflammatory cytokines and neuroprotective molecules, and the levels may be slightly elevated at the early stage of the disease to protect dopaminergic neurons from degeneration, but when the endogenesis of anti-inflammatory cytokines and neuropeptides such as PACAP or VIP is overwhelmed by an excessive inflammatory response, microglia initiate neuronal death and drive the progressive nature of PD (Wu et al., 2014). Therefore, the above analysis may explain the decrease in peripheral levels. Additionally, (Bukovics et al., 2014) found that plasma and CSF levels of PACAP display parallel patterns in traumatic brain injury survivors. Therefore, it is suggested that PACAP in peripheral blood is derived from the central nervous system (Jiang et al., 2016) and may easily be due to injury-activated release of peripheral PACAP into the serum. The same scenario is also likely for VIP. VIP is released centrally, but has many peripheral sources as well. Of course, further studies are needed to determine whether mRNA expression of PACAP and VIP in the CSF and periphery blood are decreased in PD models and patients.

This study shows that patients with PD have a significant negative correlation between PACAP levels and disease duration, suggesting that decreased serum PACAP levels may play an important role in the progression of this age-related disease, consistent with previous findings (Feher et al., 2018). Additionally, we found a negative correlation between serum VIP levels and UPDRS III scores. Not surprisingly, we found a positive correlation between serum levels of VIP and PACAP regardless of whether they were grouped. Previous studies (Hirabayashi et al., 2018) found that the structures of these two neuropeptides have high homology (∼68% amino acid identity) and exert their action through two common receptors, VPAC1 and VPAC2, while PACAP has a wider range of influence due to an additional specific receptor, PAC1. Thus, the mechanisms of the neuroprotective effects of PACAP and VIP, as well as the signaling pathways, are almost identical (Dong et al., 2019) and our study found that there was a positive correlation between PACAP and VIP levels in the serum. Additionally, serum PACAP and VIP levels showed moderate Se and Sp in differentiating PD patients from controls, which provide a basis for the diagnosis of PD.

Subsequently, we classified PD non-motor symptoms based on the NMSS and analyzed the correlation between non-motor symptoms and PACAP and VIP levels in PD patients. We found that the serum PACAP levels of PD were mainly correlated with scores for item five, assessing Attention/memory. In particular, we found significant differences in the PACAP levels between the cognitive dysfunction subgroup and the cognitively intact subgroup. Therefore, it is speculated that the occurrence of cognitive dysfunction in PD patients has a certain relationship with the reduction of PACAP levels. Clinically, although PD has long been known to be characterized by motor disturbances, cognitive dysfunction is also common in patients and is often manifested as dementia, deficits in learning and attention, or impaired executive function among others (Soles-Tarres et al., 2020). This disorder is often mediated by the extracellular or intracellular accumulation of protein aggregates that disrupt synaptic plasticity, leading to neuronal dysfunction and/or neuronal death. Several mechanisms have been involved in neuronal plasticity disturbance and neuronal cell death, such as inflammation, excitotoxicity, oxidative stress, and neurotrophic deprivation. Although human studies of PACAP are in the preliminary phase, animal studies have shown beneficial effects of PACAP on cognition and memory. Some data in animal models show that the lack of PACAP is associated with cognitive decline. Indeed, PACAP deficient mice display impaired recognition memory (Shibasaki et al., 2015). Moreover, animal studies have shown that an exogenous increase in PACAP may rescue 6-OHDA-induced degenerating dopamine neurons (Reglodi et al., 2004). Deguil et al. (2010) found that pretreatment with PACAP by intravenous injections can partially protect against the loss

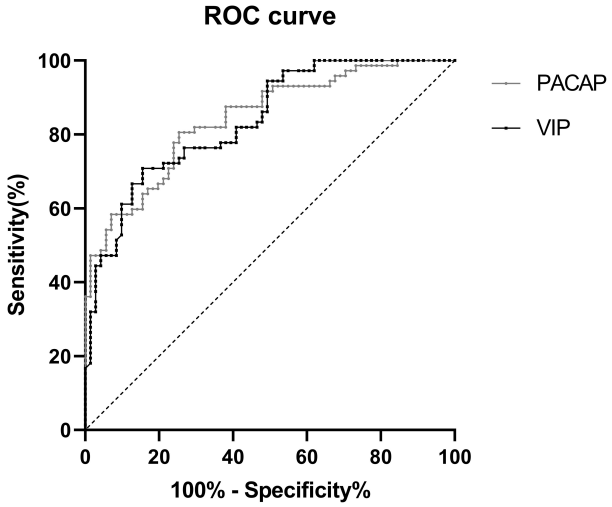

FIGURE 5 | ROC curve for serum PACAP and VIP levels comparing PD group and healthy control group. ROC curve, receiver operating characteristic curve; PD, Parkinson' s disease; AUC, area under the curve; CI, confidence interval.

	AUC	95% CI	*P*-Value	Cut-off value (pg/ml)	Sensitivity	Specificity
PACAP	0.843	0.781–0.906	<0.001	106.54	74.6%	80.6%
VIP	0.838	0.775–0.901	<0.001	114.90	84.5%	70.8%

of TH-positive neurons and improve learning and memory in MPTP-injected mice. Based on these findings, we could infer that the decrease in PACAP levels may be one of the causes of related learning and memory deficits.

We also found that the serum VIP levels of PD and some non-motor symptoms, such as cardiovascular symptoms and mood/cognition disorders, had a certain correlation, the most important being mood/cognition disorders. The remaining non-motor symptoms have not yet been found to be relevant or different. Further analysis found that serum VIP levels were not significantly different between the negative cardiovascular symptom subgroup and the cardiovascular symptom subgroup, whereas lower serum VIP levels were detected in the anxiety subgroup and depression subgroup than in the non-anxiety subgroup and non-depression subgroup. Therefore, it is speculated that the occurrence of mood disorders in PD patients has a certain relationship with internal VIP levels. Mood disorders are now considered among the main non-motor symptoms of PD and have a serious impact on quality of life (Rieu et al., 2016). Among these symptoms, the prevalence of depression ranges from 20 to 40%, and the prevalence of anxiety varies from 8 to 25% (Aarsland et al., 2009; Gallagher and Schrag, 2012). Some studies have found that symptoms of depression and anxiety are more common in patients with PD than in the general population and are related to signs of inflammation (Lindqvist et al., 2012). Decreased VIP levels have been found in patients with major depression, which has also been found in PD patients. Moreover, the lower VIP levels are consistent with reduced parasympathetic tone that has been reported in depression (Gjerris et al., 1984), considering VIP levels probably involved in the pathobiology of affective disorders. A study by Lindqvist et al. (2012) found that depression scores and anxiety scores are significantly associated with pro-inflammatory cytokines. Because of the anti-inflammatory effects of VIP, we speculate that the high VIP content in PD patients who are not accompanied by depression and anxiety symptoms may reduce the release of pro-inflammatory mediators by activated microglia through these effects, thereby reducing the occurrence of mood disorders. In addition, it was found in a 6-OHDA-induced PD rat model that intraperitoneal injection of VIP can increase the number of 5-hydroxytryptamine (5-HT)-positive cells and the relative expression of mRNA in the dorsal raphe nucleus (DRN) and reduce the expression of depression-related neuroendocrine hormones (Wang et al., 2015). A large number of studies have confirmed that the decreased release of the monoamine neurotransmitter serotonin 5-HT in the brain may be one of the causes of clinical depressive symptoms (Gavioli and Calo, 2013), and DRN is the nucleus with the largest distribution of 5-HT neurons and is closely related to stress-related mental disorders such as anxiety and depression (Vasudeva et al., 2011). Therefore, we infer that VIP may have a potential therapeutic effect on patients with PD associated with mood disorders, which also provides a new research direction for the treatment of neurodegenerative diseases with mood disorders. In addition, VIP levels are reduced in PD, and these patients may have an increased risk of cardiovascular disease. Therefore, we can infer that VIP can reduce the incidence of cardiovascular adverse events and reduce cardiovascular symptoms to a certain extent by inhibiting the release of pro-inflammatory factors.

Our study had several limitations. First, patients were collected from a single clinical center. Hence, multicentre studies with more patients will be required to further investigate the changes in serum PACAP and VIP levels. Second, whether peripheral PACAP and VIP levels reflect central-related material activity

TABLE 2 | Correlation analysis of non-motor symptoms and serum PACAP and VIP levels in PD patients.

	Medians (quartile ranges)	PACAP		VIP	
		Spearman rank	*P*	Spearman rank	*P*
NMSS total score	39.50 (24.25,63.25)	−0.086	0.474	−0.285*	0.015
NMSS component score					
Cardiovascular	1.00 (0,4)	−0.163	0.170	−0.257*	0.029
Sleep/fatigue	6.00 (3,10)	−0.012	0.921	−0.159	0.181
Mood/cognition	7.00 (3,20)	0.028	0.816	−0.373**	0.001
Perceptual Problems/hallucinations	0.00 (0,1)	0.076	0.524	−0.062	0.606
Attention/memory	2.00 (2,8)	−0.276*	0.019	−0.137	0.252
Gastrointestinal tract	6.00 (2,8.75)	−0.035	0.769	−0.095	0.427
Urinary	5.50 (2,12)	−0.054	0.654	−0.003	0.980
Sexual function	0.00 (0,0)	0.011	0.930	0.107	0.373
Miscellaneous	4.00 (1,6.75)	−0.113	0.343	−0.074	0.536

*NMSS, The Non-motor Symptoms Scale for Parkinson's disease. *P < 0.05, **P < 0.01.*

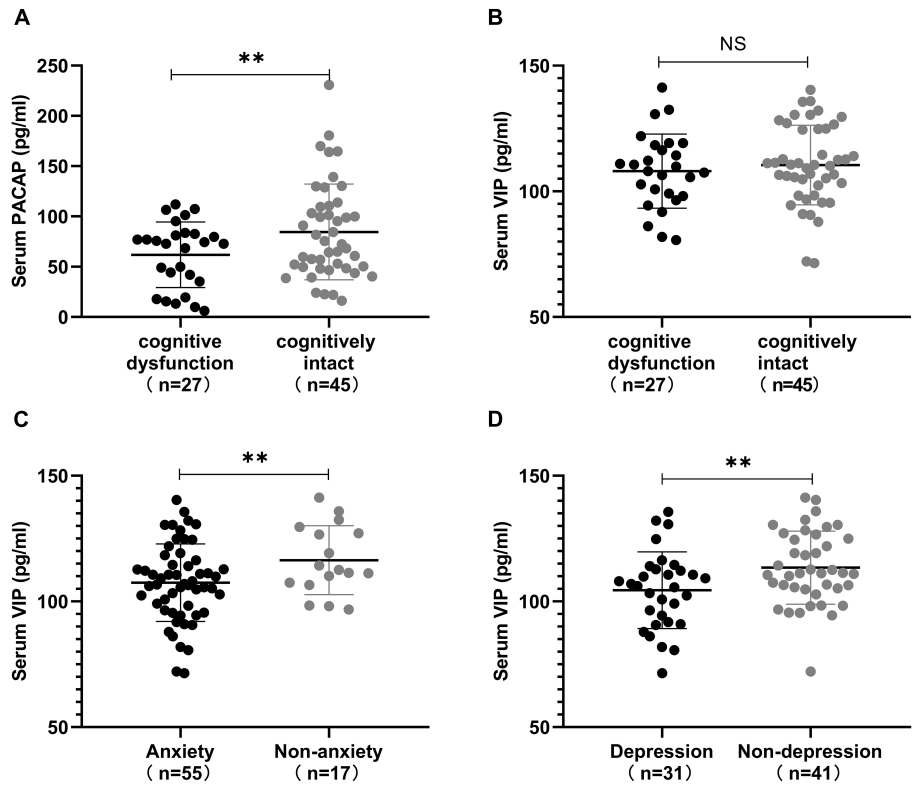

FIGURE 6 | Correlation between serum pituitary adenylate-cyclase activating polypeptide (PACAP) and vasoactive intestinal peptide (VIP) levels, and non-motor symptoms. **(A)** Serum PACAP levels in different subgroups defined by the presence or absence of cognitive dysfunction in Parkinson's disease (PD) patients. Patients in the cognitively intact subgroup showed higher levels of serum PACAP than in the cognitive dysfunction subgroup. **(B)** Serum VIP levels in different subgroups defined by the presence or absence of cognitive dysfunction in PD patients. Patients in the cognitively intact subgroup showed higher levels of serum VIP than in the cognitive dysfunction subgroup. **(C)** Serum VIP levels between the anxiety and non-anxiety subgroups in PD patients. Patients in the non-anxiety subgroup showed higher levels of serum VIP than those in the anxiety subgroup. **(D)** Serum VIP levels between the depression and non-depression subgroups in PD patients. Patients in the non-depression subgroup showed higher levels of serum VIP than those in the depression subgroup. Values are presented as the mean ± SD; NS, no significance; $^{**}P < 0.05$.

remains controversial. To further clarify the clinical significance of PACAP and VIP levels in serum, it is necessary to investigate whether PACAP and VIP levels in serum and in CSF move in parallel. Third, in contrast to cross-sectional studies, a more accurate and appropriate approach would be to assess PACAP and VIP levels in follow-up studies.

CONCLUSION

Our study found a reduction in the levels of PACAP and VIP in PD for the first time. At the same time, PACAP levels in relation to cognitive function and VIP levels in relation to mood disorders were proven. These findings suggest potential underlying link between serum PACAP and VIP levels and the non-motor symptoms in PD patients. Therefore, PACAP and VIP levels can be used to evaluate PD-related non-motor symptom–cognitive function and mood disorders, respectively.

DATA AVAILABILITY STATEMENT

The original contributions presented in the study are included in the article/supplementary material, further inquiries can be directed to the corresponding author.

ETHICS STATEMENT

The studies involving human participants were reviewed and approved by the Ethics Committee of the Henan Provincial People's Hospital. The patients/participants provided their written informed consent to participate in this study.

AUTHOR CONTRIBUTIONS

SYH and JM completed the topic selection and study design. SYH conducted the experiments. SH, DL, ZZ, and JZ conducted the literature search, acquisition of data, and study supervision. ML, ZW, WS, and XS performed the statistical analysis and interpretation of data. SYH and JM drafted the manuscript. All authors contributed to the manuscript and gave final approval.

FUNDING

This work was supported by research grants from the Henan Province Science and Technology Development Plan (192102310085) and Henan Province Medical Science and Technology Research Program (201701018).

REFERENCES

Aarsland, D., Marsh, L., and Schrag, A. (2009). Neuropsychiatric symptoms in Parkinson's disease. *Mov. Disord.* 24, 2175–2186. doi: 10.1002/mds.22589

Baranowska-Bik, A., Kochanowski, J., Uchman, D., Wolinska-Witort, E., Kalisz, M., Martynska, L., et al. (2013). Vasoactive intestinal peptide (VIP) and pituitary adenylate cyclase activating polypeptide (PACAP) in humans with multiple sclerosis. *J. Neuroimmunol.* 263, 159–161. doi: 10.1016/j.jneuroim.2013.08.012

Bukovics, P., Czeiter, E., Amrein, K., Kovacs, N., Pal, J., Tamas, A., et al. (2014). Changes of PACAP level in cerebrospinal fluid and plasma of patients with severe traumatic brain injury. *Peptides* 60, 18–22. doi: 10.1016/j.peptides.2014.07.001

Campos-Acuna, J., Elgueta, D., and Pacheco, R. (2019). T-cell-driven inflammation as a mediator of the gut-brain axis involved in Parkinson's disease. *Front. Immunol.* 10:239. doi: 10.3389/fimmu.2019.00239

Cernuda-Morollon, E., Riesco, N., Martinez-Camblor, P., Serrano-Pertierra, E., Garcia-Cabo, C., and Pascual, J. (2016). No change in interictal PACAP levels in peripheral blood in women with chronic migraine. *Headache* 56, 1448–1454. doi: 10.1111/head.12949

Chaudhuri, K. R., Martinez-Martin, P., Brown, R. G., Sethi, K., Stocchi, F., Odin, P., et al. (2007). The metric properties of a novel non-motor symptoms scale for Parkinson's disease: results from an international pilot study. *Mov. Disord.* 22, 1901–1911. doi: 10.1002/mds.21596

de Souza, F. R. O., Ribeiro, F. M., and d' Almeida Lima, P. M. (2020). Implications of VIP and PACAP in Parkinson's disease: what do we know so far? *Curr. Med. Chem.* 27, 1–12. doi: 10.2174/0929867327666200320162436

Deguil, J., Chavant, F., Lafay-Chebassier, C., Perault-Pochat, M. C., Fauconneau, B., and Pain, S. (2010). Neuroprotective effect of PACAP on translational control alteration and cognitive decline in MPTP parkinsonian mice. *Neurotox. Res.* 17, 142–155. doi: 10.1007/s12640-009-9091-4

Dong, D., Xie, J., and Wang, J. (2019). Neuroprotective effects of brain-gut peptides: a potential therapy for Parkinson's disease. *Neurosci. Bull.* 35, 1085–1096. doi: 10.1007/s12264-019-00407-3

Feher, M., Gaszner, B., Tamas, A., Gil-Martinez, A. L., Fernandez-Villalba, E., Herrero, M. T., et al. (2018). Alteration of the PAC1 receptor expression in the basal ganglia of MPTP-induced parkinsonian macaque monkeys. *Neurotox. Res.* 33, 702–715. doi: 10.1007/s12640-017-9841-7

Gallagher, D. A., and Schrag, A. (2012). Psychosis, apathy, depression and anxiety in Parkinson's disease. *Neurobiol. Dis.* 46, 581–589. doi: 10.1016/j.nbd.2011.12.041

Garcia-Esparcia, P., Llorens, F., Carmona, M., and Ferrer, I. (2014). Complex deregulation and expression of cytokines and mediators of the immune response in Parkinson's disease brain is region dependent. *Brain Pathol.* 24, 584–598. doi: 10.1111/bpa.12137

Garcia-Ruiz, P. J., Chaudhuri, K. R., and Martinez-Martin, P. (2014). Non-motor symptoms of Parkinson's disease a review from the past. *J. Neurol. Sci.* 338, 30–33. doi: 10.1016/j.jns.2014.01.002

Gavioli, E. C., and Calo, G. (2013). Nociceptin/orphanin FQ receptor antagonists as innovative antidepressant drugs. *Pharmacol. Ther.* 140, 10–25. doi: 10.1016/j.pharmthera.2013.05.008

Gelders, G., Baekelandt, V., and Van der Perren, A. (2018). Linking neuroinflammation and neurodegeneration in Parkinson's disease. *J. Immunol. Res.* 2018:4784268. doi: 10.1155/2018/4784268

Gjerris, A., Rafaelsen, O. J., Vendsborg, P., Fahrenkrug, J., and Rehfeld, J. F. (1984). Vasoactive intestinal polypeptide decreased in cerebrospinal fluid (CSF) in atypical depression. Vasoactive intestinal polypeptide, cholecystokinin and gastrin in CSF in psychiatric disorders. *J. Affect. Disord.* 7, 325–337. doi: 10.1016/0165-0327(84)90054-5

Hall, S., Janelidze, S., Surova, Y., Widner, H., Zetterberg, H., and Hansson, O. (2018). Cerebrospinal fluid concentrations of inflammatory markers in Parkinson's disease and atypical parkinsonian disorders. *Sci. Rep.* 8:13276. doi: 10.1038/s41598-018-31517-z

Han, P., Liang, W., Baxter, L. C., Yin, J., Tang, Z., Beach, T. G., et al. (2014). Pituitary adenylate cyclase-activating polypeptide is reduced in Alzheimer disease. *Neurology* 82, 1724–1728. doi: 10.1212/WNL.0000000000000417

Han, X., Dong, Z., Hou, L., Wan, D., Chen, M., Tang, W., et al. (2015). Interictal plasma pituitary adenylate cyclase-activating polypeptide levels are decreased in migraineurs but remain unchanged in patients with tension-type headache. *Clin. Chim. Acta* 450, 151–154. doi: 10.1016/j.cca.2015.08.017

Hirabayashi, T., Nakamachi, T., and Shioda, S. (2018). Discovery of PACAP and its receptors in the brain. *J. Headache Pain* 19:28. doi: 10.1186/s10194-018-0855-1

Huang, Y., Huang, C., Zhang, Q., Wu, W., and Sun, J. (2020). Serum BDNF discriminates Parkinson's disease patients with depression from without depression and reflect motor severity and gender differences. *J. Neurol.* 268, 1411–1418. doi: 10.1007/s00415-020-10299-3

Jellinger, K. A. (2002). Recent developments in the pathology of Parkinson's disease. *J. Neural Transm. Suppl.* 62, 347–376. doi: 10.1007/978-3-7091-6139-5_33

Jiang, L., Wang, W. H., Dong, X. Q., Yu, W. H., Du, Q., Yang, D. B., et al. (2016). The change of plasma pituitary adenylate cyclase-activating polypeptide levels after aneurysmal subarachnoid hemorrhage. *Acta Neurol. Scand.* 134, 131–139. doi: 10.1111/ane.12522

Joers, V., Tansey, M. G., Mulas, G., and Carta, A. R. (2017). Microglial phenotypes in Parkinson's disease and animal models of the disease. *Prog. Neurobiol.* 155, 57–75. doi: 10.1016/j.pneurobio.2016.04.006

Lindqvist, D., Kaufman, E., Brundin, L., Hall, S., Surova, Y., and Hansson, O. (2012). Non-motor symptoms in patients with Parkinson's disease – correlations with inflammatory cytokines in serum. *PLoS One* 7:e47387. doi: 10.1371/journal.pone.0047387

Lotankar, S., Prabhavalkar, K. S., and Bhatt, L. K. (2017). Biomarkers for Parkinson's disease: recent advancement. *Neurosci. Bull.* 33, 585–597. doi: 10.1007/s12264-017-0183-5

Ma, B. Q., Zhang, M., and Ba, L. (2015). Plasma pituitary adenylate cyclase-activating polypeptide concentrations and mortality after acute spontaneous basal ganglia hemorrhage. *Clin. Chim. Acta* 439, 102–106. doi: 10.1016/j.cca.2014.10.010

Miyata, A., Arimura, A., Dahl, R. R., Minamino, N., Uehara, A., Jiang, L., et al. (1989). Isolation of a novel 38 residue-hypothalamic polypeptide which stimulates adenylate cyclase in pituitary cells. *Biochem. Biophys. Res. Commun.* 164, 567–574. doi: 10.1016/0006-291x(89)91757-9

Moody, T. W., Ito, T., Osefo, N., and Jensen, R. T. (2011). VIP and PACAP: recent insights into their functions/roles in physiology and disease from molecular and genetic studies. *Curr. Opin. Endocrinol. Diabetes Obes* 18, 61–67. doi: 10.1097/MED.0b013e328342568a

Onoue, S., Endo, K., Ohshima, K., Yajima, T., and Kashimoto, K. (2002). The neuropeptide PACAP attenuates beta-amyloid (1-42)-induced toxicity in PC12 cells. *Peptides* 23, 1471–1478. doi: 10.1016/s0196-9781(02)00085-2

Panicker, N., Sarkar, S., Harischandra, D. S., Neal, M., Kam, T. I., Jin, H., et al. (2019). Fyn kinase regulates misfolded alpha-synuclein uptake and NLRP3 inflammasome activation in microglia. *J. Exp. Med.* 216, 1411–1430. doi: 10.1084/jem.20182191

Postuma, R. B., Berg, D., Stern, M., Poewe, W., Olanow, C. W., Oertel, W., et al. (2015). MDS clinical diagnostic criteria for Parkinson's disease. *Mov. Disord.* 30, 1591–1601. doi: 10.1002/mds.26424

Qian, Y., Yang, X., Xu, S., Huang, P., Li, B., Du, J., et al. (2020). Gut metagenomics-derived genes as potential biomarkers of Parkinson's disease. *Brain* 143, 2474–2489. doi: 10.1093/brain/awaa201

Reglodi, D., Lubics, A., Tamas, A., Szalontay, L., and Lengvari, I. (2004). Pituitary adenylate cyclase activating polypeptide protects dopaminergic neurons and improves behavioral deficits in a rat model of Parkinson's disease. *Behav. Brain Res.* 151, 303–312. doi: 10.1016/j.bbr.2003.09.007

Rieu, I., Houeto, J. L., Pereira, B., De Chazeron, I., Bichon, A., Chereau, I., et al. (2016). Impact of mood and behavioral disorders on quality of life in Parkinson's disease. *J. Parkinsons Dis.* 6, 267–277. doi: 10.3233/JPD-150747

Shibasaki, Y., Hayata-Takano, A., Hazama, K., Nakazawa, T., Shintani, N., Kasai, A., et al. (2015). Atomoxetine reverses locomotor hyperactivity, impaired novel object recognition, and prepulse inhibition impairment in mice lacking pituitary adenylate cyclase-activating polypeptide. *Neuroscience* 297, 95–104. doi: 10.1016/j.neuroscience.2015.03.062

Soles-Tarres, I., Cabezas-Llobet, N., Vaudry, D., and Xifro, X. (2020). Protective effects of pituitary adenylate cyclase-activating polypeptide and vasoactive intestinal peptide against cognitive decline in neurodegenerative diseases. *Front. Cell Neurosci.* 14:221. doi: 10.3389/fncel.2020.00221

Tuncel, N., Korkmaz, O. T., Tekin, N., Sener, E., Akyuz, F., and Inal, M. (2012). Antioxidant and anti-apoptotic activity of vasoactive intestinal peptide (VIP) against 6-hydroxy dopamine toxicity in the rat corpus striatum. *J. Mol. Neurosci.* 46, 51–57. doi: 10.1007/s12031-011-9618-z

Vasudeva, R. K., Lin, R. C., Simpson, K. L., and Waterhouse, B. D. (2011). Functional organization of the dorsal raphe efferent system with special consideration of nitrergic cell groups. *J. Chem. Neuroanat.* 41, 281–293. doi: 10.1016/j.jchemneu.2011.05.008

Wang, Q., Fu, W., Zhuang, W., Liu, C., Wang, X., and Li, F. (2015). The effects of VIP on the expression of 5- HT,SP,CRF,CRFR2 and its mRNA in the dorsal raphe nucleus of rats with Parkinson's disease. *Chin. J. Neuroanat.* 31, 611–616. doi: 10.16557/j.cnki.1000-7547.2015050014

Wu, W., Shao, J., Lu, H., Xu, J., Zhu, A., Fang, W., et al. (2014). Guard of delinquency? A role of microglia in inflammatory neurodegenerative diseases of the CNS. *Cell Biochem. Biophys.* 70, 1–8. doi: 10.1007/s12013-014-9872-0

Conflict of Interest: The authors declare that the research was conducted in the absence of any commercial or financial relationships that could be construed as a potential conflict of interest.

Publisher's Note: All claims expressed in this article are solely those of the authors and do not necessarily represent those of their affiliated organizations, or those of the publisher, the editors and the reviewers. Any product that may be evaluated in this article, or claim that may be made by its manufacturer, is not guaranteed or endorsed by the publisher.

frontiers in Neuroscience

ORIGINAL RESEARCH
published: 10 September 2021
doi: 10.3389/fnins.2021.663980

Serum Cystatin C as a Potential Predictor of the Severity of Multiple System Atrophy With Predominant Cerebellar Ataxia: A Case-Control Study in Chinese Population

Fei Ye[1,2†], Tianzhu Wang[3†], Huan Li[1,2†], Jie Liang[1,2], Xiaoxin Wu[1,2] and Wenli Sheng[1,2]*

[1] Department of Neurology, The First Affiliated Hospital, Sun Yat-sen University, Guangzhou, China, [2] Guangdong Provincial Key Laboratory of Diagnosis and Treatment of Major Neurological Diseases, The First Affiliated Hospital, Sun Yat-sen University, Guangzhou, China, [3] Department of Neurology, The First Affiliated Hospital of Chongqing Medical University, Chongqing, China

OPEN ACCESS

Edited by:
Henrik Zetterberg, University of Gothenburg, Sweden

Reviewed by:
Alessio Di Fonzo, IRCCS Ca 'Granda Foundation Maggiore Policlinico Hospital, Italy
Ichiro Yabe, Hokkaido University, Japan
Maria Teresa Pellecchia, University of Salerno, Italy

***Correspondence:**
Wenli Sheng
shengwl@mail.sysu.edu.cn

[†] These authors have contributed equally to this work

Specialty section:
This article was submitted to Neurodegeneration, a section of the journal Frontiers in Neuroscience

Received: *05 February 2021*
Accepted: *24 August 2021*
Published: *10 September 2021*

Citation:
Ye F, Wang T, Li H, Liang J, Wu X and Sheng W (2021) Serum Cystatin C as a Potential Predictor of the Severity of Multiple System Atrophy With Predominant Cerebellar Ataxia: A Case-Control Study in Chinese Population. Front. Neurosci. 15:663980. doi: 10.3389/fnins.2021.663980

Objective: Multiple system atrophy (MSA) is a serious neurodegenerative disease that is charactered by progressive neurological disability. The aim of this study was to investigate the correlation of serum oxidant factors with the severity of MSA.

Methods: A total of 52 MSA patients and 52 age- and gender- matched healthy subjects were retrospectively enrolled in this study. Enzymatic colorimetric methods were used to assay the concentrations of uric acid (UA), serum creatinine (Scr), blood urea nitrogen (BUN), and cystatin C (Cys-C). Disease severity was evaluated by the Unified Multiple System Atrophy Rating Scale (UMSARS). The disease progression rate was defined by the change in UMSARS-IV (global disability score, GDS) over a 1-year period.

Results: Comparisons between the two groups revealed that there were no significant differences in terms of serum Scr (70.81 ± 13.88 vs. 70.92 ± 14.19 μmol/L, $p = 0.967$). However, the serum levels of the other three biomarkers were significantly higher in the MSA patients (UA: 325.31 ± 84.92 vs. 291.19 ± 64.14 μmol/L, $p = 0.023$; BUN: 5.68 ± 1.67 vs. 4.60 ± 1.24 mmol/L, $p < 0.001$; Cys-C: 0.96 ± 0.15 vs. 0.89 ± 0.14 mg/L, $p = 0.024$). In addition, Pearson correlation analyses revealed that only serum Cys-C was significantly correlated to GDS ($r = 0.281$, $p = 0.044$). Subgroup analysis further demonstrated that serum Cys-C was the only factor that was positively associated with the disease severity in patients with MSA and predominant cerebellar ataxia (MSA-C) ($r = 0.444$, $p = 0.018$); there was no significant association in MSA patients with predominant Parkinsonism (MSA-P) ($r = 0.118$, $p = 0.582$). MSA-C patients with severe disability were shown to express higher serum levels of Cys-C than patients with mild disability (1.03 ± 0.13 vs. 0.88 ± 0.12 mg/L, $p = 0.009$). Finally, Kaplan-Meier plots revealed a significant difference in the 5-year probability of survival from severe disability between MSA-C patients with high- and low-concentrations of serum Cys-C

(Log-rank test: $X^2 = 4.154$, $p = 0.042$). ROC curve analysis confirmed that serum Cys-C exhibits good performance as a biomarker (AUC = 0.847).

Conclusion: Our research indicated that oxidative stress plays a vital role in MSA. Serum Cys-C represents a potential prognostic biomarker to evaluate the severity of disease in patients with MSA-C.

Keywords: cystatin C, multiple system atrophy, unified multiple system atrophy rating scale, disease severity, case-control study

INTRODUCTION

Multiple system atrophy (MSA) is an adult-onset, sporadic, and rapidly progressive neurodegenerative disease that is characterized by autonomic failure in connection with Parkinsonism and/or cerebellar ataxia (Stefanova et al., 2009). The generation of α-synuclein usually acts as a pathological hallmark of MSA and other Parkinson-related diseases and involves the accumulation of argyrophilic filamentous glial cytoplasmic inclusions from the cerebrospinal fluid (Stefanova et al., 2009). The misfolding of α-synuclein is increasingly being considered as a key initial event in the pathophysiological cascade of MSA. Recent studies have successfully described the epidemiological and clinical characteristics of this disease, although the specific causes and mechanisms involved still remain unclear. The rapid progression of this disease, and the lack of an appropriate therapeutic intervention, results in a serious deterioration of neurological function and a fatal outcome.

A significant body of evidence now indicates that oxidative stress plays a key role in triggering and/or exacerbating MSA (Nee et al., 1991; Vanacore et al., 2005; Fernagut and Tison, 2012; Stefanova et al., 2012; Zhou et al., 2016). Oxidative stress can contribute to neuronal damage and can modulate intracellular signaling pathways, ultimately leading to neuronal death by apoptosis or necrosis (Calabrese et al., 2010). Research has shown that several serum oxidant factors may act as important biomarkers to predict the disease severity in neurodegenerative diseases, such as Parkinson's disease (PD) (Hu et al., 2016; Sampat et al., 2016) and amyotrophic lateral sclerosis (ALS) (Tetsuka et al., 2013; Paganoni et al., 2018; van Eijk et al., 2018), including uric acid (UA), serum creatinine (Scr), and cystatin C (Cys-C). However, its controversy remains as to whether UA and Scr could act as predictive factors for MSA (Lee et al., 2011; Cao et al., 2013, 2016; Chen et al., 2015; Sakuta et al., 2016; Fukae et al., 2017). Furthermore, the roles of Cys-C and blood urea nitrogen (BUN) have yet to be investigated in patients with MSA. In this case-control study, we aimed to evaluate differences in these biomarkers between MSA patients and healthy subjects, and to evaluate the potential correlations between these biomarkers and the severity of MSA in patients from a Chinese population.

MATERIALS AND METHODS

Study Subjects

This study was a case-control study that took place between June 2013 and December 2018 and involved Chinese patients with MSA. A total of 91 Chinese patients previously diagnosed with MSA were retrospectively identified via diagnosis-specific code (ICD-10 code G90.301). Patients were eligible for inclusion in this study if they met the following criteria: (1) if diagnosis had been made on the basis of the second consensus criteria (Gilman et al., 2008), (2) there was no history of a previous diagnosis of PD and medicated with anti-PD drugs, (3) a complete set of clinical data was available. We excluded patients who were vegetarian, those with anemia and/or kidney disease, those with severe dementia, and those with advanced stages of cancer. After applying these criteria, we identified 52 MSA patients for inclusion (**Figure 1**). In addition, 52 age- and gender-matched subjects were selected from the database held by our Health Management Center as controls. These controls were neurologically normal and free of a family history of movement disorders. All participants provided written informed consent. The study was approved by the Ethics Committees of the First Affiliated Hospital of Chongqing Medical University and the First Affiliated Hospital of Sun Yat-sen University.

Sample Preparation and Methods

Serum levels of UA, Scr, BUN, and Cys-C were determined at baseline by an enzymatic colorimetric method and an automatic analyzer (Type 7600; Hitachi Ltd., Japan) in our clinical laboratory. We also recorded a range of clinical information, including gender, age, disease duration (defined as the period between symptom onset and the last hospitalization), history of hypertension, diabetes mellitus, cigarette use, and alcohol abuse. The disease severity of MSA was evaluated by the Unified Multiple System Atrophy Rating Scale (UMSARS) (Wenning et al., 2004). The disease progression rate was defined as the change in UMSARS-IV (global disability score, GDS) over a period of 1 year (Fukae et al., 2017).

Statistical Analysis

Continuous variables are presented as mean ± standard deviation for age, disease duration, UMSARS, disease progression rate, and the concentrations of UA, Scr, BUN, and Cys-C. Categorical variables are presented as percentages, including gender, history of hypertension, diabetes mellitus, cigarette use, and alcohol abuse. The Chi-squared test was used to compare categorical variables between MSA patients and healthy subjects while the *t*-test was used to identify differences in continuous variables. The Pearson correlation coefficient was used to determine the associations between serum oxidant factors and disease severity and to identify significant biomarkers in subgroup analysis.

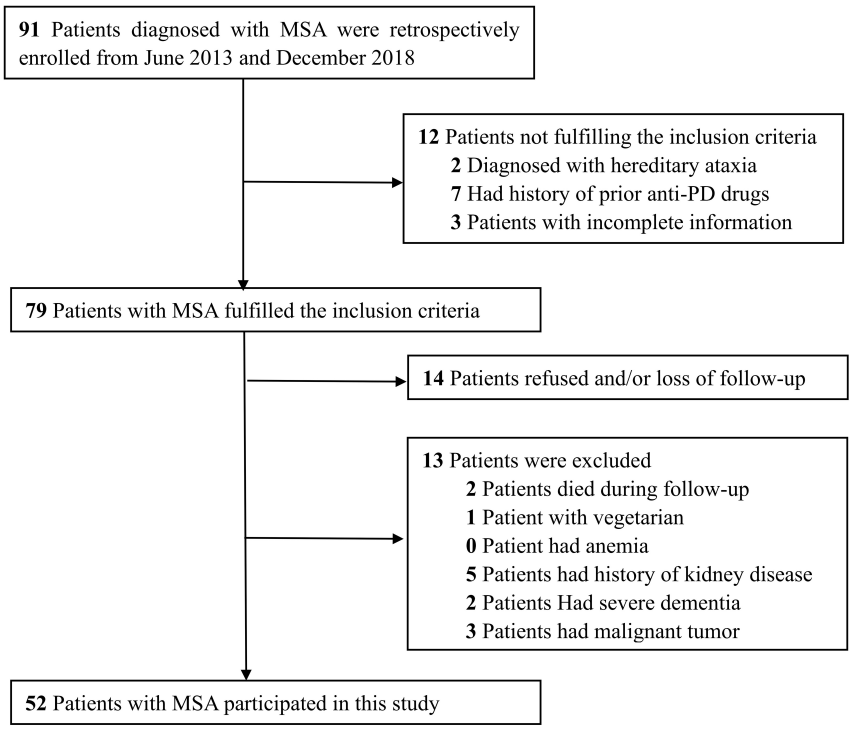

FIGURE 1 | Flow chart presenting the process of patient inclusion and exclusion of this study.

The subgroups included MSA with predominant Parkinsonism (MSA-P) and MSA with predominant cerebellar ataxia (MSA-C) (Gilman et al., 2008). The Kaplan-Meier method was used to explore the probability of survival from severe disability. Receiver operating characteristic (ROC) curves were applied to evaluate the performance of significant biomarkers. All statistical analyses were performed using the Statistical Program for Social Science (SPSS, version 26) and GraphPad Prism (version 9). The significance level was set to 0.05 for all tests.

RESULTS

Demographic Characteristics

Demographic characteristics and clinical data related to the MSA patients and healthy subjects are listed in **Table 1**. A total of 44 patients diagnosed with probable MSA and 8 of them diagnosed with possible MSA. The mean age of the MSA patients was 57.8 ± 9.1 years; over 65% of the subjects were male. The mean UMSARS-I, -II, -IV and total scores were 9.6 ± 4.3, 13.6 ± 5.1, 2.2 ± 1.1, and 25.4 ± 8.7, respectively. For these patients, the mean disease duration was 2.3 ± 1.1 years and the calculated disease progression rate was 1.4 ± 1.2. There were no significant differences between the groups in terms of age, gender distribution, or history of vascular risk factors. We also divided the patients into MSA-C ($n = 28$) and MSA-P ($n = 24$) subgroups; there were no significant differences between these groups with regards to the clinical parameters observed in this study (**Table 2**).

Serum Oxidative Biomarkers in MSA Patients

Analysis did not identify a significant difference in the levels of Scr between the MSA patients and healthy subjects, as shown in **Figure 2A** (70.81 ± 13.88 vs. 70.92 ± 14.19 μmol/L, $p = 0.967$). However, the other three oxidative biomarkers were

TABLE 1 | The clinical characteristics of MSA patients and healthy subjects.

	MSA patients ($n = 52$)	Healthy subjects ($n = 52$)	p
Age (years)	57.8 ± 9.1	57.7 ± 9.1	0.974
Male	35 (67.3%)	35 (67.3%)	1.000
Risk factors			
Hypertension	1 (1.9%)	2 (3.8%)	0.558
Diabetes mellitus	4 (7.7%)	4 (7.7%)	1.000
Smoking	17 (32.7%)	19 (36.5%)	0.680
Drinking	13 (25.0%)	14 (26.9%)	0.823
Diagnosis			
Probable MSA	44 (84.6%)		
Possible MSA	8 (51.4%)		
Disease duration	2.7 ± 2.8		
UMSARS			
UMSARS-I	9.6 ± 4.3		
UMSARS-II	13.6 ± 5.1		
UMSARS-IV	2.2 ± 1.1		
Total score	25.4 ± 8.7		
Progression rate	1.4 ± 1.2		

significantly higher in MSA patients than in healthy controls, as shown in **Figures 2B–D** (UA:325.31 ± 84.92 vs. 291.19 ± 64.14 μmol/L, $p = 0.023$; BUN:5.68 ± 1.67 vs. 4.60 ± 1.24 mmol/L, $p < 0.001$; Cys-C:0.96 ± 0.15 vs. 0.89 ± 0.14 mg/L, $p = 0.024$). Next, we compared these significantly elevated serum oxidative biomarkers between the two subgroups. Although we did not identify any significant differences, we found that the MSA-C patients exhibited relatively lower concentrations of these biomarkers than the MSA-P patients, as shown in **Supplementary Figure 1** (UA:305.82 ± 72.89 vs. 348.04 ± 93.56, $p = 0.074$; BUN:5.44 ± 1.81 vs. 5.95 ± 1.49, $p = 0.280$; Cys-C:0.92 ± 0.14 vs. 1.00 ± 0.16, $p = 0.093$).

Pearson Correlation Analysis

Pearson correlation analyses revealed that there was no significant association between either UA and BUN with the UMSARS score, disease duration, or disease progression rate (**Table 3**). The serum levels of Cys-C were not associated with disease duration or disease progression rate but were significantly and positively correlated with GDS, as shown in **Figure 3A** ($r = 0.287$, $p = 0.039$), thus suggesting that this factor could act as a potential biomarker for patients with MSA. Next, we investigated the efficacy of serum Cys-C in the MSA-C and MSA-P subgroups. This serum biomarker showed a strong association with the MSA-C subgroup (**Figure 3B**; $r = 0.444$, $p = 0.018$) but not the MSA-P subgroup (**Figure 3C**; $r = 0.118$, $p = 0.582$). In addition, we explored the relationship between serum Cys-C and UMSARS scores in MSA-C patients. This serum biomarker was significantly positive correlated with disease duration ($r = 0.407$, $p = 0.032$) and GDS ($r = 0.444$, $p = 0.018$), but its relation to UMSARS-I ($r = -0.115$, $p = 0.559$), -II ($r = 0.056$, $p = 0.779$), total score ($r = 0.042$, $p = 0.830$) or the disease progression rates ($r = -0.077$, $p = 0.696$) was not statistical significance. These results suggest that serum Cys-C may act as a predictive factor for disease severity in patients with MSA-C.

TABLE 2 | A comparison of clinical parameters between MSA-C and MSA-P subgroups.

	MSA-C ($n = 28$)	MSA-P ($n = 24$)	p
Age (years)	58.0 ± 9.4	57.5 ± 9.0	0.833
Male	16 (57.1%)	19 (79.2%)	0.091
Risk factors			
Hypertension	0 (0.0%)	1 (4.2%)	0.275
Diabetes mellitus	2 (7.1%)	2 (8.3%)	0.872
Smoking	9 (32.1%)	8 (33.3%)	0.927
Drinking	9 (32.1%)	4 (16.7%)	0.199
Diagnosis			
Probable MSA	25 (89.3%)	19 (79.2%)	0.313
Possible MSA	3 (10.7%)	5 (20.8%)	
Disease duration	2.7 ± 2.1	2.8 ± 3.5	0.838
UMSARS			
UMSARS-I	8.9 ± 3.7	10.5 ± 4.8	0.172
UMSARS-II	14.5 ± 5.3	12.5 ± 4.6	0.164
UMSARS-IV	2.2 ± 1.1	2.3 ± 1.1	0.710
Total score	25.5 ± 8.3	25.3 ± 9.4	0.921
Progression rate	1.2 ± 1.2	1.7 ± 1.2	0.301

The Predictive Value of Serum Cys-C in Patients With MSA-C

In order to explore the predictive value of serum Cys-C for the disease severity of patients with MSA-C, we first classified disease severity into mild disability (GDS 1–2) and severe disability (GDS 3–5). We found that MSA-C patients with severe disability had significantly higher concentrations of serum Cys-C than patients with mild disability (1.03 ± 0.13 vs. 0.88 ± 0.12 mg/L, $p = 0.009$; **Figure 4A**), thus suggesting that high levels of serum Cys-C represents a positive risk factor for serious functional disability. Furthermore, MSA-C patients were divided into a high-concentration group and a low-concentration group based on mean serum Cys-C (0.92 mg/L) as a cut-off value. The 5-year probability of survival, based on severe disability, showed that MSA-C patients with high levels of Cys-C were associated with a significantly shorter duration of disease with severe functional disability, as determined by the Kaplan-Meier method (**Figure 4B**; Log-rank test: $X^2 = 4.154$, $p = 0.042$). Finally, ROC curve analysis confirmed that this serum biomarker showed good performance as a predictor of disease severity in patients with MSA-C; the area under the curve (AUC) was 0.847 (**Figure 4C**).

DISCUSSION

Our analyses showed that there was no statistical difference between healthy controls and MSA patients with regards to serum Scr. However, the other three biomarkers were significantly higher in MSA patients than in controls. In addition, Pearson correlation analyses found that only serum levels of Cys-C were significantly correlated to GDS. Subgroup analysis also showed that serum Cys-C was positively associated with disease severity in patients with MSA-C; there was no association between serum Cys-C and disease severity in patients with MSA-P. Furthermore, MSA-C patients with severe disability had higher levels of serum Cys-C than those with mild disability. We also determined that the 5-year survival risk from severe disability was significantly increased in patients with MSA-C who also had high serum levels of Cys-C when compared to those with low levels of Cys-C.

Our analyses also indicated that there was a positive correlation between Cys-C concentration and disease severity in MSA patients; these findings were similar to a previous study involving other neurodegenerative disease (Hu et al., 2016). In addition, the increased Cys-C levels were found as an independent predictor for cognitive impairment via a meta-analysis including12 studies (Nair et al., 2020), and it could be used for distinguishing patients with cognitive impairment from healthy population (Wang et al., 2017). Shu et al. (2018) also revealed its predictive role in disease duration and severity in patients with anti-NMDAR encephalitis. These results suggested serum Cys-C might be a risk factor for neurological disorders. As a cysteine protease inhibitor enriched in the central nervous system, Suzuki et al. (2014) found that Cys-C was an oligodendrocyte-derived secretory protein led to MSA via overexpressing of human α-synuclein and via increased expression of the endogenous α-synuclein in a mouse model. Interestingly, Gauthier et al. (2011) reported that this serum factor played a protective role in brain damage and

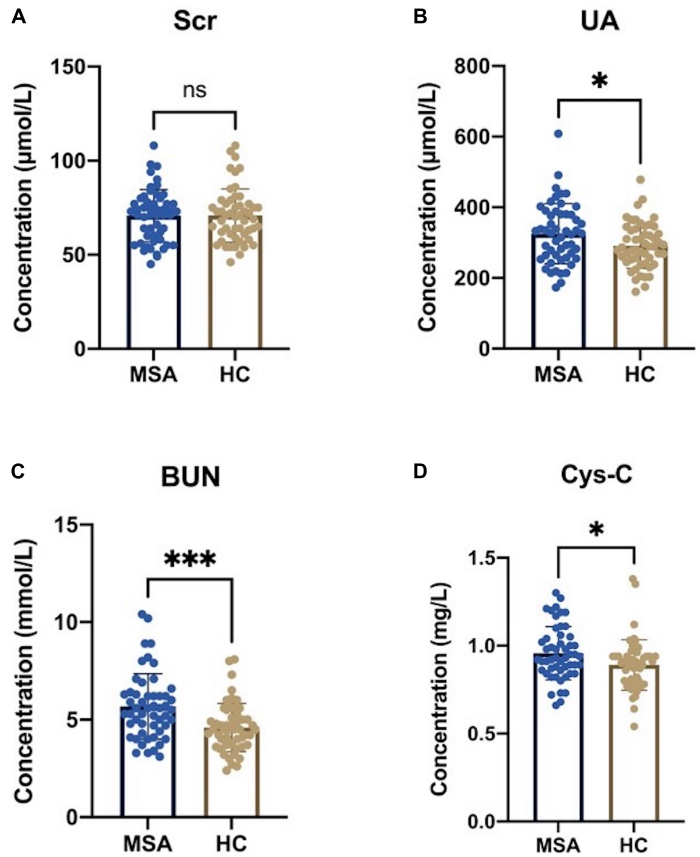

FIGURE 2 | Serum oxidative biomarkers in MSA patients and healthy subjects. **(A)** There was no statistical significance in serum Scr levels between MSA patients and healthy controls (HCs) (70.81 ± 13.88 vs. 70.92 ± 14.19 μmol/L, $p = 0.967$). **(B)** The serum levels of UA were significantly higher in MSA patients than in HCs (325.31 ± 84.92 vs. 291.19 ± 64.14 μmol/L, $p = 0.023$). **(C)** The serum levels of BUN were significantly higher in MSA patients than in HCs (5.68 ± 1.67 vs. 4.60 ± 1.24 mmol/L, $p < 0.001$). **(D)** The serum levels of Cys-C was significantly higher in MSA patients than in HCs (0.96 ± 0.15 vs. 0.89 ± 0.14 mg/L, $p = 0.024$). The symbol ns is for $P > 0.05$, * for $P < 0.05$, ** for $P < 0.01$, and *** for $P < 0.001$, retrospectively.

neurodegenerative processes by inhibiting cysteine proteases. Kaur et al. (2010) found that the over-expressed Cyst-C effectively rescued the neural injury by inhibiting the apoptosis-promoting actions of cathepsins in the mouse model of the inherited neurodegenerative disorder, progressive myoclonic epilepsy type 1 (EPM1). It's worth noting that these animal models of neurodegenerative disorders were from the knock out of a single gene, while the susceptibility gene of MSA remained unclear. Simply, the homologous repair could be explained by the increased Cys-C levels in the EPM1 mouse model via knocking down Cystatin B. Thus, in our opinion, serum Cys-C may have multiple pathophysiological regulatory mechanisms in neurodegenerative disorders. When it comes to the relationship with MSA, serum Cys-C is more likely to be considered as a bad protein.

In a former study, Urbizu et al. (2015) confirmed that the transcription of Cys-C was differentially expressed in different MSA phenotypes. The Cys-C gene (CST3) B-haplotype was significantly associated with MSA-P, while the higher expression of CST3 were found in the caudate nuclei of MSA-P and in the cerebellum of MSA-C. Although our study did not prove a statistical difference in serum Cys-C between two phenotypes (only relatively lower expression in the MSA-C patients compared with MSA-P patients), a positive correlation between Cys-C and disease severity in MSA-C patients has been found out. Therefore, the serum levels of Cys-C may have a potential to evaluate the disease severity in patients with MSA-C while other variables should be taken into consideration together.

TABLE 3 | Pearson correlation analysis of the association between elevated biomarkers and disease severity in MSA patients.

	UA		BUN		Cys-C	
	r	*p*	*r*	*p*	*r*	*p*
UMSARS-I	−0.078	0.583	−0.041	0.774	−0.077	0.587
UMSARS-II	−0.089	0.530	0.009	0.952	−0.096	0.500
UMSARS-IV	0.084	0.554	0.028	0.844	0.287	0.039
Total score	−0.081	0.567	−0.011	0.939	−0.059	0.680
Disease duration	0.053	0.710	−0.097	0.493	0.048	0.736
Progression rate	−0.031	0.829	−0.063	0.656	−0.050	0.725

In contrast to the findings reported by Lee et al. (2011) and Cao et al. (2013), our study did not reveal an increase

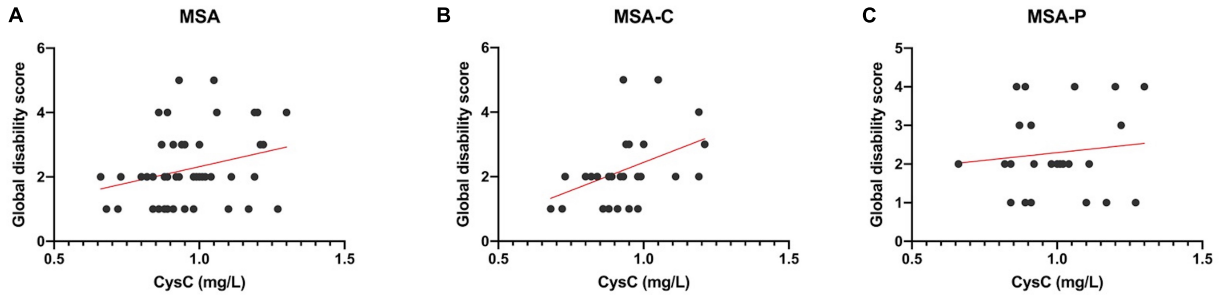

FIGURE 3 | Pearson correlation analyses of serum Cys-C levels in MSA patients and subgroups. **(A)** The serum levels of Cys-C were positively correlated to GDS in MSA patients (r = 0.287, p = 0.039). **(B)** The serum levels of Cys-C were positively correlated to GDS in MSA-C patients (r = 0.444, p = 0.018). **(C)** The serum levels of Cys-C were not correlated to GDS in MSA-P patients (r = 0.118, p = 0.582).

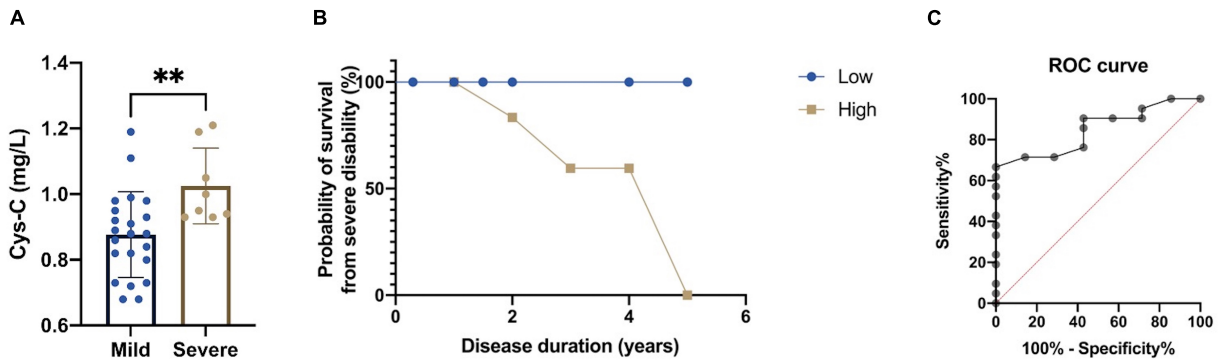

FIGURE 4 | Evaluation of the predictive value of the serum levels of Cys-C in MSA-C patients. **(A)** A comparison of serum Cys-C levels between MSA-C patients with severe disability and those with mild disability (1.03 ± 0.13 vs. 0.88 ± 0.12 mg/L, p = 0.009). **(B)** Kaplan-Meier analysis of the 5-year probability of survival from MSA-C patients with severe disability when compared between those with high levels of Cys-C and those with low levels of Cys-C (Log-rank test: X^2 = 4.154, p = 0.042). **(C)** ROC curve for serum Cys-C levels when predicting disease severity of patients with MSA-C (AUC = 0.847). The symbol ns is for $P > 0.05$, * for $P < 0.05$, ** for $P < 0.01$, and *** for $P < 0.001$, retrospectively.

in the serum levels of Scr in MSA patients. Furthermore, we did not find an association between elevations of serum UA concentrations and the severity or progression of MSA. In our study, we did not explore the correlation between different quartiles of these serum oxidative biomarkers and MSA in order to avoid misclassification bias. In addition, we excluded patients with kidney disorders so that we could avoid individual bias; it is possible that our sample selection strategy may have contributed to the differences between our study and the findings of previous studies. However, Milanesi et al. (2019) found that UA was involved in the inflammatory reaction and oxidative stress mediated by the activation of toll-like receptor 4 (TLR4); this is the final oxidation product of purine catabolism in humans and primates and is known to exert neuroprotective effects. Zhang et al. (2017) revealed that higher UA concentrations could significantly improve cell viability and apoptosis, thus reducing the production of reactive oxygen species (ROS). These results might suggest that oxidative stress plays a key role in the mechanism underlying MSA.

A number of studies have shown that oxidative stress is a major factor in MSA. Zhou et al. (2016) found that increased serum levels of homocysteine and reduced serum levels of high-density lipoprotein cholesterol were potential prognostic biomarkers associated with the disease severity of MSA patients. In another study, Herrera-Vaquero et al. (2020) observed increased levels of tubulation in the mitochondria of neural progenitor cells from MSA patients and that ROS could promote the translocation of α-synuclein into nucleus, thus suggesting that oxidative stress plays a key role in MSA at early onset. In addition, Glat et al. (2020) found that oxidative stress-related genes were up-regulated in a mouse model of MSA and that an injection of mitochondrial neurotoxin could improve motor function. Collectively, these findings indicate that oxidative toxicity could represent a potential therapeutic target for MSA patients.

There are some limitations to our study that need to be considered. First, our study was limited by a small sample size of MSA patients. This is because we recruited patients from a single teaching hospital and some patients were reluctant to be involved in clinical studies. Therefore, further studies should now be carried out with a larger sample size and a longer follow-up period; such studies should provide us with a more comprehensive evaluation. Second, we only measured the concentrations of UA, Scr, BUN, and Cys-C once in this study. UMSARS assessments were conducted by independent

neurologists. Therefore, random measurement errors may have influenced our data. Third, although MSA patients who took anti-PD drugs were excluded from this study, a few patients have previously taken oral mecobalamin (0.5 g/d). Future research should investigate the specific effect of mecobalamin on MSA patients.

CONCLUSION

In conclusion, the serum levels of Cys-C may have a potential to evaluate the disease severity in patients with MSA-C while other variables should be taken into consideration together.

DATA AVAILABILITY STATEMENT

Original data for this study are included in the article/**Supplementary Material**, requests for further information can be obtained from the corresponding author.

ETHICS STATEMENT

The studies involving human participants were reviewed and approved by the independent ethics committees of the First Affiliated Hospital of Chongqing Medical University and the First Affiliated Hospital of Sun Yat-sen University. The patients/participants provided their written informed consent to participate in this study.

AUTHOR CONTRIBUTIONS

FY designed the study, draft the manuscript, and contributed to the discussion. TW collected the data, analyzed the data, and contributed to the discussion. HL analyzed the data and draft the manuscript. JL and XW contributed to the discussion. WS designed the study and revised the manuscript. All authors contributed to the article and approved the submitted version.

FUNDING

This study was funded by the National Natural Science Foundation of China (Grant Nos. 81671132, 81471180, and 82071286).

SUPPLEMENTARY MATERIAL

The Supplementary Material for this article can be found online at: https://www.frontiersin.org/articles/10.3389/fnins.2021.663980/full#supplementary-material

Supplementary Figure 1 | Serum oxidative biomarkers in different MSA subgroups. **(A)** There was no significant difference in the serum levels of UA when compared between patients with MSA-C and MSA-P (305.82 ± 72.89 vs. 348.04 ± 93.56, $p = 0.074$). **(B)** There was no significant difference in the serum levels of BUN when compared between patients with MSA-C and MSA-P (5.44 ± 1.81 vs. 5.95 ± 1.49, $p = 0.280$). **(C)** There was no significant difference in the serum levels of Cys-C when compared between patients with MSA-C and MSA-P (0.92 ± 0.14 vs. 1.00 ± 0.16, $p = 0.093$).

REFERENCES

Calabrese, V., Cornelius, C., Mancuso, C., Lentile, R., Stella, A. M., and Butterfield, D. A. (2010). Redox homeostasis and cellular stress response in aging and neurodegeneration. *Methods Mole. Biol.* 610, 285–308. doi: 10.1007/978-1-60327-029-8_17

Cao, B., Guo, X., Chen, K., Song, W., Huang, R., Wei, Q., et al. (2016). Serum creatinine is associated with the prevalence but not disease progression of multiple system atrophy in Chinese population. *Neurol. Res.* 38, 255–260. doi: 10.1179/1743132815y.0000000095

Cao, B., Guo, X., Chen, K., Song, W., Huang, R., Wei, Q. Q., et al. (2013). Uric acid is associated with the prevalence but not disease progression of multiple system atrophy in Chinese population. *J. Neurol.* 260, 2511–2515. doi: 10.1007/s00415-013-7006-z

Chen, D., Wei, X., Zou, J., Wang, R., Liu, X., Xu, X., et al. (2015). Contra-Directional Expression of Serum Homocysteine and Uric Acid as Important Biomarkers of Multiple System Atrophy Severity: A Cross-Sectional Study. *Front. Cell. Neurosci.* 9:247.

Fernagut, P. O., and Tison, F. (2012). Animal models of multiple system atrophy. *Neuroscience* 211, 77–82. doi: 10.1016/j.neuroscience.2011.09.044

Fukae, J., Fujioka, S., Yanamoto, S., Mori, A., Nomi, T., Hatano, T., et al. (2017). Serum uric acid level is linked to the disease progression rate in male patients with multiple system atrophy. *Clin. Neurol. Neurosurg.* 158, 15–19. doi: 10.1016/j.clineuro.2017.04.002

Gauthier, S., Kaur, G., Mi, W., Tizon, B., and Levy, E. (2011). Protective mechanisms by cystatin C in neurodegenerative diseases. *Front. Biosci.* 3, 541–554. doi: 10.2741/s170

Gilman, S., Wenning, G. K., Low, P. A., Brooks, D. J., Mathias, C. J., Trojanowski, J. Q., et al. (2008). Second consensus statement on the diagnosis of multiple system atrophy. *Neurology* 71, 670–676. doi: 10.1212/01.wnl.0000324625.00404.15

Glat, M. J., Stefanova, N., Wenning, G. K., and Offen, D. (2020). Genes to treat excitotoxicity ameliorate the symptoms of the disease in mice models of multiple system atrophy. *J. Neural Transm.* 127, 205–212. doi: 10.1007/s00702-020-02158-2

Herrera-Vaquero, M., Heras-Garvin, A., Krismer, F., Deleanu, R., Boesch, S., Wenning, G. K., et al. (2020). Signs of early cellular dysfunction in multiple system atrophy. *Neuropathol. Appl. Neurobiol.* 2020:12661. doi: 10.1111/nan.12661

Hu, W. D., Chen, J., Mao, C. J., Feng, P., Yang, Y. P., Luo, W. F., et al. (2016). Elevated Cystatin C Levels Are Associated with Cognitive Impairment and Progression of Parkinson Disease. *Cogn. Behav. Neurol.* 29, 144–149. doi: 10.1097/wnn.0000000000000100

Kaur, G., Mohan, P., Pawlik, M., DeRosa, S., Fajiculay, J., Che, S., et al. (2010). Cystatin C rescues degenerating neurons in a cystatin B-knockout mouse model of progressive myoclonus epilepsy. *Am. J. Pathol.* 177, 2256–2267. doi: 10.2353/ajpath.2010.100461

Lee, J. E., Song, S. K., Sohn, Y. H., and Lee, P. H. (2011). Uric acid as a potential disease modifier in patients with multiple system atrophy. *Move. Dis.* 26, 1533–1536. doi: 10.1002/mds.23556

Milanesi, S., Verzola, D., Cappadona, F., Bonino, B., Murugavel, A., Pontremoli, R., et al. (2019). Uric acid and angiotensin II additively promote inflammation and oxidative stress in human proximal tubule cells by activation of toll-like receptor 4. *J. Cell. Phys.* 234, 10868–10876. doi: 10.1002/jcp.27929

Nair, P., Misra, S., Nath, M., Vibha, D., Srivastava, A. K., Prasad, K., et al. (2020). Cystatin C and Risk of Mild Cognitive Impairment: A Systematic Review and Meta-Analysis. *Dement. Geriatr. Cogn. Dis.* 49, 471–482.

Nee, L. E., Gomez, M. R., Dambrosia, J., Bale, S., Eldridge, R., and Polinsky, R. J. (1991). Environmental-occupational risk factors and familial associations in multiple system atrophy: a preliminary investigation. *Clin. Auton. Res.* 1, 9–13. doi: 10.1007/bf01826052

Paganoni, S., Nicholson, K., Chan, J., Shui, A., Schoenfeld, D., Sherman, A., et al. (2018). Urate levels predict survival in amyotrophic lateral sclerosis: Analysis of the expanded Pooled Resource Open-Access ALS clinical trials database. *Muscle Nerve* 57, 430–434. doi: 10.1002/mus.25950

Sakuta, H., Suzuki, K., Miyamoto, T., Miyamoto, M., Numao, A., Fujita, H., et al. (2016). Serum uric acid levels in Parkinson's disease and related disorders. *Brain Behav.* 7:e00598. doi: 10.1002/brb3.598

Sampat, R., Young, S., Rosen, A., Bernhard, D., Millington, D., Factor, S., et al. (2016). Potential mechanisms for low uric acid in Parkinson disease. *J. Neural Trans.* 123, 365–370. doi: 10.1007/s00702-015-1503-4

Shu, Y., Chang, Y., Wu, H., Li, J., Cao, B., Sun, X., et al. (2018). Serum cystatin C and anti-N-methyl-D-aspartate receptor encephalitis. *Acta Neurolog. Scand.* 137, 515–522.

Stefanova, N., Bücke, P., Duerr, S., and Wenning, G. K. (2009). Multiple system atrophy: an update. *The Lancet. Neurology* 8, 1172–1178.

Stefanova, N., Georgievska, B., Eriksson, H., Poewe, W., and Wenning, G. K. (2012). Myeloperoxidase inhibition ameliorates multiple system atrophy-like degeneration in a transgenic mouse model. *Neurotox. Res.* 21, 393–404. doi: 10.1007/s12640-011-9294-3

Suzuki, Y., Jin, C., and Yazawa, I. (2014). Cystatin C triggers neuronal degeneration in a model of multiple system atrophy. *Am. J. Pathol.* 184, 790–799. doi: 10.1016/j.ajpath.2013.11.018

Tetsuka, S., Morita, M., Ikeguchi, K., and Nakano, I. (2013). Utility of cystatin C for renal function in amyotrophic lateral sclerosis. *Acta Neurolog. Scand.* 128, 386–390. doi: 10.1111/ane.12134

Urbizu, A., Canet-Pons, J., Munoz-Marmol, A. M., Aldecoa, I., Lopez, M. T., Compta, Y., et al. (2015). Cystatin C is differentially involved in multiple system atrophy phenotypes. *Neuropathol. Appl. Neurob.* 41, 507–519. doi: 10.1111/nan.12134

van Eijk, R., Eijkemans, M., Ferguson, T. A., Nikolakopoulos, S., Veldink, J. H., and van den Berg, L. H. (2018). Monitoring disease progression with plasma creatinine in amyotrophic lateral sclerosis clinical trials. *J. Neurol. Neurosurg. Psychiatr.* 89, 156–161. doi: 10.1136/jnnp-2017-317077

Vanacore, N., Bonifati, V., Fabbrini, G., Colosimo, C., De Michele, G., Marconi, R., et al. (2005). Case-control study of multiple system atrophy. *Move. Dis.* 20, 158–163.

Wang, R., Chen, Z., Fu, Y., Wei, X., Liao, J., Liu, X., et al. (2017). Plasma Cystatin C and High-Density Lipoprotein Are Important Biomarkers of Alzheimer's Disease and Vascular Dementia: A Cross-Sectional Study. *Front. Aging Neurosci.* 9:26.

Wenning, G. K., Tison, F., Seppi, K., Sampaio, C., Diem, A., Yekhlef, F., et al. (2004). Development and validation of the Unified Multiple System Atrophy Rating Scale (UMSARS). *Move. Dis.* 19, 1391–1402. doi: 10.1002/mds.20255

Zhang, B., Yang, N., Lin, S. P., and Zhang, F. (2017). Suitable Concentrations of Uric Acid Can Reduce Cell Death in Models of OGD and Cerebral Ischemia-Reperfusion Injury. *Cell. Mole. Neurob.* 37, 931–939. doi: 10.1007/s10571-016-0430-8

Zhou, L., Jiang, Y., Zhu, C., Ma, L., Huang, Q., and Chen, X. (2016). Oxidative Stress and Environmental Exposures are Associated with Multiple System Atrophy in Chinese Patients. *Can. J. Neurolog. Sci. Le* 43, 703–709. doi: 10.1017/cjn.2016.261

Conflict of Interest: The authors declare that the research was conducted in the absence of any commercial or financial relationships that could be construed as a potential conflict of interest.

Publisher's Note: All claims expressed in this article are solely those of the authors and do not necessarily represent those of their affiliated organizations, or those of the publisher, the editors and the reviewers. Any product that may be evaluated in this article, or claim that may be made by its manufacturer, is not guaranteed or endorsed by the publisher.

frontiers in Aging Neuroscience

BRIEF RESEARCH REPORT
published: 28 September 2021
doi: 10.3389/fnagi.2021.711784

Increased Levels of Circulating Angiogenic Cells and Signaling Proteins in Older Adults With Cerebral Small Vessel Disease

*Arunima Kapoor[1], Aimée Gaubert[2], Anisa Marshall[3], Irene B. Meier[4,5], Belinda Yew[3], Jean K. Ho[2], Anna E. Blanken[3], Shubir Dutt[3], Isabel J. Sible[3], Yanrong Li[2], Jung Yun Jang[2], Adam M. Brickman[4], Kathleen Rodgers[6] and Daniel A. Nation[1,2]**

[1] Department of Psychological Science, University of California, Irvine, Irvine, CA, United States, [2] Institute for Memory Impairments and Neurological Disorders, University of California, Irvine, Irvine, CA, United States, [3] Department of Psychology, University of Southern California, Los Angeles, CA, United States, [4] Department of Neurology, Taub Institute for Research on Alzheimer's Disease and the Aging Brain, Columbia University, New York, NY, United States, [5] Chione GmbH, Binz, Switzerland, [6] Center for Innovation in Brain Science, Department of Pharmacology, The University of Arizona, Tucson, AZ, United States

OPEN ACCESS

Edited by:
Thomas K. Karikari,
University of Gothenburg, Sweden

Reviewed by:
Sina Naserian,
INSERM UMR-S-MD 1197, Hôpital Paul Brousse, France
Agathe Vrillon,
Assistance Publique–Hopitaux De Paris, France
Mark Daniel Ross,
Edinburgh Napier University, United Kingdom

***Correspondence:**
Daniel A. Nation
dnation@uci.edu

Received: 19 May 2021
Accepted: 14 July 2021
Published: 28 September 2021

Citation:
Kapoor A, Gaubert A, Marshall A, Meier IB, Yew B, Ho JK, Blanken AE, Dutt S, Sible IJ, Li Y, Jang JY, Brickman AM, Rodgers K and Nation DA (2021) Increased Levels of Circulating Angiogenic Cells and Signaling Proteins in Older Adults With Cerebral Small Vessel Disease. Front. Aging Neurosci. 13:711784. doi: 10.3389/fnagi.2021.711784

Background: Cerebral small vessel disease (SVD) is associated with increased risk of stroke and dementia. Progressive damage to the cerebral microvasculature may also trigger angiogenic processes to promote vessel repair. Elevated levels of circulating endothelial progenitor cells (EPCs) and pro-angiogenic signaling proteins are observed in response to vascular injury. We aimed to examine circulating levels of EPCs and proangiogenic proteins in older adults with evidence of SVD.

Methods: Older adults (ages 55–90) free of dementia or stroke underwent venipuncture and brain magnetic resonance imaging (MRI). Flow cytometry quantified circulating EPCs as the number of cells in the lymphocyte gate positively expressing EPC surface markers (CD34+CD133+CD309+). Plasma was assayed for proangiogenic factors (VEGF-A, VEGF-C, VEGF-D, Tie-2, and Flt-1). Total SVD burden score was determined based on MRI markers, including white matter hyperintensities, cerebral microbleeds and lacunes.

Results: Sixty-four older adults were included. Linear regression revealed that older adults with higher circulating EPC levels exhibited greater total SVD burden [$\beta = 1.0 \times 10^5$, 95% CI (0.2, 1.9), $p = 0.019$], after accounting for age and sex. Similarly, a positive relationship between circulating VEGF-D and total SVD score was observed, controlling for age and sex [$\beta = 0.001$, 95% CI (0.000, 0.001), $p = 0.048$].

Conclusion: These findings suggest that elevated levels of circulating EPCs and VEGF-D correspond with greater cerebral SVD burden in older adults. Additional studies are warranted to determine whether activation of systemic angiogenic growth factors and EPCs represents an early attempt to rescue the vascular endothelium and repair damage in SVD.

Keywords: vascular endothelial growth factor, endothelial progenitor cells, cerebral microvascular pathology, cerebral small vessel disease, aging, vascular dementia, dementia

INTRODUCTION

Cerebral small vessel disease (SVD) occurs commonly with advancing age and is associated with increased risk of cognitive impairment, vascular dementia and Alzheimer's disease, contributing to up to 45% of all cases of dementia (Gorelick et al., 2011; Lee et al., 2016). Small vessel changes often remain asymptomatic, but are evident on brain magnetic resonance imaging (MRI) (Wardlaw et al., 2019) and believed to result from pathological changes in the perforating cerebral arteries, penetrating arterioles, capillaries, and venules (Pantoni, 2010). Microvascular function is crucial to addressing cerebral metabolic demands, clearing waste products and maintaining the blood-brain barrier (Zlokovic, 2008; Chabriat et al., 2009; Wardlaw et al., 2013a, 2019; Pettersen et al., 2017; Nation et al., 2019). Reduced blood flow and hypoxia due to degradation of small blood vessels may trigger angiogenesis—the process of blood vessel growth—as a compensatory mechanism (Quick et al., 2021). While it is still debated whether the process of angiogenesis is beneficial or detrimental in the context of vascular brain injury, animal models and studies of large vessel disease show increased angiogenesis in response to vascular injury (Adamczak and Hoehn, 2015).

One feature of angiogenesis is the mobilization of cells that can repair the vasculature. Endothelial progenitor cells (EPCs) represent a heterogeneous cell population known to be mobilized in response to vascular-endothelial damage to promote vessel repair and regenesis (Medina et al., 2017). Increased levels of circulating EPCs at day 7 post-intracerebral hemorrhage predict improved functional outcome at 12 months (Pías-Peleteiro et al., 2016) and mobilization of EPCs has been observed in response to cerebral large vessel disease (Sobrino et al., 2007). Animal mouse models of ischemic stroke suggest that transplantation of *in vitro* cultured EPCs attenuates blood–brain barrier leakage, tight junction protein degradation, and neurological deficits (Geng et al., 2017; Kong et al., 2018).

Similarly, damage to the cerebral vasculature can trigger the release of signaling proteins that are involved in angiogenesis. The vascular endothelial growth factor (VEGF) family proteins, as well as other angiogenic factors, are also known to induce endothelial and neuronal remodeling after stroke (Hayakawa et al., 2017). Levels of these proteins are elevated after ischemic insult in brain tissue and serum in rodent models and in humans (Issa et al., 1999; Zhang et al., 2000; Prodjohardjono et al., 2020). However, few previous studies have evaluated whether changes in circulating angiogenic cells and proteins also occur in response to progressive and insidious cerebral SVD changes which commonly occur with advancing age.

The current study evaluated whether circulating levels of EPCs and pro-angiogenic proteins are associated with SVD burden in older adults who were otherwise neurologically healthy, with no history of clinical stroke or dementia. Consistent with prior studies, we hypothesized that higher levels of circulating angiogenic proteins and EPCs would be associated with greater cerebral SVD burden.

METHODS

Participants

Participants were recruited from the community and included if they were 55 years of age or older, independently living with no history of clinical stroke, dementia or other systemic or neurological illness that may impact central nervous system function. History of vascular risk factors, including hypertension, body mass index, dyslipidemia, diabetes, as well as history of other medical illnesses, was determined by clinical interview. This study was approved by the local Institutional Review Board; all participants gave informed consent and underwent blood draw and brain MRI.

Endothelial Progenitor Cell Quantification

Venipuncture was performed after an overnight fast. EPCs were quantified with flow cytometry. Peripheral blood mononuclear cells (PBMCs) were isolated by density gradient centrifugation and washed twice with DPBS + 2% FBS at 120 × *g* for 10 min and 300 × *g* for 8 min at room temperature. Fluorescently labeled antibodies to EPC surface antigens were utilized (Nation et al., 2018). 1 million cells were transferred to an unstained tube blank, and the remainder was transferred to the stained tube, where 5 μL of Human BD Fc Block (BD Biosciences) was added and incubated for 10– 15 min. An additional 1 μL of each of the following antibodies were then added: (Gorelick et al., 2011) CD34-PE-Vio770 (clone: AC136, Miltenyi Biotec), (Lee et al., 2016) CD133-VioBright FITC (clone: AC133, Miltenyi Biotec), (Wardlaw et al., 2019) PerCP/Cy5.5-CD309 (clone: 7D4-6, BioLegend). Tubes were incubated in the dark for 30 min at 4°C. Samples were washed with 3 mL PBS, centrifuged at 300 × *g* for 8 min, and fixed with 2% formaldehyde in PBS until analysis. Compensation controls were conducted using AbC Total Antibody Compensation Bead Kit (Thermo Fisher Scientific). Samples were acquired on a BD LSR II flow cytometer and analyzed on FlowJo software. EPCs were defined as CD34+CD133+CD309+ cells (Medina et al., 2017). Circulating EPCs were quantified by flow cytometry as the number of cells in the lymphocyte gate positively expressing EPC surface markers (CD34+CD133+CD309+). CD34+CD133+CD309+ cell concentrations were calculated as a percentage of lymphocytes.

APOE Genotyping

Apolipoprotein E (APOE) genotyping was conducted on the blood cell pellet fraction obtained from plasma separation. DNA was isolated from the pellet fraction using the PureLink Genomic DNA Mini Kit (Thermo Fisher Scientific). Genotyping was conducted on isolated DNA using the TaqMan SNP Genotyping Assay (Thermo Fisher Scientific) on an Applied Biosystems 7300 Real Time PCR System. APOE gene SNPs were assessed for dbSNP IDs rs429358 and rs7412. Allelic discrimination was conducted using the included qPCR software. The APOE-ε4 allele was designated as rs429358-C + rs7412-C.

Angiogenic Protein Levels

Levels of angiogenic proteins in plasma were determined using the Meso Scale Discovery V- PLEX Human Biomarker 40-Plex Kit Angiogenesis Panel 1 (VEGF-A, VEGF-C, VEGF-D, Tie-2, Flt-1, PIGF, and bFGF), following manufacturer's protocol without modification. Briefly, we utilized the MSD Multi-Spot 96-well 7-spot plate pre-coated with capture antibodies. Plates were washed three times with at least 150 μl/well of wash buffer. 50 μl of diluted plasma samples per well were added for the angiogenesis panel and incubated at room temperature with shaking for 2 h. Plates were then washed 3 times with at least 150 μl/well of washing buffer. 25 μl of detection antibody solution was added to each well and incubated at room temperature with shaking for 2 h. Plates were then washed three times again. 150 μl of 2X Read Buffer T was added to each well. Plates were then analyzed on an MSD instrument. Values below the lower limit of detection (LLOD) were replaced with zero.

Cerebral Small Vessel Disease Quantification

All participants underwent a comprehensive neuroimaging protocol as previously described (Nation et al., 2018). The following sequences were examined for the current analysis: 3D T1-weighted anatomical scan for qualitative assessment of brain structures and abnormalities, T2-weighted scan for identification and differentiation of lacunes, fluid-attenuated inversion recovery (T2-FLAIR) for the evaluation of white matter hyperintensities, and T2*-weighted imaging for assessment of cerebral microbleeds (Pantoni, 2010; Gorelick et al., 2011; Lee et al., 2016; Wardlaw et al., 2019). MRI markers were identified and scored in accordance with established neuroimaging standards for SVD (Wardlaw et al., 2013b). To determine total MRI SVD burden, all imaging markers were combined using a SVD score (amended version) recently developed by Amin Al Olama et al. (2020), which ranges from 0 to 7 and includes grading of white matter hyperintensities (0–3; using the Fazekas scale), number of lacunes (0–3; 0 = no lacunes, 1 = 1–2, 2 = 3–5, 3 = > 5) and presence of microbleeds (0–1; 0 = absent, 1 = present).

Statistical Analyses

All analyses were performed using IBM SPSS Statistics 27 and R Version 3.6.1. Data were initially screened for extreme values (outliers) defined as values greater than 5 standard deviations from the mean and values that were unduly affecting regression parameter estimates based on measures of distance or influence. Two participants had extreme values for CD34+CD133+CD309+ cell counts, two participants had extreme values for VEGF-C and one participant had an extreme value for VEGF-D and were excluded from analyses. We examined the relationship between circulating EPCs as well as angiogenic proteins (independent predictors) and SVD score (dependent outcome), independently and after adjusting for age and sex. In addition, we examined any significant effects of APOE4 carrier status on the relationship between angiogenic circulating cells as well as proteins and SVD burden. Significance threshold was set at $p < 0.05$ for all analyses.

RESULTS

A total of 64 participants were included in the analysis. Age of study participants ranged from 55 to 90 years [Mean (M) = 69.8, standard deviation (SD) = 7.3], education ranged from 6 to 20 years [M = 15.8, SD = 2.8] and 40.6% were male (**Table 1**). Levels of circulating angiogenic proteins can be found in **Table 2**.

Cerebral Small Vessel Disease Burden

Small vessel disease markers were evident (SVD score > 1) in 29 (45.3%) participants (**Figure 1**). SVD scores ranged from 0 to 4 (M = 1.6, SD = 1.0). Microbleeds were identified in 5 (7.8%) participants, and small lacunes in 8 (12.5%) participants. White matter hyperintensities were identified in majority of participants; 36 (56.3%) displayed mild white matter hyperintensity burden (Fazekas 1), 18 (28.1%) displayed moderate burden (Fazekas 2) and 6 (9.4%) showed severe burden (Fazekas 3).

Association Between Endothelial Progenitor Cells and Small Vessel Disease Burden

Endothelial progenitor cell count (CD34+CD133+CD309+ count per lymphocyte) and SVD score was available for 52 participants and 2 outliers were removed; 50 participants were therefore included in this analysis. Mean EPC count was 2.7×10^{-6} CD34+CD133+CD309+ cells/lymphocyte (SD = 3.4×10^{-6}). Linear regression revealed that higher levels of circulating EPCs was associated with greater SVD burden, even after accounting for age and sex in multiple regression [$\beta = 1.0 \times 10^{5}$, 95% CI (0.2, 1.9), $p = 0.019$]. The relationship remained significant even after adjusting for APOE4 carrier status and a significant positive effect of APOE4 carrier status

TABLE 1 | Participant characteristics, demographics, and vascular risk factors.

	***N* = 64**
Age (years), *M* (SD)	69.8 (7.3)
Sex male, *n* (%)	26 (40.6)
Education (years), M (SD)	15.8 (2.8)
APOE4 Carrier, *n* (%)	20 (33.3%)
Hypertension, *n* (%)	26 (40.6)
Dyslipidemia, *n* (%)	33 (51.6)
Diabetes, *n* (%)	6 (9.4)
Smoking history, *n* (%)	26 (40.6)
TIA, *n* (%)	1 (1.6)
Cardiovascular disease, *n* (%)	5 (7.9)
Atrial fibrillation, *n* (%)	3 (4.8)
Left ventricular hypertrophy, *n* (%)	1 (1.6)

**History of cardiovascular disease, atrial fibrillation, and left ventricular hypertrophy was collected for 63 (98.4%) participants and missing for one participant. APOE4 carrier status was missing for four participants and available for 60 participants.*

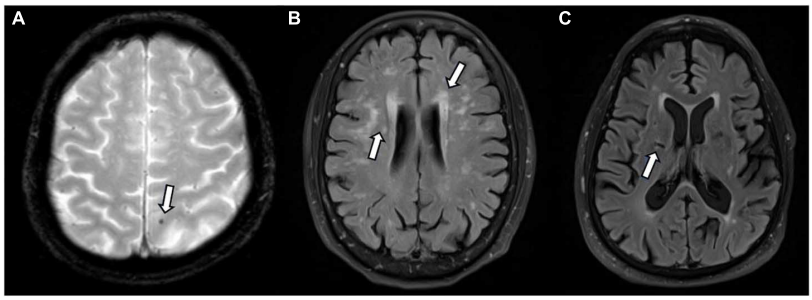

FIGURE 1 | Small vessel disease as identified on magnetic resonance imaging (MRI) by white arrows. **(A)** Microbleed identified on T2*; **(B)** white matter hyperintensities identified on FLAIR; **(C)** lacune on FLAIR.

was observed, with APOE4 carriers having greater SVD burden [$N = 48$; $\beta = 0.57$, 95% CI (0.01, 1.13), $p = 0.046$; **Table 3**].

Association Between Pro-angiogenic Proteins and Small Vessel Disease Burden

We specifically examined the relationship of VEGF-A, VEGF-C, VEGF-D, Tie-2, and Flt-1 with SVD score. Values were available for all 64 participants, however, two participants had extreme values for VEGF-C and one participant had an extreme value for VEGF-D and were excluded from the current analyses. Simple linear regression revealed a positive relationship only between circulating VEGF-D and total SVD score, which remained significant in multiple regression controlling for age and sex [$\beta = 0.001$, 95% CI (0.000, 0.001), $p = 0.048$]. The relationship remained significant even after adjusting for APOE4 carrier status (**Table 4**).

DISCUSSION

Mobilization of EPCs and release of angiogenic growth factors has been observed in response to cerebral large vessel disease (Sobrino et al., 2007). Consistent with such studies, our findings indicate increased levels of circulating EPCs and angiogenic proteins in the presence of cerebral SVD. Specifically, circulating numbers of CD34+CD133+CD309+ cells and levels of VEGF-D protein correlated with greater cerebral SVD burden based on white matter hyperintensities, cerebral microbleeds and lacunes. SVD markers were evident on MRI in almost half our sample, yet participants did not have major cognitive dysfunction at the time of assessment, suggesting that the correlation between cerebral SVD and these angiogenic factors may be observed during the preclinical disease stage. While the current study was correlational, precluding causal inference, our findings are consistent with the hypothesis that EPCs and angiogenic signaling proteins may be increased in circulation in response to cerebral SVD (Nation et al., 2018).

Studies focused on clinically symptomatic patients with more severe white matter changes, cognitive impairment and dementia indicate a limited pool of EPCs may be exhausted with the emergence and progression of clinical symptomatology (Iadecola, 2013). Based on these data and the present study findings, we hypothesize that increased circulating EPC and VEGF-D levels in asymptomatic older adults may represent preclinical markers of early-stage cerebral small vessel injury, and that later exhaustion of the EPC pool may coincide with progressive cognitive decline (Lee et al., 2009). Elevation of VEGF in the presence of cognitive impairment is supported by prior research (Mahoney et al., 2021), although the literature suggests that EPC levels deplete in correspondence with the decline in cognitive function (Lee et al., 2009). If our hypothesized model is supported, the potential for circulating EPC and VEGF-D levels biomarkers for early-stage cerebral SVD changes warrants further research. Moreover, animal studies suggest that transplantation of EPCs may attenuate blood brain barrier breakdown (Geng et al., 2017), tight junction protein degradation, and neurological deficits (Geng et al., 2017; Kong et al., 2018), suggesting that EPCs may also offer potential therapeutic opportunities. Similarly, *in vitro* studies suggest that VEGF may support EPC differentiation and vascular repair (Li et al., 2017) but additional studies are needed.

Increased levels of VEGF-D have been associated with atrial fibrillation, ischemic stroke and heart failure (Borné et al., 2018; Berntsson et al., 2019) and elevated levels are known to predict mortality in patients with coronary artery disease (Wada et al., 2020). VEGF-D is a secreted glycoprotein and one of five members of the VEGF family with high angiogenic and lymphangiogenic potential (Lohela et al., 2009). Recent animal and *in vitro* studies also suggest a role for VEGF-D in dendrite maintenance required for memory formation and other cognitive processes (Mauceri et al., 2011, 2020;

TABLE 2 | Angiogenic protein levels.

	N	Mean
VEGF (pg/mL), *M* (SD)	64	112.08 (116.97)
VEGF-C (pg/mL), *M* (SD)	64	91.53 (154.36)
VEGF-D (pg/mL), *M* (SD)	64	849.76 (818.72)
Tie-2 (pg/mL), *M* (SD)	64	3180.27 (1106.89)
Flt-1 (pg/mL), *M* (SD)	64	57.04 (21.28)
PlGF (pg/mL), *M* (SD)	35	3.08 (1.29)
bFGF (pg/mL), *M* (SD)	35	2.90 (2.70)

TABLE 3 | Association between EPCs and small vessel disease.

Variable	Unstandardized	Coefficients	Standardized	Sig.	95% confidence interval for B	
	B	Std. error	B		Lower bound	Upper bound
Age (years)	0.004	0.019	0.033	0.838	−0.035	0.043
Sex (male)	−0.153	0.269	−0.080	0.572	−0.696	0.389
APOE4 (carrier)	0.568	0.276	0.291	0.046	0.011	1.125
Circulating EPCs (CD34+CD133+CD309+/lymphocyte)	105447.5	41519.0	0.394	0.015	21716.5	189178.4

Dependent variable: SVD score.

TABLE 4 | Association between VEGF-D and small vessel disease.

Variable	Unstandardized	Coefficients	Standardized	Sig.	95% confidence interval for B	
	B	Std. error	B		Lower bound	Upper bound
Age (years)	0.031	0.018	0.236	0.092	−0.005	0.067
Sex (male)	−0.078	0.255	−0.039	0.761	−0.589	0.434
APOE4 (carrier)	0.330	0.283	0.159	0.249	−0.237	0.898
Circulating VEGF-D (pg/mL)	0.001	0.000	0.257	0.048	0.000	0.001

Dependent variable: SVD score.

Stacker and Achen, 2018). It remains unclear whether circulating EPCs may play related roles in central nervous system functions. In the present study, we demonstrate an association between circulating VEGF-D and SVD in older adults, suggesting that angiogenic and lymphangiogenic processes may be taking places. Prior studies have demonstrated a role for VEGF-A in EPC recruitment to stimulate vasculogenesis, however, no prior studies have examined the relationship between VEGF-D and EPCs, making it challenging to understand the relationship and directionality between the two based on current literature. Further studies are warranted to confirm these findings and uncover potential mechanisms.

Whether the mobilization of EPCs and angiogenic factors to promote angiogenesis is beneficial or detrimental in SVD warrants further attention. Angiogenic processes, including endothelial barrier function and cell connections that may be weakened during repair and remodeling, may lead to inflammation and increased blood–brain barrier permeability (Adamczak and Hoehn, 2015). The involvement and impact of angiogenic cells and signaling proteins in repairing cerebral SVD—often a progressive form of vascular damage which worsens with age—may be important in understanding cognitive decline in older adults.

Limitations of this study include the limited sample size and cross-sectional design. Further studies may elucidate the predictive value of these angiogenic biomarkers. Moreover, additional angiogenic markers warrant further attention. We utilized the MSD angiogenesis biomarker panel in this study; however, numerous other proteins play a significant role in mediating angiogenesis and advanced techniques could be further utilized to identify and examine additional markers of angiogenesis. Future studies could also examine the relationship between inflammation and EPCs, given that recent studies suggest that inflammation may influence EPC function (Naserian et al., 2020; Nouri Barkestani et al., 2021).

Another limitation is the lack of specificity and varying definitions of EPCs in current literature. Gating for flow cytometry and calculation of EPCs also remains inconsistent. We utilized the consensus statement and recent studies to define EPCs as CD34+CD133+CD309+ cells (Medina et al., 2017). However, inclusion of cell markers such as CD45 remains inconsistent (Medina et al., 2017) and commonly employed methods to quantify EPCs assume a high risk of cell loss. Additional studies are needed to better understand and quantify the EPC population. The findings of this study provide further insight into the potential role of angiogenesis in microvascular pathology of the aging brain.

DATA AVAILABILITY STATEMENT

The raw data supporting the conclusions of this article will be made available by the authors, upon reasonable request.

ETHICS STATEMENT

The studies involving human participants were reviewed and approved by the University of Southern California and University of California, Irvine. The patients/participants provided their written informed consent to participate in this study.

AUTHOR CONTRIBUTIONS

DN contributed to the study design. AK and DN contributed to analyzing the data and drafting the manuscript. AG, AM, IM, BY, JH, AEB, SD, IS, YL, JJ, AMB, and KR contributed to data collection. All authors contributed to manuscript revision, read, and approved the submitted version.

FUNDING

This research was supported by the National Institutes of Health grants (DN: R01AG064228, R01AG060049, P01AG052350, and P50AG016573), Alzheimer's Association (DN: AARG-17-532905), National Science Foundation (SD: DGE1418060), and Canadian Institutes of Health Research (AK: DFD-170763).

REFERENCES

Adamczak, J., and Hoehn, M. (2015). Poststroke Angiogenesis, Con. *Stroke* 2015:46. doi: 10.1161/STROKEAHA.114.007642

Amin Al Olama, A., Wason, J. M. S., Tuladhar, A. M., van Leijsen, E. M. C., Koini, M., Hofer, E., et al. (2020). Simple MRI score aids prediction of dementia in cerebral small vessel disease. *Neurology* 94, e1294–e1302. doi: 10.1212/WNL.0000000000009141

Berntsson, J., Smith, J. G., Johnson, L. S. B., Söderholm, M., Borné, Y., Melander, O., et al. (2019). Increased vascular endothelial growth factor D is associated with atrial fibrillation and ischaemic stroke. *Heart* 105, 553–558. doi: 10.1136/heartjnl-2018-313684

Borné, Y., Gränsbo, K., Nilsson, J., Melander, O., Orho-Melander, M., Smith, J. G., et al. (2018). Vascular Endothelial Growth Factor D, Pulmonary Congestion, and Incidence of Heart Failure. *J. Am. Coll. Cardiol.* 71, 580–582. doi: 10.1016/j.jacc.2017.11.058

Chabriat, H., Joutel, A., Dichgans, M., Tournier-Lasserve, E., and Bousser, M.-G. (2009). CADASIL. *Lancet Neurol.* 2009, 643–653. doi: 10.1016/S1474-4422(09)70127-9

Geng, J., Wang, L., Qu, M., Song, Y., Lin, X., Chen, Y., et al. (2017). Endothelial progenitor cells transplantation attenuated blood-brain barrier damage after ischemia in diabetic mice via HIF- 1α. *Stem Cell Res. Ther.* 8:163. doi: 10.1186/s13287-017-0605-3

Gorelick, P. B., Scuteri, A., Black, S. E., Decarli, C., Greenberg, S. M., Iadecola, C., et al. (2011). Vascular contributions to cognitive impairment and dementia: A statement for healthcare professionals from the American Heart Association/American Stroke Association. *Stroke* 42, 2672–2713. doi: 10.1161/STR.0b013e3182299496

Hayakawa, K., Seo, J. H., Miyamoto, N., Pham, L.-D. D., Navaratna, D., Lo, E. H., et al. (2017). *Brain Angiogenesis After Stroke. In: Biochemical Basis and Therapeutic Implications of Angiogenesis*. Cham: Springer International Publishing, 473–494. doi: 10.1007/978-3-319-61115-0_21

Iadecola, C. (2013). The pathobiology of vascular dementia. *Neuron* 2013, 844–866. doi: 10.1016/j.neuron.2013.10.008

Issa, R., Krupinski, J., Bujny, T., Kumar, S., Kaluza, J., and Kumar, P. (1999). Vascular endothelial growth factor and its receptor, KDR, in human brain tissue after ischemic stroke. *Lab. Invest.* 79, 417–425.

Kong, Z., Hong, Y., Zhu, J., Cheng, X., and Liu, Y. (2018). Endothelial progenitor cells improve functional recovery in focal cerebral ischemia of rat by promoting angiogenesis via VEGF. *J. Clin. Neurosci.* 55, 116–121. doi: 10.1016/j.jocn.2018.07.011

Lee, S., Viqar, F., Zimmerman, M. E., Narkhede, A., Tosto, G., Benzinger, T. L. S., et al. (2016). White matter hyperintensities are a core feature of Alzheimer's disease: Evidence from the dominantly inherited Alzheimer network. *Ann. Neurol.* 79, 929–939. doi: 10.1002/ana.24647

Lee, S.-T., Chu, K., Jung, K.-H., Park, H.-K., Kim, D.-H., Bahn, J.-J., et al. (2009). Reduced circulating angiogenic cells in Alzheimer disease. *Neurology* 72, 1858–1863. doi: 10.1212/WNL.0b013e3181a711f4

Li, L., Liu, H., Xu, C., Deng, M., Song, M., Yu, X., et al. (2017). VEGF promotes endothelial progenitor cell differentiation and vascular repair through connexin 43. *Stem Cell Res. Ther.* 8:237. doi: 10.1186/s13287-017-0684-1

Lohela, M., Bry, M., Tammela, T., and Alitalo, K. (2009). VEGFs and receptors involved in angiogenesis versus lymphangiogenesis. *Curr. Opin. Cell Biol.* 21, 154–165. doi: 10.1016/j.ceb.2008.12.012

Mahoney, E. R., Dumitrescu, L., Moore, A. M., Cambronero, F. E., De Jager, P. L., Koran, M. E. I., et al. (2021). Brain expression of the vascular endothelial growths factor gene family in cognitive aging and alzheimer's disease. *Mol Psychiatry* 26, 888–896. doi: 10.1038/s41380-019-0458-5

Mauceri, D., Buchthal, B., Hemstedt, T. J., Weiss, U., Klein, C. D., and Bading, H. (2020). Nasally delivered VEGFD mimetics mitigate stroke-induced dendrite loss and brain damage. *Proc. Natl. Acad. Sci.* 117, 8616–8623. doi: 10.1073/pnas.2001563117

Mauceri, D., Freitag, H. E., Oliveira, A. M. M., Bengtson, C. P., and Bading, H. (2011). Nuclear Calcium-VEGFD Signaling Controls Maintenance of Dendrite Arborization Necessary for Memory Formation. *Neuron* 71, 117–130. doi: 10.1016/j.neuron.2011.04.022

Medina, R. J., Barber, C. L., Sabatier, F., Dignat-George, F., Melero-Martin, J. M., Khosrotehrani, K., et al. (2017). Endothelial Progenitors: A Consensus Statement on Nomenclature. *Stem Cells Transl. Med.* 6, 1316–1320. doi: 10.1002/sctm.16-0360

Naserian, S., Abdelgawad, M. E., Afshar Bakshloo, M., Ha, G., Arouche, N., Cohen, J. L., et al. (2020). The TNF/TNFR2 signaling pathway is a key regulatory factor in endothelial progenitor cell immunosuppressive effect. *Cell Commun. Signal.* 18:94. doi: 10.1186/s12964-020-00564-3

Nation, D. A., Sweeney, M. D., Montagne, A., Sagare, A. P., D'Orazio, L. M., Pachicano, M., et al. (2019). Blood- brain barrier breakdown is an early biomarker of human cognitive dysfunction. *Nat. Med.* 25, 270–276. doi: 10.1038/s41591-018-0297-y

Nation, D. A., Tan, A., Dutt, S., McIntosh, E. C., Yew, B., Ho, J. K., et al. (2018). Circulating Progenitor Cells Correlate with Memory, Posterior Cortical Thickness, and Hippocampal Perfusion. *J. Alzheimers Dis.* 61, 91–101. doi: 10.3233/JAD-170587

Nouri Barkestani, M., Shamdani, S., Afshar Bakshloo, M., Arouche, N., Bambai, B., Uzan, G., et al. (2021). TNFα priming through its interaction with TNFR2 enhances endothelial progenitor cell immunosuppressive effect: new hope for their widespread clinical application. *Cell Commun. Signal.* 19:1. doi: 10.1186/s12964-020-00683-x

Pantoni, L. (2010). Cerebral small vessel disease: from pathogenesis and clinical characteristics to therapeutic challenges. *Lancet Neurol.* 9, 689–701. doi: 10.1016/S1474-4422(10)70104-6

Pettersen, J. A., Keith, J., Gao, F., Spence, J. D., and Black, S. E. (2017). CADASIL accelerated by acute hypotension: Arterial and venous contribution to leukoaraiosis. *Neurology* 88, 1077–1080. doi: 10.1212/WNL.0000000000003717

Pías-Peleteiro, J., Pérez-Mato, M., López-Arias, E., Rodríguez-Yáñez, M., Blanco, M., Campos, F., et al. (2016). Increased Endothelial Progenitor Cell Levels are Associated with Good Outcome in Intracerebral Hemorrhage. *Sci. Rep.* 6:28724. doi: 10.1038/srep28724

Prodjohardjono, A., Vidyanti, A. N., Susianti, N. A., Sudarmanta, S. S., and Setyopranoto, I. (2020). Higher level of acute serum VEGF and larger infarct volume are more frequently associated with post-stroke cognitive impairment. *PLoS One* 15:e0239370. doi: 10.1371/journal.pone.0239370

Quick, S., Moss, J., Rajani, R. M., and Williams, A. A. (2021). Vessel for Change: Endothelial Dysfunction in Cerebral Small Vessel Disease. *Trends Neurosci.* 44, 289–305. doi: 10.1016/j.tins.2020.11.003

Sobrino, T., Hurtado, O., Moro, M. A., Rodríguez-Yáñez, M., Castellanos, M., Brea, D., et al. (2007). The increase of circulating endothelial progenitor cells after acute ischemic stroke is associated with good outcome. *Stroke* 38, 2759–2764. doi: 10.1161/STROKEAHA.107.484386

Stacker, S., and Achen, M. (2018). Emerging Roles for VEGF-D in Human Disease. *Biomolecules* 8:1. doi: 10.3390/biom8010001

Wada, H., Suzuki, M., Matsuda, M., Ajiro, Y., Shinozaki, T., Sakagami, S., et al. (2020). Distinct Characteristics of VEGF-D and VEGF-C to Predict Mortality in Patients With Suspected or Known Coronary Artery Disease. *J. Am. Heart Assoc.* 9:9. doi: 10.1161/JAHA.119.015761

Wardlaw, J. M., Doubal, F. N., Valdes-Hernandez, M., Wang, X., Chappell, F. M., Shuler, K., et al. (2013a). Blood-brain barrier permeability and long-term clinical and imaging outcomes in cerebral small vessel disease. *Stroke* 2013, 525–527. doi: 10.1161/STROKEAHA.112.669994

Wardlaw, J. M., Smith, C., and Dichgans, M. (2019). Small vessel disease: mechanisms and clinical implications. *Lancet Neurol.* 18, 684–696. doi: 10.1016/S1474-4422(19)30079-1

Wardlaw, J. M., Smith, E. E., Biessels, G. J., Cordonnier, C., Fazekas, F., Frayne, R., et al. (2013b). Neuroimaging standards for research into small vessel disease and its contribution to ageing and neurodegeneration. *Lancet Neurol.* 12, 822–838. doi: 10.1016/S1474-4422(13)70124-8

Zhang, Z. G., Zhang, L., Jiang, Q., Zhang, R., Davies, K., Powers, C., et al. (2000). VEGF enhances angiogenesis and promotes blood-brain barrier leakage in the ischemic brain. *J. Clin. Invest.* 106, 829–838. doi: 10.1172/JCI9369

Zlokovic, B. V. (2008). The blood-brain barrier in health and chronic neurodegenerative disorders. *Neuron* 57, 178–201. doi: 10.1016/j.neuron.2008.01.003

Conflict of Interest: IM was employed by company Chione GmbH.

The remaining authors declare that the research was conducted in the absence of any commercial or financial relationships that could be construed as a potential conflict of interest.

Publisher's Note: All claims expressed in this article are solely those of the authors and do not necessarily represent those of their affiliated organizations, or those of the publisher, the editors and the reviewers. Any product that may be evaluated in this article, or claim that may be made by its manufacturer, is not guaranteed or endorsed by the publisher.

frontiers in Neuroscience

ORIGINAL RESEARCH
published: 01 October 2021
doi: 10.3389/fnins.2021.755056

Association of Serum Uric Acid Levels in Meige's Syndrome

Haochen Guan[1†], Zhi Geng[2†], Weijie Yuan[1] and Bowen Chang[3*]*

[1] Department of Nephrology, Shanghai General Hospital, Shanghai Jiao Tong University School of Medicine, Shanghai, China, [2] Department of Neurology, Second People's Hospital of Hefei City, The Hefei Affiliated Hospital of Anhui Medical University, Hefei, China, [3] Division of Life Sciences and Medicine, Department of Neurosurgery, The First Affiliated Hospital of USTC, University of Science and Technology of China, Hefei, China

Uric acid (URIC) is a natural antioxidant, and it has been shown that low levels of URIC could be a risk factor for the development of Parkinson's disease. Our aim was to investigate whether URIC also plays a role in Meige's syndrome (MS). We conducted a cohort study to compare serum URIC levels between patients with MS and healthy controls. In addition, we analyzed the impact of URIC on the risk of MS and symptom severity. Compared with normal subjects, URIC content was remarkably decreased in MS patients. In addition, URIC was regarded as a protective factor for MS, as verified by multivariate logistic regression models. We also found non-linear relationships between the levels of serum URIC and the incidence rate of MS and the Burke-Fahn-Marsden dystonia rating scale score. Our study is the first to show a connection between serum URIC levels and MS. Low serum URIC levels indicate an increased risk of MS incidence and more severe clinical symptoms. Our findings provide new insights into the prevention and treatment of MS.

Keywords: Meige's syndrome, uric acid, antioxidants, movement disorders, Burke-Fahn-Marsden dystonia rating scale score

OPEN ACCESS

Edited by:
Nicholas James Ashton, University of Gothenburg, Sweden

Reviewed by:
Carlos Henrique Ferreira Camargo, Federal University of Paraná, Brazil
Paul Matthew D. Pasco, University of the Philippines Manila, Philippines
Eduardo Joaquim Lopes Alho, University of São Paulo, Brazil
Rubens Gisbert Cury, University of São Paulo, Brazil

***Correspondence:**
Bowen Chang
changbowen21@163.com
Weijie Yuan
ywj4168@163.com

[†] These authors have contributed equally to this work

Specialty section:
This article was submitted to Neurodegeneration, a section of the journal Frontiers in Neuroscience

Received: *07 August 2021*
Accepted: *10 September 2021*
Published: *01 October 2021*

Citation:
Guan H, Geng Z, Yuan W and Chang B (2021) Association of Serum Uric Acid Levels in Meige's Syndrome. Front. Neurosci. 15:755056. doi: 10.3389/fnins.2021.755056

INTRODUCTION

Meige's syndrome (MS) is a dystonia characterized by bilateral eyelid and involuntary facial muscle movement (Greene et al., 1995; LeDoux, 2009). The incidence is approximately 100 cases per 100,000 people (Defazio et al., 2004). MS is currently considered movement disorder that commonly occurs in elderly female patients (Pandey and Sharma, 2017). Although the pathogenesis of movement disorder such as MS and Parkinson's disease (PD) remains unknown, free radical accumulation (such as reactive oxygen species) and decreased antioxidants within brain tissue may be possible mechanisms (Savitt et al., 2006; Poewe et al., 2017).

Serum uric acid (URIC) has been identified as a natural antioxidant in the human body (Stocker et al., 1987; Becker et al., 1991). Recent meta-analyses and controlled studies suggest that reduced levels of URIC are related to PD (Jesus et al., 2013; Wen et al., 2017). In addition, two prospective articles demonstrated that people showing increased URIC contents may have a lower susceptibility to PD (Davis et al., 1996; Gao et al., 2016) and a slower rate of decline of neurological function (Ascherio et al., 2009). A postmortem study revealed that the URIC content within brain tissue (particularly in the striatal substantia nigra and cortex) was remarkably decreased in PD cases compared with normal controls (Church and Ward, 1994; McFarland et al., 2013). These results suggest that URIC may be related to PD progression, since its reduction within brain tissue indicates antioxidant insufficiency. Whether serum URIC has a similar effect on MS is unknown.

TABLE 1 | Characteristics of the patients with Meige's syndrome and healthy controls.

Variables	Healthy control	Meige's syndrome	*P*-value
No.	133	80	
Gender			0.011
Male	72 (54.1%)	29 (36.2%)	
Female	61 (45.9%)	51 (63.7%)	
Age	55.5 ± 17.9	54.2 ± 10.1	0.547
Uric acid	317.2 ± 71.0	250.5 ± 66.9	< 0.001
CREA	65.2 ± 20.9	62.4 ± 13.9	0.283
BUN	5.3 ± 1.4	5.9 ± 1.5	0.013
ALB	42.0 ± 3.7	42.3 ± 4.1	0.698
Hypertension			0.109
No	94 (70.7%)	48 (60.0%)	
Yes	39 (29.3%)	32 (40.0%)	

TABLE 2 | Association between each variable and Meige's syndrome.

Variables	Statistics	Meige's syndrome OR (95% CI)	*P*-value
Gender			0.011
Male	101 (47.418%)	1.0	
Female	112 (52.582%)	2.076 (1.175, 3.668)	
Age	55.047 ± 15.397	0.994 (0.978, 1.011)	0.502
Uric acid	292.129 ± 76.528	0.985 (0.978, 0.992)	< 0.001
CREA	64.120 ± 18.626	0.991 (0.977, 1.005)	0.223
BUN	5.531 ± 1.492	1.266 (1.050, 1.526)	0.013
ALB	42.119 ± 3.875	1.014 (0.942, 1.093)	0.706
Hypertension			0.111
No	142 (66.667%)	1.0	
Yes	71 (33.333%)	1.607 (0.897, 2.877)	

TABLE 3 | Multivariate regression for effect of serum uric acid levels on Meige's syndrome.

Variable	Non-adjusted		Model I		Model II	
Uric acid	**OR (95% CI)**	***P*-value**	**OR (95% CI)**	***P*-value**	**OR (95% CI)**	***P*-value**
	0.985 (0.980, 0.990)	<0.001	0.985 (0.980, 0.991)	<0.001	0.984 (0.979, 0.990)	< 0.001

Model I adjusted for age and gender. Model II adjusted for age, gender, history of hypertension. CI, confidence interval; OR, odds ratio.

At present, the etiology and pathogenic mechanisms of MS remain unclear. It has been suggested that diverse environmental and genetic factors, mitochondrial dysfunction, and other factors are related to the oxidative stress (OS) of neurons (Steele et al., 2014). This study focused on investigating the serum URIC content in MS and evaluating its impact on the development of MS.

MATERIALS AND METHODS

Meige's Syndrome Patients and Normal Subjects

This retrospective cross-sectional study collected medical records from MS cases diagnosed at the Shanghai General Hospital and Hefei Second People's Hospital between January 2018 and February 2021. Patients meeting the following criteria were included: those with MS, the main manifestations were double blepharospasm, oral and mandibular dystonia, and involuntary movements like facial dystonia; those not receiving treatment such as opioids or non-steroidal anti-inflammatory drugs; those without hematological disorders, hyperpyrexia, concurrent infectious disease, severe heart disease, metabolic disorder, inflammatory disease or medication for inflammatory disease, autoimmune disease, severe liver/kidney disease, other malignancies; and those with sufficient data on the biochemical index of fasting blood. In addition, this study also collected medical records of age- and sex-matched healthy subjects who underwent physical examinations at the same hospital. None of the healthy control subjects took any drugs to raise or lower uric acid. Our study protocols were approved by the Institutional Ethics Committee of the hospital. All participants in this study provided informed consent.

Abbreviations: BFMDRS, Burke-Fahn-Marsden dystonia rating scale; MS, Meige's syndrome; OS, oxidative stress; PD, Parkinson's disease; URIC, uric acid.

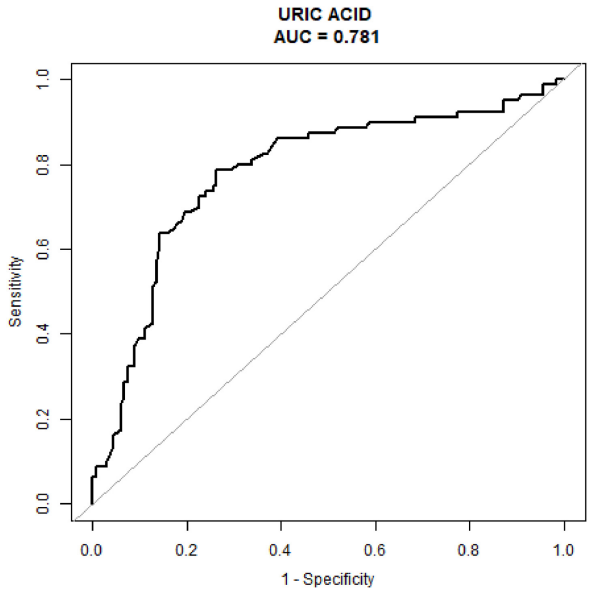

FIGURE 1 | The diagnostic value of serum uric acid levels was evaluated using receiver operating characteristic analysis testing patients with Meige's syndrome against healthy controls.

TABLE 4 | The threshold effect of serum uric acid levels on incidence rate of Meige's syndrome assessments.

	OR (95% CI)	*P*-value
Uric acid <337 μmol/L	0.975 (0.968, 0.983)	< 0.001
Uric acid ≥337 μmol/L	1.007 (0.997, 1.018)	0.186

Adjusted for age, gender, history of hypertension. CI, confidence interval; OR, odds ratio.

Data Extraction

Patient clinicopathological and demographic variables, including sex, age, BFMDRS (Burke-Fahn-Marsden dystonia rating scale) score, and history of hypertension were collected from medical records. In addition, blood samples were collected upon admission to conduct kidney and liver tests, which were part of the standard workup. Each specimen was assayed by the Department of Clinical Laboratory 2 h post-collection. Specifically, URIC, albumin (ALB), blood urea nitrogen (BUN), and creatinine (CREA) levels were examined to assess kidney and liver function. The above clinical variables were determined using standard automatic counters. The epidemiological data, clinical evaluation, and laboratory tests were extracted from the same visit of each patient.

Statistical Analyses

R[1] and Empower (R)[2] (X&Y solutions, Inc., Boston, MA, United States) software were used for statistical analysis. First, the normal distribution of variables was assessed using the Kolmogorov–Smirnov test, and normally distributed data were assessed by one-way analysis of variance or two-tailed Student's *t*-test. Simultaneously, non-parametric data were compared across diverse groups using the Mann–Whitney *U* test. A multiple logistic regression model was employed to evaluate the relationships between inflammatory markers and MS. Additionally, the value of the area under the receiver operating characteristic (ROC) curve (AUC) was determined to assess the significance of URIC in the diagnosis of MS. The two-piecewise linear regression model was also utilized to examine the role of URIC in predicting MS and BFMDRS scores using the smoothing function. Typically, trial and error were utilized to determine the threshold level (turning point), such as selecting the turning point down a preset interval and later selecting a turning point giving the maximum model likelihood. After *post hoc* analysis, we determined the outlier by adopting the value with maximal specificity and sensitivity. Statistical significance was set at $P < 0.05$.

[1]http://www.R-project.org

[2]www.empowerstats.com

RESULTS

Study Participants

Altogether, data for 80 MS cases and 133 healthy controls were collected for final analyses. **Table 1** shows the demographic data of all study participants. There were 29 (36.2%) male and 51 (63.7%) female MS patients, with ages ranging between 39 and 81 years. There were 72 (54.1%) male controls, aged between 29 and 86 years.

Comparing the Biochemical Indexes Between Meige's Syndrome Patients and Normal Subjects

Table 1 shows the features of all study participants. Differences in ALB, BUN, CREA, and diabetes history were not significant between the two groups. In contrast, URIC levels of MS cases (250.5 ± 66.9 μmol/L) decreased significantly in comparison with healthy controls (317.2 ± 71.0 μmol/L; $P < 0.05$).

Relationship of Uric Acid With Meige's Syndrome

Table 2 displays the relationships between MS and diverse variables, such as sex, age, ALB, BUN, CREA, URIC, and hypertension history. URIC content was closely related to MS, and increased URIC content served as a protective factor for MS. **Table 3** presents the above relationships assessed through multivariate analyses. As suggested by multivariate analysis, URIC content was closely related to MS (Odds ratio [OR] = 0.985; 95% confidence interval [CI]: 0.980–0.990; $P < 0.001$). After adjusting for confounders such as sex, age, and hypertension history, the results remained largely unchanged, which confirmed that the decreased URIC content served as a risk factor for CH (OR = 0.984; 95% CI: 0.979–0.990; $P < 0.001$). The value of URIC in diagnosing MS patients (ROC curves) is

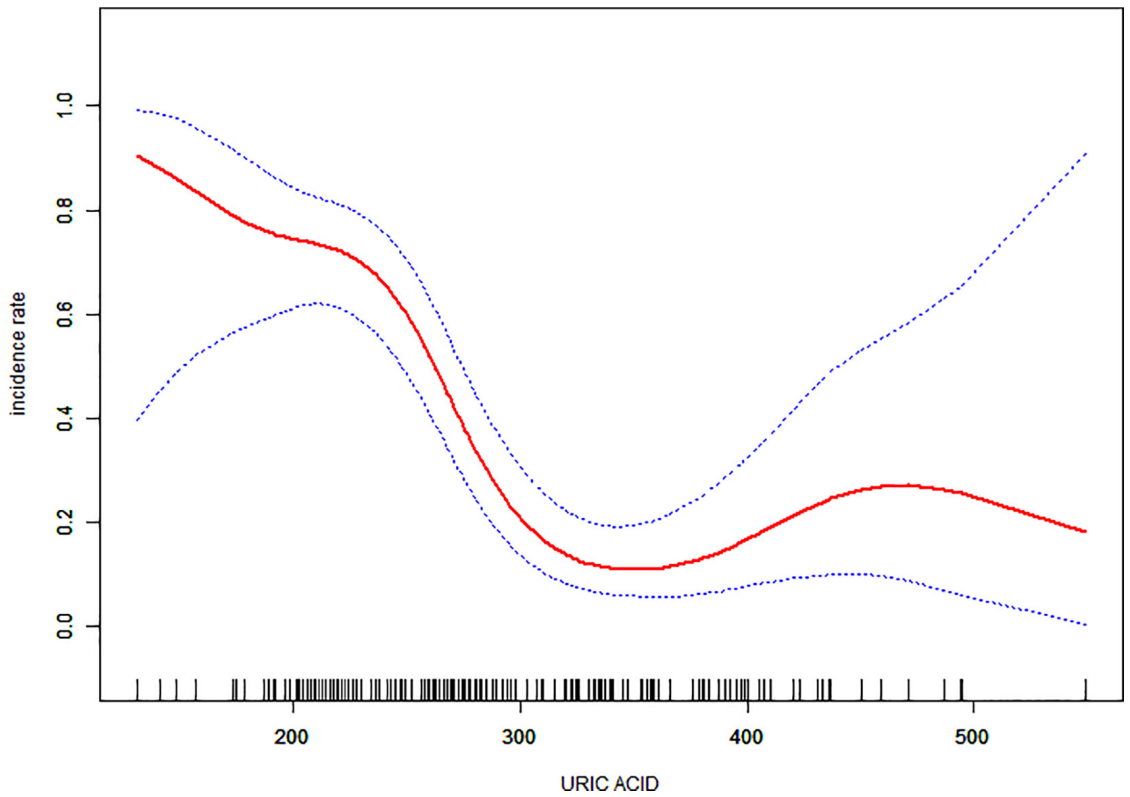

FIGURE 2 | The association of serum uric acid levels between the incidence rate of Meige's syndrome. The adjusted data for the incidence rate of Meige's syndrome is plotted against serum uric acid levels with a curve indicating the shaped relationship between the two. A threshold serum uric acid level of 337 μmol/L existed for the regulation of uric acid.

TABLE 5 | The threshold effect of serum uric acid levels on score of BFMDRS assessments.

	OR (95% CI)	*P*-value
Uric acid <330 μmol/L	−0.065 (−0.075, −0.056)	< 0.001
Uric acid ≥330 μmol/L	0.006 (−0.010, 0.021)	0.186

Adjusted for age, gender, history of hypertension. CI, confidence interval; OR, odds ratio.

shown in **Figure 1**. Our results indicated that the URIC values performed the best in diagnosis, with an AUC value of 0.781 and the specificity and sensitivity were 0.7368 and 0.7875, respectively (**Figure 1**).

Non-linear relationships between serum URIC and the incidence rate of MS and the BFMDRS score were detected. The incidence rate of MS increased as serum URIC levels decreased to the turning point (URIC = 337 μmol/L). With a URIC level ≥ 337 μmol/L, the predicted dose–response curve conformed to the horizontal line (**Table 4** and **Figure 2**). Similarly, the severity of symptoms increased with decreasing URIC levels to the turning point (URIC = 330 μmol/L). Likewise, the OR of the incidence rate of MS was 0.975 (95% CI: 0.968–0.983), and −0.065 (95% CI: −0.075 to −0.056) for BFMDRS scores (**Table 5** and **Figure 3**).

DISCUSSION

Numerous studies have been conducted on the relationship between serum URIC levels and neurological diseases. Nonetheless, the association is still controversial because of the small sample sizes; besides, other confounders such as sex and age may have a certain impact. Currently, there are disputes regarding the role of URIC content in the prognosis prediction of neurological disorders. Increased URIC content has been suggested as a protective factor for functional results (Xue et al., 2017), whereas other studies suggest URIC content as a risk factor (Jung et al., 2018). The effect of URIC levels on MS has not been investigated until now.

This study analyzed URIC contents in MS patients and normal subjects. The results suggested that MS patients had decreased serum URIC content compared with normal subjects, suggesting that decreased URIC levels might serve as an MS-related risk factor. After adjusting for sex, age, and hypertension history, the heterogeneity remained significant. This result conforms to the opinion that URIC shows neuroprotection, which may be related to its role as an iron chelator and antioxidant (Davies et al., 1986). OS is related to numerous central nervous system (CNS) diseases, such as the dopaminergic cell decomposition of PD and early neuronal characteristics

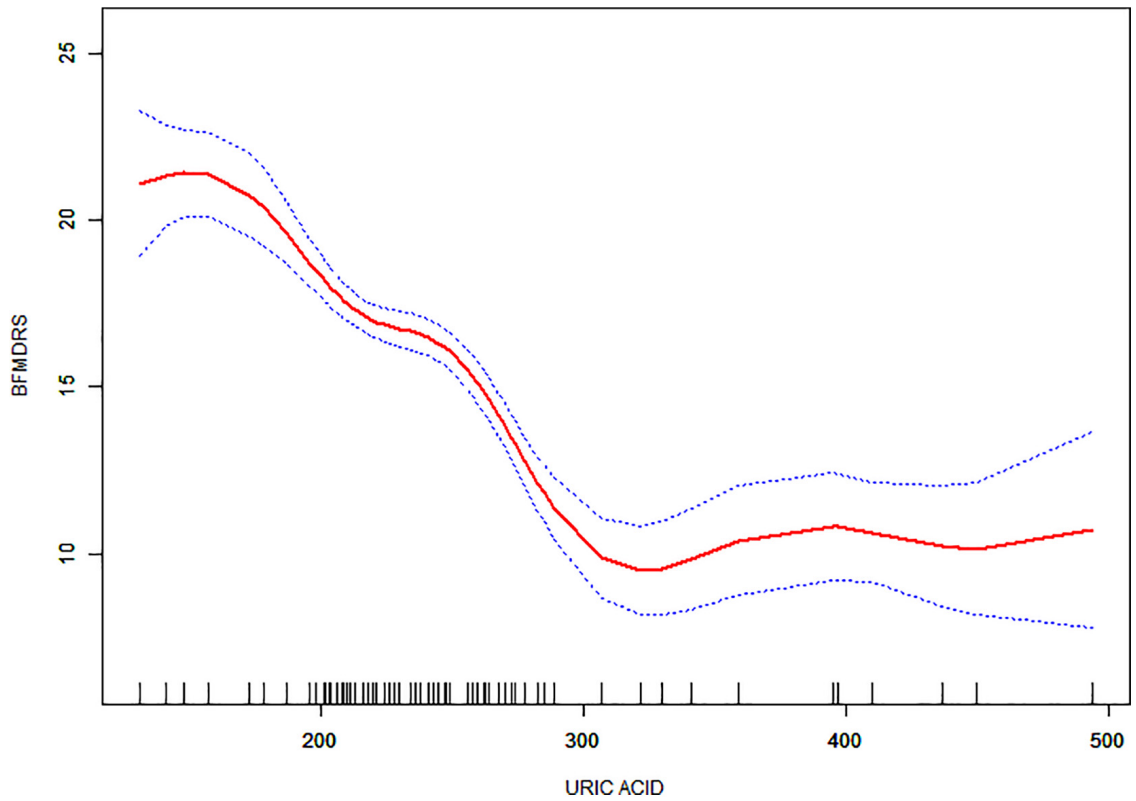

FIGURE 3 | The association between serum uric acid levels and Burke-Fahn-Marsden dystonia rating scale scores. A non-linear relationship was observed, and a threshold serum uric acid of 330 μmol/L existed for the regulation of uric acid.

in Alzheimer's disease (Moreira et al., 2006; Wei et al., 2018). Moreover, free radicals such as peroxynitrite may facilitate axonal demyelination and inflammation (Hooper et al., 2000). Therefore, the prevention of OS can delay the occurrence of such CNS diseases and improve their prognostic outcomes. URIC is a potent endogenous antioxidant that functions in resisting OS-mediated neuronal death and neurodegeneration, as suggested by *in vivo* and *in vitro* studies (Chen et al., 2013; Bartoli et al., 2017). As a result, the present work indicates that URIC exerts antioxidant and neuroprotective effects in MS.

URIC contents in MS cases are similar to those in PD cases, indicating a similar pathophysiological mechanism underlying neuronal injury. The neuroprotective effects of glutathione have been demonstrated in several studies (Fitzmaurice et al., 2003). The reduced glutathione content in PD is possibly due to the aberrant production, utilization, and catabolism of URIC and/or additional CNS antioxidants (Albers et al., 1999). Therefore, the decreased glutathione content in MS may be due to the decreased URIC content. Further studies are needed to explore this relationship.

Our study also found an interesting non-linear relationship between URIC levels, MS incidence and symptom severity, indicating that the incidence and severity of MS increased significantly when URIC was lower than 337 and 330 μmol/L. This suggests that monitoring and regulating URIC may be important for both patients with MS and healthy individuals. It is well known that the normal value of URIC is 149–416 μmol/L in males and 89–357 μmol/L in females (Maiuolo et al., 2016). When URIC is higher than normal, there is a risk of gout and cardiovascular disease (Jung et al., 2018). However, this study demonstrates that low serum URIC levels increase the risk of MS and the severity of symptoms in patients with MS. In summary, it is necessary to control serum URIC at an appropriate level. Therefore, our results suggest that controlling serum uric acid levels in the range of 337 μmol/L to the upper normal value is a reasonable goal. Thus, serum uric acid levels are a double-edged sword, and regulating URIC levels at an appropriate level is beneficial for preventing and delaying neurological diseases.

This study has some limitations. First, the MS cohort had a small sample size. Second, this study only extracted data regarding whether the study subjects had hypertension, but no information on detailed medication was gathered. Third, this study did not determine the long-term effects of URIC on MS.

The present study was the first to analyze the association of serum URIC levels with MS. Low serum URIC levels predict

a higher MS risk and serious clinical symptoms. This study sheds light on future avenues of research for the prevention and treatment of MS.

DATA AVAILABILITY STATEMENT

The raw data supporting the conclusions of this article will be made available by the authors, without undue reservation.

ETHICS STATEMENT

The studies involving human participants were reviewed and approved by Shanghai General Hospital Institutional Ethics Committee Second People's Hospital of Hefei Institutional Ethics Committee. The patients/participants provided their written informed consent to participate in this study.

AUTHOR CONTRIBUTIONS

HG and ZG jointly completed the experiment and the writing. BC and WY took overall control of the whole study. All authors contributed to the article and approved the submitted version.

ACKNOWLEDGMENTS

We would like to thank Editage for English language editing.

REFERENCES

Albers, D. S., Augood, S. J., Martin, D. M., Standaert, D. G., Vonsattel, J. P., and Beal, M. F. (1999). Evidence for oxidative stress in the subthalamic nucleus in progressive supranuclear palsy. *J. Neurochem.* 73, 881–884. doi: 10.1046/j.1471-4159.1999.0730881.x

Ascherio, A., LeWitt, P. A., Xu, K., Eberly, S., Watts, A., Matson, W. R., et al. (2009). Urate as a predictor of the rate of clinical decline in Parkinson disease. *Arch. Neurol.* 66, 1460–1468. doi: 10.1001/archneurol.2009.247

Bartoli, F., Carra, G., and Clerici, M. (2017). Purinergic dysfunction in bipolar disorder: any role for the antioxidant uric acid as a trait and state biomarker? *Psychiatry Clin. Neurosci.* 71:417. doi: 10.1111/pcn.12518

Becker, B. F., Reinholz, N., Leipert, B., Raschke, P., Permanetter, B., and Gerlach, E. (1991). Role of uric acid as an endogenous radical scavenger and antioxidant. *Chest* 100, 176S–181S. doi: 10.1378/chest.100.3_Supplement.176S

Chen, X., Burdett, T. C., Desjardins, C. A., Logan, R., Cipriani, S., Xu, Y., et al. (2013). Disrupted and transgenic urate oxidase alter urate and dopaminergic neurodegeneration. *Proc. Natl. Acad. Sci. U. S. A.* 110, 300–305. doi: 10.1073/pnas.1217296110

Church, W. H., and Ward, V. L. (1994). Uric acid is reduced in the substantia nigra in Parkinson's disease: effect on dopamine oxidation. *Brain Res. Bull.* 33, 419–425. doi: 10.1016/0361-9230(94)90285-2

Davies, K. J., Sevanian, A., Muakkassah-Kelly, S. F., and Hochstein, P. (1986). Uric acide iron ion complexes. A new aspect of the antioxidant functions of uric acid. *Biochem. J.* 235, 747–754. doi: 10.1042/bj2350747

Davis, J. W., Grandinetti, A., Waslien, C. I., Ross, G. W., White, L. R., and Morens, D. M. (1996). Observations on serum uric acid levels and the risk of idiopathic Parkinson's disease. *Am. J. Epidemiol.* 144, 480–484. doi: 10.1093/oxfordjournals.aje.a008954

Defazio, G., Abbruzzese, G., Livrea, P., and Berardelli, A. (2004). Epidemiology of primary dystonia. *Lancet Neurol.* 3, 673–678. doi: 10.1016/S1474-4422(04)00907-X

Fitzmaurice, P. S., Ang, L., Guttman, M., Rajput, A. H., Furukawa, Y., and Kish, S. J. (2003). Nigral glutathione deficiency is not specific for idiopathic Parkinson's disease. *Mov. Disord.* 18, 969–976. doi: 10.1002/mds.10486

Gao, X., O'Reilly, E. J., Schwarzschild, M. A., and Ascherio, A. (2016). Prospective study of plasma urate and risk of Parkinson disease in men and women. *Neurology* 86, 520–526. doi: 10.1212/WNL.0000000000002351

Greene, P., Kang, U. J., and Fahn, S. (1995). Spread of symptoms in idiopathic torsion dystonia. *Mov. Disord.* 10, 143–152. doi: 10.1002/mds.870100204

Hooper, D. C., Scott, G. S., Zborek, A., Mikheeva, T., Kean, R. B., Koprowski, H., et al. (2000). Uric acid, a peroxynitrite scavenger, inhibits CNS inflammation, blood–CNS barrier permeability changes, and tissue damage in a mouse model of multiple sclerosis. *FASEB J.* 14, 691–698. doi: 10.1096/fasebj.14.5.691

Jesus, S., Perez, I., Caceres-Redondo, M. T., Carrillo, F., Carballo, M., Gomez-Garre, P., et al. (2013). Low serum uric acid concentration in Parkinson's disease in southern Spain. *Eur. J. Neurol.* 20, 208–210. doi: 10.1111/j.1468-1331.2012.03745.x

Jung, J. Y., Choi, Y., Suh, C. H., Yoon, D., and Kim, H. (2018). Effect of fenofibrate on uric acid level in patients with gout. *Sci. Rep.* 8:16767. doi: 10.1038/s41598-018-35175-z

LeDoux, M. S. (2009). Meige syndrome: what's in a name? *Parkinsonism Relat. Disord.* 15, 483–489. doi: 10.1016/j.parkreldis.2009.04.006

Maiuolo, J., Oppedisano, F., Gratteri, S., Muscoli, C., and Mollace, V. (2016). Regulation of uric acid metabolism and excretion. *Int. J. Cardiol.* 15, 8–14. doi: 10.1016/j.ijcard.2015.08.109

McFarland, N. R., Burdett, T., Desjardins, C. A., Frosch, M. P., and Schwarzschild, M. A. (2013). Postmortem brain levels of urate and precursors in Parkinson's disease and related disorders. *Neurodegener Dis.* 12, 189–198. doi: 10.1159/000346370

Moreira, P. I., Honda, K., Zhu, X., Nunomura, A., Casadesus, G., Smith, M. A., et al. (2006). Brain and brawn Parallels in oxidative strength. *Neurology* 66, 97–101. doi: 10.1212/01.wnl.0000192307.15103.83

Pandey, S., and Sharma, S. (2017). Meige's syndrome: history, epidemiology, clinical features, pathogenesis and treatment. *J. Neurol. Sci.* 372, 162–170. doi: 10.1016/j.jns.2016.11.053

Poewe, W., Seppi, K., Tanner, T. M., Halliday, G. M., Brundin, P., Volkmann, J., et al. (2017). Parkinson disease. *Nat. Rev. Dis. Primer* 3, 1–21. doi: 10.1038/nrdp.2017.13

Savitt, J. M., Dawson, V. L., and Dawson, T. M. (2006). Diagnosis and treatment of Parkinson disease: molecules to medicine. *J. Clin. Invest.* 116, 1744–1754. doi: 10.1172/JCI29178

Steele, J. C., Richardson, J. C., and Olszewski, J. (2014). Progressive supranuclear palsy: a heterogeneous degeneration involving the brain stem, basal ganglia and cerebellum with vertical gaze and pseudobulbar palsy, nuchal dystonia and dementia. *Semin. Neurol.* 34, 129–150. doi: 10.1055/s-0034-1377058

Stocker, R., Yamamoto, Y., McDonagh, A. F., Glazer, A. N., and Ames, B. N. (1987). Bilirubin is an antioxidant of possible physiological importance. *Science* 235, 1043–1046. doi: 10.1126/science.3029864

Wei, Z., Li, X., Li, X., Liu, Q., and Cheng, Y. (2018). Oxidative stress in Parkinson's disease: a systematic review and meta-analysis. *Front. Mol. Neurosci.* 11:236. doi: 10.3389/fnmol.2018.00236

Wen, M., Zhou, B., Chen, Y. H., Ma, Z. L., Gou, Y., Zhang, C. L., et al. (2017). Serum uric acid levels in patients with Parkinson's disease: a meta-analysis. *PLoS One* 12:e0173731. doi: 10.1371/journal.pone.0173731

Xue, L., Liu, Y., Xue, H., Xue, J., Sun, K., Wu, L., et al. (2017). Low uric acid is a risk factor in mild cognitive impairment. *Neuropsychiatr. Dis. Treat.* 13, 2363–2367. doi: 10.2147/NDT.S145812

Conflict of Interest: The authors declare that the research was conducted in the absence of any commercial or financial relationships that could be construed as a potential conflict of interest.

Publisher's Note: All claims expressed in this article are solely those of the authors and do not necessarily represent those of their affiliated organizations, or those of the publisher, the editors and the reviewers. Any product that may be evaluated in this article, or claim that may be made by its manufacturer, is not guaranteed or endorsed by the publisher.

frontiers in Aging Neuroscience

ORIGINAL RESEARCH
published: 14 October 2021
doi: 10.3389/fnagi.2021.747686

High Blood Uric Acid Is Associated With Reduced Risks of Mild Cognitive Impairment Among Older Adults in China: A 9-Year Prospective Cohort Study

Chen Chen[1†], Xueqin Li[2†], Yuebin Lv[1], Zhaoxue Yin[3], Feng Zhao[1], Yingchun Liu[1], Chengcheng Li[1], Saisai Ji[1], Jinhui Zhou[1], Yuan Wei[1], Xingqi Cao[2], Jiaonan Wang[1,4], Heng Gu[1], Feng Lu[5], Zuyun Liu[2,6] and Xiaoming Shi[1,4]**

[1] China CDC Key Laboratory of Environment and Population Health, National Institute of Environmental Health, Chinese Center for Disease Control and Prevention, Beijing, China, [2] Department of Big Data in Health Science, School of Public Health, Zhejiang University School of Medicine, Hangzhou, China, [3] Division of Non-communicable Disease and Healthy Ageing Management, Chinese Center for Disease Control and Prevention, Beijing, China, [4] Center for Global Health, School of Public Health, Nanjing Medical University, Nanjing, China, [5] Beijing Municipal Health Commission Information Center, Beijing Municipal Health Commission Policy Research Center, Beijing, China, [6] Center for Clinical Big Data and Analytics, Second Affiliated Hospital, Zhejiang University School of Medicine, Hangzhou, China

OPEN ACCESS

Edited by:
Henrik Zetterberg, University of Gothenburg, Sweden

Reviewed by:
Hao Peng, Soochow University, China
Dongfeng Zhang, Qingdao University, China

***Correspondence:**
Zuyun Liu
zuyunliu@zju.edu.cn;
Zuyun.liu@outlook.com
Xiaoming Shi
shixm@chinacdc.cn

† These authors have contributed equally to this work

Received: *26 July 2021*
Accepted: *22 September 2021*
Published: *14 October 2021*

Citation:
Chen C, Li X, Lv Y, Yin Z, Zhao F, Liu Y, Li C, Ji S, Zhou J, Wei Y, Cao X, Wang J, Gu H, Lu F, Liu Z and Shi X (2021) High Blood Uric Acid Is Associated With Reduced Risks of Mild Cognitive Impairment Among Older Adults in China: A 9-Year Prospective Cohort Study. Front. Aging Neurosci. 13:747686. doi: 10.3389/fnagi.2021.747686

Background: It remains unsolved that whether blood uric acid (UA) is a neuroprotective or neurotoxic agent. This study aimed to evaluate the longitudinal association of blood UA with mild cognitive impairment (MCI) among older adults in China.

Methods: A total of 3,103 older adults (aged 65+ years) free of MCI at baseline were included from the Healthy Aging and Biomarkers Cohort Study (HABCS). Blood UA level was determined by the uricase colorimetry assay and analyzed as both continuous and categorical (by quartile) variables. Global cognition was assessed using the Mini-Mental State Examination four times between 2008 and 2017, with a score below 24 being considered as MCI. Cox proportional hazards models were used to examine the associations.

Results: During a 9-year follow-up, 486 (15.7%) participants developed MCI. After adjustment for all covariates, higher UA had a dose-response association with a lower risk of MCI (all $P_{for\ trend} < 0.05$). Participants in the highest UA quartile group had a reduced risk [hazard ratio (HR), 0.73; 95% (CI): 0.55–0.96] of MCI, compared with those in the lowest quartile group. The associations were still robust even when considering death as a competing risk. Subgroup analyses revealed that these associations were statistically significant in younger older adults (65–79 years) and those without hyperuricemia. Similar significant associations were observed when treating UA as a continuous variable.

Conclusions: High blood UA level is associated with reduced risks of MCI among Chinese older adults, highlighting the potential of managing UA in daily life for maintaining late-life cognition.

Keywords: uric acid, mild cognitive impairment, cognitive function, older adults, prospective cohort study

INTRODUCTION

Uric acid (UA) is a chemical which is created when the human body breaks down purines and then catalyzed by xanthine oxidase. Blood UA level is determined by the residual quantities between dietary purine intake and renal excretion. Hyperuricemia, the status of an abnormally high level of UA in the blood, is a prerequisite for gout (Zhu et al., 2011). Both hyperuricemia and gout confer a high risk for subsequent metabolic syndrome (Choi et al., 2007) and cardiovascular diseases (CVDs) (Feig et al., 2008; Richette et al., 2014). However, as a natural antioxidant, the antioxidant properties of UA may protect against the detrimental effect of oxidative stress among people with central nervous system disorders (Euser et al., 2009; Gong et al., 2012). Some debates have been raised that urate-lowering-therapies might paradoxically expose patients to a high risk of neurodegenerative disease (such as dementia) (Khan et al., 2016; Singh and Cleveland, 2018b).

To date, many studies have explored the associations between blood UA levels and cognition or dementia in developed countries, but the results remain in dispute. Positive (De Vera et al., 2008; Euser et al., 2009; Irizarry et al., 2009; Cicero et al., 2015; Lu et al., 2016; Pellecchia et al., 2016; Ye et al., 2016; Tuven et al., 2017), negative (Latourte et al., 2018; Singh and Cleveland, 2018a; Alam et al., 2020), U-shaped (Huang et al., 2019), or no associations (Iuliano et al., 2010) of blood UA levels with cognition have been reported. In China, some cross-sectional studies support the neuroprotective role of UA in cognition. However, most of them were limited to their cross-sectional nature and the relatively small sample size (Li et al., 2010; Wu et al., 2013; Liu et al., 2017; Wang F. et al., 2017; Xiu et al., 2017; Xu et al., 2017). To our best knowledge, only three relevant longitudinal studies have been conducted, with one on Parkinson's disease (PD) (Hu et al., 2020) or one on dementia (Hong et al., 2015). The only one on cognition was limited to its relatively short follow-up time (ranged from 1.3 to 2.4 years) (Wang T. et al., 2017) (For detailed information see **Supplementary Table 1**). Therefore, investigations on the long-term effect of UA on cognition in general Chinese populations are urgently needed.

Therefore, based on 9-year follow-up data from a community-based multi-wave cohort of older adults (65 years and older), the Healthy Aging and Biomarkers Cohort Study (HABCS), this study aimed to evaluate the longitudinal associations of blood UA levels with the risks of incident mild cognitive impairment (MCI) in general Chinese older population.

MATERIALS AND METHODS

Study Population

The HABCS was launched in eight longevity areas in China in 2008, collecting comprehensive data, such as health status, and behavioral, laboratory, and anthropometric measurements. The follow-up surveys were conducted in 2012, 2014, and 2017. Due to the high death rate in older adults, new participants were recruited in the follow-up surveys to maintain a stable sample size for the dynamic cohort. Details of the survey design have been described elsewhere (Lv et al., 2019). A total of 5,074 older adults from the 2008 survey and the recruits from the follow-up surveys (2012–2014 waves) from the HABCS were included in this study. We excluded 606 participants aged < 65 years, six participants with missing data on sex, 368 participants on Mini-Mental State Examination (MMSE) score, and 195 participants on UA levels, and then excluded 796 participants with prevalent CI at baseline, leaving 3,103 participants free of CI for the final longitudinal analysis (**Figure 1**). All participants or their legal representatives gave written informed consent to participate in the baseline and follow-up surveys. The HABCS was approved by the Ethics Committee of Peking University and Duke University.

Assessment of Blood Uric Acid Levels

Fasting venous blood was collected from all participants at the baseline wave (the year 2008–2014). The plasma was separated and stored at −20°C and delivered to the laboratory at Capital Medical University in Beijing for unified detection. Blood UA level was determined by uricase colorimetry assay. Details on quality control and assessments in the laboratory were described elsewhere (Yi et al., 2012). Blood UA levels > 420 μmol/L in men and UA levels > 360 μmol/L in women were defined as hyperuricemia (Zhang et al., 2011), which indicates above the UA normal range. Both continuous (i.e., per 10 μmol/L blood UA increment) and categorical (i.e., sex-specific quartiles of UA) type were constructed and used in all analyses.

Assessment of Cognition

Cognition was assessed in the years 2008, 2012, 2014, and 2017, using the modified version of the widely used MMSE questionnaire. The MMSE included six cognitive domains (orientation, working memory, concentration, memory recall, language, and visuospatial ability), with a total score ranging from 0 to 30, and the higher score indicates better cognition. In HABCS, professionally trained staff interviewed participants at the baseline survey and subsequent follow-up surveys face-to-face at their homes. We asked the trained staff to review the MMSE form before each formal interview. Trained staff asked questions in order which were listed on the form, then scored immediately and documented score in the appropriate location. For participants who were unable to complete a question, we did not ask questions again (Katzman et al., 1988; Lv et al., 2019). We categorized cognition into two levels: no MCI ($24 \leq$ MMSE ≤ 30) and MCI (MMSE < 24) as done previously (Creavin et al., 2016; Yuan et al., 2019). We set MCI as the outcome and calculated the follow-up time for each participant from baseline to either the date of incident MCI, loss to follow-up (including death), or the end of the study period, whichever came first.

Covariates

Age, sex, education, current marital status, current smoking, current alcohol consuming, regular exercise, and adequate medical service were considered. Education was categorized as having more than 1 year of schooling or no formal education. Current marital status was categorized as currently married or others. Current smoking and current alcohol consumption

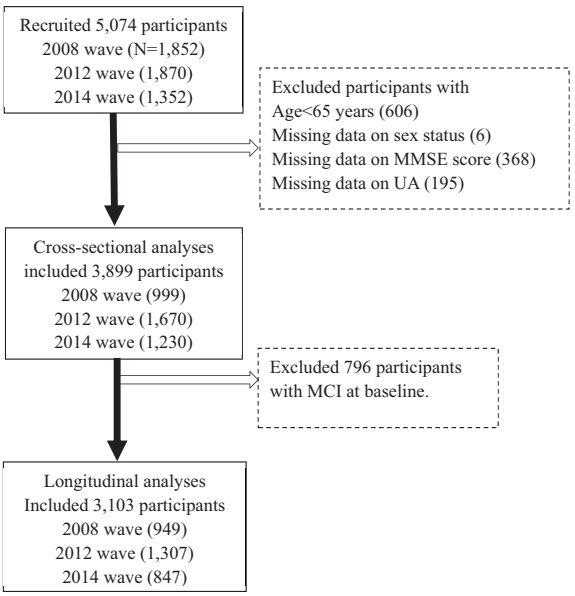

FIGURE 1 | Flowchart of study participant enrollment in this study. MMSE, Mini-Mental State Examination. UA, uric acid.

were categorized as with or without status. Regular exercise was classified into "yes" or "no" by the question "Do you do exercises regularly at present, including walking, playing ball, running, and Qigong?" Hypertension was defined as yes if a participant had an SBP $\geq$ 140 mmHg and/or a DBP $\geq$ 90, or self-reported suffering from hypertension. Diabetes mellitus was defined as yes if a participant had fasting glucose $\geq$ 7.0 mmol/L or self-reported current diabetes medication use. Self-reported history of heart disease, stroke and CVD were also considered. Standardized protocols were used to collect measurements of weight, height, and waist circumference (WC) (Lv et al., 2018). Central obesity was defined as 85 cm or larger of WC in men and 80 cm or larger of WC in women. These covariates have been demonstrated as important correlations with blood UA level (Norris et al., 2018), or cognition (Liu et al., 2018), or both (Lv et al., 2019).

Statistical Analyses

Descriptive statistics of the baseline characteristics were presented as means ± standard deviation (SD) or percentages among the full sample and by the sex-specific UA quartile groups.

First, we evaluated the associations and dose-response relationship between blood UA and baseline cognition score, to confirm the findings from previous studies using a cross-section design.

Second, we ran the main analysis (prospective analysis), i.e., examining the association between blood UA quartiles (the lowest UA quartile as a reference category) and the risk of MCI. Cox proportional hazards model was used and hazard ratios (HRs) and 95% confidence intervals (CIs) were documented. Three models were considered. In model 1, we included age, sex, and education. In model 2, we further included current smoking, current alcohol consuming, marital status, regular exercise, BMI, central obesity, and adequate medical service based on model 1. In model 3, we additionally adjusted for hypertension, diabetes mellitus, heart disease, and stroke and CVD based on model 2. Then, given the high proportion of death in older adults, we used Fine and Gray competing risk models (Fine and Gray, 1999) to re-examine the association between blood UA and risk of developing MCI, using the similar models as above. Additionally, we used restricted cubic splines (RCS) to flexibly model and visualize the dose-response association of blood UA levels with the risk of MCI with three sex-specific knots at the 5th, 50th, and 95th percentiles of blood UA distribution in model 1. We performed subgroup analyses of the association between blood UA and the risk of developing MCI by age (65–79 vs $\geq$ 80 years), sex (men vs women), and hyperuricemia (without hyperuricemia vs with hyperuricemia) using model 3. We added the interaction items (e.g., age group × UA quantiles) to determine whether the associations differed by the subgroup.

Third, as MCI is a disease state rather than an acute event, such as stroke, we also explored the longitudinal associations between baseline blood UA and the repeated MMSE scores at follow-up examinations using a mixed-effect linear model (Littell et al., 1998). We repeated the three steps of analyses above using blood UA as a continuous variable (i.e., per 10 μmol/L blood UA increment).

Two sensitivity analyses were conducted to verify the robustness of the above estimations. First, we compared the baseline characteristics of the included and excluded participants. Second, because we included new participants enrolled in the follow-up surveys, we also compared the baseline characteristics of study participants by different enrolled times. A *P*-value of less than 0.05 (two-tailed) was considered. All analyses were carried out in SAS version 9.4 (SAS Institute, Cary, NC, United States).

RESULTS

Cross-Sectional Associations of Blood Uric Acid and Cognition

We included 3,899 participants for the cross-sectional analysis and their basic characteristics were presented in **Supplementary Table 2**. We observed that higher blood UA levels were associated with higher cognitive scores ($\beta = 0.08$, for per 10 μmol/L blood UA level increment, $P < 0.010$), after fully adjusting of covariates in model 3. Additionally, compared with the participants in the lowest quartile group, those in the highest quartile group had 1.41 points higher cognitive scores (**Table 1**). We found consistent results of higher UA levels associated with higher cognition scores using dose-response testing in the cross-sectional analysis (**Supplementary Figure 1**).

Main Analysis: Prospective Associations of Blood Uric Acid With the Incidence of Mild Cognitive Impairment

For prospective analyses, we included 3,103 participants. The mean (SD) age of 3,103 older adults was 85.1 (±11.7) years, and approximately 54% ($n = 1{,}688$) were women. Participants

TABLE 1 | Cross-sectional associations of blood UA levels with the cognitive score.

Blood UA (μmol/L)	Model 1 β (SE)	Model 2 β (SE)	Model 3 β (SE)
Continuous variable			
Per 10 μmol/L increment	0.09 (0.01)**	0.08 (0.01)**	0.08 (0.01)**
By quartiles[a]			
Q_1	Ref.	Ref.	Ref.
Q_2	0.85 (0.35)	0.46 (0.35)	0.32 (0.35)
Q_3	1.53 (0.35)**	1.44 (0.36)**	1.27 (0.36)**
Q_4	1.90 (0.36)**	1.66 (0.36)**	1.41 (0.36)**
P for linear trend	<0.010	<0.010	<0.010

UA, uric acid; SE, standard estimation.
Model 1 adjusted for age, sex, and education; model 2 additionally adjusted for drinking, smoking, marital status, regular exercise, body mass index, central obesity, adequate medical service; model 3 additionally adjusted for hypertension, diabetes mellitus, self-reported history of heart disease, and stroke and cardiovascular disease.
[a]*The cutoff values were 214.2, 264.0, and 319.0 μmol/L for women, 252.0, 304.6, and 364.5 μmol/L for men.*
***P < 0.01.*

with higher blood UA were more likely to have traditional cardiovascular disease risk factors (drinking, central obesity, hypertension, and diabetes mellitus), while had a higher proportion of the assumed healthy behaviors (regular exercise) (all $P < 0.050$, **Table 2**).

During a 9-year follow-up, 486 (15.7%) participants developed MCI. From three adjusted models in **Table 3**, we found that higher UA levels had a lower risk of developing MCI. After full adjustment of covariates in model 3, compared with participants in the lowest quartile group of UA level (Q1), those in the highest quartile group (Q4) had a 27% lower risk of MCI [$HR_{Q4vsQ1} = 0.73$ (95% CIs: 0.55–0.96)]. The association was still robust after considering death as a competing risk [$HR_{Q4vsQ1} = 0.67$ (95% CIs: 0.51–0.88)]. The dose-response relationship between blood UA and the risk of MCI was shown in **Figure 2** ($P_{for\ non-linear} = 0.080$). When treated UA as a continuous variable, we observed that per 10 μmol/L blood UA increment was associated with 2% decreased risk of incident MCI in competing risk model 3 [$HR_{per10\mu\ mol/L} = 0.98$ (95% CIs: 0.97–0.99)]. Subgroup analyses stratified by age and sex are shown in **Figure 3**. The associations were more pronounced in the younger older adults (65–79 years) ($P_{for\ interaction} = 0.034$). Compared with the lowest quartile group of UA level (Q1), those in the highest quartile group (Q4) had a 50% lower risk of developing MCI [$HR_{Q4vsQ1} = 0.50$ (95% CI: 0.26–0.98)]. Partially due to the relatively small sample size, some of the associations of blood UA levels with the risk of MCI became non-significant (e.g., that in women). In addition, we observed that the association of blood UA on the risk of MCI remained statistically significant among those without hyperuricemia [$HR_{Q4vsQ1} = 0.64$ (95% CI: 0.48–0.85)] (**Supplementary Table 3**). However, no significant associations were found for older adults with UA levels above the normal range (i.e., with hyperuricemia) [$HR_{Q4vsQ1} = 2.19$ (0.81–5.88)].

Longitudinal Associations of Blood Uric Acid With Mini-Mental State Examination Score

We used the same dataset of 3,103 participants above to examine the longitudinal associations of blood UA with MMSE score. We found that higher blood UA was associated with a fewer decline in the MMSE score over time (**Supplementary Table 4**). The adjusted mean difference in annual cognitive decline rate, changed by the interaction of per 10 μmol/L increment and follow-up time, was −0.02 (0.005) points ($P < 0.001$).

Sensitivity Analyses

In sensitivity analyses: (1) Differences in demographic characteristics were found between eligible and excluded

TABLE 2 | Baseline characteristics of study participants included in the main analysis, in total and by UA quartiles[a].

Characteristics	Total (*N* = 3103)	Q_1 (*N* = 773)	Q_2 (*N* = 777)	Q_3 (*N* = 776)	Q_4 (*N* = 777)	*P* Value
Age, mean ± SD, years	85.1 ± 11.7	82.8 ± 12.2	84.8 ± 11.6	85.8 ± 11.4	86.8 ± 11.2	< 0.001
Sex, women (%)	1,688 (54.4)	422 (54.6)	421 (54.2)	424 (54.6)	421 (54.2)	0.996
More than 1 year of education, yes (%)	1,098 (36.3)	274 (36.2)	258 (33.9)	276 (36.6)	290 (38.6)	0.319
Currently married, yes (%)	1,170 (38.5)	318 (41.6)	294 (38.6)	292 (38.4)	266 (35.5)	0.113
Regular exercise, yes (%)	552 (18.4)	105 (13.9)	150 (19.7)	144 (19.0)	153 (20.8)	0.003
Current smoking, yes (%)	573 (18.8)	152 (19.9)	134 (17.4)	142 (18.5)	145 (19.3)	0.628
Current alcohol drinking, yes (%)	510 (16.8)	135 (17.6)	101 (13.3)	139 (18.2)	135 (18.0)	0.028
BMI, mean ± SD, kg/m^2	21.5 ± 10.1	20.8 ± 3.4	21.9 ± 17.2	21.4 ± 6.3	21.8 ± 7.7	0.170
Central obesity [b], yes (%)	1,303 (42.3)	308 (40.1)	315 (41.0)	318 (41.3)	362 (46.8)	0.031
Adequate medical service, yes (%)	2,864 (93.9)	706 (92.4)	722 (94.1)	728 (94.9)	708 (94.1)	0.212
Hypertension, yes (%)	1,730 (55.8)	352 (45.6)	410 (52.9)	473 (61.0)	495 (63.8)	< 0.001
Diabetes mellitus, yes (%)	331 (10.7)	74 (9.6)	65 (8.4)	99 (12.8)	93 (12.0)	0.017
Heart Disease, yes (%)	232 (7.7)	58 (7.7)	46 (6.1)	61 (8.1)	67 (8.9)	0.212
Stroke/CVD, yes (%)	165 (5.4)	50 (6.6)	35 (4.6)	35 (4.6)	45 (5.9)	0.232

UA, uric acid; SD, standard deviation; BMI, body mass index; CVD, cardiovascular disease.
Values are given as No. (%) unless otherwise stated.
[a]*The cutoff values were 213.9, 265.0, and 320.9 μmol/L for women, and 252.0, 305.6, and 365.1 μmol/L for men.*
[b]*Central obesity was defined as waist circumference ≥ 80 cm in women and waist circumference ≥ 85 cm in men.*

TABLE 3 | Longitudinal associations of blood UA levels with the risk of MCI.

Blood UA (μmol/L[a])	Model 1 HR (95% CI)	Model 2 HR (95% CI)	Model 3 HR (95% CI)
Cox proportional hazards model			
Per 10 μmol/L increment	0.99 (0.98, 0.10)	0.99 (0.98, 1.00)	0.99 (0.97, 0.10)
Q1	Ref.	Ref.	Ref.
Q2	0.84 (0.66, 1.06)	0.84 (0.66, 1.07)	0.82 (0.64, 1.06)
Q3	0.81 (0.64, 1.04)	0.83 (0.65, 1.06)	0.73 (0.56, 0.95)
Q4	0.74 (0.57, 0.96)	0.75 (0.57, 0.98)	0.73 (0.55, 0.96)
$P_{for\ trend}$	0.022	0.036	0.013
Fine and Gray competing risks model [b]			
Per 10 μmol/L increment	0.98 (0.97, 0.99)	0.98 (0.97, 0.99)	0.98 (0.97, 0.99)
Q1	Ref.	Ref.	Ref.
Q2	0.90 (0.71, 1.14)	0.89 (0.69, 1.14)	0.88 (0.68, 1.13)
Q3	0.89 (0.70, 1.13)	0.80 (0.62, 1.04)	0.79 (0.61, 1.02)
Q4	0.70 (0.54, 0.91)	0.67 (0.51, 0.88)	0.67 (0.51, 0.88)
$P_{for\ trend}$	0.014	0.018	0.003

UA, uric acid; HR, hazard, ratio; CI, confidence interval.
Model 1 adjusted for age, sex, and education; model 2 additionally adjusted for drinking, smoking, marital status, regular exercise, body mass index, central obesity, adequate medical service; model3 additionally adjusted for hypertension, diabetes mellitus, self-reported history of heart disease, and stroke and cardiovascular disease.
[a] *The cutoff values were 213.9, 265.0, and 320.9 μmol/L for women, and 252.0, 305.6, and 365.1 μmol/L for men.*
[b] *Adjusted for death as competing risk.*

participants. Those who were excluded were more likely to be younger and women, and had lower blood UA levels; and had more healthy characteristics (a higher proportion of education, and a lower proportion of smoking, central obesity, hypertension, and heart disease) (all $P < 0.05$, **Supplementary Table 5**). (2) Different characteristics of participants by enrolled time (i.e., 2008 wave, 2012 wave, and 2014 wave) were observed (**Supplementary Table 6**).

DISCUSSION

In this community-based longitudinal study of 3,103 Chinese older adults free of MCI at baseline, we found that higher UA was associated with a lower risk of developing MCI during the 9 years follow-up. Furthermore, these associations were generally stronger in the younger older adults (65–79 years) and those without hyperuricemia. The findings confirm the neuroprotective effect of UA in Chinese older populations.

The neuroprotective effects of blood UA we observed are generally consistent with that from the previous epidemiological studies. A recent cross-sectional study using data from Beijing Longitudinal Study on Aging II showed the beneficial role of high blood UA levels on CI (Xiu et al., 2017). A cohort study from Netherland, with over 11-year follow-up, found that higher serum UA levels at baseline predicted better cognition in later life (Euser et al., 2009). Similarly, another cohort (Lu et al., 2016) identified the potential neuroprotective role of UA on Alzheimer's disease in a 5-year follow-up. However, there are still some studies that failed to observe the neuroprotective role of UA in dementia (Latourte et al., 2018; Singh and Cleveland, 2018a; Alam et al., 2020). The heterogeneity in study populations and outcome measurements might partially explain the different findings across studies.

Several possible biological mechanisms may elucidate the observed association of higher normal UA levels with a lower risk of MCI in the current study. First, in a urate oxidase mouse model with hemi-parkinsonism, genic mutated urate oxidase resulted in increased brain urate concentrations and substantially attenuated toxic effects of 6-hydroxydopamine on neurochemicals and rotational behavior. Additionally, transgenic urate oxidase decreased brain urate, which exacerbated neural functional lesions (Chen et al., 2013). Second, UA exerts its important antioxidant property in human bodies by acting as a direct scavenger of oxygen and hydroperoxyl radicals and forming stable complexes with iron ions (Davies et al., 1986), which further reduces the risk of MCI (Gackowski et al., 2008; Cervellati et al., 2013). Third, nutrition status might partly play a role in the UA-cognition relationship. Hypouricemia, a status of the abnormally low level of UA in the blood, is a well-established biomarker of poor nutritional status (Tseng et al., 2012). Meanwhile, malnutrition is a serious issue in older adults with MCI or dementia (Cederholm et al., 2014).

In our study, the association of blood UA with the risk of MCI appeared to be more pronounced in the younger

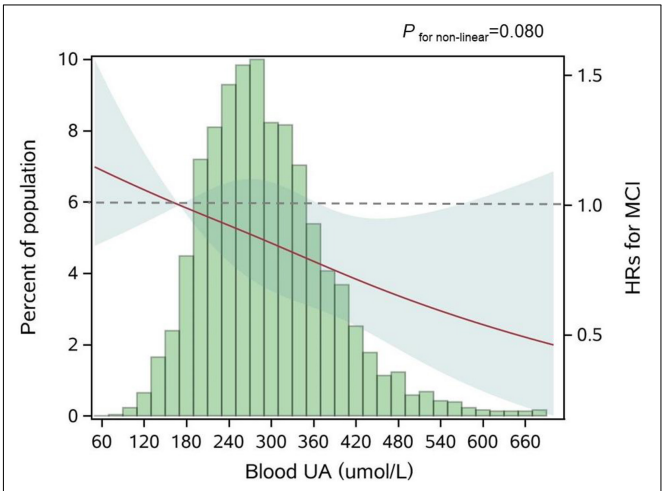

FIGURE 2 | Adjusted dose-response association between blood UA and risk for MCI. UA, uric acid; HR, hazard ratio; MCI, mild cognitive impairment. Blood UA was coded using a restricted cubic spline (RCS) function with three sex-specific knots, which approximately corresponded to the 5th (170.0 μmol/L), 50th (281.6 μmol/L), and 95th (454.3 μmol/L) percentiles of blood UA distribution. The solid red line represents the adjusted hazard ratio for the risk of MCI for any value of UA compared to participants with 170.0 μmol/L (P5) of blood UA level, with light green shaded areas showing 95% confidence intervals derived from restricted cubic spline regressions. The green histograms show the fraction of the population with the different levels of blood UA. The dashed gray line refers to the reference for the association at an HR of 1.0. *P* for non-linear = 0.080.

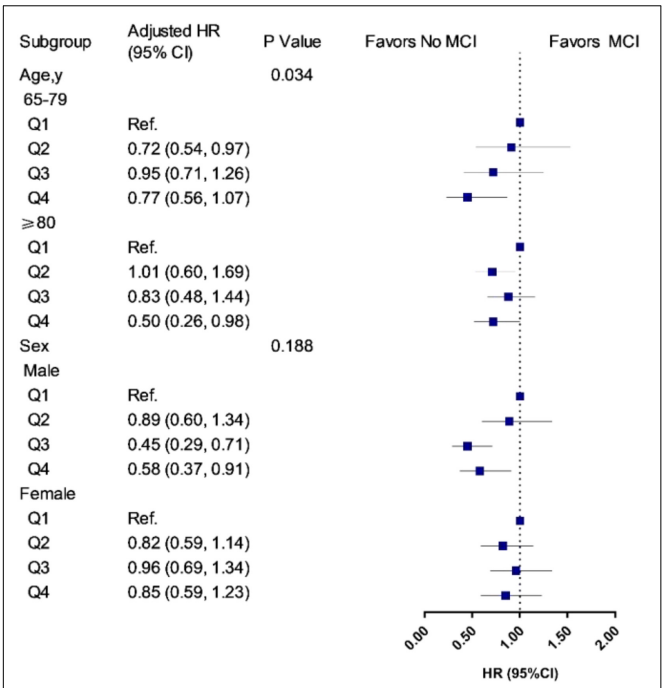

FIGURE 3 | Associations of UA quartiles with the risk of MCI in age and sex subgroups. HR, hazard ratio; CIs, confidence intervals. The model was adjusted for age (not in age subgroup) and sex (not in sex subgroup), education, drinking, smoking, marital status, regular exercise, body mass index, central obesity, adequate medical service, hypertension, diabetes mellitus, self-reported history of heart disease, and stroke/CVD. Q1 was defined as the reference group. In the age subgroup, participants aged 65–79 years, the cutoff values of UA quartiles were 245.4, 291.6, and 355.4 μmol/L for men, and 195.2, 242.0, and 296.4 μmol/L for women; participants aged 80 years and older, the cutoff values of UA quartiles were 262.0, 315.0, and 377.1 μmol/L for men, and 220.0, 270.7, and 329.8 μmol/L for women. In the sex subgroup, the cutoff values were 252.0, 305.6, and 365.1 μmol/L for men, and 213.9, 265.0, and 320.9 μmol/L for women.

older adults (65–79 years) and those without hyperuricemia. The age-specific protective effects of high blood UA on the risk of MCI might be explained by the fact that the younger older adults have a lower aging rate, and to be more sensitive to the beneficial effects of blood UA on cognition (Vauzour et al., 2017). Furthermore, survivor bias might exist in our study population. The unexpected non-significant result among those without hyperuricemia might be due to occasional chance and the relatively small sample size ($N_{hyperuricemia} = 404$). Besides, from the dose-response test (**Figure 2**), we noticed that the 95% CIs for the risk estimates became extremely wider when the UA levels were higher than about 420 μmol/L, which was around the cutoff value of the UA normal range (blood UA levels > 420 μmol/L in men and UA levels > 360 μmol/L in women were defined as hyperuricemia). These older adults with hyperuricemia might not share the same underlying etiology pathway relative to those without hyperuricemia.

The strengths of this study include its prospective cohort design and a relatively large sample size of older adults. However, several limitations should be considered. First, comprehensive neuropsychological assessments and the diagnoses of specific dementia or Parkinson's disease were not available in our study, so we could not capture the detailed aspects and clinical stage of cognition. Nevertheless, (i) we repeated measured the MMSE four times, which would allow us to capture the global patterns of cognitive fluctuation over time; (ii) the MMSE was commonly used as part of the evaluation for possible dementia (Creavin et al., 2016). Second, the UA levels were measured only once, and may not reflect the true value and ignore the fluctuation. Third, residual confounding could not be ignored, such as, we did not collect information on dietary habits and medication, which might serve as confounding factors in the UA-cognition association. Due to these limitations, we need to be cautious when interpreting our results. Given that our study focused on the Chinese older adults, more studies are warranted to further investigate the associations in other ethnic groups.

CONCLUSION

By evaluating the associations of blood UA with the risk of MCI, our findings suggest the protective role of high blood UA among Chinese older adults. The findings highlight the potential of managing UA in daily life for maintaining late-life cognition, with important clinical practice implications, and deserves further verifications.

DATA AVAILABILITY STATEMENT

The data that support the findings of this study are available from the corresponding author XS, upon reasonable request.

ETHICS STATEMENT

The studies involving human participants were reviewed and approved by the Ethics Committee of Peking University and Duke University. The patients/participants provided their written informed consent to participate in this study.

AUTHOR CONTRIBUTIONS

ZL and XS: study concept and design. CC and XL: acquisition, analysis, interpretation of data, drafting of the manuscript, and statistical analysis. YLv, XC, ZL, and XS: critical revision of the manuscript for important intellectual content. ZL and XS: funding acquisition and supervision. ZY, FZ, YLi, CL, SJ, JZ, YW, XC, JW, HG, and FL: administrative, technical, or material support. All authors contributed to the article and approved the submitted version.

FUNDING

This work was supported by the National Natural Science Foundation of China (grant numbers 82025030, 81941023, and 82171584), the 2020 Milstein Medical Asian American Partnership Foundation Irma and Paul Milstein Program for Senior Health project award (to ZL), and a project from the Natural Science Foundation of Zhejiang Province (LQ21H260003). The current study was partially conducted at the School of Public Health and the Second Affiliated Hospital, Zhejiang University School of Medicine.

ACKNOWLEDGMENTS

We would like to thank all participants who attended the Healthy Aging and Biomarkers Cohort Study (HABCS).

SUPPLEMENTARY MATERIAL

The Supplementary Material for this article can be found online at: https://www.frontiersin.org/articles/10.3389/fnagi.2021.747686/full#supplementary-material

REFERENCES

Alam, A. B., Wu, A., Power, M. C., West, N. A., and Alonso, A. (2020). Associations of serum uric acid with incident dementia and cognitive decline in the ARIC-NCS cohort. *J. Neurol. Sci.* 414:116866. doi: 10.1016/j.jns.2020.116866

Cederholm, T., Nouvenne, A., Ticinesi, A., Maggio, M., Lauretani, F., Ceda, G. P., et al. (2014). The role of malnutrition in older persons with mobility limitations. *Curr. Pharm. Des.* 20, 3173–3177. doi: 10.2174/13816128113196660689

Cervellati, C., Cremonini, E., Bosi, C., Magon, S., Zurlo, A., Bergamini, C. M., et al. (2013). Systemic oxidative stress in older patients with mild cognitive impairment or late onset Alzheimer's disease. *Curr. Alzheimer Res.* 10, 365–372. doi: 10.2174/1567205011310040003

Chen, X., Burdett, T. C., Desjardins, C. A., Logan, R., Cipriani, S., Xu, Y., et al. (2013). Disrupted and transgenic urate oxidase alter urate and dopaminergic neurodegeneration. *Proc. Natl. Acad. Sci. U.S.A.* 110, 300–305. doi: 10.1073/pnas.1217296110

Choi, H. K., Ford, E. S., Li, C., and Curhan, G. (2007). Prevalence of the metabolic syndrome in patients with gout: the Third National Health and Nutrition Examination Survey. *Arthritis Rheum.* 57, 109–115. doi: 10.1002/art.22466

Cicero, A. F., Desideri, G., Grossi, G., Urso, R., Rosticci, M., D'Addato, S., et al. (2015). Serum uric acid and impaired cognitive function in a cohort of healthy young elderly: data from the Brisighella Study. *Intern. Emerg. Med.* 10, 25–31. doi: 10.1007/s11739-014-1098-z

Creavin, S. T., Wisniewski, S., Noel-Storr, A. H., Trevelyan, C. M., Hampton, T., Rayment, D., et al. (2016). Mini-Mental State Examination (MMSE) for the detection of dementia in clinically unevaluated people aged 65 and over in community and primary care populations. *Cochrane Database Syst. Rev.* CD011145.

Davies, K. J., Sevanian, A., Muakkassah-Kelly, S. F., and Hochstein, P. (1986). Uric acid-iron ion complexes. a new aspect of the antioxidant functions of uric acid. *Biochem. J.* 235, 747–754. doi: 10.1042/bj2350747

De Vera, M., Rahman, M. M., Rankin, J., Kopec, J., Gao, X., and Choi, H. (2008). Gout and the risk of Parkinson's disease: a cohort study. *Arthritis Rheum.* 59, 1549–1554. doi: 10.1002/art.24193

Euser, S. M., Hofman, A., Westendorp, R. G., and Breteler, M. M. (2009). Serum uric acid and cognitive function and dementia. *Brain* 132(Pt. 2), 377–382. doi: 10.1093/brain/awn316

Feig, D. I., Kang, D. H., and Johnson, R. J. (2008). Uric acid and cardiovascular risk. *N. Engl. J. Med.* 359, 1811–1821.

Fine, J. P., and Gray, R. J. (1999). A proportional hazards model for the subdistribution of a competing risk. *J. Am. Stat. Assoc.* 94, 496–509. doi: 10.1080/01621459.1999.10474144

Gackowski, D., Rozalski, R., Siomek, A., Dziaman, T., Nicpon, K., Klimarczyk, M., et al. (2008). Oxidative stress and oxidative DNA damage is characteristic for mixed Alzheimer disease/vascular dementia. *J. Neurol. Sci.* 266, 57–62. doi: 10.1016/j.jns.2007.08.041

Gong, L., Zhang, Q. L., Zhang, N., Hua, W. Y., Huang, Y. X., Di, P. W., et al. (2012). Neuroprotection by urate on 6-OHDA-lesioned rat model of Parkinson's disease: linking to Akt/GSK3beta signaling pathway. *J. Neurochem.* 123, 876–885. doi: 10.1111/jnc.12038

Hong, J. Y., Lan, T. Y., Tang, G. J., Tang, C. H., Chen, T. J., and Lin, H. Y. (2015). Gout and the risk of dementia: a nationwide population-based cohort study. *Arthritis Res. Ther.* 17:139.

Hu, L. Y., Yang, A. C., Lee, S. C., You, Z. H., Tsai, S. J., Hu, C. K., et al. (2020). Risk of Parkinson's disease following gout: a population-based retrospective cohort study in Taiwan. *BMC Neurol.* 20:338. doi: 10.1186/s12883-020-01916-9

Huang, R., Tian, S., Han, J., Lin, H., Guo, D., Wang, J., et al. (2019). U-Shaped association between serum uric acid levels and cognitive functions in patients with type 2 diabetes: a cross-sectional study. *J. Alzheimers Dis.* 69, 135–144. doi: 10.3233/jad-181126

Irizarry, M. C., Raman, R., Schwarzschild, M. A., Becerra, L. M., Thomas, R. G., Peterson, R. C., et al. (2009). Plasma urate and progression of mild cognitive impairment. *Neurodegener. Dis.* 6, 23–28. doi: 10.1159/000170883

Iuliano, L., Monticolo, R., Straface, G., Spoletini, I., Gianni, W., Caltagirone, C., et al. (2010). Vitamin E and enzymatic/oxidative stress-driven oxysterols in amnestic mild cognitive impairment subtypes and Alzheimer's disease. *J. Alzheimers Dis.* 21, 1383–1392. doi: 10.3233/jad-2010-100780

Katzman, R., Zhang, M. Y., Ouang Ya, Q., Wang, Z. Y., Liu, W. T., Yu, E., et al. (1988). A Chinese version of the Mini-Mental State Examination; impact of illiteracy in a Shanghai dementia survey. *J. Clin. Epidemiol.* 41, 971–978.

Khan, A. A., Quinn, T. J., Hewitt, J., Fan, Y., and Dawson, J. (2016). Serum uric acid level and association with cognitive impairment and dementia: systematic review and meta-analysis. *Age* 38:16.

Latourte, A., Soumaré, A., Bardin, T., Perez-Ruiz, F., Debette, S., and Richette, P. (2018). Uric acid and incident dementia over 12 years of follow-up: a population-based cohort study. *Ann. Rheum. Dis.* 77, 328–335. doi: 10.1136/annrheumdis-2016-210767

Li, J., Dong, B. R., Lin, P., Zhang, J., and Liu, G. J. (2010). Association of cognitive function with serum uric acid level among Chinese nonagenarians and centenarians. *Exp. Gerontol.* 45, 331–335. doi: 10.1016/j.exger.2010.01.005

Littell, R. C., Henry, P. R., and Ammerman, C. B. (1998). Statistical analysis of repeated measures data using SAS procedures. *J. Anim. Sci.* 76, 1216–1231. doi: 10.2527/1998.7641216x

Liu, M., Wang, J., Zeng, J., and He, Y. (2017). Relationship between serum uric acid level and mild cognitive impairment in Chinese community elderly. *BMC Neurol.* 17:146. doi: 10.1186/s12883-017-0929-8

Liu, Z., Han, L., Wang, X., Feng, Q., and Gill, T. M. (2018). Disability prior to death among the oldest-old in China. *J. Gerontol. A Biol. Sci. Med. Sci.* 73, 1701–1707. doi: 10.1093/gerona/gly010

Lu, N., Dubreuil, M., Zhang, Y., Neogi, T., Rai, S. K., Ascherio, A., et al. (2016). Gout and the risk of Alzheimer's disease: a population-based, BMI-matched cohort study. *Ann. Rheum. Dis.* 75, 547–551. doi: 10.1136/annrheumdis-2014-206917

Lv, Y., Mao, C., Yin, Z., Li, F., Wu, X., and Shi, X. (2019). Healthy Ageing and Biomarkers Cohort Study (HABCS): a cohort profile. *BMJ Open.* 9:e026513. doi: 10.1136/bmjopen-2018-026513

Lv, Y.-B., Liu, S., Yin, Z.-X., Gao, X., Kraus, V. B., Mao, C., et al. (2018). Associations of body mass index and waist circumference with 3-year all-cause mortality among the oldest old: evidence from a chinese community-based prospective cohort study. *J. Am. Med. Dir. Assoc.* 19, 672–678.e4.

Norris, K. C., Smoyer, K. E., Rolland, C., Van der Vaart, J., and Grubb, E. B. (2018). Albuminuria, serum creatinine, and estimated glomerular filtration rate as predictors of cardio-renal outcomes in patients with type 2 diabetes mellitus and kidney disease: a systematic literature review. *BMC Nephrol.* 19:36. doi: 10.1186/s12882-018-0821-9

Pellecchia, M. T., Savastano, R., Moccia, M., Picillo, M., Siano, P., Erro, R., et al. (2016). Lower serum uric acid is associated with mild cognitive impairment in early Parkinson's disease: a 4-year follow-up study. *J. Neural Transm.* 123, 1399–1402. doi: 10.1007/s00702-016-1622-6

Richette, P., Perez-Ruiz, F., Doherty, M., Jansen, T. L., Nuki, G., Pascual, E., et al. (2014). Improving cardiovascular and renal outcomes in gout: what should we target? *Nat. Rev. Rheumatol.* 10, 654–661. doi: 10.1038/nrrheum.2014.124

Singh, J. A., and Cleveland, J. D. (2018b). Use of urate-lowering therapies is not associated with an increase in the risk of incident dementia in older adults. *Ann. Rheum. Dis.* 77, 1243–1245.

Singh, J. A., and Cleveland, J. D. (2018a). Gout and dementia in the elderly: a cohort study of Medicare claims. *BMC Geriatr.* 18:281. doi: 10.1186/s12877-018-0975-0

Tseng, C. K., Lin, C. H., Hsu, H. S., Ho, C. T., Huang, H. Y., Liu, C. S., et al. (2012). In addition to malnutrition and renal function impairment, anemia is associated with hyponatremia in the elderly. *Arch. Gerontol. Geriatr.* 55, 77–81. doi: 10.1016/j.archger.2011.06.019

Tuven, B., Soysal, P., Unutmaz, G., Kaya, D., and Isik, A. T. (2017). Uric acid may be protective against cognitive impairment in older adults, but only in those without cardiovascular risk factors. *Exp. Gerontol.* 89, 15–19. doi: 10.1016/j.exger.2017.01.002

Vauzour, D., Camprubi-Robles, M., Miquel-Kergoat, S., Andres-Lacueva, C., Bánáti, D., Barberger-Gateau, P., et al. (2017). Nutrition for the ageing brain: towards evidence for an optimal diet. *Ageing Res. Rev.* 35, 222–240. doi: 10.1016/j.arr.2016.09.010

Wang, F., Zhao, M., Han, Z., Li, D., Zhang, S., Zhang, Y., et al. (2017). Hyperuricemia as a protective factor for mild cognitive impairment in non-obese elderly. *Tohoku J. Exp. Med.* 242, 37–42. doi: 10.1620/tjem.242.37

Wang, T., Wu, Y., Sun, Y., Zhai, L., and Zhang, D. (2017). A prospective study on the association between uric acid and cognitive function among middle-aged and older Chinese. *J. Alzheimers Dis.* 58, 79–86. doi: 10.3233/jad-161243

Wu, Y., Zhang, D., Pang, Z., Jiang, W., Wang, S., and Tan, Q. (2013). Association of serum uric acid level with muscle strength and cognitive function among Chinese aged 50-74 years. *Geriatr. Gerontol. Int.* 13, 672–677. doi: 10.1111/j.1447-0594.2012.00962.x

Xiu, S., Zheng, Z., Guan, S., Zhang, J., Ma, J., and Chan, P. (2017). Serum uric acid and impaired cognitive function in community-dwelling elderly in Beijing. *Neurosci. Lett.* 637, 182–187. doi: 10.1016/j.neulet.2016.11.013

Xu, Y., Wang, Q., Cui, R., Lu, K., Liu, Y., and Zhao, Y. (2017). Uric acid is associated with vascular dementia in Chinese population. *Brain Behav.* 7:e00617. doi: 10.1002/brb3.617

Ye, B. S., Lee, W. W., Ham, J. H., Lee, J. J., Lee, P. H., and Sohn, Y. H. (2016). Does serum uric acid act as a modulator of cerebrospinal fluid Alzheimer's disease biomarker related cognitive decline? *Eur. J. Neurol.* 23, 948–957. doi: 10.1111/ene.12969

Yi, Z., Shi, X. M., Fitzgerald, S. M., Qian, H. Z., Kraus, V. B., Sereny, M., et al. (2012). High sensitivity C-reactive protein associated with different health predictors in middle-aged and oldest old Chinese. *Biomed. Environ. Sci.* 25, 257–266.

Yuan, J. Q., Lv, Y. B., Chen, H. S., Gao, X., Yin, Z. X., Wang, W. T., et al. (2019). Association between late-life blood pressure and the incidence of cognitive impairment: a community-based prospective cohort study. *J. Am. Med. Dir. Assoc.* 20, 177–182.e2.

Zhang, Q., Lou, S., Meng, Z., and Ren, X. (2011). Gender and age impacts on the correlations between hyperuricemia and metabolic syndrome in Chinese. *Clin. Rheumatol.* 30, 777–787.

Zhu, Y., Pandya, B. J., and Choi, H. K. (2011). Prevalence of gout and hyperuricemia in the US general population: the National Health and Nutrition Examination Survey 2007-2008. *Arthritis Rheum.* 63, 3136–3141.

Conflict of Interest: The authors declare that the research was conducted in the absence of any commercial or financial relationships that could be construed as a potential conflict of interest.

Publisher's Note: All claims expressed in this article are solely those of the authors and do not necessarily represent those of their affiliated organizations, or those of the publisher, the editors and the reviewers. Any product that may be evaluated in this article, or claim that may be made by its manufacturer, is not guaranteed or endorsed by the publisher.

frontiers in Aging Neuroscience

ORIGINAL RESEARCH
published: 22 October 2021
doi: 10.3389/fnagi.2021.753242

Plasma and CSF Neurofilament Light Chain in Amyotrophic Lateral Sclerosis: A Cross-Sectional and Longitudinal Study

Veria Vacchiano[1,2†], Andrea Mastrangelo[1†], Corrado Zenesini[2], Marco Masullo[1], Corinne Quadalti[2], Patrizia Avoni[1,2], Barbara Polischi[2], Arianna Cherici[2], Sabina Capellari[1,2], Fabrizio Salvi[2], Rocco Liguori[1,2] and Piero Parchi[2,3] on behalf of the BoReALS group*

[1] Department of Biomedical and NeuroMotor Sciences (DIBINEM), University of Bologna, Bologna, Italy, [2] IRCCS Istituto delle Scienze Neurologiche di Bologna, Bologna, Italy, [3] Department of Experimental Diagnostic and Specialty Medicine (DIMES), University of Bologna, Bologna, Italy

Background: Neurofilament light chain (NfL) is a validated biofluid marker of neuroaxonal damage with great potential for monitoring patients with neurodegenerative diseases. We aimed to further validate the clinical utility of plasma (p) vs. CSF (c) NfL for distinguishing patients with Amyotrophic Lateral Sclerosis (ALS) from ALS mimics. We also assessed the association of biomarker values with clinical variables and survival and established the longitudinal changes of pNfL during the disease course.

Methods: We studied 231 prospectively enrolled patients with suspected ALS who underwent a standardized protocol including neurological examination, electromyography, brain MRI, and lumbar puncture. Patients who received an alternative clinical diagnosis were considered ALS mimics. We classified the patients based on the disease progression rate (DPR) into fast (DPR $>$ 1), intermediate (DPR 0.5–1), and slow progressors (DPR $<$ 0.5). All patients were screened for the most frequent ALS-associated genes. Plasma and CSF samples were retrospectively analyzed; NfL concentrations were measured with the SIMOA platform using a commercial kit.

Results: ALS patients (n = 171) showed significantly higher pNfL ($p < 0.0001$) and cNfL ($p < 0.0001$) values compared to ALS mimics (n = 60). Both cNfL and pNfL demonstrated a good diagnostic value in discriminating the two groups, although cNfL performed slightly better (cNfL: AUC 0.924 ± 0.022, sensitivity 86.8%, specificity 92.4; pNfL: AUC 0.873 ± 0.036, sensitivity 84.7%, specificity 83.3%). Fast progressors showed higher cNfL and pNfL as compared to intermediate (p = 0.026 and p = 0.001) and slow progressors (both $p < 0.001$). Accordingly, ALS patients with higher baseline cNfL and pNfL levels had a shorter survival (highest tertile of cNfL vs. lowest tertile, HR 4.58, p = 0.005; highest tertile of pNfL vs. lowest tertile, HR 2.59, p = 0.015). Moreover, there were positive associations between cNfL and pNfL levels and the number of body regions displaying UMN signs (rho = 0.325, $p < 0.0001$; rho = 0.308,

OPEN ACCESS

Edited by:
Thomas K. Karikari, University of Gothenburg, Sweden

Reviewed by:
Ahmad Al Khleifat, King's College London, United Kingdom
Pamela Ferreira, University of Pittsburgh, United States

***Correspondence:**
Piero Parchi
piero.parchi@unibo.it

† These authors have contributed equally to this work

Received: *04 August 2021*
Accepted: *27 September 2021*
Published: *22 October 2021*

Citation:
Vacchiano V, Mastrangelo A, Zenesini C, Masullo M, Quadalti C, Avoni P, Polischi B, Cherici A, Capellari S, Salvi F, Liguori R and Parchi P (2021) Plasma and CSF Neurofilament Light Chain in Amyotrophic Lateral Sclerosis: A Cross-Sectional and Longitudinal Study. Front. Aging Neurosci. 13:753242. doi: 10.3389/fnagi.2021.753242

p = 0.001). Finally, longitudinal analyses in 57 patients showed stable levels of pNfL during the disease course.

Conclusion: Both cNfL and pNfL have excellent diagnostic and prognostic performance for symptomatic patients with ALS. The stable longitudinal trajectory of pNfL supports its use as a marker of drug effect in clinical trials.

Keywords: neurofilament light chain, amyotrophic lateral sclerosis, diagnosis, prognosis, longitudinal, Simoa, biofluid, biomarker

INTRODUCTION

Amyotrophic lateral sclerosis (ALS) is a heterogeneous neurodegenerative disorder affecting both the upper (UMN) and the lower motor neurons (LMN). It generally causes progressive and diffuse muscular paralysis and eventually affects the nutritional and respiratory functions leading to death. The diagnosis of ALS currently relies on the demonstration of clinical and electrophysiological signs of damage of motor neurons at both levels and the exclusion of ALS mimics (Brooks et al., 2000; de Carvalho et al., 2008). Whereas ALS in its "classical" phenotype rarely represents a diagnostic challenge for an experienced neurologist, ALS variants with prevalent UMN or LMN involvement may present with subtle, slowly progressive clinical signs and lead to misdiagnosis with alternative disorders (Swinnen and Robberecht, 2014). Thus, the definition of CSF and blood disease biomarkers is of great relevance to improve the diagnostic accuracy and the prognostic assessment of patients. Moreover, as potential disease-modifying approaches for neurodegenerative disorders are emerging, there is an urgent need for biomarkers to monitor the therapeutic effect during the disease course.

Among several candidates, neurofilament light chain (NfL), a validated marker of neuroaxonal damage that can be reliably measured in both CSF (cNfL) and plasma (pNfL) (Gray et al., 2020), showed the best performance in distinguishing patients with ALS from patients with ALS mimics (Steinacker et al., 2016; Poesen et al., 2017; Feneberg et al., 2018; Gille et al., 2019; Abu-Rumeileh et al., 2020; Ashton et al., 2021).

Moreover, several authors highlighted the potential role of cNfL and pNfL as robust prognostic biomarkers, given the significant associations between the disease progression rate (DPR) and survival and the basal biomarkers values (Lu et al., 2015; Gaiani et al., 2017; Poesen et al., 2017; Steinacker et al., 2017; Feneberg et al., 2018; Benatar et al., 2020; Thouvenot et al., 2020). Finally, a few preliminary longitudinal studies suggested that pNfL levels remain stable in the disease course (Lu et al., 2015; Skillbäck et al., 2017; Verde et al., 2019; Benatar et al., 2020), making this novel biomarker a potential candidate for the monitoring of future therapeutic approaches in ALS.

In this study, we aimed to further explore the value of cNfL vs. pNfL in distinguishing patients with ALS and ALS mimics in one of the largest cohorts studied to date. Furthermore, we assessed the association of both biomarkers with clinical variables and with survival. Finally, we sought to describe the longitudinal behavior of pNfL, analyzing the biomarker values at different disease stages in a significant group of patients.

MATERIALS AND METHODS

Ethical Approval

The study was conducted according to the revised Declaration of Helsinki and Good Clinical Practice guidelines. Written informed consent was given by study participants. The study was approved by the ethics committee of "Area Vasta Emilia Centro."

Inclusion Criteria and Clinical Assessment

We studied 171 ALS patients and 60 patients with an alternative clinical diagnosis (ALS mimics group) evaluated at the Institute of Neurological Sciences of Bologna (ISNB) between September 2014 and June 2021. We also analyzed blood and CSF samples from 57 non-neurodegenerative controls, namely 30 blood samples from healthy subjects and 27 CSF samples from patients lacking any clinical or neuroradiological evidence of central nervous system (CNS) disease.

Patients with suspected ALS were prospectively enrolled, and underwent a standardized protocol including neurological examination, electromyography (EMG), lumbar puncture and ancillary exams to exclude an alternative clinical diagnosis. We included in the ALS group patients who received a diagnosis of ALS according to the Revised El Escorial criteria at baseline or during follow-up (Brooks et al., 2000), with available clinical data and at least one between CSF and plasma samples at baseline. Patients evaluated for ALS who received an alternative clinical diagnosis during the diagnostic work-up and/or follow-up and with at least one biofluid available were included in the ALS mimics group. For ALS patients the following clinical data were collected at the time of diagnosis (baseline visit): Age at onset, sex, disease duration (time elapsed between the first referred symptom and sampling), type of onset [bulbar, spinal, pseudopolyneuritic or pyramidal (Swinnen and Robberecht, 2014)], clinical phenotype [classical, bulbar, predominant upper motor neuron (PUMN), predominant lower motor neuron (PLMN) (Chiò et al., 2011; Al-Chalabi et al., 2016)], ALS Functional Rating Scale-revised (ALSFRS-R) score, forced vital capacity (FVC) expressed as a percentage of predicted volume, and body mass index (BMI). Patients were classified according to the Revised El Escorial criteria in 31 definite ALS, 69

probable ALS, 31 probable laboratory-supported ALS and 40 possible ALS (Brooks et al., 2000), and staged in agreement with King's clinical staging system (Roche et al., 2012). All patients underwent genetic screening for the most frequent ALS genes (i.e., *SOD1*, *FUS*, *TARDBP*, and the repeats expansion of the *C9Orf72* gene) (Bartoletti-Stella et al., 2021). The degree of the UMN involvement was defined as the number of regions (bulbar, cervical and lumbosacral region) showing UMN signs at clinical examination, while for the extent of the LMN involvement both clinical and EMG assessment were considered, as stated by the Awaji criteria (de Carvalho et al., 2008). The DPR at the baseline visit was calculated as follows: (48-ALSFRS-R score at the time of sampling)/months elapsed between disease onset and sampling (Lu et al., 2015), and patients were accordingly divided into slow (DPR < 0.5), intermediate (DPR 0–5–1) and fast progressors (DPR > 1), as previously described (Lu et al., 2015). Moreover, the Medical Research Council (MRC) scale of 0–5 (calculated as the sum of 10 muscles for each side score/20; score 0–5 points) was provided for each patient at the time of clinical evaluation.

A subgroup of ALS patients underwent the Edinburgh Cognitive and Behavioral ALS Screen (ECAS) (Abrahams et al., 2014; Siciliano et al., 2017) to investigate the presence of cognitive impairment up to a full-blown frontotemporal dementia (FTD).

Baseline CSF and plasma samples were used for a cross-sectional study of NfL levels.

Fifty-seven of the 171 ALS patients had plasma samples available from two or more visits. Longitudinal plasma samples were obtained during multidisciplinary follow-up visits from ALS patients who accepted to donate further blood samples after baseline sampling. No selection criteria were applied to identify these patients. In details, 24 patients were sampled twice, 20 patients had three plasma samples, 11 patients were sampled four times and for two subjects we had five samples available. Patients were repeatedly sampled at non-standardized time points, with a median follow-up period of 12 months (IQR 8–26). We observed 55 patients for more than 3 months, 50 subjects for at least 6 months, 32 and 17 patients for at least 12 and 24 months, respectively. The most extended follow-up duration was 55 months (two patients). For patients with more than one sampling, we calculated the longitudinal disease progression rate (l-DPR), as the change in the ALSFRS-R between the last and the baseline visits divided by the number of months between the visits (Vu et al., 2020). Accordingly, ALS patients were further classified into fast progressors (l-DPR > 1), intermediate progressors (l-DPR 0.5–1), and slow progressors (l-DPR < 0.5).

CSF and Plasma Analyses

EDTA plasma samples were collected, aliquoted, and stored at −80°C according to standard procedures. CSF samples were obtained by LP following a standard procedure, centrifuged in case of blood contamination, divided into aliquots, and stored in polypropylene tubes at −80°C until analysis.

Both cNfL and pNfL concentrations, in the entire sample cohort, were determined with the Single molecule array (Simoa) technology on a Simoa SR-X instrument (Quanterix, Billerica, MA, United States) using the commercially available NF-light advantage kit (Quanterix). The mean intra- and inter-assay coefficients of variation (CVs) were below 15% for both cNfL and pNfL.

Genetic Analyses

Molecular genetic analyses were performed as previously described (Bartoletti-Stella et al., 2021). Briefly, genomic DNA (gDNA) was extracted from peripheral blood by standard procedures (Giannoccaro et al., 2017). gDNA was quantified using the Quantus Fluorometer (Promega) with QuantiFluor double stranded DNA system (Promega). Patients were screened for mutations in ALS major genes: *SOD1* (all exons), *FUS* (exons 6 and 15), *TARDBP* (exons 2, 3, and 5) genes and for pathogenic repeat expansion (RE) in the *C9orf72* gene as previously reported (Bartoletti-Stella et al., 2021).

Statistical Analyses

Statistical analyses were performed using IBM SPSS Statistics version 21 (IBM, Armonk, NY, United States), Stata SE version 14.2 (StataCorp LLC, College Station, TX, United States) and GraphPad Prism 7 (GraphPad Software, La Jolla, CA, United States) software.

Continuous variables were presented as mean and Standard Deviation (SD) or median and interquartile range (IQR), categorical variables were presented as absolute number (n) and relative frequency (%). For continuous variables, based on the data distribution, the Mann-Whitney U test or the Student *t*-test were adopted to evaluate the differences between the groups, while the Kruskal-Wallis test (followed by Dunn-Bonferroni *post hoc* test) or the one-way analysis of variance (ANOVA) (followed by Tukey's *post hoc* test) were used for multiple group comparisons. Chi-Square test was applied for categorical variables. Biomarker values were transformed into a logarithmic scale to obtain a normal data distribution.

For the analysis of diagnostic value, receiver operating characteristic (ROC) analyses were performed to establish the accuracy in the distinction between ALS and ALS mimics, as well as the sensitivity and specificity of biomarkers. The optimal cut-off value for each biomarker was calculated using the maximed Youden Index. A subgroup analysis was also carried out according to patients' median age ($\leq$55 vs. $>$ 55 years) and sex (female vs. male). De Long test was used to compare the areas under the curve of pNfL and cNfL in the whole groups and between subgroups.

For the cross-sectional analysis, Spearman's rho coefficient was used to test the correlation between cNfL and pNfL levels and clinical variables. Moreover, the association between biofluids NfL and the degree of UMN and/or LMN involvement was analyzed using univariate and multivariate linear regression models with the log-transformed biomarker values (cNfL and pNfL) as dependent variables and the extent of: (1) UMN involvement, (2) LMN involvement, (3) UMN and LMN involvement as independent variables. In the multivariable models we adjusted for age at sampling, sex, genetic status, basal ALSFRS-R score, DPR, MRC and King's scores. The results are presented as β coefficients and 95% confidence intervals (95% CI).

For the prognostic analysis the cumulative time-dependent probability of death was calculated by the Kaplan-Meier estimate. The time of entry into the analysis was the date of the first sampling (at baseline), and the time of the endpoint was the date of death/tracheostomy or the date of the last follow-up information, whichever came first. We performed univariate and multivariate Cox regression models to study the association between time to death/tracheostomy and prognostic factors in ALS. The multivariate Cox regression analysis was adjusted for age at baseline, sex, baseline ALSFRS-R score, genetic status, DPR, MRC and King' scores. The results are presented as Hazard Ratios (HR) and 95% CI. The assumption of proportional hazard was assessed by Schoenfeld residuals. Differences were considered significant at $p < 0.05$.

For the longitudinal analysis, a linear mixed effect modeling analysis with random slope and random intercept was performed to evaluate the rate of change over the time of both cNfL and pNfL in the ALS patients stratified into fast, intermediate and slow progressors, as previously described (Vu et al., 2020). The results are presented as β coefficients and 95% CI.

RESULTS

Demographic Values, Distribution and Diagnostic Performance of Plasma Neurofilament Light Chain and Cerebrospinal Fluid Neurofilament Light Chain

Demographic and clinical features of the study population are detailed in **Tables 1**, **2** and **Supplementary Table 1**.

Age at baseline and sex distribution were not significantly different among the three diagnostic groups (age, $p = 0.575$; sex, $p = 0.728$). No effect of sex and age on cNfL and pNfL values was detected in the ALS group, while there was a moderate effect of age on pNfL and cNfL levels in both the ALS mimics (age vs. pNfL: rho = 0.546, $p < 0.001$; age vs. cNfL: rho = 0.536, $p < 0.001$) and the control groups (age vs. pNfL: rho = 0.691, $p < 0.001$; age vs. cNfL: 0.451, $p = 0.018$).

ALS patients showed significantly higher pNfL ($p < 0.0001$) and cNfL ($p < 0.0001$) values compared to subjects belonging to the ALS mimics and control groups (**Figure 1A**). When evaluating the ROC curves, cNfL yielded a higher diagnostic value than pNfL ($p = 0.043$) in discriminating patients with ALS and subjects with an alternative ALS-mimicking disease (cNfL: AUC 0.924 ± 0.022, sensitivity 86.8%, specificity 92.4, cut-off 2,517 pg/ml; pNfL: AUC 0.873 ± 0.036, sensitivity 84.7%, specificity 83.3%. cut-off 32.7 pg/ml) (**Figure 1B**). After patient stratification, we found no significant influence of age ($p = 0.149$) and sex ($p = 0.644$) on the diagnostic performance of cNfL. Age but not sex ($p = 0.981$) slightly influenced the diagnostic accuracy of pNfL, although the effect did not reach statistical significance (≤ 55 years: AUC 0.939 ± 0.026 vs. > 55 years: AUC 0.804 ± 0.067; $p = 0.062$). Finally, the diagnostic accuracy of pNfL almost reached that of cNfL (AUC 0.906 ± 0.026, sensitivity 84.7%, specificity 86.4%, cut-off 32.7 pg/ml), when we limited the analysis to the subjects with alternative diseases only involving the CNS.

TABLE 1 | Demographic and clinical features of the study population.

ALS patients—clinical characteristics	**N (tot. 171)**	**%**
Sex	68 (F)	39.8
Type of onset		
Bulbar	42	24.6
Spinal	113	66.1
Pseudopolyneuritic	9	5.3
Pyramidal	7	4.1
Deceased/with tracheostomy	72	42.1
Genetic screening	(N tot. 167)	
C9Orf72 RE carriers	18	10.8
SOD1 mutation carriers	7	4.2
FUS mutation carriers	1	0.6
TARDBP mutation carriers	2	1.2
FTD status	21	12.3
		Median (IQR)
Age at first sampling (y)		65 (56–74)
DD from first symptom to sampling (m)		16 (9–27)
ALSFRS-R score		41 (34.5–44)
MRC score		4.6 (4.1–4.8)
FVC		90 (70–106)
Biomarker values		Median (IQR)
cNfL	114	6543 (3697–12719)
pNfL	170	73.0 (45.9–114.2)
ALS mimics group	**N (tot. 60)**	**%**
Sex	24 (F)	40
Age at first sampling (y)		Median (IQR)
		65 (56.3–71.8)
Biomarker values		Median (IQR)
cNfL	53	1140 (589.5–1937)
pNfL	30	22.5 (11.4–28)
Clinical and healthy controls	**N (tot. 57)***	**%**
Sex	26 (F)	45.6
Age at sampling (y)		Median (IQR)
		63 (56.5–69)
Biomarker values		Median (IQR)
cNfL	27	682.3 (498.7–934.3)
pNfL	30	9.4 (6.8–15.5)

**Clinical and healthy controls used for cNfL and pNfL analysis are presented as a single group because they did not differ significantly in median age and sex distribution. Biomarker values are in pg/ml. Key: ALS, amyotrophic lateral sclerosis; ALSFRS-R, Revised Amyotrophic Lateral Sclerosis Functional Rating; cNfL, cerebrospinal fluid neurofilament light chain; DD, disease duration; FVC, forced vital capacity; FTD, frontotemporal dementia; IQR, interquartile range; m, months; MRC, Medical Research Council; PLMN, predominant lower motor neuron; pNfL, plasma neurofilament light chain; PUMN, predominant upper motor neuron; RE, repeats expansion; y, years.*

Association Between Cerebrospinal Fluid Neurofilament Light Chain, Plasma Neurofilament Light Chain and Clinical Variables

cNfL and pNfL values strongly correlated at baseline (Spearman's rho = 0.836, $p < 0.0001$).

TABLE 2 | Diagnostic categories in the ALS mimics group.

ALS mimic diagnoses	60
Hereditary or idiopathic spastic paraplegia	12
Chronic inflammatory demyelinating polyneuropathy	5
Polyneuropathy	6
Myelopathy/myelitis	3
Multineuropathy	3
Spinal muscular atrophy 3	2
Myopathy/myositis	4
Cramp-fasciculation syndrome	1
Spinocerebellar ataxia	1
Focal amyotrophy	2
Amyloidosis	1
Myasthenia gravis	3
Post-polio syndrome	1
Caspr2 antibody-associated disease	1
Anti-IgLON5 disease	1
Meningioma	1
Hydrocephalus	1
PSP-PLS	1
Atypical parkinsonism	2
Alexander's disease	1
Lumbar spinal stenosis	1
Unclassified	7

Key: ALS, amyotrophic lateral sclerosis; PLS, primary lateral sclerosis; PSP, progressive supranuclear palsy.

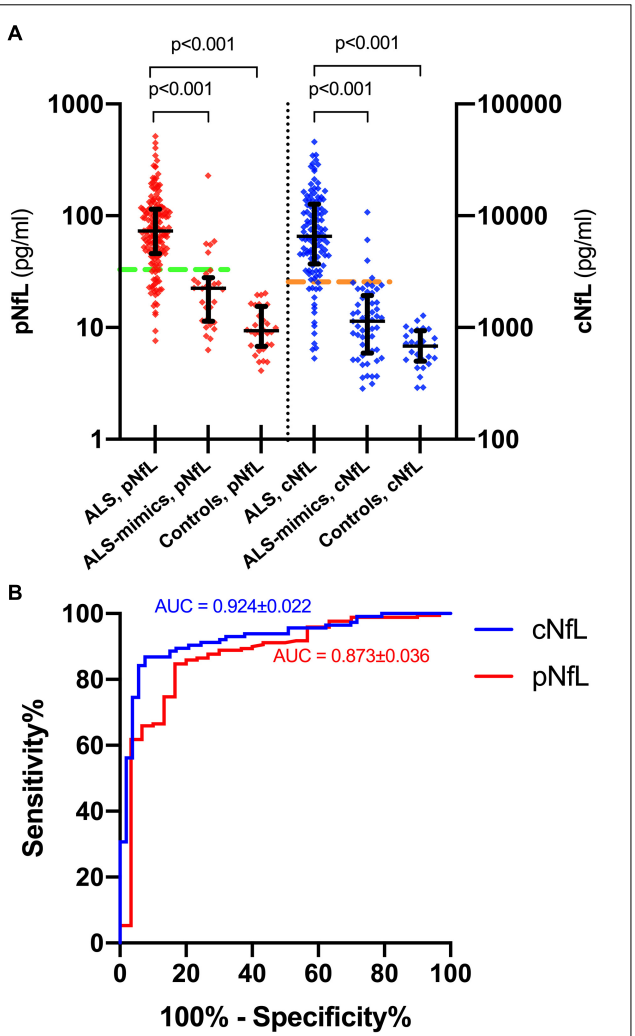

FIGURE 1 | pNfL and cNfL levels in the diagnostic groups and ROC curves for pNfL and cNfL. Both cNfL and pNfL demonstrate high diagnostic value in the distinction between ALS and ALS mimics. **(A)** pNfL and cNfL levels in ALS patients, ALS-mimics and control groups. Thick lines represent medians and interquartile ranges. Biomarker values are expressed in the logarithmic scale. Dotted horizontal lines indicate the optimal cut-off values for pNfL (green) and cNfL (orange) in the distinction between ALS and ALS-mimics patients, as calculated through the maximized Youden Index. Only *p*-values of significative comparisons are shown (Kruskal-Wallis followed by Dunn-Bonferroni *post hoc* test). **(B)** ROC curves for pNfL (red) and cNfL (blue) in the comparison between ALS patients and ALS-mimics. Key: cNfL, cerebrospinal fluid neurofilament light chain; pNfL, plasma neurofilament light chain.

When evaluating the associations between biofluid biomarkers and measures of ALS severity, we found a marked association between both cNfL and pNfL concentrations and DPR (rho = 0.493, $p < 0.0001$; rho = 0.525, $p < 0.0001$, respectively), and a weaker association of NfL values in both biofluids with the MRC score (rho = 0.231, $p = 0.014$; rho = 0.248, $p = 0.002$), FVC (rho = 0.363, $p = 0.003$; rho = 0.276, $p = 0.001$), and ALSFRS-R (rho = 0.206, $p = 0.023$; rho = 0.217, $p = 0.006$) values. cNfL levels were also weakly correlated with the King's stage (rho = 0.249, $p = 0.008$).

Moreover, fast progressors (i.e., ALS patients with DPR > 1) showed higher cNfL and pNfL compared to intermediate ($p = 0.026$ and $p = 0.001$) and slow progressors ($p < 0.001$).

In contrast, there was no significant association between pNfL/cNfL and ECAS (total, ALS-specific and ALS non- specific scores) and BMI, and between pNfL and King's stage. cNfL levels significantly differed across onset types ($p = 0.011$), and *post hoc* analysis revealed significantly higher levels in patients with bulbar than in those with spinal onset ($p = 0.038$). We found no significant differences across ALS variants, FTD, or genetic status, although cNfL resulted higher in ALS-FTD patients than in pure ALS (8637.2, IQR 6331.9-13979.9 vs. 6155.7, IQR 3231.4-12011, $p = 0.093$) and in *C9Orf72* RE carriers ($p = 0.14$) (**Table 3**).

pNfL levels did not significantly differ among ALS phenotypes and type of onset but were slightly increased in FTD-ALS patients compared to those with ALS alone, with a trend of significance (110.8, IQR 55.5-165 vs. 70.7, IQR 43.4-109.5, $p = 0.054$). Moreover, pNfL values were significantly higher in *C9Orf72* RE expansion carriers than in the other patients ($p = 0.010$) (**Table 3**).

Finally, both pNfL and cNfL levels increased according to the accuracy level of the categories of the Revised El Escorial diagnostic criteria (Brooks et al., 2000) (for pNfL: probable laboratory-supported vs. definite ALS, $p = 0.001$; probable laboratory-supported vs. probable ALS, $p = 0.002$; for cNfL: possible ALS vs. probable ALS, $p = 0.005$; probable laboratory-supported ALS vs. definite ALS, $p = 0.043$; possible ALS vs. definite ALS, $p = 0.004$, **Table 3**), likely reflecting the effect of the

TABLE 3 | pNfL and cNfL levels according to the accuracy level of the categories of the Revised El Escorial diagnostic criteria and to genetic status (i.e., wild type vs. ALS gene mutations).

Revised El *Escorial criteria*	**N**	**pNfL Median (IQR)**	**N**	**cNfL Median (IQR)**
Possible ALS	38	64.9 (27.6–101.3)	25	4536 (2232–8853)
Probable laboratory-supported ALS	31	45.8 (31.4–70.7)	24	5100 (3145.2–7760)
Probable ALS	68	86.1 (57.7–127.2)	45	7572 (4770–15569)
Definite ALS	31	100.5 (58.8–135.5)	19	10892.4 (6156–14629)
Genetic status	**N**	**pNfL Median (IQR)**	**N**	**cNfL Median (IQR)**
Wild-type	137	73.5 (43.9–113.7)	98	6317 (3574–13476)
SOD1	6	36.0 (14.0–59.4)	2	2252; 4536
TARDBP	2	32.8; 51.8	1	3018.5
FUS	1	37.2	0	NA
C9Orf72	18	107.1 (64.5–125.3)	11	10796 (7950–12031)

Biomarker values are expressed in pg/ml. Key: ALS, amyotrophic lateral sclerosis; cNfL, cerebrospinal neurofilament light chain; IQR, interquartile range; N, number; NA, not available; pNfL, plasma neurofilament light chain.

progressive spreading of the neurodegeneration and the increase of body regions involved during the disease course.

Association Between Cerebrospinal Fluid Neurofilament Light Chain, Plasma Neurofilament Light Chain and the Extent of Upper Motor Neurons and/or Lower Motor Neurons Degeneration

Both cNfL and pNfL were associated with the number of body regions displaying UMN signs (rho = 0.325, $p < 0.0001$; rho = 0.308, $p = 0.001$). Accordingly, both cNfL and pNfL levels significantly raised with increasing number of regions affected by UMN signs only ($p = 0.008$ and $p = 0.001$) or displaying both UMN and LMN signs ($p = 0.001$ and $p = 0.002$). Both results remained statistically significant after adjusting for covariates (i.e., age at sampling, sex, genetic status, basal ALSFRS-R, DPR, MRC, and King's scores) (cNfL vs. UMN, three regions vs. zero or one region: β = 0.834, CI 0.316–1.636, $p = 0.042$; pNfL vs. UMN, three regions vs. zero or one region: β = 0.609, CI 0.348–1.185, $p = 0.038$; cNfL vs. UMN + LMN, three regions vs. zero or one region: β = 1.003, CI 0.265–1.741, $p = 0.008$; pNfL vs. UMN + LMN, three regions vs. zero or one region: β = 0.529, CI 0.206–1.038, $p = 0.042$).

In contrast, there was no association with the number of LMN affected regions ($p = 0.467$ and $p = 0.537$) (**Table 4**).

Prognostic Value of Cerebrospinal Fluid Neurofilament Light Chain and Plasma Neurofilament Light Chain in Amyotrophic Lateral Sclerosis

Based on univariate Cox regression analysis (171 ALS patients; 72 dead), age at sampling ($p = 0.034$), basal ALSFRS-R ($p < 0.001$), DPR ($p < 0.001$), *C9orf72* status ($p = 0.031$), MRC score ($p = 0.001$), King's score ($p < 0.001$), FVC ($p < 0.001$), cNfL ($p < 0.001$) and pNfL ($p < 0.001$) were identified as predictors of the mortality in ALS patients (**Supplementary Table 2**). Multivariate Cox regression confirmed the value of both cNfL (HR 2.44, CI 1.52–3.90, $p < 0.001$) and pNfL (HR 2.06, CI 1.31–3.22, $p = 0.002$) as independent predictors of the mortality in ALS (see **Supplementary Table 2** for details). Accordingly, ALS patients with higher baseline cNfL and pNfL levels were associated with shorter survival (highest tertile of cNfL vs. lowest tertile of NfL, HR 4.58, CI 1.57–13.41, $p = 0.005$; highest tertile of pNfL vs. lowest tertile of NfL, HR 2.59, CI 1.20–5.58, $p = 0.015$) (**Figure 2**).

Longitudinal Trajectories of Plasma Neurofilament Light Chain During the Follow-Up

When stratifying ALS patients according to the l-DPR, baseline levels of both cNfL and pNfL were significantly higher in ALS fast progressors than the slow progressors ($p = 0.002$ and $p = 0.001$, respectively, **Table 5**). In contrast, there was no significant rise or decline in the slopes of pNfL levels during follow-up in the three ALS groups (slow β = –0.001, CI –0.009 to 0.007, $p = 0.773$; intermediate β = 0.006, CI –0.002 to 0.013, $p = 0.126$; fast β = –0.0001, CI –0.009 to 0.009, $p = 0.974$, **Figure 3**), highlighting the overall stability of the biomarker during the disease course.

DISCUSSION

In the context of motor neuron disease, biofluid markers may aid in the diagnosis of clinically subtle or atypical ALS variants, in the prognostic evaluation of patients and their stratification for clinical trials. Here we confirmed the value of cNfL in distinguishing between patients with ALS and ALS mimics in a large clinical cohort. Additionally, in line with previous studies (Gaiottino et al., 2013; Lu et al., 2015; Benatar et al., 2018; Feneberg et al., 2018; Verde et al., 2019; Ashton et al., 2021), we demonstrated a strong association between cNfL and pNfL, and showed that pNfL also provides a robust diagnostic marker for ALS, especially after excluding patients with peripheral

TABLE 4 | pNfL and cNfL levels according to the extent of UMN and/or LMN degeneration.

		N	pNfL Median (IQR)	N	cNfL Median (IQR)
UMN and LMN degeneration	Zero regions	15	51.8 (32.8–103.9)	10	4161 (2165–8816)
	One region	52	58.2 (32.7–95)	35	4938 (2926–7964)
	Two regions	65	76.8 (48–120.8)	45	7187 (4209–14901)
	Three regions	36	104.0 (64.5–139.1)	23	11052 (6970–15995)
UMN degeneration	Zero regions	10	40.9 (24.3–108.7)	7	3574 (1103–8778)
	One region	29	49.7 (35.8–72)	21	4938 (3814–6590)
	Two regions	60	67.8 (43.4–112.3)	40	5943 (3211–13758)
	Three regions	69	97.2 (58.83–136.9)	45	9440 (5624–14653)
LMN degeneration	Zero regions	6	59.0 (46.9–76.6)	3	4747 (–)
	One region	20	80.4 (22.8–116.0)	11	6263 (881.6–13732)
	Two regions	65	63.4 (38.8–117.3)	41	5784 (3392–13805)
	Three regions	77	79.2 (51.2–112.4)	58	7378 (4496–12147)

Biomarker values are expressed in pg/ml. Key: ALS, amyotrophic lateral sclerosis; cNfL, cerebrospinal neurofilament light chain; LMN, lower motor neuron; IQR, interquartile range; N, number; pNfL, plasma neurofilament light chain; UMN, upper motor neuron.

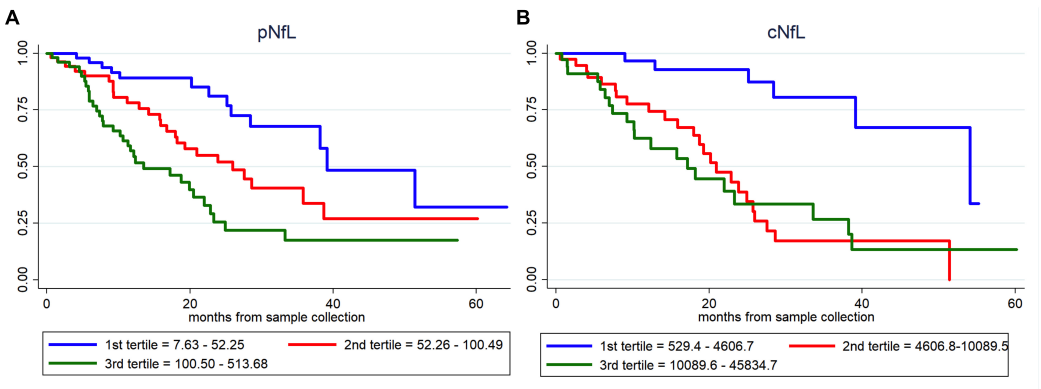

FIGURE 2 | Prognostic value of pNfL and cNfL. Survival curves in ALS patients according to the values of pNfL **(A)** and cNfL **(B)**. A greater increase in baseline cNfL and pNfL levels is associated with shorter survival in patients with ALS. Key: c-NfL, cerebrospinal fluid neurofilament light chain; pNfL, plasma neurofilament light chain.

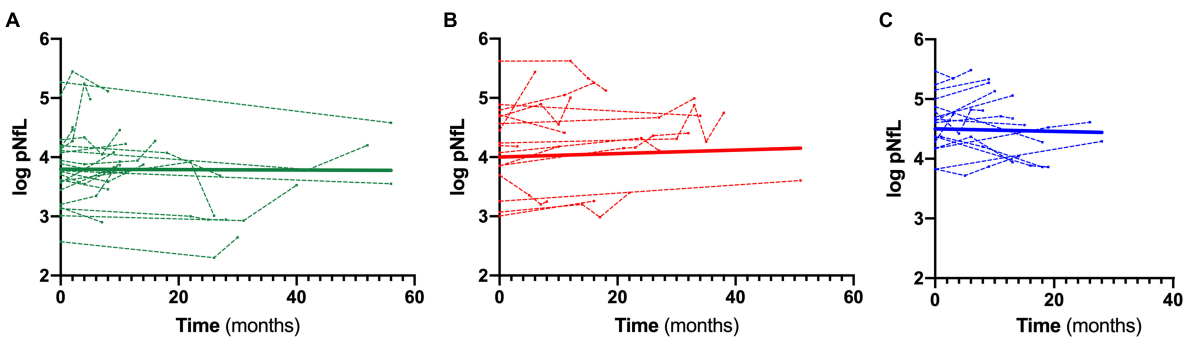

FIGURE 3 | Longitudinal trajectories of pNfL during the follow-up. Overall and single-patient longitudinal pNfL behavior in the slow **(A)**, intermediate **(B)** and fast **(C)** progressors showing a stable longitudinal biomarker trajectory Thick lines represent the overall biomarker trend. Analyses were conducted through a linear mixed effects model. Biomarker values are expressed in the logarithmic scale. Key: pNfL, plasma neurofilament light chain.

neuropathy, a condition associated with a higher increase of NfL values in plasma than in CSF (Bischof et al., 2018; Mariotto et al., 2018; Sandelius et al., 2018). Given that an extensive clinical and electrophysiological evaluation can reliably identify a PNS involvement, the diagnostic value of pNfL may be considered almost comparable to that of cNfL in the clinical routine. Furthermore, after stratification for age, we found a slight decrease of diagnostic accuracy of pNfL in elderly patients,

likely reflecting the physiological increase of the biomarker levels with age, which did not involve the ALS patients, given the marked abnormal concentrations, but that was evident in the ALS mimics cohort.

To address the still debated issue of the pathophysiology of NfL release according to the involvement of upper and lower motor neurons (Zucchi et al., 2020), we investigated the association between biomarker levels and the extent of UMN and LMN degeneration. We found that both pNfL and cNfL levels increased with the number of UMN regions, which is in line with several studies showing a significant correlation between serum (Gille et al., 2019) or CSF (Menke et al., 2015) NfL levels and clinical signs of UMN damage or the extent of corticospinal tract involvement assessed by diffusion tensor MRI (Menke et al., 2015). However, other studies, including our previous evaluation limited to CSF NfL in a smaller cohort, did not confirm this association (Steinacker et al., 2016; Gaiani et al., 2017; Abu-Rumeileh et al., 2020). Beside the possible effects of patient selection and cohort size and the type of assay chosen for the analysis, one likely explanation for these conflicting results relies on the well-known high inter-rater variability in the clinical evaluation of UMN and LMN signs. Indeed, there is still disagreement among neurologists on how to define the presence of UMN-signs given that some consider a preserved reflex in an otherwise atrophic muscle to be a sign of upper motor neuron involvement, while others require the reflex to be hyperactive to reach the same conclusion (Swinnen and Robberecht, 2014). Likewise, given that both clinical and neurophysiological assessment help evaluate LMN involvement, a between-center standardization of neurophysiological techniques is also needed.

In our cohort, both cNfL and pNfL showed higher values in *C9Orf72*-expanded ALS patients than in those with sporadic ALS, likely reflecting the more severe disease course in this patient subgroup. Notably, the current literature does not show full agreement also on this issue with three previous studies supporting our findings (Gendron et al., 2017, Benatar et al., 2020; Huang et al., 2020), and two others not detecting any difference in CSF or serum NFL levels between patients with mutations in *SOD1*, *TARDBP*, *FUS* or the RE of *C9orf72* and sporadic cases (Weydt et al., 2016; Verde et al., 2019).

Another debated issue concerns the potential effect of cognitive impairment on neurofilament levels in ALS. FTD-ALS patients in our cohort presented with higher levels of both pNfL and cNfL than ALS alone, reaching a trend of significance only for the plasma biomarker. Similarly, one study demonstrated higher, although not significant, plasma neurofilament heavy-chain levels in ALS-FTD than in ALS patients (Falzone et al., 2020). However, other studies failed to find a correlation between cognitive functions decline and NfL levels (Gaiani et al., 2017; Feneberg et al., 2018), suggesting that the increase in biomarker levels in ALS is probably relatively independent of the brain regions involved compared to the effect of progression rate. These discordances in the current literature may also be attributable to the small number of ALS-FTD patients enrolled in the available studies. Further studies are, therefore, needed to establish whether the abnormal accumulation of neurofilaments might contribute to the definition of the pathologic ALS-FTD continuum.

On another critical issue, our results confirmed the predictive value on disease progression of cNfL and pNfL assessment (De Schaepdryver et al., 2020). Indeed, our data showed a strong correlation between the biofluid levels of the biomarker and the DPR. Accordingly, when stratifying patients in fast, intermediate, and slow progressors by tertiles, score, biofluid NfL levels were significantly higher in fast progressors compared to the other two groups, in line with previous results (Poesen et al., 2017; Feneberg et al., 2018; Verde et al., 2019; Abu-Rumeileh et al., 2020; Dreger et al., 2021).

In the present study, we also confirmed that both CSF and plasma NfL levels are independent prognostic factors in ALS, even after adjusting for potential clinical prognostic predictors, such as basal ALSFRS-R, genetic status, DPR, MRC, and King's scores (Benatar et al., 2020). This implies that NfL assessment in both plasma and CSF allows an early diagnosis of ALS

TABLE 5 | Longitudinal ALS cohort: patients' characteristics and biomarkers stratification according to the I-DPR.

Groups (I-DPR)	N	Age at sample mean (SD)	Time from onset to sample (m) mean (SD)	Sex F/M	Type of onset, SPI/BUL/PSE/PYR	cNfL median (IQR)	pNfL median (IQR)
ALS Fast	17	55.6 (13.5)	14.6 (15.6)	8/9	9/6/1/1	9175 (6021–14887)	101.4 (68.7–134.7)
ALS Intermediate	16	67.4 (11.9)	20.8 (10.7)	10/6	11/3/0/2	5520 (3738–8345)	67.8 (43.7–109.9)
ALS Slow	24	64.8 (12.4)	31.7 (24.9)	13/11	17/3/2/2	3250 (2365–5193)	43.4 (31.4–64.4)
p-value		0.021*	0.021**	0.71	0.461	0.002°	0.002°°

**Post hoc analysis revealed a significant difference between Fast and Intermediate ALS patients (p = 0.028).*

***Post hoc analysis showed a significant difference between Fast and Slow ALS patients (p = 0.021).*

°Post hoc analysis revealed a significant difference between Fast and Slow ALS patients (p = 0.002).

°°Post hoc analysis revealed a significant difference between Fast and Slow ALS patients (p = 0.001).

The p-values reported directly in the table refer to the multiple-groups comparison analyses. Only the p-values of the comparisons showing a statistically significant difference at the post hoc analysis are further detailed in the table legend.

Biomarker values are expressed in pg/ml. Key: ALS, amyotrophic lateral sclerosis; BUL, bulbar; cNfL, cerebrospinal neurofilament light chain; F, females, I-DPR, longitudinal disease progression rate; IQR, interquartile range; m, months; M, Males; N, number; pNfL, plasma neurofilament light chain; PSE, pseudopolyneuritic; PYR, pyramidal; SPI, spinal; SD, standard deviation.

and a better stratification of patients for early recruitment in clinical trials, considering the high clinical variability of this devastating disease. Accordingly, a recent study (Benatar et al., 2020) showed that using the baseline serum NfL level as a pharmacodynamic biomarker instead of the ALSFRS-R slope would yield a significant patient sample size saving in a clinical trial.

While the absolute pNfL values varied between patients in our cohort, they remained largely stable in individual patients over time, consistent with previous observations (Lu et al., 2015; Verde et al., 2019). This finding further confirms the potential clinical utility of plasma NfL as a marker of drug effect, provides that the tested novel therapeutics will result in a significant reduction of NfL levels, as recently proved for nusinersen in pediatric spinal muscular atrophy (Darras et al., 2019; Johannsen et al., 2021).

The present study has some limitations. Although we enrolled a significant number of ALS patients, the well-known high variability of the disease did not allow us to draw definitive conclusions about the effect of ALS clinical variants, FTD status, and ALS gene mutations on plasma and CSF NfL levels. Moreover, our demonstration of NfL concentration stability during the disease course was based on the analysis of a relatively small cohort and on longitudinal blood samples collected at non-standardized time points, suggesting caution in interpreting these results. Another partial limitation concerns the small number of ALS patients with a recent onset of symptoms and the absence of pre-symptomatic subjects carrying mutations in ALS genes. The inclusion of such patients could provide additional information about the behavior of biofluids NfL during the pre-symptomatic and early symptomatic phases of the disease, as already pointed out in recent studies (Benatar et al., 2018). Thus, future studies on larger cohorts are needed to validate our results and better explore the NfL behavior during the entire disease course. In conclusion, the results of the present study confirm and extend the available data indicating that both cNfL and pNfL have excellent diagnostic and prognostic performance for symptomatic patients with ALS and support the use of pNfL as a pharmacodynamic marker in clinical trials. However, despite the positive results, to fully understand the diagnostic potential of biofluid NfL in ALS, it would be important to perform more detailed comparisons between ALS patients and homogeneous larger cohorts of single categories of mimic diseases. Furthermore, more extensive prospective multicentric studies on the longitudinal behavior of neurofilament based on standardized methodologies are needed to further assess the role of NfL as a disease progression marker. Finally, a better understanding of how NfL is released in response to pathology, especially in the early disease stages, would also facilitate the use of NfL in the diagnostic work-up and therapeutic trials in ALS.

DATA AVAILABILITY STATEMENT

The original contributions presented in the study are included in the article/**Supplementary Material**, further inquiries can be directed to the corresponding author/s.

ETHICS STATEMENT

The study was approved by the Ethics Committee of "Area Vasta Emilia Centro". The patients/participants provided their written informed consent to participate in this study.

AUTHOR CONTRIBUTIONS

VV, AM, and PP: conceptualization and writing—original draft preparation. PP: writing—review and editing based on the critical revision of all authors and supervision. All authors: methodology, formal analysis, and investigation.

FUNDING

This work was supported by the Italian Ministry of Health ("Ricerca Corrente").

ACKNOWLEDGMENTS

Collaborators: BoReALS group: Ilaria Bartolomei, Franca Cinelli, Vitantonio Di Stasi, Rosaria Plasmati, Francesca Pastorelli, Cecilia Celidea Quarta, David Milletti, Raffaella Nasca, Francesca Rizzi, Francesca Santoro, Luca Valeriani, Francesca Anzolin, Elisabetta Fantoni, Vincenzo Donadio, Fiorito Alessia, Silvia de Pasqua, Giovanni Rizzo, Annalisa Pession, Luca Vignatelli, Michelangelo Stanzani-Maserati, Sofia Asioli, Anna Bartoletti-Stella, Carolina Colombo, Serena Maselli, Maria Pia Giannoccaro.

SUPPLEMENTARY MATERIAL

The Supplementary Material for this article can be found online at: https://www.frontiersin.org/articles/10.3389/fnagi.2021.753242/full#supplementary-material

REFERENCES

Abrahams, S., Newton, J., Niven, E., Foley, J., and Bak, T. H. (2014). Screening for cognition and behaviour changes in ALS. *Amyotroph Later. Scler Frontotemp. Deg.* 15, 9–14. doi: 10.3109/21678421.2013.805784

Abu-Rumeileh, S., Vacchiano, V., Zenesini, C., Polischi, B., de Pasqua, S., Fileccia, E., et al. (2020). Diagnostic-prognostic value and electrophysiological correlates of CSF biomarkers of neurodegeneration and neuroinflammation in amyotrophic lateral sclerosis. *J. Neurol.* 267, 1699–1708. doi: 10.1007/s00415-020-09761-z

Al-Chalabi, A., Hardiman, O., Kiernan, M. C., Chiò, A., Rix-Brooks, B., and van den Berg, L. H. (2016). Amyotrophic lateral sclerosis: moving towards a new classification system. *Lancet Neurol.* 15, 1182–1194. doi: 10.1016/S1474-4422(16)30199-5

Ashton, N. J., Janelidze, S., Al Khleifat, A., Leuzy, A., van der Ende, E. L., Karikari, T. K., et al. (2021). A multicentre validation study of the diagnostic value of

plasma neurofilament light. *Nat. Commun.* 12:3400. doi: 10.1038/s41467-021-23620-z

Bartoletti-Stella, A., Vacchiano, V., De Pasqua, S., Mengozzi, G., De Biase, D., Bartolomei, I., et al. (2021). Targeted sequencing panels in Italian ALS patients support different etiologies in the ALS/FTD continuum. *J. Neurol.* 2021:10521. doi: 10.1007/s00415-021-10521-w

Benatar, M., Wuu, J., Andersen, P. M., Lombardi, V., and Malaspina, A. (2018). Neurofilament light: a candidate biomarker of presymptomatic amyotrophic lateral sclerosis and phenoconversion. *Ann. Neurol.* 84, 130–139. doi: 10.1002/ana.25276

Benatar, M., Zhang, L., Wang, L., Granit, V., Statland, J., Barohn, R., et al. (2020). Validation of serum neurofilaments as prognostic and potential pharmacodynamic biomarkers for ALS. *Neurology* 2020:9559. doi: 10.1212/WNL.0000000000009559

Bischof, A., Manigold, T., Barro, C., Heijnen, I., Berger, C. T., Derfuss, T., et al. (2018). Serum neurofilament light chain: a biomarker of neuronal injury in vasculitic neuropathy. *Ann. Rheum. Dis.* 77, 1093–1094. doi: 10.1136/annrheumdis-2017-212045

Brooks, B. R., Miller, R. G., Swash, M., and Munsat, T. L. (2000). El Escorial revisited: revised criteria for the diagnosis of amyotrophic lateral sclerosis. *Amyotroph Later. Scler Motor Neuron Dis.* 1, 293–299. doi: 10.1080/146608200300079536

Chiò, A., Calvo, A., Moglia, C., Mazzini, L., and Mora, G. (2011). Phenotypic heterogeneity of amyotrophic lateral sclerosis: a population based study. *J. Neurol. Neurosurg. Psychiatry* 82, 740–746. doi: 10.1136/jnnp.2010.235952

Darras, B. T., Crawford, T. O., Finkel, R. S., Mercuri, E., De Vivo, D. C., Oskoui, M., et al. (2019). Neurofilament as a potential biomarker for spinal muscular atrophy. *Ann. Clin. Transl. Neurol.* 2019, 932–944. doi: 10.1002/acn3.779

de Carvalho, M., Dengler, R., Eisen, A., England, J. D., Kaji, R., Kimura, J., et al. (2008). Electrodiagnostic criteria for diagnosis of ALS. *Clin. Neurophysiol.* 119, 497–503. doi: 10.1016/j.clinph.2007.09.143

De Schaepdryver, M., Lunetta, C., Tarlarini, C., Mosca, L., Chio, A., Van Damme, P., et al. (2020). Neurofilament light chain and C reactive protein explored as predictors of survival in amyotrophic lateral sclerosis. *J. Neurol. Neurosurg. Psychiatry* 91, 436–437. doi: 10.1136/jnnp-2019-322309

Dreger, M., Steinbach, R., Gaur, N., Metzner, K., Stubendorff, B., Witte, O. W., et al. (2021). Cerebrospinal fluid neurofilament light chain (NfL) predicts disease aggressiveness in amyotrophic lateral sclerosis: an application of the D50 disease progression model. *Front. Neurosci.* 15:651651. doi: 10.3389/fnins.2021.651651

Falzone, Y. M., Domi, T., Agosta, F., Pozzi, L., Schito, P., Fazio, R., et al. (2020). Serum phosphorylated neurofilament heavy-chain levels reflect phenotypic heterogeneity and are an independent predictor of survival in motor neuron disease. *J. Neurol.* 267, 2272–2280. doi: 10.1007/s00415-020-09838-9

Feneberg, E., Oeckl, P., Steinacker, P., Verde, F., Barro, C., Van Damme, P., et al. (2018). Multicenter evaluation of neurofilaments in early symptom onset amyotrophic lateral sclerosis. *Neurology* 90, e22–e30. doi: 10.1212/WNL.0000000000004761

Gaiani, A., Martinelli, I., Bello, L., Querin, G., Puthenparampil, M., Ruggero, S., et al. (2017). Diagnostic and prognostic biomarkers in amyotrophic lateral sclerosis: Neurofilament light chain levels in definite subtypes of disease. *JAMA Neurol.* 74, 525–532. doi: 10.1001/jamaneurol.2016.5398

Gaiottino, J., Norgren, N., Dobson, R., Topping, J., Nissim, A., Malaspina, A., et al. (2013). Increased neurofilament light chain blood levels in neurodegenerative neurological diseases. *PLoS One* 8:e75091. doi: 10.1371/journal.pone.0075091

Gendron, T. F., C9ORF72 Neurofilament Study Group, Daughrity, L. M., Heckman, M. G., Diehl, N. N., Wuu, J., et al. (2017). Phosphorylated neurofilament heavy chain: a biomarker of survival for C9ORF72-associated amyotrophic lateral sclerosis. *Ann Neurol.* 82, 139–146. doi: 10.1002/ana.24980

Giannoccaro, M. P., Bartoletti-Stella, A., Piras, S., Pession, A., De Massis, P., Oppi, F., et al. (2017). Multiple variants in families with amyotrophic lateral sclerosis and frontotemporal dementia related to C9orf72 repeat expansion: further observations on their oligogenic nature. *J. Neurol.* 264, 1426–1433. doi: 10.1007/s00415-017-8540-x

Gille, B., De Schaepdryver, M., Goossens, J., Dedeene, L., De Vocht, J., Oldoni, E., et al. (2019). Serum neurofilament light chain levels as a marker of upper motor neuron degeneration in patients with Amyotrophic Lateral Sclerosis. *Neuropathol. Appl. Neurobiol.* 45, 291–304. doi: 10.1111/nan.12511

Gray, E., Oeckl, P., Amador, M. D. M., Andreasson, U., An, J., Blennow, K., et al. (2020). A multi-center study of neurofilament assay reliability and inter-laboratory variability. *Amyotroph Later. Scler Frontotemp. Degener.* 21, 452–458. doi: 10.1080/21678421.2020.1779300

Huang, F., Zhu, Y., Hsiao-Nakamoto, J., Tang, X., Dugas, J. C., Moscovitch-Lopatin, M., et al. (2020). Longitudinal biomarkers in amyotrophic lateral sclerosis. *Ann. Clin. Transl. Neurol.* 7, 1103–1116. doi: 10.1002/acn3.51078

Johannsen, J., Weiss, D., Daubmann, A., Schmitz, L., and Denecke, J. (2021). Evaluation of putative CSF biomarkers in paediatric spinal muscular atrophy (SMA) patients before and during treatment with nusinersen. *J. Cell Mol. Med.* 2021:16802. doi: 10.1111/jcmm.16802

Lu, C. H., Macdonald-Wallis, C., Gray, E., Pearce, N., Petzold, A., Norgren, N., et al. (2015). Neurofilament light chain: A prognostic biomarker in amyotrophic lateral sclerosis. *Neurology* 84, 2247–2257.

Mariotto, S., Farinazzo, A., Magliozzi, R., Alberti, D., Monaco, S., Ferrari, S. (2018). Serum and cerebrospinal neurofilament light chain levels in patients with acquired peripheral neuropathies. *J. Peripher. Nerv. Syst.* 23, 174–177. doi: 10.1111/jns.12279

Menke, R. A., Gray, E., Lu, C. H., Kuhle, J., Talbot, K., Malaspina, A., et al. (2015). CSF neurofilament light chain reflects corticospinal tract degeneration in ALS. *Ann. Clin. Transl. Neurol.* 2, 748–755. doi: 10.1002/acn3.212

Poesen, K., De Schaepdryver, M., Stubendorff, B., Gille, B., Muckova, P., Wendler, S., et al. (2017). Neurofilament markers for ALS correlate with extent of upper and lower motor neuron disease. *Neurology* 88, 2302–2309. doi: 10.1212/WNL.0000000000004029

Roche, J. C., Rojas-Garcia, R., Scott, K. M., Scotton, W., Ellis, C. E., Burman, R., et al. (2012). A proposed staging system for amyotrophic lateral sclerosis. *Brain* 135, 847–852. doi: 10.1093/brain/awr351

Sandelius, Å., Zetterberg, H., Blennow, K., Adiutori, R., Malaspina, A., Laura, M., et al. (2018). Plasma neurofilament light chain concentration in the inherited peripheral neuropathies. *Neurology.* 90, e518–e524. doi: 10.1212/WNL.0000000000004932

Siciliano, M., Trojano, L., Trojsi, F., Greco, R., Santoro, M., Basile, G., et al. (2017). Edinburgh Cognitive and Behavioural ALS Screen (ECAS)-Italian version: regression based norms and equivalent scores. *Neurol. Sci.* 38, 1059–1068.

Skillbäck, T., Mattsson, N., Blennow, K., and Zetterberg, H. (2017). Cerebrospinal fluid neurofilament light concentration in motor neuron disease and frontotemporal dementia predicts survival. *Amyotroph Later. Scler Frontotemp. Degener.* 18, 397–403.

Steinacker, P., Feneberg, E., Weishaupt, J., Brettschneider, J., Tumani, H., Andersen, P. M., et al. (2016). Neurofilaments in the diagnosis of motoneuron diseases: a prospective study on 455 patients. *J. Neurol. Neurosurg. Psychiatry* 87, 12–20. doi: 10.1136/jnnp-2015-311387

Steinacker, P., Huss, A., Mayer, B., Grehl, T., Grosskreutz, J., Borck, G., et al. (2017). Diagnostic and prognostic significance of neurofilament light chain NF-L, but not progranulin and S100B, in the course of amyotrophic lateral sclerosis: Data from the German MND-net. *Amyotroph Later. Scler Frontotemp. Degener.* 18, 112–119. doi: 10.1080/21678421.2016.1241279

Swinnen, B., and Robberecht, W. (2014). The phenotypic variability of amyotrophic lateral sclerosis. *Nat. Rev. Neurol.* 10, 661–670. doi: 10.1038/nrneurol.2014.184

Thouvenot, E., Demattei, C., Lehmann, S., Maceski-Maleska, A., Hirtz, C., Juntas-Morales, R., et al. (2020). Serum neurofilament light chain at time of diagnosis is an independent prognostic factor of survival in amyotrophic lateral sclerosis. *Eur. J. Neurol.* 27, 251–257.

Verde, F., Steinacker, P., Weishaupt, J. H., Kassubek, J., Oeckl, P., Halbgebauer, S., et al. (2019). Neurofilament light chain in serum for the diagnosis of amyotrophic lateral sclerosis. *J. Neurol. Neurosurg. Psychiatry* 90, 157–164. doi: 10.1136/jnnp-2018-318704

Vu, L., An, J., Kovalik, T., Gendron, T., Petrucelli, L., and Bowser, R. (2020). Cross-sectional and longitudinal measures of chitinase proteins in amyotrophic lateral sclerosis and expression of CHI3L1 in activated astrocytes. *J. Neurol. Neurosurg. Psychiatry* 91, 350–358. doi: 10.1136/jnnp-2019-321916

Weydt, P., Oeckl, P., and Huss, A. (2016). Neurofilament levels as biomarkers in asymptomatic and symptomatic familial amyotrophic lateral sclerosis. *Ann. Neurol.* 79, 152–158. doi: 10.1002/ana.24552

Zucchi, E., Bonetto, V., Sorarù, G., Martinelli, I., Parchi, P., Liguori, R., et al. (2020). Neurofilaments in motor neuron disorders: towards promising diagnostic and

prognostic biomarkers. *Mol. Neurodegener.* 15:58. doi: 10.1186/s13024-020-00406-3

Conflict of Interest: The authors declare that the research was conducted in the absence of any commercial or financial relationships that could be construed as a potential conflict of interest.

Publisher's Note: All claims expressed in this article are solely those of the authors and do not necessarily represent those of their affiliated organizations, or those of the publisher, the editors and the reviewers. Any product that may be evaluated in this article, or claim that may be made by its manufacturer, is not guaranteed or endorsed by the publisher.

frontiers in Aging Neuroscience

ORIGINAL RESEARCH
published: 27 October 2021
doi: 10.3389/fnagi.2021.749649

Performance of Plasma Amyloid β, Total Tau, and Neurofilament Light Chain in the Identification of Probable Alzheimer's Disease in South China

Bin Jiao[1,2,3†], Hui Liu[1†], Lina Guo[1], Xinxin Liao[2,3,4], Yafang Zhou[2,3,4], Ling Weng[1,2,3], Xuewen Xiao[1], Lu Zhou[1], Xin Wang[1], Yaling Jiang[1], Qijie Yang[1], Yuan Zhu[1], Lin Zhou[2,3,4], Weiwei Zhang[5], Junling Wang[1,2,3], Xinxiang Yan[1,2,3], Beisha Tang[1,2,3] and Lu Shen[1,2,3,6,7,8]*

[1] Department of Neurology, Xiangya Hospital, Central South University, Changsha, China, [2] National Clinical Research Center for Geriatric Disorders, Central South University, Changsha, China, [3] Key Laboratory of Hunan Province in Neurodegenerative Disorders, Central South University, Changsha, China, [4] Department of Geriatrics, Xiangya Hospital, Central South University, Changsha, China, [5] Department of Radiology, Xiangya Hospital, Central South University, Changsha, China, [6] Key Laboratory of Organ Injury, Aging and Regenerative Medicine of Hunan Province, Changsha, China, [7] Engineering Research Center of Hunan Province in Cognitive Impairment Disorders, Central South University, Changsha, China, [8] Hunan International Scientific and Technological Cooperation Base of Neurodegenerative and Neurogenetic Diseases, Changsha, China

OPEN ACCESS

Edited by:
Nicholas James Ashton, University of Gothenburg, Sweden

Reviewed by:
Marta Mila Aloma, BarcelonaBeta Brain Research Center, Spain
Fabricio Ferreira de Oliveira, Elysian Clinic, Brazil
Alberto Benussi, University of Brescia, Italy

***Correspondence:**
Lu Shen
shenlu@csu.edu.cn;
shenlu2505@126.com

[†] These authors have contributed equally to this work

Received: *29 July 2021*
Accepted: *24 September 2021*
Published: *27 October 2021*

Citation:
Jiao B, Liu H, Guo L, Liao X, Zhou Y, Weng L, Xiao X, Zhou L, Wang X, Jiang Y, Yang Q, Zhu Y, Zhou L, Zhang W, Wang J, Yan X, Tang B and Shen L (2021) Performance of Plasma Amyloid β, Total Tau, and Neurofilament Light Chain in the Identification of Probable Alzheimer's Disease in South China. Front. Aging Neurosci. 13:749649. doi: 10.3389/fnagi.2021.749649

Background: Alzheimer's disease (AD) is the most common type of dementia and has no effective treatment to date. It is essential to develop a minimally invasive blood-based biomarker as a tool for screening the general population, but the efficacy remains controversial. This cross-sectional study aimed to evaluate the ability of plasma biomarkers, including amyloid β (Aβ), total tau (t-tau), and neurofilament light chain (NfL), to detect probable AD in the South Chinese population.

Methods: A total of 277 patients with a clinical diagnosis of probable AD and 153 healthy controls with normal cognitive function (CN) were enrolled in this study. The levels of plasma Aβ42, Aβ40, t-tau, and NfL were detected using ultra-sensitive immune-based assays (SIMOA). Lumbar puncture was conducted in 89 patients with AD to detect Aβ42, Aβ40, t-tau, and phosphorylated (p)-tau levels in the cerebrospinal fluid (CSF) and to evaluate the consistency between plasma and CSF biomarkers through correlation analysis. Finally, the diagnostic value of plasma biomarkers was further assessed by constructing a receiver operating characteristic (ROC) curve.

Results: After adjusting for age, sex, and the apolipoprotein E (*APOE*) alleles, compared to the CN group, the plasma t-tau, and NfL were significantly increased in the AD group ($p < 0.01$, Bonferroni correction). Correlation analysis showed that only the plasma t-tau level was positively correlated with the CSF t-tau levels ($r = 0.319$, $p = 0.003$). The diagnostic model combining plasma t-tau and NfL levels, and age, sex, and *APOE* alleles, showed the best performance for the identification of probable AD [area under the curve (AUC) = 0.89, sensitivity = 82.31%, specificity = 83.66%].

Conclusion: Blood biomarkers can effectively distinguish patients with probable AD from controls and may be a non-invasive and efficient method for AD pre-screening.

Keywords: Alzheimer's disease, plasma biomarkers, amyloid-beta, total-tau, neurofilament light chain

INTRODUCTION

Currently, ∼50 million people in the world are living with dementia and every 3 s a new case of dementia is diagnosed (Christina, 2018). Alzheimer's disease (AD) is the most common neurodegenerative dementia in older people and is characterized by progressive cognitive decline and behavioral defects with a complex and heterogeneous pathophysiology.

A preclinical phase of ≥20 years may occur before the clinical diagnosis of AD, during which no or only subtle symptoms appear, adding to the difficulty of early diagnosis and prevention (Jack et al., 2013; Jansen et al., 2015). At present, the most well-established AD biomarkers are mainly based on the core pathological features, including amyloid β (Aβ) deposition [detected by cerebrospinal fluid (CSF)] Aβ42 levels, amyloid positron emission tomography (PET), neurodegeneration [CSF total tau (t-tau)] and phosphorylated (p)-tau levels, structural MRI, and hypometabolism on fluorodeoxyglucose (FDG)-PET (Desikan et al., 2009; Mattsson et al., 2009; Landau et al., 2012). Nevertheless, high invasiveness, expensive costs, and limited availability hinder their clinical application. Therefore, noninvasive, cost-effective, and easily accessible biomarkers are desperately needed for the identification of AD.

To date, many studies have focused on blood-based biomarkers for the diagnosis of AD; somewhat promising results have mainly been achieved with Aβ, tau, and neurofilament light chain (NfL) in the blood. Previous studies have described the excellent performance of plasma Aβ-related peptides for the prediction of AD using different methods (Chen et al., 2019; Vergallo et al., 2019). The plasma t-tau level is a promising candidate marker because it is a brain-specific protein that is mainly expressed in central nervous system (CNS) neurons, indicates neuronal damage, and is derived from the brain parenchyma and transported to the CSF and blood (Schraen-Maschke et al., 2008). It has also been shown to enhance the prediction of dementia and is suggested to serve as a biomarker for risk stratification in dementia prevention trials (Mielke et al., 2017). NfL, the main component of the axonal cytoskeleton, is mainly expressed in large-caliber myelinated axons and released into the CSF following neuroaxonal injury (Petzold, 2005). Recently, robust studies have shown that NfL level in the peripheral blood is a promising biomarker for tracking neurodegenerative changes in patients with AD and increased levels are related to brain atrophy, brain hypometabolism, and decreased cognitive function (Zetterberg et al., 2016; Mattsson et al., 2017; Mayeli et al., 2019). Due to the poor disease specificity, the clinical application in detecting AD is limited (Wilke et al., 2016; Bridel et al., 2019). Compelling and emerging evidence has highlighted the potential of plasma p-tau181 and p-tau217, both of which have shown exceptional sensitivity and specificity to widespread AD pathology at autopsy and in patients with underlying AD pathology confirmed by other biomarkers (Janelidze et al., 2020; Karikari et al., 2020; Lantero Rodriguez et al., 2020; Palmqvist et al., 2020; Thijssen et al., 2020). However, due to technical limitations, these results are predominantly based on the Caucasian populations, and studies on blood biomarkers in Chinese populations are hard to achieve and still lacking. To our knowledge, only one study has detected plasma p-tau level in a Chinese population, which mainly focused on the correlation between p-tau181 and cognitive function (Xiao et al., 2021). Further studies are warranted to explore these biomarkers in currently underrepresented populations. Considering the heterogeneity and complexity of AD etiology, it is difficult to use a single biomarker to reflect the comprehensive pathological changes and disease diagnosis. Few domestic studies have integrated plasma Aβ, tau, and NfL simultaneously to evaluate their comprehensive diagnostic efficacy for AD and assess their consistency with classic CSF core biomarkers.

Therefore, in this cross-sectional study, we simultaneously detected the levels of classic biomarkers in the plasma of patients with AD and cognitively normal (CN) individuals from South China, including Aβ42, Aβ40, t-tau, and NfL, assessed their performance in discriminating patients with probable AD from CN participants to evaluating their ability to diagnose AD.

MATERIALS AND METHODS

Participants

A total of 430 individuals, including 277 patients with probable AD and 153 CN participants, were enrolled from the Department of Neurology, Xiangya Hospital, Central South University, between March 2017 and December 2019. The inclusion criteria for patients were as follows: (1) memory complaints from the patient or guardian; (2) ability to cooperate with physical examination and neuropsychological tests; (3) brain atrophy confirmed by CT or MRI, and (4) diagnosis of probable AD by two or more experienced neurologists from Xiangya Hospital according to the criteria of the National Institute on Aging and Alzheimer's Association (NIA-AA) (McKhann et al., 2011). In this study, the inclusion and exclusion criteria for controls were as follows: (1) no subjective cognitive complaints and no objective impairment in cognitive tests, including the Clinical Dementia Rating Scale (CDR) (CDR scores = 0) and Mini-Mental State Examination (MMSE; combined with educational attainment, illiteracy > 17, primary school > 20, and junior high school and above > 24); (2) no brain organic or functional disease; (3) no hypertension, diabetes, hyperhomocysteinemia, or other systemic diseases; and (4) matched with patients with probable AD by age and sex.

The study protocol was approved by the Institutional Review Board of Xiangya Hospital of Central South University in China. Written informed consent was obtained from each participant or guardian.

Neuropsychological and Cognitive Assessment

Participants in the AD group underwent a battery of neuropsychological tests, including the MMSE, Montreal Cognitive Assessment (MoCA), Activities of Daily Living (ADL), and Neuropsychiatric Inventory (NPI). The MMSE was also administered to the CN group.

Further, all participants were interviewed by two neurologists specializing in neurodegenerative disease, and the severity of cognitive impairment was assessed using the CDR.

The Apolipoprotein E (*APOE*) Genotyping

Venous blood was collected from all participants in tubes containing ethylenediaminetetraacetic acid (EDTA). Genomic DNA was extracted using the standard phenol-chloroform extraction method. All DNA samples were diluted to 50 ng/μl. A 581-bp fragment was amplified using the following primers: forward 5′-CCTACAAATCGGAACTGG-3′ and reverse 5′-CTCGAACCAGCTCTTGAG-3′. PCR was performed as previously described (Jiao et al., 2014). Each PCR product was sequenced using an ABI 3730xl DNA analyzer (ABI, Louis, MO, USA).

CSF Collection and Analysis

The cerebrospinal fluid was obtained from lumbar puncture samples. In this study, as lumbar puncture was carried out on a voluntary basis, a total of 188 patients refused to undergo the procedure, and 89 patients were tested for CSF core biomarkers. Briefly, participants were placed in the left lateral position for lumbar puncture. The L3–L5 intervertebral spaces were selected as the puncture site. The CSF samples were processed within 2 h after the standard lumbar puncture, and hemorrhagic samples were excluded (Teunissen et al., 2009). Each sample was centrifuged at 2,000 × *g* for 10 min, and the CSF samples were separated and stored in an enzyme-free microcentrifuge tube at −80°C. All samples were subjected to a maximum of two freeze-thaw cycles. All analyses of CSF core AD biomarkers (Aβ42, Aβ40, t-tau, and p-tau) were measured using enzyme-linked immunosorbent assay (ELISA) and performed by experienced technicians in strict accordance with the instructions of the manufacturer within 1 week of sample collection. Briefly, samples were added to the reagent wells, and the plate was incubated for 3 h at 22°C ± 2°C. After washing, horseradish peroxidase solution was added and incubated for 90 min at 22°C ± 2°C. The plate was then washed with the provided washing buffer, and substrate solution was added. After 30 min incubation protected from light, stop-solution was added, and the optical density (OD) was measured using a microplate reader (Thermo, Waltham, MA, USA), at 450 nm, corrected by the reference OD at 620 nm within 30 min of adding the stop solution. Two technical replicates are performed on samples and standards, and the average value of the replicates is used for statistical analysis. All measurements were performed in a blinded manner. Specifically, Aβ42 level in CSF < 651 pg/ml, or Aβ42/Aβ40 ratio ≤ 0.1, is defined as positive amyloidosis (corresponding to A+ in the ATN framework); p-tau > 61 pg/ml in CSF is defined as neurofibrillary tangles (corresponding to T+ in the ATN framework); t-tau ≥ 290 pg/ml in CSF is defined as nerve cell death (corresponding to A+ in the β amyloid deposition, pathologic tau, and neurodegeneration [ATN] framework).

Plasma Protein Quantification

Venous blood was collected in tubes containing EDTA and centrifuged at 2,000 × *g* for 10 min at 4°C. The obtained plasma was divided into ∼500 μl aliquots and frozen at −80°C. All samples underwent no more than three freeze-thaw cycles (Keshavan et al., 2018). The samples were rapidly thawed at 22 ± 2°C and then centrifuged at 10,000 × *g* prior to analysis to prevent any sample debris from interfering with the measurements. Plasma Aβ42, Aβ40, t-tau, and NfL concentrations were measured simultaneously using the single-molecule array (SIMOA)-HD1 platform (SIMOA; Quanterix, Billerica, MA, USA), which employed an automated SIMOA principle. Briefly, Aβ42, Aβ40, and t-tau levels were measured using a multiplex array (Neurology 3-Plex A Advantage Kit, N3PA), and NfL levels were measured using a single-analyte array (NF-light). The samples were measured using a two-step immunoassay. All analytical procedures were performed according to the protocol of the manufacturer by well-trained technicians who were blinded to the state of participant and clinical data, according to the protocol of the manufacturer. Samples with coefficients of variance (CV) of >20% were excluded from the analyses. In this study, the within-batch CV of all samples was <5%.

Statistical Analysis

The normality of the distribution of the variables was assessed. Categorical data were analyzed using the χ^2 test. Continuous variables were compared between two independent samples using the *t*-test or the Mann-Whitney *U* test, and differences between multiple independent samples were compared using the Kruskal-Wallis H test. Partial correlation analyses were performed to assess the correlations among plasma biomarkers, demographic characteristics, and clinical data. Diagnostic accuracy was evaluated using receiver operating characteristic (ROC) curve analysis and with logistic regression models. The area under the curve (AUC) and representative optimal sensitivity and specificity were used to evaluate the performance of the models. The statistical significance of the difference in AUCs between two different models was analyzed using Delong's test.

All tests were two-tailed, and $p < 0.05$ was considered statistically significant. All analyses were performed using SPSS version 24 (IBM, Armonk, NY, USA) and R (version 4.1.0). Data were visualized using Prism 8 software (GraphPad, San Diego, CA, USA).

RESULTS

Demographic Characteristics

The demographic characteristics of the patients with probable AD and CN participants are summarized in **Table 1**, including 277 patients with probable AD and 153 CN participants. The mean age at onset (AAO) was 62.23 years, and the mean disease course was approximately 2.91 years. The sex ratio (F/M) of patients with probable AD was 172/105, which matched the CN group (99/54) ($p > 0.05$). In parallel, 160 (57.8%) patients with AD carried at least one *APOE4* allele. There was no significant difference in age at diagnosis (means the age at the time of blood extraction) between patients with probable AD and CN participants, but the educational levels were significantly different between the two groups ($p < 0.001$).

TABLE 1 | Demographic and clinical characteristics of patients with probable AD and healthy controls.

	AD ($n = 277$)	Control ($n = 153$)	p
Demographic and clinical characteristics			
Age at diagnosis (Mean ± SD)	65.11 ± 10.57	64.5 ± 8.2	0.650
Age at onset (Mean ± SD)	62.23 ± 10.7	–	–
Sex (F/M, *n*)	172/105	99/54	0.591
Education level, years (Mean ± SD)	7.31 ± 4.38	8.99 ± 3.52	<0.001*
*APOE*4 (+/–, *n*)	160/117	26/127	<0.001*
Family history (+/–, *n*)	90/187	–	–
Disease course, years (Mean ± SD)	2.91 ± 2.13	–	–
MMSE (Mean ± SD)	12.0 ± 6.44	27.7 ± 2.3	<0.001*
MoCA (Mean ± SD)	7.63 ± 5.48	–	–
ADL (Mean ± SD)	36.79 ± 11.78	–	–
NPI (Mean ± SD)	19.20 ± 14.96	–	–
CDR (*n*, %)			
CDR = 0	0	153 (100)	–
CDR = 1	156 (56.3%)	0	–
CDR = 2	108 (39.0%)	0	–
CDR = 3	13 (4.7%)	0	–
Plasma biomarkers (mean ± SD)			
Aβ42 (pg/ml)	14.18 ± 3.96	14.58 ± 3.33	0.02 (0.308)
Aβ40 (pg/ml)	275.77 ± 63.25	258.48 ± 50.36	0.002 (0.062)
Aβ42/Aβ40	0.052 ± 0.014	0.057 ± 0.013	<0.001* (0.056)
t-tau (pg/ml)	4.12 ± 1.25	3.23 ± 1.12	<0.001*(<0.001#)
NfL (pg/ml)	28.76 ± 30.34	14.13 ± 10.25	<0.001* (<0.001#)

Demographic and clinical characteristics of patients with probable AD and healthy controls. Continuous variable comparisons between two independent samples were conducted via t-test or the Mann-Whitney U test. Categorical data were analyzed using the χ^2 test. The p-value in the bracket refers to the p-value after adjusting for age (means the age at diagnosis), sex, and APOE alleles. The differences of plasma biomarkers between the AD and CN groups were performed correction for multiple comparisons.

**The difference between the groups is statistically significant ($p < 0.05$).*

#The difference between the groups is statistically significant ($p < 0.01$, Bonferroni corrected).

AD, Alzheimer's disease; ADL, Activities of Daily Living; CDR, Clinical Dementia Rating Scale; MMSE, Mini-Mental State Examination; MoCA, Montreal Cognitive Assessment; NPI, Neuropsychiatric Inventory; NfL, neurofilament light chain; t-tau, total tau.

Differences in Plasma Biomarkers Levels

Before correcting for confounding factors, all detected plasma biomarkers, including Aβ42, Aβ40, Aβ42/Aβ40, t-tau, and NfL, significantly differed between the AD and CN groups. Among them, the plasma Aβ42 and Aβ42/40 levels were significantly lower in the AD group than in the CN group ($p = 0.02$ and $p < 0.001$, respectively). In parallel, the levels of Aβ42/Aβ40, t-tau, and NfL showed an increasing tendency in patients with probable AD ($p < 0.05$; **Table 1**). However, after adjusting for age, sex, and *APOE* alleles, and Bonferroni correction, compared with the CN group, plasma t-tau, and NfL were significantly increased in the AD group ($p < 0.001$), whereas other plasma biomarkers, including Aβ42 and Aβ40, showed no significant difference ($p = 0.308$ and $p = 0.062$, respectively), Aβ42/Aβ40 showed a decreasing tendency, but the difference was not significant ($p = 0.056$; **Table 1**; **Figure 1**).

Correlations Between Plasma Biomarkers and Demographic Characteristics

Next, we analyzed the correlations between plasma biomarkers and demographic data, including AAO, age at diagnosis, disease course, and education level. Associations between the levels of plasma biomarkers and demographic data were examined using partial correlation analyses with adjustment for age at diagnosis, sex, and *APOE* alleles. In addition, we compared the differences in plasma biomarkers according to sex, family history, and *APOE4* alleles distribution (**Table 2**). After adjustment for age at diagnosis, sex, and *APOE* alleles, Aβ42, Aβ40, Aβ42/Aβ40, and t-tau were not significantly associated with AAO in the probable AD group ($p > 0.05$), but NfL showed a significant association ($r = -0.183$, $p < 0.001$), which indicated that the earlier the AAO, the higher the level of NfL in plasma. In contrast, there was a significant positive correlation between age at diagnosis and the plasma NfL level ($r = 0.235$, $p < 0.001$). Meanwhile, plasma NfL was positively correlated with the disease course ($r = 0.199$, $p < 0.001$). Moreover, compared with patients with a positive family history of dementia, both plasma Aβ42 and Aβ42/Aβ40 were significantly lower in patients without a positive family history of dementia. Regarding *APOE* alleles, the Aβ42/Aβ40 ratio, and NfL were significantly lower in patients carrying the *APOE4* alleles than in non-carriers ($p = 0.033$ and $p = 0.034$, respectively), whereas there were no significant differences in other plasma biomarkers between the two subgroups (**Table 2**).

Correlations Between Plasma Biomarker Levels and Neuropsychological Assessments

We analyzed the correlations between plasma biomarkers and neuropsychological assessments, including MMSE, MoCA, ADL, and NPI (**Table 2**). Associations between the levels of plasma biomarkers and neuropsychological assessments were examined using partial correlation analyses with adjustment for age, sex, *APOE* alleles, and education level. The results showed that all the plasma biomarkers showed no significant association with neuropsychological assessments, including MMSE, MoCA, ADL, and NPI.

To further analyze the correlations between plasma biomarkers levels and disease severity, the patients with probable AD were divided into three subgroups according to the CDR score. No significant difference in plasma biomarkers was found among patients with different disease severity.

Correlations Between Plasma and CSF Biomarkers

According to the ATN diagnosis framework, not all clinically diagnosed patients with probable AD were compatible with the biologically defined AD. Specifically, among 89 patients who underwent lumbar puncture, 70 (78.7%) patients were diagnosed with AD continuum (A + T + N +: 39 cases, A + T + N–:

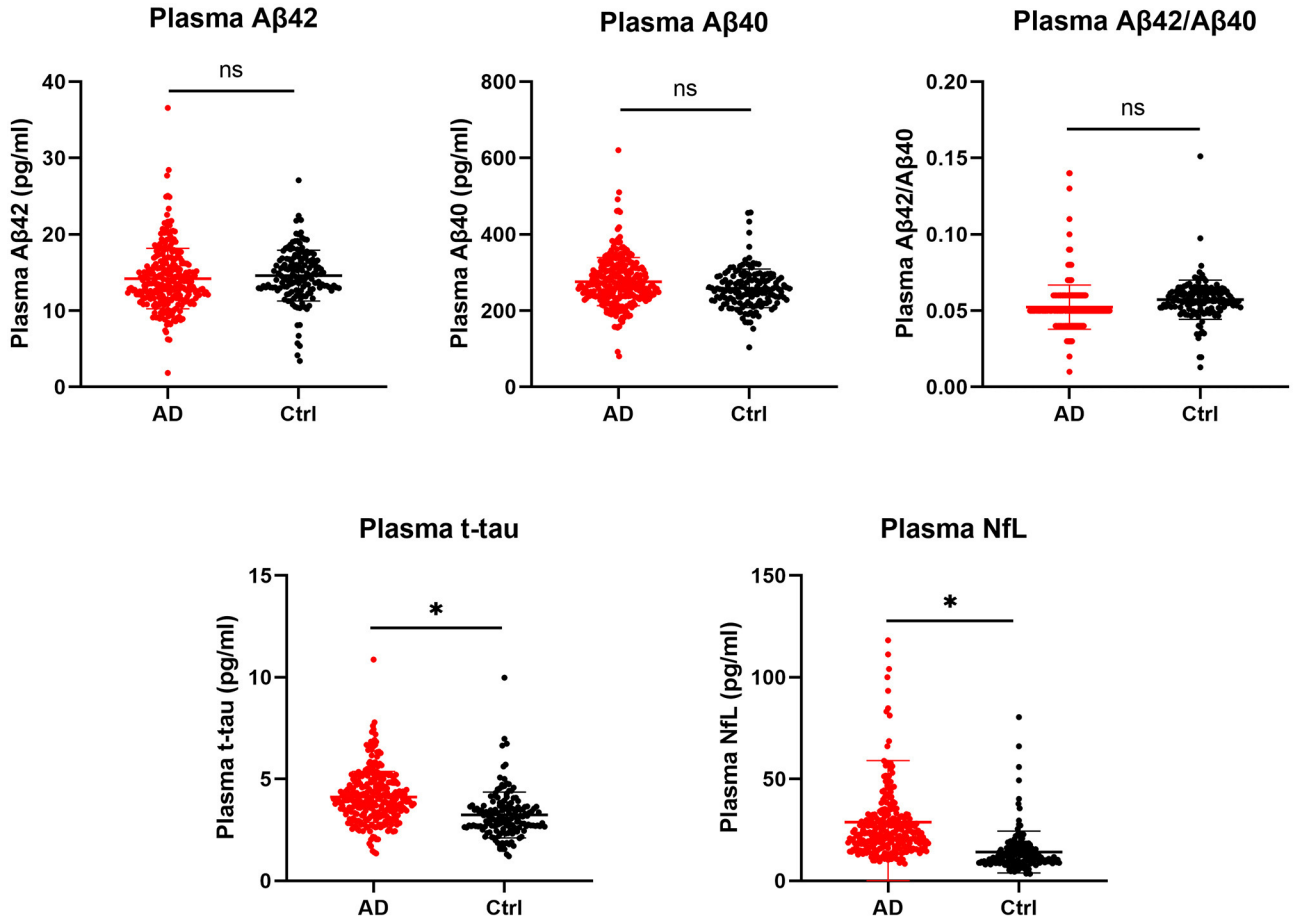

FIGURE 1 | Comparison of plasma biomarkers between the AD and CN groups. Plasma biomarkers are presented as the means ± SD. The significance of differences between groups was determined using the Mann-Whitney *U* test. AD, Alzheimer's disease; CN, cognitively normal; t-tau, total tau; NfL, neurofilament light chain; ns, not significant; *$p < 0.05$.

8 cases, A + T − N +: 9 cases, A + T − N −: 14 cases). The correlations between plasma and CSF biomarker levels in patients with probable AD were determined to assess the efficacy of plasma biomarkers in reflecting changes in brain pathology, as shown in **Table 3**. After adjusting for age, sex, and *APOE* alleles, only plasma t-tau was positively correlated with t-tau in the CSF ($r = 319$, $p = 0.003$).

Diagnostic Performance of Plasma Biomarkers

Finally, ROC curves were generated to evaluate the performance of the plasma biomarkers to discriminate patients with probable AD from controls (**Figure 2**). The cutoff value and its corresponding sensitivity and specificity were calculated using the maximum Youden index (**Table 4**). As a single plasma biomarker, NfL displayed the best diagnostic efficacy (AUC = 0.85, sensitivity = 73.28%, specificity = 83.00%). In addition, based on the results of differences in plasma biomarker levels, the model combining plasma t-tau and NfL showed the best diagnostic performance (AUC = 0.86, sensitivity = 83.75%, specificity = 76.47%). Furthermore, when age, sex, and *APOE* alleles were included in the combined model, it showed the best performance to distinguish probable AD from CN participants (AUC = 0.89, sensitivity = 82.31%, specificity = 83.66%), which was significantly better than other models ($p < 0.05$). In addition, we extracted 89 patients with AD who underwent CSF biomarker detection and analyzed the diagnostic performance of their plasma biomarkers through the ROC curve. The results showed that when plasma t-tau and NfL are included in the model, the diagnostic efficiency is better than that of any single plasma biomarker. After incorporating age, sex, and *APOE* alleles into the model, there was no statistical difference in the diagnostic performance of the two models, but the AUC of the latter reached the best (AUC = 0.89, sensitivity = 78.65%, specificity = 88.88%; **Table 4**).

DISCUSSION

This study aimed to evaluate the ability of plasma biomarkers, including Aβ, t-tau, and NfL, to detect probable AD in a Chinese population. We first determined the differences in plasma biomarkers between patients with probable AD

TABLE 2 | Correlations of plasma biomarkers with demographics and neuropsychological assessments in patients with AD.

CSF biomarkers	Plasma Aβ42		Plasma Aβ40		Plasma Aβ42/Aβ40		Plasma t-tau		Plasma NfL	
	r	*p*	*r*	*p*	*R*	*p*	*r*	*p*	*r*	*p*
Age at onset	−0.041	0.503	−0.018	0.763	−0.007	0.907	−0.025	0.682	−0.198	<0.001*
Age at diagnosis	0.040	0.513	0.081	0.184	−0.048	0.426	0.011	0.861	0.235	<0.001*
Sex (F/M)	–	0.285	–	0.097	–	0.619	–	0.425	–	0.077
Education level (years)	−0.024	0.691	−0.039	0.518	0.025	0.684	0.058	0.336	0.105	0.083
Disease course (years)	0.041	0.497	0.018	0.765	0.007	0.912	0.021	0.729	**0.199**	<0.001*
Family history (+/–)	–	<0.001*	–	0.627	–	<0.001*	–	0.630	–	0.218
*APOE*4 (+/–)	–	0.349	–	0.465	–	0.033*	–	0.666	–	0.034*
MMSE	0.054	0.375	0.078	0.198	−0.023	0.701	−0.079	0.191	−0.044	0.474
MoCA	0.069	0.258	0.085	0.160	−0.015	0.811	−0.059	0.334	0.008	0.891
ADL	−0.115	0.058	−0.090	0.139	−0.006	0.920	−0.014	0.818	−0.035	0.566
NPI	−0.051	0.402	0.021	0.731	−0.071	0.242	0.012	0.845	0.021	0.729

Correlations of plasma biomarkers with demographics and neuropsychological assessments in patients with AD. Correlations between plasma biomarkers and AAO were assessed by partial correlation with age at diagnosis, sex, and APOE alleles adjustment. Correlations between plasma biomarkers and age at diagnosis were assessed by partial correlation with AAO, sexes, and APOE alleles adjustment. Correlations between plasma biomarkers and educational level were assessed by partial correlation with age (means age at diagnosis), sexes, and APOE alleles adjustment. Correlations between plasma biomarkers and neurological assessment were assessed by partial correlation analyses with age at diagnosis, sex and APOE alleles, educational levels adjustment.

**The difference between the groups is statistically significant ($p < 0.05$).*

AD, Alzheimer's disease; ADL, Activities of Daily Living; MMSE, Mini-Mental State Examination; MoCA, Montreal Cognitive Assessment; NPI, Neuropsychiatric Inventory; NfL, neurofilament light chain; t-tau, total tau.

TABLE 3 | Correlations between plasma biomarkers and CSF biomarkers in patients with AD ($n = 89$).

CSF biomarkers	Plasma Aβ42		Plasma Aβ40		Plasma Aβ42/Aβ40		Plasma t-tau		Plasma NfL	
	r	*p*	*r*	*p*	*r*	*p*	*R*	*p*	*r*	*p*
Aβ42	0.081	0.461	0.098	0.370	−0.011	0.923	−0.061	0.579	0.017	0.875
Aβ40	−0.081	0.458	−0.090	0.410	0.024	0.823	−0.158	0.146	−0.013	0.907
Aβ42/Aβ40	0.166	0.126	0.209	0.053	0.037	0.738	−0.081	0.456	0.180	0.097
p-tau	−0.150	0.169	−0.166	0.128	−0.002	0.982	0.065	0.551	−0.141	0.197
t-tau	−0.115	0.293	−0.151	0.164	−0.019	0.862	0.319	0.003*	−0.121	0.268

Correlations between plasma biomarkers and CSF biomarkers in patients with AD ($n = 89$). Correlations between the levels of plasma biomarkers and CSF core biomarkers were assessed with partial correlation analyses with age, sexes, and APOE alleles adjustment. Age here refers to the age at diagnosis.

**The difference of the correlations between these biomarkers is statistically significant ($p < 0.05$).*

AD, Alzheimer's disease; NfL, neurofilament light chain; t-tau, total tau.

and CN participants. Second, a comprehensive model with high diagnostic efficacy of AD was constructed, including plasma t-tau, NfL, age, sex, and *APOE* alleles, which can be applied to perform preliminary screening in populations with a high risk of AD and may effectively reduce the application of lumbar puncture and PET examinations in clinical practice.

At present, a lot of efforts are devoted to comparing the difference of plasma Aβ between patients with AD and control, trying to diagnose AD through the less invasive and easily acceptable method. However, the results of different studies are still controversial. Studies adopting the SIMOA platform showed lower levels of plasma Aβ42 and Aβ42/Aβ40 in patients with AD than in controls (Janelidze et al., 2016; Li et al., 2019; Tosun et al., 2021). By contrast, some studies found that the levels of Aβ42 and Aβ42/Aβ40 were significantly increased in patients with mild cognitive impairment (MCI) or AD (Teunissen et al., 2018; Palmqvist et al., 2019). However, several studies showed that there were no significant differences in the plasma Aβ levels between patients with AD and controls (Hsu et al., 2017; Lövheim et al., 2017). The low abundance of Aβ in plasma and detection methods with different sensitivities, such as ELISA, SIMOA, immunomagnetic reduction (IMR), and Elecsys immunoassays, are the main reasons for these conflicting findings (Qu et al., 2021). To our knowledge, few domestic studies have evaluated these plasma biomarkers simultaneously in large cohorts from China or analyzed their correlations with typical AD biomarkers (Lue et al., 2017; Shi et al., 2019). In the present study, after adjusting for age, sex, and *APOE* alleles, the level of plasma Aβ42/Aβ40 showed a decreasing tendency but not a significant difference in patients with probable AD; meanwhile, the individual levels of plasma Aβ42 and Aβ40 were not significantly different from those of controls, which was consistent with the previous study (Olsson et al., 2016). Aβ40 is always used

as a reference peptide to potentially explain the difference in CSF concentrations between individuals and the difference in sample preanalytical processing (Schauer et al., 2018). As for the correlation between plasma Aβ and neuropsychological assessment, previous studies have reported the association between plasma Aβ levels and cognitive performance (Hanon et al., 2018; Chen et al., 2019), which indicates that plasma Aβ can potentially reflect the cognitive function even monitor the progression of AD. In this study, after adjusting for confounding factors, there was no significant correlation between plasma Aβ and neuropsychological assessment.

Approximately 30–50% of blood Aβ is derived from a brain-to-blood transport mechanism, and a dynamic equilibrium exists between the peripheral blood and the CNS (Roberts et al., 2014). The levels of Aβ in the plasma reflect pathological changes in the brain to some extent. Robust studies have shown that plasma Aβ levels can reflect Aβ pathology in the brain using amyloid PET or CSF Aβ levels as the positive reference (Park et al., 2017; Hanon et al., 2018; Pérez-Grijalba et al., 2019; Schindler et al., 2019). Furthermore, the ratio in plasma appears to be associated with the increased risk of progression to AD dementia (Verberk et al., 2018). However, in this study, the associations of plasma and CSF Aβ were not significant. There are several possibilities to explain these results. First, in the present study, only 89 patients with probable AD were tested for CSF core biomarkers, and the small sample size of CSF cannot reflect the true relationship of Aβ between plasma and CSF. Second, in this study, the inclusion criteria of patients with AD were the NIA-AA criteria and not all patients met the biological definition of AD. Considering that the clinical symptoms of different types of neurodegenerative dementia have a high degree of overlap, there are several clinically diagnosed patients with probable AD without Alzheimer's pathology. Third, the different detection methods used for markers in CSF and plasma may also be one of the reasons for the weak correlation. Finally, in this study, the different disease severity of patients with AD may also explain part of the results.

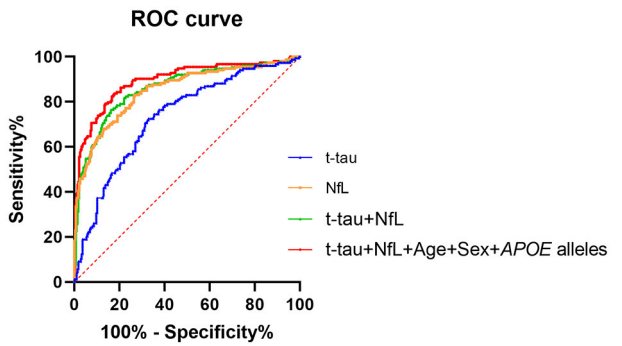

FIGURE 2 | ROC curve analysis of plasma biomarkers for the AD diagnosis. NfL levels in plasma exhibited the best diagnostic efficacy as a single indicator (AUC = 0.85, sensitivity = 73.28%%, specificity = 83.00%). Combined with t-tau and NfL levels in plasma, the diagnostic performance was significantly improved (AUC = 0.86, sensitivity = 83.75%, specificity = 76.47%). The diagnostic model combining plasma t-tau and NfL levels, age, sex, and *APOE* alleles showed the best performance for the identification of probable AD (AUC = 0.89, sensitivity = 82.31%, specificity = 83.66%). Delong test was performed to compare the difference of different diagnostic models. AUC, area under the curve; ROC, receiver operating characteristic curve; NfL, neurofilament light chain; t-tau, total tau.

In the present study, plasma t-tau levels were significantly higher in patients with probable AD than in healthy controls, similar to the findings of most published results (Mattsson et al., 2016; Lue et al., 2017), whereas several studies also found that plasma t-tau levels showed the opposite result or no significant difference between them (Sparks et al., 2012; Verberk et al., 2018; Qu et al., 2021). In a large meta-analysis, it was confirmed that patients with AD had higher plasma t-tau levels than controls, which may reflect neuronal damage as a nonspecific marker (Jack et al., 2018; Ding et al., 2021). Mattson et al. found that the higher plasma t-tau level was associated with AD dementia and showed significant correlations with poor cognition, greater atrophy, and hypometabolism during follow-up in the AD Neuroimaging Initiative study (Mattsson et al., 2016). In our study, after adjusting for age, sex, and *APOE* alleles, plasma t-tau was weakly correlated with CSF t-tau, which is consistent with previous studies that the association between plasma t-tau with CSF t-tau was weak or nonsignificant (Müller et al., 2017; Pase et al., 2019). Notably, accumulating evidence supports that plasma p-tau, the most promising biomarker for AD, shows outstanding performance in differential diagnosis, in relation to other biomarkers, neuropathology, prediction, progression monitoring, and prognosis (Mielke et al., 2018; Janelidze et al., 2020, 2021; Palmqvist et al., 2020). Due to the low concentration in the samples and limitations associated with the methodology, we did not measure p-tau levels in plasma. In our next study, we will increase the sample size to reevaluate whether plasma t-tau

TABLE 4 | Performance of plasma biomarkers for probable AD diagnosis.

Plasma biomarkers	Sensitivity (%)	Specificity (%)	AUC	95% CI	*p*
t-tau	67.14 (66.29)	72.54 (78.43)	0.73 (0.74)	0.68–0.78 (0.67–0.80)	<0.001* (<0.001*)
NfL	73.28 (77.52)	83.00 (82.35)	0.85 (0.86)	0.81–0.89 (0.78–0.90)	0.002* (0.08)
t-tau+NfL	83.75 (87.64)	76.47 (73.20)	0.86 (0.86)	0.82–0.90 (0.81–0.90)	0.007* (0.07)
t-tau + NfL + age + sex + *APOE* alleles	82.31 (78.65)	83.66 (88.88)	0.89 (0.89)	0.86–0.92 (0.86–0.94)	

*Performance of plasma biomarkers for probable AD diagnosis, including the sensitivity, specificity, AUC, and 95% CI. The values in brackets refer to the results of diagnostic efficacy analysis on a subset of patients who underwent lumbar puncture. The p-value is obtained by comparing each model with the combined model incorporating t-tau, NfL, age, sex, and APOE alleles through the Delong test. Age here refers to the age at diagnosis. AD, Alzheimer's disease; AUC, under the curve; CI, confidence interval; NfL, neurofilament light chain; t-tau, total tau. *The difference of the correlations between these biomarkers is statistically significant ($p < 0.05$).*

levels predict cognitive function and AD pathology and assess the utility of plasma p-tau levels for discriminating patients with AD from controls in the Chinese population.

Neurofilament light chain is a sensitive and promising biomarker for neurodegenerative disease, as it is released into CSF and plasma after axonal damage (Kuhle et al., 2015; Weston et al., 2017). Recently, Quiroz et al. found that plasma NfL levels increased with age and began to differentiate in *PSEN1* E280A mutation carriers from noncarriers as early as 22 years of age based on a large kindred study of patients with AD (Quiroz et al., 2020). Consistent with these results, the plasma NfL concentration was correlated with age and increased significantly as individuals aged in the present study. Meanwhile, the association between plasma NfL levels was positively correlated with disease course, which supports the hypothesis that the NfL is a sensitive marker of progressive myelinated axonal damage in the early stage of AD. However, it is not a specific indicator of the typical pathological changes associated with AD (Disanto et al., 2017). The correlation analysis showed that plasma NfL levels were not associated with AD core biomarkers in CSF, which is inconsistent with some previous study findings (Lewczuk et al., 2018; Mattsson et al., 2019). Combined with a recent longitudinal study showing that the plasma NfL level of participants who developed AD increased at a rate that was consistently higher than that of CN participants, and as early as 10 years before the clinical diagnosis of AD (de Wolf et al., 2020), these data indicate that it maybe a stable and useful biomarker for disease identification and for monitoring disease progression.

Notably, the results suggested that these plasma indicators were promising for discriminating patients with probable AD from CN participants. The peripheral biomarker panel as an initial screening strategy to identify people who should undergo further examinations, such as PET imaging or CSF testing, might be a critical step forward. Additionally, given the low concentrations of markers in plasma and the limited detection sensitivity, methodological limitations still exist. In this study, we unified the detection method by SIMOA technology to minimize possible experimental errors and promote the accurate detection of plasma biomarkers.

There are some limitations to this study. First, the study was a cross-sectional study without longitudinal follow-up to determine the differences in the trajectories of plasma biomarkers of patients in different AD stages and CN individuals. Second, due to the invasive characteristics of lumbar puncture, we failed to obtain the CSF data of all the participants in this study. Importantly, as the inclusion criteria for patients were probable AD but not biologically proven AD, there maybe several "AD" participants without Alzheimer's pathology as the primary cause of their symptoms, or controls with Alzheimer's pathology since AD is a continuum, where participants may present without any symptoms. Finally, patients with non-AD dementia were not recruited to compare differences in plasma biomarkers and verify the ability of the panel to distinguish patients with AD dementia from patients with other forms of dementia. Thus, head-to-head comparisons based on large-scale prospective studies that adopt unified and standardized inclusion criteria, detection, and analysis methods are necessary to assess the ability of plasma biomarkers for AD diagnosis in a Chinese population and their utility in monitoring pathological changes in the brain.

In summary, plasma biomarkers, including t-tau and NfL levels, were significantly different between the AD and CN groups after adjusting for age, sex, and *APOE* alleles. The diagnostic model that included t-tau, NfL levels, age, sex, and *APOE* alleles showed the best performance in discriminating patients with probable AD from CN participants. Although the accurate diagnosis of AD using plasma biomarkers is still challenging, the combination of multiple blood biomarkers can identify patients with probable AD from controls and is expected to serve as a potential method for pre-screening probable AD.

DATA AVAILABILITY STATEMENT

The raw data supporting the conclusions of this article will be made available by the authors, without undue reservation.

ETHICS STATEMENT

The studies involving human participants were reviewed and approved by the Ethics Committee of Xiangya Hospital of the Central South University. The patients/participants provided their written informed consent to participate in this study.

AUTHOR CONTRIBUTIONS

BJ, HL, and LS: study design, acquisition of data, analysis and interpretation of data, and drafting/revising the manuscript. LG, XL, and YZho: analyzed the data and revised the manuscript for intellectual content. LW, XX, LuZ, XW, YJ, QY, YZhu, WZ, LiZ, JW, XY, and BT: data collection and analysis. All authors contributed to the article and approved the submitted version.

FUNDING

This study was supported by the National Key R&D Program of China (Nos. 2020YFC2008500, 2017YFC0840100, and 2017YFC0840104 to LS, and No. 2018YFC1312003 to JW), the National Natural Science Foundation of China (Nos. 81671075 and 81971029 to LS, No. 82071216 to BJ, and No. 81901171 to XL), Hunan Innovative Province Construction Project (No. 2019SK2335 to BT), and the Youth Science Foundation of Xiangya Hospital (No. 2018Q020 to XL).

ACKNOWLEDGMENTS

The authors thank all the patients and their families, and all healthy volunteers for their involvement in this study. The authors are grateful to all our colleagues in the Department of Neurology, Xiangya Hospital, Central South University, China.

REFERENCES

Bridel, C., van Wieringen, W. N., Zetterberg, H., Tijms, B. M., Teunissen, C. E., Alvarez-Cermeño, J. C., et al. (2019). Diagnostic value of cerebrospinal fluid neurofilament light protein in neurology. *JAMA Neurol.* 76:1035. doi: 10.1001/jamaneurol.2019.1534

Chen, T., Lee, Y., Lin, S., Chen, J., Hu, C., Wang, P., et al. (2019). Plasma aβ42 and total tau predict cognitive decline in amnestic mild cognitive impairment. *Sci. Rep. UK* 9, 1–10. doi: 10.1038/s41598-019-50315-9

Christina, P. (2018). *World Alzheimer Report 2018: The State of the Art of Dementia Research: New Frontiers.* London: Alzheimer's Disease International.

de Wolf, F., Ghanbari, M., Licher, S., McRae-McKee, K., Gras, L., Weverling, G. J., et al. (2020). Plasma tau, neurofilament light chain and amyloid-β levels and risk of dementia; a population-based cohort study. *Brain* 143, 1220–1232. doi: 10.1093/brain/awaa054

Desikan, R. S., Cabral, H. J., Hess, C. P., Dillon, W. P., Glastonbury, C. M., Weiner, M. W., et al. (2009). Automated mri measures identify individuals with mild cognitive impairment and Alzheimer's disease. *Brain* 132, 2048–2057. doi: 10.1093/brain/awp123

Ding, X., Zhang, S., Jiang, L., Wang, L., Li, T., and Lei, P. (2021). Ultrasensitive assays for detection of plasma tau and phosphorylated tau 181 in Alzheimer's disease: a systematic review and meta-analysis. *Transl. Neurodegener.* 10, 1–14. doi: 10.1186/s40035-021-00234-5

Disanto, G., Barro, C., Benkert, P., Naegelin, Y., Schädelin, S., Giardiello, A., et al. (2017). Serum neurofilament light: a biomarker of neuronal damage in multiple sclerosis. *Ann. Neurol.* 81, 857–870. doi: 10.1002/ana.24954

Hanon, O., Vidal, J., Lehmann, S., Bombois, S., Allinquant, B., Tréluyer, J., et al. (2018). Plasma amyloid levels within the Alzheimer's process and correlations with central biomarkers. *Alzheimers Dement.* 14, 858–868. doi: 10.1016/j.jalz.2018.01.004

Hsu, J., Lee, W., Liao, Y., Wang, S., and Fuh, J. (2017). The clinical significance of plasma clusterin and aβ in the longitudinal follow-up of patients with Alzheimer's disease. *Alzheimers Res. Ther.* 9, 1–11. doi: 10.1186/s13195-017-0319-x

Jack, C. R., Bennett, D. A., Blennow, K., Carrillo, M. C., Dunn, B., Haeberlein, S. B., et al. (2018). NIA-AA research framework: toward a biological definition of Alzheimer's disease. *Alzheimers Dement.* 14, 535–562. doi: 10.1016/j.jalz.2018.02.018

Jack, C. R. P. D., Knopman, D. S. P., Jagust, W. J. P., Petersen, R. C. P., Weiner, M. W. P., Aisen, P. S. P., et al. (2013). Tracking pathophysiological processes in Alzheimer's disease: an updated hypothetical model of dynamic biomarkers. *Lancet Neurol.* 12, 207–216. doi: 10.1016/S1474-4422(12)70291-0

Janelidze, S., Berron, D., Smith, R., Strandberg, O., Proctor, N. K., Dage, J. L., et al. (2021). Associations of plasma phospho-tau217 levels with tau positron emission tomography in early Alzheimer disease. *JAMA Neurol.* 78, 149–156. doi: 10.1001/jamaneurol.2020.4201

Janelidze, S., Mattsson, N., Palmqvist, S., Smith, R., Beach, T. G., Serrano, G. E., et al. (2020). Plasma p-tau181 in Alzheimer's disease: relationship to other biomarkers, differential diagnosis, neuropathology and longitudinal progression to Alzheimer's dementia. *Nat. Med.* 26, 379–386. doi: 10.1038/s41591-020-0755-1

Janelidze, S., Stomrud, E., Palmqvist, S., Zetterberg, H., van Westen, D., Jeromin, A., et al. (2016). Plasma beta-amyloid in Alzheimer's disease and vascular disease. *Sci. Rep.* 6:26801. doi: 10.1038/srep26801

Jansen, W. J., Ossenkoppele, R., Knol, D. L., Tijms, B. M., Scheltens, P., Verhey, F. R. J., et al. (2015). Prevalence of cerebral amyloid pathology in persons without dementia. *JAMA* 313:1924. doi: 10.1001/jama.2015.4668

Jiao, B., Liu, X., Tang, B., Hou, L., Zhou, L., Zhang, F., et al. (2014). Investigation of trem2, pld3, and unc5c variants in patients with Alzheimer's disease from mainland china. *Neurobiol. Aging* 35, 2422–2429. doi: 10.1016/j.neurobiolaging.2014.04.025

Karikari, T. K., Pascoal, T. A., Ashton, N. J., Janelidze, S., Benedet, A. L., Rodriguez, J. L., et al. (2020). Blood phosphorylated tau 181 as a biomarker for Alzheimer's disease: a diagnostic performance and prediction modelling study using data from four prospective cohorts. *Lancet Neurol.* 19, 422–433. doi: 10.1016/S1474-4422(20)30071-5

Keshavan, A., Heslegrave, A., Zetterberg, H., and Schott, J. M. (2018). Stability of blood-based biomarkers of Alzheimer's disease over multiple freeze-thaw cycles. *Alzheimers Dement (Amst)* 10, 448–451. doi: 10.1016/j.dadm.2018.06.001

Kuhle, J., Gaiottino, J., Leppert, D., Petzold, A., Bestwick, J. P., Malaspina, A., et al. (2015). Serum neurofilament light chain is a biomarker of human spinal cord injury severity and outcome. *J. Neurol. Neurosurg. Psychiatry* 86, 273–279. doi: 10.1136/jnnp-2013-307454

Landau, S. M., Mintun, M. A., Joshi, A. D., Koeppe, R. A., Petersen, R. C., Aisen, P. S., et al. (2012). Amyloid deposition, hypometabolism, and longitudinal cognitive decline. *Ann. Neurol.* 72, 578–586. doi: 10.1002/ana.23650

Lantero Rodriguez, J., Karikari, T. K., Suárez-Calvet, M., Troakes, C., King, A., Emersic, A., et al. (2020). Plasma p-tau181 accurately predicts Alzheimer's disease pathology at least 8 years prior to post-mortem and improves the clinical characterisation of cognitive decline. *Acta Neuropathol.* 140, 267–278. doi: 10.1007/s00401-020-02195-x

Lewczuk, P., Ermann, N., Andreasson, U., Schultheis, C., Podhorna, J., Spitzer, P., et al. (2018). Plasma neurofilament light as a potential biomarker of neurodegeneration in Alzheimer's disease. *Alzheimers Res. Ther.* 10:71. doi: 10.1186/s13195-018-0404-9

Li, W., Shen, Y., Tian, D., Bu, X., Zeng, F., Liu, Y., et al. (2019). Brain amyloid-β deposition and blood biomarkers in patients with clinically diagnosed Alzheimer's disease. *J. Alzheimers Dis.* 69, 169–178. doi: 10.3233/JAD-190056

Lövheim, H., Elgh, F., Johansson, A., Zetterberg, H., Blennow, K., and Hallmans, G., et al. (2017). Plasma concentrations of free amyloid β cannot predict the development of Alzheimer's disease. *Alzheimers Dement.* 13, 778–782. doi: 10.1016/j.jalz.2016.12.004

Lue, L., Sabbagh, M. N., Chiu, M., Jing, N., Snyder, N. L., Schmitz, C., et al. (2017). Plasma levels of aβ42 and tau identified probable Alzheimer's dementia: findings in two cohorts. *Front. Aging Neurosci.* 9:226. doi: 10.3389/fnagi.2017.00226

Mattsson, N., Andreasson, U., Zetterberg, H., and Blennow, K. (2017). Association of plasma neurofilament light with neurodegeneration in patients with Alzheimer disease. *JAMA Neurol.* 74, 557–566. doi: 10.1001/jamaneurol.2016.6117

Mattsson, N., Cullen, N. C., Andreasson, U., Zetterberg, H., and Blennow, K. (2019). Association between longitudinal plasma neurofilament light and neurodegeneration in patients with Alzheimer disease. *JAMA Neurol.* 76, 791–799. doi: 10.1001/jamaneurol.2019.0765

Mattsson, N., Zetterberg, H., Hansson, O., Andreasen, N., Parnetti, L., Jonsson, M., et al. (2009). Csf biomarkers and incipient Alzheimer disease in patients with mild cognitive impairment. *JAMA* 302, 385–393. doi: 10.1001/jama.2009.1064

Mattsson, N., Zetterberg, H., Janelidze, S., Insel, P. S., Andreasson, U., Stomrud, E., et al. (2016). Plasma tau in Alzheimer disease. *Neurology* 87, 1827–1835. doi: 10.1212/WNL.0000000000003246

Mayeli, M., Mirshahvalad, S. M., Aghamollaii, V., Tafakhori, A., Abdolalizadeh, A., Rahmani, F., et al. (2019). Plasma neurofilament light chain levels are associated with cortical hypometabolism in Alzheimer disease signature regions. *J. Neuropathol. Exp. Neurol.* 78, 70–716. doi: 10.1093/jnen/nlz054

McKhann, G. M., Knopman, D. S., Chertkow, H., Hyman, B. T., Jack, C. R., Kawas, C. H., et al. (2011). The diagnosis of dementia due to Alzheimer's disease: recommendations from the national institute on aging-Alzheimer's association workgroups on diagnostic guidelines for Alzheimer's disease. *Alzheimers Dement.* 7, 263–269. doi: 10.1016/j.jalz.2011.03.005

Mielke, M. M., Hagen, C. E., Wennberg, A. M. V., Airey, D. C., Savica, R., Knopman, D. S., et al. (2017). Association of plasma total tau level with cognitive decline and risk of mild cognitive impairment or dementia in the mayo clinic study on aging. *JAMA Neurol.* 74:1073. doi: 10.1001/jamaneurol.2017.1359

Mielke, M. M., Hagen, C. E., Xu, J., Chai, X., Vemuri, P., Lowe, V. J., et al. (2018). Plasma phospho-tau181 increases with Alzheimer's disease clinical severity and is associated with tau- and amyloid-positron emission tomography. *Alzheimer's Dement.* 14, 989–997. doi: 10.1016/j.jalz.2018.02.013

Müller, S., Preische, O., Göpfert, J. C., Yañez, V. A. C., Joos, T. O., Boecker, H., et al. (2017). Tau plasma levels in subjective cognitive decline: results from the delcode study. *Sci. Rep.* 7, 1–6. doi: 10.1038/s41598-017-08779-0

Olsson, B., Lautner, R., Andreasson, U., Öhrfelt, A., Portelius, E., Bjerke, M., et al. (2016). Csf and blood biomarkers for the diagnosis of Alzheimer's disease: a systematic review and meta-analysis. *Lancet Neurol.* 15, 673–684. doi: 10.1016/S1474-4422(16)00070-3

Palmqvist, S., Janelidze, S., Quiroz, Y. T., Zetterberg, H., Lopera, F., Stomrud, E., et al. (2020). Discriminative accuracy of plasma phospho-tau217 for Alzheimer disease vs. other neurodegenerative disorders. *JAMA* 324, 772–781. doi: 10.1001/jama.2020.12134

Palmqvist, S., Janelidze, S., Stomrud, E., Zetterberg, H., Karl, J., Zink, K., et al. (2019). Performance of fully automated plasma assays as screening tests for Alzheimer disease–related β-amyloid status. *JAMA Neurol.* 76:1060. doi: 10.1001/jamaneurol.2019.1632

Park, J., Han, S., Cho, H. J., Byun, M. S., Yi, D., Choe, Y. M., et al. (2017). Chemically treated plasma aβ is a potential blood-based biomarker for screening cerebral amyloid deposition. *Alzheimers Res. Ther*. 9, 1–13. doi: 10.1186/s13195-017-0248-8

Pase, M. P., Beiser, A. S., Himali, J. J., Satizabal, C. L., Aparicio, H. J., DeCarli, C., et al. (2019). Assessment of plasma total tau level as a predictive biomarker for dementia and related endophenotypes. *JAMA Neurol.* 76:598. doi: 10.1001/jamaneurol.2018.4666

Pérez-Grijalba, V., Arbizu, J., Romero, J., Prieto, E., Pesini, P., Sarasa, L., et al. (2019). Plasma aβ42/40 ratio alone or combined with fdg-pet can accurately predict amyloid-pet positivity: a cross-sectional analysis from the ab255 study. *Alzheimers Res Ther.* 11, 1–19. doi: 10.1186/s13195-019-0549-1

Petzold, A. (2005). Neurofilament phosphoforms: surrogate markers for axonal injury, degeneration and loss. *J. Neurol. Sci.* 233, 183–198. doi: 10.1016/j.jns.2005.03.015

Qu, Y., Ma, Y., Huang, Y., Ou, Y., Shen, X., Chen, S., et al. (2021). Blood biomarkers for the diagnosis of amnestic mild cognitive impairment and Alzheimer's disease: a systematic review and meta-analysis. *Neurosci. Biobehav. Rev.* 128, 479–486. doi: 10.1016/j.neubiorev.2021.07.007

Quiroz, Y. T., Zetterberg, H., Reiman, E. M., Chen, Y., Su, Y., Fox-Fuller, J. T., et al. (2020). Plasma neurofilament light chain in the presenilin 1 e280a autosomal dominant Alzheimer's disease kindred: a cross-sectional and longitudinal cohort study. *Lancet Neurol.* 19, 513–521. doi: 10.1016/S1474-4422(20)30137-X

Roberts, K. F., Elbert, D. L., Kasten, T. P., Patterson, B. W., Sigurdson, W. C., Connors, R. E., et al. (2014). Amyloid-beta efflux from the central nervous system into the plasma. *Ann. Neurol.* 76, 837–844. doi: 10.1002/ana.24270

Schauer, S. P., Mylott, W. R., Yuan, M., Jenkins, R. G., Rodney Mathews, W., Honigberg, L. A., et al. (2018). Preanalytical approaches to improve recovery of amyloid-β peptides from csf as measured by immunological or mass spectrometry-based assays. *Alzheimers Res. Ther.* 10, 1–16. doi: 10.1186/s13195-018-0445-0

Schindler, S. E., Bollinger, J. G., Ovod, V., Mawuenyega, K. G., Li, Y., Gordon, B. A., et al. (2019). High-precision plasma β-amyloid 42/40 predicts current and future brain amyloidosis. *Neurology* 93, e1647–e1659. doi: 10.1212/WNL.0000000000008081

Schraen-Maschke, S., Sergeant, N., Dhaenens, C., Bombois, S., Deramecourt, V., Caillet-Boudin, M., et al. (2008). Tau as a biomarker of neurodegenerative diseases. *Biomark. Med.* 2, 363–384. doi: 10.2217/17520363.2.4.363

Shi, Y., Lu, X., Zhang, L., Shu, H., Gu, L., Wang, Z., et al. (2019). Potential value of plasma amyloid-beta, total tau, and neurofilament light for identification of early Alzheimer's disease. *ACS Chem. Neurosci.* 10, 3479–3485. doi: 10.1021/acschemneuro.9b00095

Sparks, D. L., Kryscio, R. J., Sabbagh, M. N., Ziolkowski, C., Lin, Y., Sparks, L. M., et al. (2012). Tau is reduced in ad plasma and validation of employed ELISA methods. *Am. J. Neurodegener. Dis*. 1, –106

Teunissen, C. E., Chiu, M. J., Yang, C. C., Yang, S. Y., Scheltens, P., Zetterberg, H., et al. (2018). Plasma amyloid-beta (abeta42) correlates with cerebrospinal fluid abeta42 in Alzheimer's disease. *J. Alzheimers Dis.* 62, 1857–1863. doi: 10.3233/JAD-170784

Teunissen, C. E., Petzold, A., Bennett, J. L., Berven, F. S., Brundin, L., Comabella, M., et al. (2009). A consensus protocol for the standardization of cerebrospinal fluid collection and biobanking. *Neurology* 73, 1914–1922. doi: 10.1212/WNL.0b013e3181c47cc2

Thijssen, E. H., La Joie, R., Wolf, A., Strom, A., Wang, P., Iaccarino, L., et al. (2020). Diagnostic value of plasma phosphorylated tau181 in Alzheimer's disease and frontotemporal lobar degeneration. *Nat. Med.* 26, 387–397. doi: 10.1038/s41591-020-0762-2

Tosun, D., Veitch, D., Aisen, P., Jack, C. R., Jagust, W. J., Petersen, R. C., et al. (2021). Detection of β-amyloid positivity in Alzheimer's disease neuroimaging initiative participants with demographics, cognition, MRI and plasma biomarkers. *Brain Commun*. 3:b8. doi: 10.1093/braincomms/fcab008

Verberk, I. M. W., Slot, R. E., Verfaillie, S. C. J., Heijst, H., Prins, N. D., van Berckel, B. N. M., et al. (2018). Plasma amyloid as prescreener for the earliest Alzheimer pathological changes. *Ann. Neurol.* 84, 648–658. doi: 10.1002/ana.25334

Vergallo, A., Mégret, L., Lista, S., Cavedo, E., Zetterberg, H., Blennow, K., et al. (2019). Plasma amyloid β 40/42 ratio predicts cerebral amyloidosis in cognitively normal individuals at risk for Alzheimer's disease. *Alzheimers Dement*. 15, 764–775. doi: 10.1016/j.jalz.2019.03.009

Weston, P., Poole, T., Ryan, N. S., Nair, A., Liang, Y., Macpherson, K., et al. (2017). Serum neurofilament light in familial Alzheimer disease: a marker of early neurodegeneration. *Neurology* 89, 2167–2175. doi: 10.1212/WNL.0000000000004667

Wilke, C., Preische, O., Deuschle, C., Roeben, B., Apel, A., Barro, C., et al. (2016). Neurofilament light chain in ftd is elevated not only in cerebrospinal fluid, but also in serum. *J. Neurol. Neurosurg. Psychiatry* 87, 1270–1272. doi: 10.1136/jnnp-2015-312972

Xiao, Z., Wu, X., Wu, W., Yi, J., Liang, X., Ding, S., et al. (2021). Plasma biomarker profiles and the correlation with cognitive function across the clinical spectrum of Alzheimer's disease. *Alzheimers Res. Ther.* 13:123. doi: 10.1186/s13195-021-00864-x

Zetterberg, H., Skillbäck, T., Mattsson, N., Trojanowski, J. Q., Portelius, E., Shaw, L. M., et al. (2016). Association of cerebrospinal fluid neurofilament light concentration with Alzheimer disease progression. *JAMA Neurol.* 73:60. doi: 10.1001/jamaneurol.2015.3037

Conflict of Interest: The authors declare that the research was conducted in the absence of any commercial or financial relationships that could be construed as a potential conflict of interest.

Publisher's Note: All claims expressed in this article are solely those of the authors and do not necessarily represent those of their affiliated organizations, or those of the publisher, the editors and the reviewers. Any product that may be evaluated in this article, or claim that may be made by its manufacturer, is not guaranteed or endorsed by the publisher.

frontiers in Aging Neuroscience

ORIGINAL RESEARCH
published: 08 November 2021
doi: 10.3389/fnagi.2021.759182

Assessing Plasma Levels of α-Synuclein and Neurofilament Light Chain by Different Blood Preparation Methods

*Kuo-Hsuan Chang[1], Kou-Chen Liu[2,3], Chao-Sung Lai[2,4,5], Shieh-Yueh Yang[6] and Chiung-Mei Chen[1]**

[1] Department of Neurology, Chang Gung Memorial Hospital, Chang Gung University College of Medicine, Taoyuan, Taiwan, [2] Department of Electronic Engineering, Artificial Intelligence and Green Technology Research Center, Chang Gung University, Taoyuan, Taiwan, [3] Division of Pediatric Infectious Disease, Department of Pediatrics, Chang Gung Memorial Hospital, Taoyuan, Taiwan, [4] Department of Nephrology, Chang Gung Memorial Hospital, Taoyuan, Taiwan, [5] Department of Materials Engineering, Ming Chi University of Technology, New Taipei City, Taiwan, [6] MagQu Co., Ltd., Taipei, Taiwan

The potential biomarkers of Parkinson's disease are α-synuclein and neurofilament light chain (NFL). However, inconsistent preanalytical preparation of plasma could lead to variations in levels of these biomarkers. Different types of potassium salts of EDTA and different centrifugation temperatures during plasma preparation may affect the results of α-synuclein and NFL measurements. In this study, we prepared plasma from eight patients with Parkinson's disease (PD) and seven healthy controls (HCs) by using di- and tri-potassium (K_2- and K_3-) EDTA tubes and recruited a separated cohort with 42 PD patients and 40 HCs for plasma samples prepared from whole blood by centrifugation at room temperature and 4°C, respectively, in K_2-EDTA tubes. The plasma levels of α-synuclein and NFL in K_2- and K_3-EDTA were similar. However, the levels of α-synuclein in the plasma prepared at 4°C (101.57 ± 43.43 fg/ml) were significantly lower compared with those at room temperature (181.23 ± 196.31 fg/ml, $P < 0.001$). Room temperature preparation demonstrated elevated plasma levels of α-synuclein in PD patients (256.6 ± 50.2 fg/ml) compared with the HCs (102.1 ± 0.66 fg/ml, $P < 0.001$), whereas this increase in PD was not present by preparation at 4°C. Both plasma preparations at room temperature and 4°C demonstrated consistent results of NFL, which are increased in PD patients compared with HCs. Our findings confirmed that K_2- and K_3-EDTA tubes were interchangeable for analyzing plasma levels of α-synuclein and NFL. Centrifugation at 4°C during plasma preparation generates considerable reduction and variation of α-synuclein level that might hinder the detection of α-synuclein level changes in PD.

Keywords: Parkinson's disease, biomarker, α-synuclein, neurofilament light chain, ethylenediaminetetraacetic acid, centrifugation temperature

OPEN ACCESS

Edited by:
Thomas K. Karikari, University of Gothenburg, Sweden

Reviewed by:
Joel Simrén, University of Gothenburg, Sweden
Giovanni Bellomo, University of Perugia, Italy

****Correspondence:***
Chiung-Mei Chen
cmchen@cgmh.org.tw

Received: *16 August 2021*
Accepted: *05 October 2021*
Published: *08 November 2021*

Citation:
Chang K-H, Liu K-C, Lai C-S, Yang S-Y and Chen C-M (2021) Assessing Plasma Levels of α-Synuclein and Neurofilament Light Chain by Different Blood Preparation Methods. Front. Aging Neurosci. 13:759182. doi: 10.3389/fnagi.2021.759182

INTRODUCTION

The development of biomarker research has driven a new avenue toward the diagnosis and prediction of the progression of Parkinson's disease (PD). PD is clinically characterized by motor dysfunction including bradykinesia, rigidity, tremor, postural instability, and freezing of gait, as well as pathologically by the progressive loss of dopaminergic neurons in substantia nigra

(Lang and Lozano, 1998). To assess disease severity in PD, different rating tools, such as the unified PD rating scale (UPDRS) or Hoehn and Yahr stage (Hoehn and Yahr, 1967; Movement Disorder Society Task Force on Rating Scales for Parkinson's Disease, 2003), are widely used in clinical practice. However, these scales demonstrate significant inter- and intra-rater variability (Shulman et al., 2010). Their non-linear properties further limit the application of these scales to precisely assess the progression of neurodegeneration. Therefore, discovery and validation of PD-specific molecular biomarkers, particularly in body fluids such as blood and cerebrospinal fluid (CSF), are important to provide objective and linear tools for diagnosing the disease at prodromal or early stages, as well as monitoring disease progression and therapeutic responses.

Among biomarker candidates for neurodegenerative diseases, α-synuclein, and neurofilament light chain (NFL) are the two most studied molecules in PD. The α-synuclein is a major constituent of Lewy bodies, the pathological intracytoplasmic inclusions in degenerative dopaminergic neurons of PD patients (Spillantini et al., 1997). As highly expressed in large-caliber myelinated axons, NFL has been suggested to be involved in axonal injury and degeneration (Petzold, 2005). Given that abnormal accumulation of α-synuclein and NFL in body fluids may reflect the abnormalities in the brains of PD patients, these proteins have gained attention as potential surrogate biomarkers for PD (Simonsen et al., 2016). Compared with CSF, plasma is relatively easy to access and preferable for biomarker analysis. However, the determinations of α-synuclein and NFL in plasma yield conflicting results. Plasma α-synuclein levels in PD patients could be increased (Lee et al., 2006; Ding et al., 2017; Lin et al., 2017; Chang et al., 2019; Ng et al., 2019), decreased (Li et al., 2007), or unchanged (Mata et al., 2010; Park et al., 2011; Foulds et al., 2013). NFL levels in the plasma of PD patients could be elevated (Lin et al., 2019), or modest increases in PD only in one of the cohorts (Hansson et al., 2017). The inconsistency of preanalytical sample preparations may affect the measurement results of α-synuclein and NFL in plasma.

Components in the blood collection tubes, such as anticoagulants, gels, and clot activators, have been recognized as significant sources, resulting in variability in the quantification of molecules in the blood (Bowen and Remaley, 2014). Plasma is usually prepared from whole blood in an EDTA-containing tube. Di- and tri-potassium (K_2 and K_3) salts of EDTA are the standard anticoagulants used for plasma preparations. It has been recognized that the type of EDTA salts may affect the accuracy of cell counting and sizing (Goossens et al., 1991). K_2-EDTA was suggested as the anticoagulant of choice for routine hematology testing in hospitals (England et al., 1993). However, K_3-EDTA tubes were used in a few biomarker studies for PD (Lin et al., 2017; Chang et al., 2019). On the other hand, centrifugation condition for quick separation of cells from the plasma is also crucial. It is recommended that plasma is ideally centrifuged at room temperature (RT) for hemostasis assays (Adcock Funk et al., 2012). Some laboratories prefer to process blood samples at refrigerated temperatures at 4°C (Mussbacher et al., 2017). In this study, we investigated whether K_2-EDTA tubes introduced any significant bias in α-synuclein and NFL measurements as compared with K_3-EDTA tubes. We further examined the effect of centrifugation temperatures during plasma preparation on the measurements of α-synuclein and NFL.

MATERIALS AND METHODS

Ethics Approval and Consent to Participate

This study was approved by the Institutional Review Boards of the Chang Gung Memorial Hospital (ethical license No: 201801049A3 and 201801051A3).

Patient Recruitment

This was a cross-sectional study and patients were recruited from July 1, 2018, to December 31, 2020, in Chang Gung Memorial Hospital-Linkou Medical Center in Taiwan. Patients were diagnosed as PD according to the UK Brain Bank criteria for PD (Hughes et al., 1992). UPDRS (Movement Disorder Society Task Force on Rating Scales for Parkinson's Disease, 2003), Hoehn and Yahr stage (Hoehn and Yahr, 1967), levodopa equivalent daily dose (LEDD) (Tomlinson et al., 2010), mini-mental state examination (Tombaugh and McIntyre, 1992), and demographic information was recorded for each patient. PD patients with Hoehn and Yahr stages 1–2 were defined as at the early stage, while those with Hoehn and Yahr stages higher than 2 were classified as at the advanced stage. Sex/age-matched healthy control (HC) subjects were randomly recruited from neurology outpatient clinics. The HC subjects visiting neurology outpatient clinics were diagnosed with insomnia, tension headache, myalgia, or low back pain. All HC subjects had no systemic infection, chronic renal failure, cardiac or liver dysfunction, malignancies, autoimmune diseases, PD, stroke, or any neurodegenerative diseases. Diagnoses were determined by two experienced neurologists in movement disorders (KH Chang and CM Chen) who were blinded to both α-synuclein and NFL levels in plasma. This was a prospective study. For the first part experiment of K_2- and K_3-EDTA tube comparison, the first eight PD patients were recruited and the seven age- and gender-matched HC were selected accordingly. Subsequently, all the 42 PD patients and the 40 age- and gender-matched HC including the subjects from the first part were included for the second part of the study in assessing sample centrifugation under RT or 4°C.

Sample Collection and Preparation

Ten-milliliter K_2- (BD vacutainer K2, 367525, BD, Franklin Lakes, NJ) or K_3-EDTA tubes (455036, Greiner Bio-One GmbH, Kremsmunster, Austria) were used for the blood draw. After blood collection, the blood collection tube was gently inverted 10 times immediately. Blood collection tubes were immediately centrifuged at 1,500–2,500 g for 15 min within 1 h. In this study, each participant was requested to donate two tubes of blood. One was centrifuged at RT, the other was centrifuged at 4°C. A swing-out (basket) rotor was used for centrifugation. By using a disposable 1 ml micropipette tip, every 1 ml of plasma

(supernatant) was transferred to a fresh 1.5 ml Eppendorf tube. All plasma samples were frozen at –80°C before measurements.

Measurement of α-Synuclein and Neurofilament Light Chain Levels in Plasma

We used an immunomagnetic reduction (IMR) assay to measure the plasma levels of total α-synuclein and NFL (Yang et al., 2016). The frozen human plasma sample was moved from –80°C to wet ice, and then to RT for 20 min. Afterward, 40 μl of plasma was mixed with 80 μl of reagent (MF-ASCd with MagQu, New Taipei City, Taiwan) for total α-synuclein assay, while 60 μl of plasma was mixed with 60 μl of reagent (MF-NFLd with MagQu, New Taipei City, Taiwan) for NFL. For each batch of measurements, calibrators (CA-DEX-0060, CA-DEX-0080, MagQu, New Taipei City, Taiwan) and control solutions (CL-ASC-000T, MagQu, New Taipei City, Taiwan) were used. The IMR analyzer (XacPro-S361, MagQu, New Taipei City, Taiwan) was utilized. For each sample, duplicated measurements were performed for assaying total α-synuclein and NFL. The averaged concentration of the duplicated measurements was reported. Plasma total α-synuclein and NFL levels were determined by technicians who were blinded to the clinical diagnosis. The limit of detection (LoD) and analytical range (total α-synuclein: 0.0014–1,020 pg/ml; NFL: 0.001–1,000 pg/ml) were determined according to Clinical and Laboratory Standards Institute (CLSI)/National Committee for Clinical Laboratory Standards (NCCLS) document, Evaluation of Detection Capability for Clinical Laboratory Measurement Procedures (EP17-A2) and Validation of analytical procedure [ICH Q2(R1)], respectively. For intra- (repeatability) and inter-assay (reproducibility), the precision testing was determined according to CLSI/NCCLs document Evaluation of Precision of Quantitative Measurement Procedures (EP5-A3). Two samples with different total α-synuclein and NFL concentrations were measured. The measurements of each concentration had been conducted a total of 80 times. Inter- (repeatability) and intra-assay (reproducibility) involved assaying two samples on 20 different working days, with two runs per day, and two replicates per run, i.e., a 20 × 2 × 2 design. The coefficient variances of inter- (repeatability) and intra-assay (reproducibility) of the total α-synuclein and NFL IMR assay are shown in **Supplementary Table 1**.

Measurement of Hemoglobin Level in Plasma

Hemoglobin was estimated by the cyanmethemoglobin methods of Drabkin (Sigma). Readings were taken at 540 nm in a spectrophotometer.

Statistical Analysis

The Statistical Program for Social Sciences [SPSS version 23 (IBM, Armonk, NY) and GraphPad Prism 8 (GraphPad, La Jolla, CA) were used to analyze all the statistics]. Data distribution normality was examined by D'Agostino-Pearson omnibus test. Mann-Whitney *U*-test, or Kruskal-Wallis test followed by Dunn *post hoc* test, was applied to compare the differences of two non-categorical variables whose distribution is not Gaussian. For the variables with Gaussian distribution, differences between two groups were examined by Student's *t*-test or analysis of covariance (ANCOVA), as appropriate. Pearson's correlation analysis was performed to analyze the linear correlation between two variables. Bland-Altman plotting was performed to assess the comparability of results obtained by different methods. Sex distribution was analyzed by χ^2-test. To examine the diagnostic accuracy of plasma α-synuclein and NFL levels, the receiver operating characteristic (ROC) curve was used to determine the area under the ROC curve (AUC) of variables, and the values of sensitivity and specificity. Each set of data was expressed as median ± *SD*. All *P*-values were two-tailed, and a $P < 0.05$ was considered significant.

RESULTS

To compare the relative influences of different potassium salts of EDTA on the measurement of α-synuclein and NFL levels in plasma by IMR we collected blood by using K_2 and K_3-EDTA tubes at RT from 8 patients with PD and 7 HCs. The plasma levels of α-synuclein (K_2: 141.5 ± 53.16 fg/ml, K_3: 146.92 ± 49.06 fg/ml, $P = 0.595$, **Figure 1A**) and NFL (K_2: 8.92 ± 2.8 pg/ml, K_3: 9.19 ± 2.58 pg/ml, $P = 0.744$, **Figure 1B**) in K_2- and K_3-EDTA were similar. The effective size to detect the difference between the levels of these molecules in K_2- and K_3-EDTA tubes was 0.1 and with a power of 0.9, and a sample size of 1,043 was needed to achieve a significant difference. Significant correlations were also demonstrated between these levels in K_2 and K_3-EDTA (α-synuclein: $R^2 = 0.918$, $P < 0.001$, **Figure 1C**; NFL: $R^2 = 0.836$, $P < 0.001$, **Figure 1D**). Bland-Altman plotting also confirmed that the differences in the tested molecule levels between K_2- and K_3-EDTA collection were small (α-synuclein: –5.42 ± 15.3 fg/ml, **Figure 1E**; NFL: –0.28 ± 1.14 pg/ml, **Figure 1F**). Compared with HCs, a significantly higher levels of α-synuclein in PD patients were detected by using either K_2- (PD: 177.1 ± 37.04 fg/ml, HC: 100.90 ± 37.16 fg/ml, $P = 0.016$, **Figure 2A**) or K_3-EDTA (PD: 183.05 ± 20.79 fg/ml, HC: 105.10 ± 35.78 fg/ml, $P = 0.001$, **Figure 2B**) collection, although the number of cases was small. Plasma levels of NFL in PD and HCs were similar by using either K_2- (PD: 8.89 ± 2.38 pg/ml, HC: 8.95 ± 3.42 pg/ml, $P = 0.961$, **Figure 2C**) or K_3-EDTA collection (PD: 9.53 ± 2.26 pg/ml, HC: 8.81 ± 3.03 pg/ml, $P = 0.61$, **Figure 2D**). These results showed no remarkable differences in plasma levels of α-synuclein and NFL between K_2- and K_3-EDTA preparations.

To further evaluate the effect of centrifugation temperature on plasma levels of α-synuclein and NFL, we prepared plasma from 42 patients with PD and 40 HCs (**Table 1**) by using centrifuging blood samples in K_2-EDTA at RT or refrigerated temperature. Under RT centrifugation, the levels of α-synuclein ($n = 82$, 181.23 ± 196.31 fg/ml) were significantly higher compared with refrigerated centrifugation ($n = 82$, 101.57 ± 43.43 fg/ml, $P < 0.001$, **Figure 3A**), and α-synuclein levels in plasma prepared from the two temperature conditions of centrifugation did not demonstrate a significant correlation ($R^2 = 0.007$, $P = 0.444$, **Figure 3B**). Bland-Altman plotting also demonstrated

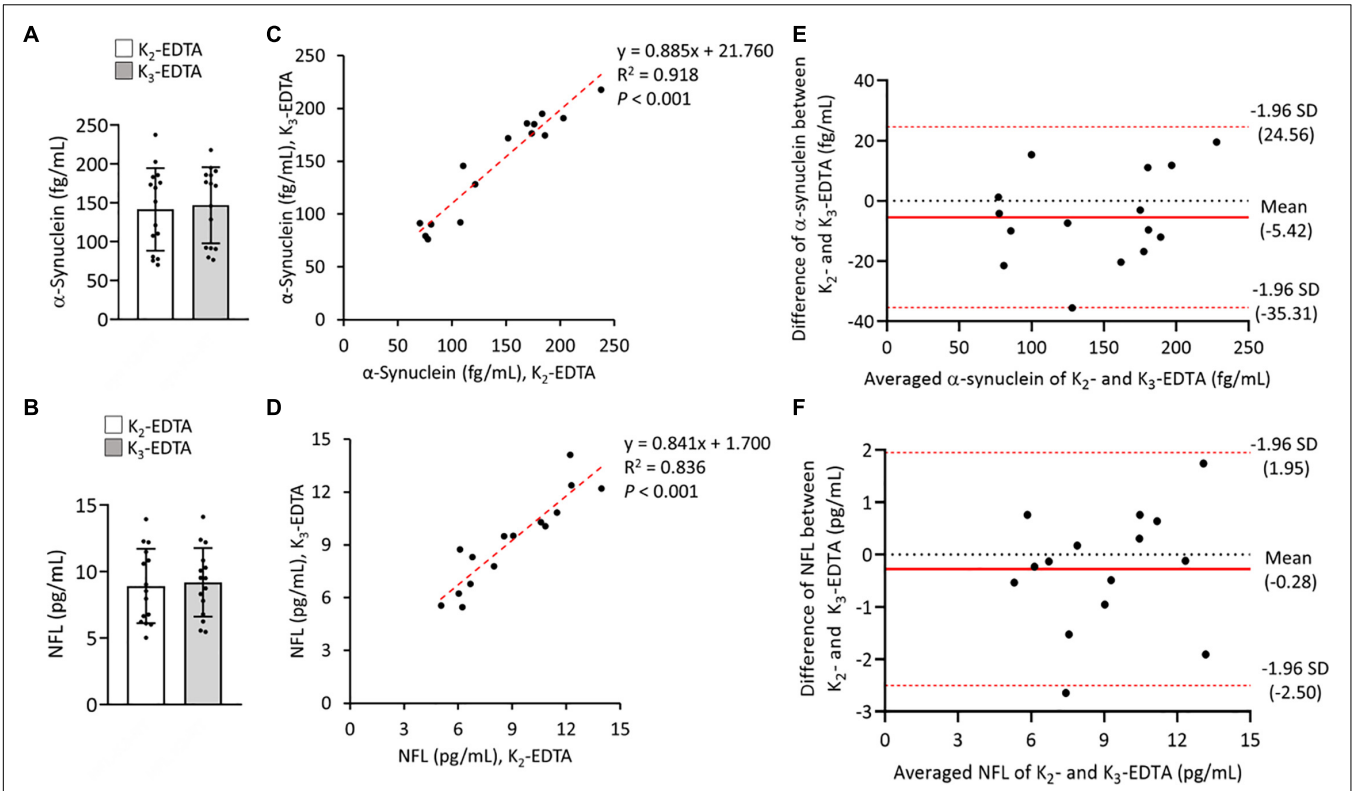

FIGURE 1 | Levels of α-synuclein and neurofilament light chain (NFL) in the plasma were prepared by using different EDTA tubes. **(A)** Plasma levels of α-synuclein in K_2- (N = 15) and K_3- (N = 15) EDTA tubes. **(B)** Plasma levels of NFL in K_2- and K_3-EDTA tubes. **(C)** Correlations between α-synuclein levels in K_2- and K_3-EDTA tubes. **(D)** Correlations between NFL levels in K_2- and K_3-EDTA tubes. **(E)** Bland-Altman plot of the comparability of α-synuclein levels in K2- and K3-EDTA tubes. The red dotted lines represent limits of agreement (mean difference ± 1.96 *SD*). **(F)** Bland-Altman plot of the comparability of NFL levels in K2- and K3-EDTA tubes. R^2, Pearson's correlation coefficient. Comparisons by Mann-Whitney *U*-test.

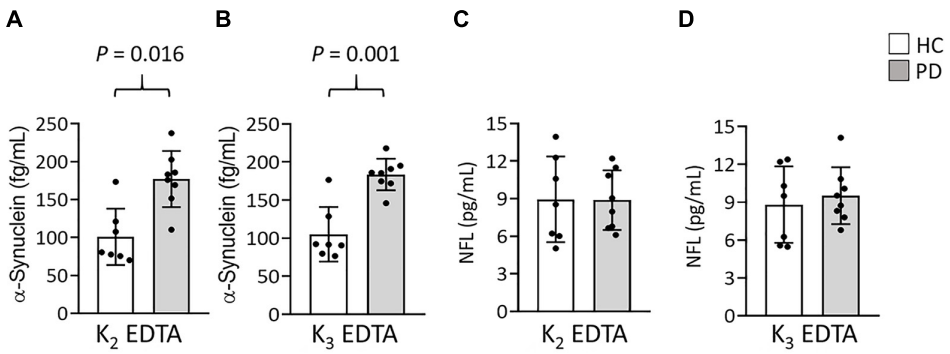

FIGURE 2 | Levels of α-synuclein and NFL in the plasma of patients with Parkinson's disease (PD) and healthy controls (HCs). **(A,B)** Plasma levels of α-synuclein in patients with PD (n = 8) and healthy controls (HCs, n = 7) in **(A)** K_2- and **(B)** K_3-EDTA tubes. **(C,D)** Plasma levels of NFL in patients with PD and HCs in **(C)** K_2- and **(D)** K_3-EDTA tubes. Error bars represent *SD*. Comparisons by Mann-Whitney *U*-test.

a huge difference in α-synuclein levels between these two conditions (79.65 ± 197.4 fg/ml, **Figure 3C**). On the other hand, NFL levels in plasma prepared from RT and refrigerated centrifugations were similar (RT: 13.92 ± 8.05 pg/ml, 4°C: 11.94 ± 7.1 pg/ml, P = 0.1, **Figure 3D**). NFL levels in plasma under RT centrifugation were highly correlated with those under refrigerated centrifugation (R^2 = 0.836, P < 0.001, **Figure 3E**). Bland-Altman plotting also confirmed that the differences between these two groups were small (1.99 ± 5.73 pg/ml, **Figure 3F**). Under RT centrifugation, the levels of α-synuclein in PD patients (256.6 ± 50.2 fg/ml) were significantly higher compared with HCs (102.1 ± 0.66 fg/ml, P < 0.001, **Figure 4A**). The sensitivity analysis confirmed the statistical significance following removing the outliers in PD group (PD:

TABLE 1 | Clinical characteristics of the patients with Parkinson's disease (PD) and healthy controls (HC).

	HC (*n* = 40)	PD		
		Early (*n* = 24)	Advanced (*n* = 18)	Total (*n* = 42)
Sex (female/male)	19/21	9/15	8/10	17/25
Age (years)	65.85 ± 7.52	61.58 ± 9.57	71.61 ± 9.15	65.88 ± 10.55
Duration (years)		5.78 ± 4.94	13.06 ± 6.58	8.88 ± 6.69
Hoehn and Yahr stage		1.54 ± 0.51	3.22 ± 0.43	2.17 ± 0.93
LEDD (mg)		549.73 ± 548.88	1422.69 ± 662.50	923.86 ± 736.32
UPDRS-total		23.38 ± 6.53	69.29 ± 21.71	42.37 ± 27.15
UPDRS-part III		13.92 ± 5.40	40.36 ± 12.54	24.88 ± 15.93
MMSE	29.62 ± 0.72	28.33 ± 2.76	22.59 ± 6.48	25.95 ± 5.42
CDR	0.13 ± 0.22	0.27 ± 0.25	0.59 ± 0.40	0.41 ± 0.36

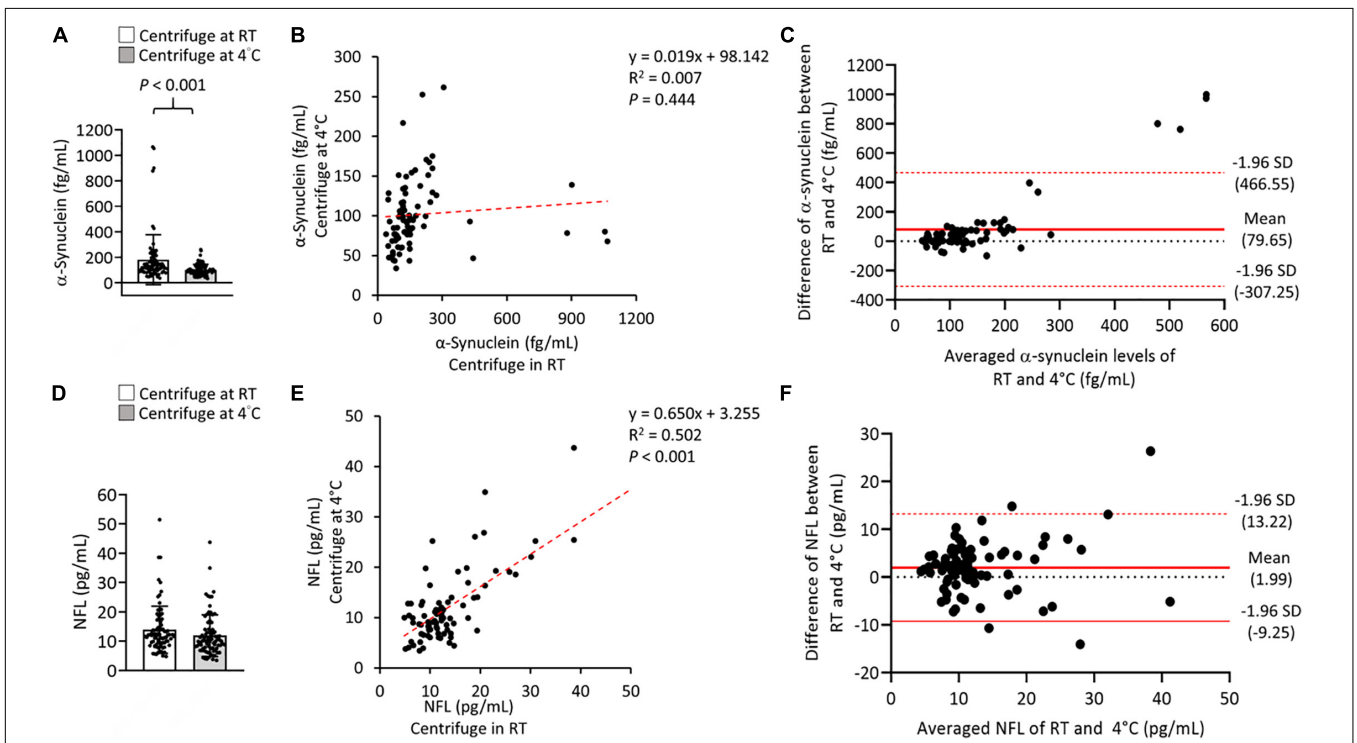

FIGURE 3 | Levels of α-synuclein and NFL in the plasma were centrifuged at different temperatures. **(A)** Plasma levels and α-synuclein in K_2-EDTA tubes were centrifuged at room temperature (RT) or 4°C. **(B)** Correlations between α-synuclein levels in K_2-EDTA tubes centrifuged at RT or 4°C. **(C)** Bland-Altman plot of the comparability of α-synuclein levels in K_2-EDTA tubes centrifuged at RT or 4°C. The red dotted lines represent limits of agreement (mean difference ± 1.96 *SD*). **(D)** Plasma levels and of NFL in K_2-EDTA tubes centrifuged at RT or 4°C. **(E)** Correlations between NFL levels in K_2-EDTA tubes centrifuged at RT or 4°C. **(F)** Bland-Altman plot of the comparability of α-synuclein levels in K_2-EDTA tubes centrifuged at RT or 4°C. R^2, Pearson's correlation coefficient. Comparisons by Student's *t*-test.

181.06 ± 102.05 pg/ml, $P < 0.001$). However, this difference was not recapitulated with refrigerated centrifugation (PD: 111.1 ± 48.69 fg/ml; HC: 91.59 ± 35 fg/ml, $P = 0.085$, **Figure 4B**). Under both RT and refrigerated centrifugations, the levels of NFL in PD patients (RT: 16.47 ± 9.96 pg/ml; 4°C: 13.92 ± 8.31 pg/ml) were significantly higher compared with HCs (RT: 11.24 ± 4.06 pg/ml, $P = 0.006$, **Figure 4C**; 4°C: 9.84 ± 4.81 pg/ml, $P = 0.017$, **Figure 4D**). To further understand whether hemolysis could affect the levels of α-synuclein in plasma, we measured hemoglobin levels in our samples. The results showed hemoglobin levels in PD (RT:0.89 ± 0.5 mg/ml; 4°C:0.90 ± 0.56 mg/ml) and HCs (RT:0.74 ± 0.41 mg/ml, $P = 0.15$; 4°C:0.74 ± 0.43 mg/ml, $P = 0.13$) were similar in both temperatures of centrifugations (**Figures 4E,F**). The levels of α-synuclein between PD patients and HC under RT centrifugation remained significantly different after ANCOVA adjustment for hemoglobin levels ($P < 0.001$). AUC showed good ability for α-synuclein under RT centrifugation (AUC = 0.873, 95% CI: 0.793–0.953, **Figure 5A**) to distinguish PD patients from HCs, whereas α-synuclein levels under refrigerated

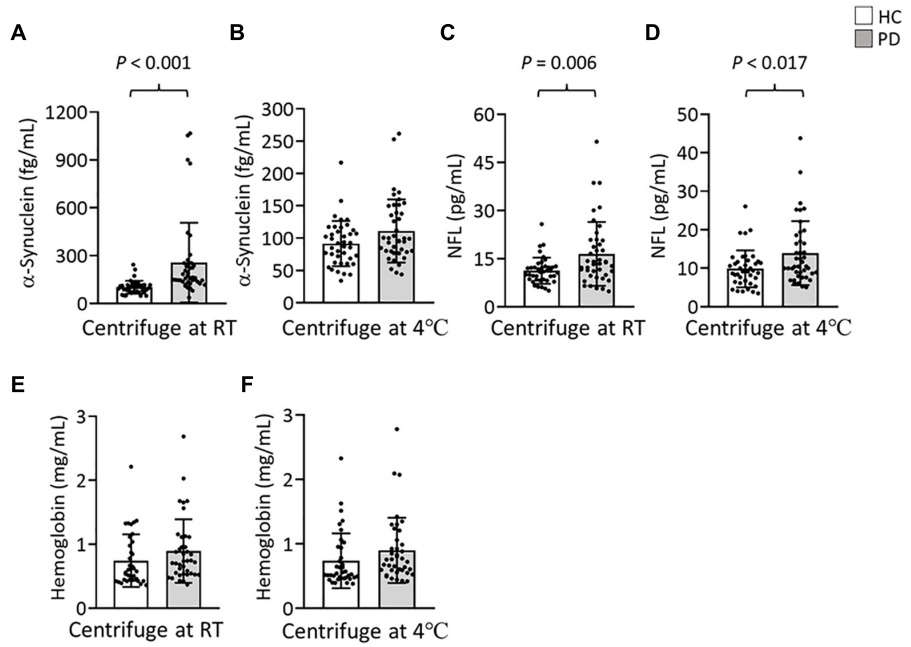

FIGURE 4 | Levels of α-synuclein and NFL in the plasma of patients with PD and HCs. **(A,B)** Plasma levels of α-synuclein in patients with PD (n = 42) and HCs (n = 40) in K_2-EDTA tubes centrifuged at **(A)** RT or **(B)** 4°C. **(C,D)** Plasma levels of NFL in patients with PD and HCs in K_2-EDTA tubes centrifuged at **(C)** RT or **(D)** 4°C. **(E,F)** Plasma levels of hemoglobin in patients with PD and HCs in K_2-EDTA tubes centrifuged at **(E)** RT or **(F)** 4°C. Error bars represent *SD*. Comparisons by Student's *t*-test.

centrifugation (AUC = 0.611, 95% CI: 0.488–0.733, **Figure 5B**), and NFL levels under RT (AUC = 0.674, 95% CI: 0.557–0.792, **Figure 5C**) and refrigerated centrifugation (AUC = 0.652, 95% CI: 0.535–0.77, **Figure 5D**) did not demonstrated adequate AUCs to separate PD from HCs.

We further stratified our patients into early and advanced PD according to their disease stages. Under RT centrifugation, the levels of α-synuclein among these groups were significant after ANCOVA adjustment for hemoglobin levels (P = 0.002). PD patients at early (285.64 ± 293.81 fg/ml, P < 0.001) and advanced PD (217.95 ± 177.41 fg/ml, P < 0.001) demonstrated higher levels of α-synuclein compared with HCs (102.05 ± 40.66 fg/ml, **Figure 6A**). These differences cannot be recapitulated under refrigerated centrifugation (early PD: 101.87 ± 35.63 fg/ml; advanced PD: 123.37 ± 61; HC: 91.59 ± 35.01, P = 0.157, **Figure 6B**). Under RT centrifugation, the levels of NFL (17.52 ± 10.37 pg/ml) in advanced PD were significantly higher compared with HCs (11.24 ± 4.06 pg/ml, P = 0.007, **Figure 6C**), but not significantly different between early PD (15.69 ± 9.74 pg/ml) and HCs (11.24 ± 4.06 pg/ml, P = 0.082). Under refrigerated centrifugation, early PD demonstrated significantly higher levels of NFL (15.23 ± 9.59 pg/ml) compared with HCs (9.84 ± 4.81 pg/ml, P = 0.028, **Figure 6D**), but not significantly different between advanced PD (12.22 ± 6.1 pg/ml) and HCs (9.84 ± 4.81 pg/ml, P = 0.669). Levels of α-synuclein and NFL in plasma under different centrifugation temperatures did not demonstrate correlations with the scores of UPDRS, Hoehn and Yahr stages or LEDDs (data not shown).

DISCUSSION

The α-synuclein and NFL levels in plasma have been widely tested to know if they can serve as potential biomarkers to indicate PD and disease progression, whereas the results are not satisfactorily consistent (Lee et al., 2006; Ding et al., 2017; Lin et al., 2017; Chang et al., 2019; Ng et al., 2019). It is noted that different assay methods including IMR, single-molecule array, and enzyme-linked immunosorbent assay may explain the different results between studies but using the same assay platform may also generate differential data caused by different preanalytical conditions. These include blood collection tubes, centrifuge, and storage temperatures. In order to identify useful markers to indicate disease onset, severity, and progression or to test the efficacy of potential treatments for future clinical trials, an optimized and standardized blood sample preparation are crucial to minimizing data variations from different centers. Therefore, the sample preparation methods should be taken into account for the establishment of reliable biochemical assessment of biomarkers for neurodegenerative diseases including PD. In this study, we evaluated the levels of α-synuclein and NFL in plasma, which were collected in K_2- or K_3-EDTA tubes and centrifuged at RT or refrigerated temperature. The results showed a linear relationship for the levels of α-synuclein and NFL between K_2- or K_3-EDTA tubes. The levels of α-synuclein in the plasma collected by both types of tubes were consistently elevated in PD patients compared with HCs. However, the temperature of centrifugation significantly affects the levels of α-synuclein. The levels of α-synuclein in the plasma prepared by RT centrifugation were

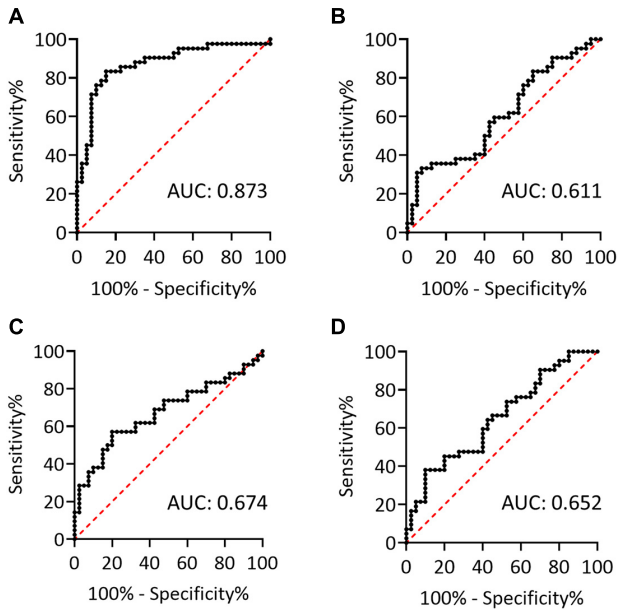

FIGURE 5 | The potentials to discriminate PD and HCs. **(A,B)** Receiver operating characteristic (ROC) curves for plasma levels of α-synuclein in K_2-EDTA tubes centrifuged at **(A)** RT or **(B)** 4°C to discriminate patients with PD from HCs. **(C,D)** ROC curves for plasma levels of NFL in K_2-EDTA tubes centrifuged at **(C)** RT or **(D)** 4°C to discriminate patients with PD from HCs. AUC, area under the ROC curve.

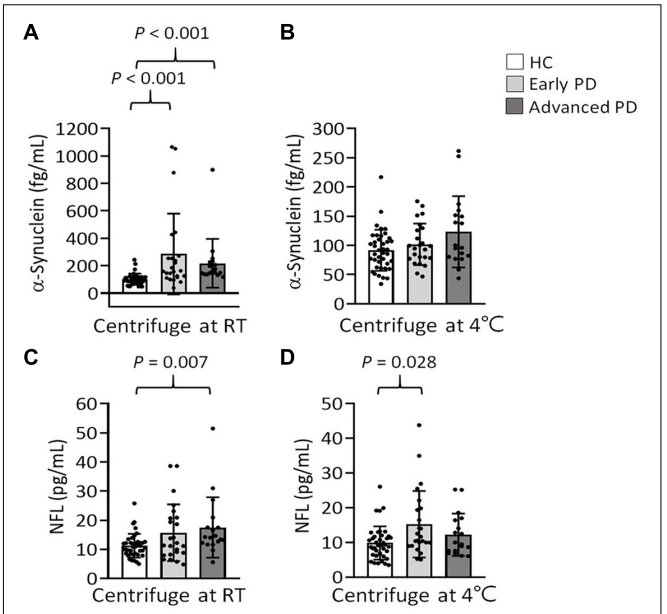

FIGURE 6 | Levels of α-synuclein and NFL in the plasma of patients with PD at early or advanced stages, and HCs. **(A,B)** Plasma levels of α-synuclein in patients with early (n = 24) and advanced PD (n = 18), and HCs (n = 40) in K_2-EDTA tubes centrifuged at **(A)** RT or **(B)** 4°C. **(C,D)** Plasma levels of NFL in patients with early and advanced PD, and HCs in K_2-EDTA tubes centrifuged at **(C)** RT or **(D)** 4°C. Error bars represent *SD*. Comparisons by Kruskal-Wallis test followed by Dunn *post hoc* test.

not significantly correlated with those in the plasma prepared by refrigerated centrifugation. Similar to those reported in the literature (Lee et al., 2006; Ding et al., 2017; Lin et al., 2017; Chang et al., 2019; Ng et al., 2019), elevated levels of α-synuclein in PD patients were observed in plasma prepared by RT centrifugation, whereas such a change for PD was not present in plasma prepared by refrigerated centrifugation. The levels of NFL in plasma prepared by RT centrifugation demonstrated a linear relationship with those in plasma prepared by refrigerated centrifugation. Both conditions consistently demonstrated higher levels of NFL in PD patients compared with HCs. Our results suggested that the K_2-EDTA tube was equivalent to the K_3-EDTA tube in collecting blood to analyze plasma levels of α-synuclein and NFL. Centrifugation temperatures during plasma preparation generated a considerable variation of α-synuclein level that might hinder the identification of α-synuclein level changes in PD. Therefore, the choice of temperature for plasma preparation is crucial for assessing biomarkers in PD.

Plasma is usually prepared from blood in EDTA-anticoagulated tubes. EDTA comes in blood tubes as K_2- and K_3-EDTA salts. K_2-EDTA is dispensed as powder, so it causes no variation in the volume/dilution of the collected sample. K_3-EDTA is placed inside the tube in liquid form, which causes a slight dilution of the sample, possibly generates an osmotic effect on blood cells, and increases the variations in hemogram studies (Goossens et al., 1991). Prolonged storage of blood in K_3-EDTA may reduce the size of red blood cells (RBCs) (Goossens et al., 1991). There is no significant difference in plasma glycohemoglobin levels between blood collections using K_2- and K_3-EDTA tubes (Vrtaric et al., 2016). In respect of biomarkers for Alzheimer's disease, there was no marked difference in the levels of amyloid β and tau between K_2- and K_3-EDTA tubes (Rozga et al., 2019). Our results provide evidence for the small discrepancy between K_2- and K_3-EDTA tubes in measuring plasma levels of α-synuclein and NFL. The differences in α-synuclein between PD and HCs are also consistently found in K_2- and K_3-EDTA tubes, suggesting that both tubes can be used interchangeably for clinical assessments of biomarkers for PD.

Centrifugation is a necessary and key step in blood processing. Although it has been recommended that blood samples should be centrifuged at RT for homeostasis assays (Adcock Funk et al., 2012), there is no evidence that centrifugation temperatures might significantly influence concentrations of tested molecules in plasma. On routine coagulation tests, centrifugation of blood at refrigerated temperature is not likely to generate significant analytical or clinical biases on activated partial thromboplastin time, fibrinogen, and D-dimer (Lippi et al., 2006). However, our results showed refrigerated centrifugation significantly reduced the level of α-synuclein in plasma, as well as undermined the differences between PD and HCs. α-Synuclein is an amyloidogenic protein, which is prone to aggregate to form specific cross-β amyloid fibrils (Araki et al., 2019). The fibrillation formation and solubility of α-synuclein may be affected by temperatures. The inhibition of α-synuclein fibril formation appears after 60°C (Ariesandi et al., 2013), while

the low temperature enhances the α-synuclein denaturation (Ikenoue et al., 2014). This cold denaturation is not seen in other amyloidogenic peptides, such as β2−microglobulin, amyloid β, and insulin (Ikenoue et al., 2014). Previous studies also showed that centrifugation temperature did not affect the levels of amyloid β in plasma (Verberk et al., 2020). Consistent with the study of Verberk, we found the level of NFL is not significantly biased by centrifugation temperatures (Verberk et al., 2020).

Lines of study have demonstrated elevation of α-synuclein in plasma of PD patients, using different assessment tools including enzyme-linked immunosorbent assay (Lee et al., 2006; Ding et al., 2017), single-molecule array (Ng et al., 2019), or IMR (Lin et al., 2017; Chang et al., 2019). Our results recapitulated this important finding by centrifuging blood at RT and demonstrated a good potential of α-synuclein in plasma to discriminate PD and HCs. However, a few studies report negative findings showing either decreased or unchanged α-synuclein levels (Mata et al., 2010; Park et al., 2011; Foulds et al., 2013). Given that 99% of α-synuclein in the blood is stored in RBCs (Barbour et al., 2008), potential hemolysis could confound the results. Blood sample preparations can be another important factor contributing to this inconsistency. This point is addressed by our results, which showed that refrigerated centrifugation reduced the level of α-synuclein, lessen the difference of α-synuclein levels between PD and HCs, and critically lowered the diagnostic potential of α-synuclein in PD. The potential mechanism underlying increased plasma levels of α-synuclein in PD remains unclear. Neurons that resided at the enteric plexus may harbor α-synuclein in PD patients since the prodromal stage (Stokholm et al., 2016). α-Synuclein released by peripheral neurons into the bloodstream may be transported to the brain and gradually seeds to form aggregations in central neurons. Therefore, assessment of α-synuclein in blood, with appropriate sample preparations and quantitative technologies, can offer a useful biomarker for the early diagnosis of PD. Further prospective studies, focusing on the patients at prodromal or early stages, may be needed to confirm the role of α-synuclein in the early diagnosis of PD.

Plasma NFL levels are elevated in several neurodegenerative diseases, including amyotrophic lateral sclerosis (Lu et al., 2015), multiple sclerosis (Piehl et al., 2018), Alzheimer's disease (Weston et al., 2017), and atypical parkinsonian syndromes (Hansson et al., 2017). However, the results of blood NFL levels were not consistent. The study of Hansson et al. (2017) reported plasma NFL levels in patients with PD were modestly elevated in the London cohort but not in the Lund cohort. Similar to our results, the work of Lin et al. (2019) reported higher blood NFL levels in patients with PD, particularly at the advanced stage. It is of interest that plasma in both RT and refrigerated centrifugations demonstrated similar levels of NFL. It has been shown that blood levels of NFL may not be affected by repeated freeze-thaw cycles, delayed processing, and long-term storage at different temperatures, suggesting the NFL is stable under the common sample preparations (Barro et al., 2020). The study of Lin et al. (2019) also demonstrated that plasma NFL levels are correlated with scores of UPDRS part III and MMSE in PD patients. Our results, with a relatively small number of patients, did not recapitulate these correlations. NFL levels in plasma centrifuged at RT were elevated in PD patients at the advanced stage, while PD patients at the early stage demonstrated higher NFL levels in plasma in refrigerated centrifugation. The reason for inconsistent results of NFL in advanced and early PD stages between RT and refrigerated centrifugation might be because of the small sample size tested, especially in the advanced stage (n = 18). A large prospective cohort or meta-analysis will be needed to consolidate the role of NFL in the disease progression of PD.

This study has some limitations. It should be noted that the sample size of this study was relatively small. The results should be further tested in well-powered cohorts. The levels of α-synuclein, which was produced by the IMR platform, should be validated by other quantitative technologies. The polymerization and phosphorylation of α-synuclein might not be properly identified. The parameters (α-synuclein and NFL), which had been shown to differentiate PD from atypical parkinsonism (Lee et al., 2006; Hansson et al., 2017; Lin et al., 2019), were not tested in patients with other parkinsonism or other neurological diseases. However, differentiation of PD from atypical parkinsonism was not the aim of our study. In the future, further studies should be conducted to examine if α-synuclein and NFL measured by applying the sample preparation used in our study can clearly distinguish PD from atypical parkinsonism. Nevertheless, this study evidently indicated that when processed in optimal conditions, K_2-and K_3-EDTA tubes used to collect blood for measurements of α-synuclein and NFL could display compatible results. Plasma should be prepared under RT centrifugation to lessen the reduction of α-synuclein. With standardized preanalytical sample preparations, both α-synuclein and NFL serve as potential biomarkers for PD. Our study results suggested that a consensus protocol of blood sample preparation was essential in quantifying α-synuclein levels if we would plan to use α-synuclein as a biomarker for PD.

DATA AVAILABILITY STATEMENT

The raw data supporting the conclusions of this article will be made available by the authors, without undue reservation.

ETHICS STATEMENT

The studies involving human participants were reviewed and approved by the Institutional Review Boards of the Chang Gung Memorial Hospital. The patients/participants provided their written informed consent to participate in this study.

AUTHOR CONTRIBUTIONS

K-HC and C-MC contributed to conception and design of the study, organized the database, and finalized and approved the submitted version. K-CL and C-SL contributed reagents, materials, analysis tools. K-HC and S-YY performed the statistical

analysis. K-HC wrote the first draft of the manuscript. All authors contributed to manuscript revision.

FUNDING

This work was supported by the Chang Gung Medical Foundation (CMRPG3H1471-2, CMRPG3H1481-2, CMRPG3H 1491-2, CORPD2J0072, and CMRPD2K0171), and Ministry of Science and Technology, Taiwan (MOST 110-2622-8-182-001-TS1 and MOST 109-2221-E-182-013-MY3).

ACKNOWLEDGMENTS

We thank all the patients for consenting to the collection of blood samples.

SUPPLEMENTARY MATERIAL

The Supplementary Material for this article can be found online at: https://www.frontiersin.org/articles/10.3389/fnagi.2021.759182/full#supplementary-material

REFERENCES

Adcock Funk, D. M., Lippi, G., and Favaloro, E. J. (2012). Quality standards for sample processing, transportation, and storage in hemostasis testing. *Semin. Thromb. Hemost* 38, 576–585. doi: 10.1055/s-0032-1319768

Araki, K., Yagi, N., Aoyama, K., Choong, C.-J., Hayakawa, H., Fujimura, H., et al. (2019). Parkinson's disease is a type of amyloidosis featuring accumulation of amyloid fibrils of α-synuclein. *Proc. Natl. Acad. Sci. U S A* 116, 17963–17969. doi: 10.1073/pnas.1906124116

Ariesandi, W., Chang, C. F., Chen, T. E., and Chen, Y. R. (2013). Temperature-dependent structural changes of Parkinson's alpha-synuclein reveal the role of pre-existing oligomers in alpha-synuclein fibrillization. *PLoS One* 8:e53487. doi: 10.1371/journal.pone.0053487

Barbour, R., Kling, K., Anderson, J. P., Banducci, K., Cole, T., Diep, L., et al. (2008). Red blood cells are the major source of alpha-synuclein in blood. *Neurodegener. Dis.* 5, 55–59. doi: 10.1159/000112832

Barro, C., Chitnis, T., and Weiner, H. L. (2020). Blood neurofilament light: a critical review of its application to neurologic disease. *Ann. Clin. Transl. Neurol.* 7, 2508–2523. doi: 10.1002/acn3.51234

Bowen, R. A., and Remaley, A. T. (2014). Interferences from blood collection tube components on clinical chemistry assays. *Biochem. Med.* 24, 31–44. doi: 10.11613/BM.2014.006

Chang, C. W., Yang, S. Y., Yang, C. C., Chang, C. W., and Wu, Y. R. (2019). Plasma and serum alpha-synuclein as a biomarker of diagnosis in patients with Parkinson's disease. *Front. Neurol.* 10:1388. doi: 10.3389/fneur.2019.01388

Ding, J., Zhang, J., Wang, X., Zhang, L., Jiang, S., Yuan, Y., et al. (2017). Relationship between the plasma levels of neurodegenerative proteins and motor subtypes of Parkinson's disease. *J. Neural. Transm.* 124, 353–360. doi: 10.1007/s00702-016-1650-2

England, J. M., Rowan, R. M., van Assendelft, O. W., Bull, B. S., Coulter, W., Fujimoto, K., et al. (1993). Recommendations of the international council for standardization in haematology for ethylenediaminetetraacetic acid anticoagulation of blood for blood cell counting and sizing. International council for standardization in haematology: Expert panel on cytometry. *Am. J. Clin. Pathol.* 100, 371–372. doi: 10.1093/ajcp/100.4.371

Foulds, P. G., Diggle, P., Mitchell, J. D., Parker, A., Hasegawa, M., Masuda-Suzukake, M., et al. (2013). A longitudinal study on alpha-synuclein in blood plasma as a biomarker for Parkinson's disease. *Sci. Rep.* 3:2540. doi: 10.1038/srep02540

Goossens, W., Van Duppen, V., and Verwilghen, R. L. (1991). K2- or K3-EDTA: the anticoagulant of choice in routine haematology? *Clin. Lab. Haematol.* 13, 291–295. doi: 10.1111/j.1365-2257.1991.tb00284.x

Hansson, O., Janelidze, S., Hall, S., Magdalinou, N., Lees, A. J., Andreasson, U., et al. (2017). Blood-based NfL: A biomarker for differential diagnosis of parkinsonian disorder. *Neurology* 88, 930–937. doi: 10.1212/wnl.0000000000003680

Hoehn, M. M., and Yahr, M. D. (1967). Parkinsonism: onset, progression and mortality. *Neurology* 17, 427–442. doi: 10.1212/wnl.17.5.427

Hughes, A. J., Daniel, S. E., Kilford, L., and Lees, A. J. (1992). Accuracy of clinical diagnosis of idiopathic Parkinson's disease: a clinico-pathological study of 100 cases. *J. Neurol. Neurosurg. Psychiatry* 55, 181–184. doi: 10.1136/jnnp.55.3.181

Ikenoue, T., Lee, Y. H., Kardos, J., Saiki, M., Yagi, H., Kawata, Y., et al. (2014). Cold denaturation of alpha-synuclein amyloid fibrils. *Angew Chem. Int. Ed. Engl.* 53, 7799–7804. doi: 10.1002/anie.201403815

Lang, A. E., and Lozano, A. M. (1998). Parkinson's Disease. *N. Engl. J. Med.* 339, 1044–1053. doi: 10.1056/NEJM199810083391506

Lee, P. H., Lee, G., Park, H. J., Bang, O. Y., Joo, I. S., and Huh, K. (2006). The plasma alpha-synuclein levels in patients with Parkinson's disease and multiple system atrophy. *J. Neural. Transm.* 113, 1435–1439. doi: 10.1007/s00702-005-0427-9

Li, Q. X., Mok, S. S., Laughton, K. M., McLean, C. A., Cappai, R., Masters, C. L., et al. (2007). Plasma alpha-synuclein is decreased in subjects with Parkinson's disease. *Exp. Neurol.* 204, 583–588. doi: 10.1016/j.expneurol.2006.12.006

Lin, C. H., Li, C. H., Yang, K. C., Lin, F. J., Wu, C. C., Chieh, J. J., et al. (2019). Blood NfL: A biomarker for disease severity and progression in Parkinson disease. *Neurology* 93, e1104–e1111. doi: 10.1212/WNL.0000000000008088

Lin, C. H., Yang, S. Y., Horng, H. E., Yang, C. C., Chieh, J. J., Chen, H. H., et al. (2017). Plasma alpha-synuclein predicts cognitive decline in Parkinson's disease. *J. Neurol. Neurosurg. Psychiatry* 88, 818–824. doi: 10.1136/jnnp-2016-314857

Lippi, G., Salvagno, G. L., Montagnana, M., Poli, G., and Guidi, G. C. (2006). Influence of centrifuge temperature on routine coagulation testing. *Clin. Chem.* 52, 537–538. doi: 10.1373/clinchem.2005.063149

Lu, C. H., Macdonald-Wallis, C., Gray, E., Pearce, N., Petzold, A., Norgren, N., et al. (2015). Neurofilament light chain: A prognostic biomarker in amyotrophic lateral sclerosis. *Neurology* 84, 2247–2257. doi: 10.1212/WNL.0000000000001642

Mata, I. F., Shi, M., Agarwal, P., Chung, K. A., Edwards, K. L., Factor, S. A., et al. (2010). SNCA variant associated with Parkinson disease and plasma alpha-synuclein level. *Arch. Neurol.* 67, 1350–1356. doi: 10.1001/archneurol.2010.279

Movement Disorder Society Task Force on Rating Scales for Parkinson's Disease (2003). The Unified Parkinson's Disease Rating Scale (UPDRS): status and recommendations. *Mov. Disord* 18, 738–750. doi: 10.1002/mds.10473

Mussbacher, M., Schrottmaier, W. C., Salzmann, M., Brostjan, C., Schmid, J. A., Starlinger, P., et al. (2017). Optimized plasma preparation is essential to monitor platelet-stored molecules in humans. *PLoS One* 12:e0188921. doi: 10.1371/journal.pone.0188921

Ng, A. S. L., Tan, Y. J., Lu, Z., Ng, E. Y. L., Ng, S. Y. E., Chia, N. S. Y., et al. (2019). Plasma alpha-synuclein detected by single molecule array is increased in PD. *Ann. Clin. Transl. Neurol.* 6, 615–619. doi: 10.1002/acn3.729

Park, M. J., Cheon, S. M., Bae, H. R., Kim, S. H., and Kim, J. W. (2011). Elevated levels of alpha-synuclein oligomer in the cerebrospinal fluid of drug-naive patients with Parkinson's disease. *J. Clin. Neurol.* 7, 215–222. doi: 10.3988/jcn.2011.7.4.215

Petzold, A. (2005). Neurofilament phosphoforms: surrogate markers for axonal injury, degeneration and loss. *J. Neurol. Sci.* 233, 183–198. doi: 10.1016/j.jns.2005.03.015

Piehl, F., Kockum, I., Khademi, M., Blennow, K., Lycke, J., Zetterberg, H., et al. (2018). Plasma neurofilament light chain levels in patients with MS switching from injectable therapies to fingolimod. *Mult. Scler.* 24, 1046–1054. doi: 10.1177/1352458517715132

Rozga, M., Bittner, T., Batrla, R., and Karl, J. (2019). Preanalytical sample handling recommendations for Alzheimer's disease plasma biomarkers. *Alzheimers Dement* 11, 291–300. doi: 10.1016/j.dadm.2019.02.002

Shulman, L. M., Gruber-Baldini, A. L., Anderson, K. E., Fishman, P. S., Reich, S. G., and Weiner, W. J. (2010). The clinically important difference on the

unified Parkinson's disease rating scale. *Arch. Neurol.* 67, 64–70. doi: 10.1001/archneurol.2009.295

Simonsen, A. H., Kuiperij, B., El-Agnaf, O. M. A., Engelborghs, S., Herukka, S.-K., Parnetti, L., et al. (2016). The utility of α-synuclein as biofluid marker in neurodegenerative diseases: a systematic review of the literature. *Biomark. Med.* 10, 19–34. doi: 10.2217/bmm.14.105

Spillantini, M. G., Schmidt, M. L., Lee, V. M., Trojanowski, J. Q., Jakes, R., and Goedert, M. (1997). Alpha-synuclein in Lewy bodies. *Nature* 388, 839–840. doi: 10.1038/42166

Stokholm, M. G., Danielsen, E. H., Hamilton-Dutoit, S. J., and Borghammer, P. (2016). Pathological alpha-synuclein in gastrointestinal tissues from prodromal Parkinson disease patients. *Ann. Neurol.* 79, 940–949. doi: 10.1002/ana.24648

Tombaugh, T. N., and McIntyre, N. J. (1992). The mini-mental state examination: a comprehensive review. *J. Am. Geriatr. Soc.* 40, 922–935. doi: 10.1111/j.1532-5415.1992.tb01992.x

Tomlinson, C. L., Stowe, R., Patel, S., Rick, C., Gray, R., and Clarke, C. E. (2010). Systematic review of levodopa dose equivalency reporting in Parkinson's disease. *Mov. Disord* 25, 2649–2653. doi: 10.1002/mds.23429

Verberk, I. M. W., Misdorp, E. O., Koelewijn, J. M. W., Shan, D., Lambrechts, C., Shaw, L. M., et al. (2020). A biorepository for the in-depth validation of pre-analytical sample handling effects on novel blood-based biomarkers for Alzheimer's disease: The first results. *Alzheimers Dement* 16:e045763. doi: 10.1002/alz.045763

Vrtaric, A., Filipi, P., Hemar, M., Nikolac, N., and Simundic, A. M. (2016). K2-EDTA and K3-EDTA Greiner tubes for HbA1c measurement. *Lab. Med.* 47, 39–42. doi: 10.1093/labmed/lmv016

Weston, P. S. J., Poole, T., Ryan, N. S., Nair, A., Liang, Y., Macpherson, K., et al. (2017). Serum neurofilament light in familial Alzheimer disease: a marker of early neurodegeneration. *Neurology* 89, 2167–2175. doi: 10.1212/WNL.0000000000004667

Yang, S. Y., Chiu, M. J., Lin, C. H., Horng, H. E., Yang, C. C., Chieh, J. J., et al. (2016). Development of an ultra-high sensitive immunoassay with plasma biomarker for differentiating Parkinson disease dementia from Parkinson disease using antibody functionalized magnetic nanoparticles. *J. Nanobiotechnology* 14:41. doi: 10.1186/s12951-016-0198-5

Conflict of Interest: S-YY was employed by company MagQu Co., Ltd.

The remaining authors declare that the research was conducted in the absence of any commercial or financial relationships that could be construed as a potential conflict of interest.

Publisher's Note: All claims expressed in this article are solely those of the authors and do not necessarily represent those of their affiliated organizations, or those of the publisher, the editors and the reviewers. Any product that may be evaluated in this article, or claim that may be made by its manufacturer, is not guaranteed or endorsed by the publisher.

frontiers in Neuroscience

ORIGINAL RESEARCH
published: 09 December 2021
doi: 10.3389/fnins.2021.680104

Assessing Causal Relationship Between Human Blood Metabolites and Five Neurodegenerative Diseases With GWAS Summary Statistics

Haimiao Chen[1†], Jiahao Qiao[1†], Ting Wang[1†], Zhonghe Shao[1], Shuiping Huang[1,2,3] and Ping Zeng[1,2,3]*

[1] Department of Epidemiology and Biostatistics, School of Public Health, Xuzhou Medical University, Xuzhou, China, [2] Center for Medical Statistics and Data Analysis, School of Public Health, Xuzhou Medical University, Xuzhou, China, [3] Key Laboratory of Human Genetics and Environmental Medicine, Xuzhou Medical University, Xuzhou, China

Background: Neurodegenerative diseases (NDDs) are the leading cause of disability worldwide while their metabolic pathogenesis is unclear. Genome-wide association studies (GWASs) offer an unprecedented opportunity to untangle the relationship between metabolites and NDDs.

Methods: By leveraging two-sample Mendelian randomization (MR) approaches and relying on GWASs summary statistics, we here explore the causal association between 486 metabolites and five NDDs including Alzheimer's Disease (AD), amyotrophic lateral sclerosis (ALS), frontotemporal dementia (FTD), Parkinson's disease (PD), and multiple sclerosis (MS). We validated our MR results with extensive sensitive analyses including MR-PRESSO and MR-Egger regression. We also performed linkage disequilibrium score regression (LDSC) and colocalization analyses to distinguish causal metabolite-NDD associations from genetic correlation and LD confounding of shared causal genetic variants. Finally, a metabolic pathway analysis was further conducted to identify potential metabolite pathways.

Results: We detected 164 metabolites which were suggestively associated with the risk of NDDs. Particularly, 2-methoxyacetaminophen sulfate substantially affected ALS (OR = 0.971, 95%CIs: 0.961 ∼ 0.982, FDR = 1.04E-4) and FTD (OR = 0.924, 95%CIs: 0.885 ∼ 0.964, FDR = 0.048), and X-11529 (OR = 1.604, 95%CIs: 1.250 ∼ 2.059, FDR = 0.048) and X-13429 (OR = 2.284, 95%CIs: 1.457 ∼ 3.581, FDR = 0.048) significantly impacted FTD. These associations were further confirmed by the weighted median and maximum likelihood methods, with MR-PRESSO and the MR-Egger regression removing the possibility of pleiotropy. We also observed that ALS or FTD can alter the metabolite levels, including ALS and FTD on 2-methoxyacetaminophen sulfate. The LDSC and colocalization analyses showed that none of the identified associations could be driven by genetic correlation or confounding by LD with common causal loci. Multiple metabolic pathways were found to be involved in NDDs, such as "urea cycle"

OPEN ACCESS

Edited by:
Henrik Zetterberg,
University of Gothenburg, Sweden

Reviewed by:
Junling Wang,
Central South University, China
David Otaegui,
Biodonostia Health Research Institute (IIS Biodonostia), Spain

***Correspondence:**
Ping Zeng
zpstat@xzhmu.edu.cn

[†]*These authors share first authorship*

Specialty section:
This article was submitted to Neurodegeneration, a section of the journal Frontiers in Neuroscience

Received: *13 March 2021*
Accepted: *22 November 2021*
Published: *09 December 2021*

Citation:
Chen H, Qiao J, Wang T, Shao Z, Huang S and Zeng P (2021) Assessing Causal Relationship Between Human Blood Metabolites and Five Neurodegenerative Diseases With GWAS Summary Statistics. Front. Neurosci. 15:680104. doi: 10.3389/fnins.2021.680104

(P = 0.036), "arginine biosynthesis" (P = 0.004) on AD and "phenylalanine, tyrosine and tryptophan biosynthesis" (P = 0.046) on ALS.

Conclusion: our study reveals robust bidirectional causal associations between servaral metabolites and neurodegenerative diseases, and provides a novel insight into metabolic mechanism for pathogenesis and therapeutic strategies of these diseases.

Keywords: metabolites, neurodegenerative diseases, Mendelian randomization, metabolic pathway, amyotrophic lateral sclerosis, frontotemporal dementia, causal association

BACKGROUND

Neurodegenerative diseases (NDDs; Blennow et al., 2010; Parnetti, 2011), such as Alzheimer's disease (AD), amyotrophic lateral sclerosis (ALS), frontotemporal dementia (FTD), Parkinson's disease (PD), and multiple sclerosis (MS), are a prominent group of progressive and fatal neurological diseases currently without an effective cure, representing one of the fastest and largest increasing categories of the global disease burden especially because of aging populations (Roth et al., 2018; Bakhta et al., 2019). Therefore, identifying potential biomarkers for early diagnosis and unraveling risk factors for prevention and treatment become critical in the clinic. Although great advances have been made in discovering biomarkers and risk factors for various NDDs over the past few years (Trojanowski, 2000; Barnham et al., 2004; Emerit et al., 2004; Rachakonda et al., 2004; Amor et al., 2010; Blennow et al., 2010; Parnetti, 2011; Doty, 2017; Leng et al., 2019), the knowledge regarding the physiological and pathological mechanism underlying these diseases remains largely unclear.

As part of efforts to understand such mechanism, the relationship between metabolites and NDDs has been attracted active research attention (Wang et al., 2012; Jové et al., 2014; To et al., 2019; Chatterjee et al., 2020; Shang et al., 2020). Metabolites are the intermediate or end products that drive essential biological functions of human bodies and reflect the physiological and pathological disease phenotypes (Johnson et al., 2016; Shang et al., 2020). There is also a growing literature indicating that profiling metabolites in biofluids offers deep insights into biomarkers of NDDs (Wang et al., 2012; Mendelsohn and Larrick, 2013; Jové et al., 2014; González-Domínguez et al., 2015; Kori et al., 2016; To et al., 2019; Chatterjee et al., 2020; Shang et al., 2020). For example, it was demonstrated lipids and amino acids were associated with cognitive decline and the progression of dementia (Jiang et al., 2019); primary fatty amides in plasma were associated with brain amyloid burden and memory (Kim et al., 2019); blood metabolite changes in the periphery reflected the asymptomatic, prodromal and symptomatic stages of memory and AD (Kiddle et al., 2014; Mapstone et al., 2014). However, due to unknown confounders and reverse causality, these findings obtained from observational studies remain problematical as to whether metabolites are subsequent or consequent to NDDs, and it is also unknown whether there is a definite association between metabolites and NDDs, and whether such relationship is causal.

Recent advances in statistical genetic approaches of causal inference, along with publicly available summary statistics from large-scale genome-wide association studies (GWASs) of metabolites and NDDs provide an unprecedented opportunity to systematically evaluate their relationship through Mendelian randomization (MR; Greenland, 2000; Thomas and Conti, 2004; Tobin et al., 2004; Wheatley and Gray, 2004; Evans and Davey Smith, 2015; Zeng et al., 2019; Zeng and Zhou, 2019b; Yu et al., 2020a,b). In brief, MR is an instrumental-variable based method, which performs the causal inference with single nucleotide polymorphisms (SNPs) as instrumental variables to assess the causal effect of an exposure of focus (i.e., metabolite) on an outcome (i.e., ALS). The attractive strength of MR is that it is often less susceptible to reverse causation and confounders compared to other study designs since the two alleles of an SNP are randomly segregated under the Mendel's law and such segregation can be considered to be independent of many unmeasured or unknown confounders. More importantly, MR can be implemented with only publicly available summary statistics of the exposure and outcome rather than individual-level genotypes and phenotypes, circumventing privacy concerns stemming from data sharing (Pasaniuc and Price, 2016). Therefore, over the past few years MR has been widely applied to disentangle the causal relationship between an exposure and an outcome in various application fields (Greenland, 2000; Thomas and Conti, 2004; Tobin et al., 2004; Wheatley and Gray, 2004; Evans and Davey Smith, 2015; Davies et al., 2018; Zeng et al., 2019; Zeng and Zhou, 2019b; Yu et al., 2020a,b).

Hereby making full use of the latest GWAS summary statistics of 486 metabolites and five major NDDs, we conducted a two-sample MR analysis to assess the causal effects of metabolites on these diseases or vice versa. Extensive sensitivity analyses, including linkage disequilibrium (LD) score regression (LDSC) and colocalization analysis (Giambartolomei et al., 2014), were also implemented to investigate whether the MR findings could be driven by genetic similarity or confounding due to LD with causal genetic loci. Overall, we found that there existed a bidirectional causal association between three metabolites and two types of NDDs (i.e., ALS and FTD). We further demonstrated that the identified associations were robust against

Abbreviations: NDD, neurodegenerative disease; GWAS, genome-wide association study; MR, Mendelian randomization; AD, Alzheimer' s Disease; ALS, amyotrophic lateral sclerosis; FTD, frontotemporal dementia; PD, Parkinson' s disease; MS, multiple sclerosis; MR-PRESSO, Mendelian Randomization Pleiotropy RESidual Sum and Outlier; LDSC, linkage disequilibrium score regression; LD, linkage disequilibrium; FDR, false discover rate; SNP, single nucleotide polymorphisms; PVE, phenotypic variance explained; IVW, inverse-variance-weighted.

TABLE 1 | Genome-wide association study data sets of neurodegenerative diseases employed in our analysis.

Disease	Sample size	Case	Control	Number of SNPs	Data source (PMID)
AD	455,258	71,880	383,378	13,144,351	Jansen (30617256)
ALS	80,610	20,806	59,804	8,563,029	AVS (29566793)
FTD	12,928	3,526	9,462	4,812,662	IFGC (24943344)
PD	1,474,097	56,306	1,417,791	15,317,976	IPDGC (31701892)
MS	68,379	32,367	36,012	7,930,010	IMSGC (30343897)

AD, Alzheimer's disease; ALS, amyotrophic lateral sclerosis; FTD, frontotemporal dementia; PD, Parkinson's disease; MS, multiple sclerosis; SNP, single nucleotide polymorphism; AVS, the ALS Variant Server; IFGC, International FTD-Genomics consortium; IPDGC, International Parkinson's Disease Genomics consortium; IMSGC, International Multiple Sclerosis Genetics consortium.

used MR approaches and instrumental pleiotropy, and were not likely driven by shared genetic components or confounded by LD with common causal SNPs. We also identified multiple significant metabolic pathways that might be involved in the development of NDDs.

MATERIALS AND METHODS

Genome-Wide Association Study Data Sources

We obtained summary statistics of metabolites from the metabolomics GWAS (Shin et al., 2014), which was the most comprehensive study performed to date on human blood metabolites and was a meta-analysis of two cohorts including TwinsUK and KORA F4. After quality control, a total of 486 metabolites and approximately 2.1 million SNPs up to 7,824 individuals of European ancestry were reserved for analysis (Shin et al., 2014). These metabolites can be classified as being known (309) or unknown (177). These unknown metabolites indicated that their chemical identity had not yet been conclusively established. All known metabolites can be further classified into eight broad metabolic groups (i.e., amino acid, carbohydrate, cofactors and vitamin, energy, lipid, nucleotide, peptide, and xenobiotic metabolism) (Kanehisa et al., 2012). The association of every genetic variant with individual metabolites was analyzed using a linear additive regression with age and sex as covariates.

In addition, we yielded European-only summary statistics of five NDDs (**Table 1**), including AD (Jansen et al., 2019), ALS (Nicolas et al., 2018), FTD (Ferrari et al., 2014), PD (Nalls et al., 2019), and MS (International Multiple Sclerosis Genetics Consortium, 2019). The Manhattan and QQ plots of *P*-values are shown in **Supplementary Figures 1, 2**. Although a marked departure is observed in the QQ plots of some diseases (i.e., $\lambda = 1.13$ for MS), the estimated λ_{1000} and the intercept obtained by LDSC (Bulik-Sullivan et al., 2015) indicate that the observed inflation is mainly due to polygenic signals rather than confounding factors such as population stratification or cryptic relatedness (**Supplementary Table 1**). Therefore, the genomic control for test statistics is not necessary for of these NDDs.

Selection of Instrumental Variables

We generated a set of uncorrelated index SNPs serving as instrumental variables for each of metabolites using the clumping procedure of PLINK (version v1.90b3.38) (Purcell et al., 2007). Specifically, we set both the primary significance level and the secondary significance level for index SNPs to be 1.00E-5, the LD, and the physical distance to be 0.10 and 500kb, respectively. Genotypes of 503 European individuals from the 1000 Genomes Project were applied as the reference panel during clumping (The 1000 Genomes Project Consortium, 2015). The relaxed statistical threshold of 1.00E-5 was employed here because of the relatively small sample size of the metabolite GWAS. In practical MR studies, a smaller significance threshold (e.g., 1.00E-5) was generally used to explain a larger variation for power enhancement when few SNPs were available for the exposure at the genome-wide significance level of 5.00E-8 (Sanna et al., 2019). In addition, to avoid horizontal pleiotropy in instrumental variables, we further removed index SNPs that were located within 1 Mb of disease-associated loci and that may be potentially related to a given neurodegenerative disease if selected genetic variants had a Bonferroni-adjusted *P*-value less than 0.05 for that disease. This was a conservative manner protecting against the pleiotropic impact of instruments to ensure valid causal inference in MR analysis (Ahmad et al., 2015; Larsson et al., 2017; Zeng et al., 2019; Zeng and Zhou, 2019a; Yu et al., 2020a).

Causal Effect Estimation With Inverse-Variance-Weighted Mendelian Randomization Methods

For each index SNP that was utilized as instrumental variable in turn, we first examined whether it was strongly associated with the metabolite. To do so, we calculated the proportion of phenotypic variance of metabolite explained (PVE) by instruments using summary statistics using the approach proposed in Shim et al. (2015) and computed the *F* statistic to quantitatively measure the strength of instruments (Cragg and Donald, 1993; Burgess et al., 2017). The Cochran's Q test was applied to examine the heterogeneity in effect sizes of instruments to determine whether fixed or random-effects IVW method would be utilized (Thompson and Sharp, 1999). We then undertook the inverse-variance-weighted (IVW) MR analysis for one metabolite at a time to estimate its causal effect on each of the five diseases (Burgess et al., 2017; Hartwig et al., 2017; Yavorska and Burgess, 2017). We declared an association to be statistically significant if the false discovery rate (FDR) <0.05 (Benjamini and Hochberg, 1995).

Sensitivity Analyses for Identified Causal Associations

Based on the IVW MR analysis, we discovered several causal associations between metabolites and NDDs. However, these significant associations may reflect four explanations including: (1) *causality* from metabolites to NDDs, which indicates that the metabolites are risk factors related to the diseases; (2) *reverse causality* from NDDs to metabolites, which implies that the metabolites are biomarkers of the diseases; (3) *undetected horizontal pleiotropy*, which suggests the diseases and the metabolites may share common genetic foundation; and (4) *confounding* by LD among leading causal SNPs shared by metabolites and NDDs, which means that the observed associations are spurious (**Supplementary Figure 3**). Therefore, it is of importance to untangle the causal association from other explanations. To this aim, for each identified association we further implemented a series of sensitivity analyses: (i) the weighted median-based method (Bowden et al., 2016b) and the maximum likelihood method (Burgess et al., 2013) to evaluate

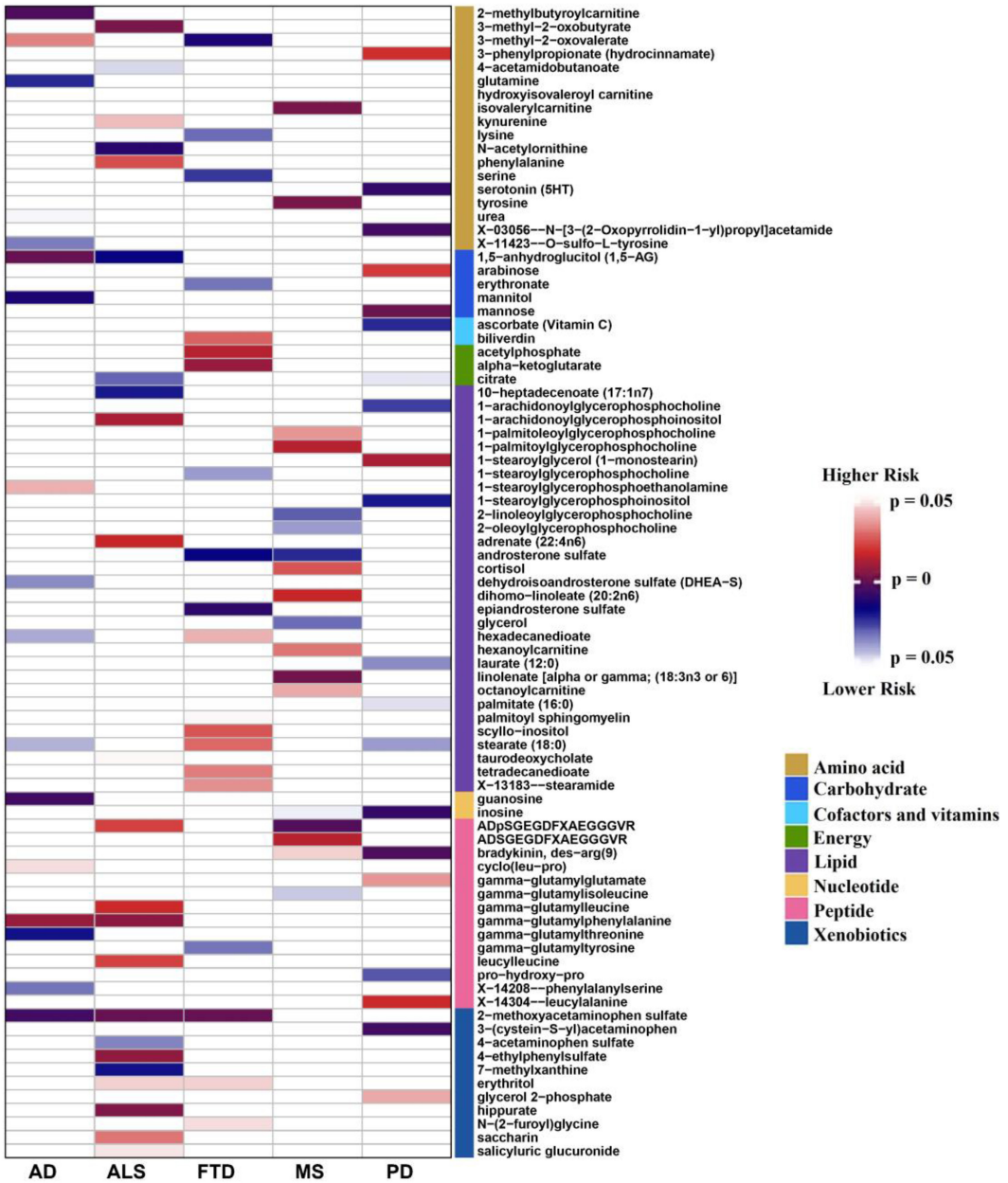

FIGURE 1 | Identified causal associations between known metabolites and the risk of five neurodegenerative diseases using the IVW MR analysis. IVW, inverse-variance weighted; AD: Alzheimer's disease; ALS: amyotrophic lateral sclerosis; FTD: frontotemporal dementia; PD: Parkinson's disease; MS: multiple sclerosis.

the robustness of the discovered associations; (ii) the MR-Egger regression (Bowden et al., 2016a; Burgess and Thompson, 2017) to detect directional pleiotropic effects of instruments; (iii) the MR-PRESSO test to assess horizontal pleiotropy and examine potential instrumental outliers (Verbanck et al., 2018); (iv) the reverse causality analysis with one of NDDs as the exposure and the identified metabolite as the outcome; the instrumental variables of these NDDs were selected *via* the similar PLINK clumping procedure described above but with a genome-wide significance level of 5E-8 (**Supplementary Material**); (v) the multivariable MR analysis to examine the independent relationship between one associated metabolite and NDDs while adjusting for the effects of other associated metabolites (Burgess et al., 2015); (vi) LDSC to assess the overall genetic correlation (r_g) using all available SNPs; (vii) the colocalization analysis to investigate whether the identified association between metabolites and NDDs was attributable to shared causal genetic variants (Giambartolomei et al., 2014; **Supplementary Material**).

Metabolic Pathway Analysis

We finally conducted a metabolic pathway analysis for identified metabolites *via* MetaboAnalyst (Chong et al., 2018) and exploited the functional enrichment analysis module to search potential metabolite pathways for metabolites that might be involved in biological processes of the five NDDs analyzed here. Our metabolic pathway analysis included two datasets: 99 metabolite sets from The Small Molecule Pathway Database (SMPDB; Frolkis et al., 2010) and 84 metabolite sets from the KEGG database (Kanehisa et al., 2012). SMPDB is designed to support pathway discovery in clinical metabolomics, transcriptomics, proteomics, and systems biology, and further provides diagrams of human metabolic and metabolite signaling pathways.

RESULTS

Causal Effects of the 486 Blood Metabolites on Neurodegenerative Diseases

The number of instrumental variables of metabolite varied from 4 to 585, with a median number of 29. These instrumental variables on average explained approximately 38.4% of phenotypic variance across all metabolites, and the minimum F statistic among all instruments was 20.8, indicating that weak instrumental bias is unlikely to occur and the used instruments for these metabolites were sufficiently informative (F statistic >10) for our MR analysis (**Supplementary Table 2**). Based on these instrumental variables we implemented the IVW MR analysis for each pair of metabolites and NDDs (**Supplementary Table 2**). We identified a total of 164 suggestive associations (136 unique metabolites) ($P < 0.05$), including 99 associations for 85 known metabolites and 65 associations for 51 unknown metabolites (**Supplementary Table 3**). Among these, 18, 23, 20, 20, and 18 associations of known metabolites (**Figure 1**) and 15, 12, 14, 13, and 11 associations of unknown metabolites (**Supplementary Figure 4**) are detected to be associated with the risk of AD, ALS, FTD, PD, and MS, respectively. However, after correcting multiple comparisons, we only obtain four significant associations (FDR < 0.05; involving three metabolites), including 2-methoxyacetaminophen sulfate with ALS [odd ratio (OR) = 0.971, 95% confidence intervals [CIs]: 0.961 $\sim$ 0.982, FDR = 1.04E-4] and FTD (OR = 0.924, 95%CIs: 0.885 $\sim$ 0.964, FDR = 0.048); X-11529 (OR = 1.604, 95%CIs: 1.250 $\sim$ 2.059, FDR = 0.048) and X-13429 (OR = 2.284, 95%CIs: 1.457 $\sim$ 3.581, FDR = 0.048) with FTD. Furthermore, we used a stricter r^2 threshold of <0.001 in the clumping procedure to avoid the inflation of test statistics. As a result, it is shown that the four associations are still significant, with consistent effects in direction magnitude (**Supplementary Table 4**). 2-methoxyacetaminophen sulfate, also known as 4-(acetylamino)-3-methoxyphenyl hydrogen sulfate, is a member of the acetamide class and has a role as a drug metabolite (Mrochek et al., 1974; Bozzoni et al., 2016). Acetamides have long been recognized to be related to levels of glutathione and N-acetylcysteine, which are known biomarkers for ALS (Przedborski et al., 1996) and other NDDs such as AD (Saharan and Mandal, 2014).

It is worth noting that 2-methoxyacetaminophen sulfate also exhibits a suggestive association with AD (OR = 0.998, 95%CIs: 0.996 $\sim$ 0.999, $P = 0.006$), implying shared metabolic mechanisms might exist among these NDDs. Moreover, 12 metabolites are suggestively related to at least two NDDs ($P < 0.05$) (**Table 2**). For example, besides 2-methoxyacetaminophen sulfate, 3-methyl-2-oxovalerate is also identified to be associated with both AD and FTD. In addition, we find the direction of causal effect sizes of some metabolites is inconsistent across NDDs, including 3-methyl-2-oxovalerate on AD (OR = 1.075, 95%CIs: 1.007 $\sim$ 1.148, $P = 0.031$) and FTD (OR = 0.148, 95%CIs: 0.033 $\sim$ 0.662, $P = 0.012$), hexadecanedioate on AD (OR = 0.971, 95%CIs: 0.945 $\sim$ 0.999, $P = 0.039$) and FTD (OR = 1.865, 95%CIs: 1.034 $\sim$ 3.362, $P = 0.038$), stearate (18:0) on AD (OR = 0.932, 95%CIs: 0.872 $\sim$ 0.997, $P = 0.040$) and FTD (OR = 4.780, 95%CIs: 1.193 $\sim$ 19.150, $P = 0.027$), ADpSGEGDFXAEGGGVR on ALS (OR = 1.363, 95%CIs: 1.048 $\sim$ 1.773, $P = 0.021$) and MS (OR = 0.580, 95%CIs: 0.407 $\sim$ 0.828, $P = 0.003$), suggesting potentially different functional roles of these metabolites implicated in NDDs. In brief, these findings provide important knowledge for understanding the metabolic mechanism underlying the relationship between metabolites and NDDs.

Results of Sensitivity Analyses

To evaluate the influence of horizontal pleiotropy on our MR estimates, we conducted sensitivity and pleiotropy analyses to examine the robustness of the four associations discovered above. Here we only show some important findings, with more complete and detailed results demonstrated in the **Supplementary Material**. First, it is displayed that these causal associations are robust against other MR methods except the MR-Egger regression (**Figure 2** and **Supplementary Table 5**). This might be that the MR-Egger method is substantially less efficient than other methods since it was proposed based on weaker modeling assumptions in causal inference. Second, the MR-PRESSO analysis offers little evidence for the presence

TABLE 2 | Overlapped known metabolites existing causal association with at least two neurodegenerative diseases.

Metabolites	AD		ALS		FTD		MS		PD	
	OR (95% CI)	*P*	OR (95% CI)	*P*	OR (95% CI)	*P*	OR (95% CI)	*P*	OR (95% CI)	*P*
M15676	1.08 (1.01 ~ 1.15)	0.031			0.15 (0.03 ~ 0.66)	0.012				
M20675	0.93 (0.89 ~ 0.97)	3.2E-4	0.71 (0.53 ~ 0.94)	0.017						
M01564			0.63 (0.41 ~ 0.96)	0.030					0.50 (0.25 ~ 0.99)	0.047
M31591					0.65 (0.46 ~ 0.93)	0.017	0.86 (0.75 ~ 0.98)	0.022		
M35678	0.97 (0.95 ~ 1.00)	0.039			1.87 (1.03 ~ 3.36)	0.038				
M01358	0.93 (0.87 ~ 1.00)	0.040			4.78 (1.19 ~ 19.2)	0.027			0.48 (0.24 ~ 0.96)	0.037
M01123							0.84 (0.71 ~ 1.00)	0.048	0.84 (0.73 ~ 0.95)	0.008
M33801			1.36 (1.05 ~ 1.77)	0.021			0.58 (0.41 ~ 0.83)	0.003		
M34420							1.14 (1.00 ~ 1.29)	0.043	0.84 (0.75 ~ 0.95)	0.004
M33422	1.10 (1.03 ~ 1.19)	0.008	1.96 (1.21 ~ 3.17)	0.006						
M33178	0.998 (0.996 ~ 0.999)	0.006	0.97 (0.96 ~ 0.98)	2.3E-7	0.92 (0.89 ~ 0.96)	2.6E-4				
M20699			1.34 (1.01 ~ 1.79)	0.043	3.14 (1.04 ~ 9.50)	0.043				

M15676, 3-methyl-2-oxovalerate; M20675, 1,5-anhydroglucitol (1,5-AG); M01564, citrate; M31591, androsterone sulfate; M35678, hexadecanedioate; M01358, stearate (18:0); M01123, inosine; M33801, ADpSGEGDFXAEGGGVR; M34420, bradykinin, des-arg(9); M33422, gamma-glutamylphenylalanine; M33178, 2-methoxyacetaminophen sulfate; M20699, erythritol, AD, Alzheimer's disease; ALS, amyotrophic lateral sclerosis; FTD, frontotemporal dementia; PD, Parkinson's disease; MS, multiple sclerosis.

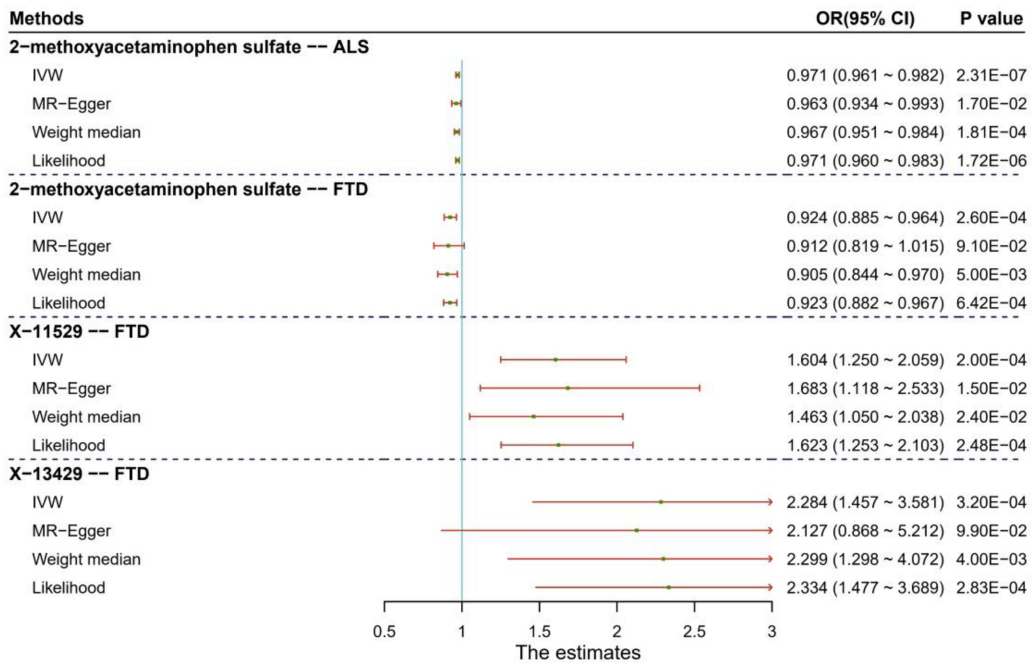

FIGURE 2 | Results of sensitivity analysis for the four significant causal associations identified between human blood metabolites and two types of neurodegenerative diseases (e.g., ALS and FTD). ALS: amyotrophic lateral sclerosis; FTD: frontotemporal dementia.

of horizontal pleiotropy ($P_{\text{MR−PRESSO global}} > 0.05$) and instrumental outliers ($P > 0.05$) (**Supplementary Figures 5, 6**). Third, the intercept of MR-Egger is not significantly deviated from zero, also indicating the absence of apparent horizontal pleiotropy (**Supplementary Table 5**). For the three associated metabolites identified above, to study whether the causal effect of one metabolite on FTD can be affected by the other two, we performed the multivariable MR analysis and find that, except X-11529, the direction and magnitude of the causal effects of other two metabolites (i.e., 2-methoxyacetaminophen sulfate and X-13429) are almost consistent with the unadjusted ones obtained *via* the IVW method (**Supplementary Table 6**), partly suggesting the independent role of these two metabolites in the risk of FTD.

We report another nine metabolites which have suggestive associations with the five NDDs ($P < 0.05$) in **Table 3**. For these associations, we also do not discover any evidence supporting horizontal pleiotropy, such as glutamine on AD ($P_{\text{MR−EggerIntercept}} = 0.065$, and $P_{\text{MR−PRESSOglobal}} = 0.444$),

TABLE 3 | Suggestive association metabolites passing all MR analyses at the nomial significance level of 0.05.

Metabolites	NDD	IVW		MR-Egger		Weight median		Likelihood	
		OR (95% CI)	*P*	OR (95% CI)	*P*	OR (95% CI)	*P*	OR (95% CI)	*P*
M00053	AD	0.81 (0.67 ∼ 0.97)	0.022	0.63 (0.45 ∼ 0.87)	0.010	0.72 (0.56 ∼ 0.93)	0.011	0.81 (0.67 ∼ 0.97)	0.021
M01573	AD	0.96 (0.92 ∼ 0.99)	0.006	0.91 (0.84 ∼ 0.99)	0.034	0.95 (0.91 ∼ 0.99)	0.024	0.96 (0.92 ∼ 0.99)	0.008
M00584	PD	2.69 (1.54 ∼ 4.70)	0.001	6.42 (1.19 ∼ 34.75)	0.032	3.62 (1.57 ∼ 8.39)	0.003	2.81 (1.46 ∼ 5.42)	0.002
M01564	PD	0.50 (0.25 ∼ 0.99)	0.047	0.10 (0.01 ∼ 0.85)	0.035	0.26 (0.09 ∼ 0.71)	0.009	0.49 (0.24 ∼ 0.99)	0.046
M34407	MS	1.71 (1.20 ∼ 2.45)	0.003	3.29 (1.02 ∼ 10.69)	0.047	2.53 (1.45 ∼ 4.42)	0.001	1.76 (1.11 ∼ 2.78)	0.016
M33782	ALS	1.17 (1.04 ∼ 1.31)	0.009	1.34 (1.05 ∼ 1.71)	0.023	1.21 (1.02 ∼ 1.44)	0.026	1.17 (1.02 ∼ 1.35)	0.027
M32855	FTD	2.22 (1.30 ∼ 3.78)	0.003	3.68 (1.35 ∼ 10.01)	0.014	2.72 (1.33 ∼ 5.57)	0.006	2.30 (1.34 ∼ 3.94)	0.002
M33163	FTD	9.54 (2.59 ∼ 35.09)	0.001	38.43 (1.71 ∼ 861.74)	0.024	11.68 (1.84 ∼ 74.03)	0.009	10.59 (2.76 ∼ 40.63)	0.001
M33192	PD	1.45 (1.16 ∼ 1.80)	0.001	1.74 (1.00 ∼ 3.02)	0.050	1.55 (1.16 ∼ 2.08)	0.003	1.46 (1.16 ∼ 1.83)	0.001

M00053, glutamine; M01573, guanosine; M00584, mannose; M01564, citrate; M34407, isovalerylcarnitine; M33782, X-10346; M32855, X-11538; M33163, X-11818; M33192, X-11847, AD, Alzheimer's disease; ALS, amyotrophic lateral sclerosis; FTD, frontotemporal dementia; PD, Parkinson's disease; MS, multiple sclerosis.

guanosine on AD ($P_{MR-Eggerintercept}$ = 0.244, and $P_{MR-PRESSOglobal}$ = 0.739), mannose on PD ($P_{MR-Eggerintercept}$ = 0.260, and $P_{MR-PRESSOglobal}$ = 0.162), citrate on PD ($P_{MR-Eggerintercept}$ = 0.115, and $P_{MR-PRESSOglobal}$ = 0.408) and isovalerylcarnitine on MS ($P_{MR-Eggerintercept}$ = 0.222, and $P_{MR-PRESSOglobal}$ = 0.410).

Bidirectional Mendelian Randomization Examining Reverse Association From Amyotrophic Lateral Sclerosis/Frontotemporal Dementia to Metabolites

For the four significant associations between metabolites and ALS/FTD identified above, we further carried out a MR analysis using instrumental variables of ALS/FTD to estimate their reverse causal effects on metabolites (**Supplementary Material**). We observe that ALS/FTD also can alter the level of metabolites at the nominal significance level of 0.05 (**Supplementary Table 7**), such as ALS on 2-methoxyacetaminophen sulfate (OR = 0.838, 95%CIs: 0.722 ∼ 0.972, *P* = 0.020), FTD on 2-methoxyacetaminophen sulfate (OR = 1.050, 95%CIs: 1.007 ∼ 1.095, *P* = 0.021), and FTD on X-11529 (OR = 0.976, 95%CIs: 0.961 ∼ 0.991, *P* = 0.002), implying that the emergence of possible bidirectional causal relationships between these metabolites and ALS/FTD.

In this reverse MR analysis, similar results are also generated by other MR tests ($P_{Likelihood}$ = 0.022 and $P_{MR-PRESSO}$ = 0.038 for ALS on 2-methoxyacetaminophen sulfate; $P_{Weight-median}$ = 0.030, $P_{Likelihood}$ = 0.021 and $P_{MR-PRESSO}$ = 3.44E-05 for FTD on 2-methoxyacetaminophen sulfate; $P_{Weight-median}$ = 0.009, $P_{Likelihood}$ = 0.002 and $P_{MR-PRESSO}$ = 0.001 for FTD on X-11529). Moreover, there is no evidence of horizontal pleiotropy for any association ($P_{MR-Egger\ intercept}$ = 0.975 and $P_{MR-PRESSO\ global}$ = 0.558 for ALS on 2-methoxyacetaminophen sulfate; $P_{MR-Egger\ intercept}$ = 0.416 and $P_{MR-PRESSO\ global}$ = 0.999 for FTD on 2-methoxyacetaminophen sulfate; $P_{MR-Egger\ intercept}$ = 0.347 and $P_{MR-PRESSO\ global}$ = 0.918 for FTD on X-11529) (**Supplementary Table 7** and **Supplementary Figures 7, 8**).

Causal Association Among Identified Metabolites

In order to acquire a much deeper insight into the association between the three metabolites and ALS/FTD, we performed an additional MR analysis to investigate the presence of causal relationship among these metabolites. Of interest, we ultimately observe several interaction associations between them (**Supplementary Table 8**), such as 2-methoxyacetaminophen sulfate on X-11529 (β = 0.012, 95%CIs: 0.002 ∼ 0.021, *P* = 0.012), X-11529 on X-13429 (β = 0.500, 95%CIs: 0.463 ∼ 0.537, *P* = 1.44E-153), suggesting that metabolites may interact to affect NDDs (**Figure 3**).

Genetic Correlation and Colocalization Analyses

To examine the alternative explanation of common genetic component, we undertook the LDSC and colocalization analyses to investigate whether the genetic associations underlying metabolites and ALS/FTD were likely due to shared causal genetic variants (**Supplementary Figure 3**). In terms of LDSC (**Supplementary Table 9**), we do not observe the existence of substantial genetic correlations (r_g = −0.107 and *P* = 0.370 between 2-methoxyacetaminophen sulfate and ALS; r_g = 0.116 and *P* = 0.589 between 2-methoxyacetaminophen sulfate and FTD; r_g = −0.151 and *P* = 0.771 between X-11529 and FTD; and r_g = −0.224 and *P* = 0.675 between X-13429 and FTD). However, we cannot fully rule out the possibility of low statistical power due to small sample sizes of metabolites. Furthermore, upon performing colocalization analysis (**Supplementary Table 10**), we do not find any evidence of colocalization for the four associations (the posterior probability that both metabolite and NDDs are associated with common causal genetic variants < 80%), suggesting that none of these MR findings could be driven by genetic confounding by LD with causal SNPs.

Metabolic Pathway Analysis

We were also interested in elucidating plausible metabolic pathways for the five NDDs. Therefore, we further carried out

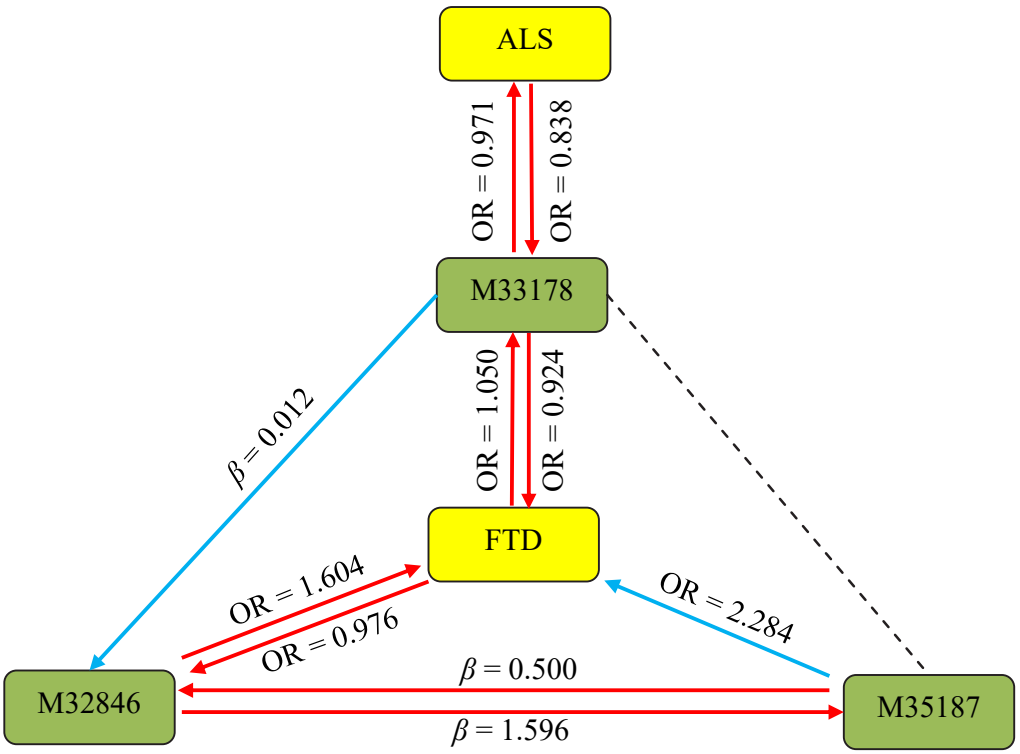

FIGURE 3 | Association pathways between three metabolites and ALS/FTD with MR analysis. M33178: 2-methoxyacetaminophen sulfate; M32846: X-11529; M35187: X-13429; ALS: amyotrophic lateral sclerosis; FTD: frontotemporal dementia. The solid arrow stands for the presence of the association, while the dot line represents the absence of the association.

the metabolic pathway analysis using all metabolites discovered through the IVW approach ($P < 0.05$), and identified seven significant metabolic pathways for these diseases except PD (**Table 4**). Among them, three pathways are separately related to ALS, FTD and MS, and four are associated with AD, including "urea cycle" ($P = 0.036$), "arginine biosynthesis" ($P = 0.004$), "purine metabolism" ($P = 0.009$), and "D-glutamine and D-glutamate metabolism" ($P = 0.042$). There exists a common metabolic pathway (i.e., phenylalanine, tyrosine and tryptophan biosynthesis) shared by ALS ($P = 0.046$) and MS ($P = 0.023$).

DISCUSSION

Leveraging genetic variants as proxies, in the present work we assessed the causal relationship between many metabolites and five NDDs using various statistical methods (Greenland, 2000; Thomas and Conti, 2004; Tobin et al., 2004; Wheatley and Gray, 2004; Evans and Davey Smith, 2015; Davies et al., 2018; Zeng et al., 2019; Zeng and Zhou, 2019b; Yu et al., 2020a,b). Totally, we discovered 164 suggestive associations, among which four were statistically significant for three metabolites, including 2-methoxyacetaminophen sulfate (known metabolite) affecting ALS and FTD, as well as X-11529 and X-13429 (unknown metabolites) affecting FTD. Genetic studies have revealed that ALS and FTD share a high extent of common genetic origin (Wood, 2011). If 2-methoxyacetaminophen sulfate is considered a promising metabolite that has an effect on both of the two diseases, then, 2-methoxyacetaminophen sulfate can be treated as a therapeutic biomarker of diseases. Due to limited understanding of the role of this metabolite in the specific pathophysiological mechanism of ALS and FTD, this would be a suggestive finding. We further demonstrated that there also existed a reverse association between these metabolites and ALS/FTD, implying a bidirectional influence on each other. Extensive sensitivity analyses showed that these associations were robust against used MR approaches and instrumental pleiotropy, and were not likely driven by shared genetic components or confounded by LD with common causal SNPs. In addition, we found these identified metabolites interacted to influence each other, implying that there might exist a complicated network among metabolites which impact NDDs in both direct and indirect manners. It needs to highlight that a complete investigation of such role of metabolites in NDDs is beyond the scope of this work as it requires additional methodological development, which we leave for future study. Furthermore, seven significant metabolic pathways involved in the five NDDs were also detected. Our metabolic pathway analysis showed that "phenylalanine, tyrosine and tryptophan biosynthesis" was associated with both ALS and MS. It should be noted that the onset age of MS is mainly 20–40 years old (Klineova and Lublin, 2018), which is relatively younger

TABLE 4 | Significant metabolic pathways involved in the five neurodegenerative diseases.

Traits	Metabolites pathway	Involved metabolites	*P*-value	Database
AD	Urea cycle	Urea, L-Glutamine	0.0364	SMPDB
AD	Arginine biosynthesis	Urea, L-Glutamine	0.0040	KEGG
AD	Purine metabolism	Guanosine, L-Glutamine	0.0093	KEGG
AD	D-Glutamine and D-glutamate metabolism	L-Glutamine	0.0421	KEGG
ALS	Phenylalanine, tyrosine and tryptophan biosynthesis	L-Phenylalanine	0.0459	KEGG
FTD	Carnitine synthesis	L-Lysine, Oxoglutaric acid	0.0441	SMPDB
MS	Phenylalanine, tyrosine and tryptophan biosynthesis	L-Tyrosine	0.0232	KEGG

AD, Alzheimer's disease; ALS, amyotrophic lateral sclerosis; FTD, frontotemporal dementia; MS, multiple sclerosis; KEGG, Kyoto encyclopedia of genes and genomes; SMPDB, small molecule pathway database.

than the average onset age of ALS. Whether phenylalanine has a mediation effect between ALS and MS needs to be further studied. In prior literature, tryptophan and competing neutral amino acid levels were found to be diminished in the plasma of patients with neurodegenerative diseases, the greatest decrease being of tryptophan (Monaco et al., 1979; Zhang et al., 2020). Evidence was also shown that higher serum phenylalanine concentrations related to immune activation are detectable in a subgroup of AD patients (Wissmann et al., 2013). The paired conversion of phenylalanine may affect not only the production of tyrosine but also the biosynthesis of the neurotransmitters dopamine, norepinephrine and epinephrine (Fernstrom and Fernstrom, 2007).

In conclusion, our findings provide an insightful perspective into the understanding of the relationship between metabolites and NDDs, and have important implications for pathology, drug development and clinical treatment. For example, given few effective drugs are available for these diseases (Al-Chalabi and Hardiman, 2013), these identified metabolites may be prioritized as candidate therapeutic targets for NDDs (Cummings et al., 2014; Lu et al., 2016), especially 2-methoxyacetaminophen sulfate for ALS or FTD. On the other hand, in terms of the findings in the reverse causality analysis, metabolites such as 2-methoxyacetaminophen sulfate can also serve as predictive biomarkers for the development of NDDs. Our study also found that some NDDs might share common metabolic mechanism, suggesting that multiple similar etiological pathways may give rise to different clinical manifestations (e.g., hexadecanedioate on AD and FTD) (Couratier et al., 2017; Ferrari et al., 2017; Broce et al., 2018; Karch et al., 2018; Abramzon et al., 2020). Overall, our study presents robust associations between multiple metabolites and NDDs, indicating the avenue for follow-up studies to improve the diagnostics, prevention and treatment of NDDs.

There are several strengths to our study. First, because it depends only on publicly available summary statistics rather than individual-level datasets, in the current work we can undertake a comprehensive MR causal inference evaluating the relationship between a large number of metabolites and NDDs in an unprecedented manner. Second, methodologically, in contrast to previous observational studies, our MR analysis implemented instrumental variable-based causal inference to assess the association between metabolites and NDDs, while minimizing the possibility of bias due to unknown confounding. Third, to provide robust MR assessment for identified associations, a wide range of sensitivity analyses were performed to distinguish causal effects from horizontal pleiotropy, reverse causation, and genetic confounding. However, this study also has some limitations. First, MR studies are generally recommended to be implemented using GWASs with large sample size; however, in our work the metabolite GWAS had a relatively small sample size, which may undermine the validity of our MR findings. Second, our study identified bidirectional causal relationships between metabolites (such as 2-methoxyacetaminophen sulfate) and NDDs (such as ALS); however, the small effect size would limit its potential utility as important biomarkers or therapeutic targets in practice. Third, we used a multivariate MR analysis to investigate whether metabolites interacted with each other to influence the causal effect of disease, but this method may be not unsuitable for unknown pleiotropy (Burgess et al., 2015). Fourth, metabolites levels are known to differ among cell and tissue types (Holmes et al., 2008; Wang et al., 2012; Shin et al., 2014); however, in this study we can only evaluate the influence of metabolites measured in blood on NDDs but unable to assess the relevance of metabolites levels in more biologically relevant tissues such as brain.

CONCLUSION

In summary, our study reveals robust bidirectional causal associations between servaral metabolites and neurodegenerative diseases, and provides a novel insight into metabolic mechanism for pathogenesis and therapeutic strategies of these diseases.

DATA AVAILABILITY STATEMENT

The original contributions presented in the study are included in the article/**Supplementary Material**, further inquiries can be directed to the corresponding author.

AUTHOR CONTRIBUTIONS

PZ conceived the idea for the study. PZ, TW, SH, and HC obtained the genetic data. PZ and SH developed the study

methods. PZ, TW, ZS, and HC performed the data analyses. PZ, ZS, JQ, and HC interpreted the results of the data analyses. PZ, JQ, and HC wrote the manuscript with suggestions from other authors. All authors contributed to the article and approved the submitted version.

FUNDING

The research of PZ was supported in part by the National Natural Science Foundation of China (82173630 and 81402765), the Youth Foundation of Humanity and Social Science funded by Ministry of Education of China (18YJC910002), the Natural Science Foundation of Jiangsu Province of China (BK20181472), the China Postdoctoral Science Foundation (2018M630607 and 2019T120465), the QingLan Research Project of Jiangsu Province for Outstanding Young Teachers, the Six-Talent Peaks Project in Jiangsu Province of China (WSN-087), the Training Project for Youth Teams of Science and Technology Innovation at Xuzhou Medical University (TD202008), and the Statistical Science Research Project from National Bureau of Statistics of China (2014LY112). The research of SH was supported in part by the Social Development Project of Xuzhou City (KC19017). The research of TW was supported in part by the Social Development Project of Xuzhou City (KC20062).

ACKNOWLEDGMENTS

We thank the complex traits genetic lab, ALS Variant Server, International FTD-Genomics consortium, International Parkinson's Disease Genomics consortium, International Multiple Sclerosis Genetics consortium for making the Alzheimer's disease, amyotrophic lateral sclerosis, frontotemporal dementia, Parkinson's disease, and multiple sclerosis summary data publicly available and are grateful of all the investigators and participants contributed to this study. The human blood metabolites data is publicly available from Metabolomics GWAS Server at http://metabolomics.helmholtz-muenchen.de/gwas/. The data analyses in the present study were carried out with the high-performance computing cluster that was supported by the special central finance project of local universities for Xuzhou Medical University. We thank two reviewers for their constructive comments, which substantially improved our manuscript.

SUPPLEMENTARY MATERIAL

The Supplementary Material for this article can be found online at: https://www.frontiersin.org/articles/10.3389/fnins.2021.680104/full#supplementary-material

REFERENCES

Abramzon, Y., Fratta, P., Traynor, B., and Chia, R. (2020). The overlapping genetics of amyotrophic lateral sclerosis and frontotemporal dementia. *Front. Neurosci.* 14:42. doi: 10.3389/fnins.2020.00042

Ahmad, O. S., Morris, J. A., Mujammami, M., Forgetta, V., Leong, A., Li, R., et al. (2015). A Mendelian randomization study of the effect of type-2 diabetes on coronary heart disease. *Nat. Commun.* 6:7060. doi: 10.1038/ncomms8060

Al-Chalabi, A., and Hardiman, O. (2013). The epidemiology of ALS: a conspiracy of genes, environment and time. *Nat. Rev. Neurol.* 9, 617–628. doi: 10.1038/nrneurol.2013.203

Amor, S., Puentes, F., Baker, D., and Van Der Valk, P. (2010). Inflammation in neurodegenerative diseases. *Immunology* 129, 154–169. doi: 10.1111/j.1365-2567.2009.03225.x

Bakhta, K., Cecillon, E., Lacombe, E., Lamy, M., Leboucher, A., and Philippe, J. (2019). Alzheimer's disease and neurodegenerative diseases in France. *Lancet* 394, 466–467. doi: 10.1016/s0140-6736(19)31633-2

Barnham, K. J., Masters, C. L., and Bush, A. I. (2004). Neurodegenerative diseases and oxidative stress. *Nat. Rev. Drug Discov.* 3, 205–214. doi: 10.1038/nrd1330

Benjamini, Y., and Hochberg, Y. (1995). Controlling the false discovery rate: a practical and powerful approach to multiple testing. *J. R. Statist. Soc. B* 57, 289–300. doi: 10.1111/j.2517-6161.1995.tb02031.x

Blennow, K., Hampel, H., Weiner, M., and Zetterberg, H. (2010). Cerebrospinal fluid and plasma biomarkers in Alzheimer disease. *Nat. Rev. Neurol.* 6, 131–144. doi: 10.1038/nrneurol.2010.4

Bowden, J., Smith, G. D., Haycock, P. C., and Burgess, S. (2016b). Consistent estimation in mendelian randomization with some invalid instruments using a weighted median estimator. *Genet. Epidemiol.* 40, 304–314. doi: 10.1002/gepi.21965

Bowden, J., Del Greco, M. F., Minelli, C., Smith, G. D., Sheehan, N. A., and Thompson, J. R. (2016a). Assessing the suitability of summary data for two-sample Mendelian randomization analyses using MR-Egger regression: the role of the I-2 statistic. *Int. J. Epidemiol.* 45, 1961–1974. doi: 10.1093/ije/dyw220

Bozzoni, V., Pansarasa, O., Diamanti, L., Nosari, G., Cereda, C., and Ceroni, M. (2016). Amyotrophic lateral sclerosis and environmental factors. *Funct. Neurol.* 31, 7–19. doi: 10.11138/fneur/2016.31.1.007

Broce, I., Karch, C. M., Wen, N., Fan, C. C., Wang, Y., Hong Tan, C., et al. (2018). Immune-related genetic enrichment in frontotemporal dementia: an analysis of genome-wide association studies. *PLoS Med.* 15:e1002487. doi: 10.1371/journal.pmed.1002487

Bulik-Sullivan, B., Finucane, H. K., Anttila, V., Gusev, A., Day, F. R., Loh, P.-R., et al. (2015). An atlas of genetic correlations across human diseases and traits. *Nat. Genet.* 47, 1236–1241. doi: 10.1038/ng.3406

Burgess, S., Butterworth, A., and Thompson, S. G. (2013). Mendelian randomization analysis with multiple genetic variants using summarized data. *Genet. Epidemiol.* 37, 658–665. doi: 10.1002/gepi.21758

Burgess, S., Dudbridge, F., and Thompson, S. G. (2015). Re: "Multivariable Mendelian randomization: the use of pleiotropic genetic variants to estimate causal effects". *Am. J. Epidemiol.* 181, 290–291. doi: 10.1093/aje/kwv017

Burgess, S., Small, D. S., and Thompson, S. G. (2017). A review of instrumental variable estimators for Mendelian randomization. *Stat. Methods Med. Res.* 26, 2333–2355. doi: 10.1177/0962280215597579

Burgess, S., and Thompson, S. G. (2017). Interpreting findings from Mendelian randomization using the MR-Egger method. *Eur. J. Epidemiol.* 32, 377–389. doi: 10.1007/s10654-017-0255-x

Chatterjee, P., Cheong, Y.-J., Bhatnagar, A., Goozee, K., Wu, Y., McKay, M., et al. (2020). Plasma metabolites associated with biomarker evidence of neurodegeneration in cognitively normal older adults. *J. Neurochem.* 159, 389–402. doi: 10.1111/jnc.15128 n/a(n/a),

Chong, J., Soufan, O., Li, C., Caraus, I., Li, S., Bourque, G., et al. (2018). MetaboAnalyst 4.0: towards more transparent and integrative metabolomics analysis. *Nucleic Acids Res.* 46, W486–W494. doi: 10.1093/nar/gky310

Couratier, P., Corcia, P., Lautrette, G., Nicol, M., and Marin, B. (2017). ALS and frontotemporal dementia belong to a common disease spectrum. *Rev. Neurol.* 173, 273–279. doi: 10.1016/j.neurol.2017.04.001

Cragg, J. G., and Donald, S. G. (1993). Testing identifiability and specification in instrumental variable models. *Econometric Theory* 9, 222–240.

Cummings, J. L., Morstorf, T., and Zhong, K. (2014). Alzheimer's disease drug-development pipeline: few candidates, frequent failures. *Alzheimers Res. Ther.* 6:37. doi: 10.1186/alzrt269

Davies, N. M., Holmes, M. V., and Davey Smith, G. (2018). Reading Mendelian randomisation studies: a guide, glossary, and checklist for clinicians. *Br. Med. J.* 362:k601. doi: 10.1136/bmj.k601

Doty, R. L. (2017). Olfactory dysfunction in neurodegenerative diseases: is there a common pathological substrate? *Lancet Neurol.* 16, 478–488. doi: 10.1016/s1474-4422(17)30123-0

Emerit, J., Edeas, M., and Bricaire, F. (2004). Neurodegenerative diseases and oxidative stress. *Biomed. Pharmacother.* 58, 39–46. doi: 10.1016/j.biopha.2003.11.004

Evans, D. M., and Davey Smith, G. (2015). Mendelian randomization: new applications in the coming age of hypothesis-free causality. *Annu. Rev. Genomics Hum. Genet.* 16, 327–350. doi: 10.1146/annurev-genom-090314-050016

Fernstrom, J. D., and Fernstrom, M. H. (2007). Tyrosine, phenylalanine, and catecholamine synthesis and function in the brain. *J. Nutr.* 137(6 Suppl. 1), 1539S–1547S. doi: 10.1093/jn/137.6.1539S discussion 1548S,

Ferrari, R., Hernandez, D. G., Nalls, M. A., Rohrer, J. D., Ramasamy, A., Kwok, J. B., et al. (2014). Frontotemporal dementia and its subtypes: a genome-wide association study. *Lancet Neurol.* 13, 686–699. doi: 10.1016/S1474-4422(14)70065-1

Ferrari, R., Wang, Y., Vandrovcova, J., Guelfi, S., Witeolar, A., Karch, C. M., et al. (2017). Genetic architecture of sporadic frontotemporal dementia and overlap with Alzheimer's and Parkinson's diseases. *J. Neurol. Neurosurg. Psychiatry* 88, 152–164. doi: 10.1136/jnnp-2016-314411

Frolkis, A., Knox, C., Lim, E., Jewison, T., Law, V., Hau, D. D., et al. (2010). SMPDB: the small molecule pathway database. *Nucleic Acids Res.* 38(Database issue), D480–D487. doi: 10.1093/nar/gkp1002

Giambartolomei, C., Vukcevic, D., Schadt, E. E., Franke, L., Hingorani, A. D., Wallace, C., et al. (2014). Bayesian test for colocalisation between pairs of genetic association studies using summary statistics. *PLoS Genet.* 10:e1004383. doi: 10.1371/journal.pgen.1004383

González-Domínguez, R., García-Barrera, T., and Gómez-Ariza, J. L. (2015). Metabolite profiling for the identification of altered metabolic pathways in Alzheimer's disease. *J. Pharm. Biomed. Anal.* 107, 75–81. doi: 10.1016/j.jpba.2014.10.010

Greenland, S. (2000). An introduction to instrumental variables for epidemiologists. *Int. J. Epidemiol.* 29, 722–729. doi: 10.1093/ije/29.4.722

Hartwig, F. P., Davey Smith, G., and Bowden, J. (2017). Robust inference in summary data Mendelian randomization via the zero modal pleiotropy assumption. *Int. J. Epidemiol.* 46, 1985–1998. doi: 10.1093/ije/dyx102

Holmes, E., Loo, R. L., Stamler, J., Bictash, M., Yap, I. K., Chan, Q., et al. (2008). Human metabolic phenotype diversity and its association with diet and blood pressure. *Nature* 453, 396–400. doi: 10.1038/nature06882

International Multiple Sclerosis Genetics Consortium (2019). Multiple sclerosis genomic map implicates peripheral immune cells and microglia in susceptibility. *Science* 365:eaav7188. doi: 10.1126/science.aav7188

Jansen, I. E., Savage, J. E., Watanabe, K., Bryois, J., Williams, D. M., Steinberg, S., et al. (2019). Genome-wide meta-analysis identifies new loci and functional pathways influencing Alzheimer's disease risk. *Nat. Genet.* 51, 404–413. doi: 10.1038/s41588-018-0311-9

Jiang, Y., Zhu, Z., Shi, J., An, Y., Zhang, K., Wang, Y., et al. (2019). Metabolomics in the development and progression of dementia: a systematic review. *Front. Neurosci.* 13:343. doi: 10.3389/fnins.2019.00343

Johnson, C. H., Ivanisevic, J., and Siuzdak, G. (2016). Metabolomics: beyond biomarkers and towards mechanisms. *Nat. Rev. Mol. Cell Biol.* 17, 451–459. doi: 10.1038/nrm.2016.25

Jové, M., Portero-Otín, M., Naudí, A., Ferrer, I., and Pamplona, R. (2014). Metabolomics of human brain aging and age-related neurodegenerative diseases. *J. Neuropathol. Exp. Neurol.* 73, 640–657. doi: 10.1097/nen.0000000000000091

Kanehisa, M., Goto, S., Sato, Y., Furumichi, M., and Tanabe, M. (2012). KEGG for integration and interpretation of large-scale molecular data sets. *Nucleic Acids Res.* 40(Database issue), D109–D114. doi: 10.1093/nar/gkr988

Karch, C. M., Wen, N., Fan, C. C., Yokoyama, J. S., Kouri, N., Ross, O. A., et al. (2018). Selective genetic overlap between amyotrophic lateral sclerosis and diseases of the frontotemporal dementia spectrum. *JAMA Neurol.* 75, 860–875. doi: 10.1001/jamaneurol.2018.0372

Kiddle, S. J., Sattlecker, M., Proitsi, P., Simmons, A., Westman, E., Bazenet, C., et al. (2014). Candidate blood proteome markers of Alzheimer's disease onset and progression: a systematic review and replication study. *J. Alzheimers Dis.* 38, 515–531. doi: 10.3233/jad-130380

Kim, M., Snowden, S., Suvitaival, T., Ali, A., Merkler, D. J., Ahmad, T., et al. (2019). Primary fatty amides in plasma associated with brain amyloid burden, hippocampal volume, and memory in the European Medical Information Framework for Alzheimer's Disease biomarker discovery cohort. *Alzheimers Dement.* 15, 817–827. doi: 10.1016/j.jalz.2019.03.004

Klineova, S., and Lublin, F. D. (2018). Clinical course of multiple sclerosis. *Cold Spring Harb. Perspect. Med.* 8:a028928. doi: 10.1101/cshperspect.a028928

Kori, M., Aydın, B., Unal, S., Arga, K. Y., and Kazan, D. (2016). Metabolic biomarkers and neurodegeneration: a pathway enrichment analysis of Alzheimer's disease, Parkinson's disease, and amyotrophic lateral sclerosis. *OMICS* 20, 645–661. doi: 10.1089/omi.2016.0106

Larsson, S. C., Burgess, S., and Michaëlsson, K. (2017). Association of genetic variants related to serum calcium levels with coronary artery disease and myocardial infarction. *JAMA* 318, 371–380. doi: 10.1001/jama.2017.8981

Leng, Y., Musiek, E. S., Hu, K., Cappuccio, F. P., and Yaffe, K. (2019). Association between circadian rhythms and neurodegenerative diseases. *Lancet Neurol.* 18, 307–318. doi: 10.1016/s1474-4422(18)30461-7

Lu, H., Le, W. D., Xie, Y.-Y., and Wang, X.-P. (2016). Current therapy of drugs in amyotrophic lateral sclerosis. *Curr. Neuropharmacol.* 14, 314–321. doi: 10.2174/1570159x14666160120152423

Mapstone, M., Cheema, A. K., Fiandaca, M. S., Zhong, X., Mhyre, T. R., MacArthur, L. H., et al. (2014). Plasma phospholipids identify antecedent memory impairment in older adults. *Nat. Med.* 20, 415–418. doi: 10.1038/nm.3466

Mendelsohn, A. R., and Larrick, J. W. (2013). Sleep facilitates clearance of metabolites from the brain: glymphatic function in aging and neurodegenerative diseases. *Rejuvenation Res.* 16, 518–523. doi: 10.1089/rej.2013.1530

Monaco, F., Fumero, S., Mondino, A., and Mutani, R. (1979). Plasma and cerebrospinal fluid tryptophan in multiple sclerosis and degenerative diseases. *J. Neurol. Neurosurg. Psychiatry* 42, 640–641. doi: 10.1136/jnnp.42.7.640

Mrochek, J. E., Katz, S., Christie, W. H., and Dinsmore, S. R. (1974). Acetaminophen metabolism in man, as determined by high-resolution liquid chromatography. *Clin. Chem.* 20, 1086–1096.

Nalls, M. A., Blauwendraat, C., Vallerga, C. L., Heilbron, K., Bandres-Ciga, S., Chang, D., et al. (2019). Identification of novel risk loci, causal insights, and heritable risk for Parkinson's disease: a meta-analysis of genome-wide association studies. *Lancet Neurol.* 18, 1091–1102. doi: 10.1016/s1474-4422(19)30320-5

Nicolas, A., Kenna, K. P., Renton, A. E., Ticozzi, N., Faghri, F., Chia, R., et al. (2018). Genome-wide analyses identify KIF5A as a novel ALS gene. *Neuron* 97, 1268–1283.e6. doi: 10.1016/j.neuron.2018.02.027

Parnetti, L. (2011). Biochemical diagnosis of neurodegenerative diseases gets closer. *Lancet Neurol.* 10, 203–205. doi: 10.1016/s1474-4422(11)70019-9

Pasaniuc, B., and Price, A. L. (2016). Dissecting the genetics of complex traits using summary association statistics. *Nat. Rev. Genet.* 18, 117–127. doi: 10.1038/nrg.2016.142

Przedborski, S., Donaldson, D., Jakowec, M., Kish, S. J., Guttman, M., Rosoklija, G., et al. (1996). Brain superoxide dismutase, catalase, and glutathione peroxidase activities in amyotrophic lateral sclerosis. *Ann. Neurol.* 39, 158–165. doi: 10.1002/ana.410390204

Purcell, S., Neale, B., Todd-Brown, K., Thomas, L., Ferreira, M. A., Bender, D., et al. (2007). PLINK: a tool set for whole-genome association and population-based linkage analyses. *Am. J. Hum. Genet.* 81, 559–575. doi: 10.1086/519795

Rachakonda, V., Pan, T. H., and Le, W. D. (2004). Biomarkers of neurodegenerative disorders: how good are they? *Cell Res.* 14, 347–358.

Roth, G. A., Abate, D., Abate, K. H., Abay, S. M., Abbafati, C., Abbasi, N., et al. (2018). Global, regional, and national age-sex-specific mortality for 282 causes of death in 195 countries and territories, 1980–2017: a systematic analysis for the Global Burden of Disease Study 2017. *Lancet* 392, 1736–1788. doi: 10.1016/S0140-6736(18)32203-7

Saharan, S., and Mandal, P. K. (2014). The emerging role of glutathione in Alzheimer's disease. *J. Alzheimers Dis.* 40, 519–529. doi: 10.3233/jad-132483

Sanna, S., van Zuydam, N. R., Mahajan, A., Kurilshikov, A., Vila, A. V., Vosa, U., et al. (2019). Causal relationships among the gut microbiome, short-chain fatty acids and metabolic diseases. *Nat. Genet.* 51, 600–+. doi: 10.1038/s41588-019-0350-x

Shang, L., Smith, J. A., and Zhou, X. (2020). Leveraging gene co-expression patterns to infer trait-relevant tissues in genome-wide association studies. *PLoS Genet.* 16:e1008734. doi: 10.1371/journal.pgen.1008734

Shim, H., Chasman, D. I., Smith, J. D., Mora, S., Ridker, P. M., Nickerson, D. A., et al. (2015). A multivariate genome-wide association analysis of 10 LDL subfractions, and their response to statin treatment, in 1868 Caucasians. *PLoS One* 10:e0120758. doi: 10.1371/journal.pone.0120758

Shin, S. Y., Fauman, E. B., Petersen, A. K., Krumsiek, J., Santos, R., Huang, J., et al. (2014). An atlas of genetic influences on human blood metabolites. *Nat. Genet.* 46, 543–550. doi: 10.1038/ng.2982

The 1000 Genomes Project Consortium (2015). A global reference for human genetic variation. *Nature* 526, 68–74. doi: 10.1038/nature15393

Thomas, D. C., and Conti, D. V. (2004). Commentary: the concept of 'Mendelian randomization'. *Int. J. Epidemiol.* 33, 21–25. doi: 10.1093/ije/dyh048

Thompson, S. G., and Sharp, S. J. (1999). Explaining heterogeneity in meta-analysis: a comparison of methods. *Stat. Med.* 18, 2693–2708. doi: 10.1002/(sici)1097-0258(19991030)18:20<2693::aid-sim235<3.0.co;2-v

To, T., Zhu, J., Stieb, D., Gray, N., Fong, I., Pinault, L., et al. (2019). Early life exposure to air pollution and incidence of childhood asthma, allergic rhinitis and eczema. *Eur. Respir. J.* 55:1900913. doi: 10.1183/13993003.00913-2019

Tobin, M. D., Minelli, C., Burton, P. R., and Thompson, J. R. (2004). Commentary: development of Mendelian randomization: from hypothesis test to 'Mendelian deconfounding'. *Int. J. Epidemiol.* 33, 26–29.

Trojanowski, J. (2000). Biochemical markers of neurodegenerative diseases: τ and synucleins. *Arch. Neurol.* 57, 1236–1236.

Verbanck, M., Chen, C. Y., Neale, B., and Do, R. (2018). Detection of widespread horizontal pleiotropy in causal relationships inferred from Mendelian randomization between complex traits and diseases. *Nat. Genet.* 50, 693–698. doi: 10.1038/s41588-018-0099-7

Wang, J., Wu, Z., Li, D., Li, N., Dindot, S. V., Satterfield, M. C., et al. (2012). Nutrition, epigenetics, and metabolic syndrome. *Antioxid. Redox Signal.* 17, 282–301. doi: 10.1089/ars.2011.4381

Wheatley, K., and Gray, R. (2004). Commentary: Mendelian randomization—an update on its use to evaluate allogeneic stem cell transplantation in leukaemia. *Int. J. Epidemiol.* 33, 15–17. doi: 10.1093/ije/dyg313

Wissmann, P., Geisler, S., Leblhuber, F., and Fuchs, D. (2013). Immune activation in patients with Alzheimer's disease is associated with high serum phenylalanine concentrations. *J. Neurol. Sci.* 329, 29–33. doi: 10.1016/j.jns.2013.03.007

Wood, H. (2011). A hexanucleotide repeat expansion in C9ORF72 links amyotrophic lateral sclerosis and frontotemporal dementia. *Nat. Rev. Neurol.* 7:595. doi: 10.1038/nrneurol.2011.162

Yavorska, O. O., and Burgess, S. (2017). MendelianRandomization: an R package for performing Mendelian randomization analyses using summarized data. *Int. J. Epidemiol.* 46, 1734–1739. doi: 10.1093/ije/dyx034

Yu, X., Wang, T., Chen, Y., Shen, Z., Gao, Y., Xiao, L., et al. (2020a). Alcohol drinking and amyotrophic lateral sclerosis: an instrumental variable causal inference. *Ann. Neurol.* 88, 195–198. doi: 10.1002/ana.25721

Yu, X., Yuan, Z., Lu, H., Gao, Y., Chen, H., Shao, Z., et al. (2020b). Relationship between birth weight and chronic kidney disease: evidence from systematics review and two-sample Mendelian randomization analysis. *Hum. Mol. Genet.* 29, 2261–2274. doi: 10.1093/hmg/ddaa074

Zeng, P., Wang, T., Zheng, J., and Zhou, X. (2019). Causal association of type 2 diabetes with amyotrophic lateral sclerosis: new evidence from Mendelian randomization using GWAS summary statistics. *BMC Med.* 17:225. doi: 10.1186/s12916-019-1448-9

Zeng, P., and Zhou, X. (2019b). Causal effects of blood lipids on amyotrophic lateral sclerosis: a Mendelian randomization study. *Hum. Mol. Genet.* 28, 688–697. doi: 10.1093/hmg/ddy384

Zeng, P., and Zhou, X. (2019a). Causal association between birth weight and adult diseases: evidence from a Mendelian randomization analysis. *Front. Genet.* 10:618. doi: 10.3389/fgene.2019.00618

Zhang, Q. J., Chen, Y., Zou, X. H., Hu, W., Ye, M. L., Guo, Q. F., et al. (2020). Promoting identification of amyotrophic lateral sclerosis based on label-free plasma spectroscopy. *Ann. Clin. Transl. Neurol.* 7, 2010–2018. doi: 10.1002/acn3.51194

Conflict of Interest: The authors declare that the research was conducted in the absence of any commercial or financial relationships that could be construed as a potential conflict of interest.

Publisher's Note: All claims expressed in this article are solely those of the authors and do not necessarily represent those of their affiliated organizations, or those of the publisher, the editors and the reviewers. Any product that may be evaluated in this article, or claim that may be made by its manufacturer, is not guaranteed or endorsed by the publisher.

frontiers in Molecular Neuroscience

REVIEW
published: 23 December 2021
doi: 10.3389/fnmol.2021.778955

Recent Advances in the Application Peptide and Peptoid in Diagnosis Biomarkers of Alzheimer's Disease in Blood

Yuxin Guo[1,2], Zhiyuan Hu[1,3,4,5] and Zihua Wang[3]**

[1] CAS Key Laboratory of Standardization and Measurement for Nanotechnology, CAS Key Laboratory for Biomedical Effects of Nanomaterials and Nanosafety, CAS Center for Excellence in Nanoscience, National Center for Nanoscience and Technology, Beijing, China, [2] University of Chinese Academy of Sciences, Beijing, China, [3] Fujian Provincial Key Laboratory of Brain Aging and Neurodegenerative Diseases, School of Basic Medical Sciences, Fujian Medical University, Fuzhou, China, [4] School of Nanoscience and Technology, Sino-Danish College, University of Chinese Academy of Sciences, Beijing, China, [5] School of Chemical Engineering and Pharmacy, Wuhan Institute of Technology, Wuhan, China

Alzheimer's disease (AD) is one of the most common neurodegenerative diseases with irreversible damage of the brain and a continuous pathophysiological process. Early detection and accurate diagnosis are essential for the early intervention of AD. Precise detection of blood biomarkers related to AD could provide a shortcut to identifying early-stage patients before symptoms. In recent years, targeting peptides or peptoids have been chosen as recognition elements in nano-sensors or fluorescence detection to increase the targeting specificity, while peptide-based probes were also developed considering their specific advantages. Peptide-based sensors and probes have been developed according to different strategies, such as natural receptors, high-throughput screening, or artificial design for AD detection. This review will briefly summarize the recent developments and trends of AD diagnosis platforms based on peptide and peptoid as recognition elements and provide insights into the application of peptide and peptoid with different sources and characteristics in the diagnosis of AD biomarkers.

Keywords: Alzheimer's disease, blood biomarkers, diagnosis, peptide, peptoid

OPEN ACCESS

Edited by:
Henrik Zetterberg,
University of Gothenburg, Sweden

Reviewed by:
Shannon Servoss,
University of Arkansas, United States
Homira Behbahani,
Karolinska Institutet (KI), Sweden

****Correspondence:***
Zhiyuan Hu
huzy@nanoctr.cn
Zihua Wang
wangzh@fjmu.edu.cn

Specialty section:
This article was submitted to Methods and Model Organisms, a section of the journal Frontiers in Molecular Neuroscience

Received: *17 September 2021*
Accepted: *06 December 2021*
Published: *23 December 2021*

Citation:
Guo Y, Hu Z and Wang Z (2021) Recent Advances in the Application Peptide and Peptoid in Diagnosis Biomarkers of Alzheimer's Disease in Blood. Front. Mol. Neurosci. 14:778955. doi: 10.3389/fnmol.2021.778955

INTRODUCTION

Alzheimer's disease (AD) is one of the most common neurodegenerative diseases, leading to a rapid decline in cognitive impairment. As a result of the aging population and the improvement of life quality, the number of people affected by AD will increase several times in the next few decades, from about 40 million at present to more than 100 million in 2050 (Scheltens et al., 2016; Hajipour et al., 2017; Hampel et al., 2018; Jia et al., 2018). AD is a chronic disease that gradually progresses over time. Before clinical symptoms appear, the patients have already had physiological changes in their brains and changes in the cerebrospinal fluid (CSF) concentration of related proteins (Blennow and Zetterberg, 2018). Diagnosis in the early stages means less disease progresses, conducive to disease intervention (Nordberg, 2015). Therefore, there is an urgent need for ideal AD diagnostic technology, which is non-invasive or minimally invasive, with high accuracy and facilitates large-scale screening to improve early diagnosis, primary care, and precision medicine (Hampel et al., 2018).

Currently, nano-biosensors and molecular probes have been developed in the field of biomarkers detection and molecular imaging with the aim of AD diagnosis (Kaushik et al., 2016; Jun et al., 2019; Yang et al., 2019; Bilal et al., 2020; Hanif et al., 2021). Due to the inherent characteristics of a high surface-area-to-volume ratio, targeting ligand surface modification and higher blood-brain barrier (BBB) permeability, nanomaterials have great potential in fast, selective and sensitive detection of biomarker (Gopalan et al., 2020). At the present time, the most widely used methods for AD fluid biomarkers detection by enzyme-linked immunosorbent assay (ELISA) based on commercial monoclonal antibodies (mAbs). However, due to the complicated production and high cost, but there are some limitations using traditional antibodies as detection receptors. The new emerging synthetic and bio-mimetic receptors such as peptide and small molecules have alternative bio-analytical approaches for AD biomarkers detection (Scarano et al., 2016).

In particular, peptide-based materials have recently been widely used in imaging, disease detection and drug delivery systems (Tweedle, 2009; Wang and Hu, 2019). Peptide and peptoid probes have also been proven to have great potential in detecting and diagnosing AD, which benefits from their small molecular weight, strong affinity and specificity, low immunogenicity, easy synthesis and modification (Baig et al., 2018b). On the one hand, as a recognition element, it binds explicitly to disease-related proteins to achieve high sensitivity and specificity, rapid, low-cost, and reliable biomarker detection (Baig et al., 2018a; Zafar et al., 2021). Due to their large number and diverse structures, it is relatively easy to find peptide ligands specifically binding to Aβ42 biomarkers compare with monoclonal antibody. On the other hand, peptide-based materials are promising to be used as Magnetic Resonance Imaging (MRI) contrast agents and imaging probes to visualize Aβ biomarkers to diagnose AD effectively (Gopalan et al., 2020). In addition, a peptide can self-assemble through intramolecular or intermolecular non-covalent bonds (such as electrostatic interaction, hydrogen bonding, van der Waals force, and π-π stacking, etc.) to form different nanostructures such as nanobelts, nanofibers, and so on (Wei et al., 2017). Peptide-based nanomaterials can provide enhanced surface area and binding sites to increase the accumulation of signal probes and bind particular peptide domains to display specific functions (Wei et al., 2017; Qi et al., 2018). As a result, self-assembled peptide nanomaterials have become one of the signal amplification strategies of biosensors in AD detection and imaging.

In this review, examples of the application of peptide-based materials to AD detection will be reported according to different sources and functions, and the method adopted for their selection and synthesis as well:

- Peptides from natural receptors or pronucleion peptides: stable artificial tiny receptors can be synthesized from known innate receptor sequences. For AD biomarkers, the most typical are cellular prion protein (PrPC), a natural Aβ oligomer receptor, and KLVFF (Aβ amino acid residues 16–20), the core area responsible for Aβ self-association and aggregation.
- Peptides from combinatorial peptide libraries: a variety of combinatorial libraries have been used for affinity peptide screening targeting AD biomarkers. Peptide library screening methods usually require little or no prior knowledge of the required sequence or structural features.
- Peptoid: peptoid is a peptide mimic with better protease resistance, stability, and enhanced pharmacological properties. Besides, peptoids have been designed as nanosheets with cyclic structures on the surface, mimicking the structure of antibodies.
- Enzyme-responsive peptides: as the Beta-secretase 1 (BACE1) enzyme also plays a vital role in AD pathology, peptides have been designed and synthesized as enzyme-responsive substrates to detect enzyme activity.

DIAGNOSIS OF ALZHEIMER'S DISEASE

At present, AD is considered to be a continuous process of neurological decline, which can be identified and staged by a combination of neuropathological findings and biomarkers in the body (Khoury and Ghossoub, 2019). Traditional AD biomarkers mainly include Aβ42, Aβ42/Aβ40, p-tau, and t-tau in CSF and blood. The accumulation and deposition of Aβ in the brain is a critical factor in the pathogenesis of AD and is used as a biomarker of AD (Selkoe et al., 1994; Nakamura et al., 2018). However, the absolute Aβ42 level is affected by many factors, and individual differences are apparent (Milà-Alomà et al., 2019). Since the concentration of Aβ40 in CSF is ten times higher than that of Aβ42 and its level usually does not change in AD (Lewczuk et al., 2017), the use of Aβ42/Aβ40 as an AD biomarker may be more reliable than the absolute value of Aβ42, that the AUC in the blood can reach 0.89 (Ovod et al., 2017). Hyperphosphorylation of tau protein leading to neurofibrillary tangles is another significant pathological sign of AD (Goedert, 1993; Alonso et al., 2001). In the brain of AD patients, the phosphorylation level is 3–4 times that of normal tau protein (Schöll et al., 2019). Among Tau-related biomarkers, t-tau has also been found to be elevated in a variety of neurological diseases, so it is considered to be a related biomarker of neuronal damage and has low specificity for AD (Schöll et al., 2019). As p-tau (especially p-tau181) is present at normal levels in most other neurodegenerative diseases, p-tau has higher sensitivity and specificity for differential diagnosis of AD and other diseases (Janelidze et al., 2020; Thijssen et al., 2020; Brickman et al., 2021). The high levels of p-tau181 in plasma and CSF may reflect early Tau abnormalities that predate tau-PET abnormalities. In addition, some new potential AD biomarkers are being studied. BACE1 is a key enzyme that initiates the formation of Aβ peptides, and studies have shown that the concentration and activity of BACE1 increase in patients with AD and Mild Cognitive Impairment (MCI) (Jankowsky et al., 2004; Zetterberg et al., 2008). In addition to senile plaques and neurofibrillary tangles (NFTs), neurodegeneration and synapse loss are also inevitable in AD and increase with the progress of AD, which is manifested by the existence of a large number of dystrophic axons and dendrites surrounded by activated glial cells in the AD brain (Serrano-Pozo et al., 2011; Park et al., 2020).

Neurofilament light chain (NfL) has been shown to be a biomarker of axon damage (Brureau et al., 2017). The destruction of the axon membrane releases NfL into the interstitial fluid, and finally into CSF and blood (Petzold, 2005). Many studies have shown that CSF and blood NfL levels increase with the progression of AD disease, and serum/plasma and cerebrospinal fluid NfL concentrations are highly correlated (Mattsson et al., 2017; Khalil et al., 2018; Preische et al., 2019). NfL has poor specificity for AD, but if combined with other indicators, it still has a high differential diagnosis value (Ashton et al., 2021; Cullen et al., 2021). Plasma NfL concentrations are increased in 13 neurodegenerative disorders and is not specific to AD.

Currently, AD diagnostic biomarkers include imaging, cerebrospinal fluid (CSF) detection and blood biomarkers. CSF biomarkers have high sensitivity and specificity and have been included in the diagnostic criteria for AD and used as biomarkers for the differential diagnosis of other types of dementia (Bjerke and Engelborghs, 2018). CSF is the most reliable and accurate biological fluid used for AD biomarker evaluation since CSF directly interacts with the extracellular space in the brain to reflect related biochemical/pathological changes (Blennow et al., 2015). However, the CSF extraction process is complex and invasive (CSF extraction requires professional equipment and lumbar puncture, which is not easy to be repeated many times), limiting its application in AD and MCI progression monitoring. Compared with CSF, the blood-based biomarkers of AD provide a cost- and time-effective way to enhance the utility of CSF (Henriksen et al., 2014; Dubois et al., 2016; Patricia et al., 2020). Because blood testing is clinical routines globally, allowing the use of existing systems to collect and process samples, blood-based AD biomarkers can meet the requirements of primary care settings to widely screen a large number of people (Hampel et al., 2018; Zou et al., 2020; Hansson, 2021). At the same time, blood biomarkers are conducive to multiple sampling and longitudinal studies. Blood-based testing would be widely available, easy and rapid to perform, and economical (Schneider et al., 2009; Crunkhorn, 2018; Hampel et al., 2018). Research on changes in biomarkers over time may show better results in AD screening and diagnosis (Weston et al., 2019; Moscoso et al., 2021). However, blood-based biomarkers have ultra-low concentrations (usually only a few to tens of pg/mL) and require ultra-sensitive sensors and analytical techniques to detect them (Andreasson et al., 2016). A recent study used immunoprecipitation-mass spectrometry (IP-MS) technology to score the ratio of APP669–711 to Aβ42 comprehensively and the ratio of Aβ40/Aβ42 to define whether the patient was AD positive or negative with 90% accuracy, further verifying the feasibility of using blood biomarkers to detect AD (Nakamura et al., 2018). AD-related imaging biomarkers mainly include MRI and Positron Emission Tomography (PET) diagnosis, which respectively reveal brain atrophy and the accumulation of amyloid, tau and other proteins in the brain (van Oostveen and de Lange, 2021). In addition to some tools and technologies currently in clinical trials, with the rapid development of optical probes, optical imaging not only has been used for fluorescence detection and imaging *in vitro* but also has become a reliable *in vivo* imaging tool (Arora et al., 2020).

PEPTIDE AND PEPTOID IN ALZHEIMER'S DISEASE DIAGNOSIS

Peptides From Natural Receptors or Pronucleon Peptides

Synthesizing stable artificial small receptors from known natural receptor sequences is one of the common methods to obtain targeted peptides. For AD biomarkers, cellular prion protein (PrP^C) is a high-affinity receptor specifically binding to Aβ oligomer (AβO), while not significantly binding to Aβ monomers or fibrils (Lauren et al., 2009; Chen et al., 2010). The core region of PrP^C interacting with AβOs is PrP_{95-110}, and the amino acid sequence is THSQWNKPSKPKTNMK, which is located in the unstructured N-terminal region of PrP^C. The peptide has been used as a recognition element in a variety of electrochemical sensing technologies such as square wave voltammetry (SWV), electrochemical impedance spectroscopy (EIS), linear sweep voltammetry (LSV) and differential pulse voltammetry (DPV), to achieve high-sensitivity detection of AD biomarkers and signal amplification, with the potential for CSF and blood detection (**Table 1**).

Rushworth et al. (2014) have conjugated the biotinylated PrP95–110 to a polymer-functionalized screen printing gold electrode through a biotin/Avidin bridge to construct a label-free electrical impedimetric biosensor. As the combination of AβO and various metal cations increases the surface current density of the sensor, the impedance decreases with the increase of AβO concentration with a linear range of 1 pM–1 μM, and a LOD of 0.5 pM. Xia et al. (2017) used AβO and AuNPs competitively combined with PrP95–110 fixed on the surface of the gold electrode to prevent AuNPs from accumulating on the surface of the electrode, thereby increasing the impedance. The charge transfer resistance is proportional to the Aβ concentration in the range of 0.1 nM–0.2 μM, and the detection limit is determined to be 45 pM (Xia et al., 2017). According to a similar principle, Xing et al. (2017) constructed an electrochemical sensor based on peptide-induced AgNPs aggregation with a detection range of 0.01–200 nM and a LOD of 6 pM. The method has been proved can be applied to the analysis of AβO in serum and artificial cerebrospinal fluid (aCSF) (Xing et al., 2017). Negahdary and Heli (2019) electrodeposited microporous gold nanostructures with high surface area to immobilize PrP95–110 with high surface concentration to amplify the electrical signal. Using ferrous/ferricyanide as the redox probe, the peak current of DPV obtained is linear with the concentration of Aβ in the range of 3–7000 pg/mL, and the detection limit is 0.2 pg/mL (Negahdary and Heli, 2019). Huang et al. (2021) proposed a new signal amplification strategy based on in-situ peptide self-assembly. They designed a cysteine-containing peptide CP4-PrP (95–110) immobilized on the surface of a gold electrode to capture AβO, and another ferrocene-coupled peptide C16-GGG-PrP (95–110)-Fc to identify the captured AβO. The C16 hydrophobic domain initiates the peptide self-assembly *in situ*, thereby generating the accumulation of ferrocene as an electroactive reporter and obtaining an amplified electrochemical signal. The SWV peak intensity of the sandwich electrochemical sensor thus constructed

TABLE 1 | Electrochemical biosensor based on Aβ peptides.

Method	Electrode	Identify element	Detection range	LOD	References
EIS	Screen printing gold electrode	PrP_{95-110}	1 pM–1 μM	0.5 pM	Rushworth et al., 2014
EIS	Gold electrode	PrP^{C}-AuNPs	0.1 nM–0.2 μM	45 pM	Xia et al., 2017
LSV	Gold electrode	Ad-PrP_{95-110}-AgNPs	0.01–200 nM	6 pM	Xing et al., 2017
DPV	Gold electrode	PrP_{95-110}	3–7000 pg/mL	0.2 pg/mL	Negahdary and Heli, 2019
SWV	Gold electrode	CP4-PrP_{95-110}, C16-GGG-PrP_{95-110}-Fc	0.005–5 μM	0.6 nM	Huang et al., 2021
SWV	Gold electrode	KLVFFEEEEEE	3.3–3300 pg/mL	1 pg/mL	Zhang et al., 2019

increases linearly with the concentration of AβO, ranging from 0.005 to 5 μM. The LOD is 0.6 nM, and the signal-to-noise ratio is 3. Zhang et al. (2019) developed an electrochemical sensor to evaluate the neurodegenerative ability of Aβ secreted by platelets in forming and catalyzing oxidative cross-linking. The detection range is 3.3–3300 pg/mL, LOD < 1 pg/mL. Li et al. (2012) constructed a peptide-based electrochemical biosensor for Aβ 42 soluble oligomer assay, and the concentration range from 480 pM to 12 nM. Matharu et al. (2015) was designed and synthesized an MRI probe R2 [Gd-(DOTA)Grffvlkrrrrrr-NH2] combining Aβ42 fragment with cell-penetrating peptide to obtain high resolution images of amyloid plaques in AD model mice. This potential peptide MRI contrast agents may give rise to lower background staining as they are hydrophilic in character, containing more clustered positively charged side chains, and chelated gadolinium ion (Matharu et al., 2015).

Studies have shown that KLVFF (amino acid residues 16–20), the central region of Aβ, is responsible for its polymerization and aggregation (Tjernberg et al., 1996). The sequence and its derived peptides are often used to selectively bind amyloid, thus developing various biosensing technologies, such as fluorescence assays, electrochemical biosensors, and immunoassays. Pradhan et al. (2015) used the aggregation-induced emission (AIE) molecule and peptide RGKLVFFGR, composed of the core region KLVFF and two terminal solubilizing components (RG–/–GR), to construct a fluorescent probe specifically binding to Aβ fibrils, which has a high signal-to-noise ratio and is not affected by traditional fluorescence quenchers. Sun et al. (2018) created a personalized array of lab-on-chip fluorescent peptide nanoparticles (f-PNPs) to detect multiple biomarkers in human blood samples. Taking Aβ as an example, the sequence of f-PNPs is WFAAACKLVFFC: KLVFF is used to bind to Aβ polypeptides, WF self-assembles into nanostructures, and cysteine cyclizes to protect the recognition sequence during self-assembly (**Figure 1A**). The change of fluorescence intensity and the morphological change of nanoparticles can significantly distinguish AD patients from healthy controls. Similarly, Liu et al. (2021) used KLVFF and Fmoc-KLVFF to self-assemble into f-PNPs through zinc coordination and π-π stacking, which can specifically detect Aβ aggregates (oligomers and fibrils) in the range of 10^{-4}-10^{-10} mg/mL, and have the potential to be used in blood sample detection of Aβ. Matveeva et al. (2017) proposed a new non-antibody detection method based on pronucleon peptides to capture Aβ oligomer called PLISA, with a similar principle to ELISA. The detection limit of PLISA is 0.35–1.5 pM, and its monomer cross-reactivity (monomer/oligomer percentage) is much lower than ELISA.

Due to its self-assembly capability, structural controllability and good biocompatibility, the sequence KLVFF is also used as a carrier for molecular probes or recognition elements to achieve the purpose of signal amplification. Lei et al. (2019) coupled sialic acid (SA) to the KLVFFAL (KL-7) sequence, and it self-assembled to form nanofibers to obtain high-density SA on the surface. They used the probe to study the interaction between SA and Aβ, as well as Aβ aggregation. The linear range is 2×10^{-5}–2×10^{1} nM, and the detection limit is 3.8×10^{-4} nM (**Figure 1B**). Subsequently, they used KL-7 loaded with Zn^{2+} specific dye AQZ and selective Cu^{2+}-responsive near-infrared quantum dots (NIR QD) to achieve multicolor imaging of the ratio of Zn^{2+} to Cu^{2+} in live cells and zebrafish (Lei et al., 2020).

In addition, this short peptide is also used as a "binding element" for the design of Aβ targeting inhibitors. Li et al. (2013) synthesized polyoxometalate (POM)-peptide mixed particles as a bifunctional Aβ inhibitor, which has an enhanced inhibitory effect on amyloid aggregation in the cerebrospinal fluid of mice. Du et al. (2018) synthesized a kind of magnetic nanoparticles (MNPs) modified with naphthimide-based fluorescent probes (NFP) and KLVFF peptides to improve the ability to recognize Aβ oligomers and penetrate BBB. While MNPs are exposed to an alternating magnetic field (AMF), Aβ aggregates decompose, the fluorescence of NFP is weakened and the morphological changes of Aβ can be monitored in real-time to realize the integration of diagnosis and treatment (**Figure 2**).

Peptides From Combinatorial Peptide Libraries

Combinatorial peptide libraries are often used for screening to identify valuable components, such as ligands and drug candidates (Gray and Brown, 2014). The main advantage of combinatorial peptide library screening is to generate many binding peptides from an utterly random library, which neither contains any designed peptide structure nor the elements of the planned construction. Unbiased screening can generally identify groups of peptides with different binding motifs. Therefore, peptide libraries provide an opportunity to discover previously unknown binding epitopes and motifs.

Phage display is one of the most commonly used methods to identify specific peptide ligands and is widely used to enhance the active targeting of nano-drug delivery vehicles, imaging probes, or as a recognition element for detection technologies (Wu et al., 2016). Phage display is to insert the DNA sequence

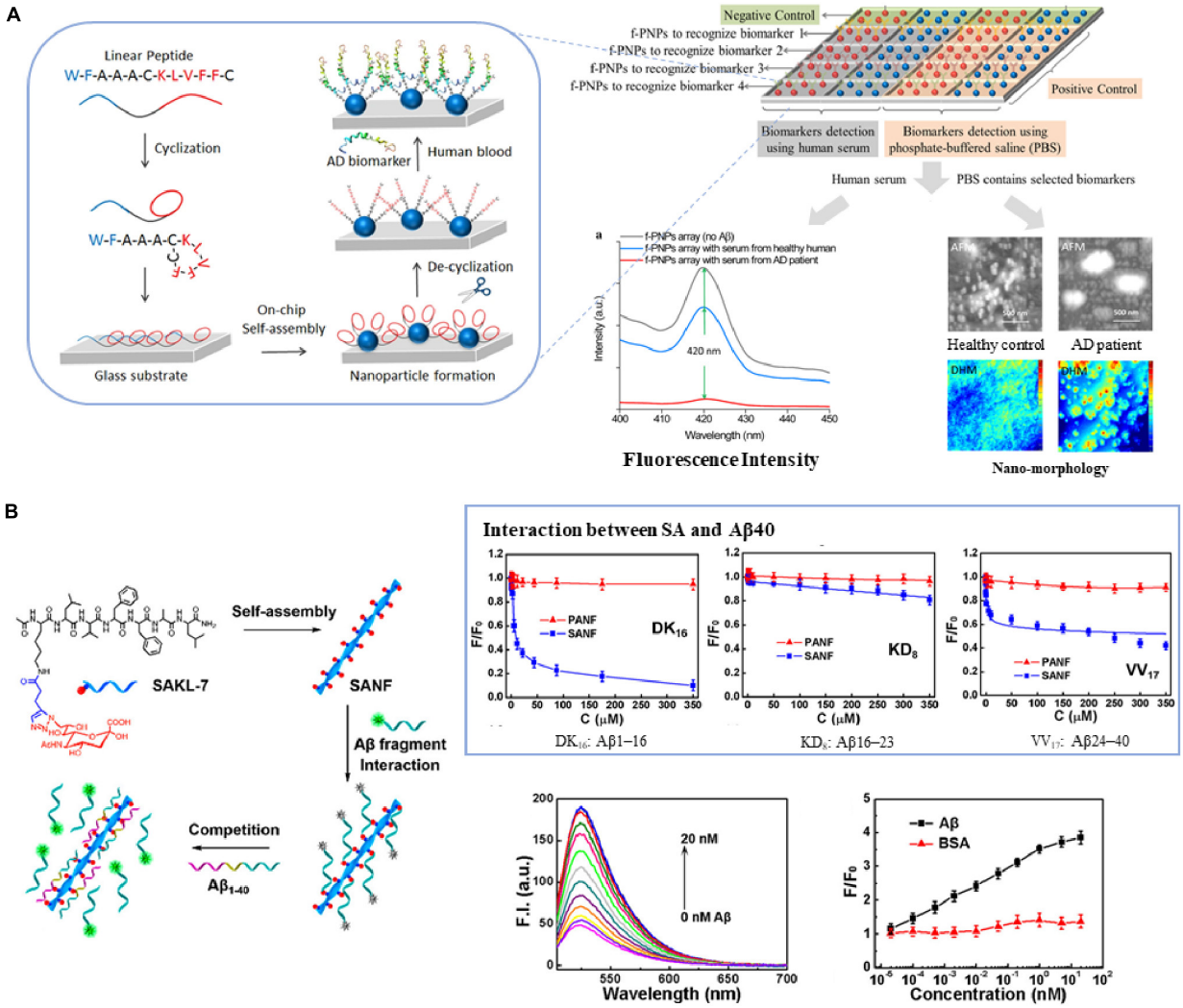

FIGURE 1 | The core region KLVFF of Aβ is used as **(A)** recognition element of biosensors (Sun et al., 2018), **(B)** carrier for signal amplification (Lei et al., 2019). Reproduced with permission.

encoding the random peptide library into the DNA of the phage coat protein. When the phage is assembled, the protein-peptide fusion is expressed and integrated on the surface of the phage so as to screen the peptide sequence that binds to the target of interest (Pande et al., 2010). Phage display libraries generally can contain 10^8 to 10^9 different peptide sequences, including cyclic peptides. Many studies have been using phage display for peptide selection *in vitro* or *in vivo* for AD detection, imaging, or drug delivery (**Table 2**).

Larbanoix et al. (2010, 2011) used phage libraries to screen Aβ-specific binding short peptides *in vitro*, and sequenced them to obtain four peptide sequences PHO, PHI, Pep1 and Pep2 with picomolar affinity. Some peptide-modified magnetic resonance imaging contrast agents can cross the blood-brain barrier and proved to be good candidates for Aβ42 imaging *in vivo*. Lee et al. (2019) used PHO and PHI peptides to design a polyvalent-directed peptide polymer (PDPP), aiming to enhance binding sensitivity and specificity by synergistically binding multiple target sites. And then, they modified it on the nanoporous zinc oxide with a high surface area to further improve the binding sensitivity and realize the detection of Aβ42 in CSF; the LOD can reach 12 ag/mL. Jokar et al. (2020) replaced all L-amino acids with D-type amino acids on the basis of Pep1, capped the C-terminus with an amide bond, and added D-proline and D-phenylalanine to the N-terminus, thus reducing the sensitivity to proteases, increasing brain uptake and inhibiting the formation of Aβ aggregates (**Figure 3A**; Jokar et al., 2020). They successfully synthesized ^{99m}Tc-Cp-GABA-D-(FPLIAIMA)-NH2 as a potential SPECT imaging agent for early detection of Aβ plaques in the brains of AD patients. In addition to the use of purified receptors for biopanning, Chen et al. (2019) chose to use the plasma of AD patients and healthy controls to obtain AD-specific peptide AD#1 and control-specific peptide Con#1. Among them, AD#1 is combined with recombinant human

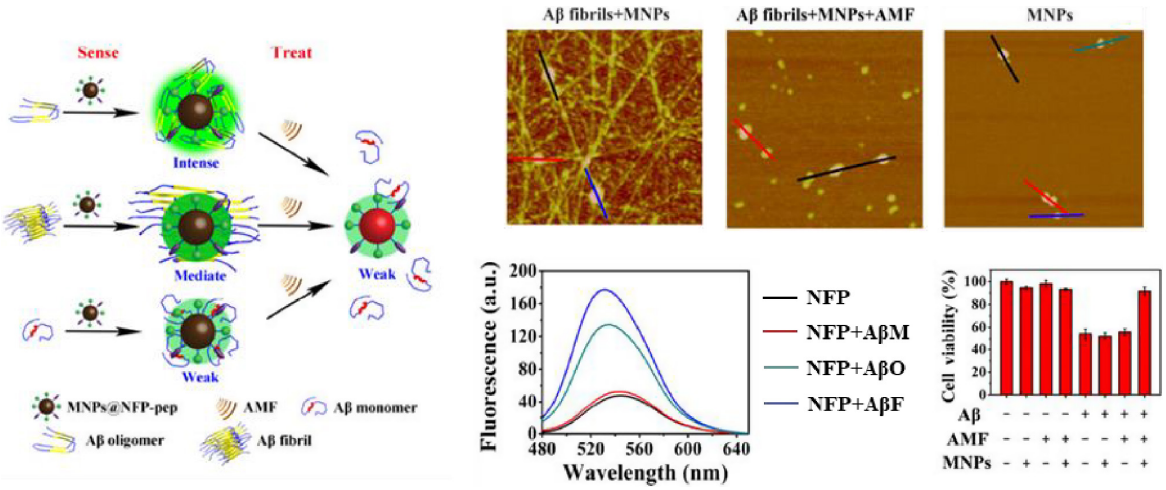

FIGURE 2 | The core region KLVFF of Aβ is used as a binding element for Aβ targeting inhibitors (Du et al., 2018). Reproduced with permission.

TABLE 2 | Aβ-targeting peptides identified from phage-display peptide libraries.

Biopanning	Sequence	Binding affinity	Application	References
Aβ42	CIPLPFYNC(PHO) CFRHMTEQC(PHI)	2.2 × 10^{-10} M 5.45 × 10^{-10} M	Detection of Aβ42 (Lee et al., 2019)	Larbanoix et al., 2010
Aβ42	LIAIMA(Pep1) IFALMG (Pep2)	2.63 × 10^{-6} M 1.11 × 10^{-6} M	SPECT imaging agent (Jokar et al., 2020)	Larbanoix et al., 2011
Recombinant Aβ42	SGVYKVAYDWQH SPHLHTSSPWER	10.09 ± 1.67 μM 1.93 ± 0.11 μM	–	Kim S.-H. et al., 2020
Plasmas	HMRQGMA (AD#1) DGARHGA (Con#1)	–	Early diagnosis of AD	Chen et al., 2019
In vivo	TPSYDTYAELR PMKSHTN TGNYKALHPHNG	–	*In vivo* optical imaging	Li et al., 2011, 2015; Yang et al., 2021
soluble Aβ42	RFRK	4.5 ± 0.5 × 10^{-5} M	Inhibit the formation of soluble Aβ42 oligomer	Kawasaki et al., 2011
D-Aβ(1–42)	QSHYRHISPAQV	0.4 μM	Probes for *in vivo* detection of Aβ	Wiesehan et al., 2003
D-enantiomeric PHF6 Fibril	D-TTSLQMRLYYPP D-APTLLRLHSLGA	–	Tau aggregation inhibitor	Dammers et al., 2016
D-enantiomeric PHF6 Fibril	NITMNSRRRRNH	–	Prohibit the formation of PHF6 fibrils	Zhang et al., 2020

YKL-40 protein in experiments *in vitro* (Chen et al., 2019). This screening method may be beneficial to obtain new valuable potential markers.

In recent years, phage display *in vivo* has received more and more attention because it completely replicates the natural physiological environment in the body and has the ability to screen peptides that target specific tissues (Andrieu et al., 2019). In this technique, the phage library is injected intravenously into live mice, rats and even humans, and then the phage is recovered from the tissues of interest. Due to the tight connection of the BBB and the efflux transport system, the delivery of drugs to the brain is severely restricted. *In vivo* phage technology facilitates screening peptides that can cross the BBB and blood-cerebrospinal fluid barrier (BCSFB). Li et al. (2011, 2015) successively used this technology to recover phage from rat cerebrospinal fluid to obtain several peptide sequences and verified their ability to pass through BBB or BCBFB by *in vivo* imaging analysis (Yang et al., 2021). They have the potential to construct drug delivery systems or imaging probes targeting the brain.

Because *E. coli* is easy to handle and multiplies, bacteria are also often used to display peptide libraries. In the *E. coli* library, the peptide gene is integrated into the membrane flagella and fimbriae protein and displayed on the surface of the bacteria. A typical library can combine up to 10^{11} different peptides (**Table 3**). Hecht and colleagues developed a method for co-expression of combined random peptides with the Aβ42-GFP fusion protein in *E. coli* (Wurth et al., 2002). When the construct is expressed recombinantly in *E. coli*, the Aβ42 sequence and the N-terminal fusion of GFP will cause aggregation and prevent proper folding and chromophore maturation, while the fused GFP can fold and emit bright fluorescence when Aβ42 is prevented from accumulation. Baine et al. (2009) used this method to screen short peptides that can inhibit the aggregation

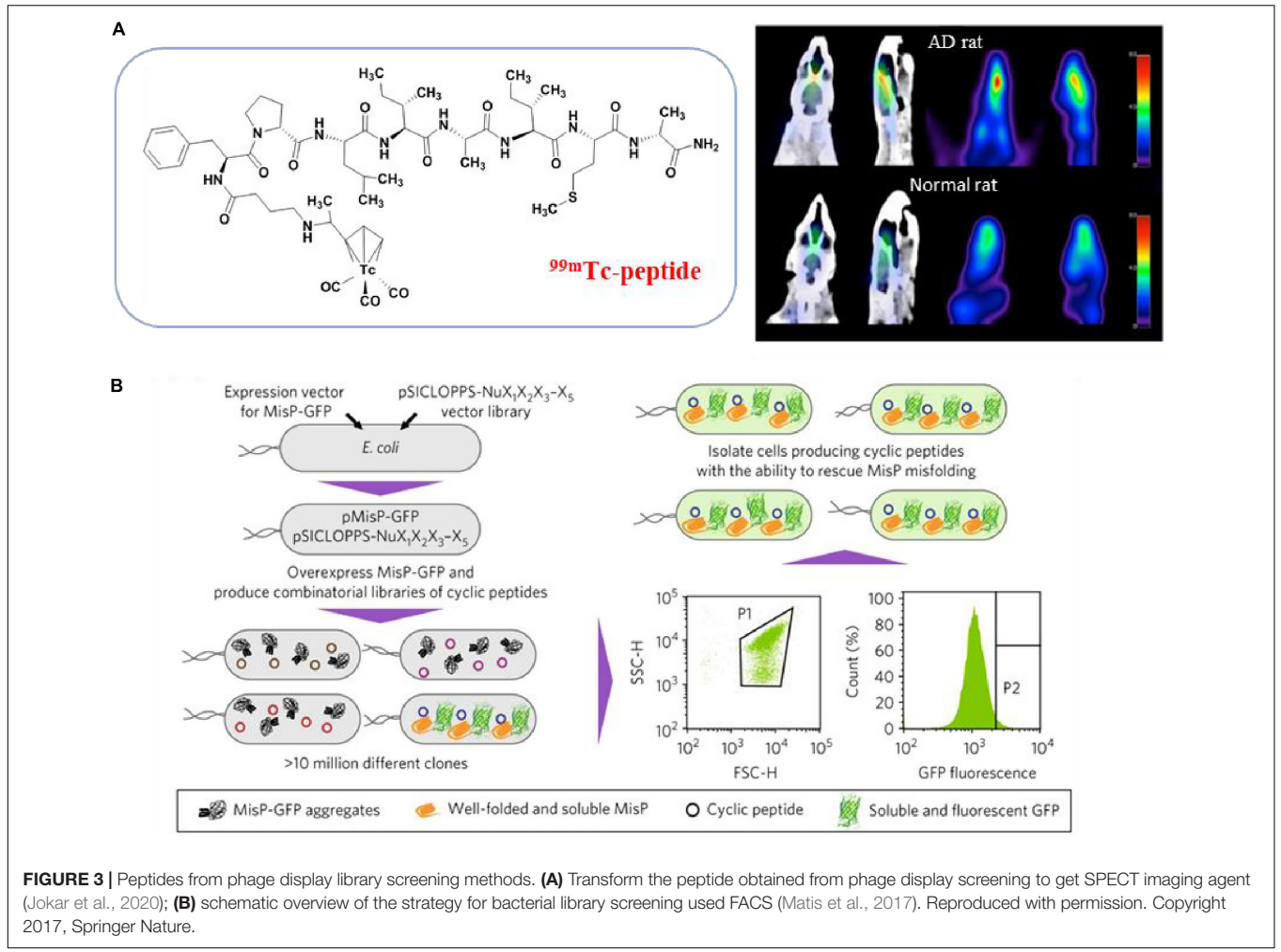

FIGURE 3 | Peptides from phage display library screening methods. **(A)** Transform the peptide obtained from phage display screening to get SPECT imaging agent (Jokar et al., 2020); **(B)** schematic overview of the strategy for bacterial library screening used FACS (Matis et al., 2017). Reproduced with permission. Copyright 2017, Springer Nature.

TABLE 3 | Aβ-targeting peptides identified from bacterial-display peptide libraries.

Receptor	Sequence	Library design	References
Aβ fibrils	NGRHVLRPKVQA VRHVLPKVQAPV	FliTrx random peptide library	Schwarzman et al., 2005
Aβ42	GDKAGAEVLAAVKAIKEK (Sv111)	Semi-random Library of Amphipathic Helices	Arslan et al., 2010
Aβ42	Peptide 1A (MSNKGASIGLMAGDVDIADSHS) Peptide 1B (MSNKGASNALMAGDGDIADSHS) Peptide 2 (MQKLDVVAEDAGSNK)	Designed to match the aggregation-prone regions of Aβ42	Baine et al., 2009
Aβ42	Cyclo-TPVWFD; cyclo-TAFDR, cyclo-TAWCR, cyclo-TTWCR, cyclo-TTVDR, cyclo-TTYAR, cyclo-TTTAR, and cyclo-SASPT	Combinatorial libraries of random cyclic tetra-, penta-, and hexapeptides	Matis et al., 2017
Aβ42	Cyclo-CKVWQLL (AβC7-1) cyclo-CRIVPSL (AβC7-14)	Random head-to-tail cyclic heptapeptide library	Delivoria et al., 2019

of Aβ42, and proved that the Peptide 2 they screened is one of the few peptides known to decompose preformed Aβ42 fibers. Arslan et al. (2010) predicted that the amphipathic helix could convert Aβ into a natural-like protein and inhibit the initiation of oligomerization and aggregation. They screened a semi-random amphipathic helix sequence library and replaced GFP with YFP to optimize the signal-to-noise ratio further. They also proved that the selected SV111 peptide could induce the natural-like structure in Aβ42 and inhibit the formation of amyloid fibrils. Since bacteria can be modified to incorporate fluorescent labels, another major advantage of bacterial libraries is the ability to use fluorescence activated cell sorting (FACS)

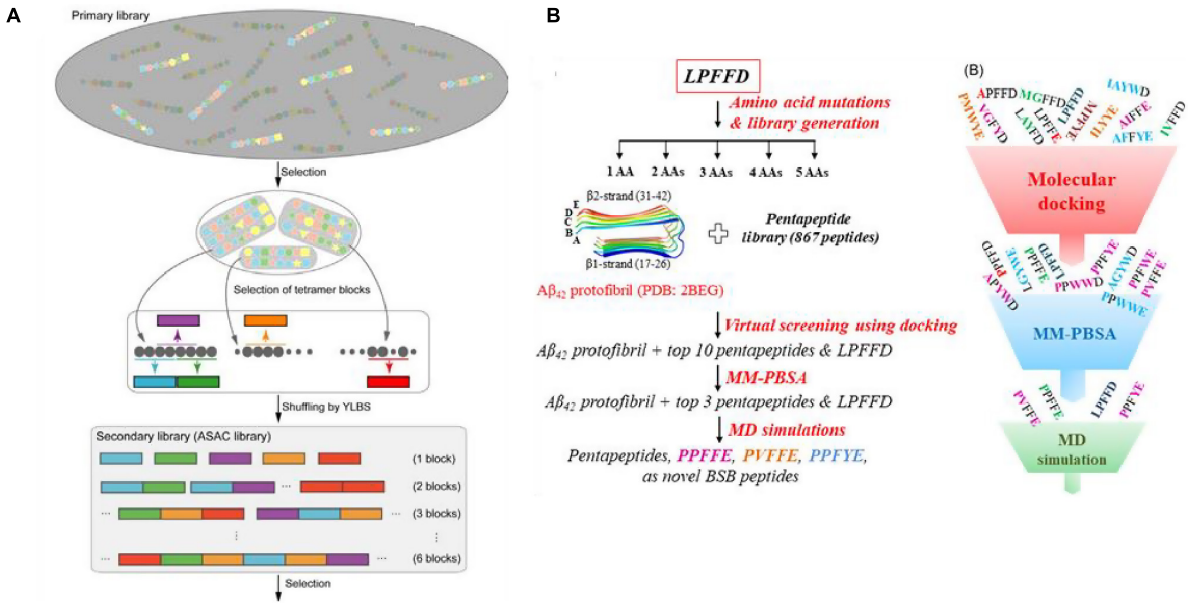

FIGURE 4 | (A) Illustration of the designated progressive library method (PLM) (Tsuji-Ueno et al., 2011; Ghimire Gautam et al., 2015); **(B)** schematic illustration of the *in silico* screening workflow for designing novel β-sheet breaker peptides (Shuaib et al., 2019). Reproduced with permission.

library screening, allowing quantification of clone binding. Skretas and colleagues synthesized large combinatorial libraries of macrocyclic molecules in *E. coli* cells, and used flow cytometry to screen cyclic peptides with the ability to rescue pathogenic protein misfolding and aggregation in an ultra-high-throughput manner (**Figure 3B**; Matis et al., 2017; Delivoria et al., 2019).

The cDNA display library has also been used for the screening of high-affinity Aβ binding peptides. Koichi and colleagues developed a systematic evolution *in vitro* and designated progressive library method (PLM) to obtain high-affinity peptide aptamers, which is to screen a diversified secondary peptide library constructed based on the information obtained from the primary library selection (**Figure 4A**; Tsuji-Ueno et al., 2011; Ghimire Gautam et al., 2015). In addition, computer screening has gradually begun to be applied in recent years. Based on the known β-sheet disruptor peptide LPFFD, Shuaib et al. (2019) used virtual screening based on molecular docking to identify pentapeptides with stronger binding affinity than LPFFD and utilized the MM-PBSA method to evaluate the binding free energy of the first 10 pentapeptides. Subsequently, molecular dynamics simulations were used to determine that the pentapeptides PPFFE, PVFFE, and PPFYE are potential BSB peptides for destroying the stability of the Aβ42 fibril structure (**Figure 4B**). Sievers et al. (2011) developed a non-natural D-peptide tau inhibitor (D)-TLKIVW (TLK) through a computational design based on the atomic structure of the tau aggregation motif (VQIVYK), and proved that it could be combined with tau aggregates instead of tau monomers through hydrogen bonding and hydrophobic interaction. Zhu et al. (2021) modified the multivalent TLK peptide to the surface of a multifunctional nanoinhibitor with core hydrophobic PCL and shell hydrophilic PEG. By capturing tau aggregates multivalently, the inhibitor not only effectively inhibits the growth of tau protein aggregates and prevents their spread across cells, but also promotes the proteolytic degradation of tau aggregates, and offers a potent and straightforward way to realize the tau-targeted treatment of AD.

Peptoid

In general, most peptides cannot be administered orally, have a short half-life, potential immunogenicity, and poor *in vivo* metabolic stability. Therefore, they are challenging to utilize directly in the biomedical field, often requiring delivery, modification or development of peptide mimics (Patch and Barron, 2002). As a synthetic, convenient, modular peptide mimic, peptoid developed in the late 1980s (Simon et al., 1992), has the same molecular skeleton as the peptide, but its side chain is attached to the amide nitrogen instead of the α-carbon, accompanied by loss of main chain chirality and amide hydrogens, as shown in **Figure 5A** (Ganesh et al., 2017). The peptide backbone is entirely composed of triamides, and the presentation of peptoid side chains is roughly equidistant, which may allow for an appropriate simulation of the spacing of critical groups of bioactive peptides. Besides, this modification confers protease resistance because natural proteases do not recognize N-substituted amide bonds (Saini and Verma, 2017). The lack of backbone chirality and amide hydrogens avoids the challenges of limiting production and interferes with the secondary structure, conferring much conformational flexibility in the main chain (Sun and Zuckermann, 2013). In the past few decades, the introduction of submonomer method has made the design and synthesis of peptoids more convenient and efficient, making the structure of peptoids flexible and rich in types (Zuckermann et al., 1992). In this strategy, peptoid monomers are synthesized

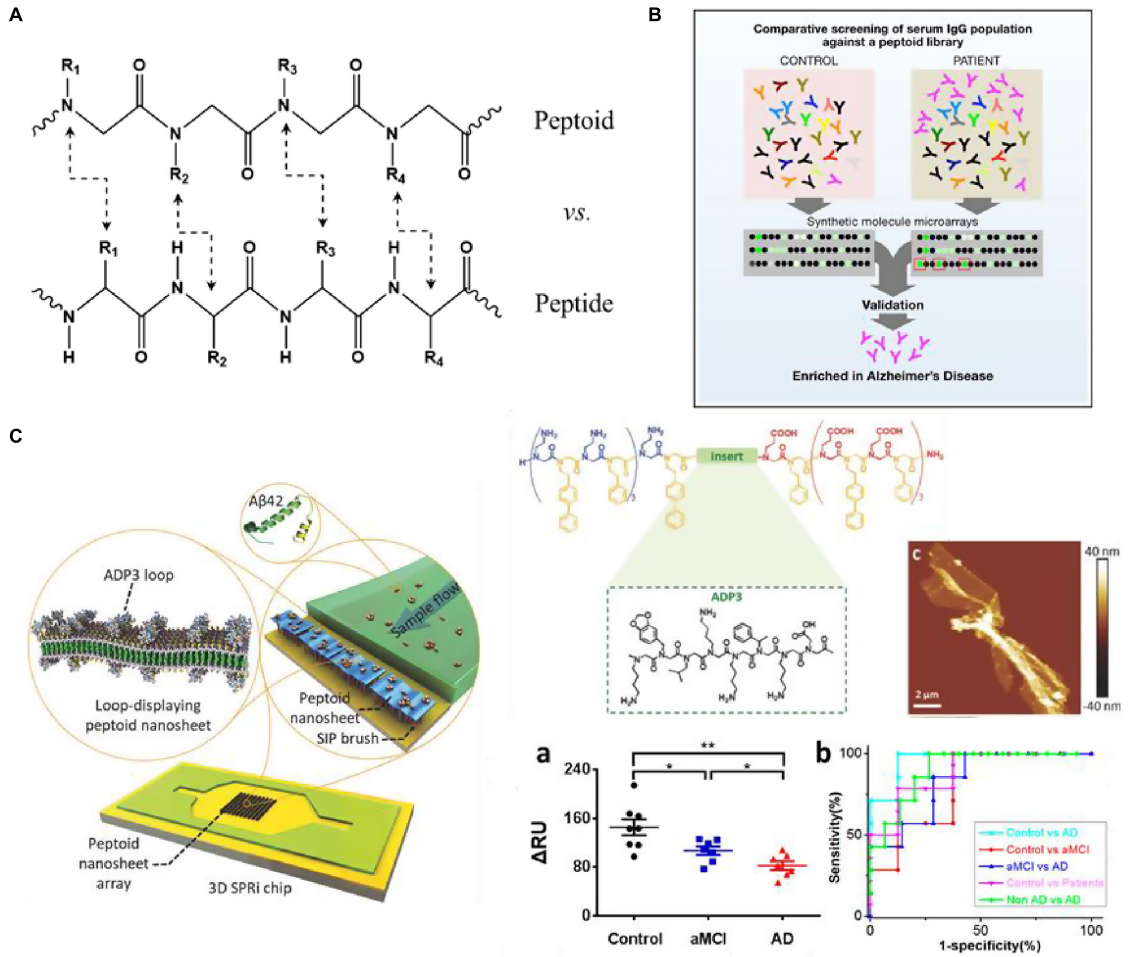

FIGURE 5 | (A) Chemical structure comparison of peptide and peptoid; **(B)** schematic overview of the process employed to screen peptoids that bind to antibodies present at higher levels in AD patients (Reddy et al., 2011); **(C)** structure of ADP3 microarray on 3D SPRi chip to develop a rapid, label-free sensor (Zhu et al., 2017; Gao et al., 2020). Reproduced with permission. Significance comparisons between groups were calculated by one-tailed unpaired *t*-test with Welch's correction. $^{*}P < 0.05$, $^{**}P < 0.01$.

in two steps: acylation reactions with bromoacetic acid followed by nucleophilic displacement of bromine with a primary amine. Coupled to better protease resistance and stability and enhanced pharmacological properties and activity, peptoids for biomedical applications can be an excellent platform as probes and sensors, also has broad application prospects in the field of AD detection and treatment (Vanderstichele and Kodadek, 2014).

2D nanomaterials have attracted widespread attention and research in recent years. The characteristics of engineered ability at the molecular level, chemical diversity, and synthesis flexibility compared to natural proteins and peptides make peptoids seem more suitable to fabricate highly tunable two-dimensional nanostructures through self-assembly (Lau, 2014). Zuckermann et al. (1992) used a water-soluble nanosheet with two molecular layers as an antibody simulation platform. At the gas-liquid interface, the amphiphilic peptoid molecules are tightly arranged to form a monomolecular layer under extrusion conditions (Nam et al., 2010). Then the monomolecular layer collapses toward the liquid surface, so that the hydrophilic part is exposed to the outside and the hydrophobic component is wrapped inside to form a stable Nanosheet structure. Then insert oligopeptide fragments with known recognition characteristics between the peptidomimetic sequences with periodic self-assembly motifs to create a nanosheet with a cyclic structure on the surface (Knight et al., 2015). This structure has better stability and lower cost than antibodies, thus having a good application prospect.

Reddy et al. (2011) used peptoid arrays to screen AD biomarkers, aiming to screen out a large number of synthetic molecules that can target antigen-binding sites without prior knowledge of natural antigens. Through the screening serum samples of six AD patients, six Parkinson's disease (PD) patients and 6 normal controls, they successfully selected 3 peptoids (ADP1-3) that specifically bind to IgG in AD serum from 4608 peptoids molecules (**Figure 5B**). And in the screening of 50 patients' serum samples, these three peptides showed good sensitivity and specificity for the diagnosis of AD (all

over 90%). Zhao et al. (2015) combined ADP3 microarray with surface plasmon resonance imaging (SPRi) to develop a rapid and label-free diagnostic method for AD, and demonstrated that high concentrations of ADP3 can recognize AD by binding to Aβ42 in serum. As shown in **Figure 5C**, they further inserted ADP3 into the amphiphilic peptoid to construct antibody mimics self-assembled peptoid nanosheets, including the surface-exposed Aβ42 recognition loop, as a label-free sensor used to detect AD serum (Zhu et al., 2017). The dense distribution of molecular recognition loops on the sturdy peptoid nanosheet scaffold mimics the structure of antibodies and reduces non-specific binding when detecting multi-component samples, further improving the sensitivity and accuracy of AD serum detection. Gao et al. (2020) used the peptoid nanosheet-SPRi sensor to measure the serum and plasma of patients with aMCI and AD and healthy controls. They proved that each group could be distinguished significantly with high sensitivity and specificity (AUC: 0.8–0.96) (Gao et al., 2020, 2021). This system is exquisitely sensitive, highly specific for AβOs and facilitates detection of biologically-relevant species in a complex matrix. Yazdani et al. (2016) identified a peptoid PD2 that can be useful for the early-stage identification of PD and serve as an indicator of disease severity. Gao et al. (2019) identified a peptoid ASBP-7 that recognizes α-synuclein in serum and provides a method for blood-based PD detection. Author further confirmed that ASBP-7 through specifically binding to α-synuclein in the serum can be effectively distinguished Parkinson's disease from serum of normal persons.

In addition, Luo et al. (2013) constructed a combinatorial peptide library with a library capacity of 38416 and obtained Aβ42 specific ligand IAM1 and its dimer (IAM1)2. Through dimerization, (IAM1)2 has a higher affinity with Aβ42 than (IAM)1. Both are promising to be used in the development of Aβ42 detection reagents or as lead therapeutic compounds, as they can effectively inhibit the aggregation of Aβ42 and reduce the neurotoxicity caused by Aβ42 *in vivo*.

Enzyme-Responsive Peptides

In recent years, enzyme-responsive peptides have been served as the "switch" of fluorescent probes as a simple and sensitive fluorescent biosensing platform for enzyme detection. BACE1 catalyzes the hydrolysis of the amyloid precursor protein, which is the rate-determining step of Aβ production; thus, it plays an essential role in the occurrence of AD and is considered a vital AD detection and therapeutic target (Esler and Wolfe, 2001; Luo et al., 2001; Evin et al., 2010). Using peptide substrates to develop a simple and rapid method to detect BACE1 and screen its inhibitors is conducive to AD's clinical diagnosis and treatment.

The APP Swedish mutation sequence (EVNLDAEF, representing residues 668-675) is a better BACE substrate than natural APP, and the enzyme cleavage between leucine and aspartic acid residues (Folk and Franz, 2010). Zuo et al. (2018) constructed a sensor platform based on WS2 nanosheets and the FAM-labeled peptide substrate, which can be adsorbed on the surface of the WS2 nanosheet to quench its fluorescence. In the presence of BACE1, BACE1 hydrolyzes the peptide substrate to release short FAM-linked peptide fragments, thereby restoring the fluorescent signal. The fluorescence sensing platform can be used to monitor BACE1 with a detection limit of 66 pM and has been proven to be suitable for screening BACE1 inhibitors. Kim S. et al. (2020) constructed a magnetic graphite oxide (MGO) alkenyl FRET biosensor, on which they synthesized an N-terminal FITC-labeled peptide specific to BACE1 (EVNLDA). The resonance energy transfer from FITC to MGO results in the quenching of the fluorescence generated from FITC. The fluorescence is restored after the BACE1 cleavage releases the FITC-peptide fragment. This method could successfully measure BACE1 in the range of 0.125 ng/mL to 1.2 μg/mL and construct imaging probes. Ge et al. (2020) developed a two-photon ratio fluorescent probe for the imaging and sensing of BACE1 in living cells and deep tissues, in which the peptide substrate connects the two-photon donor cyanine derivative (mCyd) with the acceptor Alexa Fluor 633 (AF633). The fluorescence emission ratio of AF633mCyd shows good linearity in the range of 0.1–40.0 nM, and LOD is reduced to 65.3 ± 0.1 pM. They successfully applied the probe to the imaging and sensing of BACE1 in different areas of the brain tissue of AD mice with a depth greater than 300 μm.

CONCLUSION AND PERSPECTIVE

In AD, although cerebrospinal fluid biomarkers are the most well-researched and widely accepted, blood biomarkers show greater prospects in the diagnosis of AD. The widespread application of blood biomarkers relies on the development and application of ultra-sensitive detection methods (Karki et al., 2021), so their accurate detection and quantification will greatly facilitate current and future diagnostic and therapeutic efforts. This review introduces the application of peptides or peptide mimics of different sources and functions as identification elements or carriers of biosensors or molecular probes in the highly sensitive detection and diagnosis of AD. The peptide is used as a non-antibody replacement recognition molecule with low immunogenicity, lower manufacturing cost, and easier access to chemical diversity. Also, because of its small size, it has a better ability to pass through the blood-brain barrier. Self-assembled peptides provide enhanced surface area and binding sites to increase the accumulation of signal probes and bind to special peptide domains to display specific functions, serving as a signal amplification strategy in biosensors. A variety of peptide-based biosensors have been shown potential for detecting blood biomarkers due to their pg-level detection sensitivity.

Nevertheless, there has been no success in the clinical translation of these peptide-based approaches, which require further development to meet the needs of early detection and clinical diagnosis. Future studies should consider the following significant items. First, screening for higher-affinity peptides targeting AD biomarkers remains a considerable challenge, with currently the most reliable peptides for biosensors still derived from native ligands. And most of the peptides or peptoids now used in AD detection are for Aβ or Tau-related biomarkers, but studies have shown that new biomarkers are needed to track non-Aβ and non-tau pathology (Park et al., 2020). Second,

future detection methods should be established closer to the clinical standards, rigorous control of assay performance is essential (Andreasson et al., 2015). The standard calibration curve and LOD measurements of some approaches are based on a simple system with pure proteins, which does not effectively indicate whether it is still effective on complex fluids. In contrast, others use the standard addition method in which the use of labeled proteins may prevent these studies from comparing to each other. Alternatively, differences between the calibrator and the endogenous analyte can make the specificity of the assay difficult to determine, so it's usually necessary to investigating the parallelism. The repeatability and reproducibility of the test method should also be checked. Recently, the ultrasensitive immunoassay technique (single-molecule array, Simoa) has achieved great progress in the sensitive detection of plasma A β and p-tau (Chatterjee et al., 2021). However, early and effective diagnosis of AD remains a challenge due to the complexity of AD pathogenesis, which leads to production of several related biomarkers and lack of reproducibility. In addition, the combination of multiple biomarkers can greatly improve diagnostic sensitivity and specificity (Kim K. et al., 2020; Cullen et al., 2021). The challenge is to use peptide ligand with different specificities to develop multiple devices and establish multiple detection of several AD biomarkers in the same sample solution.

Due to the differences in sensitivity and detection thresholds reported in different studies, it is difficult to use the same standard to evaluate. To confirm the validity of AD candidate blood biomarkers, the sampling, processing and analysis methods should be standardized to ensure reproducibility of results while minimizing variability between laboratories. In addition, large samples should be evaluated to assess the concentration range of biomarkers in the clinical routine. With the establishment of more and more AD biomarkers and the development of detection methods, peptide nanomaterials are currently under-utilized in the early diagnosis of AD and its potential warrants further exploration (Scarano et al., 2016). In the future, blood-based biomarkers could potentially be applied to clinical routine practice and point-of-care testing to monitor the AD progress and efficacy of disease therapies in individual patients.

AUTHOR CONTRIBUTIONS

YG and ZW wrote the manuscript. ZH revised the manuscript and supervision. All the authors approved the manuscript.

FUNDING

This work was supported financially by the National Natural Science Foundation of China (Grant Nos. 32027801, 81801766, and 31870992), the Joint Funds for the innovation of Science and Technology Fujian Province (Grant No. 2019Y9001), the Natural Science Foundation of Fujian Province (Grant No. 2020J01599), the Strategic Priority Research Program of Chinese Academy of Sciences (Grant Nos. XDB36000000 and XDB38010400), Science and Technology Service Network Initiative of the Chinese Academy of Sciences (Grant No. KFJ-STS-ZDTP-079), CAS-JSPS (Grant No. GJHZ2094), Fujian Medical University Foundation for the Introduction of Talents (Grant Nos. XRCZX 2019018, XRCZX2017020, and XRCZX2019005), and Key Laboratory of Biomedical Effects of Nanomaterials and Nanosafety, CAS (Grant No. NSKF202018).

REFERENCES

Alonso, A. D., Zaidi, T., Novak, M., Grundke-Iqbal, I., and Iqbal, K. (2001). Hyperphosphorylation induces self-assembly of tau into tangles of paired helical filaments/straight filaments. *Proc. Natl. Acad. Sci. U.S.A.* 98, 6923–6928. doi: 10.1073/pnas.121119298

Andreasson, U., Blennow, K., and Zetterberg, H. (2016). Update on ultrasensitive technologies to facilitate research on blood biomarkers for central nervous system disorders. *Alzheimers Dement.* 3, 98–102. doi: 10.1016/j.dadm.2016.05.005

Andreasson, U., Perret-Liaudet, A., Van Waalwijk Van Doorn, L. J. C., Blennow, K., Chiasserini, D., Engelborghs, S., et al. (2015). A practical guide to immunoassay method validation. *Front. Neurol.* 6:179. doi: 10.3389/fneur.2015.00179

Andrieu, J., Re, F., Russo, L., and Nicotra, F. (2019). Phage-displayed peptides targeting specific tissues and organs. *J. Drug Targeting* 27, 555–565. doi: 10.1080/1061186X.2018.1531419

Arora, H., Ramesh, M., Rajasekhar, K., and Govindaraju, T. (2020). Molecular tools to detect alloforms of Aβ and Tau: implications for multiplexing and multimodal diagnosis of alzheimer's disease. *Bull. Chem. Soc. Jpn* 93, 507–546.

Arslan, P. E., Mulligan, V. K., Ho, S., and Chakrabartty, A. (2010). Conversion of Aβ42 into a folded soluble native-like protein using a semi-random library of amphipathic helices. *J. Mol. Biol.* 396, 1284–1294. doi: 10.1016/j.jmb.2009.12.019

Ashton, N. J., Janelidze, S., Al Khleifat, A., Leuzy, A., Van Der Ende, E. L., Karikari, T. K., et al. (2021). A multicentre validation study of the diagnostic value of plasma neurofilament light. *Nat. Commun.* 12:3400. doi: 10.1038/s41467-021-23620-z

Baig, M. H., Ahmad, K., Saeed, M., Alharbi, A. M., Barreto, G. E., Ashraf, G. M., et al. (2018b). Peptide based therapeutics and their use for the treatment of neurodegenerative and other diseases. *Biomed. Pharmacother.* 103, 574–581. doi: 10.1016/j.biopha.2018.04.025

Baig, M. H., Ahmad, K., Rabbani, G., and Choi, I. (2018a). Use of peptides for the management of alzheimer's disease: diagnosis and inhibition. *Front. Aging Neurosci.* 10:21. doi: 10.3389/fnagi.2018.00021

Baine, M., Georgie, D. S., Shiferraw, E. Z., Nguyen, T. P. T., Nogaj, L. A., and Moffet, D. A. (2009). Inhibition of Aβ42 aggregation using peptides selected from combinatorial libraries. *J. Peptide Sci.* 15, 499–503.

Bilal, M., Barani, M., Sabir, F., Rahdar, A., and Kyzas, G. Z. (2020). Nanomaterials for the treatment and diagnosis of Alzheimer's disease: an overview. *NanoImpact* 20:100251.

Bjerke, M., and Engelborghs, S. (2018). Cerebrospinal fluid biomarkers for early and differential alzheimer's disease diagnosis. *J. Alzheimers Dis.* 62, 1199–1209. doi: 10.3233/JAD-170680

Blennow, K., and Zetterberg, H. (2018). Biomarkers for Alzheimer's disease: current status and prospects for the future. *J. Intern. Med.* 284, 643–663. doi: 10.1111/joim.12816

Blennow, K., Dubois, B., Fagan, A. M., Lewczuk, P., De Leon, M. J., and Hampel, H. (2015). Clinical utility of cerebrospinal fluid biomarkers in the diagnosis of early Alzheimer's disease. *Alzheimers Dement.* 11, 58–69. doi: 10.1016/j.jalz.2014.02.004

Brickman, A. M., Manly, J. J., Honig, L. S., Sanchez, D., Reyes-Dumeyer, D., Lantigua, R. A., et al. (2021). Plasma p-tau181, p-tau217, and other blood-based Alzheimer's disease biomarkers in a multi-ethnic, community study. *Alzheimers Dement.* 17, 1353–1364. doi: 10.1002/alz.12301

Brureau, A., Blanchard-Bregeon, V., Pech, C., Hamon, S., Chaillou, P., Guillemot, J.-C., et al. (2017). NF-L in cerebrospinal fluid and serum is a biomarker of neuronal damage in an inducible mouse model of neurodegeneration. *Neurobiol. Dis.* 104, 73–84. doi: 10.1016/j.nbd.2017.04.007

Chatterjee, P., Pedrini, S., Ashton, N. J., Tegg, M., Goozee, K., Singh, A. K., et al. (2021). Diagnostic and prognostic plasma biomarkers for preclinical Alzheimer's disease. *Alzheimers Dement.* doi: 10.1002/alz.12447 [Epub ahead of print].

Chen, J., Huang, Y., Zhu, C., Li, Q., Wu, Y., Liu, Q., et al. (2019). Early detection of Alzheimer's disease by peptides from phage display screening. *Brain Res.* 1721:146306. doi: 10.1016/j.brainres.2019.146306

Chen, S. G., Yadav, S. P., and Surewicz, W. K. (2010). Interaction between human prion protein and amyloid-beta (A beta) Oligomers role of N-terminal residues. *J. Biol. Chem.* 285, 26377–26383. doi: 10.1074/jbc.M110.145516

Crunkhorn, S. (2018). Identification of blood-based biomarkers. *Nat. Rev. Drug Discov.* 17, 166–166.

Cullen, N. C., Leuzy, A., Janelidze, S., Palmqvist, S., Svenningsson, A. L., Stomrud, E., et al. (2021). Plasma biomarkers of Alzheimer's disease improve prediction of cognitive decline in cognitively unimpaired elderly populations. *Nat. Commun.* 12:3555. doi: 10.1038/s41467-021-23746-0

Dammers, C., Yolcu, D., Kukuk, L., Willbold, D., Pickhardt, M., Mandelkow, E., et al. (2016). Selection and characterization of tau binding d-enantiomeric peptides with potential for therapy of Alzheimer disease. *PLoS One* 11:18. doi: 10.1371/journal.pone.0167432

Delivoria, D. C., Chia, S., Habchi, J., Perni, M., Matis, I., Papaevgeniou, N., et al. (2019). Bacterial production and direct functional screening of expanded molecular libraries for discovering inhibitors of protein aggregation. *Sci. Adv.* 5:eaax5108. doi: 10.1126/sciadv.aax5108

Du, Z., Gao, N., Guan, Y. J., Ding, C., Sun, Y. H., Ren, J. S., et al. (2018). Rational design of a "sense and treat" system to target amyloid aggregates related to Alzheimer's disease. *Nano Res.* 11, 1987–1997.

Dubois, B., Hampel, H., Feldman, H. H., Scheltens, P., Aisen, P., Andrieu, S., et al. (2016). Preclinical Alzheimer's disease: definition, natural history, and diagnostic criteria. *Alzheimers Dement.* 12, 292–323. doi: 10.1016/j.jalz.2016.02.002

Esler, W. P., and Wolfe, M. S. (2001). A portrait of alzheimer secretases–new features and familiar faces. *Science* 293:1449. doi: 10.1126/science.1064638

Evin, G., Barakat, A., and Masters, C. L. (2010). BACE: therapeutic target and potential biomarker for Alzheimer's disease. *Int. J. Biochem. Cell Biol.* 42, 1923–1926. doi: 10.1016/j.biocel.2010.08.017

Folk, D. S., and Franz, K. J. (2010). A prochelator activated by β-secretase inhibits aβ aggregation and suppresses copper-induced reactive oxygen species formation. *J. Am. Chem. Soc.* 132, 4994–4995. doi: 10.1021/ja100943r

Ganesh, S. D., Saha, N., Zandraa, O., Zuckermann, R. N., and Sáha, P. (2017). Peptoids and polypeptoids: biomimetic and bioinspired materials for biomedical applications. *Polym. Bull.* 74, 3455–3466. doi: 10.1007/s00289-016-1902-1

Gao, H., Liu, M., Zhao, Z., Yang, C., Zhu, L., Cai, Y., et al. (2020). Diagnosis of mild cognitive impairment and Alzheimer's disease by the plasma and serum amyloid-beta 42 assay through highly sensitive peptoid nanosheet sensor. *ACS Appl. Mater. Interfaces* 12, 9693–9700. doi: 10.1021/acsami.0c00370

Gao, H., Wang, J., Liu, J., Ye, S., Meng, X., Song, S., et al. (2021). Peptoid nanosheet-based sensing system for the diagnosis and surveillance of amnestic mild cognitive impairment and Alzheimer's disease. *ACS Chem. Neurosci.* 12, 4257–4264. doi: 10.1021/acschemneuro.1c00613

Gao, H., Zhao, Z., He, Z., Wang, H., Liu, M., Hu, Z., et al. (2019). Detection of Parkinson's Disease through the peptoid recognizing α-synuclein in serum. *ACS Chem. Neurosci.* 10, 1204–1208. doi: 10.1021/acschemneuro.8b00540

Ge, L., Liu, Z., and Tian, Y. (2020). A novel two-photon ratiometric fluorescent probe for imaging and sensing of BACE1 in different regions of AD mouse brain. *Chem. Sci.* 11, 2215–2224. doi: 10.1039/c9sc05256a

Ghimire Gautam, S., Komatsu, M., and Nishigaki, K. (2015). Strong inhibition of beta-amyloid peptide aggregation realized by two-steps evolved peptides. *Chem. Biol. Drug Design* 85, 356–368. doi: 10.1111/cbdd.12400

Goedert, M. (1993). Tau protein and the neurofibrillary pathology of Alzheimer's disease. *Trends Neurosci.* 16, 460–465. doi: 10.1016/0166-2236(93)90078-z

Gopalan, D., Pandey, A., Udupa, N., and Mutalik, S. (2020). Receptor specific, stimuli responsive and subcellular targeted approaches for effective therapy of Alzheimer: role of surface engineered nanocarriers. *J. Control. Release* 319, 183–200. doi: 10.1016/j.jconrel.2019.12.034

Gray, B. P., and Brown, K. C. (2014). Combinatorial peptide libraries: mining for cell-binding peptides. *Chem. Rev.* 114, 1020–1081. doi: 10.1021/cr400166n

Hajipour, M. J., Santoso, M. R., Rezaee, F., Aghaverdi, H., Mahmoudi, M., and Perry, G. (2017). Advances in Alzheimer's diagnosis and therapy: the implications of nanotechnology. *Trends Biotechnol.* 35, 937–953. doi: 10.1016/j.tibtech.2017.06.002

Hampel, H., O'bryant, S. E., Molinuevo, J. L., Zetterberg, H., Masters, C. L., Lista, S., et al. (2018). Blood-based biomarkers for Alzheimer disease: mapping the road to the clinic. *Nat. Rev. Neurol.* 14, 639–652. doi: 10.1038/s41582-018-0079-7

Hanif, S., Muhammad, P., Niu, Z., Ismail, M., Morsch, M., Zhang, X., et al. (2021). Nanotechnology-based strategies for early diagnosis of central nervous system disorders. *Adv. NanoBiomed. Res.* 1:2100008. doi: 10.1002/anbr.202100008

Hansson, O. (2021). Biomarkers for neurodegenerative diseases. *Nat. Med.* 27, 954–963. doi: 10.1093/jnen/nlaa041

Henriksen, K., O'bryant, S. E., Hampel, H., Trojanowski, J. Q., Montine, T. J., Jeromin, A., et al. (2014). The future of blood-based biomarkers for Alzheimer's disease. *Alzheimers Dement.* 10, 115–131.

Huang, Y., Zhang, B., Yuan, L., and Liu, L. (2021). A signal amplification strategy based on peptide self-assembly for the identification of amyloid-β oligomer. *Sens. Actuators B Chem.* 335:129697. doi: 10.1016/j.snb.2021.129697

Janelidze, S., Mattsson, N., Palmqvist, S., Smith, R., Beach, T. G., Serrano, G. E., et al. (2020). Plasma P-tau181 in Alzheimer's disease: relationship to other biomarkers, differential diagnosis, neuropathology and longitudinal progression to Alzheimer's dementia. *Nat. Med.* 26, 379–386. doi: 10.1038/s41591-020-0755-1

Jankowsky, J. L., Fadale, D. J., Anderson, J., Xu, G. M., Gonzales, V., Jenkins, N. A., et al. (2004). Mutant presenilins specifically elevate the levels of the 42 residue beta-amyloid peptide in vivo: evidence for augmentation of a 42-specific gamma secretase. *Hum. Mol. Genet.* 13, 159–170. doi: 10.1093/hmg/ddh019

Jia, J. P., Wei, C. B., Chen, S. Q., Li, F. Y., Tang, Y., Qin, W., et al. (2018). The cost of Alzheimer's disease in China and re-estimation of costs worldwide. *Alzheimers Dement.* 14, 483–491. doi: 10.1016/j.jalz.2017.12.006

Jokar, S., Behnammanesh, H., Erfani, M., Sharifzadeh, M., Gholami, M., Sabzevari, O., et al. (2020). Synthesis, biological evaluation and preclinical study of a novel 99mTc-peptide: a targeting probe of amyloid-β plaques as a possible diagnostic agent for Alzheimer's disease. *Bioorg. Chem.* 99:103857. doi: 10.1016/j.bioorg.2020.103857

Jun, Y. W., Cho, S. W., Jung, J., Huh, Y., Kim, Y., Kim, D., et al. (2019). Frontiers in probing Alzheimer's disease biomarkers with fluorescent small molecules. *ACS Cent. Sci.* 5, 209–217. doi: 10.1021/acscentsci.8b00951

Karki, H. P., Jang, Y., Jung, J., and Oh, J. (2021). Advances in the development paradigm of biosample-based biosensors for early ultrasensitive detection of Alzheimer's disease. *J. Nanobiotechnol.* 19:72.

Kaushik, A., Jayant, R. D., Tiwari, S., Vashist, A., and Nair, M. (2016). Nano-biosensors to detect beta-amyloid for Alzheimer's disease management. *Biosens. Bioelectron.* 80, 273–287. doi: 10.1016/j.bios.2016.01.065

Kawasaki, T., Onodera, K., and Kamijo, S. (2011). Identification of novel short peptide inhibitors of soluble 37/48 kda oligomers of amyloid β42. *Biosci. Biotechnol. Biochem.* 75, 1496–1501. doi: 10.1271/bbb.110198

Khalil, M., Teunissen, C. E., Otto, M., Piehl, F., Sormani, M. P., Gattringer, T., et al. (2018). Neurofilaments as biomarkers in neurological disorders. *Nat. Rev. Neurol.* 14, 577–589. doi: 10.1038/s41582-018-0058-z

Khoury, R., and Ghossoub, E. (2019). Diagnostic biomarkers of Alzheimer's disease: a state-of-the-art review. *Biomarkers Neuropsychiatry* 1:100005. doi: 10.1016/j.bionps.2019.100005

Kim, K., Kim, M.-J., Kim, D. W., Kim, S. Y., Park, S., and Park, C. B. (2020). Clinically accurate diagnosis of Alzheimer's disease via multiplexed sensing of core biomarkers in human plasma. *Nat. Commun.* 11:119. doi: 10.1038/s41467-019-13901-z

Kim, S., Lee, S.-M., Yoon, J. P., Lee, N., Chung, J., Chung, W.-J., et al. (2020). Robust magnetized graphene oxide platform for in situ peptide synthesis and FRET-based protease detection. *Sensors* 20:5275. doi: 10.3390/s20185275

Kim, S.-H., Lee, E.-H., Lee, S.-C., Kim, A. R., Park, H.-H., Son, J.-W., et al. (2020). Development of peptide aptamers as alternatives for antibody in the detection of amyloid-beta 42 aggregates. *Anal. Biochem.* 609:113921. doi: 10.1016/j.ab.2020.113921

Knight, A. S., Zhou, E. Y., Francis, M. B., and Zuckermann, R. N. (2015). Sequence programmable peptoid polymers for diverse materials applications. *Adv. Mater.* 27, 5665–5691. doi: 10.1002/adma.201500275

Larbanoix, L., Burtea, C., Ansciaux, E., Laurent, S., Mahieu, I., Vander Elst, L., et al. (2011). Design and evaluation of a 6-mer amyloid-beta protein derived phage display library for molecular targeting of amyloid plaques in Alzheimer's disease: comparison with two cyclic heptapeptides derived from a randomized phage display library. *Peptides* 32, 1232–1243. doi: 10.1016/j.peptides.2011.04.026

Larbanoix, L., Burtea, C., Laurent, S., Van Leuven, F., Toubeau, G., Elst, L. V., et al. (2010). Potential amyloid plaque-specific peptides for the diagnosis of Alzheimer's disease. *Neurobiol. Aging* 31, 1679–1689. doi: 10.1016/j.neurobiolaging.2008.09.021

Lau, K. H. A. (2014). Peptoids for biomaterials science. *Biomater. Sci.* 2, 627–633. doi: 10.1039/c3bm60269a

Lauren, J., Gimbel, D. A., Nygaard, H. B., Gilbert, J. W., and Strittmatter, S. M. (2009). Cellular prion protein mediates impairment of synaptic plasticity by amyloid-beta oligomers. *Nature* 457, 1128–U1184. doi: 10.1038/nature07761

Lee, S.-C., Park, H.-H., Kim, S.-H., Koh, S.-H., Han, S.-H., and Yoon, M.-Y. (2019). Ultrasensitive fluorescence detection of Alzheimer's disease based on polyvalent directed peptide polymer coupled to a nanoporous zno nanoplatform. *Anal. Chem.* 91, 5573–5581. doi: 10.1021/acs.analchem.8b03735

Lei, L., Geng, R., Xu, Z., Dang, Y., Hu, X., Li, L., et al. (2019). Glycopeptide nanofiber platform for aβ-sialic acid interaction analysis and highly sensitive detection of aβ. *Anal. Chem.* 91, 8129–8136. doi: 10.1021/acs.analchem.9b00377

Lei, L., Li, M., Wu, S., Xu, Z., Geng, P., Tian, Y., et al. (2020). Noninvasive in situ ratiometric imaging of biometals based on self-assembled peptide nanoribbon. *Anal. Chem.* 92, 5838–5845. doi: 10.1021/acs.analchem.9b05490

Lewczuk, P., Matzen, A., Blennow, K., Parnetti, L., Molinuevo, J. L., Eusebi, P., et al. (2017). Cerebrospinal fluid Aβ 42/40 corresponds better than Aβ 42 to amyloid PET in Alzheimer's Disease. *J. Alzheimers Dis.* 55, 813–822. doi: 10.3233/jad-160722

Li, H., Cao, Y., Wu, X., Ye, Z., and Li, G. (2012). Peptide-based electrochemical biosensor for amyloid β 1–42 soluble oligomer assay. *Talanta* 93, 358–363. doi: 10.1016/j.talanta.2012.02.055

Li, J., Feng, L., and Jiang, X. (2015). In vivo phage display screen for peptide sequences that cross the blood–cerebrospinal-fluid barrier. *Amino Acids* 47, 401–405. doi: 10.1007/s00726-014-1874-0

Li, J., Feng, L., Fan, L., Zha, Y., Guo, L., Zhang, Q., et al. (2011). Targeting the brain with PEG–PLGA nanoparticles modified with phage-displayed peptides. *Biomaterials* 32, 4943–4950. doi: 10.1016/j.biomaterials.2011.03.031

Li, M., Xu, C., Wu, L., Ren, J., Wang, E., and Qu, X. (2013). Self-assembled peptide–polyoxometalate hybrid nanospheres: two in one enhances targeted inhibition of amyloid β-peptide aggregation associated with Alzheimer's disease. *Small* 9, 3455–3461. doi: 10.1002/smll.201202612

Liu, D., Fu, D., Zhang, L., and Sun, L. (2021). Detection of amyloid-beta by Fmoc-KLVFF self-assembled fluorescent nanoparticles for Alzheimer's disease diagnosis. *Chin. Chem. Lett.* 32, 1066–1070. doi: 10.1039/c6cc09085k

Luo, Y., Bolon, B., Kahn, S., Bennett, B. D., Babu-Khan, S., Denis, P., et al. (2001). Mice deficient in BACE1, the Alzheimer's β-secretase, have normal phenotype and abolished β-amyloid generation. *Nat. Neurosci.* 4, 231–232. doi: 10.1038/85059

Luo, Y., Vali, S., Sun, S., Chen, X., Liang, X., Drozhzhina, T., et al. (2013). Aβ42-binding peptoids as amyloid aggregation inhibitors and detection ligands. *ACS Chem. Neurosci.* 4, 952–962. doi: 10.1021/cn400011f

Matharu, B., Spencer, N., Howe, F., and Austen, B. (2015). Gadolinium-complexed Aβ-binding contrast agents for MRI diagnosis of Alzheimer's Disease. *Neuropeptides* 53, 63–70. doi: 10.1016/j.npep.2015.07.001

Matis, I., Delivoria, D. C., Mavroidi, B., Papaevgeniou, N., Panoutsou, S., Bellou, S., et al. (2017). An integrated bacterial system for the discovery of chemical rescuers of disease-associated protein misfolding. *Nat. Biomed. Eng.* 1, 838–852. doi: 10.1038/s41551-017-0144-3

Mattsson, N., Andreasson, U., Zetterberg, H., Blennow, K., and Alzheimer's Disease Neuroimaging Initiative (2017). Association of plasma neurofilament light with neurodegeneration in patients with Alzheimer disease. *JAMA Neurol.* 74, 557–566. doi: 10.1001/jamaneurol.2016.6117

Matveeva, E. G., Moll, J. R., Khan, M. M., Thompson, R. B., and Cliff, R. O. (2017). Surface assay for specific detection of soluble amyloid oligomers utilizing pronucleon peptides instead of antibodies. *ACS Chem. Neurosci.* 8, 1213–1221. doi: 10.1021/acschemneuro.6b00381

Milà-Alomà, M., Suárez-Calvet, M., and Molinuevo, J. L. (2019). Latest advances in cerebrospinal fluid and blood biomarkers of Alzheimer's disease. *Ther. Adv. Neurol. Disord.* 12:1756286419888819. doi: 10.1177/1756286419888819

Moscoso, A., Grothe, M. J., Ashton, N. J., Karikari, T. K., Lantero Rodríguez, J., Snellman, A., et al. (2021). Longitudinal associations of blood phosphorylated tau181 and neurofilament light chain with neurodegeneration in Alzheimer disease. *JAMA Neurology* 78, 396–406. doi: 10.1001/jamaneurol.2020.4986

Nakamura, A., Kaneko, N., Villemagne, V. L., Kato, T., Doecke, J., Doré, V., et al. (2018). High performance plasma amyloid-β biomarkers for Alzheimer's disease. *Nature* 554, 249–254.

Nam, K. T., Shelby, S. A., Choi, P. H., Marciel, A. B., Chen, R., Tan, L., et al. (2010). Free-floating ultrathin two-dimensional crystals from sequence-specific peptoid polymers. *Nat. Mater.* 9, 454–460. doi: 10.1038/nmat2742

Negahdary, M., and Heli, H. (2019). An electrochemical peptide-based biosensor for the Alzheimer biomarker amyloid-β(1–42) using a microporous gold nanostructure. *Microchim. Acta* 186:766. doi: 10.1007/s00604-019-3903-x

Nordberg, A. (2015). Towards early diagnosis in Alzheimer disease. *Nat. Rev. Neurol.* 11, 69–70. doi: 10.1038/nrneurol.2014.257

Ovod, V., Ramsey, K. N., Mawuenyega, K. G., Bollinger, J. G., Hicks, T., Schneider, T., et al. (2017). Amyloid β concentrations and stable isotope labeling kinetics of human plasma specific to central nervous system amyloidosis. *Alzheimers Dement.* 13, 841–849. doi: 10.1016/j.jalz.2017.06.2266

Pande, J., Szewczyk, M. M., and Grover, A. K. (2010). Phage display: concept, innovations, applications and future. *Biotechnol. Adv.* 28, 849–858. doi: 10.1016/j.biotechadv.2010.07.004

Park, S. A., Han, S. M., and Kim, C. E. (2020). New fluid biomarkers tracking non-amyloid-β and non-tau pathology in Alzheimer's disease. *Exp. Mol. Med.* 52, 556–568. doi: 10.1038/s12276-020-0418-9

Patch, J. A., and Barron, A. E. (2002). Mimicry of bioactive peptides via non-natural, sequence-specific peptidomimetic oligomers. *Curr. Opin. Chem. Biol.* 6, 872–877. doi: 10.1016/s1367-5931(02)00385-x

Patricia, R. M., Izabela, P. V., Rafaela, P., Marina, M. G., Renata, V. P., Carla, M. C. N., et al. (2020). Blood-based biomarkers of Alzheimer's disease: the long and winding road. *Curr. Pharm. Design* 26, 1300–1315. doi: 10.2174/1381612826666200114105515

Petzold, A. (2005). Neurofilament phosphoforms: surrogate markers for axonal injury, degeneration and loss. *J. Neurol. Sci.* 233, 183–198. doi: 10.1016/j.jns.2005.03.015

Pradhan, N., Jana, D., Ghorai, B. K., and Jana, N. R. (2015). Detection and monitoring of amyloid fibrillation using a fluorescence "Switch-On" Probe. *ACS Appl. Mater. Interfaces* 7, 25813–25820. doi: 10.1021/acsami.5b07751

Preische, O., Schultz, S. A., Apel, A., Kuhle, J., Kaeser, S. A., Barro, C., et al. (2019). Serum neurofilament dynamics predicts neurodegeneration and clinical progression in presymptomatic Alzheimer's disease. *Nat. Med.* 25, 277–283. doi: 10.1038/s41591-018-0304-3

Qi, G. B., Gao, Y. J., Wang, L., and Wang, H. (2018). Self-assembled peptide-based nanomaterials for biomedical imaging and therapy. *Adv. Mater.* 30:34. doi: 10.1002/adma.201703444

Reddy, M. M., Wilson, R., Wilson, J., Connell, S., Gocke, A., Hynan, L., et al. (2011). Identification of candidate IgG biomarkers for Alzheimer's disease via combinatorial library screening. *Cell* 144, 132–142. doi: 10.1016/j.cell.2010.11.054

Rushworth, J. V., Ahmed, A., Griffiths, H. H., Pollock, N. M., Hooper, N. M., and Millner, P. A. (2014). A label-free electrical impedimetric biosensor for the specific detection of Alzheimer's amyloid-beta oligomers. *Biosens. Bioelectron.* 56, 83–90. doi: 10.1016/j.bios.2013.12.036

Saini, A., and Verma, G. (2017). "Chapter 10 – peptoids: tomorrow's therapeutics," in *Nanostructures for Novel Therapy*, eds D. Ficai and A. M. Grumezescu (Amsterdam: Elsevier), 251–280.

Scarano, S., Lisi, S., Ravelet, C., Peyrin, E., and Minunni, M. (2016). Detecting Alzheimer's disease biomarkers: From antibodies to new bio-mimetic receptors and their application to established and emerging bioanalytical platforms – a critical review. *Anal. Chim. Acta* 940, 21–37. doi: 10.1016/j.aca.2016.08.008

Scheltens, P., Blennow, K., Breteler, M. M. B., De Strooper, B., Frisoni, G. B., Salloway, S., et al. (2016). Alzheimer's disease. *Lancet* 388, 505–517.

Schneider, P., Hampel, H., and Buerger, K. (2009). Biological marker candidates of Alzheimer's disease in blood, plasma, and serum. *CNS Neurosci. Ther.* 15, 358–374. doi: 10.1111/j.1755-5949.2009.00104.x

Schöll, M., Maass, A., Mattsson, N., Ashton, N. J., Blennow, K., Zetterberg, H., et al. (2019). Biomarkers for tau pathology. *Mol. Cell. Neurosci.* 97, 18–33.

Schwarzman, A. L., Tsiper, M., Gregori, L., Goldgaber, D., Frakowiak, J., Mazur-Kolecka, B., et al. (2005). Selection of peptides binding to the amyloid b-protein reveals potential inhibitors of amyloid formation. *Amyloid* 12, 199–209. doi: 10.1080/13506120500350762

Selkoe, D. J., Citron, M., Yamazaki, T., Teplow, D., and Haass, C. (1994). Physiological production of amyloid beta-peptide as a route to the mechanism and treatment of Alzheimers-disease. *Neurobiol. Aging* 15, S69–S70. doi: 10.1111/j.1471-4159.2004.02778.x

Serrano-Pozo, A., Frosch, M. P., Masliah, E., and Hyman, B. T. (2011). Neuropathological alterations in Alzheimer disease. *Cold Spring Harb. Perspect. Med.* 1:a006189. doi: 10.1101/cshperspect.a006189

Shuaib, S., Narang, S. S., Goyal, D., and Goyal, B. (2019). Computational design and evaluation of β-sheet breaker peptides for destabilizing Alzheimer's amyloid-β42 protofibrils. *J. Cell. Biochem.* 120, 17935–17950. doi: 10.1002/jcb.29061

Sievers, S. A., Karanicolas, J., Chang, H. W., Zhao, A., Jiang, L., Zirafi, O., et al. (2011). Structure-based design of non-natural amino-acid inhibitors of amyloid fibril formation. *Nature* 475, 96–100. doi: 10.1038/nature10154

Simon, R. J., Kania, R. S., Zuckermann, R. N., Huebner, V. D., Jewell, D. A., Banville, S., et al. (1992). Peptoids: a modular approach to drug discovery. *Proc. Natl. Acad. Sci. U.S.A.* 89:9367. doi: 10.1073/pnas.89.20.9367

Sun, J., and Zuckermann, R. N. (2013). Peptoid polymers: a highly designable bioinspired material. *ACS Nano* 7, 4715–4732. doi: 10.1021/nn4015714

Sun, L., Fan, Z., Yue, T., Yin, J., Fu, J., and Zhang, M. (2018). Additive nanomanufacturing of lab-on-a-chip fluorescent peptide nanoparticle arrays for Alzheimer's disease diagnosis. *Bio Design Manuf.* 1, 182–194. doi: 10.1007/s42242-018-0019-9

Thijssen, E. H., La Joie, R., Wolf, A., Strom, A., Wang, P., Iaccarino, L., et al. (2020). Diagnostic value of plasma phosphorylated tau181 in Alzheimer's disease and frontotemporal lobar degeneration. *Nat. Med.* 26, 387–397. doi: 10.1038/s41591-020-0762-2

Tjernberg, L. O., Naslund, J., Lindqvist, F., Johansson, J., Karlstrom, A. R., Thyberg, J., et al. (1996). Arrest of beta-amyloid fibril formation by a pentapeptide ligand. *J. Biol. Chem.* 271, 8545–8548. doi: 10.1074/jbc.271.15.8545

Tsuji-Ueno, S., Komatsu, M., Iguchi, K., Takahashi, M., Yoshino, S., Suzuki, M., et al. (2011). Novel high-affinity Aβ-binding peptides identified by an advanced in vitro evolution, progressive library method. *Protein Pept. Lett.* 18, 642–650. doi: 10.2174/092986611795222678

Tweedle, M. F. (2009). Peptide-targeted diagnostics and radiotherapeutics. *Acc. Chem. Res.* 42, 958–968. doi: 10.1021/ar800215p

van Oostveen, W. M., and de Lange, E. C. M. (2021). Imaging techniques in Alzheimer's disease: a review of applications in early diagnosis and longitudinal monitoring. *Int. J. Mol. Sci.* 22:2110. doi: 10.3390/ijms22042110

Vanderstichele, H., and Kodadek, T. (2014). Roadblocks for integration of novel biomarker concepts into clinical routine: the peptoid approach. *Alzheimers Res. Ther.* 6:23. doi: 10.1186/alzrt253

Wang, W. Z., and Hu, Z. Y. (2019). Targeting peptide-based probes for molecular imaging and diagnosis. *Adv. Mater.* 31:8. doi: 10.1002/adma.201804827

Wei, G., Su, Z. Q., Reynolds, N. P., Arosio, P., Hamley, I. W., Gazit, E., et al. (2017). Self-assembling peptide and protein amyloids: from structure to tailored function in nanotechnology. *Chem. Soc. Rev.* 46, 4661–4708.

Weston, P. S. J., Poole, T., O'connor, A., Heslegrave, A., Ryan, N. S., Liang, Y., et al. (2019). Longitudinal measurement of serum neurofilament light in presymptomatic familial Alzheimer's disease. *Alzheimers Res. Ther.* 11:19. doi: 10.1186/s13195-019-0472-5

Wiesehan, K., Buder, K., Linke, R. P., Patt, S., Stoldt, M., Unger, E., et al. (2003). Selection of D-Amino-Acid peptides that bind to alzheimer's disease amyloid peptide aβ1–42 by mirror image phage display. *ChemBioChem* 4, 748–753. doi: 10.1002/cbic.200300631

Wu, C. H., Liu, I. J., Lu, R. M., and Wu, H. C. (2016). Advancement and applications of peptide phage display technology in biomedical science. *J. Biomed. Sci.* 23:14. doi: 10.1186/s12929-016-0223-x

Wurth, C., Guimard, N. K., and Hecht, M. H. (2002). Mutations that reduce aggregation of the Alzheimer's aβ42 peptide: an unbiased search for the sequence determinants of aβ amyloidogenesis. *J. Mol. Biol.* 319, 1279–1290. doi: 10.1016/S0022-2836(02)00399-6

Xia, N., Wang, X., Yu, J., Wu, Y., Cheng, S., Xing, Y., et al. (2017). Design of electrochemical biosensors with peptide probes as the receptors of targets and the inducers of gold nanoparticles assembly on electrode surface. *Sens. Actuators B Chem.* 239, 834–840.

Xing, Y., Feng, X. Z., Zhang, L. P., Hou, J. T., Han, G. C., and Chen, Z. C. (2017). A sensitive and selective electrochemical biosensor for the determination of beta-amyloid oligomer by inhibiting the peptide-triggered in situ assembly of silver nanoparticles. *Int. J. Nanomed.* 12, 3171–3179. doi: 10.2147/IJN.S132776

Yang, H.-L., Fang, S.-Q., Tang, Y.-W., Wang, C., Luo, H., Qu, L.-L., et al. (2019). A hemicyanine derivative for near-infrared imaging of β-amyloid plaques in Alzheimer's disease. *Eur. J. Med. Chem.* 179, 736–743. doi: 10.1016/j.ejmech.2019.07.005

Yang, X., Li, Y., Zhu, Z., Huang, X., Wang, T., Yuan, J., et al. (2021). Identification of a peptide that crosses the blood-cerebrospinal fluid barrier by phage display technology. *Amino Acids* 53, 1181–1186. doi: 10.1007/s00726-021-03016-5

Yazdani, U., Zaman, S., Hynan, L. S., Brown, L. S., Dewey, R. B., Karp, D., et al. (2016). Blood biomarker for Parkinson disease: peptoids. *NPJ Parkinsons Dis.* 2:16012. doi: 10.1038/npjparkd.2016.12

Zafar, S., Beg, S., Panda, S. K., Rahman, M., Alharbi, K. S., Jain, G. K., et al. (2021). Novel therapeutic interventions in cancer treatment using protein and peptide-based targeted smart systems. *Semin. Cancer Biol.* 69, 249–267. doi: 10.1016/j.semcancer.2019.08.023

Zetterberg, H., Andreasson, U., Hansson, O., Wu, G., Sankaranarayanan, S., Andersson, M. E., et al. (2008). Elevated cerebrospinal fluid BACE1 activity in incipient Alzheimer disease. *Arch. Neurol.* 65, 1102–1107. doi: 10.1001/archneur.65.8.1102

Zhang, K., Yang, Q., Fan, Z., Zhao, J., and Li, H. (2019). Platelet-driven formation of interface peptide nano-network biosensor enabling a non-invasive means for early detection of Alzheimer's disease. *Biosens. Bioelectron.* 145:111701. doi: 10.1016/j.bios.2019.111701

Zhang, X., Zhang, X., Zhong, M., Zhao, P., Guo, C., Li, Y., et al. (2020). Selection of a d-enantiomeric peptide specifically binding to PHF6 for inhibiting tau aggregation in transgenic mice. *ACS Chem. Neurosci.* 11, 4240–4253. doi: 10.1021/acschemneuro.0c00518

Zhao, Z., Zhu, L., Bu, X., Ma, H., Yang, S., Yang, Y., et al. (2015). Label-free detection of Alzheimer's disease through the ADP3 peptoid recognizing the serum amyloid-beta42 peptide. *Chem. Commun.* 51, 718–721. doi: 10.1039/c4cc07037b

Zhu, L., Xu, L., Wu, X., Deng, F., Ma, R., Liu, Y., et al. (2021). Tau-targeted multifunctional nanoinhibitor for Alzheimer's disease. *ACS Appl. Mater. Interfaces* 13, 23328–23338. doi: 10.1021/acsami.1c00257

Zhu, L., Zhao, Z., Cheng, P., He, Z., Cheng, Z., Peng, J., et al. (2017). Antibody-mimetic peptoid nanosheet for label-free serum-based diagnosis of Alzheimer's disease. *Adv. Mater.* 2:1700057. doi: 10.1002/adma.201700057

Zou, K., Abdullah, M., and Michikawa, M. (2020). Current biomarkers for Alzheimer's disease: from CSF to blood. *J. Pers. Med.* 10:85. doi: 10.3390/jpm10030085

Zuckermann, R. N., Kerr, J. M., Kent, S. B. H., and Moos, W. H. (1992). Efficient method for the preparation of peptoids [oligo(N-substituted glycines)] by submonomer solid-phase synthesis. *J. Am. Chem. Soc.* 114, 10646–10647. doi: 10.1021/ja00052a076

Zuo, X., Dai, H., Zhang, H., Liu, J., Ma, S., and Chen, X. (2018). A peptide–WS2 nanosheet based biosensing platform for determination of β-secretase and screening of its inhibitors. *Analyst* 143, 4585–4591. doi: 10.1039/c8an00132d

Conflict of Interest: The authors declare that the research was conducted in the absence of any commercial or financial relationships that could be construed as a potential conflict of interest.

Publisher's Note: All claims expressed in this article are solely those of the authors and do not necessarily represent those of their affiliated organizations, or those of the publisher, the editors and the reviewers. Any product that may be evaluated in this article, or claim that may be made by its manufacturer, is not guaranteed or endorsed by the publisher.

frontiers in Molecular Neuroscience

CORRECTION
published: 21 February 2022
doi: 10.3389/fnmol.2022.865110

Corrigendum: Recent Advances in the Application Peptide and Peptoid in Diagnosis Biomarkers of Alzheimer's Disease in Blood

Yuxin Guo[1,2], *Zhiyuan Hu*[1,3,4,5]* *and Zihua Wang*[3]*

[1] CAS Key Laboratory of Standardization and Measurement for Nanotechnology, CAS Key Laboratory for Biomedical Effects of Nanomaterials and Nanosafety, CAS Center for Excellence in Nanoscience, National Center for Nanoscience and Technology, Beijing, China, [2] University of Chinese Academy of Sciences, Beijing, China, [3] Fujian Provincial Key Laboratory of Brain Aging and Neurodegenerative Diseases, School of Basic Medical Sciences, Fujian Medical University, Fuzhou, China, [4] School of Nanoscience and Technology, Sino-Danish College, University of Chinese Academy of Sciences, Beijing, China, [5] School of Chemical Engineering and Pharmacy, Wuhan Institute of Technology, Wuhan, China

OPEN ACCESS

Approved by:
Frontiers Editorial Office,
Frontiers Media SA, Switzerland

***Correspondence:**
Zhiyuan Hu
huzy@nanoctr.cn
Zihua Wang
wangzh@fjmu.edu.cn

Specialty section:
This article was submitted to Methods and Model Organisms, a section of the journal Frontiers in Molecular Neuroscience

Received: 29 January 2022
Accepted: 31 January 2022
Published: 21 February 2022

Citation:
Guo Y, Hu Z and Wang Z (2022) Corrigendum: Recent Advances in the Application Peptide and Peptoid in Diagnosis Biomarkers of Alzheimer's Disease in Blood. Front. Mol. Neurosci. 15:865110. doi: 10.3389/fnmol.2022.865110

Keywords: Alzheimer's disease, blood biomarkers, diagnosis, peptide, peptoid

A Corrigendum on

Recent Advances in the Application Peptide and Peptoid in Diagnosis Biomarkers of Alzheimer's Disease in Blood

by Guo, Y., Hu, Z., and Wang, Z. (2021). Front. Mol. Neurosci. 14:778955. doi: 10.3389/fnmol.2021.778955

In the published article, there was an error regarding the affiliations for Yuxin Guo. As well as having affiliation 1, they should also have "University of Chinese Academy of Sciences, Beijing, China".

The authors apologize for this error and state that this does not change the scientific conclusions of the article in any way. The original article has been updated.

frontiers in Molecular Neuroscience

ORIGINAL RESEARCH
published: 17 January 2022
doi: 10.3389/fnmol.2021.752403

Aerobic Exercise Training-Induced Changes on DNA Methylation in Mild Cognitively Impaired Elderly African Americans: Gene, Exercise, and Memory Study - GEMS-I

*Julius S. Ngwa[1], Evaristus Nwulia[2], Oyonumo Ntekim[3], Fikru B. Bedada[4], Bernard Kwabi-Addo[5], Sheeba Nadarajah[6,7,8], Steven Johnson[9], William M. Southerland[5], John Kwagyan[10] and Thomas O. Obisesan[9]**

[1] Division of Cardiovascular Medicine, Department of Internal Medicine, Howard University, Washington, DC, United States, [2] Department of Psychiatry and Behavioral Sciences, Howard University, Washington, DC, United States, [3] Department of Nutritional Sciences, Howard University, Washington, DC, United States, [4] Department of Clinical Laboratory Sciences, Howard University, Washington, DC, United States, [5] Department of Biochemistry and Molecular Biology, Howard University, Washington, DC, United States, [6] Division of Nursing, Howard University, Washington, DC, United States, [7] School of Nursing and Allied Health Sciences, Howard University, Washington, DC, United States, [8] Department of Medicine, Howard University, Washington, DC, United States, [9] Division of Geriatrics, Department of Medicine and Clinical/Translational Science Program, Howard University Hospital, Washington, DC, United States, [10] Georgetown-Howard U Center for Clinical and Translation Science (GHUCCTS), Howard University Hospital, Washington, DC, United States

OPEN ACCESS

Edited by:
Thomas K. Karikari,
University of Gothenburg, Sweden

Reviewed by:
Homira Behbahani,
Karolinska Institutet (KI), Sweden
Victor Bustos,
The Rockefeller University,
United States

***Correspondence:**
Thomas O. Obisesan
Tobisesan@howard.edu

Specialty section:
This article was submitted to Brain Disease Mechanisms, a section of the journal Frontiers in Molecular Neuroscience

Received: 05 August 2021
Accepted: 16 December 2021
Published: 17 January 2022

Citation:
Ngwa JS, Nwulia E, Ntekim O, Bedada FB, Kwabi-Addo B, Nadarajah S, Johnson S, Southerland WM, Kwagyan J and Obisesan TO (2022) Aerobic Exercise Training-Induced Changes on DNA Methylation in Mild Cognitively Impaired Elderly African Americans: Gene, Exercise, and Memory Study - GEMS-I. Front. Mol. Neurosci. 14:752403. doi: 10.3389/fnmol.2021.752403

Background: DNA methylation at CpG sites is a vital epigenetic modification of the human genome affecting gene expression, and potentially, health outcomes. However, evidence is just budding on the effects of aerobic exercise-induced adaptation on DNA methylation in older mild cognitively impaired (MCI) elderly African American (AAs). Therefore, we examined the effects of a 6-month aerobic exercise-intervention on genome-wide DNA methylation in elderly AA MCI volunteers.

Design: Elderly AA volunteers confirmed MCI assigned into a 6-month program of aerobic exercise (eleven participants) underwent a 40-min supervised-training 3-times/week and controls (eight participants) performed stretch training. Participants had maximal oxygen consumption (VO_2max) test and Genome-wide methylation levels at CpG sites using the Infinium HumanMethylation450 BeadChip assay at baseline and after a 6-month exercise program. We computed false discovery rates (FDR) using Sidak to account for multiplicity of tests and performed quantitative real-time polymerase chain-reaction (qRT-PCR) to confirm the effects of DNA methylations on expression levels of the top 5 genes among the aerobic participants. CpG sites identified from aerobic-exercise participants were similarly analyzed by the stretch group to quantify the effects of exercise-induced methylation changes among the group of stretch participants.

Results: Eleven MCI participants (aerobic: 73% females; mean age 72.3 ± 6.6 years) and eight MCI participants (stretch: 75% female; mean age 70.6 ± 6.7 years) completed the training. Aerobic exercise-training was associated with increases in VO_2max and

with global hypo- and hypermethylation changes. The most notable finding was CpG hypomethylation within the body of the *VPS52* gene ($P = 5.4 \times 10^{-26}$), a Golgi-associated protein, involved in intracellular protein trafficking including amyloid precursor protein. qRT-PCR confirmed a nearly twofold increased expression of *VPS52*. Other top findings with FDR q-value $< 10^{-5}$, include hypomethylations of *SCARB1* (8.8×10^{-25}), *ARTN* (6.1×10^{-25}), *NR1H2* (2.1×10^{-18}) and *PPP2R5D* (9.8×10^{-18}).

Conclusion: We conclude that genome-wide DNA methylation patterns is associated with exercise training-induced methylation changes. Identification of methylation changes around genes previously shown to interact with amyloid biology, intracellular protein trafficking, and lipoprotein regulations provide further support to the likely protective effect of exercise in MCI. Future studies in larger samples are needed to confirm our findings.

Keywords: African Americans, Alzheimer's disease, CPG Islands, DNA methylation, mild cognitive impairment, VO_2max

BACKGROUND

Epigenetic mechanisms and their effects on gene activation and silencing are becoming increasingly relevant to phenotype expression and the development of different diseases (Bird, 2007; Gluckman et al., 2009). The epigenome, along with the genome, instructs the unique gene expression program of each cell type in order to define its functional identity during development or disease (Rivera and Ren, 2013). While epigenetic changes are functionally relevant to the genome, they do not involve changes in a DNA sequence. One of such epigenetic modifications is the methylation of cytosine molecule, usually at CG dinucleotides (CpGs), called DNA methylation. Thus, the addition of methyl groups to the DNA molecules, motivate changes in the DNA segment activity without changing its sequence. When the CpGs of promoter regions are methylated, gene expression are often silenced (Hashimshony et al., 2003). Specifically, DNA methylation may affect the transcription of genes in two ways: (a) physically impede the binding of transcriptional proteins to the gene; (b) may be bound by proteins known as methyl-CpG-binding domain proteins resulting in compact, inactive chromatin (heterochromatin) (Choy et al., 2010). There is a growing understanding that environmental manipulation (e.g., diet and exercise) can influence cell behavior and disease states through epigenetic alterations of gene expression.

Exercise is a well-known physiological stimulus resulting in health and functional improvements. Regular exercise has numerous health benefits and can help reduce the risk of common ailments such as cardiovascular disease, type II diabetes, several forms of cancer (Matheson et al., 2013), and importantly, neurodegeneration and cognitive deterioration. Until recently, there has been paucity of knowledge on how aerobic exercise can induce epigenetic modifications in humans. A global study of DNA methylation in human skeletal muscle from relatives of Type 2 Diabetes patients demonstrated that a 6-month exercise resulted in epigenetic changes (Nitert et al., 2012). However, whether aerobic exercise can influence DNA methylations in elderly AA MCI participants has not been examined. It is also unknown whether such changes will include genes having essential roles in neurodegeneration and cognitive decline.

Therefore, we examined the impact of a 6-month aerobic exercise-training on human DNA methylation in mild cognitively impaired (MCI) elderly African Americans (AA)s; identify DNA methylated genes affected by aerobic exercise, and investigated the biological pathways affected by aerobic exercise training-related changes in CpG intensities. We then used quantitative real-time polymerase chain reaction (qRT-PCR) to confirm the effects of these methylation changes on the mRNA levels of the associated genes.

MATERIALS AND METHODS

The Howard University Institutional Review Board (IRB) approved the protocols used for this investigation. As required for studies involving human subjects, all participants completed a signed informed consent form before enrollment in the study. The details of the Gene, Exercise, and Memory Study (GEMS-I) protocol have previously been published (Iyalomhe et al., 2015).

Screening

Eligibility criteria consisted of age $\geq$ 55 years, ability to exercise vigorously without difficulty, have no chronic medical condition, met Petersen MCI criteria (Petersen et al., 1997) (age and education adjusted Score 24–30 inclusive), have memory complaints and objective memory loss (Mungas et al., 1996). Demographic and general medical history were obtained from volunteers after completing informed consent (Iyalomhe et al., 2015). Randomization of subjects to the intervention (aerobic participants) and control (stretch participants) groups occurred

Abbreviations: AA, African American; AD, Alzheimer's disease; CpG, CG dinucleotide; FDR, false discovery rate; GEMS, gene, exercise, and memory study; GO, gene ontology; MCI, mild cognitively impaired; RT-PCR, reverse transcription polymerase chain reaction; VO2max, maximal oxygen consumption.

before baseline tests. All staff, except those directly monitoring exercise-training, were blinded to group assignments. The data were de-identified using assigned unique identifiers for labeling and tracking.

Baseline Testing

Qualified participants underwent a maximal treadmill exercise test using the Bruce protocol (Bruce and Hornsten, 1969). Before randomization and baseline testing, participants maintained regular caloric intake and were instructed to continue throughout the study period. Except for those directly administering exercise-training, staff was blinded to group assignments. Baseline VO_2max and endurance capacity were obtained using a modified Bruce protocol (Chaitman, 2001). Participants were instructed to abstain from alcohol, smoking, and anti-inflammatory medications 24 h before the blood draw. Fasting blood samples were obtained using sterile techniques and stored in heparinized collection tubes to enable gene expression analyses.

Aerobic Exercise-Training Protocol

Individual maximal heart rate was inferred for both the intervention (aerobic exercise) and control (stretch exercise) groups from baseline VO_2max tests before undergoing supervised training 3 times/week using the American College of Sports Medicine Guidelines (ACSM) (Pollock and Froelicher, 1990). Aerobic participants performed exercise training included a warm-up period followed by treadmill walking or jogging, stair-stepping, and elliptical, and an appropriate cool-down period. Initial training sessions lasted 20 min at 50% VO_2max while monitoring protocol adherence using individual exercise heart rate and duration. Training duration increased by 5 min/week to 40 min at 50% VO_2max, and then, incrementally by 5% VO_2max/week until 70% VO_2max was achieved. Additionally, participants underwent unsupervised 45–60 min lower intensity walk on weekends after the initial 4–6 weeks' training.

Stretch Training Protocol

Training of the stretch group consisted of maintaining exercise positions for 15–30 s to produce a slight pull on the muscle but not to the point of triggering the sensation of pain. Using different positions for a total of about 40 min, each stretch was directed at often tight muscles (e.g., hamstrings, hip flexors, calves, and chest) and repeated slowly, 3–5 times on each body side 3 days/week (Pollock et al., 1998).

Follow-Up Test at 6 Months

After subjects completed the 6-month aerobic exercise or stretch training protocol, all baseline tests (VO_2max, blood tests) were repeated.

Sample Processing and Assessment of Methylation

Total DNA was isolated from clotted blood samples using a clotspin basket (Qiagen, Germany) to disperse the clot and then extracted using the MasterPure Complete DNA and RNA Purification Kit (Epicenter, cat#MC85200) according to the manufacturer's instructions. DNA concentration and purity (OD260/280) were measured using NanoDrop ND-1000 spectrophotometer (Thermo Fischer Scientific, United States). A minimum of 500 ng DNA was used for bisulfite conversion using the EZ DNA Methylation kit (Zymo Research, United States) and a GeneAmp PCR system 9,700 (Applied Biosystems, United States), and cleaned up per manufacturer's instructions. To confirm successful bisulfite modification, we subjected the DNA to PCR using methylation-specific primers. Methylation analysis was performed using the Illumina Infinium HumanMethylation450 Beadchip platform (Illumina Inc., United States). Briefly, bisulfite-modified DNA was fragmented into 300–600 bp fragments, purified by isopropanol precipitation, and resuspended in a hybridization buffer. The sample was then hybridized to an Illumina Infinium HumanMethylation450 Beadchip. The BeadChips were subsequently washed, stained, and dried according to the manufacturer's instructions. The BeadChips were then scanned using a HiScanSQ System (Illumina Inc., United States). Methylation data were processed through Illumina GenomeStudio (Illumina Inc., United States) and analyzed in Partek (Partek Inc., St. Louis, MO, United States). Included in the methylation analysis are those who completed 6 months of intervention with methylation data.

Pathway Analysis of CG Dinucleotide Sites in Aerobic Participants

We investigated the biological relevance of the genome-wide CpG sites associated with VO_2max by considering the 248 CpG sites and performing Ingenuity Pathway Analysis on the gene annotated sites. Among these 248 CpG sites, 165 annotated to the human reference genome build 37 (hg19). We performed a Gene Ontology (GO) enrichment analysis for the genes encompassing or adjacent to these differentially methylated CpG sites.

Quantitative Real-Time Polymerase Chain-Reaction

For quantitative RT-PCR analysis, total RNA was isolated from clotted blood samples using Trizol reagent according to the manufacturer's instructions (Thermo Fisher Scientific, MA, United States). In the reverse transcription (RT) step, cDNA was reverse transcribed from 300 ng total RNA samples in 20 μl reaction buffer using the High-Capacity RT-kit (Thermo Fisher Scientific, MA, United States). Gene expression level was assessed through TaqMan expression assay system using standard 2x master mixes and 20x FAM-MGM labeled probe sets. The 20x FAM-MGM labeled probe sets used in the study have the following Assay IDs: Hs00987064_m1 for VPS52, Hs01027208_m1 for NR1H2, Hs00605059_m1 for PPP2R5D, and Hs00969821_m1 for SCARB1 and Hs99999905_m1 for GAPDH (Thermo Fisher Scientific, MA, United States). All qPCR assays were performed in duplicate samples and normalized against GAPDH and baseline control. Relative quantitation analysis of gene expression was conducted according to the $2^{(-\Delta\Delta CT)}$ relative expression method as described (Livak and Schmittgen, 2001; Bedada et al., 2014). GAPDH was used as an endogenous internal standard for expression analysis to determine the

abundance of amplified target genes within the same sample. Reactions were monitored on Applied Biosystems ViiA^{TM} 7 Real-Time PCR System and analyzed data with corresponding ViiA 7 RUO software.

STATISTICAL ANALYSIS

Genome-wide methylation levels at CpG sites from participants at baseline and at 6 months after aerobic and stretch training were profiled using the Infinium HumanMethylation450 BeadChip assay (Illumina, San Diego, CA, United States). The raw intensity data of all samples were imported into the software Partek (St. Louis, MO, United States). SWAN method (Maksimovic et al., 2012) was selected to normalize array intensities. SWAN-normalized β values, which correspond to the percentage of methylation at a CpG site, were then calculated. Premised on the exclusion of probes with a detection p-value > 0.01 in one or more of the 22 samples for the downstream analysis, we discarded 6,942 probes while 478,570 probes remained.

Analyses examining baseline genome-wide CpG methylation and the influence of a 6-month aerobic exercise-training on methylations were conducted in STATA 14 software (StataCorp, 2015). First, all variables measured at baseline and post-6 months of exercise were examined descriptively, and their distributions were further inspected using Boxplots and Scatterplots (McGill et al., 1978; Royston and Cox, 2005). Student's t-test was used to compute mean estimates of continuous variables between groups of baseline measures; nonparametric Mann–Whitney rank test to derive p-values for group differences in non-normal continuous variables; and Chi-square and Exact tests to compare group differences in categorical variables. For continuous measures, and within each group (aerobic and stretch), a paired t-test was used to assess significant differences in means between baseline and six months.

Effects of exercise-induced changes in VO_2max (i.e., VO_2max at baseline and after a 6-month training) on genome-wide CpG methylation were examined within-individual level using linear mixed-effects analysis (West et al., 2014), and robust variance-covariance approach adjusted for standard errors of the coefficients. This is robust to differences in variances between groups and to violation of normality assumption. Because sampling distributions of test statistics are known to be t and F-distributed in simple cases in small sample studies, we also used Satterthwaite and Kenward-Roger denominator-degrees-of-freedom (DDF) adjustments for small-sample inference. Given the sample size, we report standard errors derived from Kenward-Roger DDF more closely similar to the bootstrap estimation of standard errors of randomly selected CpG methylations (Satterthwaite, 1946; Kenward and Roger, 1997).

To account for the multiplicity of tests from the genome-wide inquiry, we used the frequentist q–values approach. The q-value package inputs a variable of p–values and outputs a variable of q-values, equal in each observation to the minimum FWER or FDR that would result in the inclusion of the corresponding p-value in the discovery set if the specified multiple–test procedure was applied to the complete set of input p–values (Newson, 2010). We computed false discovery rates (FDR) using Sidak approaches (Šidák, 1967).

RESULTS

Characteristics of Aerobic and Stretch Participants

The baseline demographic characteristics (**Table 1**) were limited to aerobic participants ($n = 11$), and stretch participants ($n = 8$) who completed aerobic exercise- and stretch training had data for VO_2max and methylation data. Continuous measures were summarized using means and proportions for categories. The aerobic sample consisted of 72.7% females (mean age of 71.3 ± 6.6 years) and BMI (mean 26.8 ± 4.5 kg/m^2) at baseline. As anticipated, the participants had significant decreases in mean body weight ($p = 0.007$) after a 6-month training (158.8 ± 37.9 lbs.) compared to baseline (165.1 ± 6.0 lbs.). Although participants had increases in mean relative VO_2max after 6 months (25.1 ± 7.8) compared to baseline (22.7 ± 2.7), the differences were not statistically significant ($p = 0.414$). The stretch sample consisted of 75.0% females (mean age of

TABLE 1 | Baseline characteristics of participants (completers with methylation data).

Characteristics	Aerobic ($N = 11$)			Stretch ($N = 8$)		
	Baseline	6 Months	P-value	Baseline	6 Months	P-value
Age–years.	72.35 (6.63)		–	70.58 (6.69)		–
Gender (Female%)	8 (72.73%)		–	6 (75.00%)		–
Weight (lb.)	165.09 (38.56)	158.82 (37.94)	0.007	190.63 (20.19)	189.00 (18.69)	0.871
BMI (kg/m^2)	26.77 (4.55)	25.33 (3.69)	0.075	32.34 (5.47)	30.74 (3.33)	0.913
Max VO_2 (Relative)	22.74 (2.69)	25.08 (7.82)	0.414	24.72 (8.68)	22.84 (3.93)	0.442
Max VO_2 (Absolute)	1550.26 (532.42)	1870.75 (856.47)	0.252	2109.00 (597.85)	1934.00 (193.10)	0.411
Max systolic BP (mmHg)	169.89 (9.80)	–	–	200.00 (0.00)	–	–
Max diastolic BP (mmHg)	90.11 (11.94)	–	–	96.50 (9.19)	–	–
Max heart rate	147.91 (6.36)	146.80 (6.97)	0.003	149.63 (6.46)	145.43 (13.04)	0.302

Values are mean ± SD when appropriate. P-values were computed with paired t-tests.

70.58 ± 6.7 years) and BMI (mean 32.3 ± 5.5 kg/m^2) at baseline. After 6 months of training, mean body weight remained relatively unchanged ($p = 0.871$) in the stretch group.

Genome-Wide DNA Methylation of CG Dinucleotide Sites in Aerobic Participants

We examined the association between the intensity changes in 478,570 individual CpG sites and VO_2max after 6 months of aerobic exercise-training with adjustment for Age. As illustrated in genome-wide DNA methylation analysis of CpG intensities in **Figure 1A**, the distribution is based on the location and chromosomal position for all 478,570 probes in the Infinium HumanMethylation450 BeadChip assay. With the overall genomic inflation factor of all CpG sites being 1.03, the CpG sites exhibiting the most significant association with VO_2max was cg00160018 (beta = −0.002, se = 0.0002, $p = 5.38e-26$), located in the body of the nearest gene *VPS52* (**Table 2**). Several other CpG sites nearest to *SCARB1*, *ARTN*, *NR1H2*, *PPP2R5D* genes exhibited significant associations ($p < 10e-15$). After applying FDR correction (Sidak q-value < 0.1), we identified 248 CpG sites that exhibited differential DNA methylation after the 6-month aerobic exercise-training. Among these 248 CpG sites, 89 were located in the body; 35 in TSS1500; 17 in TSS200; 15 in 5′ UTR; 5 in 1st Exon; and 4 in the 3′ UTR regions to the nearest gene (**Figure 1B**). A total of 214 CpG sites had a decrease in intensities after exercise compared to 34 CpG sites showing an increase. Pathway analysis of the top 248 CpG sites identified several biological pathways, including the top 4 biological networks depicted in **Figure 2**. To determine whether the top 10 CpG sites identified in the aerobic-exercise group were similarly influenced by stretch exercise, we performed a linear mixed-effects comparative analysis to quantify the effects of exercise-induced methylation changes in the stretch participants. However, the stretch group failed to demonstrate significant training-related changes for the top 10 CpG sites observed in the aerobic group, providing additional evidence that the observed changes in the aerobic exercise group was motivated by fitness adaptation (**Supplementary Table 1**).

Gene Expression by Quantitative Real-Time Polymerase Chain-Reaction

Validation of Methylation Study

We examined mRNA levels of the top 5 hypomethylated genes—*VPS52*; *NR1H2*; *PPP2R5D*; *SCARB1* and *ARTN*—at baseline and post-exercise, normalized to *GADPH* (housekeeping gene) levels. As expected, mRNA levels of *VPS52* and *NR1H2* increased significantly compared to baseline levels (**Figures 3A,B**). However, the level of *PPP2R5D* was significantly reduced following exercise intervention compared to the baseline (**Figure 3C**), and the 6-month expression level of *SCARB1* remained unchanged compared to baseline (**Figure 3D**). ARTN primers failed to amplify in the blood samples.

DISCUSSION

In this sample of elderly AA MCI study participants, a 6-month standardized, and supervised aerobic exercise-training influenced global DNA methylation changes. While the most significant hypomethylations involved *VSP52*, *SACRB1*, *ARTN*, *NR1H2,* and *PPPLR5D* genes (**Table 2**), these genes were not similarly influenced by training effects in the stretch exercise group. We discuss the biological plausibility of our most important findings, consistency with previous studies, and coherence with the known roles of exercise on our molecular findings, and therefore on the pathophysiology of age-associated cognitive decline.

It is now acknowledged that physical activity can enhance brain plasticity and improve cognition and wellbeing

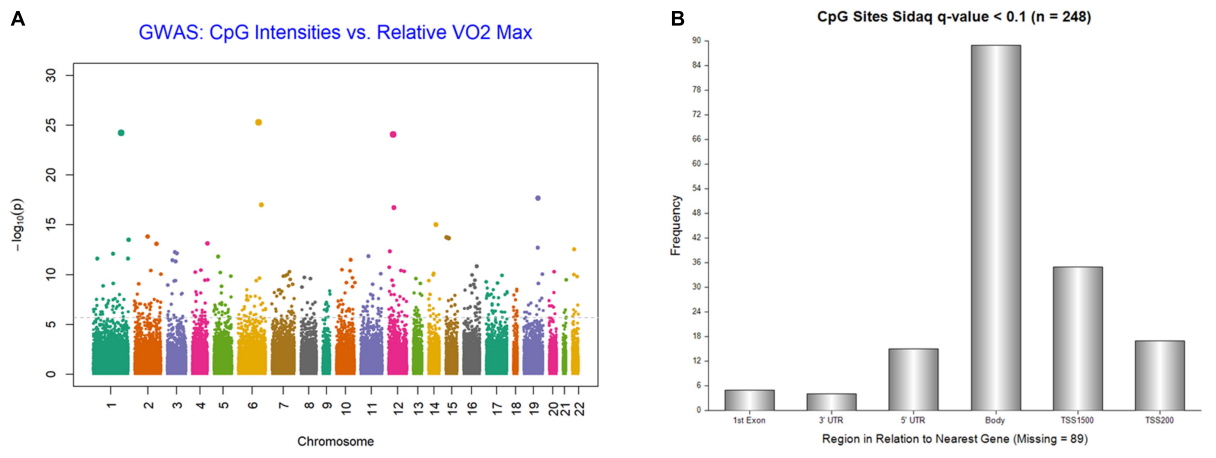

FIGURE 1 | (A) Genome-wide plot for DNA methylation analysis of CpG intensities and relative VO_2Max; distribution is based on location and chromosomal position for all 478,570 probes in Infinium HumanMethylation450 BeadChip assay. **(B)** Frequency of 248 CpG Islands by region to nearest Gene (sidakq < 0.1) that exhibited differential DNA methylation after 6-month aerobic exercise-training; 89 located in the Body; 35 in TSS1500; 17 in TSS200; 15 in 5′ UTR; 5 in 1st Exon; and 4 in the 3′ UTR regions to the nearest gene.

TABLE 2 | A 6-Month Aerobic Exercise Training–Induced Changes in DNA Methylation in African American MCI Subjects – Top 20 CpG Sites.

CpG	CHR	Gene Symbol	Gene Region	Percent	beta	se	*p*	sidakq
cg00160018	6	VPS52	Body	−0.71	−0.0020	0.0002	5.38E-26	0.00
cg11198639	12	SCARB1	Body	−2.55	−0.0063	0.0006	8.83E-25	0.00
cg17414508	1	ARTN	TSS1500	−1.23	−0.0049	0.0005	6.10E-25	0.00
cg24440997	19	NR1H2	TSS1500	−3.89	−0.0029	0.0003	2.06E-18	0.00
cg14385961	6	PPP2R5D	TSS200	−0.95	−0.0007	0.0001	9.83E-18	0.00
cg11132661	12			−0.92	−0.0018	0.0002	2.01E-17	0.00
cg02170785	14			−2.09	−0.0044	0.0006	9.71E-16	4.85E-10
cg02469461	2	CAB39	5′UTR	−0.48	−0.0015	0.0002	1.42E-14	6.90E-09
cg22988430	15	SNORD115-41	TSS200	−1.95	−0.0052	0.0007	1.84E-14	8.95E-09
cg08732418	15	DLL4	Body	−3.73	−0.0061	0.0008	2.13E-14	1.03E-08
cg14166197	1	CTNNBIP1	5′UTR	−1.11	−0.0027	0.0004	2.96E-14	1.44E-08
cg07794230	4			−0.66	−0.0018	0.0002	6.90E-14	3.35E-08
cg11124652	2			−2.05	−0.0064	0.0009	7.76E-14	3.77E-08
cg12104982	19	SAFB2	Body	−1.83	−0.0051	0.0007	1.95E-13	9.48E-08
cg15146966	22	XBP1	TSS1500	−1.78	−0.0011	0.0001	2.91E-13	1.41E-07
cg18926450	12	GIT2	3′UTR	−0.94	−0.0022	0.0003	4.69E-13	2.28E-07
cg22314684	3	PLD1	5′UTR	−1.39	−0.0033	0.0005	5.48E-13	2.66E-07
cg07403865	3	BCL6	5′UTR	−4.51	−0.0035	0.0005	7.48E-13	3.63E-07
cg24499975	1	MTR	TSS1500	4.54	0.0028	0.0004	8.38E-13	4.07E-07
cg24431486	11	CD81	Body	−1.39	−0.0023	0.0003	1.40E-12	6.79E-07

(Weinberg and Gould, 1999). Also, physical exercise can induce structural and functional changes in the brain and protect against neurodegeneration (Mandolesi et al., 2018). In a recent comprehensive review, Mandolesi et al. (2018) acknowledged the positive biological and psychological effects of physical activity on the brain through its enhancement of cognition, while Buchman et al. (2012) showed that physical activity reduced inflammation and improved memory in MCI and potentially Alzheimer's Disease patients (Buchman et al., 2012). However, the mechanisms underlying this beneficial effect of exercise on memory are poorly understood. The present study is a logical extension of our previously published work on the effects of aerobic exercise on global array expression in AA MCI volunteers, showing that aerobic-exercise can down-regulate the expression of pro-inflammatory genes, concomitantly up-regulate anti-inflammatory genes, and promoted the expression of genes involved in axonal growth and neuronal survival (Iyalomhe et al., 2015). While the aerobic group underwent progressive exercise intensity and duration to achieve individualized 70% VO2 Max and endurance capacity, the stretch (control) group only undergone progressive stretch exercise. Overall, exercise training-induced increases in endurance capacity and reduced body weight in the aerobic exercise group affirmed training effects. Conversely, a slight decline in VO2max and unchanged body weight, in the stretch group, underscore less fitness effects. Collectively, this methylation study provides additional insights into the mechanism underlying the advantageous effect of exercise on memory.

While the biological mechanisms contributing to the health benefits of exercise are well-acknowledged, the exact mechanism underlying its effects on memory remains mostly unknown. Exercise can reshape the epigenome and induce significant changes in DNA methylation (Lindholm et al., 2014). Its ability to activate or silence specific genes may, therefore, explain its effects on health. For example, acute intensity exercise can alter the methylation of exercise-responsive genes, resulting in DNA hypomethylation in skeletal muscle (Barres et al., 2012). In contrast, a 6-month exercise program in previously sedentary middle-aged men increased methylation in adipose tissue (Rönn et al., 2013). For example, Rönn et al. (2013) provided a detailed map of the genome-wide DNA methylation pattern in human adipose tissue and linked exercise to altered adipose tissue DNA methylation. Therefore, these epigenetic changes can alter gene expression and metabolism and thus inform the advantageous effects of exercise on health (Ling and Ronn, 2014). Nonetheless, understanding the consequent biologic cascade resulting in long-lasting effects of regular exercise-training on DNA methylation needs a more nuanced understanding. For example, Soci et al. (2017) showed that exercise-induced changes in DNA methylation could alter several molecular mechanisms such as muscle contraction, increased mitochondrial mass, oxidative and non-oxidative mechanisms as well as cardiac and skeletal hypertrophy (Soci et al., 2017). Interestingly, some of these mechanisms have implications for fitness and cerebral hemodynamics.

The most significant effect of a 6-month exercise in our study is the hypomethylation of vacuolar protein sorting homolog 52 (*VPS52*) gene, supported by a corresponding increase in its mRNA levels. *VPS52* is a crucial part of the Golgi-associated retrograde complex that plays an important role in cellular inter-compartment transport and is highly expressed in the brain[1]. In one experiment, the cortex of Amyloid Precursor Protein (APP)

[1]https://www.ncbi.nlm.nih.gov/gene/6293

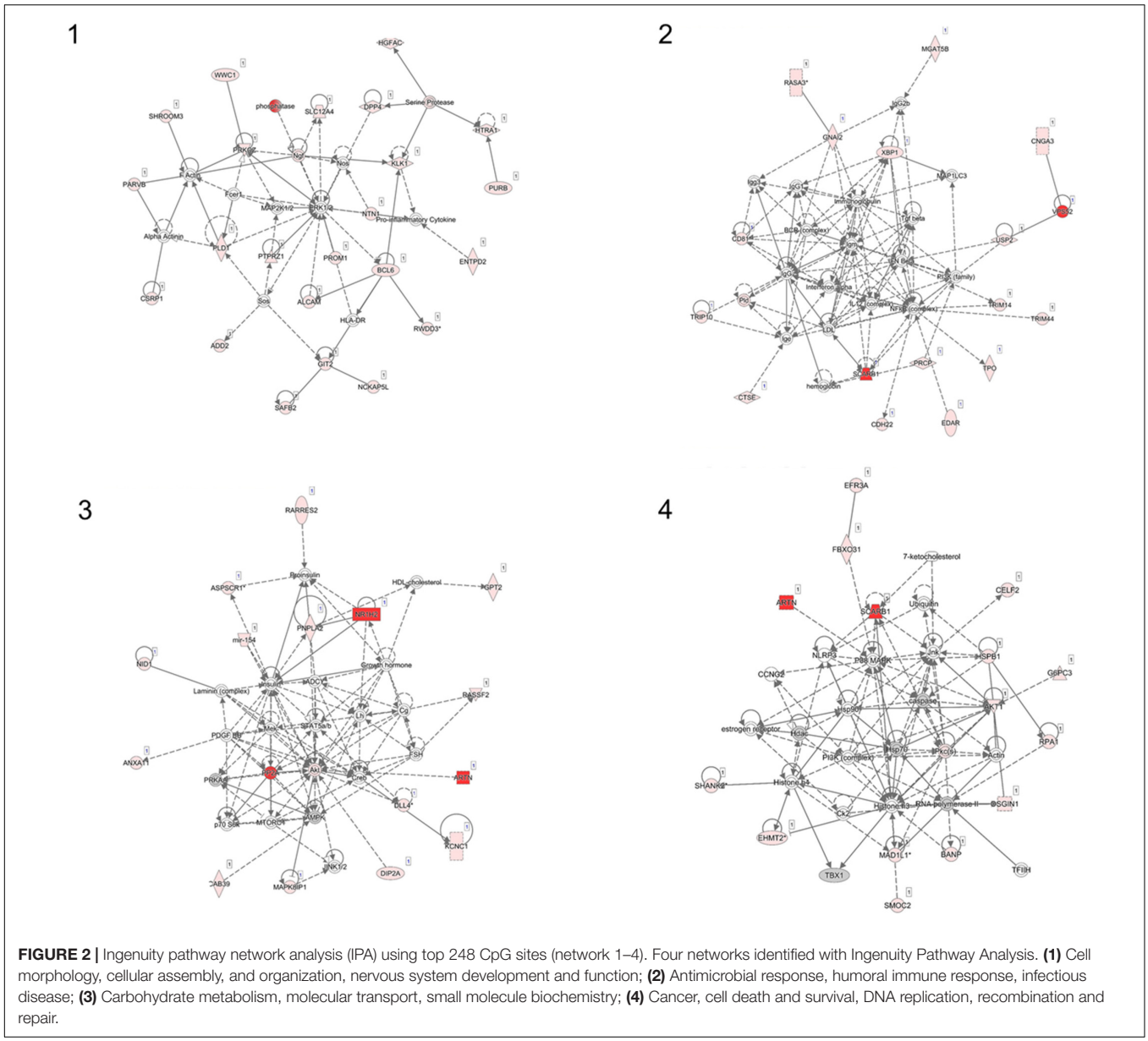

FIGURE 2 | Ingenuity pathway network analysis (IPA) using top 248 CpG sites (network 1–4). Four networks identified with Ingenuity Pathway Analysis. **(1)** Cell morphology, cellular assembly, and organization, nervous system development and function; **(2)** Antimicrobial response, humoral immune response, infectious disease; **(3)** Carbohydrate metabolism, molecular transport, small molecule biochemistry; **(4)** Cancer, cell death and survival, DNA replication, recombination and repair.

knockout mice exhibited the upregulation of *VPS52* and a related protein. Conversely, lipid dysregulation and elevated cerebral APP are associated with decreased expression of *VPS52* (Castello, 2015). Therefore, given *VPS52* complex interaction with lipid regulation in the context of changing APP build-up, studies are needed to understand the role of *VPS52* on memory and human aging.

Hypomethylation near Nuclear Receptor Subfamily 1 Group H Member 2 (NR1H2) gene was also associated with exercise-associated increases in its mRNA expression. This observation is likely significant in that dysfunctionality of the NR1H2 gene can promote late-onset AD (Patel and Forman, 2004; Adighibe et al., 2016). Because dysregulated cholesterol levels can induce amyloidogenesis (Infante et al., 2010), NR1H2-mediated cellular efflux of cholesterol may protect against AD development.

Although exercise-training was associated with methylation changes in Scavenger receptor class B member 1 (SCARB1), Protein Phosphatase 2 Regulatory Subunit B'Delta (PPP2R5D), and Artemin (ARTN), corresponding changes in gene expression remained non-significant in our study. Therefore, further studies are needed to discern their biological roles. For instance, SCARB1 encodes high-density lipoprotein receptor that regulates cholesterol efflux from the peripheral tissue to the liver, is present in astrocytes and vascular smooth muscle cells in AD brain, and has been demonstrated to mediate adhesion of microglia to fibrillar amyloid-β (Aβ) (El Khoury et al., 1996; Thanopoulou et al., 2010; Jawaid and Khalil, 2011; Mulder et al., 2012). PPP2R5D is an interesting finding because its mutations can promote intellectual disability (Houge et al., 2015) and the development of spatially restricted tauopathy by deregulating

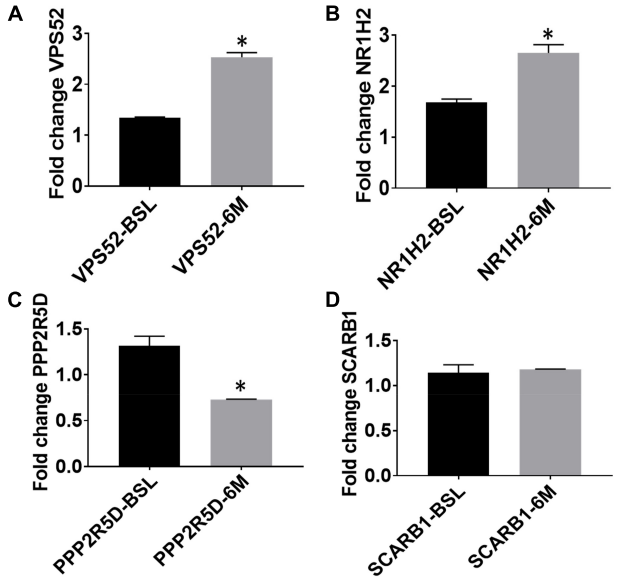

FIGURE 3 | Expression levels of top exercise induced hypomethylated genes at baseline and following aerobic exercise intervention (**A**, VPS52; **B**, NR1H2; **C**, PPP2R5D; **D,** SCARB1). Gene expression by quantitative RT-PCR; mRNA levels of top 4 hypomethylated genes for VPS52; NR1H2; PPP2R5D; SCARB1 at baseline and post-exercise. Note: * Indicates statistically significant training-induced changes in gene expression levels.

CDK5 and GSK3-beta in mice lacking PPP2R5D subunits (Louis et al., 2011). The PPP2R5D gene encodes the protein B56-delta (B56δ), a part of (B subunit) of the phosphatase 2A (PP2A) enzyme, which dephosphorylates other specific proteins, to control their activation. Since most of the affected proteins are involved in active signaling, the activation/inhibition of PPP2R5D is often tightly controlled (Wang et al., 2008); thereby making its expression levels less informative. Further, ARTN may be critical to neuronal survival, given that protein signals through the RET receptor and GFR alpha three coreceptors encoded by ARTN support the survival of several peripheral neurons and a population of dopaminergic CNS neurons (Zihlmann et al., 2005).

However, we note that gene (ARTN) did not amplify in blood cells, and an alternative primer yielded a similar result. Also, we verified from GeneCards (Stelzer et al., 2016) that, while the ARTN gene is widely expressed in nervous tissues, it is not expressed in blood cells. Because phosphatases and kinases (e.g., PPP2R5D and GSK3β) are regulated more by post-translational modifications, increases in their activities are often associated with compensatory decreased mRNA levels through other pathways, and vice versa. While our methylation result is consistent with an expectation of increased levels of PPP2R5D, the incongruent decrease in mRNA levels suggests other regulatory factors may be involved. Also, our finding of training-induced changes in SCARB1 methylation is notable, given its expression in astrocytes (Mulder et al., 2012). Nonetheless, our findings are significant to current knowledge on exercise training-induced changes on blood methylation profile in MCI subjects.

The inaccessibility of living human brain tissue in AD studies motivated our consideration for using human peripheral blood to evaluate methylation profile following exercise intervention. Several studies have reported that DNA methylation patterns in human blood parallel epigenetic changes in the brain (Horvath et al., 2012; Walton et al., 2016). For example, Horvath et al. (2012) noted a correlation r = 0.9 across whole-blood and postmortem brain tissue methylation datasets, suggesting that blood DNA methylation profiles may be a promising surrogate for brain tissue (Horvath et al., 2012). Using blood obtained premortem, Davies et al. (2012) showed that individual methylation profile correlated with relevant postmortem brain tissue (cortex and cerebellum) methylation levels (correlation coefficient = 0.66–0.76) (Davies et al., 2012). Further, a recent systematic review of the DNA methylation studies showed that epigenetics changes in the peripheral blood of AD patients correlated with AD pathology (Wei et al., 2020). Acknowledged associations of DNA methylation in peripheral blood cells of AD patients with poor cognitive performances and APOE ε4 polymorphism are consistent with this report (Di Francesco et al., 2015). Thus, our approach to investigate methylation changes in peripheral blood following exercise intervention provides valuable insight into the mechanism underlying the effects of fitness adaptation on methylation, and potentially, on experimentally inaccessible human brain and neurodegeneration.

CONCLUSION AND LIMITATION

Our study revealed global changes in DNA methylations following 6 months of standardized and supervised aerobic exercise training in MCI subjects. The relevance of some of these genes to AD pathophysiology provides further evidence to the likely significance of aerobic exercise in moderating AD pathophysiology in MCI populations. An important limitation of this pilot study is the relatively small sample size. Nonetheless, we provide novel insight into the effect of aerobic exercise on the epigenome. Our plan includes testing these findings in larger samples and informing the genes' relationship with cognitive phenotype and disease progression spectrum.

DATA AVAILABILITY STATEMENT

The datasets presented in this study can be found in online repositories. The names of the repository/repositories and accession number(s) can be found below: https://www.ebi.ac.uk/arrayexpress/ with accession E-MTAB-11166.

ETHICS STATEMENT

The studies involving human participants were reviewed and approved by the Howard University Institutional Review Board (IRB). The patients/participants provided their written informed consent to participate in this study.

AUTHOR CONTRIBUTIONS

JN, EN, and TO conceived the study, cleaned, and analyzed the data. FB performed RNA isolation, cDNA preparation, conducted Q-PCR gene expression experimental setup, and analysis. JN, EN, FB, and TO wrote the manuscript. All authors contributed to study design and strategies for analyses, and participated in the review of the final manuscript.

FUNDING

This work was supported by the National Institute on Aging at the National Institutes of Health (NIH) grant R01 5R01AG31517 and 5R01AG045058 to TO, and in part by Grant #UL1TR000101 from National Center for Advancing Translational Sciences/NIH through the Clinical and Translational Science Award Program (CTSA). The funders had no role in the design, data collection, and interpretation of this study, and the content is solely the responsibility of the authors and does not necessarily represent the official views of the National Institutes of Health.

ACKNOWLEDGMENTS

We thank all our colleagues in the Division of Geriatrics, Department of Medicine and Clinical/Translational Science Program, Howard University Hospital. We are grateful to all the participants included in the study. We also acknowledge that an abstract of the current work has been published in Alzheimer's and Dementia, The Journal of Alzheimer's Association. DOI: https://doi.org/10.1016/j.jalz.2017.07.582.

SUPPLEMENTARY MATERIAL

The Supplementary Material for this article can be found online at: https://www.frontiersin.org/articles/10.3389/fnmol.2021.752403/full#supplementary-material

REFERENCES

Adighibe, O., Leek, R. D., Fernandez-Mercado, M., Hu, J., Snell, C., Gatter, K. C., et al. (2016). Why some tumours trigger neovascularisation and others don't: the story thus far. *Chin. J. Cancer* 35:18. doi: 10.1186/s40880-016-0082-6

Barres, R., Yan, J., Egan, B., Treebak, J. T., Rasmussen, M., Fritz, T., et al. (2012). Acute exercise remodels promoter methylation in human skeletal muscle. *Cell Metab.* 15, 405–411. doi: 10.1016/j.cmet.2012.01.001

Bedada, F. B., Chan, S. S., Metzger, S. K., Zhang, L., Zhang, J., Garry, D. J., et al. (2014). Acquisition of a quantitative, stoichiometrically conserved ratiometric marker of maturation status in stem cell-derived cardiac myocytes. *Stem Cell Rep.* 3, 594–605. doi: 10.1016/j.stemcr.2014.07.012

Bird, A. (2007). Perceptions of epigenetics. *Nature* 447, 396–398.

Bruce, R. A., and Hornsten, T. R. (1969). Exercise stress testing in evaluation of patients with ischemic heart disease. *Prog. Cardiovasc. Dis.* 11, 371–390. doi: 10.1016/0033-0620(69)90027-9

Buchman, A., Boyle, P., Yu, L., Shah, R., Wilson, R., and Bennett, D. (2012). Total daily physical activity and the risk of AD and cognitive decline in older adults. *Neurology* 78, 1323–1329.

Castello, M. A. (2015). *Lipid Regulation as a Critical Factor in the Development of Alzheimer's Disease*. Electronic thesis. Loma Linda, CA: Loma Linda University.

Chaitman, B. (2001). "Exercise stress testing," in *Heart Disease: A Textbook of Cardiovascular Medicine*, Vol. 5, ed. E. Braunwald (Philadelphia, PA: WB Saunders), 153–177.

Choy, M.-K., Movassagh, M., Goh, H.-G., Bennett, M. R., Down, T. A., and Foo, R. S. (2010). Genome-wide conserved consensus transcription factor binding motifs are hyper-methylated. *BMC Genomics* 11:519. doi: 10.1186/1471-2164-11-519

Davies, M. N., Volta, M., Pidsley, R., Lunnon, K., Dixit, A., Lovestone, S., et al. (2012). Functional annotation of the human brain methylome identifies tissue-specific epigenetic variation across brain and blood. *Genome Biol.* 13, 1–14. doi: 10.1186/gb-2012-13-6-r43

Di Francesco, A., Arosio, B., Falconi, A., Micioni Di Bonaventura, M. V., Karimi, M., Mari, D., et al. (2015). Global changes in DNA methylation in Alzheimer's disease peripheral blood mononuclear cells. *Brain Behav. Immun.* 45, 139–144. doi: 10.1016/j.bbi.2014.11.002

El Khoury, J., Hickman, S. E., Thomas, C. A., Cao, L., Silverstein, S. C., and Loike, J. D. (1996). Scavenger receptor-mediated adhesion of microglia to β-amyloid fibrils. *Nature* 382:716. doi: 10.1038/382716a0

Gluckman, P. D., Hanson, M. A., Buklijas, T., Low, F. M., and Beedle, A. S. (2009). Epigenetic mechanisms that underpin metabolic and cardiovascular diseases. *Nat. Rev. Endocrinol.* 5, 401–408. doi: 10.1038/nrendo.2009.102

Hashimshony, T., Zhang, J., Keshet, I., Bustin, M., and Cedar, H. (2003). The role of DNA methylation in setting up chromatin structure during development. *Nat. Genet.* 34, 187–192. doi: 10.1038/ng1158

Horvath, S., Zhang, Y., Langfelder, P., Kahn, R. S., Boks, M. P., van Eijk, K., et al. (2012). Aging effects on DNA methylation modules in human brain and blood tissue. *Genome Biol.* 13:R97. doi: 10.1186/gb-2012-13-10-r97

Houge, G., Haesen, D., Vissers, L. E., Mehta, S., Parker, M. J., Wright, M., et al. (2015). B56δ-related protein phosphatase 2A dysfunction identified in patients with intellectual disability. *J. Clin. Invest.* 125, 3051–3062. doi: 10.1172/JCI79860

Infante, J., Rodríguez-Rodríguez, E., Mateo, I., Llorca, J., Vázquez-Higuera, J. L., Berciano, J., et al. (2010). Gene–gene interaction between heme oxygenase-1 and liver X receptor-β and Alzheimer's disease risk. *Neurobiol. Aging* 31, 710–714. doi: 10.1016/j.neurobiolaging.2008.05.025

Iyalomhe, O., Chen, Y., Allard, J., Ntekim, O., Johnson, S., Bond, V., et al. (2015). A standardized randomized 6-month aerobic exercise-training down-regulated pro-inflammatory genes, but up-regulated anti-inflammatory, neuron survival and axon growth-related genes. *Exp. Gerontol.* 69, 159–169. doi: 10.1016/j.exger.2015.05.005

Jawaid, M., and Khalil, H. A. (2011). Cellulosic/synthetic fibre reinforced polymer hybrid composites: a review. *Carbohydr. Polym.* 86, 1–18. doi: 10.1016/j.carbpol.2011.04.043

Kenward, M. G., and Roger, J. H. (1997). Small sample inference for fixed effects from restricted maximum likelihood. *Biometrics* 53, 983–997. doi: 10.2307/2533558

Lindholm, M. E., Marabita, F., Gomez-Cabrero, D., Rundqvist, H., Ekström, T. J., Tegnér, J., et al. (2014). An integrative analysis reveals coordinated reprogramming of the epigenome and the transcriptome in human skeletal muscle after training. *Epigenetics* 9, 1557–1569. doi: 10.4161/15592294.2014.982445

Ling, C., and Ronn, T. (2014). Epigenetic adaptation to regular exercise in humans. *Drug Discov. Today* 19, 1015–1018. doi: 10.1016/j.drudis.2014.03.006

Livak, K. J., and Schmittgen, T. D. (2001). Analysis of relative gene expression data using real-time quantitative PCR and the $2^{-\Delta\Delta CT}$ method. *methods* 25, 402–408. doi: 10.1006/meth.2001.1262

Louis, J. V., Martens, E., Borghgraef, P., Lambrecht, C., Sents, W., Longin, S., et al. (2011). Mice lacking phosphatase PP2A subunit PR61/B'δ (Ppp2r5d) develop spatially restricted tauopathy by deregulation of CDK5 and GSK3β. *Proc. Natl. Acad. Sci. U.S.A.* 108, 6957–6962. doi: 10.1073/pnas.1018777108

Maksimovic, J., Gordon, L., and Oshlack, A. (2012). SWAN: subset-quantile within array normalization for illumina infinium HumanMethylation450 BeadChips. *Genome Biol.* 13:R44. doi: 10.1186/gb-2012-13-6-r44

Mandolesi, L., Polverino, A., Montuori, S., Foti, F., Ferraioli, G., Sorrentino, P., et al. (2018). Effects of physical exercise on cognitive functioning and wellbeing: biological and psychological benefits. *Front. Psychol.* 9:509. doi: 10.3389/fpsyg.2018.00509

Matheson, G. O., Klügl, M., Engebretsen, L., Bendiksen, F., Blair, S. N., Börjesson, M., et al. (2013). Prevention and management of non-communicable disease: the IOC consensus statement, Lausanne 2013. *Br. J. Sports Med.* 47, 1003–1011. doi: 10.1136/bjsports-2013-093034

McGill, R., Tukey, J. W., and Larsen, W. A. (1978). Variations of box plots. *Am. Stat.* 32, 12–16. doi: 10.2307/2683468

Mulder, S. D., Veerhuis, R., Blankenstein, M. A., and Nielsen, H. M. (2012). The effect of amyloid associated proteins on the expression of genes involved in amyloid-β clearance by adult human astrocytes. *Exp. Neurol.* 233, 373–379. doi: 10.1016/j.expneurol.2011.11.001

Mungas, D., Marshall, S., Weldon, M., Haan, M., and Reed, B. (1996). Age and education correction of mini-mental state examination for English-and Spanish-speaking elderly. *Neurology* 46, 700–706. doi: 10.1212/wnl.46.3.700

Newson, R. B. (2010). Frequentist q-values for multiple-test procedures. *Stata J.* 10, 568–584. doi: 10.1177/1536867x1101000403

Nitert, M. D., Dayeh, T., Volkov, P., Elgzyri, T., Hall, E., Nilsson, E., et al. (2012). Impact of an exercise intervention on DNA methylation in skeletal muscle from first-degree relatives of patients with type 2 diabetes. *Diabetes* 61, 3322–3332. doi: 10.2337/db11-1653

Patel, N. V., and Forman, B. M. (2004). Linking lipids, Alzheimer's and LXRs? *Nucl. Recept. Signal.* 2:02001. doi: 10.1621/nrs.02001

Petersen, R. C., Smith, G. E., Waring, S. C., Ivnik, R. J., Kokmen, E., and Tangelos, E. G. (1997). Aging, memory, and mild cognitive impairment. *Int. Psychogeriatr.* 9(Suppl. 1), 65–69. doi: 10.1017/s1041610297004717

Pollock, M. L., and Froelicher, V. F. (1990). Position stand of the american college of sports medicine: the recommended quantity and quality of exercise for developing and maintaining cardiorespiratory and muscular fitness in healthy adults. *J. Cardiopulm. Rehabil. Prev.* 10, 235–245.

Pollock, M. L., Gaesser, G. A., Butcher, J. D., Després, J. P., Dishman, R. K., Franklin, B. A., et al. (1998). ACSM position stand: the recommended quantity and quality of exercise for developing and maintaining cardiorespiratory and muscular fitness, and flexibility in healthy adults. *Med. Sci. Sports Exerc.* 30, 975–991. doi: 10.1097/00005768-199806000-00032

Rivera, C. M., and Ren, B. (2013). Mapping human epigenomes. *Cell* 155, 39–55. doi: 10.1016/j.cell.2013.09.011

Rönn, T., Volkov, P., Davegårdh, C., Dayeh, T., Hall, E., Olsson, A. H., et al. (2013). A six months exercise intervention influences the genome-wide DNA methylation pattern in human adipose tissue. *PLoS Genet.* 9:e1003572. doi: 10.1371/journal.pgen.1003572

Royston, P., and Cox, N. J. (2005). A multivariable scatterplot smoother. *Stata J.* 5, 405–412. doi: 10.1177/1536867x0500500309

Satterthwaite, F. E. (1946). An approximate distribution of estimates of variance components. *Biometr. Bull.* 2, 110–114. doi: 10.2307/3002019

Šidák, Z. (1967). Rectangular confidence regions for the means of multivariate normal distributions. *J. Am. Stat. Assoc.* 62, 626–633. doi: 10.1080/01621459.1967.10482935

Soci, U. P. R., Melo, S. F. S., Gomes, J. L. P., Silveira, A. C., Nobrega, C., and de Oliveira, E. M. (2017). Exercise training and epigenetic regulation: multilevel modification and regulation of gene expression. *Adv. Exp. Med. Biol.* 1000, 281–322. doi: 10.1007/978-981-10-4304-8_16

StataCorp (2015). *Stata Statistical Software (Version Release 14)*. College Station, TX: StataCorp LP.

Stelzer, G., Rosen, N., Plaschkes, I., Zimmerman, S., Twik, M., Fishilevich, S., et al. (2016). The GeneCards suite: from gene data mining to disease genome sequence analyses. *Curr. Protoc. Bioinformatics* 54, 1–1.30.33. doi: 10.1002/cpbi.5

Thanopoulou, K., Fragkouli, A., Stylianopoulou, F., and Georgopoulos, S. (2010). Scavenger receptor class B type I (SR-BI) regulates perivascular macrophages and modifies amyloid pathology in an Alzheimer mouse model. *Proc. Natl. Acad. Sci. U.S.A.* 107, 20816–20821. doi: 10.1073/pnas.1005888107

Walton, E., Hass, J., Liu, J., Roffman, J. L., Bernardoni, F., Roessner, V., et al. (2016). Correspondence of DNA methylation between blood and brain tissue and its application to schizophrenia research. *Schizophr. Bull.* 42, 406–414. doi: 10.1093/schbul/sbv074

Wang, B., Zhang, P., and Wei, Q. (2008). Recent progress on the structure of Ser/Thr protein phosphatases. *Sci. China Ser. C Life Sci.* 51, 487–494. doi: 10.1007/s11427-008-0068-y

Wei, X., Zhang, L., and Zeng, Y. (2020). DNA methylation in Alzheimer's disease: in brain and peripheral blood. *Mech. Ageing Dev.* 191:111319. doi: 10.1016/j.mad.2020.111319

Weinberg, R., and Gould, D. (1999). *Foundations of Sport and Exercise Psychology*. Stanningley: Human Kinetics Publishers (UK) Ltd.

West, B. T., Welch, K. B., and Galecki, A. T. (2014). *Linear Mixed Models: A Practical Guide Using Statistical Software*. Boca Raton, FL: Chapman and Hall/CRC.

Zihlmann, K. B., Ducray, A. D., Schaller, B., Huber, A. W., Krebs, S. H., Andres, R. H., et al. (2005). The GDNF family members neurturin, artemin and persephin promote the morphological differentiation of cultured ventral mesencephalic dopaminergic neurons. *Brain Res. Bull.* 68, 42–53. doi: 10.1016/j.brainresbull.2004.10.012

Conflict of Interest: The authors declare that the research was conducted in the absence of any commercial or financial relationships that could be construed as a potential conflict of interest.

Publisher's Note: All claims expressed in this article are solely those of the authors and do not necessarily represent those of their affiliated organizations, or those of the publisher, the editors and the reviewers. Any product that may be evaluated in this article, or claim that may be made by its manufacturer, is not guaranteed or endorsed by the publisher.

frontiers in Aging Neuroscience

ORIGINAL RESEARCH
published: 28 January 2022
doi: 10.3389/fnagi.2021.790939

Changes in Serum Cystatin C Levels and the Associations With Cognitive Function in Alzheimer's Disease Patients

*Xueping Chen, Yan Huang, Ting Bao, Fu Jia, Ruwei Ou, Qianqian Wei, Yongping Chen, Jiao Liu, Jing Yang and Huifang Shang**

West China Hospital, Sichuan University, Chengdu, China

Background and Objective: Cystatin C is indicated to be involved in the pathogenesis of Alzheimer's disease (AD) and cognitive impairment. Our objective is to examine the serum Cystatin C levels, and to clarify the correlations between serum Cystatin C and cognitive performance in Chinese AD patients.

Methods: The serum Cystatin C concentrations in AD patients and age, sex, and body mass index (BMI) matched-healthy controls were measured. The cognitive functions of the AD patients were evaluated by using the Mini-mental State Examination (MMSE) and the Montreal Cognitive Assessment (MoCA). The severity of dementia was determined with clinical dementia rating (CDR).

Results: A total of 463 AD patients and 1,389 matched healthy subjects were included. AD patients had higher serum Cystatin C than healthy controls. Serum cystatin C levels were correlated with MoCA scores in AD patients. In an ordinal logistic regression model, AD patients with higher serum cystatin C levels had increased odds of severe cognitive dysfunction.

Conclusion: Our study suggested that AD patients had higher levels of serum cystatin C than age/sex/BMI-matched normal control subjects. Higher serum cystatin C may be associated with worse cognitive performance, but more studies are required to verify such association.

Keywords: neurodegenerative diseases, Alzheimer's disease, cystatin C, cognition, association analysis

OPEN ACCESS

Edited by:
Henrik Zetterberg,
University of Gothenburg, Sweden

Reviewed by:
Roberta Ghidoni,
San Giovanni di Dio Fatebenefratelli Center (IRCCS), Italy
Wei Ling Lau,
University of California, Irvine, United States

****Correspondence:***
Huifang Shang
hfshang2002@163.com

Specialty section:
This article was submitted to Alzheimer's Disease and Related Dementias, a section of the journal Frontiers in Aging Neuroscience

Received: *07 October 2021*
Accepted: *20 December 2021*
Published: *28 January 2022*

Citation:
Chen X, Huang Y, Bao T, Jia F, Ou R, Wei Q, Chen Y, Liu J, Yang J and Shang H (2022) Changes in Serum Cystatin C Levels and the Associations With Cognitive Function in Alzheimer's Disease Patients. Front. Aging Neurosci. 13:790939. doi: 10.3389/fnagi.2021.790939

INTRODUCTION

Cystatin C is highly expressed in the brain and cerebrospinal fluid (CSF) (Löfberg and Grubb, 1979), and it is indicated to play many roles in the risk and pathobiology for Alzheimer's disease (AD) (Taupin et al., 2000; Palmer et al., 2001; Gauthier et al., 2011). Genetically, the CST3 B haplotype of cystatin C was considered to be a risk factor for AD, frontotemporal dementia (FTD), and Lewy body dementia (LBD) (Finckh et al., 2000; Bertram et al., 2007; Maetzler et al., 2010; Hua et al., 2012). Clinically, in patients with FTD and LBD, a reduction of CSF cystatin C was found, and it was associated with an anticipation of dementia onset (Rüetschi et al., 2005; Sundelöf et al., 2008; Maetzler et al., 2010).

Specifically, in patients with AD, cystatin C levels in CSF were found to be reduced, compared to individuals without dementia (Simonsen et al., 2007; Hansson et al., 2009; Zhong et al., 2013), and CSF cystatin C levels were positively correlated with tau and Aβ levels (Sundelöf et al., 2010; Zhong et al., 2013). However, another study found increased cystatin C levels in CSF of AD patients compared to those in controls (Carrette et al., 2003). In plasma, a study found that AD patients had higher plasma cystatin C levels than healthy control subjects (Wang R. et al., 2017). The association of serum cystatin C with risk of mild cognitive impairment (MCI) or dementia was inconsistent. The Health ABC Study showed that high levels of serum cystatin C increased the risk of cognitive impairment and individuals with higher levels of cystatin C had poorer performance on cognitive examinations (Yaffe et al., 2008). In contrast, the Uppsala Longitudinal Study found that high levels of serum cystatin C were related to a decreased risk of AD in men aged between 70 and 77 years-old (Sundelöf et al., 2008), and a study also found that MCI patients with higher serum cystatin C levels remained stable, without developing to dementia (Romero-Sevilla et al., 2018). Moreover, the Osteoporotic Fractures study reported a *U*-shape association between serum cystatin C and cognitive impairment in elderly women, but the association no longer existed after adjusting for covariates (Slinin et al., 2015). However, there is no study focusing on the association of serum cystatin C levels with cognitive performance in AD patients.

In this study we are aiming to examine the levels of serum cystatin C in AD patients and compare to those in matched healthy subjects, and trying to determine whether serum cystatin C levels are associated with the severity of the dementia.

MATERIALS AND METHODS

Patients and Ethics Statement

This study was performed at the Department of Neurology, Sichuan University West China Hospital, Chengdu, China. From Jan 2014 to Dec 2019, a total of 463 patients with probable AD were enrolled. The diagnosis of AD was based on the criteria issued by the National Institute of Neurological and Communicative Disorders and Stroke-Alzheimer's Disease and Related Disorders Association (NINCDS-ADRDA) The individual, semistructured interviews were conducted with participants and their close informants. Demographic data, including sociodemographic characteristics, lifestyle, medical history, current medications, and family history, were collected. Clinical data related to cognitive impairments, including time of onset, possible triggers, course of condition, impact on daily activities, changes in mood or behavior, and treatment and its effects, were also recored. Last, standardized general and neurological examinations were performed. The diagnoses were made at the end of each interviews according to the NINCDS-ADRDA criteria (McKhann et al., 1984). AD patients participated in the standardized assessments, including the Mini-mental State Examination (MMSE), the Montreal Cognitive Assessment (MoCA), and magnetic resonance imaging (MRI). AD patients with MMSE score higher than 25 were excluded. A total of 1,389 healthy controls (HCs) were also recruited from the Medical Examination Centre of West China Hospital, and they were 3:1 and age/gender/body mass index (BMI)-matched to the AD patients. The HCs also received MMSE and MoCA evaluation. Since MMSE has shown not to be adequate in detecting MCI and clinical signs of dementia, and MoCA is superior to MMSE in the identification of MCI (Pinto et al., 2019), HCs with MMSE score higher than 25 and MoCA sore higher than 22 were included in the present study. Participants, including both AD patients and HCs, who were diagnosed with vascular dementia (VaD), cardiopathy, hypertension, diabetes mellitus, and renal dysfunction, were also excluded. All participants underwent hematological examinations considered to be part of the diagnostic workshop. Peripheral blood samples from the cubital vein were acquired from each AD patient and HCs. Samples were taken by venipuncture, performed between 9:00 and 11:00 a.m., after fasting from midnight. The blood specimens were left at room temperature for 30 min to clot and centrifuged for 10 min at 1,200 g. The cystatin C levels were measured by the automated particle-enhanced immunoturbidimetric method, and the measurement were completed in the Olympus AU5400 analyzer (Olympus, Tokyo, Japan) using the manufacturer's reagents and according to the manufacturer's instructions. The quality of all analyses was assured by appropriate quality control. The kidney function was evaluated using the estimated glomerular filtration rate (eGFR); the calculation of eGFR was completed using the abbreviated Modification of Diet in Renal Disease (MDRD) formula, recommended by K/DOQI as the preferred equation for eGFR (Lameire et al., 2006). When eGFR was 60/mL/min/1.73 m^2 or less, an impaired renal function was considered. DNA was isolated from blood cells. Samples were amplified by polymerase chain reaction (ABI 7500 FAST, Applied Biosystem, Thermofisher, Waltham, USA). APOE haplotypes were determined according to the manufacturer's instruction with the use of ViennaLab ApoE Strip Assay (Memorigen, Xiamen, China).

This study was approved by the Ethical Committee of West China Hospital of Sichuan University. All AD patients and control subjects gave their written informed consent to participate in the investigation.

Clinical Evaluation

The following variables were collected: age of onset, sex, BMI, education level, frequent physical activity, smoke, and alcohol consumption. The Clinical Dementia Rating (CDR) is an informant-based global assessment scale with established reliability and validity, and it is utilized as a severity-ranking scale in AD patients in the present study. The cognitive performance was rated in six domains: memory, orientation, judgment and problem solving, community affairs, home and hobbies, and personal care. Each domain is rated according to one of five levels of impairment, and the cognitive dysfunction was defined as follow: mild (CDR = 0.5 or 1), moderate (CDR = 2) and severe (CDR = 3).

Statistical Analysis

Comparisons of continuous variables between two groups were made using Student's *t*-test. The Kolmogorov-Smirnov

test was applied in all continuous variables to verify the presence of normality. A $\chi 2$ test was used to compare the categorical variables. One-way ANOVA was performed for three group comparisons of normally-distributed continuous variables. Pearson's non-parametric correlation was applied to investigate the existence of linear association of the serum cystatin C levels and eGFR values to the cognitive performance. The association between cystatin C levels with CDR grading was assessed using ordinal logistic regression model, which was used to predict the CDR stage using serum cystatin C levels in a single model, potential confounders, including age of onset, sex, disease duration, and carriage of the APOE4 allele were allowed in the analyses. This method makes the parallel regression assumption for all variables across the grading of CDR stage. All data were presented in the form of mean ± standard deviation, and they were analyzed using SPSS 17.0. A p-value of <0.05 was considered to be statistically significant.

RESULTS

This cross-sectional study included 463 AD patients [231 males (49.9%) and 232 (50.1%) females], and 1,389 healthy subjects [693 males (49.9%) and 696 females (50.1%)]. The MRI scan supported the diagnosis of the included AD patients, who had medial temporal 146 lobe atrophy, and the Fazekas scale of white matter lesions was <2. The mean age at examination of the AD patients and HCs were 69.00 ± 11.31 and 69.08 ± 11.28 years, respectively. Serum cystatin C levels in AD patients were significantly higher than those in normal subjects (1.034 ± 0.254 vs. 1.010 ± 0.248, $p = 0.0362$). The cognitive performances evaluated by MMSE or MoCA were poorer in AD patients compared to those in HCs (**Table 1**).

In order to determine the association between serum cystatin C levels and cognitive impairment, we stratified the cohort based on the CDR grade (mild CDR = 0.5 or 1, moderate CDR = 2, severe CDR = 3). The one-way ANOVA analyses showed that the serum cystatin C levels were not significantly different among AD patients with different severities of dementia ($p = 0.6588$). In addition, the correlation analyses were utilized to investigate the correlations between serum cystatin C levels and cognitive performance assessed by MMSE and MoCA (**Table 2**), and a significant correlation between serum cystatin C levels and MoCA scores was identified ($r_s = -0.1326$, $p = 0.046$). However, the correlation analyses showed that serum cystatin C levels were not correlated to the cognitive performance in HCs (MMSE: $r_s = -0.09827$, $p = 0.1728$; MoCA: $r_s = -0.1455$, $p = 0.0798$). Serum cystatin C levels was also found to be significantly associated with age at examination in both AD patients and HCs (AD patients: $r_s = 0.4869$, $p < 0.0001$; HCs: $r_s = 0.5033$, $p < 0.0001$). The ordinal logistic regression stratified by CDR grade was conducted, and the results of the model for predicting CDR grade using cystatin C level showed age at onset, sex, disease duration and presence of *APOE* $\varepsilon 4$ allele were not significant risk factors in this model. However, serum cystatin C levels were slightly associated with severity of cognitive impairment (OR = 1.438, 95% CI 0.017–2.858, $p = 0.047$). With regard to the cognitive predictors, AD patients with a 1-point increase in cystatin C levels were 48% more likely to have a higher CDR grade, indicating the AD patients with higher cystatin C levels may have increased odds of severe cognitive dysfunction.

DISCUSSION

Cystatin C, a cysteine protease inhibitor, is produced by most nucleated cells and present in all body fluids. In the present study, we found that serum cystatin C levels were increased in AD patients than healthy controls, which was supported by some studies (Straface et al., 2005; Wang R. et al., 2017). In contrast, a previous study reported that the plasma cystatin C levels were lower in AD patients than in controls (Chuo et al., 2007), and another studies did not find significant differences in plasma cystatin C levels between AD patients and healthy controls (Kálmán et al., 2000; Ghidoni et al., 2010; Zhong et al., 2013). Plasma cystatin C was also indicated to modulate the clinical expression of cognitive decline; a significant anticipation of the conversion to dementia was observed in MCI subjects, when the detected plasma cystatin C levels were below 1,067 ng/ml (Ghidoni et al., 2010). Such discrepancy may be caused by the differences in sample sizes, characters of participants and genetic backgrounds. To our knowledge, the current study included the largest sample to determine the difference in serum cystatin C levels between AD patients and healthy subjects.

Cystatin C is an inhibitor of cathepsins. Cathepsin D is suggested to be involved in the pathogenesis of AD, and the cathepsin D level is increased in AD patients (Nixon, 2000). The increase of this cathepsin-inhibitory enzyme in AD patients may represent a compensatory activity aimed at counteracting the increased presence of cathepsin D. Cystatin C levels were also increased in response to injury and oxidative stress (Finckh et al., 2000; Nishio et al., 2000). In the central nervous system (CNS), cystatin C can protect neuronal cells from degeneration induced by fibrillar and oligomeric Aβ (Tizon et al., 2010). Co-incubate cystatin C with monomeric Aβ42 can attenuate the formation of Aβ oligomers and protofibrils (Sastre et al., 2004; Selenica et al., 2007), and increase the cystatin C expression can reduce parenchymal Aβ load in CNS (Kaeser et al., 2007; Mi et al., 2007). In addition, the peripheral production of Aβ can be derived from peripheral organs and tissues, including various blood and endothelial cells (Wang J. et al., 2017). The accumulation of Aβ deposits in the peripheral system may stimulate the expression of cystatin C. However, the exact mechanism of increased serum cystatin C in AD patients is not clear. We have to notice that the serum cystatin C is cleared from the circulation by glomerular filtration, and it can be affected by renal function, but the increase of serum cystatin C level in AD patients cannot be simply attributable to the changes of renal function since we did not find any difference in eGFR between AD patients and controls. Furthermore, ANCOVA adjusting for eGFR showed consistent result of significantly higher serum cystatin C levels in AD patients. The findings of the association of serum cystatin C with cognitive impairment were inconsistent: one study did not find any associations in AD patients (Zhong et al., 2013), but another

TABLE 1 | Demographic and clinical characteristics of patients with AD and healthy controls.

Characteristics	AD ($n = 463$)	Controls ($n = 1,389$)	p-value
Male, *n* (%)	231 (49.9)	693 (49.9)	1
Age at examination, yr	69.00 ± 11.31	69.08 ± 11.28	0.9016
BMI	22.36 ± 3.63	22.58 ± 3.89	0.8321
eGFR (ml/min)	101.13 ± 21.16	104.76 ± 19.53	0.5961
APOE 4 allele carriers (%)	33.48%		
Serum cystatin C (mg/l)	1.034 ± 0.254	1.010 ± 0.248	**$P = 0.0362$**
MMSE	15.92 ± 7.33	27.18 ± 3.23	**$p < 0.001$**
MoCA	10.33 ± 6.45	24.98 ± 1.13	**$p < 0.001$**
Age at onset, yr	67.58 ± 10.12		
Disease duration, mo	17.61		
CDR staging (0.5 or 1/2/3)	148/163/152		
MMSE according to CDR staging	22.88 ± 2.93/15.47 ± 3.29/6.68 ± 3.33		
MoCA according to CDR staging	17.65 ± 4.22/10.19 ± 3.35/5.25 ± 2.85		

yr, year; mo, month; MMSE, Mini-Mental State Examination; MoCA, Montreal Cognitive Assessment (MoCA); CDR, clinical dementia rating. The meaning of the bold values is $P < 0.05$.

TABLE 2 | Correlations of serum cystatin C levels and eGFR values with cognitive performance.

	Serum cystatin C		eGFR values	
	r	p-value	R	p-value
MMSE	−0.08484	0.1496	−0.03495	0.6295
MoCA	−0.1326	**0.0460**	−0.1282	0.1230

The meaning of the bold values is $P < 0.05$.

study found a significant correlation between serum cystatin C levels and MMSE scores in female AD patients (Wang R. et al., 2017). In the current study, we found that serum cystatin C levels were negatively associated with cognitive function assessed by MoCA, higher serum cystatin C levels were weakly related to poorer cognitive performance. In addition, we found a significant positive correlation between serum cystatin C and age in both AD patients and healthy subjects. Previous studies also found this association in AD patients (Chuo et al., 2007; Zhong et al., 2013). Therefore, the association between serum cystatin C and age is not disease-specific. Since age is the biggest risk factor for AD (McCartney et al., 2018), we compared the age-at-examination among AD patients with different CDR score, but the differences in age-at-examination were not significant in patients with different level of cognitive dysfunction. We also compared the serum cystatin C levels among AD patients with different severity of dementia, and we did not find any differences in serum cystatin C levels among patients with mild, moderate, or severe dementia evaluated by CDR. However, using ordinal logistic regression models, we found that serum cystatin C levels were slightly associated with cognitive dysfunction; patients with higher cystatin C levels had increased odds of severe cognitive impairment. Similarly, a previous study found that among community-resident elders, those with increased serum cystatin C levels had poorer performance in cognitive tests evaluated by the Modified Mini-Mental State Examination (3MS) and the Digit Symbol Substitution Test (DSST) (Yaffe et al., 2008). Another study also evaluated the cystatin C levels in 193 participants older than 90, and found that higher tertiles of cystatin C was related with poorer global cognition, executive function and visual-spatial ability (Lau et al., 2020). Similarly, the Cardiovascular Health Study Cognition Study reported that high serum levels of cystatin C were related to poorer cognitive performance 6 years later (Riverol et al., 2015). However, the results of previous studies that correlated cystatin C with AD required careful interpretation. First, the association between cystatin C and cognition may underscore the connection between kidney function and cognitive function. Studies have shown that subjects with renal dysfunction had an elevated risk of developing dementia and poorer performance on cognitive function (Seliger et al., 2004; Martens et al., 2017). Cystatin C was found to be associated with cognitive performance in 90+ year-olds; among them nearly 90% had cystatin C levels more than 1.0, indicating that the kidney function is impaired. Further study also gave 308 individuals aged 90 or older a PET scan and obtained the brain indices of Aβ deposition using a statistically defined region of interest (statROI), and found that PET statROI was not correlated with cystatin C and eGFR, indicating an independent association between cognition and chronic kidney disease (CKD), and the CKD-associated cognitive dysfunction largely reflects vascular rather than Aβ pathology (Lau et al., 2021). Second, the correlation between serum cystatin C and cognitive function may not only depend on kidney function. In the present study, no significant differences in eGFR were found among patients with different degrees of dementia stratified by CDR grade, and the eGFR values were not associated with cognition evaluated by MMSE and MoCA. In addition, a previous study also found that elders with high serum cystatin C levels had higher risks of cognitive impairment whether or not they had CKD (Yaffe et al., 2008).

There are some limitations in the present study which should not be ignored: (1) the genetic CST3 genotypes were not considered; (2) the results of the present cannot be extrapolated to other populations since our patients were recruited from a

single specialized unit. On the other hand, some of the strengths of our study are the strict inclusion criteria, the examination of APOE genotype, and the fact that the specialized neurologists conducted all the data collections and manifestation assessments.

CONCLUSION

In summary, the findings of the current study support the idea that cystatin C plays an essential role in the pathogenesis of AD. Our results suggest AD patients had higher levels of serum cystatin C when compared to age/sex/BMI-matched normal controls, and higher serum cystatin C levels were weakly associated with worse cognitive performance in AD patients. Our findings strengthen the evidence that serum cystatin C may be involved in modulating the clinical expression of cognitive decline. Further longitudinal studies in larger cohorts and distinct ethnic groups will be needed to validate our findings, and to determine the mechanisms underlying this association.

DATA AVAILABILITY STATEMENT

The original contributions presented in the study are included in the article/supplementary material, further inquiries can be directed to the corresponding author/s.

AUTHOR CONTRIBUTIONS

HS conceived this study. YH, TB, RO, QW, YC, JL, and JY did the patient evaluation and data collection. FJ did the statistical analysis. XC and HS wrote the manuscript while all authors revised and discussed to the final edition. All authors contributed to the article and approved the submitted version.

FUNDING

This study was supported by grant from National key Research and development program of China (Grant No. 2017YFC09007703), grant from science and technology planning project in Sichuan Province (Grant No. 2020YJ0281), grant from 1·3·5 project for disciplines of excellence West China Hospital Sichuan University (Grant No. ZYJC18038), and the grant from cadres health care project in Sichuan Province (Grant No. 2019-112).

ACKNOWLEDGMENTS

The authors gratefully acknowledge the AD patients for their participation in this study.

REFERENCES

Bertram, L., McQueen, M. B., Mullin, K., Blacker, D., and Tanzi, R. E. (2007). Systematic meta-analyses of Alzheimer disease genetic association studies: the AlzGene database. *Nat. Genet.* 39, 17–23. doi: 10.1038/ng1934

Carrette, O., Demalte, I., Scherl, A., Yalkinoglu, O., Corthals, G., Burkhard, P., et al. (2003). A panel of cerebrospinal fluid potential biomarkers for the diagnosis of Alzheimer's disease. *Proteomics* 3, 1486–1494. doi: 10.1002/pmic.200300470

Chuo, L. J., Sheu, W. H., Pai, M. C., and Kuo, Y. M. (2007). Genotype and plasma concentration of cystatin C in patients with late-onset Alzheimer disease. *Dement. Geriatr. Cogn. Disord.* 23, 251–257. doi: 10.1159/000100021

Finckh, U., von der Kammer, H., Velden, J., Michel, T., Andresen, B., Deng, A., et al. (2000). Genetic association of a cystatin C gene polymorphism with late-onset Alzheimer disease. *Arch. Neurol.* 57, 1579–1583. doi: 10.1001/archneur.57.11.1579

Gauthier, S., Kaur, G., Mi, W., Tizon, B., and Levy, E. (2011). Protective mechanisms by cystatin C in neurodegenerative diseases. *Front. Biosci.* 3, 541–554. doi: 10.2741/s170

Ghidoni, R., Benussi, L., Glionna, M., Desenzani, S., Albertini, V., Levy, E., et al. (2010). Plasma cystatin C and risk of developing Alzheimer's disease in subjects with mild cognitive impairment. *J. Alzheimers Dis.* 22, 985–991. doi: 10.3233/JAD-2010-101095

Hansson, S. F., Andréasson, U., Wall, M., Skoog, I., Andreasen, N., and Wallin, A. (2009). Reduced levels of amyloid-beta-binding proteins in cerebrospinal fluid from Alzheimer's disease patients. *J. Alzheimers Dis.* 16, 389–397. doi: 10.3233/JAD-2009-0966

Hua, Y., Zhao, H., Lu, X., Kong, Y., and Jin, H. (2012). Meta-analysis of the cystatin C(CST3) gene G73A polymorphism and susceptibility to Alzheimer's disease. *Int. J. Neurosci.* 122, 431–438. doi: 10.3109/00207454.2012.672502

Kaeser, S. A., Herzig, M. C., Coomaraswamy, J., Kilger, E., Selenica, M. L., Winkler, D. T., et al. (2007). Cystatin C modulates cerebral beta-amyloidosis. *Nat. Genet.* 39, 1437–1439. doi: 10.1038/ng.2007.23

Kálmán, J., Márki-Zay, J., Juhász, A., Sántha, A., Dux, L., and Janka, Z. (2000). Serum and cerebrospinal fluid cystatin C levels in vascular and Alzheimer's dementia. *Acta Neurol. Scand.* 101, 279–282. doi: 10.1034/j.1600-0404.2000.101004279.x

Lameire, N., Adam, A., Becker, C. R., Davidson, C., McCullough, P. A., Stacul, F., et al. (2006). Baseline renal function screening. *Am J Cardiol.* 98, 21K−26K. doi: 10.1016/j.amjcard.2006.01.021

Lau, W. L., Fisher, M., Fletcher, E., DeCarli, C., Troutt, H., Corrada, M. M., et al. (2021). Kidney function is not related to brain amyloid burden on PET imaging in the 90+ Study Cohort. *Front. Med.* 8, 671945. doi: 10.3389/fmed.2021.671945

Lau, W. L., Fisher, M., Greenia, D., Floriolli, D., Fletcher, E., Singh, B., et al. (2020). Cystatin, C., cognition, and brain MRI findings in 90+-year-olds. *Neurobiol. Aging* 93, 78–84. doi: 10.1016/j.neurobiolaging.2020.04.022

Löfberg, H., and Grubb, A. O. (1979). Quantitation of gamma-trace in human biological fluids: indications for production in the central nervous system. *Scand. J. Clin. Lab. Invest.* 39, 619–626. doi: 10.3109/00365517909108866

Maetzler, W., Schmid, B., Synofzik, M., Schulte, C., Riester, K., Huber, H., et al. (2010). The CST3 BB genotype and low cystatin C cerebrospinal fluid levels are associated with dementia in Lewy body disease. *J. Alzheimers Dis.* 19, 937–942. doi: 10.3233/JAD-2010-1289

Martens, R. J., Kooman, J. P., Stehouwer, C. D., Dagnelie, P. C., van der Kallen, C. J., Koster, A., et al. (2017). Estimated GFR, albuminuria and cognitive performance: The Maastricht Study. *Am. J. Kidney Dis.* 69, 179–191. doi: 10.1053/j.ajkd.2016.04.017

McCartney, D. L., Stevenson, A. J., Walker, R. M., Gibson, J., Morris, S. W., Campbell, A., et al. (2018). Investigating the relationship between DNA methylation age acceleration and risk factors for Alzheimer's disease. *Alzheimers Dement.* 10, 429–437. doi: 10.1016/j.dadm.2018.05.006

McKhann, G., Drachman, D., Folstein, M., Katzman, R., Price, D., and Stadlan, E. M. (1984). Clinical diagnosis of Alzheimer's disease: report of the NINCDS-ADRDA Work Group under the auspices of Department of Health and Human Services Task Force on Alzheimer's Disease. *Neurology* 34, 939–944. doi: 10.1212/WNL.34.7.939

Mi, W., Pawlik, M., Sastre, M., Jung, S. S., Radvinsky, D. S., Klein, A. M., et al. (2007). Cystatin C inhibits amyloid-beta deposition in Alzheimer's disease mouse models. *Nat. Genet.* 39, 1440–1442. doi: 10.1038/ng.2007.29

Nishio, C., Yoshida, K., Nishiyama, K., Hatanaka, H., and Yamada, M. (2000). Involvement of cystatin C in oxidative stress-induced apoptosis of cultured rat CNS neurons. *Brain Res.* 873, 252–262. doi: 10.1016/S0006-8993(00)02540-3

Nixon, R. A. (2000). A "protease activation cascade" in the pathogenesis of Alzheimer's disease. *Ann. N. Y. Acad. Sci.* 924:117–131. doi: 10.1111/j.1749-6632.2000.tb05570.x

Palmer, T. D., Schwartz, P. H., Taupin, P., Kaspar, B., Stein, S. A., and Gage, F. H. (2001). Cell culture. Progenitor cells from human brain after death. *Nature* 411, 42–43. doi: 10.1038/35075141

Pinto, T. C. C., Machado, L., Bulgacov, T. M., Rodrigues-Júnior, A. L., Costa, M., Ximenes, R., et al. (2019). Is the Montreal Cognitive Assessment (MoCA) screening superior to the Mini-Mental State Examination (MMSE) in the detection of mild cognitive impairment (MCI) and Alzheimer's Disease (AD) in the elderly? *Int. Psychogeriatr.* 31, 491–504. doi: 10.1017/S1041610218001370

Riverol, M., Becker, J. T., López, O. L., Raji, C. A., Thompson, P. M., Carmichael, O. T., et al. (2015). Relationship between systemic and cerebral vascular disease and brain structure integrity in normal elderly individuals. *J. Alzheimers Dis.* 44, 319–328. doi: 10.3233/JAD-141077

Romero-Sevilla, R., Casado-Naranjo, I., Portilla-Cuenca, J. C., Duque-de San Juan, B., Fuentes, J. M., and Lopez-Espuela, F. (2018). Vascular risk factors and lesions of vascular nature in magnetic resonance as predictors of progression to dementia in patients with mild cognitive impairment. *Curr. Alzheimer Res.* 15, 671–678. doi: 10.2174/1567205015666180119100840

Rüetschi, U., Zetterberg, H., Podust, V. N., Gottfries, J., Li, S., Hviid Simonsen, A., et al. (2005). Identification of CSF biomarkers for frontotemporal dementia using SELDI-TOF. *Exp. Neurol.* 196, 273–281. doi: 10.1016/j.expneurol.2005.08.002

Sastre, M., Calero, M., Pawlik, M., Mathews, P. M., Kumar, A., Danilov, V., et al. (2004). Binding of cystatin C to Alzheimer's amyloid beta inhibits *in vitro* amyloid fibril formation. *Neurobiol. Aging* 25, 1033–1043. doi: 10.1016/j.neurobiolaging.2003.11.006

Selenica, M. L., Wang, X., Ostergaard-Pedersen, L., Westlind-Danielsson, A., and Grubb, A. (2007). Cystatin C reduces the *in vitro* formation of soluble Abeta1-42 oligomers and protofibrils. *Scand. J. Clin. Lab. Invest.* 67, 179–190. doi: 10.1080/00365510601009738

Seliger, S. L., Siscovick, D. S., Stehman-Breen, C. O., Gillen, D. L., Fitzpatrick, A., Bleyer, A., et al. (2004). Moderate renal impairment and risk of dementia among older adults: the Cardiovascular Health Cognition Study. *J. Am. Soc. Nephrol.* 15, 1904–1911. doi: 10.1097/01.ASN.0000131529.60019.FA

Simonsen, A. H., McGuire, J., Podust, V. N., Hagnelius, N. O., Nilsson, T. K., Kapaki, E., et al. (2007). A novel panel of cerebrospinal fluid biomarkers for the differential diagnosis of Alzheimer's disease versus normal aging and frontotemporal dementia. *Dement. Geriatr. Cogn. Disord.* 24, 434–440. doi: 10.1159/000110576

Slinin, Y., Peters, K. W., Ishani, A., Yaffe, K., Fink, H. A., Stone, K. L., et al. (2015). Cystatin C and cognitive impairment 10 years later in older women. *J. Gerontol. A Biol. Sci. Med. Sci.* 70, 771–778. doi: 10.1093/gerona/glu189

Straface, E., Matarrese, P., Gambardella, L., Vona, R., Sgadari, A., Silveri, M. C., et al. (2005). Oxidative imbalance and cathepsin D changes as peripheral blood biomarkers of Alzheimer disease: a pilot study. *FEBS Lett.* 579, 2759–2766. doi: 10.1016/j.febslet.2005.03.094

Sundelöf, J., Arnlöv, J., Ingelsson, E., Sundström, J., Basu, S., Zethelius, B., et al. (2008). Serum cystatin C and the risk of Alzheimer disease in elderly men. *Neurology* 71, 1072–1079. doi: 10.1212/01.wnl.0000326894.40353.93

Sundelöf, J., Sundström, J., Hansson, O., Eriksdotter-Jönhagen, M., Giedraitis, V., Larsson, A., et al. (2010). Cystatin C levels are positively correlated with both Abeta42 and tau levels in cerebrospinal fluid in persons with Alzheimer's disease, mild cognitive impairment, and healthy controls. *J. Alzheimers Dis.* 21, 471–478. doi: 10.3233/JAD-2010-091594

Taupin, P., Ray, J., Fischer, W. H., Suhr, S. T., Hakansson, K., Grubb, A., et al. (2000). FGF-2-responsive neural stem cell proliferation requires CCg, a novel autocrine/paracrine cofactor. *Neuron* 28, 385–397. doi: 10.1016/S0896-6273(00)00119-7

Tizon, B., Ribe, E. M., Mi, W., Troy, C. M., and Levy, E. (2010). Cystatin C protects neuronal cells from amyloid-beta-induced toxicity. *J. Alzheimers Dis.* 19, 885–894. doi: 10.3233/JAD-2010-1291

Wang, J., Gu, B. J., Masters, C. L., and Wang, Y. J. (2017). A systemic view of Alzheimer disease - insights from amyloid-β metabolism beyond the brain. *Nat. Rev. Neurol.* 13, 612–623. doi: 10.1038/nrneurol.2017.111

Wang, R., Chen, Z., Fu, Y., Wei, X., Liao, J., Liu, X., et al. (2017). Plasma cystatin C and high-density lipoprotein are important biomarkers of Alzheimer's disease and vascular dementia: a cross-sectional study. *Front. Aging Neurosci.* 9, 26. doi: 10.3389/fnagi.2017.00026

Yaffe, K., Lindquist, K., Shlipak, M. G., Simonsick, E., Fried, L., Rosano, C., et al. (2008). Cystatin C as a marker of cognitive function in elders: findings from the health ABC study. *Ann. Neurol.* 63, 798–802. doi: 10.1002/ana.21383

Zhong, X. M., Hou, L., Luo, X. N., Shi, H. S., Hu, G. Y., He, H. B., et al. (2013). Alterations of CSF cystatin C levels and their correlations with CSF Aβ40 and Aβ42 levels in patients with Alzheimer's disease, dementia with lewy bodies and the atrophic form of general paresis. *PLoS ONE* 8, e55328. doi: 10.1371/journal.pone.0055328

Conflict of Interest: The authors declare that the research was conducted in the absence of any commercial or financial relationships that could be construed as a potential conflict of interest.

Publisher's Note: All claims expressed in this article are solely those of the authors and do not necessarily represent those of their affiliated organizations, or those of the publisher, the editors and the reviewers. Any product that may be evaluated in this article, or claim that may be made by its manufacturer, is not guaranteed or endorsed by the publisher.

frontiers in Aging Neuroscience

ORIGINAL RESEARCH
published: 21 February 2022
doi: 10.3389/fnagi.2022.812169

Identification and Analysis of *BCAS4/hsa-miR-185-5p/SHISA7* Competing Endogenous RNA Axis in Late-Onset Alzheimer's Disease Using Bioinformatic and Experimental Approaches

Hani Sabaie[1,2], Mahnaz Talebi[3], Jalal Gharesouarn[2], Mohammad Reza Asadi[2], Abbas Jalaiei[2], Shahram Arsang-Jang[4], Bashdar Mahmud Hussen[5,6], Mohammad Taheri[7], Reza Jalili Khoshnoud[8,9]* and Maryam Rezazadeh[1,2]**

[1] Clinical Research Development Unit of Tabriz Valiasr Hospital, Tabriz University of Medical Sciences, Tabriz, Iran, [2] Department of Medical Genetics, Faculty of Medicine, Tabriz University of Medical Sciences, Tabriz, Iran, [3] Neurosciences Research Center (NSRC), Tabriz University of Medical Sciences, Tabriz, Iran, [4] Cancer Gene Therapy Research Center, Zanjan University of Medical Sciences, Zanjan, Iran, [5] Department of Pharmacognosy, College of Pharmacy, Hawler Medical University, Erbil, Iraq, [6] Center of Research and Strategic Studies, Lebanese French University, Erbil, Iraq, [7] Institute of Human Genetics, Jena University Hospital, Jena, Germany, [8] Skull Base Research Center, Loghman Hakim Hospital, Shahid Beheshti University of Medical Sciences, Tehran, Iran, [9] Functional Neurosurgery Research Center, Shahid Beheshti University of Medical Sciences, Tehran, Iran

Alzheimer's disease (AD) is a heterogeneous degenerative brain disorder with a rising prevalence worldwide. *SHISA7* (*CKAMP59*) has emerged as one of the most intriguing new members of the SHISA family, in that, unlike other CKAMP counterparts, it exhibits a direct function in inhibitory synaptic GABAAR regulation. We used bioinformatics and experimental methods in this research to explore competing endogenous RNA (ceRNA) regulation of *BCAS4* and *SHISA7* in tau pathogenesis and their capacity as peripheral biomarkers linked to an abnormal inflammatory response in AD. The Gene Expression Omnibus database included two microarray datasets, including information on mRNAs (GSE106241) and miRNAs (GSE157239) from individuals with AD with different degrees of AD-associated neurofibrillary pathology in the temporal cortex (TC) tissue specimens and corresponding controls were downloaded from the Gene Expression Omnibus database. The limma package in the R software was used to identify differently expressed mRNAs (DEmRNAs) and miRNAs (DEmiRNAs) associated with AD-related neurofibrillary pathology. Additionally, we used the quantitative polymerase chain reaction technique to examine the expression of the *BCAS4/hsa-miR-185-5p/SHISA7* ceRNA axis in the peripheral blood (PB) of fifty AD patients and fifty control subjects. *BCAS4* was shown to act as a ceRNA to control the *SHISA7* expression throughout AD-associated neurofibrillary pathology in TC tissue specimens by sponging *hsa-miR-185-5p*, based on our bioinformatics study. Furthermore, in PB specimens from individuals suffering from AD and normal controls, we found no substantial differences in *BCAS4* expression patterns. *SHISA7* expression in AD patients' PB was found to be reduced, as was the case in the TC. On the other hand, we discovered reduced amounts of *hsa-miR-185-5p* in AD patients' PB samples compared to control subjects, unlike in TC tissue, where it had been demonstrated to be overexpressed. *BCAS4* and

OPEN ACCESS

Edited by:
Henrik Zetterberg, University of Gothenburg, Sweden

Reviewed by:
Rezvan Noroozi, Jagiellonian University, Poland
Amin Safa, Complutense University of Madrid, Spain

***Correspondence:**
Mohammad Taheri
mohammad.taheri@uni-jena.de
Reza Jalili Khoshnoud
drkhoshnoud@gmail.com
Maryam Rezazadeh
rezazadehma@tbzmed.ac.ir

Specialty section:
This article was submitted to Alzheimer's Disease and Related Dementias, a section of the journal Frontiers in Aging Neuroscience

Received: *09 November 2021*
Accepted: *18 January 2022*
Published: *21 February 2022*

Citation:
Sabaie H, Talebi M, Gharesouarn J, Asadi MR, Jalaiei A, Arsang-Jang S, Hussen BM, Taheri M, Jalili Khoshnoud R and Rezazadeh M (2022) Identification and Analysis of BCAS4/hsa-miR-185-5p/SHISA7 Competing Endogenous RNA Axis in Late-Onset Alzheimer's Disease Using Bioinformatic and Experimental Approaches. Front. Aging Neurosci. 14:812169. doi: 10.3389/fnagi.2022.812169

SHISA7 expression levels showed a strong positive correlation, suggesting the presence of an interconnected network, most likely as a result of ceRNA regulation among PB specimens. The present study is the first evidence to highlight the expression of the *BCAS4/miR-185-5p/SHISA7* ceRNA axis in the brain and PB of AD patients, and offers a new viewpoint on molecular processes underlying AD pathogenic mechanisms.

Keywords: Alzheimer's disease, *BCAS4*, competing endogenous RNA, miR-185, *SHISA7*

INTRODUCTION

Alzheimer's disease (AD) is known as a type of dementia and a progressive neurodegenerative disorder (NDD), causing memory, thinking, and behavioral problems (Kang et al., 2020). According to the Alzheimer's Association, AD accounts for 60–80 percent of dementia people. Nowadays, 50 million individuals worldwide suffer from AD and other types of dementia. After the age of 65, every 5 years, the incidence of AD doubles (Fan et al., 2019). Symptoms usually appear gradually and worsen with time. Regarding genetic aspects, AD is a heterogeneous polygenic disorder. The illness has been divided into two types based on the age of onset: early-onset AD (EOAD) and late-onset AD (LOAD). The most prevalent type of dementia is LOAD, commonly known as sporadic AD (SAD). AD is a complicated disease caused by susceptible genes and also environmental variables (Rezazadeh et al., 2019). Epigenetic alterations such as non-coding RNA regulation, DNA methylation, and histone modification may all impact tau phosphorylation regulation directly or indirectly, hence contributing to the development and progression of AD (Yu et al., 2019; Noroozi et al., 2021). On the other hand, genes have an important influence on AD. LOAD has a heritability of 58–79 percent, whereas EOAD has over 90 percent. The genetic association studies have helped us comprehend the etiology of AD. There are now around 50 loci linked to AD. These data strongly imply that AD is a complicated illness (Sims et al., 2020). The buildup of β-amyloid peptide (Aβ) within the brain and hyperphosphorylated and cleaved microtubule-associated protein tau are two core pathologies of AD. It is documented that neurofibrillary tangles (NFTs) and senile plaques are formed due to metabolic malfunction of Aβ precursor protein (APP) and aberrant phosphorylation of the protein tau (Kang et al., 2020) or maybe their interaction with each other (Busche and Hyman, 2020). Genetic, biochemical, and behavioral studies show that the pathologic formation of the neurotoxic Aβ peptide following serial APP proteolysis is a key stage in AD pathogenesis. Furthermore, APP is quickly and intricately processed by sequential secretases, including β-site APP-cleaving enzyme 1 (BACE1), γ-secretase, and the ADAM family as α-secretases. In terms of tau proteolysis, this mechanism is critical in tau aggregation and neurodegeneration. The Microtubule-Associated Protein Tau (*MAPT*) gene encodes tau, a microtubule-associated protein primarily generated in neurons. Intracellular tau is occasionally hyperphosphorylated, forming dangerous oligomers and observable aggregates as NFTs (Kang et al., 2020). During the last decade, a third fundamental characteristic of AD has arisen, which may give insight into the pathogenesis of AD and a connection between the two types of main pathologies (Kinney et al., 2018). The pathogenesis of AD affects a variety of inflammatory molecules, with aberrant amounts in several brain areas (Akiyama et al., 2000; Wilson et al., 2002). Aβ and APP stimulate the production of cytokines and chemokines from neurons, microglia, and astrocytes; chemokines and cytokines also increase the synthesis and accumulation of Aβ, therefore activating the vicious cycle (Solfrizzi et al., 2006). Moreover, neuroinflammation, defined by microglial activation prior to tau tangle development, might be an early occurrence and play a critical role in the pathology of tau. In P301S transgenic mice, immunosuppression improved tau pathology (Metcalfe and Figueiredo-Pereira, 2010). Furthermore, the peripheral level of inflammation-associated cytokines varies throughout the pathogenesis of AD and is substantially associated with disease development (Motta et al., 2007; Holmes et al., 2009; Leung et al., 2013). As a result, to decipher the mechanism of the pathogenesis of AD, the crosstalk between aberrant phenomena in the central and the peripheral immune system should be understood (Dionisio-Santos et al., 2019; Park et al., 2020). Irrespective of the pathological features, synaptic dysfunction is largely regarded as a causative phenomenon in AD. There are two primary synapses (glutamatergic and GABAergic) in the central nervous system (CNS), which produce excitatory and inhibitory responses, respectively. A large body of evidence suggests that the glutamatergic system is compromised throughout disease progression. Nonetheless, new data suggest that the GABAergic pathway experiences pathogenic changes and contributes to AD development (Li et al., 2016).

SHISA7 (*CKAMP59*) has emerged as an intriguing SHISA family because, unlike other CKAMPs, Shisa7 directly affects the regulation of GABAARs at inhibitory synapses (Castellano et al., 2021). It co-localizes in hippocampal neurons with GABAARs and gephyrin (Castellano et al., 2021), whereas other CKAMPs are found at glutamatergic synapses (von Engelhardt et al., 2010; Klaassen et al., 2016; Peter et al., 2020). Moreover, it controlled GABAAR trafficking and inhibitory transmission while having no effect on excitatory synaptic transmission. Interestingly, Shisa7 influences GABAAR kinetics as well as its pharmacological characteristics (Castellano et al., 2021). The activation of the GABAAR may promote tau phosphorylation by decreasing the interaction of protein phosphatase 2A (PP2A) with tau, increasing intracellular NFTs within neurons and contributing to AD development. Hyperphosphorylated tau, on the other hand, may increase GABAergic neurotransmission. In the neurological system, there may be a feedback loop between the activation of the GABAAR and phosphorylation of tau (Li et al., 2016).

Furthermore, recent research demonstrates the dual involvement of the GABAA receptor in neuroinflammation and peripheral inflammation, implying a complex interplay between GABAergic systems and immunity systems (Malaguarnera et al., 2021). To the best of our knowledge, regulating the expression of *SHISA7* in AD development has not been investigated yet. Salmena et al. (2011) suggested a novel regulatory mechanism termed competing endogenous RNA (ceRNA). This hypothesis refers to the existence of a reversed RNA → microRNA function, in which RNAs actively control one another via direct competition for miRNA complementary sequences known as miRNA response elements (MREs) (Salmena et al., 2011; Tay et al., 2011). According to the ceRNA hypothesis, if two RNA transcripts control one another via a ceRNA-mediated mechanism, the expression of the two RNA transcripts will correlate negatively with the expression level of target miRNAs and positively with one another (Salmena et al., 2011). Several investigations in recent years have confirmed the ceRNA hypothesis. Disruptions to the ceRNA crosstalk equilibrium are well recognized to be involved in NDDs. In addition, ceRNAs were studied as biomarkers in NDDs (Moreno-García et al., 2020). Amongst NDDs, ceRNA interactions in AD have received a great deal of attention (Cai and Wan, 2018). A study on the human cell line indicated that *BCAS4*, as a *SHISA7* ceRNA, modulates the *SHISA7* expression level through a miRNA-dependent mechanism (Marques et al., 2012). Based on the as-mentioned theoretical concepts, the *BCAS4*/*SHISA7* ceRNA pair may be significantly involved in AD development.

This study aimed to examine the ceRNA regulation of *SHISA7* and *BCAS4* in tau pathogenesis and their usefulness as peripheral biomarkers associated with aberrant inflammation in the development of AD, according to bioinformatics and experimental approaches.

MATERIALS AND METHODS

Bioinformatics Analysis Based on Brain Microarray Dataset

Gene Expression Profile Data Collection

In this research, a bioinformatics approach was employed to mine data from a microarray dataset of human temporal cortical (TC) tissue samples with different degrees of AD-related neurofibrillary pathology (GSE106241). We intended to identify expression changes of *SHISA7* and *BCAS4* in human TC tissue samples. The above gene expression profile was obtained from the NCBI Gene Expression Omnibus database (GEO[1]). A chip-based platform GPL24170 Agilent-044312 Human 8 × 60K Custom Exon array (Probe Name version) was used for the dataset. The GSE106241 included 60 human TC tissue samples split into seven groups according to Braak staging (Braak 0: $n = 6$, Braak I: $n = 11$, Braak II: $n = 11$, Braak III: $n = 6$, Braak IV: $n = 7$, Braak V: $n = 12$, Braak VI: $n = 7$) reflecting the severity of the disease (Marttinen et al., 2019). Braak staging is a type of neuropathological staging that distinguishes between early, middle, and advanced AD according to the development of NFTs within the medial temporal lobe memory circuit. Braak Stage 0 corresponds to the absence of NFTs, Stages I-II to entorhinal-perirhinal cortex NFTs, Stages III-IV to NFTs additionally in the hippocampus, and Stages V-VI to NFTs dispersed across the neocortical regions (Braak and Braak, 1991).

Data Preprocessing and Differentially Expressed Genes (DEGs) Identification

Using the normexp method, background correction was performed (Silver et al., 2009) with an offset of 15, and between-array normalization was performed utilizing the quantile algorithm using normalizeBetweenArrays() function from linear models for microarray data (limma) R package (Ritchie et al., 2015). Only spots with signal minus background flagged as "positive and significant" (field name gIsPosAndSignif) and not flagged as ControlType or IsManualFlag were utilized. The AgiMicroRna Bioconductor package (version 2.40.0) was used to evaluate the quality. The principal component analysis (PCA) was used for a dimensional reduction analysis (Yeung and Ruzzo, 2001) to find similarities between each sample group by the ggplot2 package in R software version 4.0.3. Differentially expressed gene analysis (DEGA) was performed comparing AD samples with normal samples using the linear models for microarray data (limma) R package (Ritchie et al., 2015) in Bioconductor[2] (Huber et al., 2015). Student's *t*-test was used to identify statistically significant genes. Also, the cut-off for aberrantly expressed mRNAs was established as follows: (Kang et al., 2020) a false discovery rate (adjusted *P*-value) < 0.01, and (Fan et al., 2019) $|\log2 \text{ fold change (log2FC)}| > 0.3$. The volcano plot for DEGs and heat map for *BCAS4* and *SHISA7* genes were created using the Enhanced Volcano (version 1.8.0) and Pheatmap (version 1.0.12) R packages.

Identification of miRNAs Associated With Alzheimer's Disease-Related Neurofibrillary Pathology

To discover the differentially expressed miRNAs (DEmiRNAs) linked to AD-related neurofibrillary pathology, we employed a bioinformatics method identical to the one described above. GSE157239 miRNA profile data were acquired from the NCBI GEO. The platform GPL21572 (miRNA-4) Affymetrix Multispecies miRNA-4 Array (ProbeSet ID version) was applied for the dataset. The GSE157239 comprised eight TC samples from AD patients (Braak stage III or above) and eight from control subjects. The Robust Multichip Average (RMA), an effective tool in the affy Bioconductor package, was used for background correction and quantile normalization of the entire raw data files (Irizarry et al., 2003). An interquartile range filter (IQR across the samples on the log base two scale greater than median IQR) was used to lower the number of analyzed genes, which was followed by an intensity filter (a minimum of >100 expression signals in a minimum of 25% of the arrays) to remove insignificant probe sets that are not expressed or changing (von Heydebreck et al., 2005). The quality was assessed by the AgiMicroRna Bioconductor package. The PCA was used for a dimensional reduction analysis

[1]https://www.ncbi.nlm.nih.gov/geo/

[2]https://www.bioconductor.org/

(Yeung and Ruzzo, 2001) by the ggplot2 package in R software. The DEGA was conducted using the limma R package (Ritchie et al., 2015) in Bioconductor (Huber et al., 2015) on normal and AD samples. To transform the miRNA names to miRbase v22, the miRNAmeConverter Bioconductor package (Haunsberger et al., 2017) was utilized. Student's *t*-test was used to identify statistically significant miRNAs. Also, the cut-off for aberrantly expressed miRNAs were set as follows: (Kang et al., 2020) a false discovery rate (adjusted *P*-value) < 0.01, and (Fan et al., 2019) $|\log2$ fold change (log2FC)$| > 0.3$. The DEmiRNA heat map was created utilizing R's Pheatmap package.

Prediction of miRNA-mRNA Interactions

We used miRWalk (version 3) to identify interactions among miRNAs linked to AD-related neurofibrillary pathology with *BCAS4*/*SHISA7* (Sticht et al., 2018). Binding sites 3′UTR and score ≥ 0.95 were considered as criteria for the miRWalk query.

Correlation Analysis Between *BCAS4* and *SHISA7*, and Competing Endogenous RNA Axes Construction

The Pearson correlation analysis was performed to determine if there were any positive correlations between *BCAS4* and *SHISA7* in the ceRNA regulatory axes. The Hmisc and psych packages were used to calculate the correlations and visualization. The ceRNA regulatory axes were built according to the co-expression relation and miRNA-mRNA interactions.

Identification and Differential Analysis of *BCAS4*/*SHISA7* Competing Endogenous RNA Axis as an Inflammatory Biomarker in Peripheral Blood

Participants and Peripheral Blood Samples

This case-control research included 100 individuals, 50 AD patients as well as 50 healthy controls who were gender and age-matched. The present investigation was approved by Tabriz University of Medical Sciences' clinical research ethics committee (Ethical code: IR.TBZMED.REC.1398.1264). The participants were recruited from the Department of Neurology of Tabriz University of Medical Sciences' Imam Reza Hospital. A neurology specialist identified the individuals using the Diagnostic and Statistical Manual of the American Psychiatric Association (DSM-V) criteria (Association, 2013). The criteria for inclusion were 65 years of age and older and no other psychiatric/neurologic diagnoses other than AD. The control group was chosen from aged 65 years and above individuals without AD in the same department. Diabetes, active or chronic infectious diseases, thyroid disorders, cancer, renal and liver failure, inflammatory diseases or receiving anti-inflammatory drugs, metabolic disease, severe ischemic heart disease, alcohol abuse, cerebrovascular accident, and having received corticosteroids in the past 8 weeks of evaluation were all exclusion criteria. Mini-mental state examination (MMSE) was used to assess cognitive ability in both groups. Written informed consent was obtained from all participants or their primary caregivers before enrolling in the research. Finally, 5-ml of peripheral blood was taken from each participant in EDTA-treated tubes.

Expression Assays

Total RNA was isolated from whole blood utilizing the Hybrid-R^{TM} Blood RNA purification kit according to the manufacturer's instructions (GeneALL, Seoul, South Korea) and treated with DNase I to remove DNA contamination. NanoDrop was employed to assess the quantity and quality of extracted RNA (Thermo Scientific, Wilmington, DE, United States). The synthesis of cDNA was done by the cDNA synthesis Kit (GeneALL) according to the manufacturer's guidelines. The cDNA was stored at −20°C for further investigation. The primer sequences used in reverse transcription, as well as qPCR reactions, are listed in **Table 1**. *U6* and Ubiquitin C (*UBC*) were employed as internal controls to normalize miRNA and mRNA levels, respectively. The Step OnePlus^{TM} Real-Time PCR and the RealQ Plus2x Master Mix (Ampliqon, Odense, Denmark) were used for the qPCR. All qPCR reactions were performed in duplicate.

Statistical Analysis for qPCR

The data analysis was performed using the R v.4 software packages brms, stan, pROC, and GGally. The Bayesian regression model was employed to investigate the relative expressions of *BCAS4*, *SHISA7*, and *hsa-miR-185-5p* in AD patients and healthy controls, as well as subgroups. Age and gender impacts were adjusted. The adjusted *P*-values of less than 0.05 were considered significant. The expression of the abovementioned genes was also studied across age groups and between males and females. The Spearman correlation coefficients were utilized to evaluate the connections between the variables in the research. The genes' diagnostic power was determined using a receiver operating characteristic (ROC) curve analysis.

RESULTS

Brain Microarray Dataset Reanalysis

Differentially Expressed Genes Identification

Background correction, batch modification, gene filtering, and normalization were all performed prior to DEGA. The AgiMicroRna Bioconductor package was utilized to monitor the quality. The gene expression dataset's box plots were used to evaluate the distribution of data after normalization (**Supplementary File 1**). Distinct arrays in the box plots had similar expression level medians, suggesting that the correction was done properly. A PCA plot was also used to illustrate the spatial dispersion of samples (**Supplementary File 1**). PCA displays the specifics of the investigated data's structure and aids in the discovery of similarities across samples.

According to the results, *BCAS4* was significantly downregulated in Braak stages I-VI, while *SHISA7* was significantly downregulated only in Braak stage V. Thus, Braak stage V was the only one in which both the *BCAS4* (log2FC = −0.95, adj.P.Val = 1.71E-09) and the *SHISA7* (log2FC = −0.32, adj.P.Val = 0.000685865) genes were

TABLE 1 | Sequences of primers used in reverse transcription (RT) and qPCR reactions.

Gene name	Gene reference ID	Primer sequences
hsa-miR-185-5p	–	RT primer: GTCGTATCCAGTGCAGGGTCCGAGGTATTCGCACTGGATACGACTCAGGAA Forward primer: AATCGGCGTGGAGAGAAAGGC Reverse primer: GTCGTATCCAGTGCAGGGTCC
U6	–	RT primer: GTCGTATCCAGTGCAGGGTCCGAGGTATTCGCACTGGATACGACAAAAATAT Forward primer: GCTTCGGCAGCACATATACTAAAAT Reverse primer: CGCTTCACGAATTTGCGTGTCAT
BCAS4	NM_198799.4 XM_017027932.1 XM_011528887.2 XM_011528886.2 NM_017843.4 NM_001010974.2	Forward primer: ATGCTCCTCAGGCTGGAAGAGT Reverse primer: CCACGCATTTCTGTCAGTTTGGC
SHISA7	NM_001145176.2	Forward primer: TGAAGACCCCCAACCTCGACTG Reverse primer: TCCTTCTCGGCCAGCCTCTTG
UBC	NM_021009.7	Forward primer: CAGCCGGGATTTGGGTCG Reverse primer: CACGAAGATCTGCATTGTCAAGT

dysregulated. **Supplementary File 2** summarizes the information of the genes addressed in each step. A total of 18,590 DEGs were found in patients in Braak stage V using the criteria of adjusted *P*-value < 0.01, and (Fan et al., 2019) | log2 fold change (log2FC)| > 0.3. **Figure 1** depicts a volcano plot of DEGs as well as a hierarchical clustering heatmap of *BCAS4* and *SHISA7* genes in Braak stage V.

Identification of miRNAs Associated With Alzheimer's Disease-Related Neurofibrillary Pathology

Before conducting DEGA, gene filtering, normalization, batch adjustment, and background correction were performed. The AgiMicroRna Bioconductor program was utilized to monitor the quality. Box plots for gene expression profiles were shown after normalization to evaluate the distribution of data (**Supplementary File 1**). Distinct arrays in the box plots had similar expression level medians, suggesting a proper correction. In addition, a PCA plot was utilized to depict the distribution pattern of samples (**Supplementary File 1**). PCA displays the specifics of the investigated data structure. It also aids in determining the similarity of samples. A total of 68 human DEmiRNAs (38 up-regulated and 30 down-regulated) were discovered in GSE157239 comparing AD and control TC samples using the criteria [adjusted *P*-value < 0.01, and (Fan et al., 2019) | log2 fold change (log2FC)| > 0.3]. **Figure 2** depicts a hierarchical clustering heatmap of DEmiRNAs. The details of DEmiRNAs are summarized in **Supplementary File 2**.

Prediction of miRNA-mRNA Interactions

We employed miRWalk database to find interactions between miRNAs linked to AD-related neurofibrillary pathology and *BCAS4*/*SHISA7* and later showed that three (*hsa-miR-185-5p*, *hsa-miR-423-5p*, *hsa-miR-5787*) and 14 miRNAs (*hsa-miR-145-5p*, *hsa-miR-150-5p*, *hsa-miR-185-5p*, *hsa-miR-3620-5p*, *hsa-miR-4270*, *hsa-miR-4463*, *hsa-miR-4507*, *hsa-miR-4508*, *hsa-miR-4739*, *hsa-miR-485-3p*, *hsa-miR-5100*, *hsa-miR-762*, *hsa-miR-769-3p*, *hsa-miR-937-5p*) obtained from GSE157239 dataset reanalysis may target *BCAS4* and *SHISA7*, respectively. Of those miRNAs, *hsa-miR-185-5p* targeted both genes *BCAS4* and *SHISA7*. The *hsa-miR-185-5p* expression levels in TC samples of AD were statistically higher than those in controls (log2FC = 0.37, adj.P.Val = 7.89E-24).

Correlation Analysis Between *BCAS4* and *SHISA7*, and Competing Endogenous RNA Axis Construction

The Pearson correlation analysis was conducted between *BCAS4* and *SHISA7* to validate the ceRNA axes theory, which states that ceRNAs are positively regulated by each other via interactions with miRNAs. A significant positive correlation was found between the levels of expression of the evaluated genes ($r = 0.91$, $P < 0.001$) (**Figure 3**). Based on the co-expression and miRNA-mRNA interactions, *BCAS4* was shown to act as a ceRNA to control the *SHISA7* expression via sponging *hsa-miR-185-5p*.

Identification and Differential Analysis of *BCAS4/hsa-miR-185-5p/SHISA7* Competing Endogenous RNA Axis as an Inflammatory Biomarker in Peripheral Blood

General Demographic Data

Following consideration of the inclusion and exclusion criteria, 50 AD patients (male/female%: 31.4/68.6) with age [mean ± standard deviation (SD)] of 76.36 ± 6.26 and 50 healthy controls (male/female%: 30.6/69.4) with age (mean ± SD) of 74.3 ± 6.22 were included in the study. The MMSE scores (mean ± SD) of the patient and control groups were 14.2 ± 5.94 and 27.5 ± 0.76, respectively.

Expression Assays

Figure 4 depicts *BCAS4*, *SHISA7*, and *hsa-miR-185-5p* genes' relative expression levels in patients with AD and controls. The *BCAS4* expression levels demonstrated no significant differences in PB samples among AD patients and healthy controls (adjusted

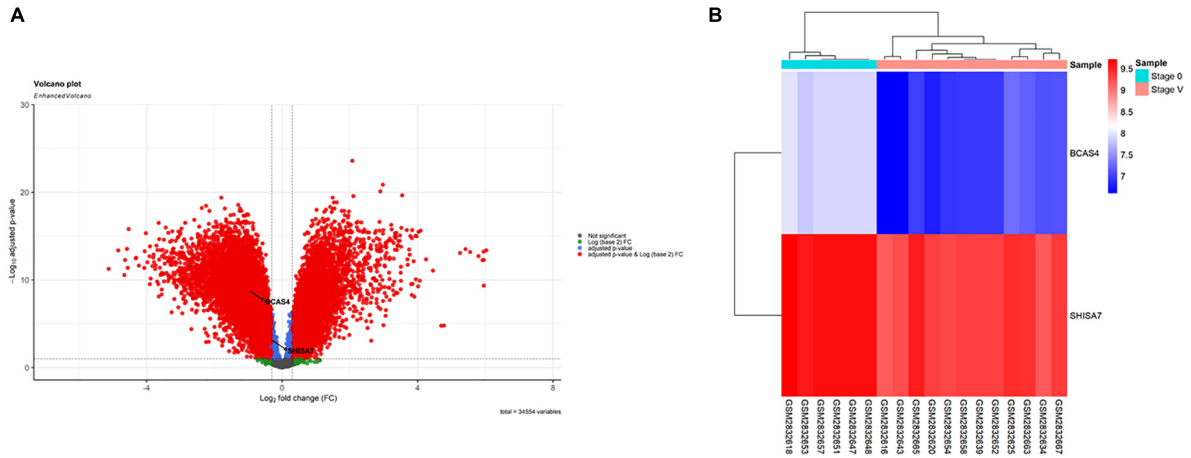

FIGURE 1 | Differentially expressed mRNAs between brain samples of Alzheimer's disease (AD) patients in Braak stage V and control (CTL) samples. **(A)** Volcano plot for the DEGs. The DEGs were screened based on a | (log2FC) | > 0.3 and an adjusted *P*-value < 0.01. **(B)** Heatmap for BCAS4 and SHISA7 genes. High expressed genes are shown in red, while those expressed at low levels are blue.

P-value = 0.967), as well as subgroups. *SHISA7* expression was significantly lower in PB samples from AD patients compared to controls (posterior beta = −1.035, adjusted *P*-value < 0.003). Such decreased expression was found between male and female subgroups too (posterior beta = −0.927, adjusted *P*-value = 0.035 and posterior beta = −0.932, adjusted *P*-value = 0.022, respectively). The *hsa-miR-185-5p* expression was found to be significantly lower (posterior beta = −0.849, adjusted *P*-value < 0.029) when PB samples from AD patients were compared to controls. Male and female subgroups also had lower expression (posterior beta = −0.857, adjusted *P*-value = 0.01 and posterior beta = −0.857, adjusted *P*-value = 0.01, respectively). **Tables 2–4** provide comprehensive data on relative expressions of *BCAS4*, *SHISA7*, and *hsa-miR-185-5p*, respectively.

Correlation Analysis

The *BCAS4*, *SHISA7*, and *hsa-miR-185-5p* expressions were not correlated to the patients' age. In AD patients, expression of *BCAS4* were correlated positively with *SHISA7* (r = 0.624, P < 0.001). In the PB of patients, our correlation results between *hsa-miR-185-5p* and *SHISA7* showed a weak positive correlation (r = 0.397, P < 0.01) instead of a negative correlation. Furthermore, the expressed levels of *hsa-miR-185-5p* and *BCAS4* were not correlated significantly in AD cases (**Figure 5**).

Receiver Operating Characteristic Curve Analysis

The diagnostic power of *SHISA7* and *hsa-miR-185-5p* were tested for their ability to distinguish AD patients from the controls. We obtained significant diagnostic powers of 0.758 and 0.779 from the transcript levels of *SHISA7* and *hsa-miR-185-5p*, respectively, by evaluating the area under the curve (AUC) (**Figure 6**).

DISCUSSION

According to growing research-based data, GABAergic neurotransmission faced serious pathological alterations in AD, and it might be a successful therapeutic candidate for this NDD (Li et al., 2016). Moreover, ceRNA regulation has biologically profound impacts in a variety of NDDs (e.g., Parkinson's disease, AD, spinocerebellar ataxia type 7, amyotrophic lateral sclerosis, and multiple sclerosis), so it can explain the pathogenic processes and provides new options for therapy. Because of the multifactorial character of ceRNA interacting networks, they may be useful in the research of complicated diseases like AD. As a result, our efforts to comprehend various aspects of ceRNA regulation processes in AD pathology elucidate possible molecular targets, identify biomarkers based on ceRNA, and develop ceRNA-based therapeutic options (Cai and Wan, 2018; Moreno-García et al., 2020; Sabaie et al., 2021). In this study, we employed bioinformatics and experimental approaches to investigate the *BCAS4*/*SHISA7* verified ceRNA axis in AD development.

BCAS4/*SHISA7* Competing Endogenous RNA Axis in Tau Pathology in Alzheimer's Disease

Our bioinformatics analysis showed that *BCAS4* could serve as a ceRNA to regulate the expression of *SHISA7* in AD-related neurofibrillary pathology via sponging *hsa-miR-185-5p*. To our knowledge, this would be the first report of a possible role of the *BCAS4*/*hsa-miR-185-5p*/*SHISA7* axis in the tau pathology of AD.

Our *in silico* analysis showed that the expression levels of *BCAS4* were substantially lower in TC samples from AD patients and the control group. *BCAS4* is a new gene, which is cloned from breast cancer cells, encoding a cytoplasmic protein (211 aa) with no substantial homology to known proteins (Bärlund et al., 2002). A recent piece of research employing machine learning approaches and various microarray datasets revealed that *BCAS4* might be a ceRNA regulator for the development of intervertebral disc degeneration (Chang et al., 2020). To the best of our knowledge, this is the first study on *BCAS4* expression in

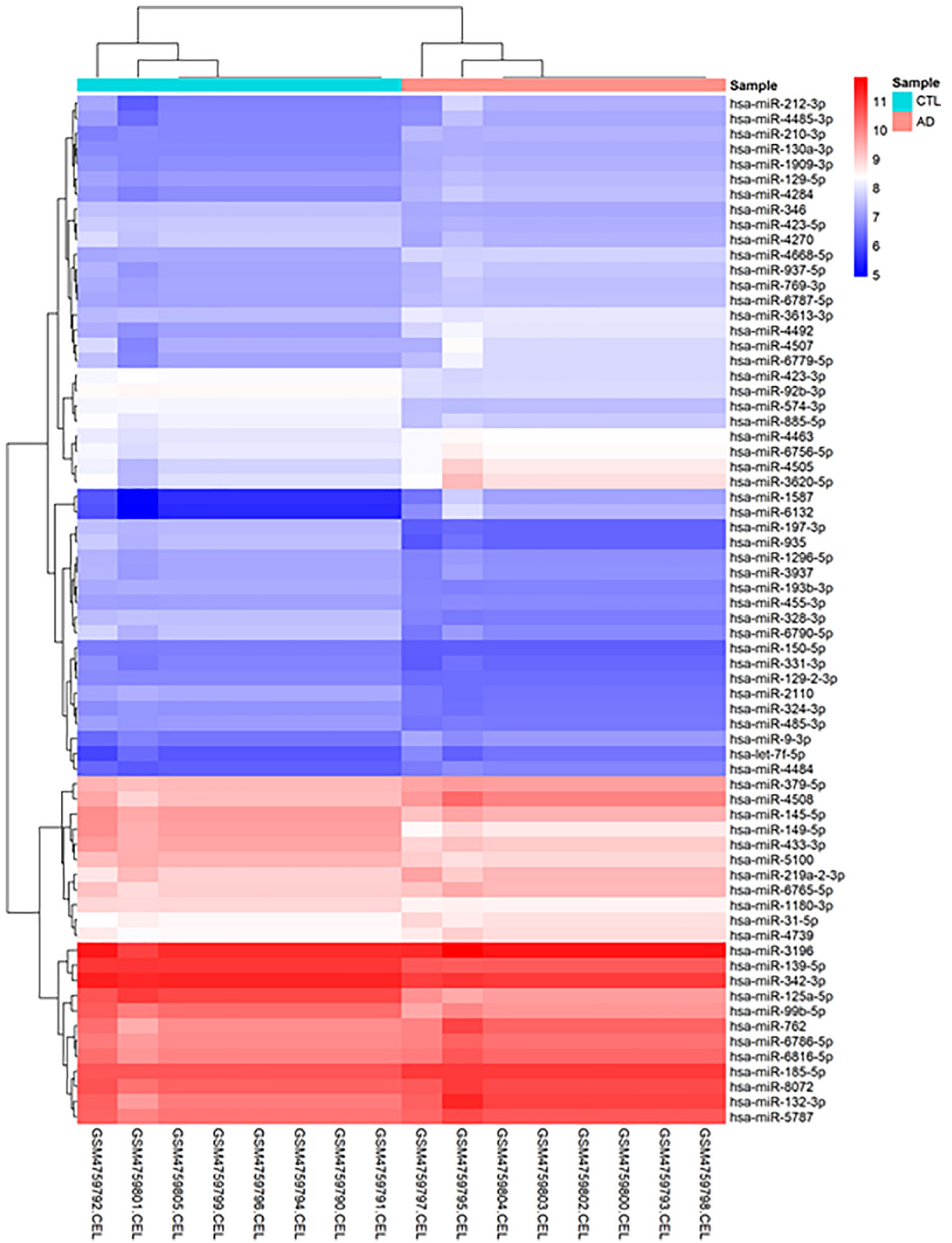

FIGURE 2 | Hierarchical clustering heatmap differentially expressed human miRNAs between brain samples of Alzheimer's disease (AD) and control (CTL) samples. High expressed genes are shown in red, while those expressed at low levels are blue.

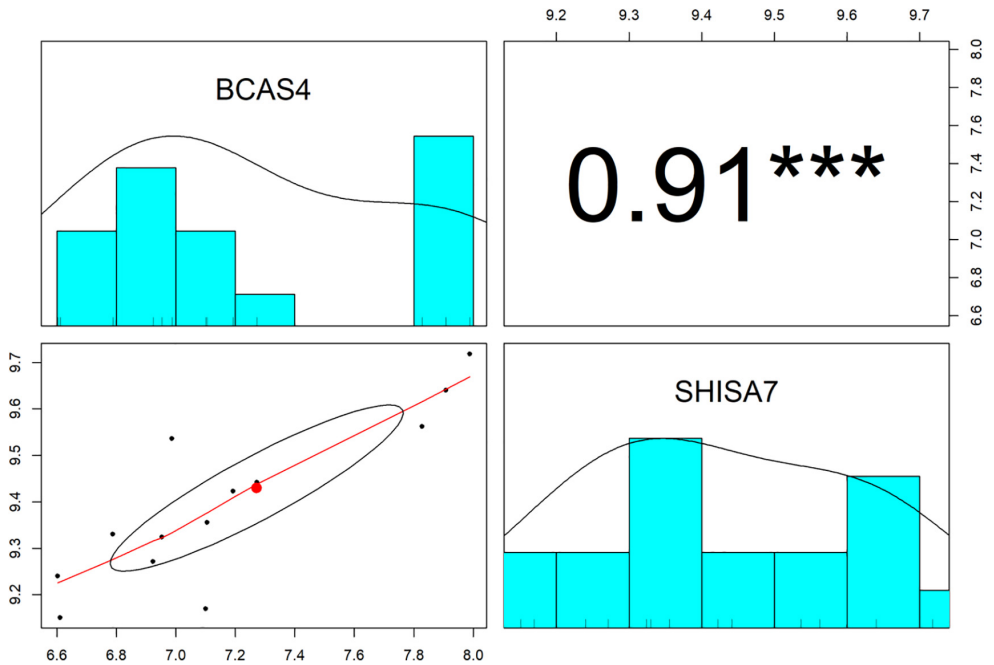

FIGURE 3 | The distribution of each variable is shown on the diagonal. The lower portion of the diagonal shows bivariate scatter plots with a fitted line. On the upper part of the diagonal, the correlation coefficients plus the significance level as stars are displayed. *** is significant correlation at *P*-value < 0.001.

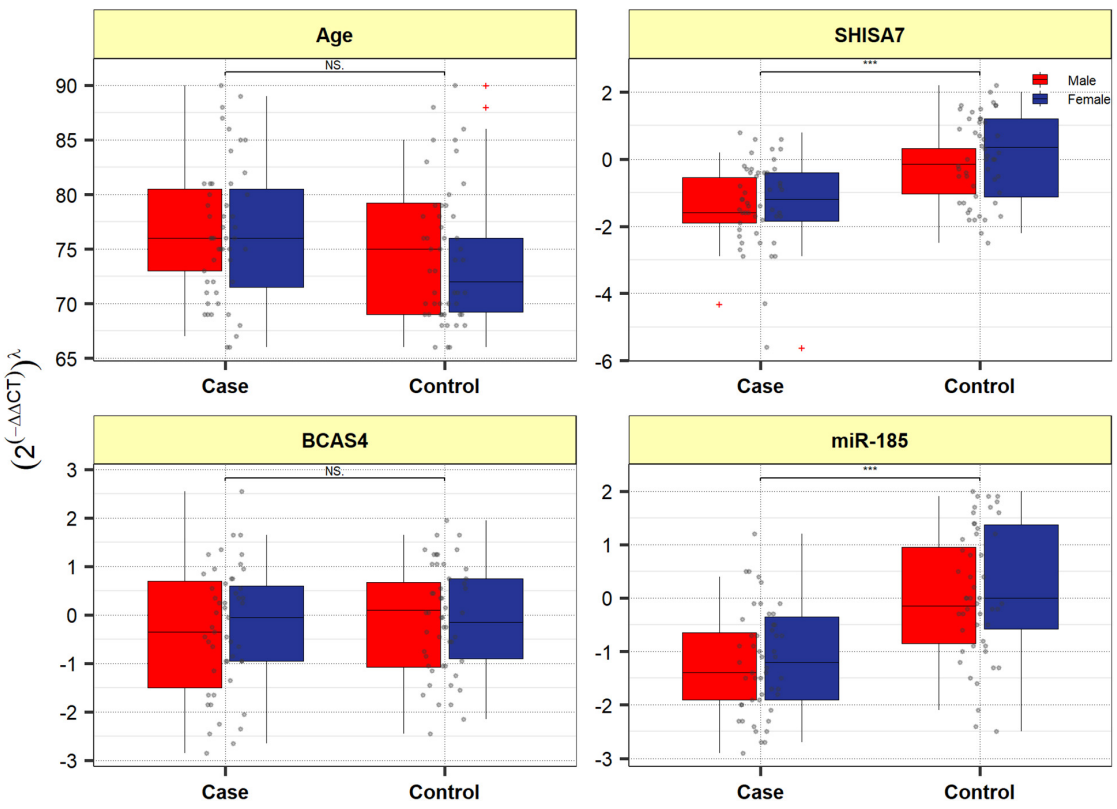

FIGURE 4 | Expression of BCAS4, SHISA7, and hsa-miR-185-5p in cases and controls' peripheral blood samples. Values are depicted as gray dots. Means of expression levels and interquartile range are displayed.

TABLE 2 | Relative levels of *BCAS4* in AD cases and controls according to the Bayesian quantile regression model.

	BCAS4	**Posterior Beta of $(2^{(-ddct)})^{\lambda}$**	**SE**	**Adjusted *P*-Value***	**95% CrI for Beta**
Total	Group, Case vs. control	−0.124	0.26	0.967	[−0.57, 0.42]
	Sex, Female vs. Male	−0.061	0.29	0.647	[−0.59, 0.51]
	Age (years)	−0.011	0.02	0.801	[−0.04, 0.02]
	Group * Sex	0.017	0.4	0.427	[−0.78, 0.76]
Male	Case vs. control	−0.138	0.17	0.495	[−0.48, 0.2]
	Age	−0.012	0.01	0.886	[−0.04, 0.02]
Female	Case vs. control	−0.132	0.17	>0.999	[−0.46, 0.22]
	Age	−0.012	0.01	0.686	[−0.04, 0.02]

**Estimated from frequentist methods; CrI: Credible interval, $^{\lambda}$: Power transformation value estimated from Box-cox or Yeo-Johnson method. AD, Alzheimer's disease.*

TABLE 3 | Relative levels of *SHISA7* in AD cases and controls according to the Bayesian quantile regression model.

	SHISA7	**Posterior Beta of $(2^{(-ddct)})^{\lambda}$**	**SE**	**Adjusted *P*-Value***	**95% CrI for Beta**
Total	Group, Case vs. control	−1.035	0.23	0.003	[−1.48, −0.58]
	Sex, Female vs. Male	0.217	0.25	0.26	[−0.26, 0.68]
	Age (years)	0.015	0.02	0.175	[−0.02, 0.04]
	Group * Sex	0.2	0.37	0.868	[−0.51, 0.93]
Male	Case vs. control	−0.927	0.18	0.035	[−1.28, −0.55]
	Age	0.019	0.02	0.389	[−0.01, 0.05]
Female	Case vs. control	−0.932	0.18	0.022	[−1.29, −0.56]
	Age	0.019	0.02	0.601	[−0.01, 0.05]

**Estimated from frequentist methods; CrI: Credible interval, $^{\lambda}$: Power transformation value estimated from Box-cox or Yeo-Johnson method. AD, Alzheimer's disease.*

TABLE 4 | Relative levels of *miR-185* in AD cases and controls according to the Bayesian quantile regression model.

	miR-185	**Posterior Beta of $(2^{(-ddct)})^{\lambda}$**	**SE**	**Adjusted *P*-Value***	**95% CrI for Beta**
Total	Group, Case vs. control	−0.849	0.21	0.029	[−1.28, −0.46]
	Sex, Female vs. Male	0.068	0.25	0.906	[−0.45, 0.55]
	Age (years)	0.016	0.01	0.195	[−0.01, 0.04]
	Group * Sex	−0.028	0.35	>0.999	[−0.69, 0.68]
Male	Case vs. control	−0.857	0.16	0.01	[−1.18, −0.56]
	Age	0.015	0.01	0.814	[−0.01, 0.04]
Female	Case vs. control	−0.857	0.15	0.01	[−1.17, −0.56]
	Age	0.014	0.01	0.288	[−0.01, 0.04]

**Estimated from frequentist methods; CrI: Credible interval, $^{\lambda}$: Power transformation value estimated from Box-cox or Yeo-Johnson method. AD, Alzheimer's disease.*

TC samples of AD cases. In line with our results, a prior study on a human neuroblastoma cell line found that ceRNA regulation between *BCAS4* and *SHISA7* by *hsa-miR-185-5p* is conserved in humans (Marques et al., 2012).

Moreover, we discovered a decreased *SHISA7* expression level in TC samples from AD patients compared to controls. *Shisa7* controlled GABAAR trafficking and also inhibitory transmission while having no effect on excitatory synaptic transmission (Han et al., 2019). Interestingly, *Shisa7* influences the kinetics and pharmacological characteristics of the GABAAR. Although *Shisa7* lowered deactivation time constants for α1β2γ2 and α2β3γ2 receptors in heterologous cells, *Shisa7* KO increased decay time constants for GABAergic transmission in hippocampal neurons (Han et al., 2019). Eventually, *Shisa7* enhanced GABAAR potentiation induced by diazepam in heterologous cells, but *Shisa7* KO substantially decreased diazepam effects *in vivo* (Han et al., 2019). To the best of our knowledge, this is the first study on the expression level of *SHISA7* in AD patients. As previously stated, recent research using human neuroblastoma cell lines found that *hsa-miR-185-5p* regulates *BCAS4* and *SHISA7* in a ceRNA manner, which is consistent with our findings (Marques et al., 2012).

In addition to finding changed expression of *SHISA7* and *BCAS4* genes in tau pathogenesis, we discovered DEmiRNAs related to AD-associated neurofibrillary pathology. Among those miRNAs, just *hsa-miR-185-5p* targeted both *SHISA7* and *BCAS4* genes. Compared to controls, individuals with AD indicated higher *hsa-miR-185-5p* expression. In mice and humans, *MiR-185* mediates conserved crosstalk among *Pbcas4*, *BCAS4*, and protein-coding gene ceRNAs like *SHISA7* (Marques et al., 2012). A recent research study anticipated that the SNP rs5848 [C/T] created a 6 mer target site/MRE for *hsa-miR-185-5p* in the 3′UTR

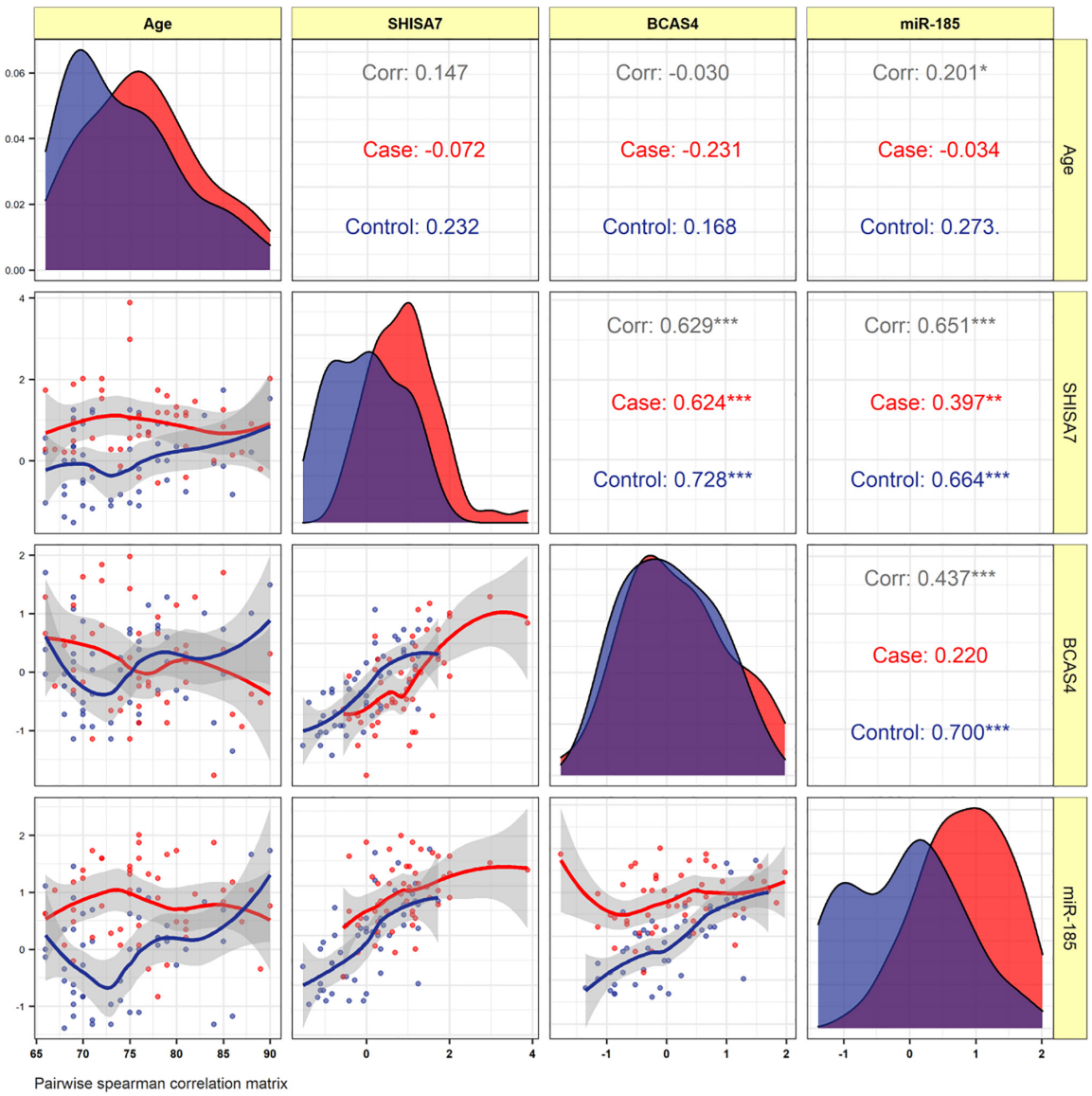

FIGURE 5 | The distribution of variables is depicted on the diagonal. The correlation coefficients plus the significance level as stars are shown. *, **, and *** is significant correlation at $P < 0.05$, $P < 0.01$, and $P < 0.001$, respectively.

of granulin (proepithelin or *GRN*). They hypothesized that the development of this novel 6 mer MRE would lead to the observed *GRN* downregulation in LOAD (Roy and Mallick, 2017). The rs5848 GRN variant has been identified as a risk factor for AD in Taiwanese people (Lee et al., 2011), although the specific mechanism by which it affects the disease is unknown.

BCAS4/hsa-miR-185-5p/SHISA7 Competing Endogenous RNA Axis as an Inflammatory Biomarker in Peripheral Blood of Alzheimer's Disease Patients

Due to the multifactorial nature of ceRNA interacting networks, they may be useful in investigations of complex NDDs like AD, particularly at levels of biomarkers (Moreno-García et al., 2020). As a result, we used qPCR to look into the expression level of the *BCAS4/hsa-miR-185-5p/SHISA7* ceRNA axis in our PB samples.

In PB samples, we found no significant differences in expression levels of *BCAS4* between AD patients and controls. Based on the literature, this is a study on the expression of *BCAS4* in PB samples from AD patients for the first time. Previous research has shown that the unique DNA methylation of *BCAS4* works as an epigenetic marker might be utilized to differentiate saliva from other types of body fluids. Moreover, it is utilized extensively in forensic investigations (Taki and Kibayashi, 2015; Silva et al., 2016).

SHISA7 expression was reduced in the PB sample of patients with AD, just as it was in brain tissue. The current study

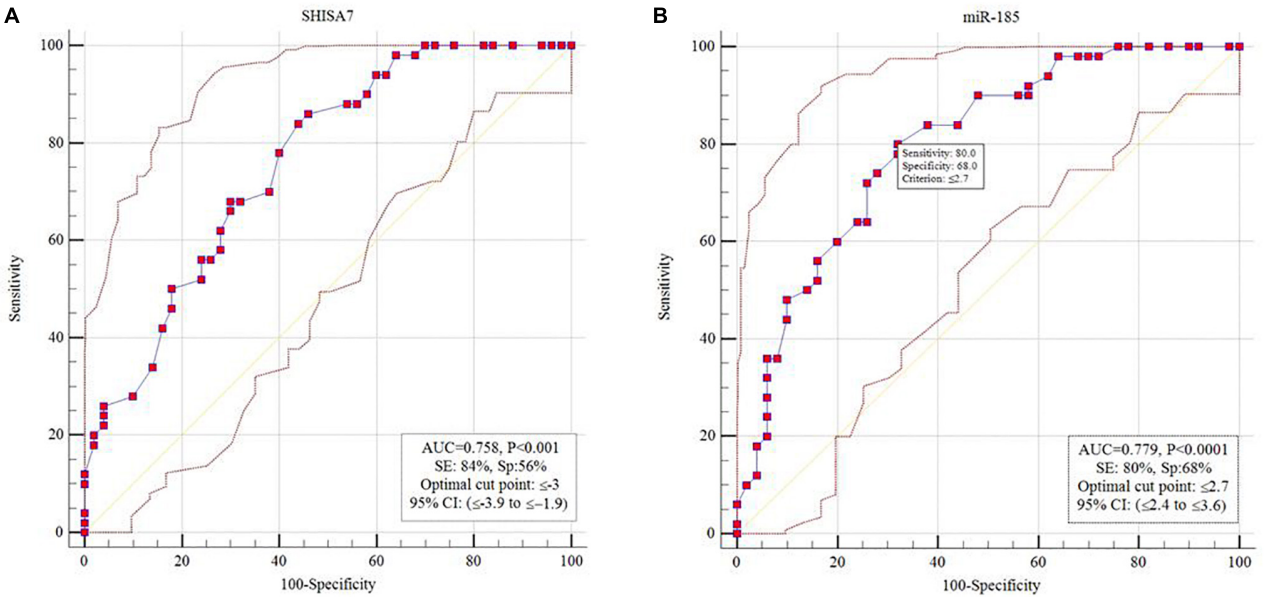

FIGURE 6 | Receiver operating characteristic (ROC) curve analysis. **(A)** SHISA7 transcript levels displayed diagnostic power of 0.758. **(B)** Hsa-miR-185-5p transcript levels displayed diagnostic power of 0.779.

is the first report considering the expression level of *SHISA7* in PB samples from AD patients. This concurrent reduction in the *SHISA7* expression level in the PB and brain might represent changes in AD patients' brains in their periphery, making it a promising candidate for biomarker research (Ma et al., 2019).

Besides, in contrast to TC tissue, where *hsa-miR-185-5p* was found to be overexpressed, we found reduced levels of *hsa-miR-185-5p* in PB of AD patients compared to the healthy control group. These findings may imply that the biological role of this miRNA in PB differs from that in TC. More study is needed to validate these findings. In a newly published study (Lugli et al., 2015), lower amounts of *hsa-miR-185-5p* were seen in the plasma of individuals with AD when compared with healthy controls. Our findings are consistent with these results.

Expression levels of *SHISA7* and *BCAS4* were shown to have a strong positive correlation, suggesting an interacting network, possibly owing to the regulation of ceRNA in PB samples. Whereas *SHISA7* and *BCAS4* are closely correlated in a direct manner, implying an interactional network, their activities in the development of AD should be reassessed considering whole blood specimens because the altered patterns of *BCAS4* expression were not strong enough to be meaningful. Nevertheless, the results obtained are just preliminary. One possible explanation for this could be our small sample size. Contrary to the common belief that miRNAs are repressive, we discovered a weak positive correlation between *SHISA7* and *hsa-miR-185-5p* in AD patients' PB samples. Although it is unusual, both negative and positive miRNA-mRNA correlations have been witnessed in many studies, suggesting the presence of a complicated network encompassing miRNA target inhibition (resulting in negative miRNA-mRNA correlations) besides feed-forward regulation provoked by widely known transcription factors (resulting in positive miRNA-mRNA correlations) (Friard et al., 2010; Chen et al., 2011; Chien et al., 2014; Diaz et al., 2015). The *hsa-miR-185-5p*, as previously mentioned, suppresses the expression of *SHISA7* in neuroblastoma cells (human and murine) (Marques et al., 2012). This finding is inconsistent with our result. In line with our result, another study found that *hsa-miR-3681-5p* acts as a super-enhancer by employing alternative enhancers and promoters, transcription factors, activators, mediators, and RNA Pol II. Further, its enhancing activity acts as an inhibitor of variable number tandem repeats (VNTRs) functions in the *SHISA7* 3′ UTR (Lee et al., 2020). More studies are needed to establish whether *hsa-miR-185-5p* functions as an enhancer in AD patients' PB.

Eventually, we determined that *SHISA7* and *hsa-miR-185-5p* had a diagnostic value of 0.758 and 0.779, in turn, in differentiating patients with AD from healthy subjects. Because of the small sample size, the obtained findings should be interpreted with caution. If future research supports the findings of the present study, the *SHISA7* and *hsa-miR-185-5p* transcription levels might be utilized as AD-associated markers.

Limitations

Our research has several limitations. Firstly, various aspects, such as diverse methods, sample preparation, platforms, data analysis, and patient characteristics, may impact expression patterns of genes. Second, a limited sample size might lead to a lack of statistical validity. Furthermore, our bioinformatics analysis must be verified by confirmatory experimental techniques. Finally, we

did not examine expressions of *SHISA7*, *BCAS4*, and *hsa-miR-185-5p* in the PB cell subpopulation.

CONCLUSION

Competing endogenous RNA regulation has biologically significant consequences in a variety of illnesses, which can help to explain pathogenic processes and provide possibilities for novel treatments. As a result, our attempts to comprehend various aspects of ceRNA regulation processes in AD pathogenesis give new insights into possible molecular targets and lead to the discovery of ceRNA-based biomarkers. The present study is the first evidence to highlight the expression of the *BCAS4*/*miR-185-5p*/*SHISA7* ceRNA axis in the brain and PB of AD patients. The obtained results are preliminary, and further *in vitro* and *in vivo* research might strengthen these results. Whereas the possible roles of this ceRNA axis require more exploration, this research advances the current insights into the GABAergic system associated with GABAAR and provides a novel viewpoint on the molecular processes behind AD development.

DATA AVAILABILITY STATEMENT

The original contributions presented in the study are included in the article/**Supplementary Material**, further inquiries can be directed to the corresponding authors.

ETHICS STATEMENT

The studies involving human participants were reviewed and approved by Tabriz University of Medical Sciences' Clinical Research Ethics Committee (Ethical code: IR.TBZMED.REC.1398.1264). The patients/participants provided their written informed consent to participate in this study.

AUTHOR CONTRIBUTIONS

HS, MR, and MoT wrote the draft and revised it. SA-J and JG analyzed the data. MA, AJ, and MaT performed the experiments. BH and RJ collected the data and corresponding clinical information. All authors read and approved the submitted version.

ACKNOWLEDGMENTS

We would like to thank the Clinical Research Development Unit of Tabriz Valiasr Hospital, Tabriz University of Medical Sciences, Tabriz, Iran for their assistance in this research.

SUPPLEMENTARY MATERIAL

The Supplementary Material for this article can be found online at: https://www.frontiersin.org/articles/10.3389/fnagi.2022.812169/full#supplementary-material

REFERENCES

Akiyama, H., Barger, S., Barnum, S., Bradt, B., Bauer, J., Cole, G. M., et al. (2000). Inflammation and Alzheimer's disease. *Neurobiol. Aging.* 21, 383–421.

Association, A. P. (2013). *Diagnostic and Statistical Manual of Mental Disorders (DSM-5®)*. Washington: American Psychiatric Pub.

Bärlund, M., Monni, O., Weaver, J. D., Kauraniemi, P., Sauter, G., Heiskanen, M., et al. (2002). Cloning of BCAS3 (17q23) and BCAS4 (20q13) genes that undergo amplification, overexpression, and fusion in breast cancer. *Genes Chromosomes Cancer* 35, 311–317. doi: 10.1002/gcc.10121

Braak, H., and Braak, E. (1991). Neuropathological stageing of Alzheimer-related changes. *Acta Neuropathol.* 82, 239–259. doi: 10.1007/BF00308809

Busche, M. A., and Hyman, B. T. (2020). Synergy between amyloid-β and tau in Alzheimer's disease. *Nat. Neurosci.* 23, 1183–1193.

Cai, Y., and Wan, J. (2018). Competing Endogenous RNA Regulations in Neurodegenerative Disorders: current Challenges and Emerging Insights. *Front. Mol. Neurosci.* 11:370. doi: 10.3389/fnmol.2018.00370

Castellano, D., Shepard, R. D., and Lu, W. (2021). Looking for Novelty in an "Old" Receptor: recent Advances Toward Our Understanding of GABA(A)Rs and Their Implications in Receptor Pharmacology. *Front. Neurosci.* 14:616298. doi: 10.3389/fnins.2020.616298

Chang, H., Yang, X., You, K., Jiang, M., Cai, F., Zhang, Y., et al. (2020). Integrating multiple microarray dataset analysis and machine learning methods to reveal the key genes and regulatory mechanisms underlying human intervertebral disc degeneration. *PeerJ.* 8:e10120. doi: 10.7717/peerj.10120

Chen, C.-Y., Chen, S.-T., Fuh, C.-S., Juan, H.-F., and Huang, H.-C. (2011). Coregulation of transcription factors and microRNAs in human transcriptional regulatory network. *BMC Bioinform.* 12:S41. doi: 10.1186/1471-2105-12-S1-S41

Chien, C. H., Chiang-Hsieh, Y. F., Tsou, A. P., Weng, S. L., Chang, W. C., and Huang, H. D. (2014). Large-scale investigation of human TF-miRNA relations based on coexpression profiles. *Biomed. Res. Int.* 2014:623078. doi: 10.1155/2014/623078

Diaz, G., Zamboni, F., Tice, A., and Farci, P. (2015). Integrated ordination of miRNA and mRNA expression profiles. *BMC Genomics* 16:767. doi: 10.1186/s12864-015-1971-9

Dionisio-Santos, D. A., Olschowka, J. A., and O'Banion, M. K. (2019). Exploiting microglial and peripheral immune cell crosstalk to treat Alzheimer's disease. *J. Neuroinflamm.* 16:74. doi: 10.1186/s12974-019-1453-0

Fan, L., Mao, C., Hu, X., Zhang, S., Yang, Z., Hu, Z., et al. (2019). New Insights Into the Pathogenesis of Alzheimer's Disease. *Front. Neurol.* 10:1312. doi: 10.3389/fneur.2019.01312

Friard, O., Re, A., Taverna, D., De Bortoli, M., and Corá, D. (2010). CircuitsDB: a database of mixed microRNA/transcription factor feed-forward regulatory circuits in human and mouse. *BMC Bioinform.* 11:435. doi: 10.1186/1471-2105-11-435

Han, W., Li, J., Pelkey, K. A., Pandey, S., Chen, X., Wang, Y. X., et al. (2019). Shisa7 is a GABA(A) receptor auxiliary subunit controlling benzodiazepine actions. *Science* 366, 246–250. doi: 10.1126/science.aax5719

Haunsberger, S. J., Connolly, N. M., and Prehn, J. H. (2017). miRNAmeConverter: an R/bioconductor package for translating mature miRNA names to different miRBase versions. *Bioinformatics* 33, 592–593. doi: 10.1093/bioinformatics/btw660

Holmes, C., Cunningham, C., Zotova, E., Woolford, J., Dean, C., Kerr, S., et al. (2009). Systemic inflammation and disease progression in Alzheimer disease. *Neurology* 73, 768–774. doi: 10.1212/wnl.0b013e3181b6bb95

Huber, W., Carey, V. J., Gentleman, R., Anders, S., Carlson, M., Carvalho, B. S., et al. (2015). Orchestrating high-throughput genomic analysis with Bioconductor. *Nat. Methods* 12, 115–121. doi: 10.1038/nmeth.3252

Irizarry, R. A., Hobbs, B., Collin, F., Beazer-Barclay, Y. D., Antonellis, K. J., Scherf, U., et al. (2003). Exploration, normalization, and summaries of high density oligonucleotide array probe level data. *Biostatistics* 4, 249–264.

Kang, S. S., Ahn, E. H., and Ye, K. (2020). Delta-secretase cleavage of Tau mediates its pathology and propagation in Alzheimer's disease. *Exp. Mol. Med.* 52, 1275–1287. doi: 10.1038/s12276-020-00494-7

Kinney, J. W., Bemiller, S. M., Murtishaw, A. S., Leisgang, A. M., Salazar, A. M., and Lamb, B. T. (2018). Inflammation as a central mechanism in Alzheimer's disease. *Alzheimers* 4, 575–590.

Klaassen, R. V., Stroeder, J., Coussen, F., Hafner, A. S., Petersen, J. D., Renancio, C., et al. (2016). Shisa6 traps AMPA receptors at postsynaptic sites and prevents their desensitization during synaptic activity. *Nat. Commun.* 7:10682.

Lee, H. E., Park, S. J., Huh, J. W., Imai, H., and Kim, H. S. (2020). Enhancer Function of MicroRNA-3681 Derived from Long Terminal Repeats Represses the Activity of Variable Number Tandem Repeats in the 3′. UTR of SHISA7. *Mol. Cells* 43, 607–618. doi: 10.14348/molcells.2020.0058

Lee, M.-J., Chen, T.-F., Cheng, T.-W., and Chiu, M.-J. (2011). rs5848 variant of progranulin gene is a risk of Alzheimer's disease in the Taiwanese population. *Neurodegener. Dis.* 8, 216–220. doi: 10.1159/000322538

Leung, R., Proitsi, P., Simmons, A., Lunnon, K., Güntert, A., Kronenberg, D., et al. (2013). Inflammatory proteins in plasma are associated with severity of Alzheimer's disease. *PLoS One* 8:e64971. doi: 10.1371/journal.pone.0064971

Li, Y., Sun, H., Chen, Z., Xu, H., Bu, G., and Zheng, H. (2016). Implications of GABAergic Neurotransmission in Alzheimer's Disease. *Front. Aging Neurosci.* 8:31. doi: 10.3389/fnagi.2016.00031

Lugli, G., Cohen, A. M., Bennett, D. A., Shah, R. C., Fields, C. J., Hernandez, A. G., et al. (2015). Plasma Exosomal miRNAs in Persons with and without Alzheimer Disease: altered Expression and Prospects for Biomarkers. *PLoS One* 10:e0139233. doi: 10.1371/journal.pone.0139233

Ma, G., Liu, M., Du, K., Zhong, X., Gong, S., Jiao, L., et al. (2019). Differential Expression of mRNAs in the Brain Tissues of Patients with Alzheimer's Disease Based on GEO Expression Profile and Its Clinical Significance. *Biomed. Res. Int.* 2019:8179145. doi: 10.1155/2019/8179145

Malaguarnera, M., Balzano, T., Castro, M. C., Llansola, M., and Felipo, V. (2021). The Dual Role of the GABAA Receptor in Peripheral Inflammation and Neuroinflammation: a Study in Hyperammonemic Rats. *Int. J. Mol. Sci.* 22:6772. doi: 10.3390/ijms22136772

Marques, A. C., Tan, J., Lee, S., Kong, L., Heger, A., and Ponting, C. P. (2012). Evidence for conserved post-transcriptional roles of unitary pseudogenes and for frequent bifunctionality of mRNAs. *Genome Biol.* 13, R102. doi: 10.1186/gb-2012-13-11-r102

Marttinen, M., Paananen, J., Neme, A., Mitra, V., Takalo, M., Natunen, T., et al. (2019). A multiomic approach to characterize the temporal sequence in Alzheimer's disease-related pathology. *Neurobiol. Dis.* 124, 454–468.

Metcalfe, M. J., and Figueiredo-Pereira, M. E. (2010). Relationship between tau pathology and neuroinflammation in Alzheimer's disease. *Mt. Sinai J. Med.* 77, 50–58. doi: 10.1002/msj.20163

Moreno-García, L., López-Royo, T., Calvo, A. C., Toivonen, J. M., de la Torre, M., and Moreno-Martínez, L. (2020). Competing Endogenous RNA Networks as Biomarkers in Neurodegenerative Diseases. *Int. J. Mol. Sci.* 21:9582.

Motta, M., Imbesi, R., Di Rosa, M., Stivala, F., and Malaguarnera, L. (2007). Altered plasma cytokine levels in Alzheimer's disease: correlation with the disease progression. *Immunol. Lett.* 114, 46–51. doi: 10.1016/j.imlet.2007.09.002

Noroozi, R., Ghafouri-Fard, S., Pisarek, A., Rudnicka, J., Spólnicka, M., Branicki, W., et al. (2021). DNA methylation-based age clocks: from age prediction to age reversion. *Ageing Res. Rev.* 68:101314. doi: 10.1016/j.arr.2021.101314

Park, J.-C., Han, S.-H., and Mook-Jung, I. (2020). Peripheral inflammatory biomarkers in Alzheimer's disease: a brief review. *BMB Rep.* 53, 10–19. doi: 10.5483/BMBRep.2020.53.1.309

Peter, S., Urbanus, B. H. A., Klaassen, R. V., Wu, B., Boele, H. J., Azizi, S., et al. (2020). AMPAR Auxiliary Protein SHISA6 Facilitates Purkinje Cell Synaptic Excitability and Procedural Memory Formation. *Cell Rep.* 31:107515. doi: 10.1016/j.celrep.2020.03.079

Rezazadeh, M., Hosseinzadeh, H., Moradi, M., Salek Esfahani, B., Talebian, S., Parvin, S., et al. (2019). Genetic discoveries and advances in late-onset Alzheimer's disease. *J. Cell Physiol.* 234, 16873–16884. doi: 10.1002/jcp.28372

Ritchie, M. E., Phipson, B., Wu, D., Hu, Y., Law, C. W., Shi, W., et al. (2015). limma powers differential expression analyses for RNA-sequencing and microarray studies. *Nucleic Acids Res.* 43:e47. doi: 10.1093/nar/gkv007

Roy, J., and Mallick, B. (2017). Altered gene expression in late-onset Alzheimer's disease due to SNPs within 3′UTR microRNA response elements. *Genomics* 109, 177–185. doi: 10.1016/j.ygeno.2017.02.006

Sabaie, H., Amirinejad, N., Asadi, M. R., Jalaiei, A., Daneshmandpour, Y., Rezaei, O., et al. (2021). Molecular Insight Into the Therapeutic Potential of Long Non-coding RNA-Associated Competing Endogenous RNA Axes in Alzheimer's Disease: a Systematic Scoping Review. *Front. Aging Neurosci.* 13:742242. doi: 10.3389/fnagi.2021.742242

Salmena, L., Poliseno, L., Tay, Y., Kats, L., and Pandolfi, P. P. (2011). A ceRNA hypothesis: the Rosetta Stone of a hidden RNA language? *Cell* 146, 353–358. doi: 10.1016/j.cell.2011.07.014

Silva, D., Antunes, J., Balamurugan, K., Duncan, G., Alho, C. S., and McCord, B. (2016). Developmental validation studies of epigenetic DNA methylation markers for the detection of blood, semen and saliva samples. *Forensic. Sci. Int. Genet.* 23, 55–63. doi: 10.1016/j.fsigen.2016.01.017

Silver, J. D., Ritchie, M. E., and Smyth, G. K. (2009). Microarray background correction: maximum likelihood estimation for the normal-exponential convolution. *Biostatistics* 10, 352–363. doi: 10.1093/biostatistics/kxn042

Sims, R., Hill, M., and Williams, J. (2020). The multiplex model of the genetics of Alzheimer's disease. *Nat. Neurosci.* 23, 311–322.

Solfrizzi, V., D'Introno, A., Colacicco, A. M., Capurso, C., Todarello, O., Pellicani, V., et al. (2006). Circulating biomarkers of cognitive decline and dementia. *Clin. Chim. Acta.* 364, 91–112. doi: 10.1016/j.cca.2005.06.015

Sticht, C., De La Torre, C., Parveen, A., and Gretz, N. (2018). miRWalk: an online resource for prediction of microRNA binding sites. *PLoS One* 13:e0206239. doi: 10.1371/journal.pone.0206239

Taki, T., and Kibayashi, K. (2015). Characterization of cellular and extracellular DNA in saliva. *Leg. Med.* 17, 471–474. doi: 10.1016/j.legalmed.2015.10.003

Tay, Y., Kats, L., Salmena, L., Weiss, D., Tan, S. M., Ala, U., et al. (2011). Coding-independent regulation of the tumor suppressor PTEN by competing endogenous mRNAs. *Cell* 147, 344–357. doi: 10.1016/j.cell.2011.09.029

von Engelhardt, J., Mack, V., Sprengel, R., Kavenstock, N., Li, K. W., Stern-Bach, Y., et al. (2010). CKAMP44: a brain-specific protein attenuating short-term synaptic plasticity in the dentate gyrus. *Science* 327, 1518–1522. doi: 10.1126/science.1184178

von Heydebreck, A., Huber, W., and Gentleman, R. (2005). "Differential expression with the Bioconductor Project"in *Technical Report 7, Bioconductor Project Working Papers, 2004*. Available online at www.bepress.com/bioconductor/paper7 (accessed october 23, 2021).

Wilson, C. J., Finch, C. E., and Cohen, H. J. (2002). Cytokines and cognition–the case for a head-to-toe inflammatory paradigm. *J. Am. Geriatr. Soc.* 50, 2041–2056. doi: 10.1046/j.1532-5415.2002.50619.x

Yeung, K. Y., and Ruzzo, W. L. (2001). Principal component analysis for clustering gene expression data. *Bioinformatics* 17, 763–774. doi: 10.1093/bioinformatics/17.9.763

Yu, C.-C., Jiang, T., Yang, A.-F., Du, Y.-J., Wu, M., and Kong, L.-H. (2019). Epigenetic Modulation on Tau Phosphorylation in Alzheimer's Disease. *Neural. Plast.* 2019:6856327. doi: 10.1155/2019/6856327

Conflict of Interest: The authors declare that the research was conducted in the absence of any commercial or financial relationships that could be construed as a potential conflict of interest.

Publisher's Note: All claims expressed in this article are solely those of the authors and do not necessarily represent those of their affiliated organizations, or those of the publisher, the editors and the reviewers. Any product that may be evaluated in this article, or claim that may be made by its manufacturer, is not guaranteed or endorsed by the publisher.

frontiers in Aging Neuroscience

ORIGINAL RESEARCH
published: 01 March 2022
doi: 10.3389/fnagi.2022.811059

Genetically Predicted Levels of Circulating Inflammatory Cytokines and the Risk and Age at Onset of Parkinson's Disease: A Two-Sample Mendelian Randomization Study

Yating Zhao[1†], Xiaoqian Zhang[1†], Na Guo[1], Dandan Tian[1], Chenguang Zhang[1], Changqing Mu[1], Chen Han[1], Ruixia Zhu[1], Jian Zhang[2,3] and Xu Liu[1]*

[1] Department of Neurology, First Affiliated Hospital of China Medical University, Shenyang, China, [2] Key Laboratory of Cell Biology, Ministry of Public Health, Department of Cell Biology, China Medical University, Shenyang, China, [3] Key Laboratory of Medical Cell Biology, Ministry of Education, China Medical University, Shenyang, China

OPEN ACCESS

Edited by:
Robert Petersen,
Central Michigan University,
United States

Reviewed by:
Pingyi Xu,
First Affiliated Hospital of Guangzhou Medical University, China
Zhaoqi Yan,
Gladstone Institutes, United States

***Correspondence:**
Xu Liu
valentine1120@126.com

[†] These authors have contributed equally to this work and share first authorship

Specialty section:
This article was submitted to Parkinson's Disease and Aging-related Movement Disorders, a section of the journal Frontiers in Aging Neuroscience

Received: 08 November 2021
Accepted: 31 January 2022
Published: 01 March 2022

Citation:
Zhao Y, Zhang X, Guo N, Tian D, Zhang C, Mu C, Han C, Zhu R, Zhang J and Liu X (2022) Genetically Predicted Levels of Circulating Inflammatory Cytokines and the Risk and Age at Onset of Parkinson's Disease: A Two-Sample Mendelian Randomization Study. Front. Aging Neurosci. 14:811059. doi: 10.3389/fnagi.2022.811059

Parkinson's disease (PD) is widely considered to be a disabling neurodegenerative disorder, which has been ranked second worldwide just after Alzheimer's disease. Until present, a wide range of studies has focused on the role of circulating inflammatory cytokines in the development of PD. However, the causal relationship between circulating inflammatory cytokines and the risk and age at the onset of PD has not been elucidated. Hence, to evaluate the effects of circulating inflammatory cytokines on the risk or age at the onset of PD more accurately, we conducted this two-sample Mendelian randomization (MR) study involving summary statistics from genome-wide association studies (GWASs). Totally, we included a GWAS for inflammatory cytokines (8,293 participants), a meta-analysis of GWASs for PD risk (482,730 participants), and a GWAS dataset for age at the onset of PD (17,996 patients with PD). A total of 149 and 131 polymorphisms for exploring relationships between 19 inflammatory cytokines and the risk and age at the onset of PD were obtained as instrumental variants. Then, we used a total of five MR methods, including inverse-variance weighted (IVW), Wald ratio, MR Egger regression, weighted median, and MR-pleiotropy residual sum and outlier (MR-PRESSO) methods. Finally, we found a causal association between circulating levels of macrophage inflammatory protein-1 beta (MIP1b) and PD risk in the IVW method (OR: 1.06; 95% CI: 1.02–1.10; P = 0.001). Meanwhile, other MR estimates by weighted median and MR-PRESSO methods yielded similar effect estimates. Besides, we identified a suggestive association of interleukin-16 (IL-16) levels with PD risk (OR: 1.08; 95% CI: 1.00–1.17; P = 0.037). For age at PD onset, there was no evidence supporting its correlation with inflammatory cytokines. Our findings implied that MIP1b and IL-16 may be novel biomarkers and promising therapeutic targets for PD development.

Keywords: cytokines, inflammation, Mendelian randomization, macrophage inflammatory protein-1 beta, interleukin-16, Parkinson's disease

INTRODUCTION

Parkinson's disease (PD) is considered to be an aging-related neurodegenerative disease, characterized by a broad spectrum of clinical features, including tremor, bradykinesia, rigidity, postural instability, and dysautonomia (Jankovic, 2008). During the past decades, the number of individuals suffering from PD increased from 2.5 million in 1990 to 6.1 million in 2016 globally, and it brought great distress and economic burden to society and families (GBD 2016 Parkinson's Disease Collaborators, 2018). In the United States alone, the overall annual cost related to PD was estimated to be US$51.9 billion in 2017 and was projected to continually increase and eventually surpass US$79 billion by 2037 (Yang et al., 2020). Thus, huge efforts have been made for exploring possible biomarkers and clarifying the pathogenesis for PD development (Schapira and Jenner, 2011; Lotankar et al., 2017).

Presently, an increasing number of evidence supported the vital role of inflammation in the pathogenesis of PD (Marogianni et al., 2020; Kline et al., 2021). It has been reported that systematic inflammation may destroy the permeability of the blood-brain barrier (BBB), activate microglia, and trigger neuroinflammation, which ultimately led to the degeneration of dopaminergic neurons and PD occurrence (Villaran et al., 2010; Joshi and Singh, 2018). Thus, as an indispensable part of the pathophysiological process of inflammation, inflammatory cytokines are suggested to be involved in PD development. Previous observational studies have demonstrated that circulating levels of several inflammatory cytokines were higher in individuals with PD than in healthy controls. For example, Pochmann et al. (2018) indicated that higher levels of monocyte chemotactic protein-1 (MCP-1) were detected in patients with PD than those in the control group. In a meta-analysis involving 2,654 individuals, elevated concentrations of interleukin-6 (IL-6) and IL-1β were observed in patients with PD but not in healthy controls (Qin et al., 2016). Moreover, several genetic polymorphisms near genes encoding MCP-1 and IL-1β were also indicated to be related to an increased risk of PD (Wahner et al., 2007; Wang et al., 2019). Additionally, it has been reported that higher expression of tumor necrosis factor-α (TNF-α) was associated with earlier onset of PD (Lindenau et al., 2017). However, due to the confounding factors, reverse causation, and limited sample size in these observational studies, the relationships between inflammatory cytokines and the risk and age at the onset of PD may be misled.

Mendelian randomization (MR) is considered to be a robust method, which could overcome the limitations of observational studies mentioned earlier by using genetic variants as instrumental variables and large-scale data from genome-wide association studies (GWASs). Hence, in this study, we introduced the MR method to assess the causal relationship between inflammatory cytokines and the risk and age at the onset of PD.

MATERIALS AND METHODS

Study Design

In **Figure 1**, the overall design of this two-sample MR analysis is displayed. The study was based on publicly available data from GWASs on circulating inflammatory cytokines and PD, with detailed information listed in **Supplementary Table 1**. Since we used summary statistics from published studies, no additional ethical approval was required.

Data Sources and Instrument Selection

Concerning PD risk, we included summary data from a GWAS meta-analysis involving IPDGC-NeuroX, UK Biobank, SGPD and IPDGC study with 33,674 cases and 449,056 controls (contributing studies outlined in **Supplementary Table 1**; Nalls et al., 2019). As for age at the onset of PD, estimates were extracted from a GWAS dataset including 17 cohorts with 17,996 cases with PD (Blauwendraat et al., 2019).

Regarding the instrument variables of inflammatory cytokines, we obtained genetic variants from one recently published GWAS on circulating inflammatory cytokines involving 8,293 European participants (Ahola-Olli et al., 2017). First, we obtained 6,368 single-nucleotide polymorphisms (SNPs) according to a genome-wide significance threshold of $P < 5 \times 10^{-8}$ and the false discovery rate (FDR) less than 5%. Then, for each cytokine, we pruned all selected SNPs in linkage disequilibrium (LD) ($r^2 < 0.1$ in the European 1,000 genomes reference panel), retaining 199 genetic polymorphisms with the lowest *P*-value as an independent instrument. Next, to avoid pleiotropic effects, 38 SNPs associated with concentrations of more than one cytokine were excluded, leaving 161 polymorphisms focusing on 19 inflammatory cytokines for use. Finally, since 30 SNPs related to the circulating levels of cytokines were not available in the PD risk or age of PD onset datasets, we selected other SNPs in high LD for replacement in further MR analysis (r^2 varying between 0.8 and 1). In the end, a total of 149 SNPs and 131 SNPs for detecting relationships between inflammatory cytokines and the risk and age at the onset of PD were included in this study separately. The detailed information of 19 cytokines and their related SNPs used as instrument variables is displayed in **Supplementary Table 2**.

Statistical Analyses

First, for those cytokines with only one related SNP, the Wald ratio method was used to compute the MR estimates for the association between one-SD elevated circulating cytokine levels and PD risk or age of PD onset, respectively. When over one variant was included, the inverse-variance weighted (IVW) method, as principal analysis, was used to evaluate the potential causal relationships between circulating levels of inflammatory cytokines and the risk and age at the onset of PD. For further assessing the heterogeneity of the causal estimates across different SNPs, Cochran's *Q*-test was applied in the IVW method. Subsequently, we evaluated the possibility that the

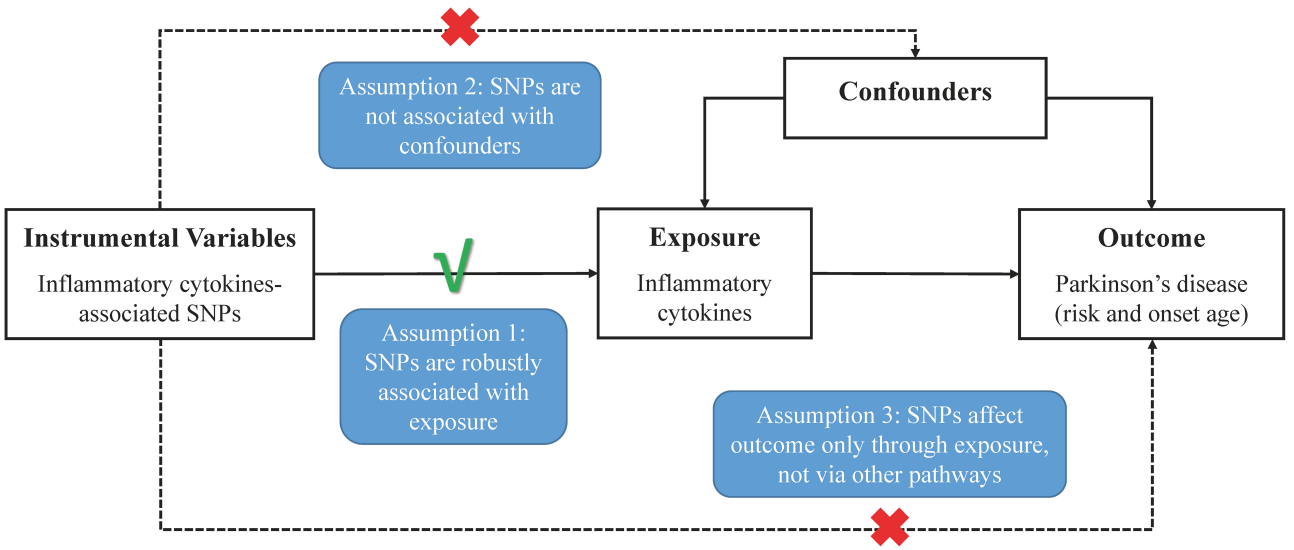

FIGURE 1 | Schematic representation of two-sample Mendelian randomization analyses for circulating levels of inflammatory cytokines and risk of Parkinson's disease.

overall MR estimate was driven by a single SNP using leave-one-out analysis (Noyce et al., 2019). Specifically, we reran the MR analysis by using all SNPs and excluding only one outlier SNP at each time. Furthermore, three supplementary analyses, including MR Egger regression, weighted median, and MR-pleiotropy residual sum and outlier (MR-PRESSO) approaches, were performed for investigating the presence of pleiotropy and further evaluating the causal relationships (Bowden et al., 2015, 2016; Verbanck et al., 2018). In addition, we calculated the *F*-statistics to quantify the strength of the selected instruments, all of which were above the threshold of the *F*-statistics ($F > 10$) typically recommended for MR analyses. As 19 exposures were involved, we set the statistically significant *P*-value threshold to 2.63×10^{-3} (0.05/19) after the Bonferroni correction. The suggestive association was identified as a *P*-value between the conventional significance level (0.05) and the Bonferroni-corrected significance level. All above statistical analyses were conducted by using the *R*-statistical software (version 4.0.3) with related *R* packages, including MR, two-sample MR, as well as MR-PRESSO.

RESULTS

Circulating Inflammatory Cytokines and Parkinson's Disease Risk

As displayed in **Table 1** and **Supplementary Figure 1**, by using a significant threshold of 2.63×10^{-3} (Bonferroni correction for the correlation test of 19 cytokines), we found that genetically predicted one-SD increment in circulating MIP1b levels was associated with 6% higher risk of PD based on 74 SNPs in the IVW method (*OR*: 1.06; 95% *CI*: 1.02–1.10; $P = 0.001$). Furthermore, we did not observe any significant heterogeneity as measured by Cochran's *Q*-test ($I^2 = 0.5\%$, $P = 0.465$). Subsequent leave-one-out analysis showed that no single SNP dominated the IVW point estimate (**Supplementary Figure 2**). Similarly, a significant association was found between circulating levels of MIP1b and PD risk in the MR-PRESSO method (*OR*: 1.06; 95% *CI*: 1.02–1.10; $P = 0.002$). Consistent with these results, suggestive evidence of an adverse effect of circulating MIP1b levels on PD risk was also observed by the weighted median method (*OR*: 1.08; 95% *CI*: 1.02–1.14; $P = 0.014$). Although the significant statistical association was not detected by MR Egger regression, the estimate was directionally consistent with other principal and supplementary analyses (**Table 1** and **Figure 2**). Additionally, there was no evidence for potential pleiotropy according to the intercept assessed by MR Egger regression; meanwhile, no outlier SNP was detected using the MR-PRESSO method.

Regarding interleukin-16 (IL-16), we identified a suggestive association between circulating IL-16 levels and PD risk in IVW analysis. Specifically, for one SD increment of IL-16 levels, the OR of PD risk was 1.08 (95% *CI*: 1.00–1.17; $P = 0.037$). Further analysis showed a lack of evidence of heterogeneity among SNPs in the suggestive association of IL-16 with PD risk ($I^2 = 0$, $P = 0.705$). Meanwhile, additional supplementary analysis displayed a similar causal trend with the estimation using the IVW method. In addition, no potential pleiotropy was detected using the MR Egger method (**Table 1**).

Apart from MIP1b and IL-16, the other 17 cytokines (TRAIL, MCP1, GROa, eotaxin, TNFb, CTACK, IL2ra, IP10, IFNg1, IL10, IL12p70, IL18, IL17, MCSF, MIF, MIG, and RANTES) were not shown to be associated with PD risk in the main IVW analysis and three supplementary analyses (**Table 1**). For each cytokine, no marked heterogeneity was found between related SNPs, except for TRAIL ($I^2 = 41.7\%$, $P = 0.016$). Meanwhile, the *P*-values for the intercepts from Egger regression did not demonstrate any pleiotropy, while IL-18 was the exception ($P = 0.037$). Further,

TABLE 1 | MR analyses of genetically predicted levels of circulating inflammatory cytokines and risk of Parkinson's disease.

Cytokines	No. of SNPs	OR (95% CI)	*P* for association	Heterogeneity test (I^2, *P*)	MR-Egger (intercept, *P*)	*P* for MR-PRESSO global test
MIP1b						
Inverse variance weighted	74	1.06 (1.02–1.10)	0.001	0.5%, 0.465		
MR egger	74	1.06 (0.99–1.14)	0.088		–0.001, 0.908	
Weighted median	74	1.08 (1.02–1.14)	0.014			
MR-PRESSO (raw, 0 outliers)	74	1.06 (1.02–1.10)	0.002			0.491
TRAIL						
Inverse variance weighted	25	0.98 (0.91–1.05)	0.556	41.7%, 0.016		
MR egger	25	0.93 (0.84–1.03)	0.177		0.019, 0.200	
Weighted median	25	0.99 (0.91–1.07)	0.813			
MR-PRESSO (raw, 0 outliers)	25	0.98 (0.91–1.05)	0.562			0.016
IL18						
Inverse variance weighted	8	1.07 (0.97–1.19)	0.182	36.7%, 0.136		
MR egger	8	1.39 (1.07–1.79)	0.012		–0.061, 0.037	
Weighted median	8	1.10 (0.98–1.23)	0.103			
MR-PRESSO (raw, 0 outliers)	8	1.07 (0.97–1.19)	0.224			0.144
MCP1						
Inverse variance weighted	7	0.97 (0.86–1.10)	0.657	0.0%, 0.776		
MR egger	7	1.13 (0.86–1.49)	0.376		–0.022, 0.233	
Weighted median	7	1.01 (0.86–1.18)	0.923			
MR-PRESSO (raw, 0 outliers)	7	0.97 (0.89–1.06)	0.569			0.726
GROa						
Inverse variance weighted	6	0.98 (0.91–1.06)	0.634	0.0%, 0.455		
MR egger	6	1.01 (0.81–1.27)	0.898		–0.009, 0.755	
Weighted median	6	0.94 (0.85–1.04)	0.224			
MR-PRESSO (raw, 0 outliers)	6	0.98 (0.91–1.06)	0.644			0.451
Eotaxin						
Inverse variance weighted	5	0.94 (0.82–1.09)	0.441	0.0%, 0.805		
MR egger	5	0.94 (0.49–1.82)	0.855		0.001, 0.988	
Weighted median	5	1.01 (0.85–1.21)	0.894			
MR-PRESSO (raw, 0 outliers)	5	0.94 (0.86–1.04)	0.293			0.743
TNFb						
Inverse variance weighted	4	1.02 (0.95–1.10)	0.541	0.0%, 0.434		

(Continued)

TABLE 1 | (Continued)

Cytokines	No. of SNPs	OR (95% CI)	*P* for association	Heterogeneity test (I^2, *P*)	MR-Egger (intercept, *P*)	*P* for MR-PRESSO global test
MR egger	4	1.11 (0.79–1.56)	0.532		–0.088, 0.612	
Weighted median	4	1.03 (0.95–1.12)	0.430			
MR-PRESSO (raw, 0 outliers)	4	1.02 (0.95–1.10)	0.568			0.644
CTACK						
Inverse variance weighted	4	1.03 (0.92–1.15)	0.593	21.8%, 0.280		
MR egger	4	1.05 (0.77–1.44)	0.746		–0.007, 0.877	
Weighted median	4	1.05 (0.93–1.17)	0.444			
MR-PRESSO (raw, 0 outliers)	4	1.02 (0.92–1.15)	0.630			0.363
IL16						
Inverse variance weighted	3	1.08 (1.00–1.17)	0.037	0.0%, 0.705		
MR egger	3	1.06 (0.94–1.19)	0.339		0.010, 0.613	
Weighted median	3	1.07 (0.99–1.17)	0.095			
IL2ra						
Inverse variance weighted	3	1.03 (0.95–1.11)	0.538	0.0%, 0.574		
MR egger	3	0.91 (0.69–1.20)	0.506		0.062, 0.376	
Weighted median	3	1.03 (0.95–1.12)	0.511			
IP10						
Inverse variance weighted	2	0.92 (0.73–1.15)	0.448	0.0%, 0.934		
IFNg1						
Wald ratio	1	0.88 (0.56–1.40)	0.599			
IL10						
Wald ratio	1	0.87 (0.59–1.28)	0.474			
IL12p70						
Wald ratio	1	1.13 (0.77–1.65)	0.531			
IL17						
Wald ratio	1	0.99 (0.65–1.51)	0.979			
MCSF						
Wald ratio	1	0.83 (0.65–1.06)	0.127			
MIF						
Wald ratio	1	0.98 (0.79–1.23)	0.877			
MIG						
Wald ratio	1	1.04 (0.82–1.32)	0.754			
RANTES						
Wald ratio	1	0.95 (0.62–1.44)	0.803			

SNP, single-nucleotide polymorphism; OR, odds ratio; CI, confidence interval; MR-PRESSO, Mendelian randomization pleiotropy residual sum and outlier.

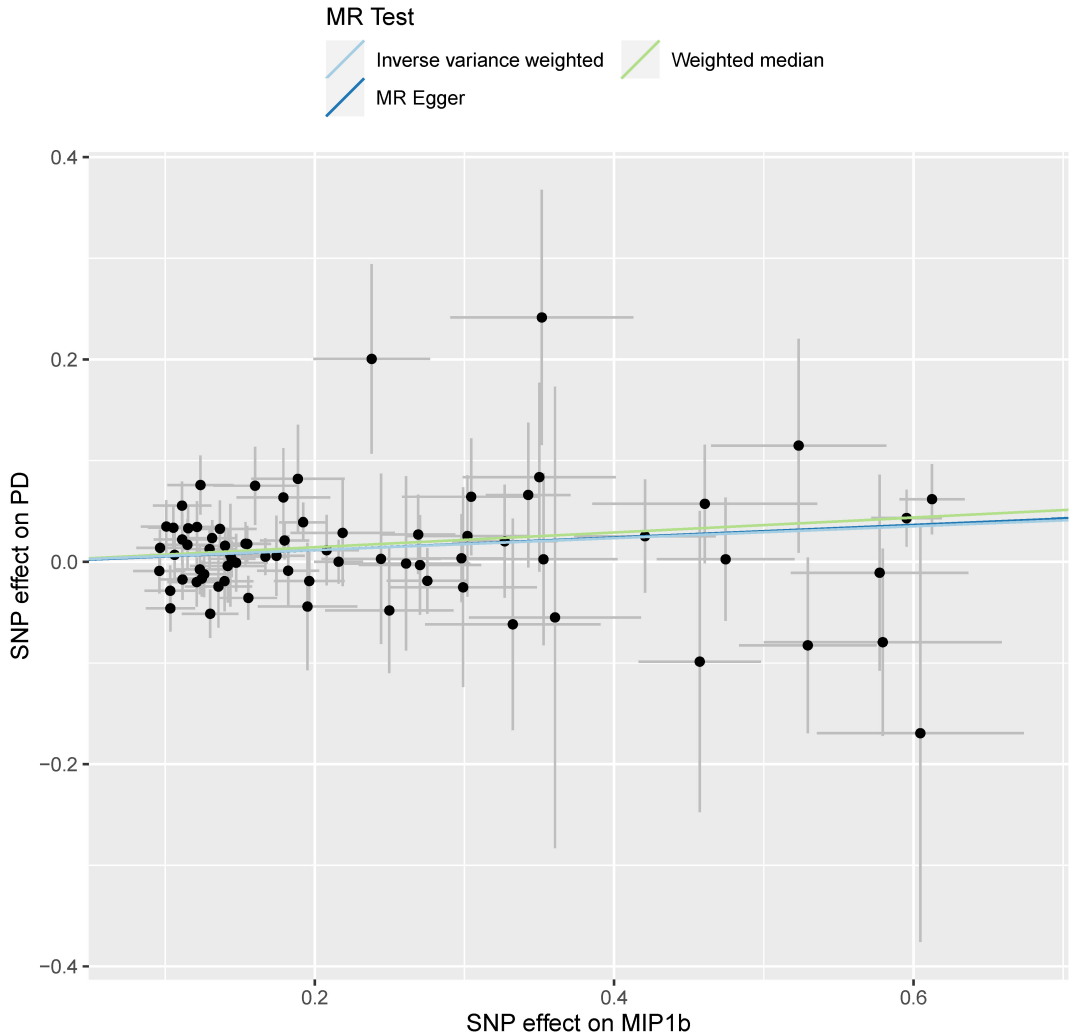

FIGURE 2 | Scatterplot of genetic association with circulating levels of MIP1b against the genetic association with PD risk. Each black dot indicates an SNP, plotted by the estimate of SNP on the MIP1b levels and the estimate of SNP on PD risk with standard error bars. The slope of the line represents the causal relationship, and each method has a different line. PD, Parkinson's disease; SNP, single-nucleotide polymorphism.

the MR-PRESSO test showed that no outlier was found for all cytokines, except for TRAIL ($P = 0.016$).

Circulating Inflammatory Cytokines and Age at the Onset of Parkinson's Disease

Except for identifying the correlation between inflammatory cytokines and PD risk mentioned earlier, we also detected the causal relationships between the circulating levels of these cytokines and the age of PD onset. Unfortunately, there was no evidence to support the causal relationships between these 19 cytokines and age at the onset of PD (**Table 2**). Moreover, no statistical evidence of instrument heterogeneity was detected using Cochran's *Q*-test except for IP10 ($I^2 = 79.1\%$, $P = 0.029$). When applying MR Egger regression, evidence of potential pleiotropy was only observed in GROa ($P = 0.029$), while other inflammatory cytokines did not show any pleiotropy. Besides, no SNP was detected as an outlier through the MR-PRESSO test (**Table 2**).

DISCUSSION

Parkinson's disease is a progressive and disabling neurodegenerative disease that mainly affects individuals in their later years of life and its course may vary from 6.9 to 14.3 years (Macleod et al., 2014; Marras et al., 2018). It has been reported that in 2016 alone, PD caused 211,296 deaths and 3.2 million disability-adjusted life-years globally (GBD 2016 Parkinson's Disease Collaborators, 2018). Despite the long course of the disease and its huge impact on life expectance for elders, the intervention for PD prevention and therapy is still deficient, and the biological mechanism underlying PD etiology is not yet well understood. Thus, we took advantage of a two-sample MR

TABLE 2 | MR analysis of genetically predicted levels of circulating inflammatory cytokines and age at onset of Parkinson's disease.

Cytokines	No. of SNPs	Beta (95% CI)	*P* for association	Heterogeneity test (I^2, *P*)	MR-egger (intercept, *P*)	*P* for MR-PRESSO global test
MIP1b						
Inverse variance weighted	65	–0.02 (–0.26–0.21)	0.854	0.0%, 0.516		
MR egger	65	0.00 (–0.49–0.48)	0.986		–0.004, 0.934	
Weighted median	65	–0.04 (–0.40–0.32)	0.840			
MR-PRESSO (raw, 0 outliers)	65	–0.02 (–0.26–0.21)	0.853			0.534
TRAIL						
Inverse variance weighted	21	–0.01 (–0.36–0.33)	0.938	0.0%, 0.939		
MR Egger	21	–0.26 (–0.77–0.26)	0.324		0.095, 0.208	
Weighted median	21	0.04 (–0.42–0.50)	0.861			
MR-PRESSO (raw, 0 outliers)	21	–0.01 (–0.27–0.25)	0.919			0.950
IL18						
Inverse variance weighted	7	–0.19 (–0.80–0.43)	0.553	20.5%, 0.273		
MR Egger	7	–0.44 (–2.43–1.54)	0.661		0.061, 0.787	
Weighted median	7	–0.29 (–0.98–0.40)	0.411			
MR-PRESSO (raw, 0 outliers)	7	–0.19 (–0.80–0.43)	0.575			0.328
MCP1						
Inverse variance weighted	7	–0.39 (–1.19–0.41)	0.342	0.0%, 0.917		
MR egger	7	0.33 (–1.56–2.22)	0.732		–0.106, 0.409	
Weighted median	7	–0.13 (–1.09–0.83)	0.796			
MR-PRESSO (raw, 0 outliers)	7	–0.39 (–0.86-0.08)	0.153			0.922
GROa						
Inverse variance weighted	6	–0.52 (–1.14–0.11)	0.104	33.9%, 0.182		
MR egger	6	0.90 (–0.47–2.28)	0.197		–0.397, 0.029	
Weighted median	6	–0.43 (–1.07–0.21)	0.184			
MR-PRESSO (raw, 0 outliers)	6	–0.52 (–1.14–0.11)	0.165			0.216
Eotaxin						
Inverse variance weighted	4	–0.10 (–1.12–0.91)	0.844	0.0%, 0.966		
MR egger	4	0.57 (–4.24–5.38)	0.816		–0.087, 0.779	
Weighted median	4	0.00 (–1.20–1.21)	0.995			
MR-PRESSO (raw, 0 outliers)	4	–0.10 (–0.40–0.20)	0.556			0.966
CTACK						
Inverse variance weighted	4	0.12 (–0.54–0.78)	0.715	11.5%, 0.335		

(Continued)

TABLE 2 | (Continued)

Cytokines	No. of SNPs	Beta (95% CI)	*P* for association	Heterogeneity test (I^2, *P*)	MR-egger (intercept, *P*)	*P* for MR-PRESSO global test
MR egger	4	0.67 (–1.08–2.42)	0.453		–0.165, 0.500	
Weighted median	4	0.25 (–0.51–1.01)	0.516			
MR-PRESSO (raw, 0 outliers)	4	0.12 (–0.54–0.78)	0.739			0.390
IL16						
Inverse variance weighted	3	0.41 (–0.11–0.93)	0.125	0.0%, 0.839		
MR egger	3	0.59 (–0.22–1.40)	0.151		–0.079, 0.558	
Weighted median	3	0.40 (–0.17–0.96)	0.166			
TNFb						
Inverse variance weighted	2	0.03 (–0.53–0.60)	0.905	0.0%, 0.902		
IL2ra						
Inverse variance weighted	2	0.45 (–0.33–1.22)	0.107	50.2%, 0.156		
IP10						
Inverse variance weighted	2	0.43 (–2.65–3.51)	0.547	79.1%, 0.029		
IFNg1						
Wald ratio	1	–0.79 (–4.24–2.67)	0.654			
IL10						
Wald ratio	1	–0.06 (–2.57–2.46)	0.965			
IL12p70						
Wald ratio	1	0.44 (–2.12–2.99)	0.738			
IL17						
Wald ratio	1	–1.18 (–3.80–1.45)	0.379			
MCSF						
Wald ratio	1	–0.02 (–1.56–1.52)	0.983			
MIF						
Wald ratio	1	–1.09 (–2.60–0.41)	0.153			
MIG						
Wald ratio	1	–0.53 (–2.12–1.06)	0.510			
RANTES						
Wald ratio	1	0.87 (–1.56–3.30)	0.484			

SNP, single-nucleotide polymorphism; CI, confidence interval; MR-PRESSO, Mendelian randomization pleiotropy residual sum and outlier.

analysis to investigate the causal role of circulating inflammatory cytokines in the risk and age at the onset of PD. In this study, higher MIP1b levels showed a causal relationship with the increased risk of PD, whereas another cytokine, IL-16, displayed a suggestive association.

Macrophage inflammatory protein-1 beta, also known as CCL4, is a chemotactic protein with 69 amino acids produced by various cells, including natural killer cells, T cells, B cells, and neutrophils (Menten et al., 2002; Mukaida et al., 2020). A previous study by Zhu et al. (2014) demonstrated that in the transgenic mice model of Alzheimer's disease, MIP1b mRNA was 18 times higher than that of wild-type mice, indicating that MIP1b might be involved in the development of Alzheimer's disease. In addition, MIP1b was also reported to be

related to other neurodegenerative diseases, including multiple system atrophy and amyotrophic lateral sclerosis (Compta et al., 2019; Martinez et al., 2020). This evidence implied that MIP1b might participate in the initiation and progression of a neurodegenerative disorder. As for PD, in the past few decades, limited observational studies provided evidence of a possible association between MIP1b and PD risk. According to a previous case-control study involving 50 participants by Calvani et al. (2020), circulating levels of MIP1b were 2-fold higher in patients with PD than in controls, suggesting that it could be considered a possible biomarker for PD occurrence. Additionally, according to Brockmann's study of 142 patients with PD, higher serum levels of MIP1b may be associated with more severe non-motor symptoms of PD, including cognitive impairment, sleep behavior disorder, and orthostatic dysfunction (Brockmann et al., 2017). Although these studies indicated an association between circulating levels of MIP1b and the occurrence and progression of PD, these results from observational studies were ambiguous and questionable. The reasons were as follows: due to the small sample size and potential confounding, the results of observational studies may be biased. Besides, the relationship between circulating levels of MIP1b and PD risk obtained from observational studies could not be determined as a causal association or even may even be a reverse causality. Therefore, we conducted this MR analysis and reached a reliable result that one-SD increment in the circulating levels of MIP1b may increase the risk of PD by 6%, indicating that lowering the levels of MIP1b may be a promising therapeutic strategy for PD.

From the perspective of biological mechanism, MIP1b may participate in the pathophysiology process of PD through the following pathways. On the one hand, MIP1b could induce the activation of macrophages by binding to its specific receptor, CCR5 (Cheung et al., 2009; Saika et al., 2012). Then, the activated macrophage might release high levels of pro-inflammatory cytokines, such as IL-1β, TNF-α, IL-6, and MIP-1α (Saika et al., 2012; Shapouri-Moghaddam et al., 2018). These cytokines could further disrupt the permeability of brain microvascular endothelial cells and the integrity of BBB (Al-Obaidi and Desa, 2018; Morris et al., 2018). On the other hand, MIP1b not only can immobilize glycosaminoglycans on the apical surface of microvascular endothelial cells but can also bind to the basal surfaces of endothelial cells as well as the subendothelial matrix. Both of the connections contributed to the establishment and maintenance of MIP1b gradients to help various circulating inflammatory cells pass through the BBB and enter the central nervous system (CNS) (Shukaliak and Dorovini-Zis, 2000). Subsequently, in response to these inflammatory mediators, microglia were activated and functionally polarized toward the pro-inflammatory M1 phenotype, which further induced the secretion of inflammatory cytokines, such as TNF-α, MCP-1, and IL-1β (Qin et al., 2007; Jo et al., 2017; Pajares et al., 2020). These chronically elevated inflammatory cytokines and activated inflammatory cells may, in turn, lead to chronic self-perpetuating neuroinflammation and eventually end up in the development of PD (Collins et al., 2012).

Regarding IL-16, it is a protein with 631 amino acids and is generally accepted to be a chemotactic cytokine for T cells (Cruikshank et al., 2000; Skundric et al., 2015). In our study, we found a suggestive association that one-SD increment in the circulating levels of IL-16 was associated with an 8% increase in PD risk. This could be explained by the following reasons: Similar to MIP1b, elevated IL-16 levels might also promote macrophages to release higher levels of pro-inflammatory cytokines and contribute to BBB breakdown (Persidsky et al., 2006; Huang et al., 2019). Besides, IL-16 could induce the activation of protein kinase C (PKC) and its translocation from cytosol to the membrane (Parada et al., 1996). Later, the PKC might phosphorylate the tight junction proteins of BBB leading to BBB damage (Li et al., 2018). Moreover, IL-16 could potentiate the inflammatory response by stimulating T cells to produce more pro-inflammatory cytokines (Skundric et al., 2015). Altogether, the production of pro-inflammatory cytokines, activation of immune cells, and continuous chronic inflammatory response could lead to PD occurrence.

There were several advantages involved in our study. This was the first MR analysis for clarifying the causality of inflammatory cytokines levels with the risk and age at the onset of PD. Another merit was the two-sample MR method that provided robust causal associations by minimizing confounding factors and avoiding reverse causality. Besides, we used data from publicly available GWASs, which included a large number of patients with PD and controls, thus affording a great power to explore the causal relationship. Finally, except for the IVW method, we also used three supplementary analyses, including MR Egger regression, weighted median, and MR-PRESSO approaches. Directional consistency of the results across multiple MR approaches reinforced the reliability of associations. Nevertheless, the results of this MR analysis should be noted in the context of the following limitations. First, since potential pleiotropy, outlier, and heterogeneity can be detected, the relationship between inflammatory cytokines, including TRAIL, IP10, IL-18, and GROa, and the risk or age at the onset of PD should be interpreted with caution. Second, we used summary data from GWASs of mostly European adults, which limited the generality of the observed causal associations to other populations with different genetic backgrounds. Third, cytokines are not something constitutively expressed in the body. During inflammation, specific inflammatory cytokines are induced to a high level but for only a short period. All of those dynamic changes cannot be addressed by MR analysis. Fourth, we focused on the causal effect of peripheral cytokines levels on the risk or age at the onset of PD and supported that systematic peripheral inflammation and chronic cytokine disturbance may contribute to the development of PD. However, a recent study by Wijeyekoon et al. (2020) suggested that some cytokines in the CSF did not correlate well with blood. Thus, our analysis cannot reveal the potential causal relationship between the levels of inflammatory cytokines in CSF and the risk or age at the onset of PD. Last but not the least, not all inflammatory cytokines were analyzed in our MR analysis due to the exclusion criteria and the limited number of cytokines analyzed in the previous GWAS.

CONCLUSION

In conclusion, this MR analysis showed a causal relationship between circulating levels of MIP1b and PD risk and a suggestive association between IL-16 and PD. Additionally, there was no evidence in support of causality between inflammatory cytokines and age at the onset of PD. Our findings brought new insights into the pathogenesis of PD and indicated that MIP1b and IL-16 could be regarded as novel biomarkers and potential therapeutic targets for PD development.

DATA AVAILABILITY STATEMENT

The original contributions presented in the study are included in the article/**Supplementary Material**, further inquiries can be directed to the corresponding author/s.

AUTHOR CONTRIBUTIONS

XL designed the research. YZ and XZ had full access to all the data in the study and took responsibility for the integrity of the data and the accuracy of the data analysis. YZ and NG wrote the manuscript and performed the data analysis. All authors contributed to the statistical analysis, critically reviewed the manuscript during the writing process, and approved the final version to be published.

FUNDING

This work was supported by the National Natural Science Foundation of China (grant nos. 81400950, 81801053, and 81872044) and the Natural Science Foundation of Liaoning Province (grant no. 2019-MS-365).

SUPPLEMENTARY MATERIAL

The Supplementary Material for this article can be found online at: https://www.frontiersin.org/articles/10.3389/fnagi.2022.811059/full#supplementary-material

Supplementary Figure 1 | Forest plot of the causal effect estimates of MIP1b-associated SNPs on PD risk. Each black dot indicates the causal estimate of MIP1b on PD using an SNP by the Wald ratio method with 95% confidence interval bars. The MR estimate using all SNPs with the IVW method is also shown (red dot with 95% confidence interval bars). PD, Parkinson's disease; SNP, single-nucleotide polymorphism; MR, Mendelian randomization; IVW, inverse-variance weighted.

Supplementary Figure 2 | Leave-one-out analysis of MIP1b-associated SNPs on PD risk. It was conducted to determine whether the causal effect of circulating MIP1b levels on PD risk was disproportionately influenced by a single SNP. The black dot and bars indicate the MR estimate and 95% confidence interval when the specific SNP is removed. The overall MR analysis, including all SNPs, is also presented for comparison (red dot with 95% confidence interval bars). SNP, single-nucleotide polymorphism; PD, Parkinson's disease; MR, Mendelian randomization.

REFERENCES

Ahola-Olli, A. V., Wurtz, P., Havulinna, A. S., Aalto, K., Pitkanen, N., Lehtimaki, T., et al. (2017). Genome-wide association study identifies 27 loci influencing concentrations of circulating cytokines and growth factors. *Am. J. Hum. Genet.* 100, 40–50. doi: 10.1016/j.ajhg.2016.11.007

Al-Obaidi, M. M. J., and Desa, M. N. M. (2018). Mechanisms of blood brain barrier disruption by different types of bacteria, and bacterial-host interactions facilitate the bacterial pathogen invading the brain. *Cell Mol. Neurobiol.* 38, 1349–1368. doi: 10.1007/s10571-018-0609-2

Blauwendraat, C., Heilbron, K., Vallerga, C. L., Bandres-Ciga, S., von Coelln, R., Pihlstrom, L., et al. (2019). Parkinson's disease age at onset genome-wide association study: defining heritability, genetic loci, and alpha-synuclein mechanisms. *Mov. Disord.* 34, 866–875. doi: 10.1002/mds.27659

Bowden, J., Davey Smith, G., and Burgess, S. (2015). Mendelian randomization with invalid instruments: effect estimation and bias detection through egger regression. *Int. J. Epidemiol.* 44, 512–525. doi: 10.1093/ije/dyv080

Bowden, J., Davey Smith, G., Haycock, P. C., and Burgess, S. (2016). Consistent estimation in mendelian randomization with some invalid instruments using a weighted median estimator. *Genet. Epidemiol.* 40, 304–314. doi: 10.1002/gepi.21965

Brockmann, K., Schulte, C., Schneiderhan-Marra, N., Apel, A., Pont-Sunyer, C., Vilas, D., et al. (2017). Inflammatory profile discriminates clinical subtypes in LRRK2-associated Parkinson's disease. *Eur. J. Neurol.* 24, 427–e426. doi: 10.1111/ene.13223

Calvani, R., Picca, A., Landi, G., Marini, F., Biancolillo, A., Coelho-Junior, H. J., et al. (2020). A novel multi-marker discovery approach identifies new serum biomarkers for Parkinson's disease in older people: an EXosomes in PArkiNson Disease (EXPAND) ancillary study. *Geroscience* 42, 1323–1334. doi: 10.1007/s11357-020-00192-2

Cheung, R., Malik, M., Ravyn, V., Tomkowicz, B., Ptasznik, A., and Collman, R. G. (2009). An arrestin-dependent multi-kinase signaling complex mediates MIP-1beta/CCL4 signaling and chemotaxis of primary human macrophages. *J. Leukoc. Biol.* 86, 833–845. doi: 10.1189/jlb.0908551

Collins, L. M., Toulouse, A., Connor, T. J., and Nolan, Y. M. (2012). Contributions of central and systemic inflammation to the pathophysiology of Parkinson's disease. *Neuropharmacology* 62, 2154–2168. doi: 10.1016/j.neuropharm.2012.01.028

Compta, Y., Dias, S. P., Giraldo, D. M., Perez-Soriano, A., Munoz, E., Saura, J., et al. (2019). Cerebrospinal fluid cytokines in multiple system atrophy: a cross-sectional Catalan MSA registry study. *Parkinsonism. Relat. Disord.* 65, 3–12. doi: 10.1016/j.parkreldis.2019.05.040

Cruikshank, W. W., Kornfeld, H., and Center, D. M. (2000). Interleukin-16. *J. Leukoc. Biol.* 67, 757–766.

GBD 2016 Parkinson's Disease Collaborators (2018). Global, regional, and national burden of Parkinson's disease, 1990-2016: a systematic analysis for the Global Burden of Disease Study 2016. *Lancet Neurol.* 17, 939–953. doi: 10.1016/S1474-4422(18)30295-3

Huang, Y., Du, K. L., Guo, P. Y., Zhao, R. M., Wang, B., Zhao, X. L., et al. (2019). IL-16 regulates macrophage polarization as a target gene of mir-145-3p. *Mol. Immunol.* 107, 1–9. doi: 10.1016/j.molimm.2018.12.027

Jankovic, J. (2008). Parkinson's disease: clinical features and diagnosis. *J. Neurol. Neurosurg. Psychiatry* 79, 368–376.

Jo, M., Kim, J. H., Song, G. J., Seo, M., Hwang, E. M., and Suk, K. (2017). Astrocytic Orosomucoid-2 modulates microglial activation and neuroinflammation. *J. Neurosci.* 37, 2878–2894. doi: 10.1523/JNEUROSCI.2534-16.2017

Joshi, N., and Singh, S. (2018). Updates on immunity and inflammation in Parkinson disease pathology. *J. Neurosci. Res.* 96, 379–390. doi: 10.1002/jnr.24185

Kline, E. M., Houser, M. C., Herrick, M. K., Seibler, P., Klein, C., West, A., et al. (2021). Genetic and environmental factors in Parkinson's disease converge on immune function and inflammation. *Mov. Disord.* 36, 25–36. doi: 10.1002/mds.28411

Li, H., Zhu, L., Feng, J., Hu, X., Li, C., and Zhang, B. (2018). Hydrogen sulfide decreases blood-brain barrier damage via regulating protein Kinase C and tight junction after cardiac arrest in rats. *Cell Physiol. Biochem.* 47, 994–1006. doi: 10.1159/000490166

Lindenau, J. D., Altmann, V., Schumacher-Schuh, A. F., Rieder, C. R., and Hutz, M. H. (2017). Tumor necrosis factor alpha polymorphisms are associated with Parkinson's disease age at onset. *Neurosci. Lett.* 658, 133–136. doi: 10.1016/j.neulet.2017.08.049

Lotankar, S., Prabhavalkar, K. S., and Bhatt, L. K. (2017). Biomarkers for Parkinson's disease: recent advancement. *Neurosci. Bull.* 33, 585–597. doi: 10.1007/s12264-017-0183-5

Macleod, A. D., Taylor, K. S., and Counsell, C. E. (2014). Mortality in Parkinson's disease: a systematic review and meta-analysis. *Mov. Disord.* 29, 1615–1622.

Marogianni, C., Sokratous, M., Dardiotis, E., Hadjigeorgiou, G. M., Bogdanos, D., and Xiromerisiou, G. (2020). Neurodegeneration and inflammation-an interesting interplay in Parkinson's disease. *Int. J. Mol. Sci.* 21:8421. doi: 10.3390/ijms21228421

Marras, C., Beck, J. C., Bower, J. H., Roberts, E., Ritz, B., Ross, G. W., et al. (2018). Prevalence of Parkinson's disease across North America. *NPJ Parkinsons Dis.* 4:21. doi: 10.1038/s41531-018-0058-0

Martinez, H. R., Escamilla-Ocanas, C. E., Camara-Lemarroy, C. R., Gonzalez-Garza, M. T., Moreno-Cuevas, J., and Garcia Sarreon, M. A. (2020). Increased cerebrospinal fluid levels of cytokines monocyte chemoattractant protein-1 (MCP-1) and macrophage inflammatory protein-1beta (MIP-1beta) in patients with amyotrophic lateral sclerosis. *Neurologia* 35, 165–169. doi: 10.1016/j.nrl.2017.07.020

Menten, P., Wuyts, A., and Van Damme, J. (2002). Macrophage inflammatory protein-1. *Cytokine Growth Factor Rev.* 13, 455–481.

Morris, G., Fernandes, B. S., Puri, B. K., Walker, A. J., Carvalho, A. F., and Berk, M. (2018). Leaky brain in neurological and psychiatric disorders: drivers and consequences. *Aust. N. Z. J. Psychiatry* 52, 924–948. doi: 10.1177/0004867418796955

Mukaida, N., Sasaki, S. I., and Baba, T. (2020). CCL4 Signaling in the tumor microenvironment. *Adv. Exp. Med. Biol.* 1231, 23–32. doi: 10.1007/978-3-030-36667-4_3

Nalls, M. A., Blauwendraat, C., Vallerga, C. L., Heilbron, K., Bandres-Ciga, S., Chang, D., et al. (2019). Identification of novel risk loci, causal insights, and heritable risk for Parkinson's disease: a meta-analysis of genome-wide association studies. *Lancet Neurol.* 18, 1091–1102. doi: 10.1016/S1474-4422(19)30320-5

Noyce, A. J., Bandres-Ciga, S., Kim, J., Heilbron, K., Kia, D., Hemani, G., et al. (2019). The Parkinson's disease mendelian randomization research portal. *Mov. Disord.* 34, 1864–1872. doi: 10.1002/mds.27873

Pajares, M., Rojo, A. I., Manda, G., Bosca, L., and Cuadrado, A. (2020). Inflammation in Parkinson's disease: mechanisms and therapeutic implications. *Cells* 9:1687. doi: 10.3390/cells9071687

Parada, N. A., Cruikshank, W. W., Danis, H. L., Ryan, T. C., and Center, D. M. (1996). IL-16- and other CD4 ligand-induced migration is dependent upon protein kinase C. *Cell Immunol.* 168, 100–106. doi: 10.1006/cimm.1996.0054

Persidsky, Y., Ramirez, S. H., Haorah, J., and Kanmogne, G. D. (2006). Blood-brain barrier: structural components and function under physiologic and pathologic conditions. *J. Neuroimmune Pharmacol.* 1, 223–236. doi: 10.1007/s11481-006-9025-3

Pochmann, D., Peccin, P. K., da Silva, I. R. V., Dorneles, G. P., Peres, A., Nique, S., et al. (2018). Cytokine modulation in response to acute and chronic aquatic therapy intervention in Parkinson disease individuals: a pilot study. *Neurosci. Lett.* 674, 30–35. doi: 10.1016/j.neulet.2018.03.021

Qin, L., Wu, X., Block, M. L., Liu, Y., Breese, G. R., Hong, J. S., et al. (2007). Systemic LPS causes chronic neuroinflammation and progressive neurodegeneration. *Glia* 55, 453–462. doi: 10.1002/glia.20467

Qin, X. Y., Zhang, S. P., Cao, C., Loh, Y. P., and Cheng, Y. (2016). Aberrations in peripheral inflammatory cytokine levels in parkinson disease: a systematic review and meta-analysis. *JAMA Neurol.* 73, 1316–1324. doi: 10.1001/jamaneurol.2016.2742

Saika, F., Kiguchi, N., Kobayashi, Y., Fukazawa, Y., and Kishioka, S. (2012). CC-chemokine ligand 4/macrophage inflammatory protein-1beta participates in the induction of neuropathic pain after peripheral nerve injury. *Eur. J. Pain* 16, 1271–1280. doi: 10.1002/j.1532-2149.2012.00146.x

Schapira, A. H., and Jenner, P. (2011). Etiology and pathogenesis of Parkinson's disease. *Mov. Disord.* 26, 1049–1055.

Shapouri-Moghaddam, A., Mohammadian, S., Vazini, H., Taghadosi, M., Esmaeili, S. A., Mardani, F., et al. (2018). Macrophage plasticity, polarization, and function in health and disease. *J. Cell. Physiol.* 233, 6425–6440. doi: 10.1002/jcp.26429

Shukaliak, J. A., and Dorovini-Zis, K. (2000). Expression of the beta-chemokines RANTES and MIP-1 beta by human brain microvessel endothelial cells in primary culture. *J. Neuropathol. Exp. Neurol.* 59, 339–352. doi: 10.1093/jnen/59.5.339

Skundric, D. S., Cruikshank, W. W., Montgomery, P. C., Lisak, R. P., and Tse, H. Y. (2015). Emerging role of IL-16 in cytokine-mediated regulation of multiple sclerosis. *Cytokine* 75, 234–248. doi: 10.1016/j.cyto.2015.01.005

Verbanck, M., Chen, C. Y., Neale, B., and Do, R. (2018). Publisher Correction: Detection of widespread horizontal pleiotropy in causal relationships inferred from Mendelian randomization between complex traits and diseases. *Nat. Genet.* 50:1196. doi: 10.1038/s41588-018-0164-2

Villaran, R. F., Espinosa-Oliva, A. M., Sarmiento, M., De Pablos, R. M., Arguelles, S., Delgado-Cortes, M. J., et al. (2010). Ulcerative colitis exacerbates lipopolysaccharide-induced damage to the nigral dopaminergic system: potential risk factor in Parkinson's disease. *J. Neurochem.* 114, 1687–1700. doi: 10.1111/j.1471-4159.2010.06879.x

Wahner, A. D., Sinsheimer, J. S., Bronstein, J. M., and Ritz, B. (2007). Inflammatory cytokine gene polymorphisms and increased risk of Parkinson disease. *Arch. Neurol.* 64, 836–840. doi: 10.1001/archneur.64.6.836

Wang, Y., Zhou, M., Wang, Y., Jiang, D., and Deng, X. (2019). Association of polymorphisms in the MCP-1 and CCR2 genes with the risk of Parkinson's disease. *J. Neural. Transm.* 126, 1465–1470. doi: 10.1007/s00702-019-02072-2

Wijeyekoon, R. S., Moore, S. F., Farrell, K., Breen, D. P., Barker, R. A., and Williams-Gray, C. H. (2020). Cerebrospinal fluid cytokines and neurodegeneration-associated proteins in Parkinson's disease. *Mov. Disord.* 35, 1062–1066. doi: 10.1002/mds.28015

Yang, W., Hamilton, J. L., Kopil, C., Beck, J. C., Tanner, C. M., Albin, R. L., et al. (2020). Current and projected future economic burden of Parkinson's disease in the U.S. *NPJ Parkinsons Dis.* 6:15. doi: 10.1038/s41531-020-0117-1

Zhu, M., Allard, J. S., Zhang, Y., Perez, E., Spangler, E. L., and Becker, K. G. (2014). Age-related brain expression and regulation of the chemokine CCL4/MIP-1beta in APP/PS1 double-transgenic mice. *J. Neuropathol. Exp. Neurol.* 73, 362–374. doi: 10.1097/NEN.0000000000000060

Conflict of Interest: The authors declare that the research was conducted in the absence of any commercial or financial relationships that could be construed as a potential conflict of interest.

Publisher's Note: All claims expressed in this article are solely those of the authors and do not necessarily represent those of their affiliated organizations, or those of the publisher, the editors and the reviewers. Any product that may be evaluated in this article, or claim that may be made by its manufacturer, is not guaranteed or endorsed by the publisher.

frontiers in Molecular Neuroscience

ORIGINAL RESEARCH
published: 02 March 2022
doi: 10.3389/fnmol.2022.762544

Blood SSR1: A Possible Biomarker for Early Prediction of Parkinson's Disease

Wen Zhang[1†], Jiabing Shen[1†], Yuhui Wang[2], Kefu Cai[1], Qi Zhang[3] and Maohong Cao[1]**

[1]Department of Neurology, Affiliated Hospital of Nantong University, Nantong, China, [2]Department of Microelectrics, Peking University, Peking, China, [3]Key Laboratory of Neuroregeneration of Jiangsu and Ministry of Education, Co-innovation Center of Neuroregeneration, Nantong University, Nantong, China

Parkinson's disease (PD) is the second most common neurodegenerative disease associated with age. Early diagnosis of PD is key to preventing the loss of dopamine neurons. Peripheral-blood biomarkers have shown their value in recent years because of their easy access and long-term monitoring advantages. However, few peripheral-blood biomarkers have proven useful. This study aims to explore potential peripheral-blood biomarkers for the early diagnosis of PD. Three substantia nigra (SN) transcriptome datasets from the Gene Expression Omnibus (GEO) database were divided into a training cohort and a test cohort. We constructed a protein–protein interaction (PPI) network and a weighted gene co-expression network analysis (WGCNA) network, found their overlapping differentially expressed genes and studied them as the key genes. Analysis of the peripheral-blood transcriptome datasets of PD patients from GEO showed that three key genes were upregulated in PD over healthy participants. Analysis of the relationship between their expression and survival and analysis of their brain expression suggested that these key genes could become biomarkers. Then, animal models were studied to validate the expression of the key genes, and only SSR1 (the signal sequence receptor subunit1) was significantly upregulated in both animal models in peripheral blood. Correlation analysis and logistic regression analysis were used to analyze the correlation between brain dopaminergic neurons and SSR1 expression, and it was found that SSR1 expression was negatively correlated with dopaminergic neuron survival. The upregulation of SSR1 expression in peripheral blood was also found to precede the abnormal behavior of animals. In addition, the application of artificial intelligence technology further showed the value of SSR1 in clinical PD prediction. The three classifiers all showed that SSR1 had high predictability for PD. The classifier with the best prediction accuracy was selected through AUC and MCC to construct a prediction model. In short, this research not only provides potential biomarkers for the early diagnosis of PD but also establishes a possible artificial intelligence model for predicting PD.

Keywords: Parkinson's disease, SSR1, biomarker, early diagnosis, artificial intelligence, machine learning

OPEN ACCESS

Edited by:
Nicholas James Ashton, University of Gothenburg, Sweden

Reviewed by:
Juan Atilio Gerez, ETH Zürich, Switzerland
Meera Srikrishna, University of Gothenburg, Sweden

****Correspondence:***
Maohong Cao
Cmhongnt@sina.com
Qi Zhang
zhangqi@ntu.edu.cn

[†]These authors have contributed equally to this work

Specialty section:
This article was submitted to Brain Disease Mechanisms, a section of the journal Frontiers in Molecular Neuroscience

Received: *22 August 2021*
Accepted: *14 January 2022*
Published: *02 March 2022*

Citation:
Zhang W, Shen J, Wang Y, Cai K, Zhang Q, and Cao M (2022) Blood SSR1: A Possible Biomarker for Early Prediction of Parkinson's Disease. Front. Mol. Neurosci. 15:762544. doi: 10.3389/fnmol.2022.762544

INTRODUCTION

Parkinson's disease (PD) is a neurodegenerative disease principally defined by the motor symptoms of resting tremor, rigidity, and bradykinesia. These symptoms occur mainly because of the progressive loss of dopaminergic neurons in the substantia nigra pars compacta (SN; Damier et al., 1999; Kalia and Lang, 2015). However, the mechanism behind this neuronal loss remains largely unclear (Dauer and Przedborski, 2003). There is no cure for PD. The mainstay of its management is symptomatic treatment with drugs that increase dopamine concentrations or directly stimulate dopamine receptors (Kalia and Lang, 2015). Clinical diagnosis of PD is based on the presence of Parkinsonian motor features, but a significant proportion of nigral neurons are lost before the onset of motor symptoms (Lang and Lozano, 1998), meaning that clinical diagnosis is likely to occur too late for the administration of disease-modifying therapies. Therefore, in the management of PD, it is urgent to find reliable diagnostic and prognostic biomarkers of PD to prevent the loss of dopaminergic neurons at an early stage (Parnetti et al., 2019).

The latest biomarkers mainly detect α-synuclein (Visanji et al., 2014) and neuroimaging modalities (Brooks and Pavese, 2011). Cerebrospinal fluid (CSF) is close to the central nervous system, making it an ideal source of diagnostic markers for ongoing pathological processes. CSF α-synuclein appears to be reasonably sensitive and specific for PD (Hong et al., 2010; Mollenhauer et al., 2011). Total α-synuclein levels have been significantly decreased in PD patients compared with controls (Mollenhauer et al., 2011, 2013). However, obtaining CSF is difficult, and repeated lumbar puncture is not conducive to long-term monitoring. The detection of α-synuclein in plasma and serum remains controversial; some researchers found that it was unaffected in PD patients (Smith et al., 2012), while another study found that it was lower in them than controls (Besong-Agbo et al., 2013). Dopamine transporter imaging and magnetic resonance imaging of the SN are sensitive and specific tools for PD (Benamer et al., 2000; Kagi et al., 2010; Lehericy et al., 2012). Although these techniques are very sensitive, they are expensive and involve radiation exposure, and it is not known how useful they are for the early detection of atypical PD (Frosini et al., 2017). As blood is easier, cheaper, and less invasive to obtain than cerebrospinal fluid (Thambisetty and Lovestone, 2010), people have focused on biomarkers in blood (Chahine et al., 2014; Lin et al., 2019; Grossi et al., 2021), especially for longitudinal evaluation. Uric acid, miR-124, and other molecules can be used as biomarkers for the diagnosis of PD in peripheral blood (Angelopoulou et al., 2019; Lawton et al., 2020). However, a single biochemical marker is unlikely to be sufficient for the early diagnosis of PD, while a combination of them may be useful. Therefore, there is a need to find more PD biomarkers in peripheral blood, and the development of reliable and accurate peripheral-blood biomarkers will greatly promote the early detection of PD and the identification of its biological characteristics.

Massively parallel microarray analysis can reliably assess the relationships between gene expression and clinical manifestations on a global scale and reveal the etiology of complex diseases by identifying abnormalities in genes or pathways (Schadt et al., 2005). Weighted gene co-expression network analysis (WGCNA) and protein–protein interaction networks (PPI) were constructed here to identify hub genes underlying PD. Longitudinal studies over time are a common method for studying degenerative diseases. We established a time axis to explore the dynamic changes in hub gene expression in a PD model and their potential as biomarkers in the early stage of the model. Finally, machine learning is a key method of modern medical research, and it is often used to diagnose diseases or to screen biomarkers of them (Deo, 2015). In this study, we used random forest (RF), K-nearest neighbor (KNN) and support vector machine (SVM) to establish a PD prediction model (Zhang, 2016; Kriegeskorte and Golan, 2019). A previous study combined KNN with a genetic algorithm to achieve high classification accuracy (Zhang et al., 2018). Here, after comparing the AUC and MCC of three classifiers, an SVM was selected to build an artificial intelligence prediction model of PD in the early stage.

MATERIALS AND METHODS

Gene Expression Data and Subsequent Processing Based on GEO Databases

The Gene Expression Omnibus (GEO[1]) is a public functional genomics data repository of high-throughput gene expression data, chips, and microarrays. As shown in the flow chart (**Figure 1**), we searched GEO with the following keywords: "(Parkinson's disease) and (substantia nigra striatum)", which yielded many datasets (Edgar et al., 2002). Four gene expression datasets [GSE28894, GSE20141, GSE20295, and GSE20292] were chosen and downloaded from GEO. The GSE28894 dataset contained 60 PD samples and 86 normal samples. GSE20141 contained 10 PD samples and eight normal samples. GSE20295 contained 40 PD samples and 53 normal samples. First, GSE20141 was chosen to run WGCNA to identify candidate hub genes. Second, GSE28894, GSE20141, and GSE20295 were used to construct a PPI network. GSE20292 was used to do external verification (**Supplementary Figure 2**). Then we searched for the keywords "(Parkinson's disease) and (whole blood) and (early stage)" and obtained three datasets: GSE6613 GSE72267, and GSE99039. We performed whole blood verification of the hub genes in all the three datasets. GSE6613 was used to calculate the area under the receiver operating characteristic curve (AUC) of SSR1 and to build our machine learning model. We finally retrieved the datasets GSE85426, GSE51759, GSE89093, GSE138118, and GSE167914 for Alzheimer's disease (AD), Huntington's disease (HD), endometrial carcinoma, bladder cancer, and thyroid carcinoma, respectively, which were used to calculate the specificity of SSR1 to PD. Detailed of all data sets can be seen in **Table 1**.

[1]http://www.ncbi.nlm.nih.gov/geo

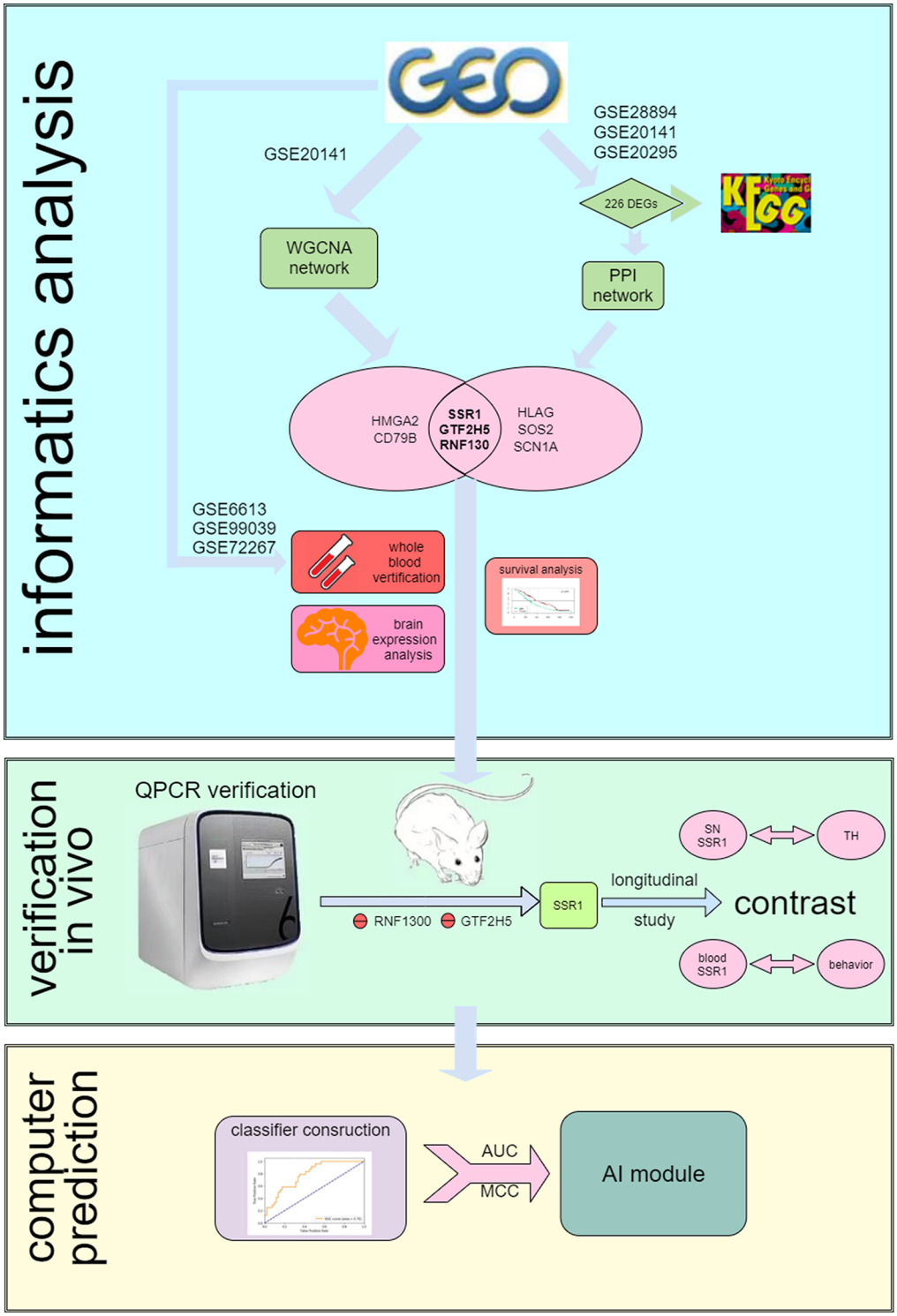

FIGURE 1 | Flow chart of the analysis process.

WGCNA

In WGCNA, the correlation between modules and clinical subtypes is calculated according to the feature vector of each network module. Module eigengenes actually formulate the expression patterns of all genes within a given module into a single characteristic expression profile. Module eigengenes can be regarded as the first principal component of the gene module. The correlation between each gene in these modules

TABLE 1 | The information of Gene Expression Omnibus (GEO) datasets.

GEO datasets	Tissue	Disease	Application
GSE20141	SN	Parkinson's disease	WGCNA analysis, PPI network
GSE28894	SN	Parkinson's disease	PPI network
GSE20295	SN	Parkinson's disease	PPI network
GSE6613	Whole blood	Parkinson's disease	External verification machine learning
GSE72267	Whole blood	Parkinson's disease	External verification
GSE99039	Whole blood	Parkinson's disease	External verification
GSE85426	Whole blood	Alzheimer's disease	machine learning (specificity of SSR1 to PD)
GSE51759	Whole blood	Huntington's Disease	machine learning (specificity of SSR1 to PD)
GSE89093	Whole blood	Endometrial Carcinoma	machine learning (specificity of SSR1 to PD)
GSE138118	Whole blood	Bladder Cancer	machine learning (specificity of SSR1 to PD)
GSE167914	Whole blood	Thyroid Carcinoma	machine learning (specificity of SSR1 to PD)

was quantified by the gene significance (GS) value. Accordingly, the module significance (MS) of a certain module is defined as the averaged GS values of all genes included in it. Modules are ranked according to the MS score, and the top five modules are considered key modules relevant to clinical outcomes for further analysis. Hub genes in the co-expression network are a class of genes that have high connectivity within a network module and are significantly correlated with biological function (Chen et al., 2017). In this study, we measured the absolute value of the gene significance (GS) score, which represents the correlation between the genes in these modules and each phenotype (Yang et al., 2018). We screened candidate genes using the cutoff criteria $|MM| \geq 0.8$ and $|GS| \geq 0.5$ because such genes are biologically meaningful. $|MM| \geq 0.8$ indicates that the gene is strongly related to the module, and $|GS| \geq 0.5$ requires that the gene expression profile be closely related to each module.

PPI Network Construction and Module Analysis

The differentially expressed genes (DEGs) between PD and normal samples were screened using GEO2R[2]). GEO2R is an interactive web tool that allows users to compare two or more datasets in a GEO series to identify DEGs across experimental conditions (Edgar et al., 2002). The adjusted *P*-values ($P_{adj.}$) and Benjamini and Hochberg false discovery rates were applied to provide a balance between the discovery of statistically significant genes and the limitation of false positives. An absolute value of the logarithm of the fold change (logFC) >1 and $P_{adj.} < 0.01$ were considered statistically significant.

The PPI network was predicted using the Search Tool for the Retrieval of Interacting Genes (STRING[3]) online database. Analyzing the functional interactions between proteins may provide insights into the mechanisms of the generation or development of diseases. The PPI network of DEGs was constructed using the STRING database, and an interaction with a combined score >0.4 was considered statistically significant. Cytoscape is an open source bioinformatics software platform for visualizing molecular interaction networks. The plug-in Molecular Complex Detection (MCODE) of Cytoscape is an app for clustering a given network based on its topology to find densely connected regions. The PPI networks were drawn using Cytoscape, and the most significant module in the PPI networks was identified using MCODE. The criteria for selection were as follows: MCODE scores >5, degree cutoff = 2, node score cutoff = 0.2, max depth = 100 and *k*-score = 2. The hub genes in the PPI network were those with degree ≥10.

Functional Analysis of Hub Genes and Enrichment Analysis of DEGs

The overall survival and disease-free survival analyses of hub genes were performed using Kaplan-Meier curves in cBioPortal[4]. The expression levels of six hub genes in the brain were determined from the NCBI database. The Database for Annotation, Visualization, and Integrated Discovery (DAVID[5]) is an online biological information database that integrates biological data and analysis tools and provides a comprehensive set of functional annotation information on genes and proteins for users to extract biological information. The Kyoto Encyclopedia of Genes and Genomes (KEGG) is a database resource for understanding high-level functions and biological systems from large-scale molecular datasets generated by high-throughput experimental technologies. Gene Ontology (GO) is a major bioinformatics tool to annotate genes and analyze the biological processes of these genes. To analyze the functions of DEGs, biological analyses were performed using the DAVID online database. $P < 0.01$ was considered statistically significant.

Classifier Construction and Machine Learning

Three ML algorithms, SVM (De Martino et al., 2008), kNN (Cover and Hart, 1967), and RF (Ho, 1998) were built both to verify if SSR1 can distinguish PD patients well and to determine which best classifies SSR1 in PD datasets. The RF method is a commonly-used classification method containing a number of decision trees. A final classification label was determined based on the class with the most votes from all trees. RF is easily parallelizable and can be enhanced with boosting or bagging. kNN performs classification by assigning a point to the class that

[2]https://www.ncbi.nlm.nih.gov/geo/geo2r/
[3]http://string-db.org
[4]http://www.cbioportal.org/
[5]http://david.ncifcrf.gov

is most prevalent out of the k points closest to it. At the same time, kNN is simple to implement and can utilize Multi-task learning. SVM maps each data item into an n-dimensional feature space where n is the number of features. It then identifies the hyperplane that separates the data items into two classes while maximizing the marginal distance for both classes and minimizing the classification errors. It is important to note that each technique has its own advantages and disadvantages. We hope to use different algorithms for verification with complementary advantages to more comprehensively verify the feasibility of SSR1 as a biomarker.

All models were learned from the same training data generated by selecting 80% of the data, and the remaining 20% were used as validation data to measure and compare the performance of the model. Each algorithm was also tested with combinations of parameters; finally, we found that $c = 2$ for the SVM, $k = 4$ for the kNN, 60 trees for RF produced the best results. To evaluate the overall performance of each model, a 10-fold cross validation was performed. Of the 10 divided sets from the data, the process by which the learned model predicts the remaining one set was repeated 10 times, and eventually, all data were used for validation. All ML algorithms were implemented in the python package *sklearn*.

Performance Evaluation

In order to find out the best classifier for further study, the performance of data validation was calculated according to the area under the curve (AUC) from 0.5 to 1 and the Matthews Correlation Coefficient (MCC) from −1 to 1, a parameter able to reflect classifier effectiveness (Chicco and Jurman, 2020).

$$MCC = \frac{TP \times TN - FP \times FN}{\sqrt{(TP + FP)(TP + FN)(TN + FP)(TN + FN)}}$$

TP is the number of samples correctly predicted as PD in PD samples, FN is the number of samples incorrectly predicted as NORMAL in PD samples, FP is the number of samples incorrectly predicted as PD in normal samples, and TN is the number of samples correctly predicted as NORMAL in normal samples. MCC ranges from −1 to 1, with a completely wrong classification at −1 and perfect classification at 1.

MCC of classification is defined as:

$$MCC = \frac{c \times s - \sum_k^K p_k \times t_k}{\sqrt{(S^2 - \sum_k^K P_k^2) \times (S^2 - \sum_k^K t_k^2)}}$$

s is the total number of samples, c is the total number of correctly predicted samples, $t_k = \sum_i^K C_{ik}$ is the number of all samples in class k, and $p_k = \sum_i^K C_{ki}$ and is the number of correctly predicted samples in class k. MCC of pan-cancer classification for perfect prediction is 1, but the minimum is somewhere between −1 and 0, depending on the number and distribution of the actual labels (Kim et al., 2020). Eventually, the classifier with the greatest AUC and MCC value was identified as the optimal PD classifier.

Animal Experiments

All experimental protocols were performed following the guidelines on animal research provided by the institutional ethics committee at Nantong University and were approved by the committee.

6-OHDA Lesion: Adult C57BL/6J male mice (25–30 g) were maintained under a 12-h light/12-h dark cycle in cages and acclimated to the experimental environment for 1 week before modeling. The mice received a unilateral intrastriatal injection of 6-OHDA (Sigma-Aldrich, St. Louis, MO, USA). The animals were pretreated with desipramine (Sigma-Aldrich, St. Louis, MO, USA). A total dose of 12 μg of 6-OHDA dissolved in 3 μl PBS (16 μmol/ml) was infused into the right striatum at the following coordinates: anterior-posterior (AP), +0.09 cm; medial-lateral (ML), +0.22 cm; dorsal-ventral (DV), −0.25 cm relative to the bregma.

MPTP model: In the same mice, MPTP (Sigma-Aldrich, St. Louis, MO, USA) was intraperitoneally injected four times at an individual dose of 12 mg/kg dissolved in 200 μl PBS with a 2-h interval between the injections. Te control animals received saline only.

Behavioral Testing: All the tests were performed 0 d, 1 d, 3 d, 5 d, 7 d, 14 d, and 28 d after 6-OHDA injection in comparison with the normal group. **In the pole test**, the mice were placed head-upward on top of a rough-surfaced iron pole (50 cm in length and 1.0 cm in diameter) and could climb down to the base of the pole. The time that it took for each mouse to turn completely downward and then reach the floor was measured, with a cutoff of 120 s. The average of three measurements was taken as the result. **In apomorphine-induced rotation**, the mice were allowed to habituate for 10 min in a white 30 × 30-cm chamber. After an intraperitoneal injection of 0.5 mg/kg apomorphine hydrochloride (Sigma-Aldrich, St. Louis, MO, USA), the full rotations in the chamber were recorded with a video camera for 30 min and counted by a blinded examiner.

Tissue Preparation: Perfusion was performed with a cold saline solution, and fixation was then performed with 4% paraformaldehyde in 0.1 M phosphate buffer. Each brain was dissected, postfixed overnight in buffered 4% paraformaldehyde at 4°C and stored in a 30% sucrose solution at 4°C until it sank. Frozen sectioning was performed on a freezing microtome (Leica, CM3050S) to generate 20-μm-thick coronal sections.

Mouse Plasma Extraction: The researcher grabbed the scruff of the mouse with the left thumb, index finger, and middle finger, and the little finger and ring finger fixed the tail. The skin of the eye that needed to be removed was lightly pressed to make the eyeball become congested and prominent. Surgical scissors were used to cut off the beard of the mouse to prevent blood from leaving the beard and causing hemolysis. The eyeball was grasped with tweezers and quickly removed, and the blood flowed from the eye socket into an Eppendorf tube, which was supplemented with a 1:9 ratio of the anticoagulant. The supernatant obtained after centrifugation at 3,000 rpm for 5–10 min was plasma.

Immunohistochemistry

The prepared tissue sections were washed with PBS, permeabilized with 0.25% Triton X-100 for 10 min at RT, and treated with 10% goat serum blocking buffer for 2 h at RT. Tissue sections were costained with primary antibody against

tyrosine hydroxylase (TH; 1:300, Abcam, UK) as a marker for dopaminergic neurons overnight at 4°C. After washing, indirect fluorescence by incubating sections at room temperature in the dark for 1 h with goat anti-rabbit IgG conjugated with Alexa Fluor 568 (1:1,000, Life Technologies). The coverslips were then washed with PBST and treated with an antifade mounting medium with Hoechst 33342. Images were obtained under a microscope (Zeiss LSM700, Carl Zeiss Microimaging GmbH, Jena, Germany). All photographs were taken using the same exposure time. For immunocytochemistry, six to nine fields (two to three fields × three independent samples) were selected randomly from each group, and for immunohistochemistry, three sections from each animal (three mice) were randomly selected.

Western Blotting Analysis

The brain tissue was homogenized in RIPA lysis buffer (EpiZyme, China), protease inhibitor cocktail (MCE, USA), and phosphatase inhibitor cocktail I (MCE, USA) and then centrifuged at 1,600× *g* at 4°C for 20 min. The supernatant was collected, and the protein concentration was determined using a BCA Protein Assay Kit (Beyotime, China). An aliquot of the supernatant was diluted in SDS-PAGE Sample Loading Buffer 28 (Beyotime, China), and the proteins were separated in Omni-PAGE^{TM} HEPES-Tris Gels (EpiZyme, China) and transferred to a polyvinylidene difluoride membrane (Millipore, USA). The membrane was blocked for 1 h at RT in blocking buffer comprising TBS with 5% Difco^{TM} skim milk (Becton, Dickinson and 606 Company, USA) and 0.1% Tween 20. It was then incubated with the following primary antibodies overnight at 4°C: rabbit anti-GAPDH (Abcam, UK), and rabbit anti-TH (Abcam, UK). The membrane was washed in TBST and incubated with goat anti-rabbit IgG (H + L) and cross-adsorbed secondary antibody (conjugated to horseradish peroxidase; Thermo Fisher, USA) for 1 h at RT. The membrane was then washed three times in TBST for 5 min. The antigen–antibody peroxidase complex was detected using High-sig ECL Western Blotting Substrate (Tanon^{TM}, China) according to the manufacturer's instructions, and images were obtained using the Tanon^{TM} 5200CE Chemi-Image System. The intensity of each band was determined with ImageJ Fiji 1.53c.

RNA Extraction and Quantitative Real-Time PCR

Total RNA of the SN was extracted using TRIzol reagent (Tiangen, Beijing, China). The total RNA of plasma was extracted using an EZ-press Serum/Plasma RNA Purification Kit (EZBioscience, Beijing, China). The RNA of 3 mice was filtered through a filter column. Reverse transcription of the RNA into cDNA and quantitative polymerase chain reaction (qPCR) were performed according to the instructions of the PrimeScript RT Reagent Kit with gDNA Eraser (Takara, Dalian, China) and TB Green Premix Ex *Taq* II (Takara). Relative expression levels were obtained by normalizing glyceraldehyde phosphate dehydrogenase (GAPDH). Each reaction was performed in triplicate. The relative mRNA expression level was calculated by the comparative $2^{-\Delta\Delta Ct}$ method.

Statistical Analysis

All data are presented as the means ± SEM and were analyzed using GraphPad Prism 8.0. The difference between two groups was analyzed by a two-tailed Student's *t*-test, and one-way ANOVA followed by Tukey's *post hoc* analysis was used for multiple comparisons among two or more groups. Significant difference among groups was assessed as ns $p > 0.05$, $^{*}p < 0.05$, $^{**}p < 0.01$, and $^{***}p < 0.001$.

RESULTS

Determination of Hub Modules and Genes in WGCNA

The expression profiles of several modules are included in **Figure 2E**, and each gene was classified into different modules (**Figure 2A**). We processed the gene expression profiles using variance analysis on the GSE20141 dataset, which included the most genes. The top five gene modules were used to select the hub gene module. To ensure that the network was a scale-free network, we ran an empirical analysis to choose an optimal parameter β. Both the scale-free topology model fit index and mean connectivity reached the steady state when β was equal to 4 (**Figures 2B,C**). A total of five gene modules were identified *via* average link age hierarchical clustering, and each module is represented in different colors. We drew a heat map to explore the correlations between module eigengenes and clinical traits (**Figure 2D**). Each column in **Figure 2D** displays the correlation and corresponding *p*-value: the darker the color, the stronger the correlation coefficient. We found that five module eigengenes had the highest correlations. Scatter plots of the degree and *P*-value of Cox regression in the five modules are shown in the **Supplementary Figure**. Accordingly, we selected the genes that had cutoff criteria $|MM| \geq 0.8$ and $|GS| \geq 0.5$, which are SSR1, RNF130, GTF2H5, HMGA2, and CD79B. WGCNA can reflect the continuity of potential co-expression information and avoid information loss by setting artificial threshold parameters (Langfelder and Horvath, 2008). However, WGCNA only focuses on a single dataset, so it lacks universality. To make up for this, we also performed a PPI network analysis.

PPI Network Analysis and Hub Gene Selection

After standardization of the microarray results, DEGs were identified. The overlap between the three datasets contained 226 genes, as shown in the Venn diagram (**Figure 3B**), consisting of 154 downregulated genes and 72 upregulated genes in PD patients vs. healthy controls. We performed KEGG and GO analysis on the 226 genes and listed the top eight pathways in both analyses (**Figure 4**). GO function annotation results displayed that changes at the biological process (BP) were observably focused in dendrite morphogenesis, dendrite development, negative regulation of catabolic process, neuron projection organization, axonogenesis, and negative regulation of protein catabolic process (**Figure 4A**). Changes of DEGs significantly in cell component (CC) were mostly in transport vesicle, transport vesicle membrane, membrane raft, membrane

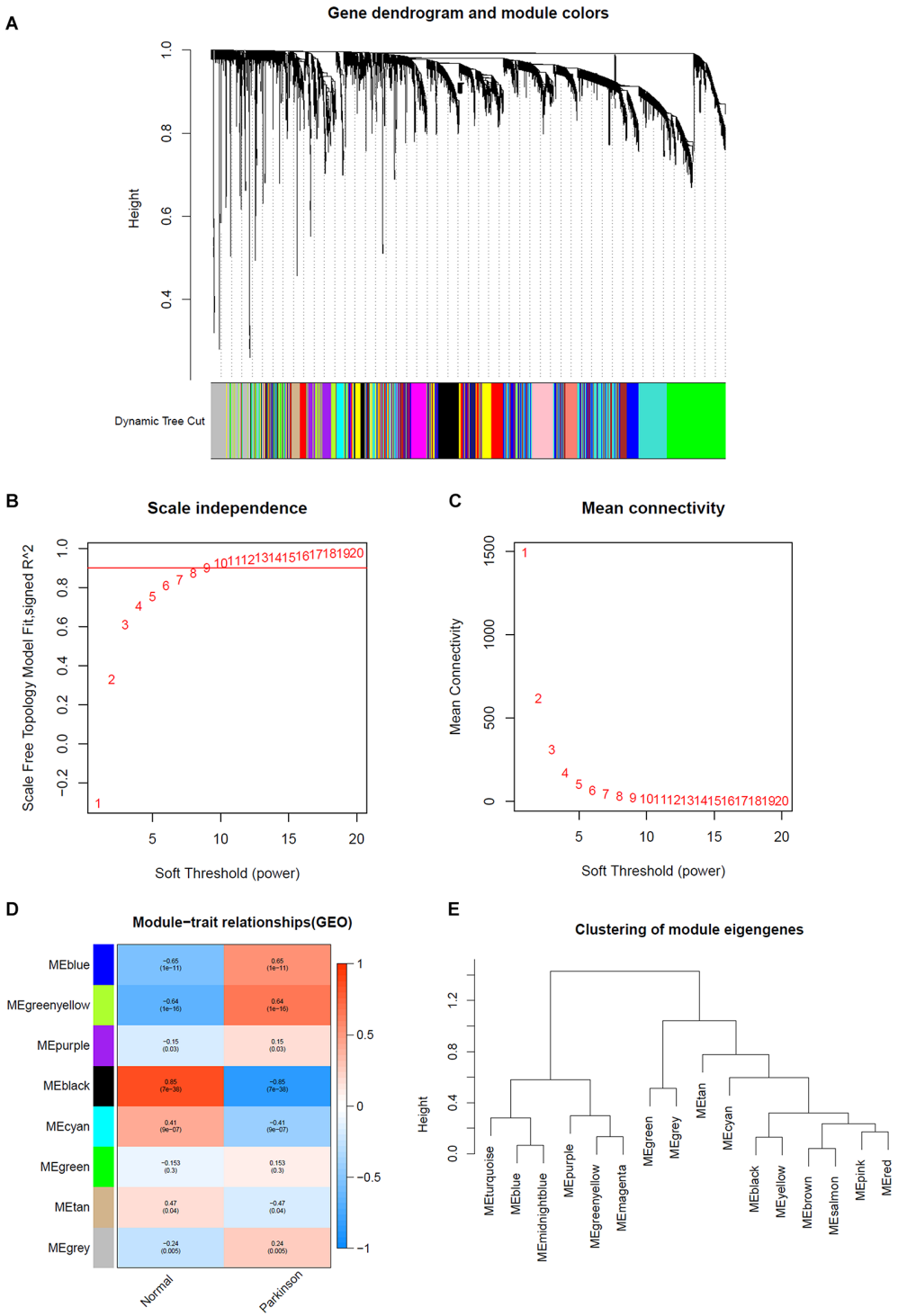

FIGURE 2 | Determination of soft-thresholding power in WGCNA analysis. **(A)** Dendrogram of all differentially expressed genes clustered based on a dissimilarity measure. **(B)** Analysis of the scale-free fit index for various soft-thresholding powers β. **(C)** Analysis of the mean connectivity for various soft thresholding powers. **(D)** Heatmap of the correlation between module eigengenes and clinical traits of Parkinson. **(E)** Clustering of module eigengenes.

microdomain, synaptic vesicle, and membrane region. The most enriched molecular function (MF) annotations were hormone receptor binding, dystroglycan binding, vinculin binding, ATPase regulator activity, nuclear hormone receptor binding, and protein transmembrane transporter activity. In addition, the results of the KEGG pathway analysis in the bubble chart revealed that DEGs were remarkably concentrated in the Viral myocarditis, Adherens junction, Arrhythmogenic right

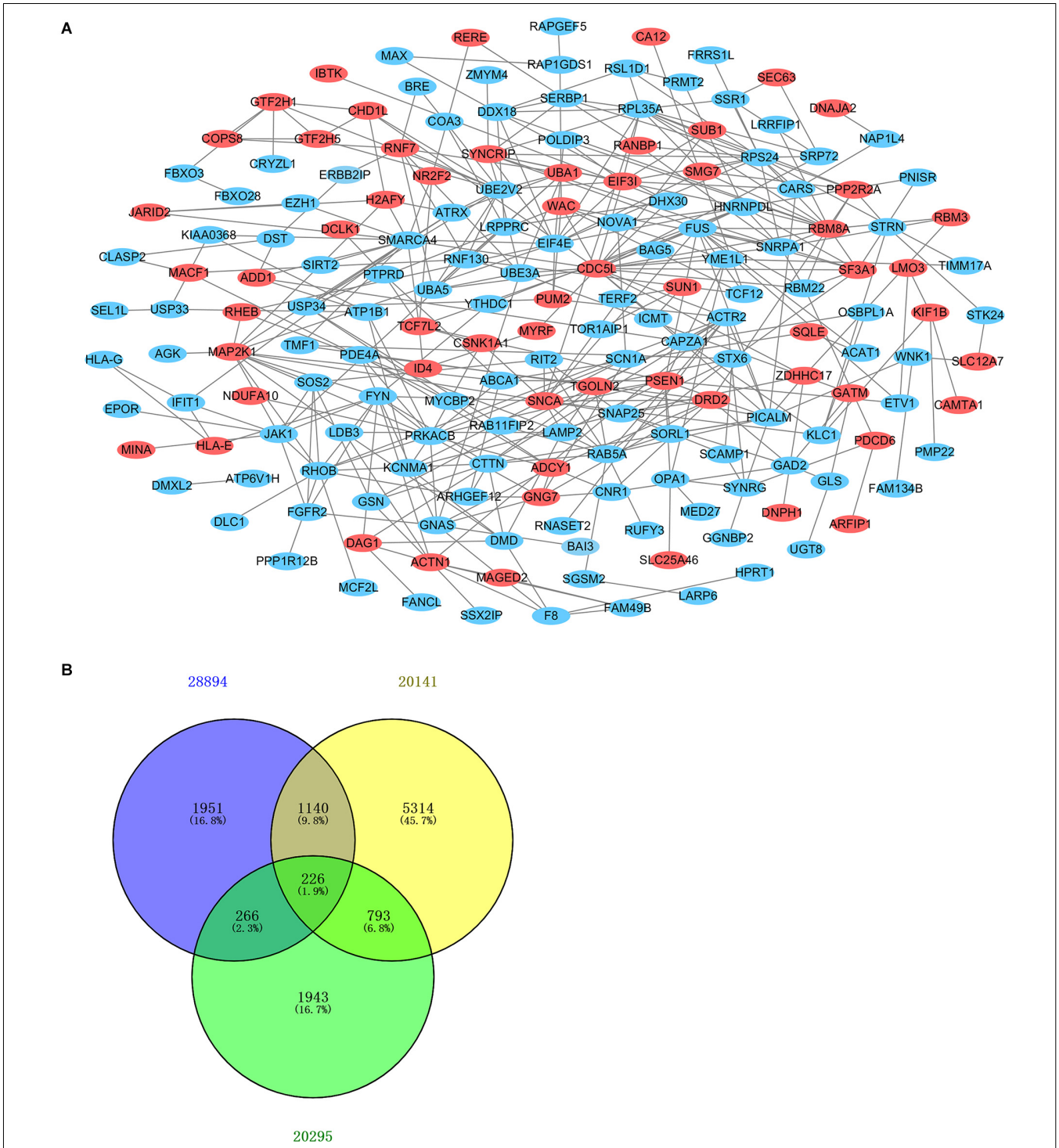

FIGURE 3 | Venn diagram and PPI network. **(A)** The PPI network of DEGs was constructed using Cytoscape. Upregulated genes are marked in light red; downregulated genes are marked in light blue. **(B)** DEGs were selected with the absolute value of fold change >1 and *P*-value <0.01 among the mRNA expression profiling sets GSE28894, GSE20141, and GSE20295. The three datasets showed an overlap of 226 genes.

ventricular cardiomyopathy (ARVC), Vasopressin-regulated water reabsorption, Vascular smooth muscle contraction, and protein processing in the endoplasmic reticulum (**Figure 4B**). The pathways of hub genes were further investigated to determine the mechanism by which hub genes can act as biomarkers of PD. The PPI network of DEGs was constructed, and the most significant module was obtained using Cytoscape (**Figure 3A**). The results showed that the network contained six

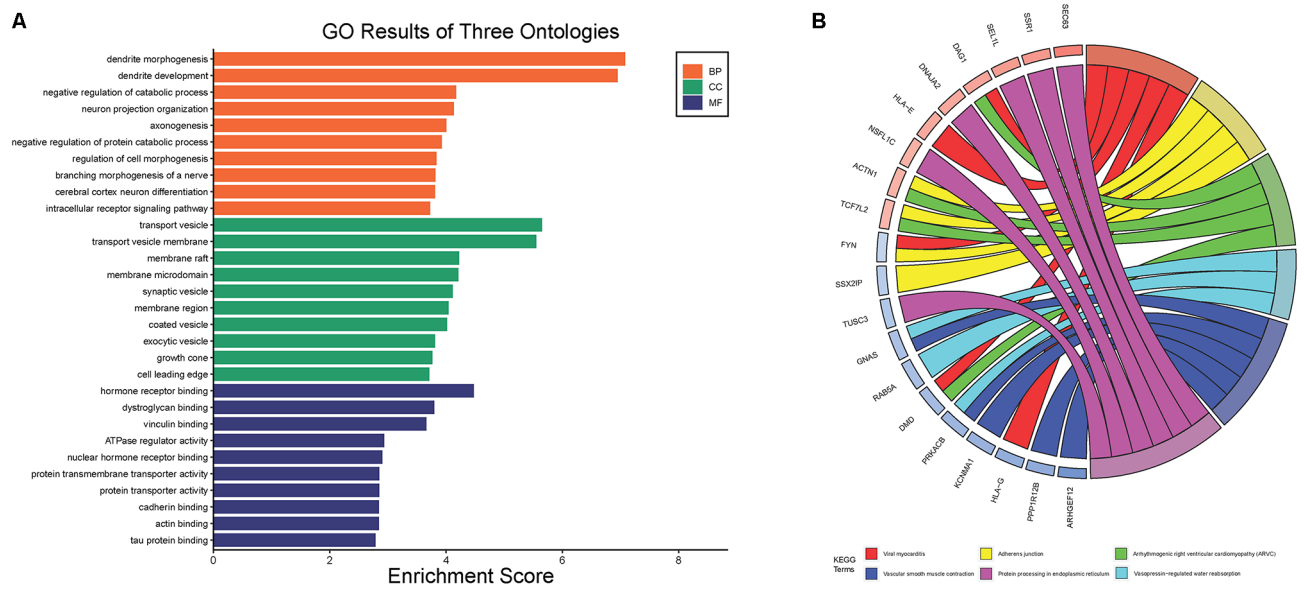

FIGURE 4 | The Go terms and KEGG pathways enrichment analysis of 226 DEGs in PD. **(A)** The Go terms conclude the biological process, cellular component, and molecular function. **(B)** KEGG pathway revealed that DEGs were remarkably concentrated in the viral myocarditis, adherens junction, arrhythmogenic right ventricular cardiomyopathy (ARVC), vasopressin-regulated water reabsorption, vascular smooth muscle contraction, and protein processing in endoplasmic reticulum.

TABLE 2 | Three hub genes and functions.

No.	Gene symbol	Full name	Function
1	RNF130	ring finger protein 130	The protein encoded by this gene contains a RING finger motif and is similar to g1, a Drosophila zinc-finger protein that is expressed in mesoderm and involved in embryonic development. This gene may regulate growth factor withdrawal-induced apoptosis of myeloid precursor cells.
2	SSR1	signal sequence receptor subunit 1	The signal sequence receptor (SSR) is a glycosylated endoplasmic reticulum (ER) membrane receptor associated with protein translocation across the ER membrane. This gene generates several mRNA species as a result of complex alternative polyadenylation.
3	GTF2H5	general transcription factor IIH subunit 5	This gene encodes a subunit of transcript!on/repair factor TFIIH, which functions in gene transcription and DNA repair. This protein stimulates ERCC3/XPB ATPase activity to trigger DNA opening during DNA repair, and is implicated in regulating cellular levels of TFIIH.

hub genes. These genes were identified as hub genes by virtue of having a degree ≥10. The genes shared in common by the WGCNA and PPI analysis were SSR1, GTF2H5, and RNF130. Since these genes were identified by two analytical methods, they will be the most reliable and representative of genes for our purposes. The names, abbreviations and functions of these hub genes are listed in **Table 2**.

Whole-Blood Sample Verification and Hub Gene Analysis

To further explore whether the abnormally expressed hub genes in the brain could be detected in peripheral blood in patients at an early stage (at the onset of motor symptoms), we observed the difference in expression between the normal group and PD group in three whole-blood datasets and found that all three genes showed significantly upregulated in peripheral blood (**Figures 5A–C**). Their differential expression in peripheral blood was basically consistent with that in the brain. The overall survival analysis of the hub genes was performed using Kaplan-Meier curves. PD patients whose period blood highly expressed these genes showed good overall survival and disease-free survival (**Figures 5D–F**). SSR1, GTF2H5, and RNF130 were expressed highly in brain tissue (**Figure 5G**), which means they meet the fundamental requirements of biomarkers of PD.

Expression Levels of Hub Genes *In vivo*

To analyze the accuracy and reliability of the above bioinformatic analysis, Quantitative Real-Time PCR was used to detect the expression levels of the hub genes in the SN and period blood of PD model mice. We used 6-OHDA and MPTP models for tissue verification. Compared with the value in normal SN tissue (non injected mice) and SHAM group, the expression level of SSR1 was significantly upregulated ($P < 0.05$) after 6-OHDA, as well as after MPTP injury (**Figures 6A,D**). GTF2H5 showed no significant difference in the 6-OHDA model and MPTP

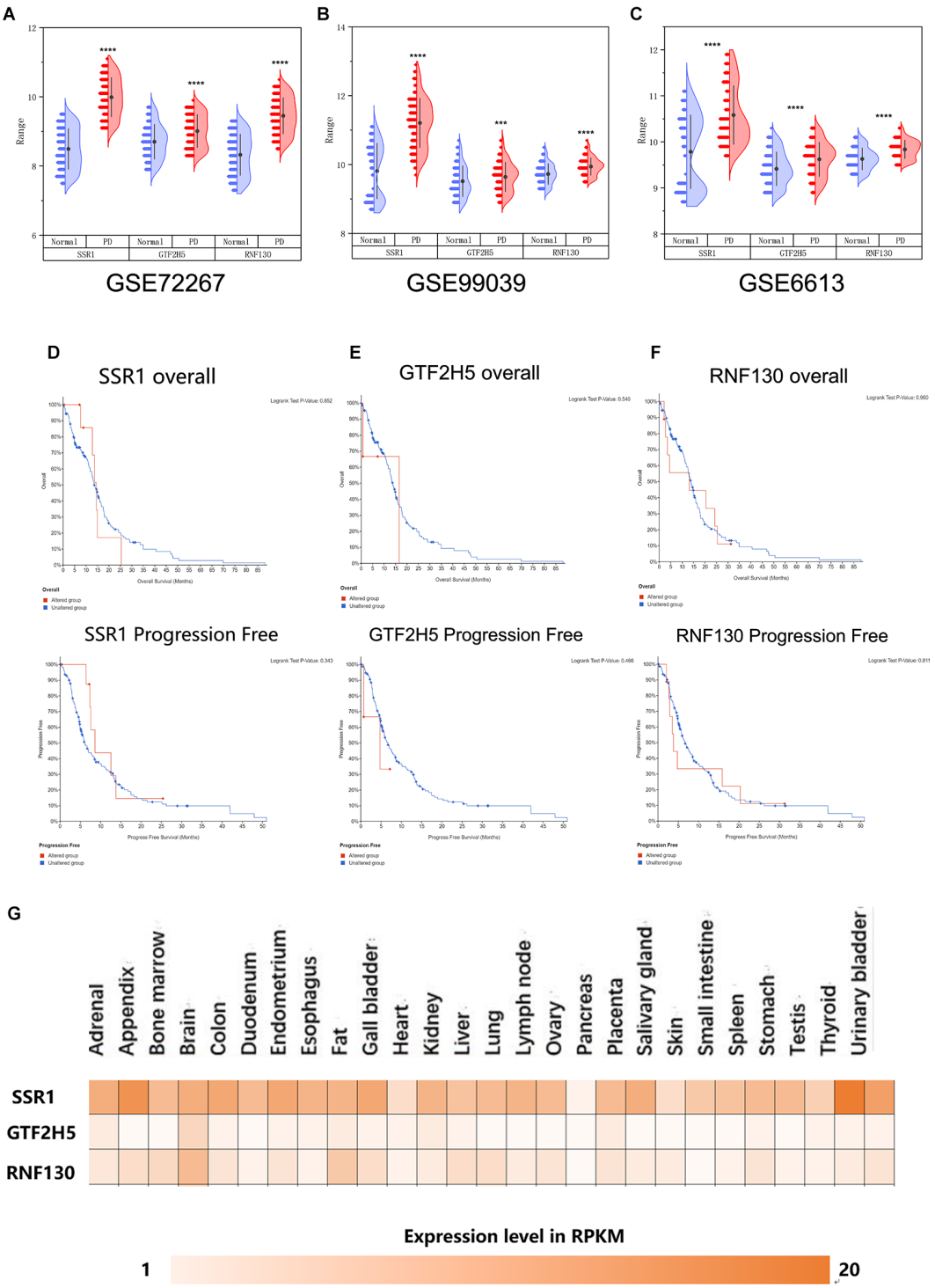

FIGURE 5 | Analysis of the correlation between three hub genes and PD based on bioinfarmatics. **(A–C)** Verification of hub genes based on peripheral blood datasets: GSE72267, GSE99039, and GSE6613. **(D–F)** Overall survival and disease-free survival analyses of three hub genes were performed using cBioPortal online platform. $P < 0.05$ was considered statistically significant. **(G)** Expression level of three hub genes in brain.

model (**Figures 6C,F**). RNF130 was not different in either model (**Figures 6B,E**). Considering the results above, we chose the 6-OHDA model to detect blood changes in hub genes. Surprisingly, SSR1 and GTF2H5 were both upregulated to varying degrees (**Figures 6G–I**). However, because they showed no obvious change in brain tissue, we thought that the changes

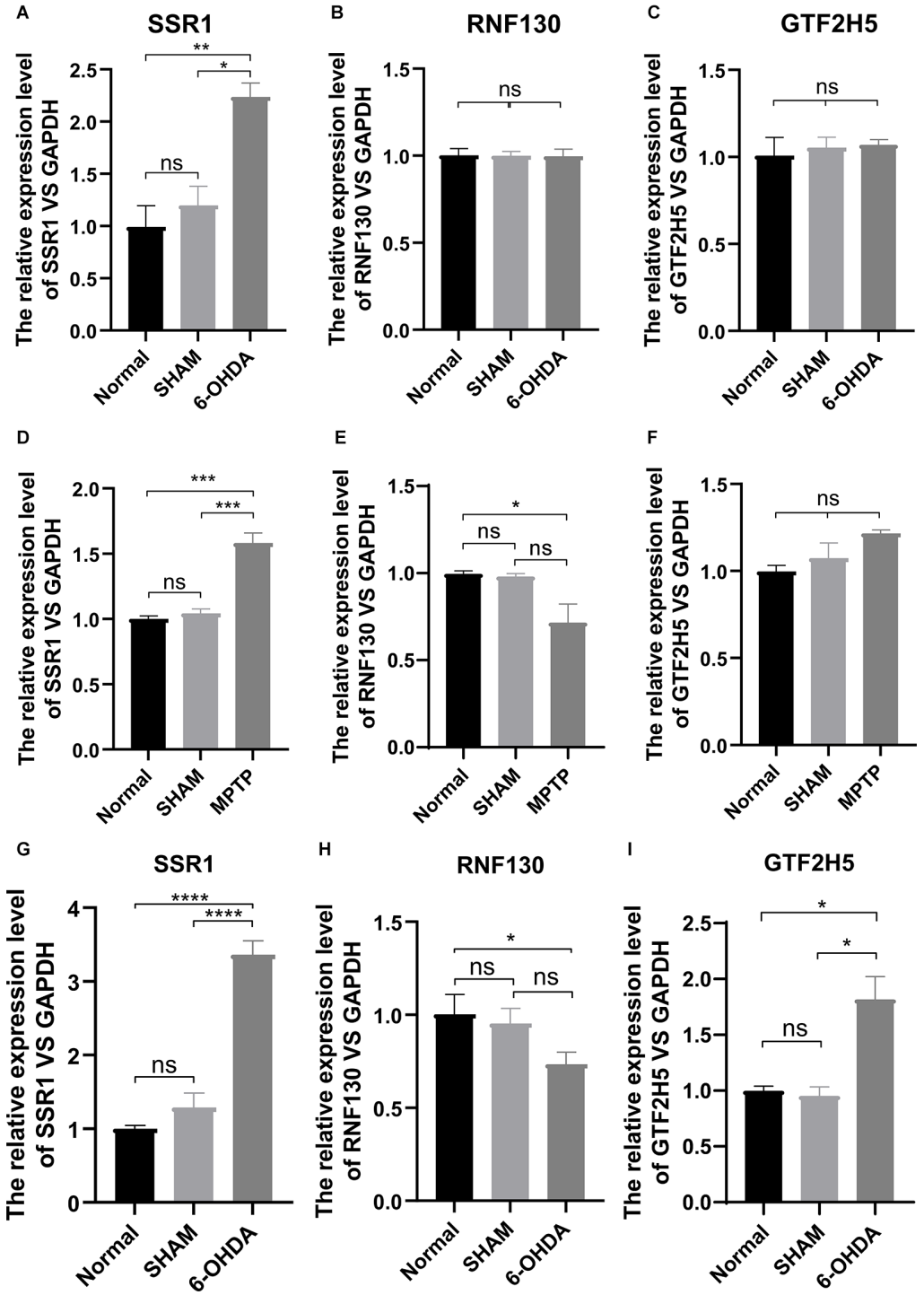

FIGURE 6 | The mRNA relative expression levels of SSR1, GTF2H5, and RNF130 in PD model mice. **(A–C)** The expression levels of SSR1, GTF2H5, and RNF130 in SN (substantia nigra) *in vivo* in PD animal model constructed with 6-OHDA. **(D–F)** The expression levels of SSR1, GTF2H5, and RNF130 in SN (substantia nigra) *in vivo* in PD animal model constructed with MPTP. **(G–I)** The expression levels of SSR1, GTF2H5, and RNF130 in whole blood *in vivo* in PD animal model constructed with 6-OHDA. Norrnal group (non injected mice), SHAM group (PBS injected mice); ns $p > 0.05$, *$p < 0.05$, **$P < 0.01$, ***$P < 0.001$, ****$P < 0.0001$ vs. each group.

in peripheral blood of GTF2H5 might not be directly related to PD. The imbalance of SSR1 both in the tissues and in peripheral blood after injury suggested that it may play an important role in the occurrence and progression of PD.

Longitudinal Study of SSR1 Expression *In vivo*

To further explore the relationship between the hub gene SSR1 and dopaminergic neurons in the SN, we established a time axis of 0, 3, 5, 7, 14, and 28 d (**Figure 7A**). We detected TH and SSR1 in the SN tissue of 6-OHDA-injured mice and with PBS-injected mice. We used Western blot and immunohistochemistry to analyze the change in TH. Immunohistochemical fluorescence showed that on day 7 after injury, dopaminergic neuron number began to decrease significantly. In the following days, the number of dopamine neurons remained low (**Figure 7B**). Western blot showed similar results: TH decreased below 60% of the control level at day 7, and from day 14 to day 28, it was lower than 20% (**Figure 7C**). Using qPCR to detect the expression trend of SSR1 at the same time, we found that the increase in SSR1 was divided into three stages (**Figure 7D**). It increased significantly from 0 d to 3 d, remained stable from 3 d to 7 d, and increased again from 7 d to 28 d, which was consistent with the decreasing trend of dopamine neurons. Then we performed a correlation analysis of SSR1 and TH in SN (**Figure 7E**). Regression of TH neuron number on SSR1 concentration showed a negative correlation, with a goodness of fit (R^2) of 0.8834. The results show that in animal models, SSR1 has a strong negative correlation with TH neurons. SSR1 may be related to damage to TH neurons and to a certain extent can reflect the degree of damage to them.

To explore whether SSR1 could be a biomarker in the early stage of PD, we measured the correlation between changes in animal behavior and SSR1 expression in blood. Most preclinical experiments have focused on late-stage, chronic, fully DA-depleted states (Stanic et al., 2003; Grealish et al., 2010; Boix et al., 2015; Zhang et al., 2017). Few studies have focused specifically on the early-phase behavioral responses after 6-OHDA lesions in the SNc (Fornaguera and Schwarting, 1999; Rosa et al., 2020). In the 6-OHDA model, few researchers have focused on behavioral disorders in the first week after SN striatum injury. We thought it would be interesting to study the early time course of changes occurring in the emergence of the parkinsonian lesion in the standard 6-OHDA model and whether SSR1 might be predictive of the severity of the lesion. Behavioral changes began to appear at 7 days after 6-OHDA injection, and significant differences appeared from 14 days to 28 days. There were few abnormalities in 3D and 5D (in apomorphine-induced rotation, when the number of rotations is >7 r/min, it is considered a successful model; **Figure 7F**). The rotation experiment induced by apomorphine further suggested that the number of dopamine neurons decreased to less than 20% of the control level at 14D-28D. The expression of SSR1 in peripheral blood began to be upregulated as early as day 3, when behavioral disorders were not obvious (**Figure 7G**). As the course of the disease progressed, the expression of SSR1 in peripheral blood stayed high. These results show that in the early stage of a PD model (with few or no behavioral abnormalities), SSR1 is significantly upregulated in both the brain and blood. This abnormal expression may indicate the degree of damage to dopaminergic neurons and make SSR1 a promising biomarker of early PD.

Machine Learning

RF, KNN, and SVM were used to construct classifiers to distinguish PD patients from healthy controls based on GSE6613, which shows the best performance in both classifiers (**Supplementary Figure 1**). To identify the best predictors of each classifier, we added these upregulated genes to each classifier one by one in order of rank. The RF classifier based on SSR1 had good predictive power (AUC: 0.91; **Figure 8A**). In addition, we validated the PD specificity of our gene expression classifier by testing it on two different protein aggregation disease datasets: one Alzheimer's disease dataset (GSE85426) and one Huntington's disease expression dataset (GSE51799). The AUCs of SSR1 for AD and HD were low (**Figures 8B,C**), which indicates that our expression classifier has no prediction power for Alzheimer's disease or Huntington's disease but is efficient and specific for PD. Given that the expression level of SSR1 in other organs (**Figure 6B**), such as the bladder, thyroid, and endometrium, was similar to that in the brain, we chose three datasets of these diseases and tested the AUC power of SSR1 in cases not specific to PD. As expected, these curves had AUCs lower than 0.6 (**Figures 8D–F**), which means that SSR1 has extreme specificity to Parkinson's disease, while it behaves normally in other diseases. The KNN and SVM classifier yielded similar results as the RF classifier (**Figures 8A–F**). By comparing the AUC value of three classifiers: RF(AUC:0.91), KNN (AUC:0.89), SVM(AUC:0.93), we can find SVM classifier behaviors best. To confirm the results above, MCC was implemented to select the optimal classifier to use in clinical applications. As illustrated in **Figure 9**, SVM had the highest MCC all the time, which represents high recognition accuracy and precision. To sum up, the SVM classifier has the best precision of SSR1 in PD.

DISCUSSION

Studies on PD biomarkers based on the GEO datasets have mostly used the peripheral-blood datasets (Wang et al., 2017, 2019; Wu et al., 2020; Yuan et al., 2020). Biomarkers corresponding to PD molecular neuropathological characteristics based on its pathogenesis can not only predict PD at an early stage but also assess the condition of PD patients and judge their prognosis. Therefore, it would b valuable to find biomarkers that are not only related to the pathogenesis of PD but also abnormally expressed in peripheral blood. This study is the first to combine brain tissue and peripheral-blood datasets to find potential biomarkers of PD. We used WGCNA to select five hub genes and constructed a PPI network through GEO data analysis to find six key genes that are abnormally expressed in the brain tissue of PD patients. We selected the three upregulated genes shared by the two analytical methods for further study. Since the ultimate goal was to find peripheral-blood markers, we verified the expression of the three hub genes in the peripheral-blood datasets. This combined with survival analysis showed that all three hub genes

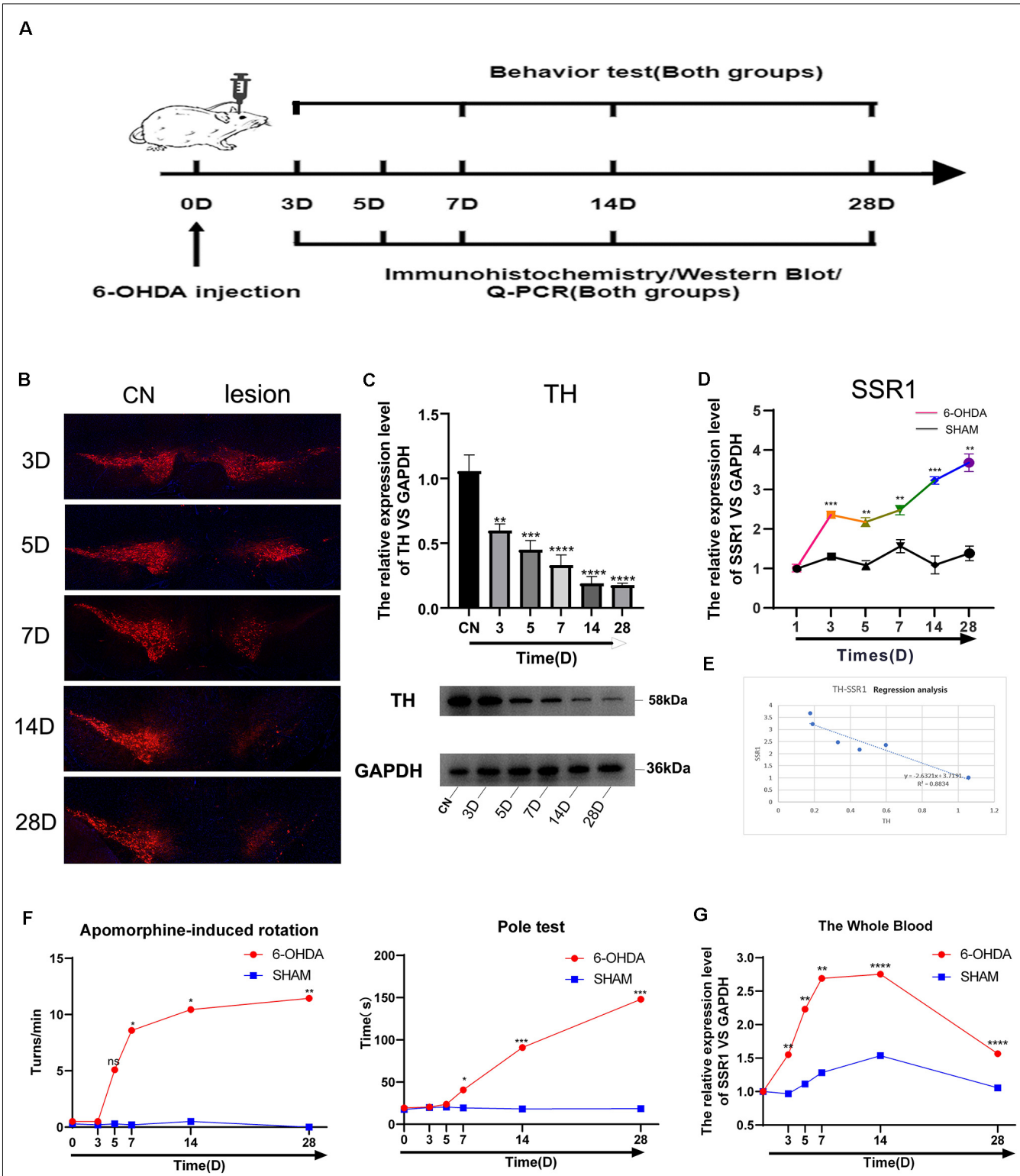

FIGURE 7 | Longitudinal study of SSR1 expression *in vivo*. **(A)** The flowchart of the construction of the 6-OHDA subacute model, behavioral tests, and sacrifice. **(B)** Tyrosine hydroxylase (TH) staining of the substantia nigra (SN) of the above mice. Scale bars: 200 μm. **(C)** Western blot analyses of TH in SN of the above mice. **(D)** The mRNA relative expression levels of SSR1 in SN of the above mice. **(E)** The correlation analysis of SSR1 and TH in SN. **(F)** Pole tests and apomorphine-induced rotation were conducted by a blinded observer after 6-OHDA treatment. **(G)** The mRNA relative expression levels of SSR1 in the whole blood of the above mice. ns $p > 0.05$, $^{*}P < 0.05$, $^{**}P < 0.01$, $^{***}P < 0.001$, $^{****}P < 0.0001$ vs. Control group.

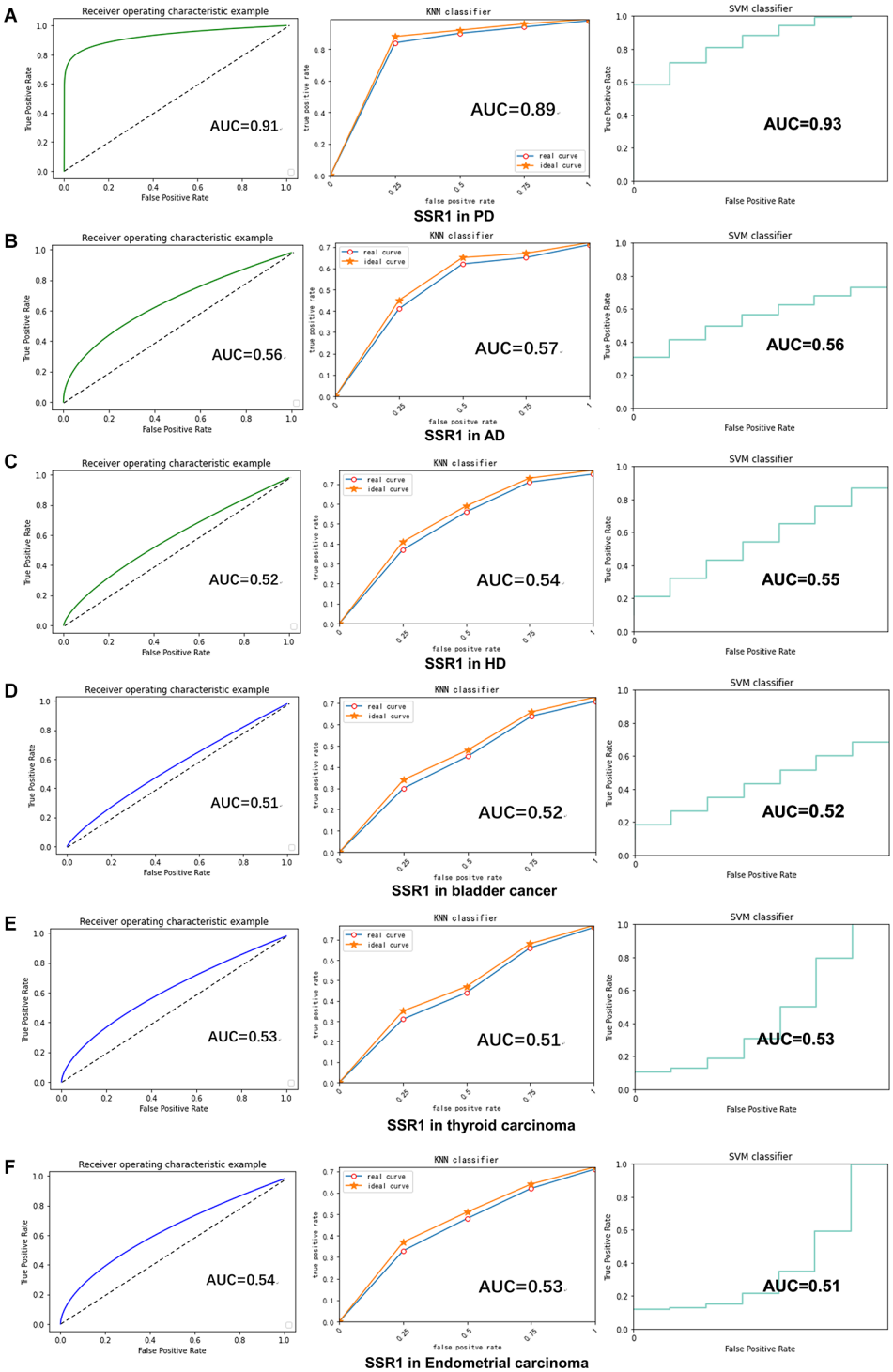

FIGURE 8 | SSR1 in artificial intelligence prediction model. **(A)** The ROC curve of the sensitivity for the diagnosis of PD based on SSR1 from RF (left), KNN analysis (middle), and SVM analysis (right). **(B–F)** The ROC curve of the specificity for the diagnosis of PD based on SSR1 in AD **(B)**, HD **(C)**, Bladder cancer **(D)**, Thyroid carcinoma **(E)**, and Endometrial carcinoma **(F)**.

were significantly upregulated and were associated with the overall survival of patients. Through bioinformatics analysis, we further confirmed the applicability of the hub genes in animal models, which suggests they can be useful in the clinic. Through qPCR verification, we successfully reproduced the SSR1 disorders in the mouse SN, which was consistent with the

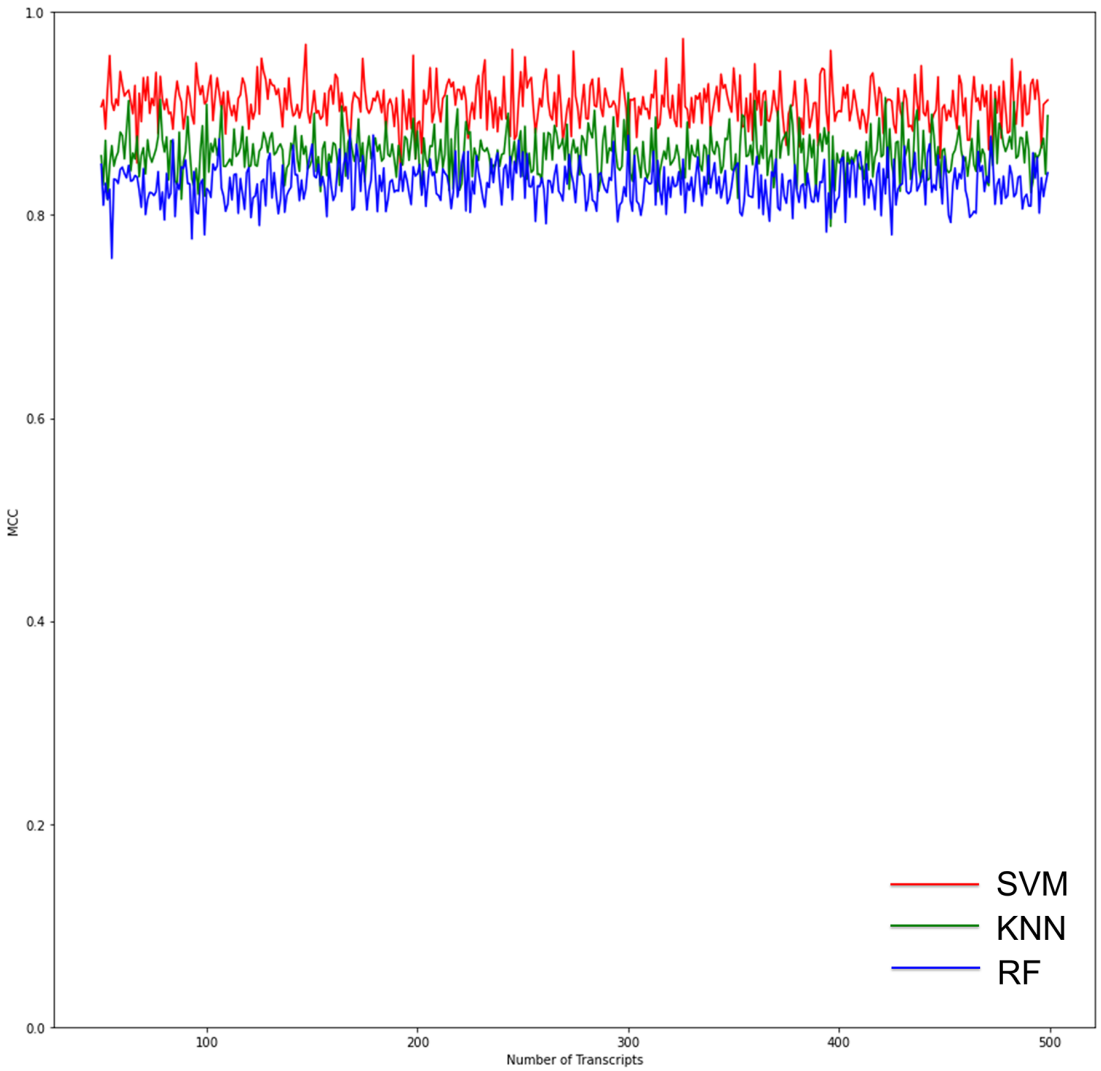

FIGURE 9 | Graphs show the performance of the three ML models according to the number of genes for binary classification. The red curves indicate SVM classifiers. The green curves indicate KNN classifiers. The blue curves indicate RF classifiers. The SVM classifier had the highest Matthews correlation coefficient (MCC) value, which means the highest recognition accuracy and precision.

bioinformatic analysis. However, GTF2H5 and RNF130 were verified in only one model, and we were unable to verify their value in both models, so we will not further study them in PD.

From the loss of dopamine neurons and the time curve of SSR1 brain expression, the imbalance of SSR1 expression is closely related to the loss of dopamine neurons. The more dopamine neurons are lost, the higher the expression of SSR1. Although we have not fully proven that SSR1 is involved in the damage to TH neurons, our experimental results do show that SSR1 is highly correlated with the damage to TH neurons and may indicate the severity of TH damage. Our results also show that when TH neuronal damage was below 20%, SSR1 expression was maintained to a certain degree. This suggests that the expression of SSR1 may be the response of glial cells to TH neuron damage. We also compared the behavioral curve with the curve of SSR1 expression in peripheral blood. SSR1 was upregulated in the early PD model or even when there is no obvious abnormality in behavior. SSR1 showed a certain degree of predictive power for PD in animal models.

The signal sequence receptor subunit (SSR) is a glycosylated endoplasmic reticulum (ER) membrane receptor associated with protein translocation across the ER membrane. The SSR consists of two subunits, one of which is SSR1. The main function of the endoplasmic reticulum is the synthesis and folding of secretory proteins. Changes in ER function will increase oxidative stress or protein N-glycosylation dysfunction, leading to the accumulation of misfolded proteins in the ER and triggering ER stress. Through KEGG analysis, we found that SSR1 was involved in ER stress. In a recent model of ER stress, it was found that long-term endoplasmic reticulum stress can induce the upregulation of mRNA encoding TARPa, namely, SSR1

(Nguyen et al., 2018). However, the significance of SSR1 in the PD model has never been confirmed. The impact of ER stress in PD has been a concern in recent years. It was first discovered in the PD model induced by MPP + rotenone. Long-term ER stress participates in the unfolded protein response (UPR) through high expression of genes involved in the pathological process of PD (Ryu et al., 2002). UPR-related signaling pathways are an adaptive cellular mechanism designed to restore ER homeostasis. Misfolded proteins can activate it to limit ER stress (Hetz et al., 2011). The activation of the UPR is controlled by the PERK, IRE1α, and ATF6 receptors on the ER membrane. Under normal circumstances, BiP binds to related receptors to inhibit its phosphorylation and the activation of downstream pathways. Under pathological conditions, α-synuclein directly interacts with BiP to trigger the phosphorylation of BiP, promote the dissociation of BiP from related receptors, and activate the UPR (Cooper et al., 2006; Jiang et al., 2010; Bellucci et al., 2011), thereby inducing downstream activation of the PERK axis, the IRE1α-XBP1 axis, and the EIF2α axis (Prell et al., 2012). Autopsy analysis of Parkinson's patients has found that compared with the control group, patients with PD showed more phosphorylated PERK in the SN dopaminergic neurons. eIF2α, phosphorylated PERK, and α-synuclein coexist in the dopaminergic neurons of PD patients (Hoozemans et al., 2007), which further suggests that α-synuclein and long-term ER stress in PD patients are closely linked. The ER stress induced by tunicamycin can also lead to the accumulation of oligomeric α-synuclein (Jiang et al., 2010), indicating that the ER stress may also reversely aggravate the aggregation and toxicity of α-syn, forming a vicious cycle and exacerbating PD deterioration. We speculate that SSR1 may be a UPR-related mRNA that reflects the degree of ER stress. In the early stage of injury, abnormally aggregated α-synuclein activates the UPR to promote the upregulation of the SSR1 gene by binding to BiP to relieve acute ER stress. Therefore, the compensatory effect of dopamine neuron damage is not obvious at this time. When the ER stress becomes chronic, it exacerbates the accumulation of oligomeric α-synuclein, and the compensatory effect of the UPR cannot counteract the increasing accumulation of abnormal α-synuclein, which further triggers inflammation. At this time, dopamine neurons are significantly reduced, and animal behavior is also significantly abnormal. The expression of SSR1 continues to be upregulated. α-Synuclein activates the PERK axis in astrocytes, and the regulation of the UPR by α-synuclein is not limited to neurons. Considering that astrocytes participate in a variety of brain functions and support neuronal activity, activation of the UPR in these cells by α-synuclein may lead to harmful consequences. This may explain why SSR1 is still highly expressed when the expression of TH neurons in late PD is extremely low. Therefore, SSR1, which has abnormal expression in the early stage of PD (before obvious movement disorders), can be used not only as an early marker but also as an effective indicator of the severity, progression, and prognosis of PD.

For the first time, we applied the timeline of an animal model to the verification and exploration of hub genes, instead of knocking out target genes in an organelle. Exploration in mice may also lay the foundation for the next step toward clinical application. The most commonly used machine learning includes SVM, KNN, RF, and ANN (Artificial Neural Network). Since ANN is a multivariate input, it has no way to predict only SSR1. So we choose the other three classifiers to analyze SSR1 temporarily. Based on our analysis, we selected SVM to construct a computer model for clinical prediction. The application of artificial intelligence to the medical industry has gradually progressed, especially in the fields of early PD prediction and severity prediction (Zhan et al., 2018; Gupta et al., 2020). Recent advances in SVM have enabled the creation of computer models that can accurately perform many tasks involving prognosis of the disease and early diagnosis (Kaya, 2019). SVM has identified PD patients' dopaminergic imaging markers (Prashanth et al., 2016), walking protocols (Rehman et al., 2019) and idiopathic REM sleep behavior disorder (Christensen et al., 2014) for early prediction. In this study, we established a SVM classifier model by identifying the peripheral-blood data of different samples that were from healthy or PD patients and continuously consolidated and improved the accuracy of the model through continuous calculation and screening of the data. In the future, as the number of clinical data samples increases, we can further improve the training results.

In future studies, we would like to further investigate whether the abnormal expression of SSR1 in PD patients is dominated by dopaminergic neurons or astrocytes. We also plan to study the possible mechanisms within cells. To improve the accuracy and sensitivity of diagnosis, the combination of neuroimaging and peripheral-blood biomarkers can provide better discrimination between parkinsonisms. The SVM can combine peripheral-blood data and images and differentially weight the two kinds of data to form an accurate judgment classifier model. This method is easily accessible and clinically applicable. It provides opportunities to develop an early diagnostic tool for PD patients, helping to save their dopaminergic neurons as early as possible.

DATA AVAILABILITY STATEMENT

The datasets presented in this study can be found in online repositories. The names of the repository/repositories and accession number(s) can be found in the article/**Supplementary Material**.

ETHICS STATEMENT

The animal study was reviewed and approved by Animal experiment ethics committee of Nantong University. Written informed consent was obtained from the individual(s) for the publication of any potentially identifiable images or data included in this article.

AUTHOR CONTRIBUTIONS

MC and QZ designed the experiments. WZ and YW performed the experiments. WZ, YW, KC, and JS analyzed

the data. MC and JS contributed to reagents, materials, and analysis tools. WZ and QZ wrote the article. All authors contributed to the article and approved the submitted version.

FUNDING

This work was supported by the National Natural Science Foundation of China (81771404 and 81901195).

ACKNOWLEDGMENTS

We thank American Journal Experts for their support in editing this article.

SUPPLEMENTARY MATERIALS

The Supplementary Material for this article can be found online at: https://www.frontiersin.org/articles/10.3389/fnmol.2022.762544/full#supplementary-material.

REFERENCES

Angelopoulou, E., Paudel, Y. N., and Piperi, C. (2019). miR-124 and Parkinson's disease: a biomarker with therapeutic potential. *Pharmacol. Res.* 150:104515. doi: 10.1016/j.phrs.2019.104515

Bellucci, A., Navarria, L., Zaltieri, M., Falarti, E., Bodei, S., Sigala, S., et al. (2011). Induction of the unfolded protein response by α-synuclein in experimental models of Parkinson's disease. *J. Neurochem.* 116, 588–605. doi: 10.1111/j.1471-4159.2010.07143.x

Benamer, T. S., Patterson, J., Grosset, D. G., Booij, J., de Bruin, K., van Royen, E., et al. (2000). Accurate differentiation of parkinsonism and essential tremor using visual assessment of [123I]-FP-CIT SPECT imaging: the [123I]-FP-CIT study group. *Mov. Disord.* 15, 503–510. doi: 10.1002/1531-8257(200005)15:3%3C503::AID-MDS1013%3E3.0.CO;2-V

Besong-Agbo, D., Wolf, E., Jessen, F., Oechsner, M., Hametner, E., Poewe, W., et al. (2013). Naturally occurring α-synuclein autoantibody levels are lower in patients with Parkinson disease. *Neurology* 80, 169–175. doi: 10.1212/WNL.0b013e31827b90d1

Boix, J., Padel, T., and Paul, G. (2015). A partial lesion model of Parkinson's disease in mice – characterization of a 6-OHDA-induced medial forebrain bundle lesion. *Behav. Brain Res.* 284, 196–206. doi: 10.1016/j.bbr.2015.01.053

Brooks, D. J., and Pavese, N. (2011). Imaging biomarkers in Parkinson's disease. *Prog. Neurobiol.* 95, 614–628. doi: 10.1016/j.pneurobio.2011.08.009

Chahine, L. M., Stern, M. B., and Chen-Plotkin, A. (2014). Blood-based biomarkers for Parkinson's disease. *Parkinsonism Relat. Disord.* 20, S99–103. doi: 10.1016/S1353-8020(13)70025-7

Chen, L., Yuan, L., Wang, Y., Wang, G., Zhu, Y., Cao, R., et al. (2017). Co-expression network analysis identified FCER1G in association with progression and prognosis in human clear cell renal cell carcinoma. *Int. J. Biol. Sci.* 13, 1361–1372. doi: 10.7150/ijbs.21657

Chicco, D., and Jurman, G. (2020). The advantages of the Matthews correlation coefficient (MCC) over F1 score and accuracy in binary classification evaluation. *BMC Genomics* 21:6. doi: 10.1186/s12864-019-6413-7

Christensen, J. A., Kempfner, J., Zoetmulder, M., Leonthin, H. L., Arvastson, L., Christensen, S. R., et al. (2014). Decreased sleep spindle density in patients with idiopathic REM sleep behavior disorder and patients with Parkinson's disease. *Clin. Neurophysiol.* 125, 512–519. doi: 10.1016/j.clinph.2013.08.013

Cooper, A. A., Gitler, A. D., Cashikar, A., Haynes, C. M., Hill, K. J., Bhullar, B., et al. (2006). α-synuclein blocks ER-Golgi traffic and Rab1 rescues neuron loss in Parkinson's models. *Science* 313, 324–328. doi: 10.1126/science.1129462

Cover, T. M., and Hart, P. E. (1967). Nearest neighbor pattern classification. *IEEE Trans. Inform. Theory* 13, 21–27. doi: 10.1109/TIT.1967.1053964

Damier, P., Hirsch, E. C., Agid, Y., and Graybiel, A. M. (1999). The substantia nigra of the human brain. II. Patterns of loss of dopamine-containing neurons in Parkinson's disease. *Brain* 122, 1437–1448. doi: 10.1093/brain/122.8.1437

Dauer, W., and Przedborski, S. (2003). Parkinson's disease: mechanisms and models. *Neuron* 39, 889–909. doi: 10.1016/s0896-6273(03)00568-3

De Martino, F., Valente, G., Staeren, N., Ashburner, J., Goebel, R., and Formisano, E. (2008). Combining multivariate voxel selection and support vector machines for mapping and classification of fMRI spatial patterns. *Neuroimage* 43, 44–58. doi: 10.1016/j.neuroimage.2008.06.037

Deo, R. C. (2015). Machine learning in medicine. *Circulation* 132, 1920–1930. doi: 10.1161/CIRCULATIONAHA.115.001593

Edgar, R., Domrachev, M., and Lash, A. E. (2002). Gene Expression Omnibus: NCBI gene expression and hybridization array data repository. *Nucleic Acids Res.* 30, 207–210. doi: 10.1093/nar/30.1.207

Fornaguera, J., and Schwarting, R. K. (1999). Early behavioral changes after nigro-striatal system damage can serve as predictors of striatal dopamine depletion. *Prog. Neuropsychopharmacol. Biol. Psychiatry* 23, 1353–1368. doi: 10.1016/s0278-5846(99)00071-8

Frosini, D., Cosottini, M., Volterrani, D., and Ceravolo, R. (2017). Neuroimaging in Parkinson's disease: focus on substantia nigra and nigro-striatal projection. *Curr. Opin. Neurol.* 30, 416–426. doi: 10.1097/WCO.0000000000000463

Grealish, S., Mattsson, B., Draxler, P., and Bjorklund, A. (2010). Characterisation of behavioural and neurodegenerative changes induced by intranigral 6-hydroxydopamine lesions in a mouse model of Parkinson's disease. *Eur. J. Neurosci.* 31, 2266–2278. doi: 10.1111/j.1460-9568.2010.07265.x

Grossi, I., Radeghieri, A., Paolini, L., Porrini, V., Pilotto, A., Padovani, A., et al. (2021). MicroRNA34a5p expression in the plasma and in its extracellular vesicle fractions in subjects with Parkinson's disease: an exploratory study. *Int. J. Mol. Med.* 47, 533–546. doi: 10.3892/ijmm.2020.4806

Gupta, U., Bansal, H., and Joshi, D. (2020). An improved sex-specific and age-dependent classification model for Parkinson's diagnosis using handwriting measurement. *Comput. Methods Programs Biomed.* 189:105305. doi: 10.1016/j.cmpb.2019.105305

Hetz, C., Martinon, F., Rodriguez, D., and Glimcher, L. H. (2011). The unfolded protein response: integrating stress signals through the stress sensor IRE1α. *Physiol. Rev.* 91, 1219–1243. doi: 10.1152/physrev.00001.2011

Ho, T. K. (1998). The random subspace method for constructing decision forests. *IEEE Trans. Pattern Anal. Mach. Intell.* 20, 832–844. doi: 10.1109/34.709601

Hong, Z., Shi, M., Chung, K. A., Quinn, J. F., Peskind, E. R., Galasko, D., et al. (2010). DJ-1 and α-synuclein in human cerebrospinal fluid as biomarkers of Parkinson's disease. *Brain* 133, 713–726. doi: 10.1093/brain/awq008

Hoozemans, J. J., van Haastert, E. S., Eikelenboom, P., de Vos, R. A., Rozemuller, J. M., and Scheper, W. (2007). Activation of the unfolded protein response in Parkinson's disease. *Biochem. Biophys. Res. Commun.* 354, 707–711. doi: 10.1016/j.bbrc.2007.01.043

Jiang, P., Gan, M., Ebrahim, A. S., Lin, W. L., Melrose, H. L., and Yen, S. H. (2010). ER stress response plays an important role in aggregation of α-synuclein. *Mol. Neurodegener.* 5:56. doi: 10.1186/1750-1326-5-56

Kagi, G., Bhatia, K. P., and Tolosa, E. (2010). The role of DAT-SPECT in movement disorders. *J. Neurol. Neurosurg. Psychiatry* 81, 5–12. doi: 10.1136/jnnp.2008.157370

Kalia, L. V., and Lang, A. E. (2015). Parkinson's disease. *Lancet* 386, 896–912. doi: 10.1016/S0140-6736(14)61393-3

Kaya, D. (2019). Optimization of SVM parameters with hybrid CS-PSO algorithms for Parkinson's disease in labVIEW environment. *Parkinsons Dis.* 2019:2513053. doi: 10.1155/2019/2513053

Kim, B. H., Yu, K., and Lee, P. C. W. (2020). Cancer classification of single-cell gene expression data by neural network. *Bioinformatics* 36, 1360–1366. doi: 10.1093/bioinformatics/btz772

Kriegeskorte, N., and Golan, T. (2019). Neural network models and deep learning. *Curr. Biol.* 29, R231–R236. doi: 10.1016/j.cub.2019.02.034

Lang, A. E., and Lozano, A. M. (1998). Parkinson's disease. First of two parts. *N. Engl. J. Med.* 339, 1044–1053. doi: 10.1056/NEJM199810083391506

Langfelder, P., and Horvath, S. (2008). WGCNA: an R package for weighted correlation network analysis. *BMC Bioinform.* 9:559. doi: 10.1186/1471-2105-9-559

Lawton, M., Baig, F., Toulson, G., Morovat, A., Evetts, S. G., Ben-Shlomo, Y., et al. (2020). Blood biomarkers with Parkinson's disease clusters and prognosis: the oxford discovery cohort. *Mov. Disord.* 35, 279–287. doi: 10.1002/mds.27888

Lehericy, S., Sharman, M. A., Dos Santos, C. L., Paquin, R., and Gallea, C. (2012). Magnetic resonance imaging of the substantia nigra in Parkinson's disease. *Mov. Disord.* 27, 822–830. doi: 10.1002/mds.25015

Lin, C. H., Li, C. H., Yang, K. C., Lin, F. J., Wu, C. C., Chieh, J. J., et al. (2019). Blood NfL: a biomarker for disease severity and progression in Parkinson disease. *Neurology* 93, e1104–e1111. doi: 10.1212/WNL.0000000000008088

Mollenhauer, B., Locascio, J. J., Schulz-Schaeffer, W., Sixel-Doring, F., Trenkwalder, C., and Schlossmacher, M. G. (2011). α-Synuclein and tau concentrations in cerebrospinal fluid of patients presenting with parkinsonism: a cohort study. *Lancet Neurol.* 10, 230–240. doi: 10.1016/S1474-4422(11)70014-X

Mollenhauer, B., Trautmann, E., Taylor, P., Manninger, P., Sixel-Doring, F., Ebentheuer, J., et al. (2013). Total CSF α-synuclein is lower in *de novo* Parkinson patients than in healthy subjects. *Neurosci. Lett.* 532, 44–48. doi: 10.1016/j.neulet.2012.11.004

Nguyen, D., Stutz, R., Schorr, S., Lang, S., Pfeffer, S., Freeze, H. H., et al. (2018). Proteomics reveals signal peptide features determining the client specificity in human TRAP-dependent ER protein import. *Nat. Commun.* 9:3765. doi: 10.1038/s41467-018-06188-z

Parnetti, L., Gaetani, L., Eusebi, P., Paciotti, S., Hansson, O., El-Agnaf, O., et al. (2019). CSF and blood biomarkers for Parkinson's disease. *Lancet Neurol.* 18, 573–586. doi: 10.1016/S1474-4422(19)30024-9

Prashanth, R., Dutta Roy, S., Mandal, P. K., and Ghosh, S. (2016). High-accuracy detection of early Parkinson's disease through multimodal features and machine learning. *Int. J. Med. Inform.* 90, 13–21. doi: 10.1016/j.ijmedinf.2016.03.001

Prell, T., Lautenschlager, J., Witte, O. W., Carri, M. T., and Grosskreutz, J. (2012). The unfolded protein response in models of human mutant G93A amyotrophic lateral sclerosis. *Eur. J. Neurosci.* 35, 652–660. doi: 10.1111/j.1460-9568.2012.08008.x

Rehman, R. Z. U., Del Din, S., Shi, J. Q., Galna, B., Lord, S., Yarnall, A. J., et al. (2019). Comparison of walking protocols and gait assessment systems for machine learning-based classification of Parkinson's disease. *Sensors (Basel)* 19:5363. doi: 10.3390/s19245363

Rosa, I., Di Censo, D., Ranieri, B., Di Giovanni, G., Scarnati, E., Alecci, M., et al. (2020). Comparison between tail suspension swing test and standard rotation test in revealing early motor behavioral changes and neurodegeneration in 6-OHDA hemiparkinsonian rats. *Int. J. Mol. Sci.* 21:2874. doi: 10.3390/ijms21082874

Ryu, E. J., Harding, H. P., Angelastro, J. M., Vitolo, O. V., Ron, D., and Greene, L. A. (2002). Endoplasmic reticulum stress and the unfolded protein response in cellular models of Parkinson's disease. *J. Neurosci.* 22, 10690–10698. doi: 10.1523/JNEUROSCI.22-24-10690.2002

Schadt, E. E., Lamb, J., Yang, X., Zhu, J., Edwards, S., Guhathakurta, D., et al. (2005). An integrative genomics approach to infer causal associations between gene expression and disease. *Nat. Genet.* 37, 710–717. doi: 10.1038/ng1589

Smith, L. M., Schiess, M. C., Coffey, M. P., Klaver, A. C., and Loeffler, D. A. (2012). α-Synuclein and anti-α-synuclein antibodies in Parkinson's disease, atypical Parkinson syndromes, REM sleep behavior disorder and healthy controls. *PLoS One* 7:e52285. doi: 10.1371/journal.pone.0052285

Stanic, D., Finkelstein, D. I., Bourke, D. W., Drago, J., and Horne, M. K. (2003). Timecourse of striatal re-innervation following lesions of dopaminergic SNpc neurons of the rat. *Eur. J. Neurosci.* 18, 1175–1188. doi: 10.1046/j.1460-9568.2003.02800.x

Thambisetty, M., and Lovestone, S. (2010). Blood-based biomarkers of Alzheimer's disease: challenging but feasible. *Biomark. Med.* 4, 65–79. doi: 10.2217/bmm.09.84

Visanji, N. P., Marras, C., Hazrati, L. N., Liu, L. W., and Lang, A. E. (2014). Alimentary, my dear Watson? The challenges of enteric α-synuclein as a Parkinson's disease biomarker. *Mov. Disord.* 29, 444–450. doi: 10.1002/mds.25789

Wang, C., Chen, L., Yang, Y., Zhang, M., and Wong, G. (2019). Identification of potential blood biomarkers for Parkinson's disease by gene expression and DNA methylation data integration analysis. *Clin. Epigenetics* 11:24. doi: 10.1186/s13148-019-0621-5

Wang, J., Liu, Y., and Chen, T. (2017). Identification of key genes and pathways in Parkinson's disease through integrated analysis. *Mol. Med. Rep.* 16, 3769–3776. doi: 10.3892/mmr.2017.7112

Wu, Y., Yao, Q., Jiang, G. X., Wang, G., and Cheng, Q. (2020). Identification of distinct blood-based biomarkers in early stage of Parkinson's disease. *Neurol. Sci.* 41, 893–901. doi: 10.1007/s10072-019-04165-y

Yang, Q., Wang, R., Wei, B., Peng, C., Wang, L., Hu, G., et al. (2018). Candidate biomarkers and molecular mechanism investigation for glioblastoma multiforme utilizing WGCNA. *Biomed. Res. Int.* 2018:4246703. doi: 10.1155/2018/4246703

Yuan, Q., Zhang, S., Li, J., Xiao, J., Li, X., Yang, J., et al. (2020). Comprehensive analysis of core genes and key pathways in Parkinson's disease. *Am. J. Transl. Res.* 12, 5630–5639.

Zhan, A., Mohan, S., Tarolli, C., Schneider, R. B., Adams, J. L., Sharma, S., et al. (2018). Using smartphones and machine learning to quantify Parkinson disease severity: the mobile Parkinson disease score. *JAMA Neurol.* 75, 876–880. doi: 10.1001/jamaneurol.2018.0809

Zhang, Z. (2016). Introduction to machine learning: k-nearest neighbors. *Ann. Transl. Med.* 4:218. doi: 10.21037/atm.2016.03.37

Zhang, S., Li, X., Zong, M., Zhu, X., and Wang, R. (2018). Efficient kNN classification with different numbers of nearest neighbors. *IEEE Trans. Neural Netw. Learn. Syst.* 29, 1774–1785. doi: 10.1109/TNNLS.2017.2673241

Zhang, W., Zhang, L., Liu, L., and Wang, X. (2017). Time course study of fractional anisotropy in the substantia nigra of a parkinsonian rat model induced by 6-OHDA. *Behav. Brain Res.* 328, 130–137. doi: 10.1016/j.bbr.2017.03.046

Conflict of Interest: The authors declare that the research was conducted in the absence of any commercial or financial relationships that could be construed as a potential conflict of interest.

Publisher's Note: All claims expressed in this article are solely those of the authors and do not necessarily represent those of their affiliated organizations, or those of the publisher, the editors and the reviewers. Any product that may be evaluated in this article, or claim that may be made by its manufacturer, is not guaranteed or endorsed by the publisher.

Advantages of publishing in Frontiers

OPEN ACCESS
Articles are free to read for greatest visibility and readership

FAST PUBLICATION
Around 90 days from submission to decision

HIGH QUALITY PEER-REVIEW
Rigorous, collaborative, and constructive peer-review

TRANSPARENT PEER-REVIEW
Editors and reviewers acknowledged by name on published articles

Frontiers
Avenue du Tribunal-Fédéral 34
1005 Lausanne | Switzerland

Visit us: www.frontiersin.org
Contact us: frontiersin.org/about/contact

REPRODUCIBILITY OF RESEARCH
Support open data and methods to enhance research reproducibility

DIGITAL PUBLISHING
Articles designed for optimal readership across devices

FOLLOW US
@frontiersin

IMPACT METRICS
Advanced article metrics track visibility across digital media

EXTENSIVE PROMOTION
Marketing and promotion of impactful research

LOOP RESEARCH NETWORK
Our network increases your article's readership